HIGH VALENT URANIUM DIOXO AND IMIDO COMPLEXES: SYNTHESIS AND STRUCTURE

A Dissertation
Presented to
The Faculty of the Graduate School
University of Missouri-Columbia

In Partial Fulfillment
of the Requirements for the Degree
Doctor of Philosophy

---

by
ANTHONY E. VAUGHN
Dr. Paul B. Duval, Dissertation Supervisor
MAY 2008

AThe undersigned, appointed by the Dean of the Graduate School, have examined the dissertation entitled

HIGH VALENT URANIUM DIOXO AND IMIDO COMPLEXES: SYNTHESIS AND STRUCTURE

Presented by ANTHONY E. VAUGHN

A candidate for the degree of Doctor of Philosophy

And hereby certify that in their opinion it is worthy of acceptance.

_____

Professor Paul Duval

_____

Professor Paul Sharp

_____

Professor Steve Keller

_____

Professor Silvia Jurisson

_____

Professor Judy Wall

In loving memory of Maxine Vaughn and Melvin Felber

Acknowledgements

First I would like to thank my graduate advisor Professor Paul B. Duval for support and guidance in his research laboratory and graduate courses, and for spreading awareness of the flourishing field of f-element science. I would also like to thank the members of my dissertation committee: Professors Paul Sharp, Silvia Jurisson, Steven Keller, and Judy Wall for helping me think about my project from different angles.

I am grateful to my wife Ashley our beautiful daughter Aubrey for making every day worth living. For the love and support of my family throughout my academic career. I am especially grateful to my parents, Mark and Karen Vaughn for continual encouragement, and allowing me to shop for groceries in their pantry.

I would like to acknowledge the talented scientists I've had the opportunity to learn from and collaborate with at MU: Drs. Charles Barnes, Wei Wycoff, Jody Turner, Steve Bockhold, Daniel Bassil, and Tuck Wong. A special thanks to the talented group of scientist at LANL for helping develop my scientific intuition and making chapter 4 in this text possible: Drs. Jaqueline L. Kiplinger, David E. Morris, Christopher R. Graves, Eric J. Schelter, Brian L. Scott, and Joe D. Thompson. Finally, I would like to thank the current and former Duval research group members for helpful discussions: Eric M. Weis, Chad L. Magee, Morgan A. Moody, Leah Arrigo, Dr. S. Kannan, Levi Banks, and Joy Biswas.

High Valent Uranium Dioxo and Imido Complexes: Synthesis and Structure

Anthony E. Vaughn

Dr. Paul B. Duval, Dissertation Advisor

Abstract

Early actinide elements have attracted considerable attention in recent years due to the need for rigorous advancements in spent nuclear fuel recycling and remediation technologies, and for their emerging versatility in organometallic chemistry. Whereas high oxidation state ions dominate environmental speciation, the corresponding high-valent organometallics are rare. These hexa- and pentavalent ions are often stabilized by the isoelectronic oxo or imido ligands, which result in robust molecular properties due to 5f/6d orbital involvement in multiple covalent bonding. The research discussed in this dissertation surveys the synthesis, isolation, and molecular and electronic structural characterization of uranyl(VI) and uranium(V)-imide complexes, and uncovers the influences imparted by a variety of functional ligand designs. In the opening report, salicylidene derived Schiff base chelates adapt to equatorial coordination and control uranyl(VI) photo- and electrochemical activity. In the second study, a ferrocenylcarboxylate ligand undergoes a transformation that renders an unprecedented bent uranyl(VI) moiety supported in a reversible coordination polymer. The final segment focuses on the rare uranium(V) oxidation state supported by pentamethylcyclopentadienyl and imido ancillary ligands in mono- and bimetallic complexes geared to elucidate the effects of ligand substitution and metal-metal communication on the $5f^1$ electronic configuration. Future directions and applications for each area are summarized.

TABLE OF CONTENTS

Acknowledgments ……. iv

Abstract ……. v

List of Figures ……..……. x

List of Schemes ……..……... xiv

List of Tables ……...…….. xv

List of Nomenclature …… xvi

Chapter 1. Introduction

1.1 Light Actinide Chemistry …… 1

1.2 The Dioxouranium Ion ……. 3

1.3 Organometallic Uranium Chemistry …….. 9

1.4 Overview 11

Uranyl(VI) Schiff base-Phenolate Complexes ……..…….. 12

A Bent Uranyl Moiety ……..……... 15

Mono- and Bimetallic Organouranium(V)-Imido Complexes ……..…….. 17

References ……. 20

Chapter 2. Structural, Electrochemical, and Photochemical Trends Among Three Types of Uranyl(VI) Schiff Base-Phenolate Complexes and Related Derivatives

Abstract …… 27

2.1 Introduction …….. 29

2.2 Results and Discussion …… 32

Synthesis and Structural Characterization ……..……... 32

Electrochemistry ……..……... 49

Electronic Spectroscopy ……. 55

2.3 Photosynthetic Generation of 1d ……. 63

2.4 Conclusion ……. 67

2.5 Experimental ……. 69

General Considerations ……..…… 69

Sample and Instrumentation Protocol ……..…….. 71

Synthetic Details ……..……... 73

References ……. 78

Chapter 3. Structure and Bending in the Uranyl Ion: A Terminal *cis*-Dioxo Uranyl(VI) Moiety Supported in a Reversible Coordination Polymer

Abstract …… 83

3.1 Introduction …….. 85

3.2 Results and Discussion ……. 88

Synthesis and Structural Characterization ……..……... 88

Electrochemistry ……..……... 105

Electronic Spectroscopy ……..……... 106

3.3 Conclusion ……. 109

3.4 Experimental ……. 111

General Considerations ……..…… 111

Sample and Instrumentation Protocol ……..…….. 111

Synthetic Details ……..……... 114

References ……. 116

Chapter 4. Organouranium(V)-Imido Complexes

Part I. Ligand Substitution Effects on the Electronic Structure of Organouranium(V)-Imido Complexes

Abstract …… 120

4.1 Introduction ……... 122

4.2 Results and Discussion ……. 125

Synthesis and Structural Characterization ……. 125

Synthesis of $(C_5Me_5)_2U(=N\text{-}2,6\text{-}^{i}Pr_2\text{-}C_6H_3)(=N\text{-}C_6H_5)$ (**16**) …….. 134

Electrochemistry ……. 137

Electronic spectroscopy …….. 140

Magnetism ……...……... 147

4.3 Conclusion ……. 150

Part II. Exploring Electronic Communication in Homobimetallic High Valent Uranium Organo-Imido Complexes

Abstract …… 152

4.4 Introduction …….. 154

4.5 Results and Discussion ……. 158

Synthesis and Structural Characterization ……. 158

Electrochemistry ……. 167

Electronic spectroscopy …….. 177

Magnetism ……...……... 179

4.6 Conclusion ……. 182

4.7 Experimental ……. 185

General Considerations …….. 185

Sample and Instrumentation Protocol …… 186

Synthetic Details ……. 187

References ……. 193

Chapter 5. Concluding Remarks

5.1 Uranyl(VI) Schiff base-Phenolate Chemistry …… 201

5.2 A Bent Uranyl(VI) Moiety ……... 205

5.3 Mono- and Homobimetallic Organouranium(V)-Imido Complexes ……... 210

VITA …….. 215

Appendices. Supporting Information

Appendix 1 ……..…….. 216

Appendix 2 ……...……. 299

Appendix 3 ……...……. 316

LIST OF FIGURES

Figure	Caption	Page
1.1	The general set of seven f-orbitals and their polynomial descriptions…….	2
1.2	The molecular orbitals that compose the triple An=O bond order for the $D_{\infty h}$ actinyl unit include combined σ and π overlap between O(2p) with An(5f) and An(6d) atomic valence orbitals along the z-axis……...	4
1.3	A generic uranyl N_2O_2 sal-type Schiff base complex. The variables in this equation include backbone conformation and the capping ligand (L)…….....	13
1.4	*Cis* (bent) and *trans* (linear) dioxo metal geometry…….	15
2.1	*t*-Butyl substituted sal-type ligands saloph (**H_2L^1**), salbinap (**H_2L^2**), saltren (**H_3L^3**) salhpn (**H_3L^7**)……...	31
2.2	Ethylenediamine derived ligands salen (**H_4L^4**), BAP (**H_2L^5**), and salNMe_2 (**HL^6**)……	31
2.3	Molecular structure for [UO_2(^{t}Bu_4-saloph)OH][$CoCp_2$] (**1d**) with thermal ellipsoids depicted at the 50% probability level……...	36
2.4	Molecular structure of UO_2(^{t}Bu_4-salbinap)THF (**2**) with thermal ellipsoids represented at the 50% probability level. Four *t*-butyl fragments are omitted for clarity……..	40
2.5	Ball-and-stick model for **2** depicting the distorted equatorial plane. All atoms except those bound directly to central uranium omitted for clarity…...	40
2.6	Complexes UO_2(^{t}Bu_6-saltrenH) (**3**) and UO_2(^{t}Bu_4-BAPH)$_2$ (**4**). Two *t*-butyl groups per salicylidene moiety not shown……...	42
2.7	The molecular unit UO_2(^{t}Bu_4-H_2salen)(OH_2) (**5**) held together by weak N-H···O=U contacts……..	44
2.8	Molecular structure of (^{t}Bu_4-salhpn)(UO_2)$_2$(μ^2-OMe)(MeOH)$_2$ (**7**) with thermal ellipsoids depicted at the 50% probability level…….	47

2.9 a) Cyclic Voltammogram for $UO_2(^tBu_4\text{-saloph})THF$ (**1a**) in ~0.1 M $[Bu_4N][PF_6]$/MeCN solution at room temperature within a scan rate range of 50-250 mV/s……. 50
b) Cyclic Voltammogram for $UO_2(^tBu_4\text{-saloph})THF$ (**1a**) in 2 ml of ~0.1 M $[Bu_4N][PF_6]/CH_2Cl_2$ solution (red) with THF administered dropwise until a total 3 ml solution (blue) with a constant scan rate of 250 mV/s……. 51

2.10 Cyclic Voltammogram for $[UO_2(^tBu_4\text{-saloph})OH][CoCp_2]$ (**1d**) in ~0.1 M $[Bu_4N][PF_6]$/MeCN solution with a scan rate range of 50-250 mV/s…….. 53

2.11 a) UV-visible absorption spectra for $\mathbf{H_2L^1}$ (dashed) vs. **1a** (solid) in THF…. 56
b) UV-visible absorption spectra for uranyl(VI) Schiff base-phenolate complexes (solid) and amino-phenolate complexes (dashed)…….. 57

2.12 Excitation (dashed) and emission (solid) spectra for **1a** in toluene (blue) versus THF (red)…….. 59

2.13 Excitation (dashed) and emission (solid) spectra for complex **2** in toluene (blue) versus THF (red)…… 62

2.14 Excitation (dashed) and emission (solid) spectra for ligand $\mathbf{H_3L^3}$ (purple) versus complex **3** in toluene or THF (orange)…….. 62

3.1 The molecular structures of $UO_2(NCN)_2(THF)$ (**i**), $[Cp^*UO_2(CN)_3][NEt_4]_2$ (**ii**), and $(Cp^‡)_4U_6O_{13}(Bpy)_2$ (**iii**)……... 87

3.2 Molecular structure of the repeating unit in **1a** with thermal ellipsoids depicted at the 50% probability level. Disordered THF carbons omitted for clarity…… 91

3.3 Top: Ball and stick model of the one-dimensional polymer chain along the a-axis. Bottom: Peering down the c-axis illustrating the alternating UO_2-fcdc arrangement. Disordered THF carbons omitted for clarity…….. 92

3.4 Two-dimensional cross-section of the network peering down the polymer chains (a-axis) showing interstitial ferrocene units……. 94

3.5 Solid-state infrared spectrum of **1b**…….. 95

3.6 Thermogravimetric analysis (TGA) curve for **1a** conducted with a thermal ramp of 5 ºC/min to 500 ºC under a constant N_2 stream…….. 96

3.7 ^{57}Fe Mössbauer spectrum for **1a** at 295K and 85K referenced to metallic Fe. 98

3.8 VT-^{1}H NMR of **1a** in MeOH-d_4. Asterisks (*) denote coordinated protic MeOH whereas hash (#) marks are attributed to an impurity of unknown composition…….. 102

3.9 Cyclic Voltammogram for **1a** in ~0.1 M $[Bu_4N][PF_6]/MeCl_2$ solution at room temperature with a scan rate range of 50-275 mV/s……... 106

3.10 UV-visible absorption spectra for **FCA** (dashed) and **1a** (solid) in MeOH. Inlay (top right) depicts the respective solid state diffuse reflectance absorption profiles…… 107

3.11 Excitation (dashed) and emission (solid) spectra for **1a** in MeOH. Fc based luminescence in blue, and emission of possible cis-uranyl origin in pink…... 108

4.1 Molecular structure of complexes **13** and **15** with thermal ellipsoids represented at the 50% probability level……..……. 130

4.2 Molecular structure of **16** with thermal ellipsoids shown at 50% probability. 136

4.3 Cyclic (solid) and square wave (dashed) voltammetric curves for complex **13** in ~1.0 M [TBA][BAr_f]/THF solution obtained room temperature with variable scan rates between 0.50 and 5.0 V/s……... 138

4.4 UV-visible absorption spectra for **7**-**14** obtained at room temperature in toluene-d_8 solution…… 142

4.5 The NIR portion of the electronic absorption spectra overlying traces for complexes **7**-**14** obtained under ambient conditions in toluene-d_8 solution…. 144

4.6 Generic energy level diagram depicting the Russell-Sanders spin orbit and O_h ligand field splittings where each level represents a pair of Kramer's doublets. This description is dependent on the strength of the ligand field, the energy separation between states dictates the thermal population, and the degree of admixture of excited and ground levels……. 146

4.7 Variable temperature magnetic susceptibility for **13** (blue) and **14** (pink). χ vs T (triangular markers) shows the gradual temperature variant, whereas χT vs T (circular markers) illustrates pronounced temperature regions……... 148

4.8 Organouranium(V)-imido bridged bimetallics reported by Andersen and co-workers……. 156

4.9 Molecular structure of **18** with thermal ellipsoids depicted at 50% probability…… 164

4.10 Molecular structure of **20** with thermal ellipsoids depicted at 50% probability. The structure of **19** is similar and provided in the supporting information……... 165

4.11 Cyclic voltammetric data for **18** with variable scan rates between 0.05 and 5.0 V/s…….. 169

4.12 Square wave voltammogram for **18** obtained for the same solution used in cyclic voltammetric studies in Figure 4.10……...……... 171

4.13 Peak current dependence on the scan-rate for **18**. $U^{VI/V}$ oxidation (purple), U(V/IV) reduction (pink) and ligand based reduction (green). The slopes for the lines were extracted from a linear least-squares fit for data points at each scan rate……...……. 171

4.14 Cyclic (red) and square wave (green and blue) voltammetric plots for **19**….. 173

4.15 Peak current dependence on the scan-rate for **19**. $U^{VI/V}$ oxidation (green), U(V/IV) reductions (blue and black) and ligand based reduction (red). The slopes for the lines were extracted from a linear least-squares fit for data points at each scan rate……. 174

4.16 Cyclic voltammetric waves for U^{VI} bis-imido complexes **16** (dashed) and **20** (solid)……..……. 176

4.17 NIR portion of the electronic absorption spectra for U^{V} bimetallic complexes **18** (solid) and **19** (dashed) obtained at room temperature in toluene-d_8 solution…… 178

4.18 UV-visible spectra for the bimetallic complexes **18**, **19**, and **20** (solid) and the monometallic **16** (dashed) obtained at room temperature in toluene-d_8 solution……. 179

4.19 Variable temperature magnetic susceptibility for **18** (green) and **19** (orange) with χ vs T curve (triangular markers) and χT vs T plot (circular markers) from 2 K to 350 K…… 181

4.20 Variable temperature magnetic susceptibility for U^{V} bimetallics with respect to monometallic analogues from 2 K to 350 K…… 181

5.1 Heterobimetallic uranyl(VI) Schiff base-phenolate complexes with redox active transition metal contained within the chelate backbone. R = ^{t}Bu, ^{i}Pr, CF_3, C_6F_5, adamantyl, $^{t}Bu_3Ar$, mesityl, *p*-tolyl…… 202

5.2 Sterically demanding carboxylate ligands…… 207

5.3 Bridging ligand varitation for the high valent bimetallic complexes……... 213

LIST OF SCHEMES

Scheme	Caption	Page
1.1	Steps involved in the photolytic activation cycle for the uranyl(VI)-oxylate fragment……...	7
1.2	Popular oxidative procedures used to prepare high-valent bent metallocene uranium-oxo (i) and -imido (ii) complexes. Py = pyridine, THF = tetrahydrofuran, Ad = adamantyl……	10
2.1	The synthesis of category 1 complexes **1a-c**……...	33
2.2	Benchtop synthesis of the acetate bridged bimetallic complex **6**……	46
2.3	Color-coded mechanism monitoring the tentative photochromic rearrangement for uranyl(VI) Schiff base-phenolate complexes……	61
2.4	Photosynthesis of **1d**……...	65
3.1	Benchtop synthesis of the coordination polymers **1a** and **1b**……..	89
3.2	Solvent-dependent mechanism describing the carboxylate abstraction responsible for the formation and reversible solubility of **1**……...	100
4.1	Synthesis of U^{V}-imido complexes via Cu^{I} salt oxidation of **2**…….....	124
4.2	Salt metathesis substitution preparation of **13** and **14**…….	126
4.3	Salt metathesis (i) followed by protonolysis (ii) to generate **15**……..……...	127
4.4	The synthesis of **16** is reminiscent of PCET..…..……..…….	135
4.5	Synthesis of the U^{V}-amide bridged bimetallic **18**……...	160
4.6	Synthesis of U^{V} and U^{VI}-imide bridged bimetallics **19** and **20**……...	161
5.1	A synthetic route to access a uranyl(VI) amido-phenolate complex……...	203
5.2	Prospective synthesis of organouranium(V)-phosphinidene complexes…….	211
5.3	Potential synthesis of a multimetallic U^{V} cluster……..……..	214

LIST OF TABLES

Table	Caption	Page
2.1	Selected crystallographic parameters for **1a-1d** ……	35
2.2	Selected metrical parameters for complexes **1a-d** ……	38
2.3	Selected metrical parameters for complexes **2, 3, 4, 6 and 7** ……...	45
2.4	Selected crystallographic parameters for **2-7** ……	48
2.5	Summary of redox potential data for uranyl(VI) Schiff base-phenolate complexes **1-7** in ~0.1 M $[Bu_4N][PF_6]$/MeCN, THF, or CH_2Cl_2. $E_{1/2}$ values are referenced to $Fc^{+/0}$ and were determined from the average of the cathodic and anodic peaks. R = Reversible; QR = Quasireversible; I = Irreversible …..	55
3.1	Selected crystallographic data for **1a** ……	90
3.2	Mössbauer spectral hyperfine parameters for **1a** ……..……...	99
4.1	Selected crystallographic data for **13, 15,** and **16** …….	129
4.2	Pertinent metrical parameters for complexes **11-15** ……..	131
4.3	Summary of redox potential data for U^V complexes **3-15** …….……...	139
4.4	Summary of magnetic susceptibility data for **3-14** in comparison to reported U^V complexes. Derivatives **11** and **12** will be disclosed in a forthcoming manuscript but fit the expected trend observed here …….	149
4.5	Selected metrical parameters for complexes **18-20,** where L represents the ancillary donor ligand present in the wedge ……..	164
4.6	Selected crystallographic parameters for **18** and **20** …….	167
4.7	Summary of redox potential data for complexes **16-20** reported in V versus $Fc^{+/0}$ ……	176

NOMENCLATURE ABBREVIATIONS

Uranyl(VI) = dioxouranium(VI), UO_2^{2+}

THF = tetrahydrofuran

DMSO = dimethylsulfoxide

$MeCl_2$ = methylene chloride

DMF = dimethyl formamide

MeOH = methanol

TMPO = trimethylphosphineoxide

OAc = acetate

OTf = triflate

TBA = tetrabutylammonium

Cp* = permethylatedcyclopentadienyl

^{i}Pr = isopropyl

Bz = benzyl

Me = methyl

^{t}Bu = t-butyl

Ph = phenyl

Ar = aryl

Ad = adamantyl

Sal = salicylidene

Tren = tris(2-aminoethyl)amine

en = ethylenediamine

$CoCp_2$ = cobaltocene

FCA = ferrocenemonocarboxylic acid

Fc = ferrocene

Fcdc = 1,2-ferrocenedicarboxylic acid

$*UO_2^{2+}$ = uranyl(VI) excited state

-yl ion = MO_2^{n+} (M = d or 5f transition ion, n = 1, 2)

LMCT = Ligand-to-Metal Charge Transfer

PCET = Proton-Coupled electron transfer

Chapter 1

Introduction

1.1 Light Actinide Chemistry

The f-elements comprise more than one-quarter of the Periodic Table. Assembled in the lower left between the s- and d-blocks, their placement on the Periodic Table is the result of combined innovations by Dmitri Mendeleev during the 19th century and G. T. Seaborg following the second world war.[1] Lanthanide and actinide elements share striking chemical similarities with the alkali, alkaline earth and early transition metal series, however, their significantly larger radii coupled with the presence of valence f-orbitals (**Figure 1.1**) distinguish f-element chemistry from any other group of metallic elements. The central themes in contemporary f-element research focus on the use of both aqueous and non-aqueous conditions to investigate the production of fuel materials for weapons and reactors, separation sciences, environmental speciation, redox and photoactive capabilities, mangnetochemical properties, occurrences of multiple bonding, and unique reactivity.[2-4] In particular, the early actinide series (Th, Pa, U, Np, Pu, Am) possess 5f orbitals that function to house valence electrons and participate in bonding and reactivity patterns. The large radial distribution of outermost 5f, 6d, 6p, 7s, and 7p orbitals blur the actinide valence orbital manifold.[5-7] This description is complicated by the multitude of f-orbital lobes (i.e. high

degree of nodality) under the influences of relativistic and spin-orbit effects that render them available to interact with the surrounding environment.

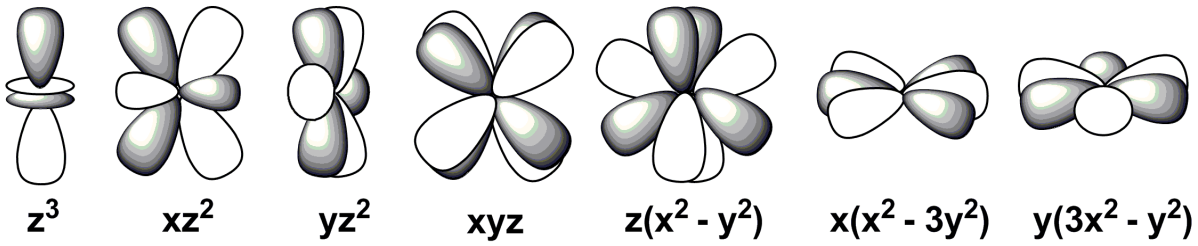

Figure 1.1. The general set of seven f-orbitals and their polynomial descriptions.

For the early actinide elements, active 5f orbitals impart the ability to access multiple oxidation states and contribute covalent overlap in support of actinide-ligand single and multiple bonds. Uranium presents an opportune platform to examine the rich electronic structure and bonding properties for a range of oxidation states, principally III, IV, V, and VI. Early actinide chemistry is of tremendous importance due to the improper treatment and disposal of actinide-bearing materials from the proliferation of nuclear fuel technology, and current concerns are focused on the development of effective *back-end* nuclear fuel cycle strategies, including: spent fuel separations and recycling, interim and long term waste stewardship, and pollution remediation and environmental restoration.[1,8,9] This chemistry is dominated by the actinyl ions, AnO_2^{n+} (An = U, Np, Pu, Am; n = 1, 2), whose redox ability, photochemical activity, and ligand binding retention are all qualities that arise from involvement of actinide valence orbitals. Organometallic actinide chemistry is a similarly bourgeoning facet of inquiry that is currently concentrated on the role of 5f orbitals in bonding and reactivity.[10] The lack of a formal 18 electron rule coupled with the range of accessible oxidation states and large ionic radii together furnish novel chemical applications

not witnessed in conventional organometallic systems.[11] This dichotomy of actinyl versus organoactinide chemistries, both of which are exemplified in this body of work, unfold an exciting challenge to acquire diverse perspectives on the extent and limitations of f-orbital participation in physicochemical properties.

1.2 The Dioxouranium Ion

The complexities of 5f orbital behavior are perhaps most clearly manifested in the dioxouranium(VI) ion, UO_2^{2+}. This molecular ion is isostructural with the rest of the actinyl series, and possesses short U=O bonds (1.73-1.84 Å) that are typically terminal and always arranged in an essentially linear (*trans*) O=U=O configuration. The U^{VI}-oxide distances are anomalously short in comparison to the transition metal congener MoO_2^{2+}, and since U^{VI} has a larger ionic radii the short bonds are a testament to the multiple bond order and robust chemical tendencies.[4] An orbital overlap match between the hard U^{VI} ion satisfied by strong π-donor oxide ligands results in remarkable stability and inert chemical behavior. The dual oxide ligands engage in π-bonding between $U(5f_{xz^2})$-$O(2p_x)$ and $U(5f_{yz^2})$-$O(2p_y)$, however, the predominant component consists of a $U(5f_{z^3})$-$O(2p_z)$ σ-bonding molecular orbital along the z-axis depicted in **Figure 1.2**.[5] This bonding motif is supported by U(6d)-O(2p) σ- and π-overlap regimes common for –yl type ions.[5] However, in the uranyl instance σ-bonding supported by 5f orbitals account for the short U=O contacts and invariably linear geometry, which together equip the uranyl(VI) ion with rich physicochemical characteristics.

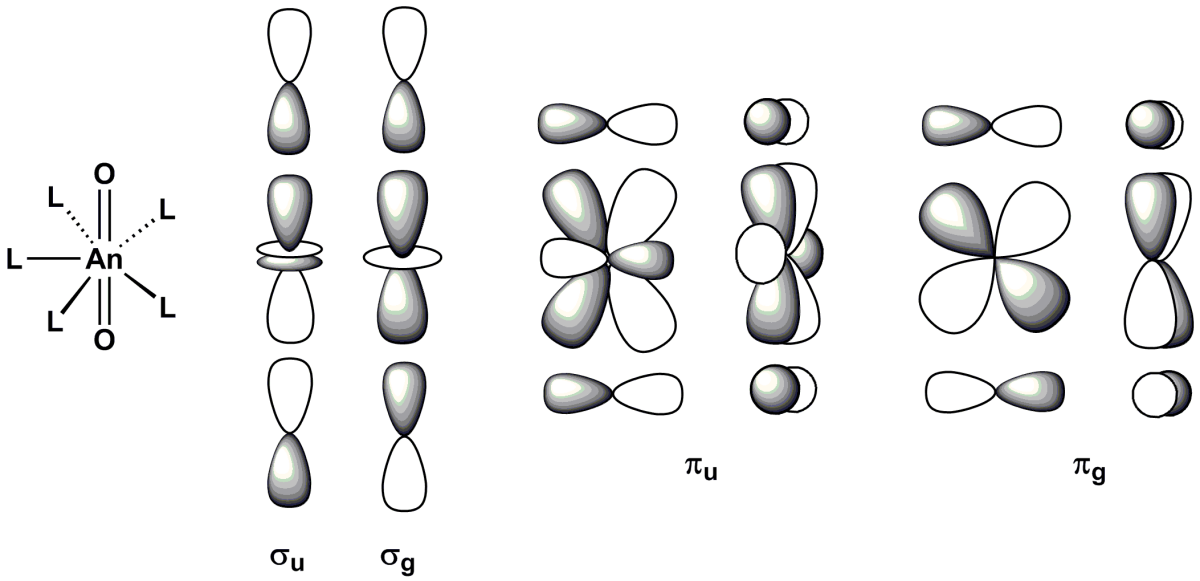

Figure 1.2. The molecular orbitals that compose the triple An=O bond order for the $D_{\infty h}$ actinyl unit include combined σ and π overlap between O(2p) with An(5f) and An(6d) atomic valence orbitals along the z-axis. Metal valence orbital labels (from left to right): $5f_{z3}$, $6d_{z2}$, $5f_{xz2}$, $5f_{yz2}$, $6d_{xz}$, $6d_{yz}$.

The axial bonding motif is reinforced by involvement of a filled *pseudo*-core U($6p_z$) orbital that mixes with the U($5f_{z3}$)-O($2p_z$) overlap via repulsion from below.[7] The combined effect from this admixture results in the σ interaction that is higher in energy to create a highest occupied molecular orbital of σ-bond character, where π-bonding is treated as auxiliary support.[5,12] The filled *pseudo*-core orbital ability to mix with the valence manifold is due to an *indirect relativistic expansion* of outermost orbitals that occupy similar spatial symmetries.[3,5] Apart from contributions to covalent bonding, *pseudo*-core orbitals also play a subtle yet important role to direct reactivity.[5-7] Specifically, an inverse *trans* influence arises from polarization effects induced by the surrounding ligand field such that the presence of one oxide ligand supports the other along the axis. The orbitals left nonbonding in the linear UO_2^{2+} arrangement accommodate interactions with ligands situated exclusively orthogonal to the oxide ligands in the equatorial plane to create five, six, or seven coordinate

bipyramidal geometries. Equatorial contacts are attenuated in accord with the inverse *trans* influence, and the effects are reflected in facile equatorial exchange reactions. This structural feature is advantageous for the development of ligands suited to separate the actinyl ions from the mix of spent nuclear fuel materials.[13] In contrast, the central UO_2^{2+} unit is much less susceptible to chemical transformation. Activation of U=O bonds is accompanied by metal ion reduction and scrambling of the coordination sphere, whereas it is common for equatorial electron density to impart nucleophilic oxides capable of bridging electropositive species.[14-16]

Uranyl(VI) electronic and molecular structural properties enable redox and photochemical aspects for uranyl ion complexes. Uranyl(VI) is a well known chromophore, where LMCT occurs in the UV-visible region and is responsible for the bright yellow, red, and orange colors often observed for these species.[17] Intense transitions arise between the ground σ-bond molecular orbital of O(2p) character to a nonbonding U(5f) excited state manifold that is both reactive and fluorescent. The nature of the uranyl(VI) excited state is dependent on equatorial ligand design to assist in the competition between radiative versus non-radiative energy decay, and the process results in green luminescence with prolonged lifetimes (μs) and potent photooxidant properties ($E^o \sim 2.6$ V) capable of oxidizing a range of organic and inorganic substrates.[18] $*UO_2^{2+}$ has been exploited as a means to disrupt the central O=U=O unit and as a route to access the uranyl(V) ion.[19] A more reliable method to produce uranyl(V) is via one electron electrolytic or chemical reduction of uranyl(VI) species by direct population of the vacant 5f nonbonding manifold. Electrochemical energetics and kinetics for the uranyl(VI/V) redox couple are dependent on equatorial ligands, however in order to stabilize the pentavalent species the ligand environment must prevent

disproportionation inherent to the uranyl(V) ion.[20] Isolation of a discrete uranyl(V) species has long been sought to confirm that the unit has longer U=O bonds than the hexavalent analogue arranged in a linear geometry like uranyl(VI), and the formal $5f^1$ electronic configuration serves as a handle to probe 5f nonbonding orbital properties.

The environmental fate of actinyl ions is important due to the accidental discharge from uranium mining and spent nuclear fuel repositories. Migration in aqueous media is dependent on solubility, and hexavalent actinyl ions ($An^{VI}O_2^{2+}$) ions are soluble whereas pentavalent species ($An^{V}O_2^{+}$) are considerably more soluble due to their lower charge and low affinity for ligand binding.[21] Therefore, pentavalent actinyl ions present an extremely potent ecological threat due to mobility in natural aquifers that could lead to biological consumption of these radioactive hazards in excess of natural abundances.[21,22] Although uranyl(V) is prone to undergo redox decomposition, it can survive in solution under a narrow conditional margin; for example, in acidic media in low concentrations in the presence of excess uranyl(VI).[23] Together these traits render uranyl(V) exceedingly evasive, making it a relevant environmental concern and a provocative synthetic objective. In this respect, neptunyl(V) chemistry is an eminent focal point since Np^{V} is the preferred oxidation state in air. However, uranyl chemistry serves as a laboratory surrogate to study Np and Pu since their isotopes have more hazardous radionuclear properties than depleted uranium (^{238}U). Accordingly, accounts documenting the preparation and isolation of uranyl(V) species have emerged in the past few years.[24]

Actinide pollution immobilization and recovery techniques transform actinyl ions into insoluble low valent species (An^{4+}) that lack the ability to migrate through aquifers due to their high cationic charge. The methods contrived for actinide contaminant remediation

utilize microbial reduction,[25] retention on redox active metal-oxide surfaces,[26] and photochemical reduction.[17,18,27,28] The photolytic route utilizes the long-lived and potent oxidizing ability of the uranyl(VI) excited state to oxidize carboxylate ligand functionalities using sunlight, producing benign gaseous CO and CO_2 byproducts with concomitant precipitation of tetravalent uranium oxide ($U^{IV}O_2$) that can be quarantined (**Scheme 1.1**).[28]

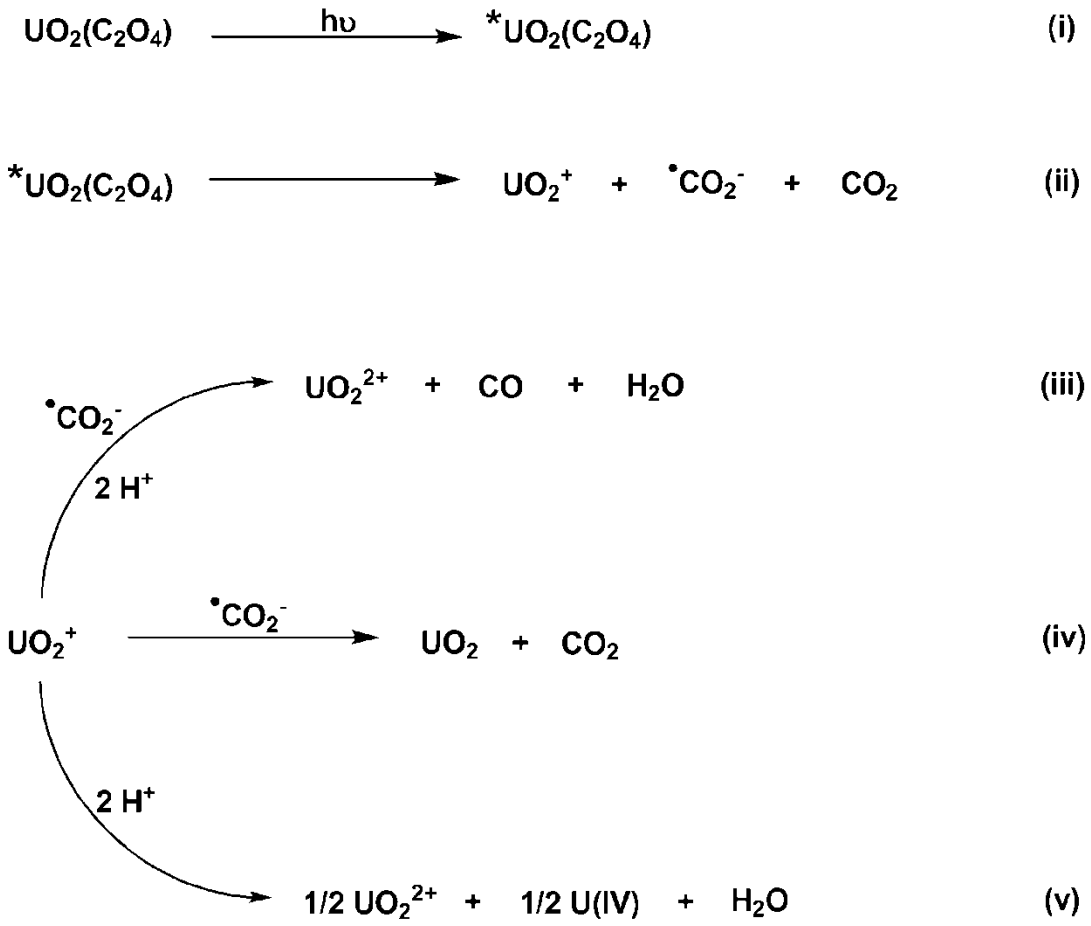

Scheme 1.1. Steps involved in the photolytic activation cycle for the uranyl(VI)-oxalate fragment. Following exposure to an intense ultraviolet light source (i) the photoexcited uranyl(VI) ion is reduced by the coordinated oxalate (ii) and the consequential uranyl(V) species can be consumed by three possible routes including oxidation back to uranyl(VI) (iii), reduction to insoluble uranium(IV) (iv), or disproportionation (v). This technique is susceptible to ambient pH, concentration, radical recombination, and air oxidation to determine overall efficiency.

An important vantage in actinyl chemistry that has experienced multi-decadal development is the incorporation of non-aqueous conditions to exploit a broad scope of reagents and synthetic pathways unavailable in aqueous media. Uranyl(VI) chemistry is inherently restricted to equatorial coordination, however only a small variety of bichelating oxyanions (i.e., carbonate, nitrate, phosphate, sulfate, fulvates, etc.) are bioavailable. In addition, aqua coordination and hydrolysis are commonplace. On the other hand, non-aqueous systems support ligand designs favorably suited for tunable uranyl properties. Interests in elucidating these systems are two-fold: to gain insight on actinide valence orbitals under varied conditions, and to apply this information to aspects associated with nuclear waste separation and remediation practices. Advances in this field have emerged to include the preparation of an arsenal of uranyl halide,[29] amide,[14] thiolate,[30] cyanide,[31] phosphinimine,[32] and alkoxide and aryloxide derivatives,[33] and have matured to include amidinate,[15] triamidoamine,[34] calixpyrrole,[16] η^5-pentamethylcyclopentadienyl (Cp^*),[35] methine,[36] and *n*-heterocyclic carbene[37] complexes. It is apparent that the Cp^* ligand is not clearly compatible with η^5 coordination to the uranyl equator, and the uranyl-carbon attachment in the uranyl(VI) Cp*, methine, *n*-heterocyclic carbene, and cyanide complexes are recent discoveries that represent significant feats in actinide chemistry that could reveal new directions in organouranyl bonding and novel reactivity pathways. Notably, it is curious that attempts to synthesize actinyl-cyclopentadienyl complexes have failed on a few occasions in the past[30,38] since the bent metallocene framework is known to host multiply bound functionalities (i.e., oxide, imide, phosphinidene) for a variety of oxidation states.[39]

1.3 Organometallic Uranium Chemistry

Organouranium chemistry is a flourishing field founded on the same fundamental principles as the dioxo uranyl system: uranium is highly electropositive and oxophilic and can exist in a group valent oxidation state range with large ionic radii and a variety of valence orbital lobes available to facilitate chemistry. The lack of a formal 18 electron rule coupled with the range of available oxidation states allows for chemical capabilities not possible for organotransition metal congeners.[11,40,41] In general, the actinide-carbon bond is extremely polar and stimulates reactivity that can be controlled through the use of steric and electronic stabilization. For example, the synthesis of simple homoleptic uranium-alkyl complexes at the onset of air-free actinide chemistry was plagued by U-C and C-H bond activation, and these quandaries were not resolved until the mid-1980's.[42] This chemistry is not limited to a planar equatorial region as in uranyl, but is rather geared to direct reactivity at available metal sites protected by an ancillary chelate. The popular auxiliary ligands in this arena include triamidoamines,[43] triazacyclononane,[44] scorpionates,[45] calixpyrrole and polypyrrolides,[46] calixarene and polyphenoxides[47] and an assortment of cyclopentadienyl and cyclooctatetraenyl metallocene derivatives in the piano-stool and linear and bent sandwich arrangements.[41,48] This field has mushroomed over the past few decades, and the canonical bent metallocene framework has fostered extensive fundamental and catalytic insights.[49] Accordingly, respective complexes encompass the full suite of uranium oxidation sates for an array of p-block donor ligands situated in the metallocene wedge.[41,50]

Numerous reports have probed tri- and tetravalent bent-sandwich uranium species, whereas high-valent derivatives are rare by comparison. Hexa- and pentavalent complexes are commonly prepared via oxidation of low valent precursors and stabilized by π-donor

oxide, imide, aryloxide, amide, and ketimide co-ligands.[39,51] For example, classic synthetic procedures used to engender the U^{V}-oxo and U^{VI} bis-imido (and oxo-imido) bent-sandwich complex via oxidation by *N*-oxide and azide substrates, respectively, are shown in **Scheme 1.2**.[52] U^{V} is considerably less stable than other oxidation states due to the proclivity for oxidative and reductive decomposition.[53] On similar grounds, recall that uranyl(V) is known to undergo facile disproportionation, and few have accomplished methodical access to the pentavalent oxidation state.[41,51,53] The multiply bound ligands (imido, oxo) that stabilize the high-valent uranium complexes are not prone to chemical attack, whereas transition metal analogues are renowned for metal-imido and metal-oxo fragment participation in exceptional chemical activity.[54-56] This is deciphered as enhanced multiple bonding in the former due to the presence of both f and d valence orbitals functioning as ligand acceptors. Overall, the high-valent collective presents an opportune platform to assess the nature of 5f orbital involvement in electronic and molecular structure, bonding, and reactivity.

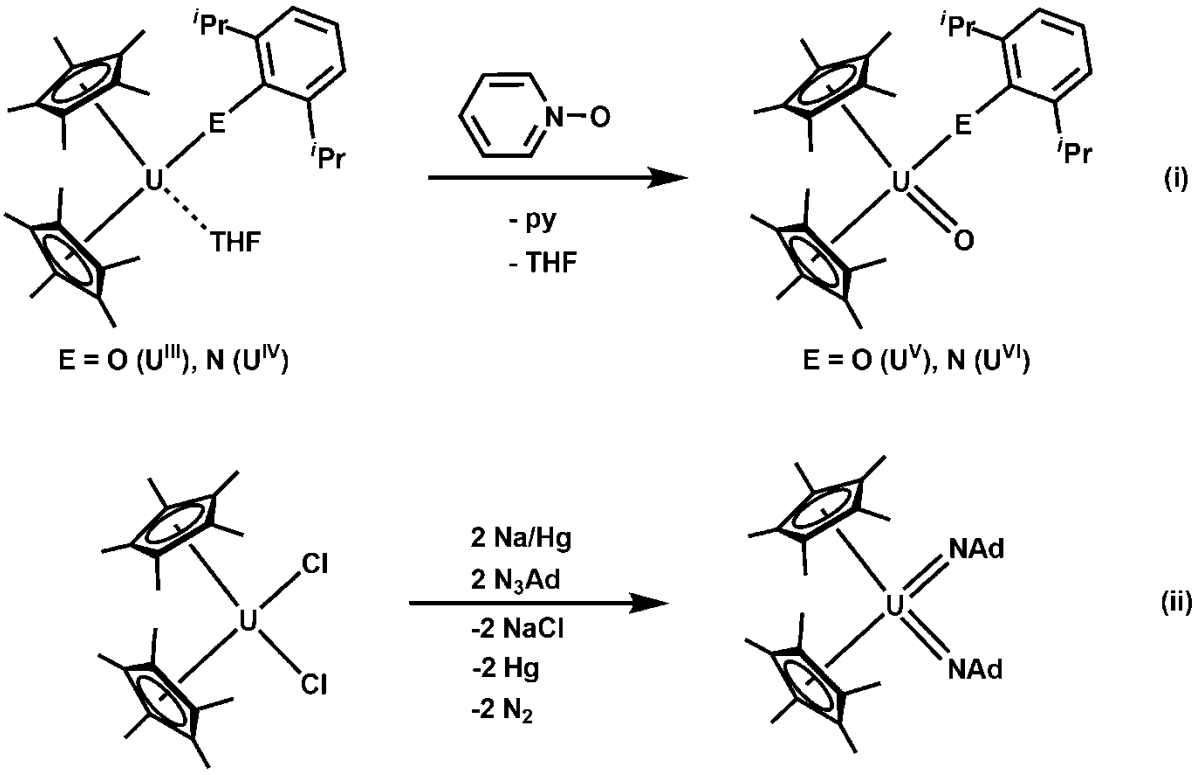

Scheme 1.2. Popular oxidative procedures used to prepare high valent bent-metallocene uranium-oxo (i) and -imido (ii) complexes. Py = pyridine, THF = tetrahydrofuran, Ad = adamantyl.

1.4 Overview

The underlying theme conserved for each of the three individual studies presented herein are founded on high-valent uranium ions stabilized by isoelectronic π-donor oxo and imido ancillary ligands. These robust core units are supported by multiple bonding through uranium based 5f and 6d valence orbitals. This chapter documents a brief overview of the current understanding of actinyl and organoactinide-imido chemistries. The perspectives encompassed in this chapter set the scope for the research that follows, with a general objective to gain insight on the tunability of electronic and molecular structural features of uranyl(VI) and U^{V}-imido units when they are transplanted into an assortment of coordination environments with different steric and electronic designs.

The first investigation employs a group of Schiff base-phenolate chelates supported by various backbone architectures (i.e., en, tren, binapthyl, *o*-phenylene) tailored to gain exquisite control of uranyl(VI) electro- and photochemical properties. In the second study, the synthesis and structural characterization of a uranyl(VI) coordination polymer with a ferrocenylcarboxylate ligand is discussed. This ligand is considerably more sterically demanding than those previously seen in uranyl(VI) carboxylate complexes, and in turn a bent dioxo unit is produced and the structural characteristics are elucidated relative to the breadth of information on linear uranyl complexes. The third segment examines the synthesis of bent metallocene U^{V}-imido complexes as a platform to assess the electronic structure of the $5f^{1}$ configuration, and extends to include bimetallic assemblies to probe metal-metal communication. The final chapter summarizes the experimental findings and sets the landscape for future directions to pursue on this course of study. Specific goals for each section are addressed below in more sophisticated detailed.

Uranyl(VI) Schiff base-Phenolate Complexes

Schiff base-phenolate chelates, often referred to as sal-type ligands due to their derivation from salicylaldehyde, contain donor compartments well suited for uranyl(VI) equatorial coordination to form archetypal bipyramidal complexes with square or pentagonal equators. This genre of ligands are easily prepared via condensation reactions between di-*t*-butyl substituted salicylidene and polyamines, and provide a variety of supportive architectures dependent on backbone design.[57] Synthetic routes employed for the production of uranyl(VI) Schiff base-phenolate complexes include protonolysis, templation, and ligand deprotonation followed by salt metathesis, that result in inherently stable complexes as

represented in **Figure 1.3**.[58] The uranyl(VI)-Schiff base framework has received substantial attention in light of the capacity to act as a host for neutral and anionic guest molecule recognition and to govern catalytic processes at the capping equatorial position.[59-61] Since equatorial ligand composition governs uranyl(VI) electro- and photochemical properties, we were motivated to conjoin the uranyl(VI) ion with these Schiff base chelates and related derivatives, that possess their own photochemical reactivity,[62] to enhance uranyl(VI) excited state fluorescence and reactivity pathways. This competitive photochemistry, much like introducing the photo-antenna effect on a metal unit that is photoactive on its own, is not ambiguous nor does it obscure uranyl photochemistry but rather complements it.[63] The survey in Chapter 2 embarks on an examination of the influences of variable chelate backbone design and the introduction of capping ligand and solvent effects on the uranyl(VI/V) redox couple and uranyl(VI) excited state to gain exquisite control of chemical and photochemical reduction processes associated with environmental contaminant immobilization.

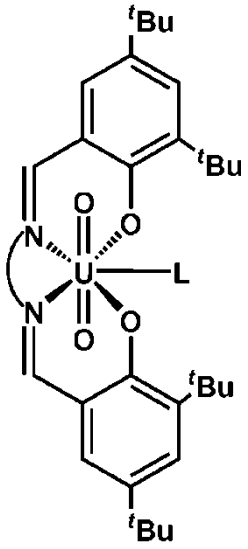

Figure 1.3. A generic uranyl N_2O_2 sal-type Schiff base complex. The variables in this equation include backbone conformation and the capping ligand (L).

The bulky *t*-butyl substituted salicylidene periphery is tailored to inhibit uranyl(V) disproportionation upon reduction of uranyl(VI) Schiff base-phenolate precursors in non-aqueous solution. Few reports have examined uranyl(VI) electro- and photochemical trends under rigorous exclusion of air,[64] which is surprising since the pentavalent oxidation state is susceptible to facile decomposition in air. In this respect, the group of complexes presented here provides a suitable platform to study the electrochemical generation of uranyl(V), and a viable option to extend to synthetic chemical reduction with the possibility of assistance from the photoexcitation operative. In whole, these complexes are enormously less reactive under photolytic reducing conditions than other dioxouranium(VI) complexes since the oxidizing ability of uranyl(VI) is quenched, however, they do present a practical opportunity to stabilize the uranyl(V) ion. This aim of stabilizing uranyl(V) is to gain a fundamental understanding of multiple bonding for the pentavalent oxidation state, and to use the $5f^1$ electronic configuration as a spectroscopic and paramagnetic marker.

A Bent Uranyl(VI) Moiety

It has been postulated that the bent dioxo actinyl geometry could be stabilized in polar solvents, or supported by a ligand field that influences actinide based valence 5f and 6d orbitals from favoring the *trans* configuration (**Figure 1.4**).[65] Nonetheless, all of the actinyl ions adopt the linear geometry regardless of f electron count (f^{1-4}) in a variety of ligand fields. Therefore, it is apparent that electronic factors are unable to overpower the resilient σ-bonding that locks the linear oxide ligands in place, resulting in the inability to redirect the dioxo geometry as dπ-pπ bonding does for transition metal –yl ion analogues.[66] Therefore, use of the proper steric design might act to disrupt the linear geometry and direct oxide

ligands to rearrange into the *cis* conformation. The U^{VI} valence 5f and 6d orbitals provide a hard-acid overlap match with oxide 2p orbitals, which is demonstrative of the oxophilic nature of uranium and leads to the false assumption that uranium should be capable of accepting oxide ligands in any arrangement possible, including *cis* or *trans* and bridging or terminal. The limiting factor in structural uranyl chemistry is that ligand coordination must be compatible with equatorial coordination, and accordingly ligands are often tailored for planar coordination. The select few that have published attempts to augment the *trans* dioxo geometry have ultimately failed to achieve their goal.[35,38] A few studies have reported structural or spectroscopic evidence for the *cis*-uranyl(VI) unit, however none have furnished experimental details in unambiguous agreement with these claims.[67-69] Thus, a synthetic strategy to stabilize a bonafide *cis*-uranyl moiety has remained a daunting challenge.

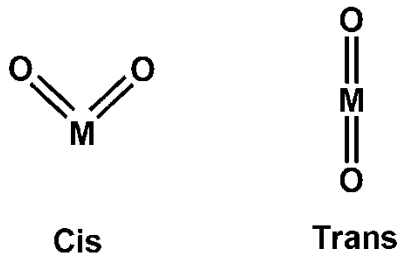

Figure 1.4. *Cis* (bent) and *trans* (linear) dioxo metal geometry.

It is especially peculiar that linear dioxo uranyl ions retain their rigid geometry in solution and in the solid state, whereas in the isoelectronic U^{VI} bis-imido and mixed oxo-imido units can adopt either *cis* or *trans* geometries.[39,70] The imide (RN^{2-}) and oxide (O^{2-}) ligands are isoelectronic, however the imido group offers the benefit of the tunable R group to gain steric and electronic control, and this structural difference contributes stability to

high-valent uranium ion complexes. One example of a discrete bent-sandwich U^{IV} dimer with dual bridging oxide ligands situated adjacent to one another in the metallocene wedge has been reported, however the study failed to reveal any electronic structural data informative of putative ionic, covalent, or steric attributes associated with the lack of directional bonding preference.[71]

An extensive number of uranyl(VI)-carboxylate species have been isolated as discrete complexes and coordination polymers.[72,73] In these cases, the carboxylate ligands always contain aryl or alkyl substituents distal to the binding site, geared to engineer uranyl(VI) coordination to bridge along the equatorial plane. However, none have approached the use of sterically demanding carboxylate substituents to interfere with common binding modes. Ferrocenemonocarboxylic acid (FCA) is commercially available, and provides a simple carboxylate ligand that bears a bulky ferrocene moiety. FCA has been applied to the uranyl system in the past, however, the report contained minimal characterization data about the product, which was speculated to be a coordination polymer on the basis of intractability and elemental analysis.[74] To revisit, our selection of the FCA ligand was to create a uranyl(VI) attachment to a stable and remote bulky redox active unit capable of shielding the uranyl(VI) ion, as a model to prevent radical reduction in the nuclear fuel stream.[75] This model relies on FCA offering free rotation about the Cp-CO_2^- connection, and redox interplay with the uranyl(VI) ion could turn out to be a viable option. However, when reacted with uranyl(VI) a novel chemical transformation takes place that displaces the dioxo unit into a severely bent arrangement with short terminal U=O bonds supported in a reversible coordination polymer. Examination of the molecular and electronic structure, bonding, and reactivity for this species pose exciting new aspects of actinide chemistry discussed in chapter 3. For example,

elucidation of U^{VI} 5f versus 6d valence orbitals that support the bent geometry in comparison and contrast to established actinyl species might, in retrospect, shed light on interpretation of actinide-ligand multiple bonding and the effects on coordination, redox, and photochemical behaviors. This platform has the potential to unveil the *cis*-dioxo role in ligand redistribution schemes,[76] to ascertain activation pathways for U=O fragments, and could lead to advantageous properties for nuclear fuel recycling strategies.

Mono- and Bimetallic Organouranium(V)-Imido Complexes

An unresolved issue that has emerged in actinide science is the clarification of 5f electronic orbital involvement in covalent bonding as a function of the spin-orbit/crystal-field continuum. In general, higher oxidation states tend to extract covalency from surrounding ligand electron density and are stabilized by π-donor ligands, whereas lower oxidation states breed enhanced covalent overlap due to larger covalent radii.[10] In both cases, bonding is supported by a significant ionic component, yet some workers harbor bonding in actinide complexes as strictly ionic like the rest of the f-block.[77] In this respect, U^{V} ion complexes offer the $5f^{1}$ configuration, simplest of all f electron configurations, with no electron-electron repulsion to gain a spectroscopic, electrochemical, and paramagnetic handle to measure high-valent 5f orbital perturbations of the orbital in which the sole electron resides.

An ensemble of organouranium(V)-imido halide complexes were recently reprted by Graves and co-workers from copper(I) oxidation of tetravalent oganouranium-imido precursors.[78] This work dispels the preconceived notion that U^{V} chemistry is unmanageable due to redox instability. In comparison to the paucity of routes used to engender quinquivalent uranium ion complexes, this facile and affordable reaction process achieves

convenient access to a full suite of halide complexes that in turn provide suitable entry to explore ligand substitution. A variety of derivatives (i.e., amide, aryloxide, ketimide, thiolate, triflate) were prepared via salt metathesis and protonolysis reactions to study the ligand field adjustment as a function of exchanging one ligand while the remainder of the coordination sphere is held constant. By inspecting structural, electrochemical, magnetic, and spectroscopic data for this series of complexes in reference to scarce reports on the molecular and electronic structure and bonding in U^{V} and other $5f^{1}$ complexes,[79] the collaborative study in Chapter 4 sheds light on the nature of 5f sensitivity to the ambient ligand field. Interpretation of these data distinguishes the extent to which the 5f orbital that houses the single valence electron is perturbed by the monoanionic unidentate ligand in the wedge.

The work performed on monometallic organouranium(V)-imido complexes establishes the underpinnings for further studies that craft discrete bimetallic analogues to investigate the potential for electronic communication between metal ions. Intramolecular metal-metal interactions have been relentlessly interrogated for discrete transition metal ion complexes.[80] Metal-metal communication phenomena have been uncovered in actinide-transition metal intermetallic extended solid materials,[81] however only a handful of reports exist that have developed rigorous synthetic, structural characterization, and metal-metal electronic communication diagnostics for well-defined lanthanide,[82] mixed 5f-4f and 5f-3d heterobimetallics,[83] and actinide multimetallic complexes.[84] The lack of focus on this subject is surprising due to the incentive to explore complexities in 5f electronic behavior, however the stagnant development of this field is in large part due to synthetic challenges imposed by the large ionic radii and lack of directional coordination preferences and required steric constraints.[84] Thus the use of bent metallocene building blocks has recently come into

focus to assemble actinide ions into specific structural topologies to predict properties based on monometallic fragments.

The factors that limit metal-metal interactions include the distance and symmetry between the metal ions, the orientation of electronic density across the bridging ligand, and the type of donor atom presented at each metal site.[85] For the 5f elements, the extensive radial distribution of valence electron density from the nucleus could be utilized to enhance electronic interactions through space or by superexchange across a conjugated bridging ligand.[83] Fortunately, the U^{V} f^{1} electronic configuration leads to simplified electronic properties. As a suitable reference point, homobimetallic organouranium(V) imido-bridged complexes have been reported to display antiferromagnetic coupling dependent on the distance between metal ions and substitutive arrangement of phenylene based bridging ligands (i.e., ortho, meta, para), however exact structural, electrochemical, spectroscopic, and theoretical details were unfortunately not reported.[86] Researchers are interested in understanding the fundamental properties of the rarely divulged pentavalent oxidation state to harness their redox instability for novel reactivity, and to probe complicated material properties to shed light on actinide-bearing materials in relation to the composition of nuclear material stockpiles. These ideas will be further discussed in more detail in the context of Chapter 4 of this chronicle.

References

[1] Seaborg, G. T. *J. Chem. Soc., Dalton Trans.* **1996**, 3899-3907.

[2] *The Chemistry of the Actinide and Transactinide Elements*, 3rd ed.; Morss, L. R., Edelstein, N. M., Fuger, J., The Netherlands, **2006**; Vol. 1-5, and references therein.

[3] Cotton, S. *Lanthanide and Actinide Chemistry*, England, 2006. (b) Kaltsoyannis, N.; Scott, P. *The f elements*, Oxford, **1999**.

[4] For more on covalent bonding in f-element complexes, refer to (a) Burns, C. J. *Science* **2005**, *309*, 1823-1824. (b) Griesbreht, G. R.; Gordon, J. C. *Dalton Trans.* 2004, 2387-2393. (c) Clark, D. L.; Gordon, J. C.; Hay, P. J.; Poli, R. *Organomet.* **2005**, *24*, 5747-5758.

[5] (a) Clark, D. L. *Los Alamos Science* **2000**, *26*, 364-381. (b) Denning, R. G. *Struct. Bonding* **1992**, *79*, 215-275. (c) King, R. B. *Inorg. Chem.* **1992**, *31*, 1978-1980.

[6] (a) Pyykko, P.; Desclaux, J. P. *Acct. Chem. Res.* **1979**, *12*, 276-281. (b) Kaltsoyannis, N. *J. Chem. Soc., Dalton Trans.* **1996**, 1-11.

[7] (a) Pyykko, P.; Runeberg, L. J. *J. Phys. Chem.* **1994**, *98*, 4809. (b) Kaltsoyannis, N. *Chem. Soc. Rev.* **2003**, *32*, 9-16.

[8] *The Nuclear Fuel Cycle* in *Radiochemistry and Nuclear Chemistry*, Choppin, G.; Rydberg, J.; Liljenzin, J. O., 2nd ed, **1995**, ch 21, Butterworth-Heinemann Ltd., pp 581-639.

[9] Francis, A. J.; Dodge, C. J. *Environ. Sci. & Technol.* **1998**, *32*, 3993-3998, and references therein.

[10] (a) Burns, C. J.; Bursten, B. E. *Comments Inorg. Chem.* **1989**, *9*, 61-93. (b) Choppin, G. R. *J. Alloy Compd.* **2002**, *344*, 54-59.

[11] (a) Marks, T. J. *Science* **1982**, *217*, 989-997. (b) Evans, W. J. *Inorg. Chem.* **2007**, *46*, 3435-3449, and references therein. (c) Peters, R. G.; Warner, B. P. Burns, C. J. *J. Am. Chem. Soc.* **1999**, *121*, 5585-5586.

[12] (a) Tatsumi, K.; Hoffman, R. *Inorg. Chem.* **1980**, *19*, 2656-2658. (b) Wadt, W. R. *J. Am. Chem. Soc.* **1981**, *103*, 6054-6057. (c) Teterin, Y. A.; Terehov, V. A.; Ryzhkov, M. V.; Utkin, I. O.; Ivanov, K. E.; Teterin, A. Y..; Nikitin, A. S. *J. Elect. Spec.* **2001**, *114-116*, 915-923.

[13] Paiva, A. P.; Malki, P. *J. Radioanal. Nucl. Chem.* **2004**, *261*, 485-496.

[14] (a) Burns, C. J.; et al. *Inorg. Chem.* **2000**, *39*, 5464-5468. (b) Vaughn, A. E.; Barnes, C. L.; Duval, P. B. *J. Chem. Crystallogr.* **2007**, *37*, 779-782.

[15] (a) Sarsfield, M. J.; Helliwell, M.; Raftery, J. *Inorg. Chem.* **2004**, *43*, 3170-3179. (b) Sarsfield, M. J.; Helliwell, M. *J. Am. Chem. Soc.* **2004**, *126*, 1036-1037.

[16] (a) Sessler, J. L.; et al. *Angew. Chem. Int. Ed.* **2001**, *40*, 591-594. (b) Arnold, P. L.; Blake, A. J.; Wilson, C. Love, J. B. *Inorg. Chem.* **2004**, *43*, 8206-8208. (c) Arnold, P. L.; et al. *J. Am. Chem. Soc.* **2006**, *128*, 9610-9611. (d) Marks, T. J.; Stojakovic, D. R. *J. Am. Chem. Soc.* **1978**, *100*, 10696-1705. (e) Sessler, J. L.; Mody, T. D.; Lynch, V. Inorg. Chem. **1992**, *31*, 529-531. (f) Melfi, P. J.; Kim, S. K.; Lee, J. T.; Bolze, F.; Seidel, D.; Lynch, V. M.; Veauthier, J. M.; Gaunt, A. J.; Neu, M. P.; Ou, Z.; Kadish, K. M.; Fukuzumi, S.; Ohkubo, K.; Sessler, J. L. *Inorg. Chem.* **2007**, *46*, 5143-5145.

[17] Burrows, H. D. *Chem. Soc. Rev.*, **1974**, 139-165.

[18] Baird, C. P.; Kemp, T. J. *Prog. React. Kinet.* **1997**, *22*, 87-139.

[19] (a) Kannan, S.; Vaughn, A. E.; Weis, E. M.; Barnes, C. L.; Duval, P. B. *J. Am. Chem. Soc.* **2006**, *128*, 14024-14025, and unpublished results extending this topic. (b) Kannan, S.; Moody, M. A.; Barnes, C. L.; Duval, P. B. *Inorg. Chem.* **2006**, *45*, 9206-9212.

[20] (a) Morris, D. E. *Inorg. Chem*. **2002**, 41, 3542-3547. (b) Mizuoka, K.; Tsushima, S.; Hasegawa, M.; Hoshi, T.; Ikeda, Y. *Inorg. Chem.* **2005**, *44*, 6211-6218, and references therein. (c) Steele, H.; Taylor, R. J. *Inorg. Chem.* **2007**, *46*, 6311-6318. (d) Ekstrom, A. *Inorg. Chem.* **1974**, *13*, 2237-2241.

[21] Renshaw, J. C.; Butchins, L. J. C.; Livens, F. R.; May, I.; Charnock, J. M.; Lloyd, J. R. *Environ. Sci. & Technol.* **2005**, *39*, 5657-5660. (b) Wander, M. C. F.; Kerisit, S.; Rosso, K. M.; Schoonen, M. A. A. *J. Phys. Chem. A* **2006**, *110*, 9691-9701.

[22] Craft, E. S.; Abu-Qare, A.; Flaherty, M.; Garofolo, M.; Rincavage, H.; Abou-Donia, M.*J. Toxicol. Env. Heal. B* **2004**, *7*, 297-317.

[23] Ilton, E. S.; Haiduc, A.; Cahill, C. L.; Felmy, A. R. *Inorg. Chem.* **2005**, *44*, 2986-2988, and references therein.

[24] (a) Hayton, T. W.; Wu, G. *J. Am. Chem. Soc.* **2008**, *130*, 2005-2014. (b) Arnold, P. L.; Patel, D.; Wilson, C.; Love, J. B. Nature **2008**, 451, 315-317. (c) Berthet, J. C.; Nierlich, M.; Ephritikhine, M. *Angew. Chem. Int. Ed.* **2003**, *42*, 1952-1954. (d) Burdet, F.; Pecaut, J.; Mazzanti, M. *J. Am. Chem. Soc.* **2006**, *128*, 16512-16513. (e) Natrajan, L.; Burdet, F.; Pecaut, J.; Mazzanti, M. *J. Am. Chem. Soc.* **2006**, *128*, 7152-7153. (f) Berthet, J. C.; Siffredi, G.; Thuery, P.; Ephritikhine, M. *Chem. Commun.* **2006**, 3184-3186.

[25] Spear, J. R.; Figueroa, L. A.; Honeyman, B. D. *Appl. Environ. Microbiol.* **2000**, *66*, 3711-3721, and references therein.

[26] (a) O'Loughlin, E. J.; Kelly, S. D.; Cook, R. E.; Csencsits, R.; Kemner, K. M. *Environ. Sci. & Technol.* **2003**, *37*, 721-727. (b) Walter, M.; Arnold, T.; Reich, T.; Bernhard, G. *Environ. Sci. & Technol.* **2003**, *37*, 2898-2904. (c) Dodge, C. J.; Francis, A. J.; Gillow, J. B.; Halada, G. P.; Eng, C.; Clayton, C. R. *Environ. Sci. & Technol.* **2002**, *36*, 3504-3511. (d) Morris, D. E.; Allen, P. G.; Berg, J. M.; Chisholm-Brause, C. J.; Conradson, S. D.; Donohoe, R. J.; Hess, N. J.; Musgrave, J. A.; Tait, C. D. *Environ. Sci. & Technol.* **1996**, *30*, 2322-2331.

[27] Francis, A. J.; Dodge, C. J. *Environ. Sci. & Technol.* **1998**, *32*, 3993-3998.

[28] McCleskey, T. M.; Foreman, T. M.; Hallman, E. E.; Burns, C. J.; Sauer, N. N. *Environ. Sci. & Technol.* **2001**, *35*, 547-551.

[29] (a) Wilkerson, M. P.; Burns, C. J.; Paine, R. T.; Scott, B. L. *Inorg. Chem.* **1999**, *38*, 4156-4158. (b) Duval, P. B.; Kannan, S.; Barnes, C. L. *Inorg. Chem. Commun.* **2006**, *9*, 426-428. (c) Kannan, S.; Barnes, C. L.; Duval, P. B. *Chem. Commun.* **2005**, 5997-5998. (d) Gaunt, A. J.; Reilly, S. D.; Hayton, T. W.; Scott, B. L.; Neu, M. P. *Chem. Commun.* **2007**, 1659-1661.

[30] Kannan, S.; Barnes, C. L.; Duval, P. B. *Inorg. Chem.* **2005**, *44*, 9137-9139.

[31] Berthet, J. C.; Thuery, P.; Ephritikhine, M. *Chem. Commun.* **2007**, 604-606.

[32] (a) Haller, L. J. L; Kaltsoyannis, N.; Sarsfield, M. J.; May, I.; Cornet, S. M.; Redmond, M. P.; Helliwell, M. *Inorg. Chem.* **2007**, *46*, 4868-4875. (b) Sarsfield, M. J.; May, I.; Cornet, S. M.; Helliwell, M. *Inorg. Chem.* **2005**, *44*, 7310-7312.

[33] (a) Wilkerson, M. P.; Burns, C. J.; Dewey, H. J.; Martin, J. M.; Morris, D. E.; Paine, R. T.; Scott, B. L. *Inorg. Chem.* **2000**, *39*, 5277-5285. (b) Wilkerson, M. P.; Burns, C. J.; Morris, D. E.; Paine, R. T.; Scott, B. L. *Inorg. Chem.* **2002**, *41*, 3110-3120. (c) Barnhart, D. M.; Burns, C. J.; Sauer, N. N.; Watkin, J. G. *Inorg. Chem.* **1995**, *34*, 4079-4084. (d) Burns, C. J.; Smith, D. C.; Sattelberger, A. P.; Gray, H. B. *Inorg. Chem.* **1992**, *31*, 3724-3727.

[34] Duval, P. B.; Burns, C. J.; Buschmann, W. E.; Clark, D. L.; Morris, D. E.; Scott, B. L *Inorg. Chem.* **2001**, *40*, 5491-5496.

[35] Maynadié, J.; Berthet, J. C.; Thuéry, P.; Ephritikhine, M. *Chem. Commun.* **2007**, 486 – 488.

[36] Sarsfield, M. J.; Helliwell, M.; Collison, D. *Chem. Commun.* **2002**, 2264-2265.

[37] (a) Mangur, S. A. *Chem. Commun.* **2004**, 2738-2739. (b) Arnold, P.; Liddle, S. T. *Chem. Commun.* **2006**, 3959-3971.

[38] Duval, P. B.; et al. *Angew. Chem. Int. Ed.* **2001**, *40*, 3357-3361.

[39] (a) Arney, D. S. J.; Burns, C. J. *J. Am. Chem. Soc.* **1995**, *117*, 9448-9460. (b) Arney, D. S. J.; Schnabel, R. C.; Scott, B. L.; Burns, C. J. *J. Am. Chem. Soc.* **1996** *128*, 6780-6781. (c) Brown, D. R.; Denning, R. G.; Jones, R. H. *J. Chem. Soc., Chem. Commun.* **1994**, 2601-2602.

[40] (a) Jantunen, K. C.; Scott, B. L.; Kiplinger, J. L. *J. Alloy Compd.* **2007** *444–445*, 363–368. (b) Dognon, J. P.; Clavaguera, C.; Pyykko, P. *Agnew. Chem. Int. Ed.* **2007**, *46*, 1427-1430. (c) Pool, J. A.; Scott, B. L.; Kiplinger, J. L. *J. Am. Chem. Soc.* **2005**, *127*, 1338-1339.

[41] (a) Burns, C. J.; Eisen, M. S. Organoactinide Chemistry: Synthesis and Characterization. In *The Chemistry of the Actinide and Transactinide Elements*, 3rd ed.; Morss, L. R., Edelstein, N. M., Fuger, J., The Netherlands, 2006; Vol. 5, pp 2799-2910, and references therein. (b) Ephritikhine, M. *J. Chem. Soc., Dalton Trans.* **2006**, 2501-2516.

[42] (a) Evans, W. J.; Wink, D. J.; Stanley, D. R. *Inorg. Chem.* **1982**, *21*, 2565-2573. (b) Lauke, H.; Swepston, P. J.; Marks, T. J. *J. Am. Chem.* Soc. **1984**, *106*, 6841-6843.

[43] Roussel, P.; Scott, P. *J. Am. Chem. Soc.* **1998**, *120*, 1070-1071, and references therein.

[44] Castro-Rodriguesz, I.; Nakai, H.; Zakharov, L. N.; Rheingold, A. L.; Meyer, K. *Science*, **2004**, *305*, 1757-1759, and references therein.

[45] Antunes, M. A.; Ferrence, G. M.; Domingos, A.; McDonald, R.; Burns, C. J.; Takats, J.; Marques, N. *Inorg. Chem.* **2004**, *43*, 6640-6643.

[46] (a) Korobkov, I.; Gambarotta, S.; Yap, G. P. A. *Organomet.* **2001**, *20*, 2552-2559. (b) Sessler, J. L.; Melfi, P. J.; Pantos, G. D. *Coord. Chem. Rev.* **2006**, *250*, 816-843.

[47] (a) Korobkov, I.; Gambarotta, S.; Yap, G. P. A. *Angew. Chem. Int. Ed.* **2003**, *42*, 4958-4961. (b) Salmon, L.; Thuery, P.; Ephritikhine, M. *Dalton Trans.* **2006**, 3629-3637. (c) Kawaguchi, H.; Matsuo, T. *J. Organomet. Chem.* **2004**, *689*, 4228-4243.

[48] Maynadié, J.; Barros, N.; Berthet, J. C.; Thuéry, P. C.; Maron, L.; Ephritikhine, M. *Angew. Chem. Int. Ed.* **2007**, *119*, 2056-2058, and references therein.

[49] Barnea, E.; Eisen, M. S. *Coord. Chem. Rev.* **2006**, *250*, 855-899

[50] Berthet, J. C.; Ephritikhine, M. *Coord. Chem. Rev.* **1998**, *178-180*, 83-117.

[51] (a) Arney, D. S. J.; Burns, C. J. *J. Am. Chem. Soc.* **1993**, *115*, 9840. (b) Arney, D. S. J.; Burns, C. J.; Smith, D. C. *J. Am. Chem. Soc.* **1992**, *114*, 10068-10069. (c) Burns, C. J.; Smith, w. H.; Huffman, J. C.; Sattelberger, A. P. *J. Am. Chem. Soc.* **1990**, *112*, 3237-3239. (d) Berthet, J. c.; Ephritikhine, M. *J. Chem. Soc., Chem. Commun.* **1993**, 1566-1567. (e) Zalkin, A.; Brennan, J. G.; Andersen, R. A. *Acta Cryst.* **1988**, *C44*, 1553-1554. (f) Castro-Rodriguez, I.; Nakai, H.; Meyer, K. *Angew. Chem. Int. Ed.* **2006**, *118*, 2449-2452. (g) Roussel, P.; Boaretto, R.; Kingsley, A. J.; Alcock, N. W. ;. Scott, P. J. *J. Chem. Soc., Dalton Trans.* **2002**, 1423-1428. Also see reference [36]

[52] Warner, B. P.; Scott, B. L.; Burns, C. J. *Angew. Chem. Int. Ed.* **1998**, *37*, 959-960.

[53] For a review on pentavalent uranium, see Selbin, J.; Ortego, J. D. *Chem. Rev.* **1969**, *69*, 657-671.

[54] Kiplinger, J. L.; Morris, D. E.; Scott, B. L.; Burns, C. J. *Chem. Commun.* **2002**, 30-31.

[55] Holm, R. H. *Chem. Rev.* **1987**, *87*, 1401-1449.

[56] (a) Walsh, P. J.; Hollander, F. J.; Bergman, R. G. *J. Am. Chem. Soc.* **1988**, *110*, 8729-8731. (b) Cummins, C. C.; Baxter, S. M.; Wolczanski, P. T. *J. Am. Chem. Soc*. **1988**, *110*, 8731-8733. (c) Duncan, A. P.; Bergman, R. G. *The Chem. Rec.* **2002**, *2*, 431-445.

[57] For a variety of Schiff base-phenolate ligands and related derivatives and their respective uranyl(VI) complexes, see Chapter 2 and references therein.

[58] For representative examples of uranyl(VI) sal-type complexes, see (a) Bandolini, G.; Clemente, D.; Croatto, U.; Vidali, M.; Vigato, P. A. *J. Chem. Soc., Chem. Commun.* **1971**, 1330-1331. (b) Benetollow, F.; Bombieri, G. *Acta Cryst.* **1979**, *B35*, 3091-3093. (c) Bandolini, G.; Clemente, D. A.; *J. Chem. Soc., Dalton Trans.* **1974**, 612-615. (d) Brock, A. M.; et al *J. Inorg. and Nucl. Chem.* **1978**, *40*, 1551-1559.

[59] Cametti, M.; Nissinen, M.; Dalla Cort, A.; Mandolini, L.; Rissanen, K. *J. Am. Chem. Soc.* **2005**, *127*, 3831-3837. (b) Rudkevich, D. M.; et al. *J. Am. Chem. Soc.* **1994**, *116*, 4341-4351. (c) Staveren, C. J. V.; Eerden, J. V.; Van Veggel, F. C. J. M; Harkema, S.; Reinhoudt, D. N. *J. Am. Chem. Soc.* **1988**, *110*, 4994-5008. (d) Rudkevich, D. M.; Stauthamer, W. P. R. V.; Verboom, W.; Engbersen, J. F. J.; Harkema, S.; Reinhoudt, D. N. *J. Am. Chem. Soc.* **1992**, *114*, 9671-9673.

[60] Cort, A. D.; Mandolini, L.; Schiaffino, L. *Chem. Commun.* **2005**, 3867-3869.

[61] Castelli, V. A.; Cort, A. D.; Mandolini, L.; Reinhoudt, D. N.; Schiaffino, L. *Eur. J. Org. Chem.* **2003**, 627-633.

[62] (a) Evangelio, E.; Ruiz-Molina, D. *Eur. J. Inorg. Chem.* **2005**, 2957-2971. (b) Khudyakov, I. V.; Turro, N. J.; Yakushenko, I. K. *J. Photochem. Photobiol. A: Chem.* **1992**, *63*, 25-31. (c) Hadjoidis, E.; Mavridis, I. M. *Chem. Soc. Rev*., **2004**, *33*, 579-588.

[63] Vaughn, A. E.; Bassil, D. B.; Barnes, C. L.; Tucker, S. A.; Duval, P. B. *J. Am. Chem. Soc.* **2006**, 128, 10656.

[64] (a) Mizuoka, K.; Kim, S.-Y.; Hasegawa, M.; Hoshi, T.; Uchiyama, G.; Ikeda, Y. *Inorg. Chem.* **2003**, *42*, 1031-1038. (b) Mizuoka, K.; Ikeda, Y. *Inorg. Chem.* **2003**, *42*, 3396-2298. (c) Mizuoka, K.; Tsushima, S.; Hasegawa, M.; Hoshi, T.; Ikeda, Y. *Inorg. Chem.* **2005**, *44*, 6211-6218.

[65] (a) Schreckenbach, G.; Hay, P. J.; Martin, R. L. *Inorg. Chem.* **1998**, *37*, 4442-4451. (b) Schreckenbach, G.; Hay, P. J.; Martin, R. L. *J. Comp. Chem.* **1999**, *20*, 70-90. (c) Hay, P. J.; Martin, R. L. *Los Alamos Science* **2000**, *26*, 382-391.

[66] (a) Barea, G.; Liedox, A.; Maseras, F.; Jean, Y. *Inorg. Chem.* **1998**, *37*, 3321-3325. (b) Odom, A. L.; Mindiola, D. J.; Cummins, C. C. *Inorg. Chem.* **1999**, *38*, 3290-3295, and references therein. (c) DuMez, D. D.; Mayer, J. M. *Inorg. Chem.* **1998**, *37*, 445-453.

[67] (a) Alcock, N. W.; Flanders, D. J.; Brown, D. *J. Chem. Soc., Dalton Trans.* **1984**, 679-681. (b) Brock, A. M.; Cook, D. H.; Fenton, D. E.; Bombieri, G.; Forsellini, E.; Benetolo, F *J. Inorg. Nucl. Chem.* **1978**, *40*, 1551-1559.

[68] (a) Bagnall, K.; du Preez, J.; Gellatly, B. J.; Holloway, J. H. *J. Chem. Soc. A* **1966**, 1963-1968. (b) Frasson, E.; Bombieri, G.; Panattoni, C. *Nature* **1964**, *202*, 1325-1326.

[69] Duval, P. B.; Burns, C. J.; Clark D. Unpublished result.

[70] (a) Hayton, T. W.; et al. *Science*, **2005**, *310*, 1941-1943. (b) Hayton, T. W.; Boncella, J. M.; Scott, B. L.; Batista, E. R.; Hay, P. J.*J. Am. Chem. Soc.* **2006**, *128*, 10549-10559. (c) Hayton, T. W.; Boncella, J. M.; Scott, B. L.; Batista, E. R. *J. Am. Chem. Soc.* **2006**, *128*, 12622-12623.

[71] Lukens, W. W.; et al. *J. Am. Chem. Soc.* **1996**, *118*, 901-902.

[72] For representative examples of discrete uranyl carboxylate complexes, refer to (a) Bombieri, G.; Croatto, U.; Graziani, R.; Forsellini, E.; Magon, L. *Acta Cryst.* **1974**, *B30*, 407-411. (b) Alcock, N. W.; Errington, W.; Kemp, T. J.; Leceiejewicz, J. *Acta Cryst.* **1996**, *C52*, 615-617, and references therein.

[73] For representative examples of uranyl carboxylate polymers, refer to (a) Thuery, P. *Chem. Commun.* **2006**, 853-855. (b) Frisch, M.; Cahill, C. L. *Dalton Trans.* **2006**, 4679-4690, and references therein.

[74] Vigato, P. A.; Casellato, U.; Clemente, D. A.; Bandoli, G. *J. Inorg. Nucl. Chem.* **1973**, *35*, 4131-4139.

[75] Runde, W. *Los Alamos Science* **2000**, *26*, 392-411.

[76] Burns, C. J.; Sattelberger, A. P. *J. Am. Chem. Soc.* **1988**, *27*, 3692-3693

[77] Eisenstein, J. C. *J. Chem. Phys.* **1956**, *25*, 142-146, and references therein.

[78] (a) Graves, C. R.; Scott, B. L.; Morris, D. E.; Kiplinger, J. L. *J. Am. Chem. Soc.* **2007**, *129*, 11914-11915. (b) Graves, C. R.; Yang, P.; Kozimor, S. A.; Vaughn, A. E.; Clark, D. L.; Conradson, S. D.; Schelter, E. J.; Scott, B. L.; Thompson, J. D.; Hay, P. J.; Morris, D. E.; Kiplinger, J. L. *J. Am. Chem. Soc.* **2008**, 130, 5272-5285.

[79] (a) Reisfeld, M. J.; Crosby, G. *Inorg. Chem.* **1965**, *4*, 65-70. (b) Penneman, R. A.; Sturgeon, G. D.; Asprey, L. B. *Inorg. Chem.* **1964**, *3*, 126-129. (c) Ryan, J. L. *J. Inorg. Nucl. Chem.* **1971**, *33*, 153-177. (d) Gourier, D.; Caurant, D.; Berthet, J. C.; Boisson, C.; Ephritikhine, M. *Inorg. Chem.* **1997**, *36*, 5931-5936. Also see reference [67].

[80] Ward, M. D. *Chem. Soc. Rev.* **1995**, 121-133, and references therein.

[81] (a) Petit, L.; Savane, A.; Timmerman, W. M.; Sazotek, Z. *Phys. Rev. Let.* **2002**, *88*, 216403(1-4) (b) Moore, K. T.; Laan, G. V.; Haire, R. G.; Wall, M. A.; Schwartz, A. J.; Söderlind, P. *Phys. Rev. Let.* **2007**, *98*, 236401(1-3)

[82] (a) Carlson, C. N.; Scott, B. L.; Martin, R. L.; Thompson, J. D.; Morris, D. E.; John, K. D. *Inorg. Chem.* **2007**, *46*, 5013-5022. (b) Carlson, C. N.; Kuehl, C. J.; Ogallo, L.; Shultz, D. A.; Thompson, J. D.; Kirk, M. L.; Martin, R. L.; John, K. D.; Morris, D. E. *Organomet.* **2007**, *26*, 4234-4242.

[83] (a) Schelter, E. J.; Veauthier, J. M.; Thompson, J. D.; Scott, B. L.; John, K. D.; Morris, D. E.; Kiplinger, J. L. *J. Am. Chem. Soc.* **2006**, *128*, 2198-2199. (b) Kozimor, S. A.; Bartlet, B. A.; Rinehard, J. D.; Long, J. R. *J. Am. Chem. Soc.* **2007**, *129*, 10672-10674.

[84] Kiplinger, J. L.; Pool, J. A.; Schelter, E. J.; Thompson, J. D.; Scott, B. L.; Morris, D. E. *Angew. Chem. Int. Ed.* **2006**, *45*, 2036-2041. (b) Evans, W. J.; Kozimor, S. A.; Ziller, J. W. *Science* **2005**, *309*, 1835-1838.

[85] (a) Ward, M. D.; McCleverty, J. A. *J. Chem. Soc., Dalton Trans.* **2002**, 275-288. (b) McCleverty, J. A.; Ward, M. D. *Acc. Chem. Res.* **1998**, *31*, 842-851.

[86] Rosen, R. K.; Andersen, R. A.; Edelstien, N. M. *J. Am. Chem. Soc.* **1990**, *112*, 4588-4590.

Chapter 2

Structural, Electrochemical, and Photochemical Trends Among Three Types of Uranyl(VI) Schiff Base-Phenolate Complexes and Related Derivatives

Abstract

A series of ten uranyl(VI) Schiff base complexes have been prepared and isolated in good yield and characterized by NMR spectroscopy, infrared spectroscopy, cyclic voltammetry, UV-visible electronic absorption and emission spectrophotometry, elemental analysis, and single crystal X-ray diffraction. The Schiff base-phenolate and amino-phenolate ligands (**H_2L^1**-**H_3L^7**) employed in this investigation are derived from di-*t*-butyl functionalized salicylidene sidearm moieties with varied chelate backbones. The corresponding collection of complexes are grouped into three categories based on structural, electro-, and photochemical similarities. Category 1 complexes are constructed from the $UO_2(^tBu_4$-saloph)L framework, where the capping ligand adduct L = THF (**1a**), TMPO (**1b**), Cl (**1c**) and OH (**1d**) has noticeable effects on the redox energetics and kinetics of the $U^{VI}O_2^{2+}/U^{V}O_2^{+}$ couple. Luminescence among this category cannot be attributed to the uranyl or chelate units exclusively, but rather depend on the combined properties of the two. In the absence of L, a saloph based photochromic transformation is observed for **1a.** This structural rearrangement is effectively blocked by the presence of L, which redirects photoexcitation energy and a new luminescence is observed at 365 nm

that coincides with a saloph → UO_2 charge transfer feature in the absorption spectrum. In one instance, these factors contribute to generate a photochemical pathway that produces **1d** from **1a** in the presence of cobaltocene. Ligands in category 2 are supported by the more flexible backbones binapthylenediimine, tris(triethylamino)imine, and ethylenediimine and the corresponding uranyl(VI) complexes in this category are structurally related to those in category 1. Again, electrochemical and photophysical measurements indicate a salient dependence on the influence of equatorial capping ligands. For example, in UO_2(^{t}Bu$_6$-saltren) (**3**) the equatorial region is saturated by the H_3L^3 chelate and does not need a monodentate ligand to complete the UO_2^{2+} coordination sphere, resulting in a $U^{VI}O_2^{2+}/U^{V}O_2^{+}$ redox couple and luminescent properties that are not reliant on the participation of the capping ligand or solvent effects. Category 3 includes two bimetallic derivatives (**6**, **7**) in which two uranyl(VI) moieties are bridged in close proximity (~4 and 6 Å, respectively). Although intramolecular electronic communication between the metal units was anticipated, the dimers display sluggish electron transfer kinetics on the voltammetric timescale and electronic spectral features indicate that absorption and emission appear to be solely ligand based. A striking similarity between all of the complexes disclosed here is the lack of photochemical reaction with mild reducing agents (i.e., methanol) whereas in general uranyl(VI) complexes are prone to undergo photolysis under such conditions.

2.1 Introduction

A substantial body of work exists on the synthesis and structural characterization of metal Schiff base complexes constructed from salicylidene sidearms.[1] Interests in the application of sal-type compartmental ligands towards the uranyl(VI) ion were initiated in the late 1970's and have since been investigated as a suitable platform to support a variety of chemical processes at available metal binding sites.[2,3] In light of the high degree of solubility imparted by the functionalized salicylidene units, advances in the use of Schiff base-phenolate chelates in actinyl chemistry have extended to focus on selectively binding actinyl ions in the presence of other metal ions as a potential application for spent nuclear fuel separations.[4]

Electrochemical analysis of the uranyl(VI/V), $U^{VI}O_2^{2+}/U^{V}O_2^{+}$, redox couple has become a subject of considerable interest since both ions are relevant to the fate of nuclear fuel materials accidentally released into the environment.[5] A series of experiments performed on UO_2(saloph)L (L = DMSO, MeOH) monitored spectroscopic changes that identified the $U^{VI}O_2^{2+}/U^{V}O_2^{+}$ redox transformation via electrolysis.[6] In addition, the potent oxidizing ability of the excited state of the $^{*}UO_2^{2+}$ ion has been employed to access uranyl(V) species and to immobilize uranium contaminants in the environment.[7,8] The photochemical activity of uranyl(VI) ion coordination complexes is determined by the composition of the equatorial ligand environment, however there are a scarce number of studies that have probed these properties when the ligands themselves demonstrate peculiar photophysical properties, such as photochromism.[9-11] Since both uranyl(VI) and Schiff base-phenolate systems individually display fluorescent and reactive photoexcited state properties, it is surprising that the combined photophysical

and photochemical characteristics of these complexes have remained unexplored. Information acquired from the electro- and photochemical pathways generated from the combination of uranyl(VI) and Schiff base-phenolate components may shed light on factors previously unrecognized in uranyl(VI) chemical processes.

This account focuses on a series of di-*t*-butyl substituted salicylidene derived uranyl(VI)-Schiff base complexes and related derivatives constructed from a host of ligand backbones (**Figures 2.1** and **2.2**). The corresponding uranyl(VI) complexes are segregated into three categories based on structural similarities. Category 1 is confined to the $UO_2(^tBu_4$-saloph)L framework where complexes **1a-d** contain different monodentate capping ligands denoted by L. Category 2 complexes (**2-5**) consist of chelates constructed from flexible backbones (**H_2L^2-H_2L^5**), whereas category 3 includes two bimetallic uranyl-Schiff base derivatives (**6**,**7**) with ligands (**H_2L^6** and **H_2L^7**). The complexes reported here were synthesized using a variety of standard non-aqueous and benchtop techniques and characterized by single crystal X-ray diffraction, NMR spectroscopy, IR spectroscopy, elemental analysis, cyclic voltammetry, and UV-visible absorption and emission spectrophotometry. Interpretation of these data suggest that the three types of complexes provide structural diversities that result in significant effects on the photo- and electrochemical behavior for each category.

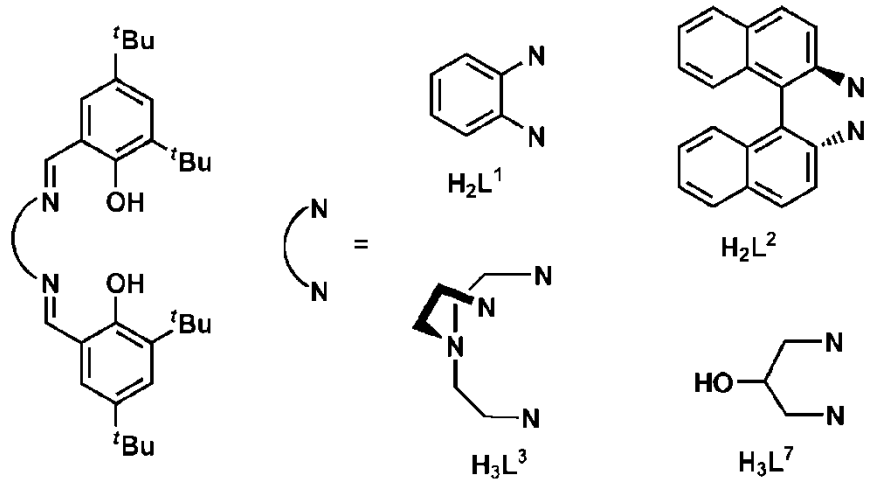

Figure 2.1. *t*-Butyl substituted sal-type ligands saloph (**H_2L^1**), salbinap (**H_2L^2**), saltren (**H_3L^3**), salhpn (**H_3L^7**).

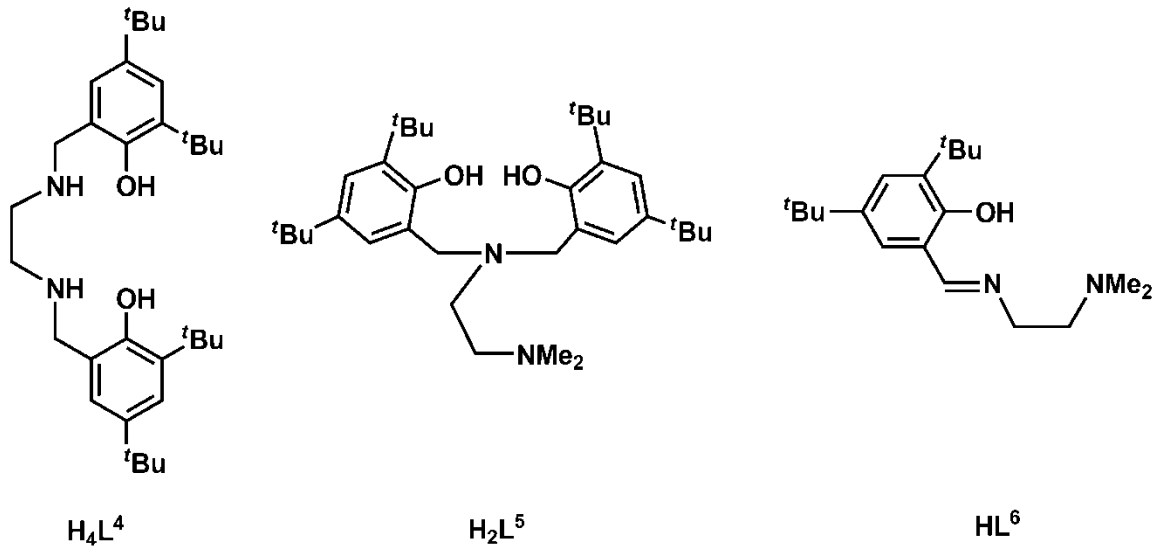

Figure 2.2. Ethylenediamine derived ligands salen (**H_4L^4**), BAP (**H_2L^5**), and salNMe$_2$ (**HL^6**).

A main objective of this report is to expand upon past work by treating uranyl(VI) Schiff base-phenolate derivatives with chemical reductants capable of accessing and stabilizing the uranyl(V) ion. Rationale for this approach is founded on supplying a chelate ligand, with a metal binding compartment saturated with a sterically demanding *t*-

butyl substituted periphery, designed to prevent uranyl(V) disproportionation in non-aqueous media. Gaining access to the pentavalent uranyl ion has a two-fold return: (i) to understand the nature of this elusive oxidation state as it pertains to environmental transport and remediation, and (ii) to utilize the $5f^1$ electronic configuration in the linear dioxo geometry as a spectroscopic and magnetic probe to provide crucial information on 5f orbital perturbations in relation to established molecular orbital theories that elucidate structure and bonding in the uranyl(VI) unit. One account has recently furnished a discrete uranyl(V) complex that uses a synthetic approach that extends from our initial communication on the one electron photochemical reduction of uranyl(VI)-saloph complexes using cobaltocene, whereas pentavalent uranyl species have surfaced in the literature on a frequent basis in recent years.[12]

2.2 Results and Discussion

Synthesis and Structural Characterization

Category 1. The synthetic protocol used for the preparation of uranyl(VI)-saloph derivatives **1a-c** is outlined in **Scheme 2.1**. Unless otherwise stated this procedure was generalized to the production of **2-7**. $UO_2(^tBu_4$-saloph)THF (**1a**) is the parent species for complexes in this category. The synthesis of **1a** involved deprotonation of ligand $\mathbf{H_2L^1}$ in tetrahydrofuran (THF) with excess sodium hydride followed by addition of a solution of $UO_2Cl_2(THF)_3$. The reaction mixture immediately changed in color from yellow to blood red, and following work-up in toluene **1a** was afforded as a red crystalline solid in good yield (77%). Complex **1b** was prepared via substitution of one equivalent of trimethylphosphine oxide (TMPO) for THF at the capping position. The reaction was

carried out in benzene and crystalline material was obtained in low yield (47%) from evaporation of the reaction mix. Likewise, **1c** was synthesized by addition of tetraphenylphosphonium chloride (PPh_4Cl) to a solution of **1a** in THF, and the resulting orange material isolated in analytically pure form in 83% yield after workup in acetonitrile (MeCN). Complex **1d** was prepared by photochemical reaction between **1a** and cobaltocene in THF solution and is described in full detail later in the discussion (**Scheme 2.4**). Following photolysis, **1d** was obtained as an orange crystalline solid in 69% yield from evaporation of an MeCN solution.

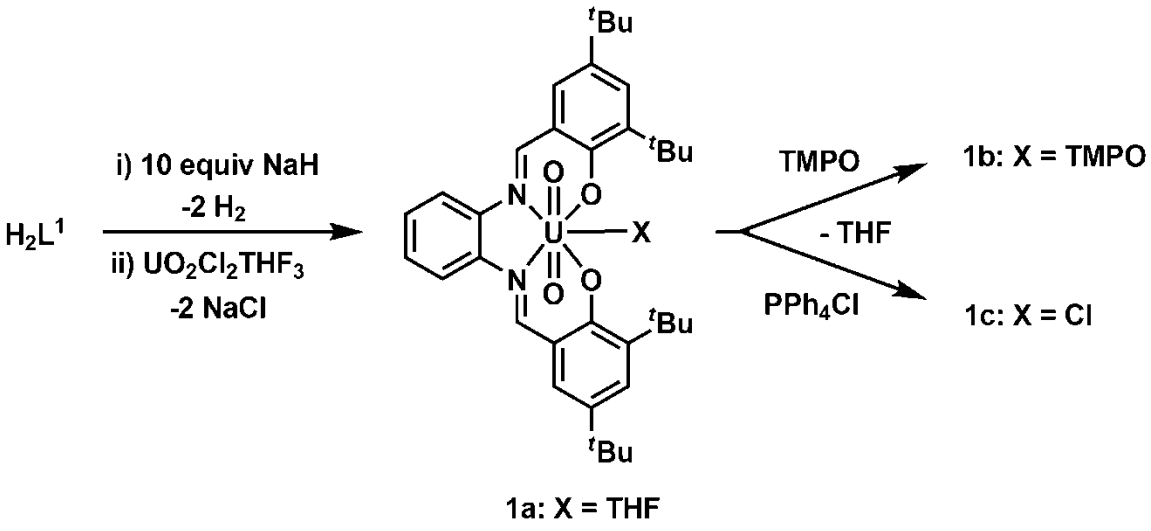

Scheme 2.1. The synthesis of category 1 complexes **1a-c**.

A few uranyl(VI)-saloph derivatives have been structurally characterized,[2-4,13] however **1a-d** represent new examples with incorporation of the *t*-butyl substituted ligand periphery and a variety of capping donors. Single crystal X-ray diffraction analysis confirmed that the $UO_2(^tBu_4$-saloph) framework is isostructural in **1a-d**, with a slightly distorted seven coordinate pentagonal bipyramidal geometry in each case. The solid-state

structure of $[UO_2(^tBu_4\text{-saloph})OH][CoCp_2]$ (**1d)** shown in **Figure 2.3** depicts the typically planar saloph ligand slightly bent around the uranyl(VI) moiety. This puckered *boat*-type conformation has been reported in previous uranyl-saloph derivatives and is attributed to the ligand cavity stretching to accommodate the large $O=U=O^{2+}$ unit.[14] The N_2O_2 donor cavity occupies the equatorial plane along with a neutral capping hydroxide anion that completes the pentagonal equator. The average $U\text{-}O_{Ar}$ distance of 2.29 Å is within the range reported for uranyl(VI)-aryloxide attachments, including structurally characterized saloph derivatives.[13,15] Average $U\text{-}N_{Im}$ (~2.63 Å) contacts are slightly elongated in comparison. Two oxide ligands reside in the axial positions with U(1)-O(4) distance of ~1.801(4) Å and an O(3)-U-O(4) angle of 175.99(17)º. The short and nearly linear U=O bonds are further evidence by the presence of the single asymmetric stretch in the solid state infrared spectrum near ~900 cm^{-1}. These data fall within the range of parameters reported for the majority uranyl(VI) complexes.[16] The metrical parameters of the $UO_2(^tBu_4\text{-saloph})$ framework are consistent across the category 1 series as listed in **Table 2.2** and complete structural details are provided in **Table 2.1** and the supporting information in appendix 1.

Table 2.1. Selected crystallographic parameters for **1a-1d**.

	1a	**1b**	**1c**	**1d**
formula	$C_{40}H_{54}N_2O_5U$	$C_{39}H_{55}N_2O_5PU$	$C_{60}H_{62}N_2O_4ClPU$	$C_{46}H_{57}N_2O_5UCo$
color	red	red	orange	orange
a (Å)	17.420(2)	12.2285(18)	19.753(6)	17.896(2)
b (Å)	17.420(2)	26.340(4)	22.563(7)	19.084(3)
c (Å)	11.7664(16)	14.886(2)	12.048(4)	17.980(2)
α (º)	90	90	90	90
β (º)	102.788(2)	107.239(2)	90	113.337(2)
γ (º)	90	90	90	90
V (Å ^{3})	4508.7(10)	4579.3(12)	5370(3)	5638.2(13)
Z	4	4	5	4
FW	880.91	900.88	1179.62	1014.93
crystal system	monolinic	monoclinic	orthorhombic	monoclinic
space group	P$2_1/c$	P$2_1/n$	Pnma	P$2_1/c$
T (K)	173(2)	173(2)	173(2)	173(2)
λ (Å)	0.71073	0.71073	0.71073	0.71073
F(000)	1960	1968	2404	2020
ρ_{calc} (g•cm^{-1})	1.433	1.420	1.507	1.194
μ (mm^{-1})	3.645	3.622	3.153	3.198
θ range (º)	1.50-27.11	1.55-27.21	1.81-27.16	1.63-27.08
total reflections	32051	32765	37252	38611
unique reflections	9912	10117	6112	12335
parameters	451	502	355	496
R_1	0.0326	0.0514	0.0472	0.0460
wR_2 (all data)	0.0886	0.0860	0.1452	0.1228
max, min peaks eÅ^{-3}	1.695, -1.665	1.234, -1.139	1.487, -1.451	2.632, -1.202
GOF on F^2	1.049	1.013	1.054	0.950

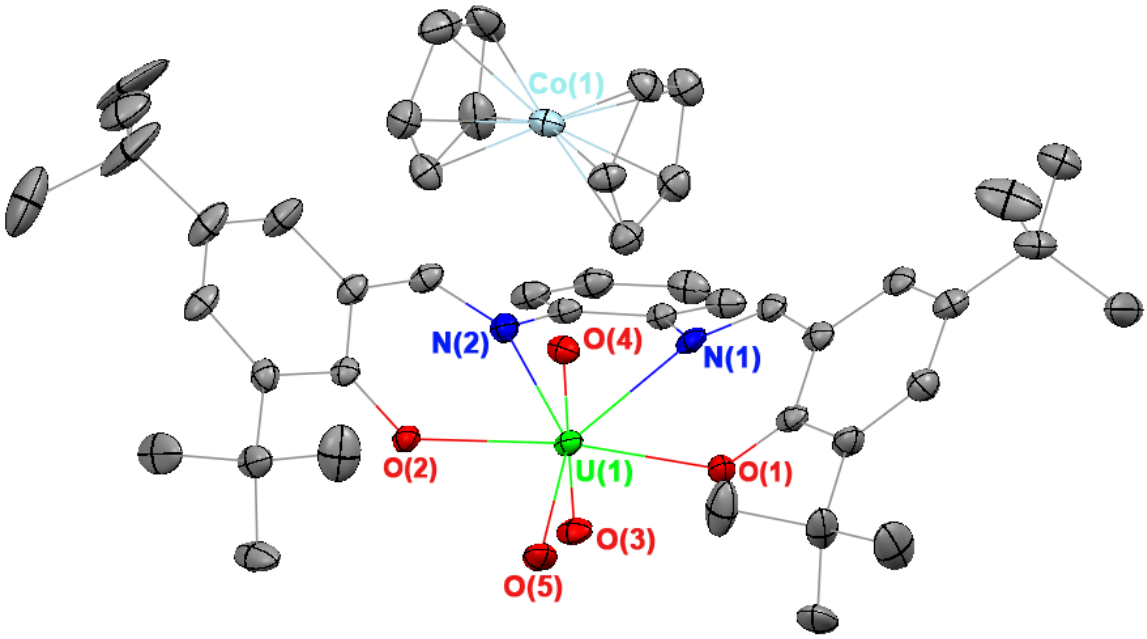

Figure 2.3. Molecular structure for $[UO_2(^tBu_4\text{-saloph})OH][CoCp_2]$ (**1d**) with thermal ellipsoids depicted at the 50% probability level. H-atoms omitted for clarity.

The $UO_2(^tBu_4\text{-saloph})$ framework has close to C_s symmetry since the only allowed symmetry operation is a mirror plane that bisects the U-X contact perpendicular to the slightly distorted equatorial plane generated by the N_2O_2 compartment. Evidence for the retention of C_s symmetry in solution is reflected in the ^1H NMR spectra for complexes **1a-d,** where a single azomethine peak near ~9 ppm is observed downfield relative to two aryl peaks and two *t*-butyl signals.

The most significant structural deviations between **1a-d** are the bond lengths associated with the monodentate ligand that occupy the equatorial position left open by the saloph chelate. The $U(1)\text{-}O(5)_{THF}$ distance in complex **1a** of 2.481(3) Å is characteristic of a uranyl-THF linkage.[17] The TMPO adduct (**1b**) is bound slightly tighter (2.364(3) Å) than the THF in **1a** due to the increased affinity for phosphine oxide donor species, which is commonplace in uranyl chemistry.[18] The intraligand P=O bond

distance of 1.519(4) Å is consistent with other bound phosphine oxide species.[19] Bulky *t*-butyl substituents on the aryloxide groups directed near the substitution site restrict TMPO coordination, reflected in the U(1)-O(5)-P(1) angle of 132.0(2)º. Distances for these types of U-O bonds, consisting of neutral donors, are slightly longer than U-O_{Ar} bonds. $^{31}P\{^{1}H\}$ NMR for **1b** displays a resonance at 63.8 ppm, characteristic of a uranyl phosphine oxide chemical shift.[20] This peak shows no sign of TMPO dissociation nor exchange between coordinated TMPO and free phophine oxide at room temperature, however the ^{1}H NMR spectrum of **1a** reveals the capping THF ligand dissociates upon dissolution.

Complexes **1c** and **1d** contain monoanionic $UO_2(^{t}Bu_4$-saloph)L units due to the presence of the anionic capping ligands. Despite this fact, the salient metrical parameters within the $UO_2(^{t}Bu_4$-saloph) framework are unperturbed. The uranium-chloride length U(1)-Cl(1) of 2.718(3) Å in **1c** is comparable to other reported uranyl(VI)-chloride bond distances,[21] and the tetraphenylphosphonium countercation is situated above the $UO_2(^{t}Bu_4$-saloph)Cl adduct and displays a peak at 24.3 ppm in the $^{31}P\{^{1}H\}$ NMR spectrum that is characteristic of a phosphonium cation.[22] In complex **1d** $UO_2(^{t}Bu_4$-saloph) is capped with a hydroxide anion, and the cobaltocenium countercation resides above the anion at about 3.79 Å (**Figure 2.3**) oriented perpendicular to the mirror plane. The Co-$C_{centroid}$ average distances of 1.635 Å in the $CoCp_2^{+}$ cation are consistent with other reported cobaltocenium cations, and the Cp ring protons appear in the NMR spectrum at 5.66 ppm.[23] Complex **1d** represents an uncommon example of a uranyl unit bound with a terminal hydroxide ligand. The short bond length U-O(5) of 2.240(4) Å is comparable to other structurally characterized uranyl hydroxide species .[24] Together the

U-X bond distances follow the expected trend decreasing across the series Cl > THF > TMPO > OH. The trend in affinity to uranyl(VI) coordination is a simple consequence of the contributions of the respective donor atom charge and radius.

Table 2.2. Selected metrical parameters for complexes **1a-d**.

	1a X = THF	**1b** X = TMPO	**1c** X = Cl	**1d** X = OH
U=O (Å)	1.784(3)	1.778(5)	1.780(5)	1.797(4)
O=U=O (º)	178.98	176.26(16)	175.2(2)	175.99(17)
υ_{as} (cm^{-1})	903	907	886	865
U-O_{Ar} (Å)	2.274(3)	2.272(14)	2.279(4)	2.288(4)
O_{Ar}-U-O_{Ar} (º)	158.22(1)	159.03(13)	160.7(2)	162.96(14)
U-N_{Im} (Å)	2.535(3)	2.557(4)	2.579(4)	2.597(5)
U-L (Å)	2.481(3)	2.364(3)	2.718(3)	2.240(4)

Category 2. The synthesis of complexes **2-4** are described in the supplementary experimental details (*vide infra*) and follow the same general protocol outlined in **Scheme 2.1** with similar high yield (75-86%) isolation. In contrast, complex **5** was prepared on the benchtop via protonolysis between $\mathbf{H_4L^5}$ and uranyl acetate dihydrate, and the air stable product was obtained in moderate yield (63 %) by concentration of the reaction solution. The ligands used in category 2 contain a variety of backbones that provide flexible chelate conformations to assist in gaining control of uranyl(VI) properties by encompassing the equatorial plane. Although $\mathbf{H_2L^4}$ and $\mathbf{H_4L^5}$ are not formal Schiff bases, they are closely related and form uranyl complexes that share several common structural features. Single crystal X-ray diffraction studies performed on complexes **2** and **3** verified their molecular structures as uranyl(VI) Schiff base-phenolate

complexes. Crystal structure analysis of **4** and **5** confirmed their structures as the corresponding uranyl(VI) amino-phenolate species. Pertinent crystallographic information is listed in **Table 2.4** and complete crystallographic parameters are given in Appendix 1.

$^{t}Bu_4$-salbinapH_2 (**H_2L^2**) offers rotation of the bridged aryl backbone that has been shown to enforce the *cisoidal* coordination isomer in octahedral transition metal ion complexes,[25] yet no accounts have extended this chelate to any f-element. Upon complexation the N_2O_2 ligand compartment twists open around the UO_2^{2+} equatorial region due to rotation about the aryl bridged backbone in complex **2**. Consequently, the two U(1)-N(1) and U(1)-N(1A) contacts are puckered out of the equatorial plane by about ~12°, giving significant distortion to the pentagonal bipyramidal geometry as depicted in **Figures 2.4** and **2.5**. The aryloxide and THF donors that complete the five coordinate equator are mutually perpendicular to the axial uranyl unit, and all bond distances are within the normal ranges. Puckering has been reported in the uranyl equatorial region in crowded situations involving small bis-chelates,[26] however, incorporation of a puckered geometry within the ligand compartment constitutes, to the best of our knowledge, a new coordination mode in uranyl chemistry.

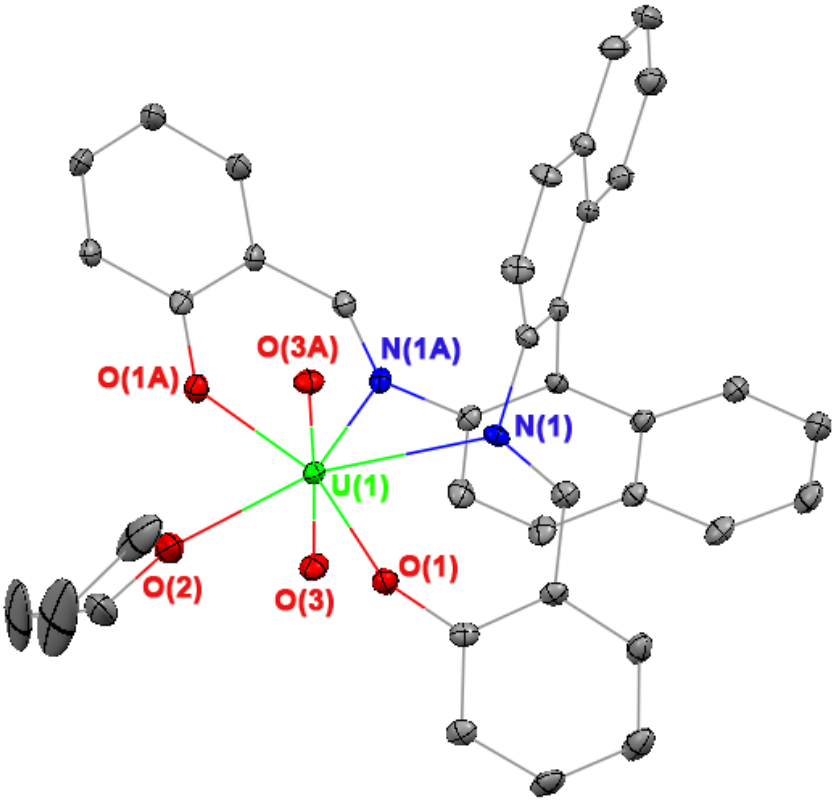

Figure 2.4. Molecular structure of UO_2(^{t}Bu$_4$-salbinap)THF (**2**) with thermal ellipsoids represented at the 50% probability level. Four *t*-butyl fragments are omitted for clarity.

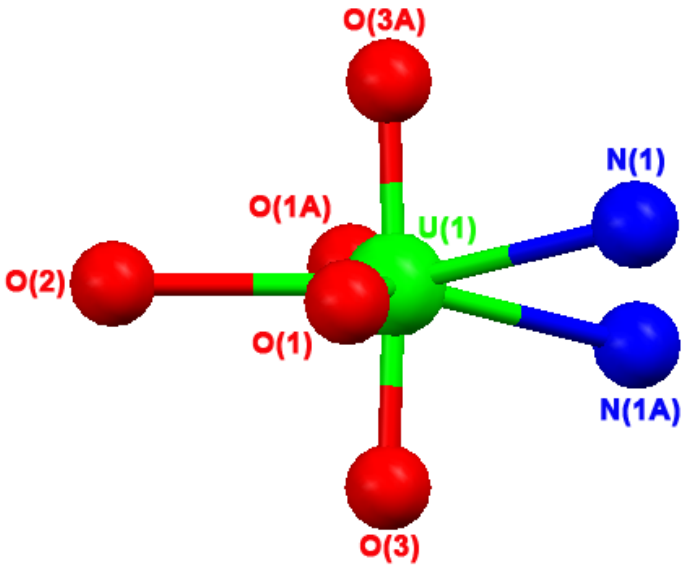

Figure 2.5. Ball-and-stick model for **2** depicting the distorted equatorial plane. All atoms except those bound directly to central uranium omitted for clarity.

Like transition metal salbinap complexes, rotation across the bi-aryl ligand backbone causes **2** to be a chiral complex with a C_2 rotation axis along the U(1)-O(2) bond. This symmetry is evidenced by the presence of a single sharp C=N stretch near 1603 cm^{-1} in the infrared spectrum. This is also in agreement with the ^1H NMR spectrum, where only one azomethine peak is observed near 9 ppm and two *t*-butyl resonances appear upfield. Only the racemic mixture could be isolated and attempts to resolve the mixture by exclusively synthesizing the *S*-enantiomer were unsuccessful since **2** is much less soluble in organic solvents than other *t*-butyl substituted uranyl-Schiff base complexes studied here. The skewed pentagonal N_2O_2 equator for complex **2** is capped by a neutral THF ligand, and since the capping position on chiral uranyl-saloph derivatives have been reported to mediate asymmetric organic catalysis and selectively recognize small molecules,[27] we attempted to stabilize various adducts of **2** by introducing TMPO, PPh_4Cl, and a variety of organic amides. In all cases the $UO_2(^tBu_4$-salbinap) framework did not withstand the donor species and resulted in dissociation of the salbinap ligand. Likewise, complex **2** slowly turned yellow in solution when removed from the drybox (whereas category 1 complexes are air stable), and this behavior is indicative of the hydrolytic decomposition of uranyl complexes to form uranyl-aqua and hydroxide species.[28] This lack of structural integrity is likely caused by strain across the C(10)-C(10A) link in the binapthyl backbone.

$^tBu_6$-saltrenH_3 (**H_3L^3**), is a potentially seven coordinate trianionic chelate designed to encapsulate a metal ion in a monocapped trigonal prismatic arrangement.[29] **H_3L^3** is composed of three phenolate donors, three imine donors, and one tertiary amine donor supported by the flexible tren backbone. In contrast to the N_2O_2 ligands discussed

thus far, the tripodal compartment is endowed with an extra side-arm and more binding functionalities than needed to satisfy uranyl(VI) equatorial complexation. Once coordinated, the chelate donors lie approximately in the plane perpendicular to the axial uranyl oxo groups giving a geometry in **3** of a slightly distorted pentagonal bipyramid (**Figure 2.6**). Average U=O (1.770(6) Å), U-O_{Ar} (2.255(6) Å), and U-N_{Im} (2.551(8) Å) bond parameters in complex **3** lie within the expected range.

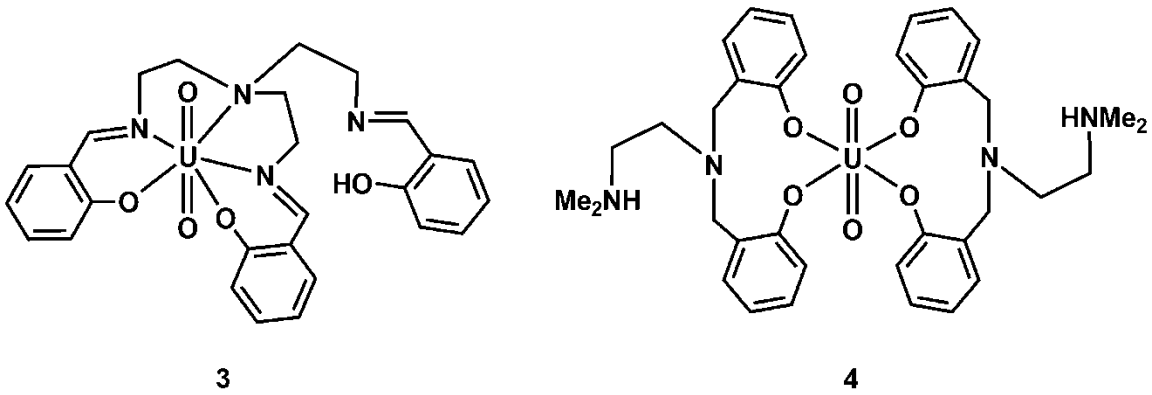

3 **4**

Figure 2.6. Complexes UO_2(^{t}Bu$_6$-saltrenH) (**3**) and UO_2(^{t}Bu$_4$-BAPH)$_2$ (**4**). Two *t*-butyl groups per salicylidene moiety not shown.

The saltren cavity serves to completely surround the UO_2^{2+} equator since the apical tertiary amine provided in the tren backbone functions as the capping unit. The U(1)-$N(2)_{Amino}$ bond distance of 2.704(8) Å is elongated in comparison to the U(1)-$N(1)_{Im}$ distance. The absence of an additional monodentate cap can further be attributed to the shortage of equatorial space left available by the acute O_{Ar}-U-O_{Ar} angle of 91.5(7)^o compared to ~160^o in complexes **1** and **2**. This lack of a unidentate capping functionality has profound effects on the electro- and photochemical properties of complex **3** in comparison to those in category 1.

The uranyl site in **3** is sterically congested from the *t*-butyl saturated phenolate sidearms, resulting in an uncoordinated pendant arm. The phenolate pendant arm dangles in close proximity to the central uranyl unit, poised to attach, however there is no room unless the robust UO_2(^{t}Bu$_6$-saltrenH) unit is disrupted. During the course of our examinations into synthetic and structural aspects of early actinide Schiff base-phenolate complexes, we often encountered multi-phenolic species that remain partially protonated in the presence of strong bases.[30]

Ligands $\mathbf{H_4L^4}$ and $\mathbf{H_2L^5}$ are both derived from the traditional ethylenediamine backbone. The amine-bis(phenolate) ligand ($\mathbf{H_2L^5}$), is a dianionic tripodal chelate when coordinated in transition metal and lanthanide complexes.[31] In the present case two of the ligands bind UO_2^{2+} equatorially through a total of four aryloxide donors, and the dimethyl substituted amino pendant arms remain uncoordinated in **4**. Complex **4** is the only species in this report that bears only four equatorial donors resulting in a six coordinate centrosymmetric square bipyramidal environment. With four aryloxides and a formal U^{VI} oxidation state assignment, the uranium sits at a dianionic center. No obvious countercation is present in the crystal lattice and therefore charge balance must be provided by intraligand protons, making **4** a zwitterionic complex. As shown in **Tables 2.2** and **2.3**, the U=O bond parameters in **4** fit within the expected range for the uranyl(VI) moiety, however the average U-O_{Ar} length of 2.26 Å is modestly elongated in comparison to aryloxide contacts observed in complexes **1**-**7**. This discrepancy is attributed to the dibasic character at the uranium center along with steric crowding around the equator. However, the U(1)-$O(1)_{Ar}$ distance of 2.2578(18) Å is slightly shorter than U(1)-$O(2)_{Ar}$ length of 2.2634(17) Å and this subtle elongation is within the range of

phenolic ligands in uranyl(VI) complexes. Two sharp peaks appear near 2 ppm in the ambient temperature NMR spectrum provide evidence that the elusive extra protons are attatched to the amino pendant arms, and possibly bifurcated between the two tertiary amines as shown in Figure 2.6.

In complex **5** the N_2O_2 donor compartment of the $\mathbf{H_4L^4}$ chelate donor is arranged around the uranyl(VI) equatorial region to form the typical pentagonal bipyramidal geometry (**Figure 2.7**) with approximate metrical parameters comparable to complexes **1**-**7**. In this case, the pentagonal equator is completed by a capping water molecule remnant from the benchtop synthesis. Discrete $UO_2(^t Bu_4\text{-salen}H_2)$ units are held together by hydrogen bonds between N-H functionalities directed near the oxide of a neighboring uranyl moiety. The poor quality of x-ray data collected on single crystals of complex **5** precluded conclusive structural assignments beyond molecular connectivity.

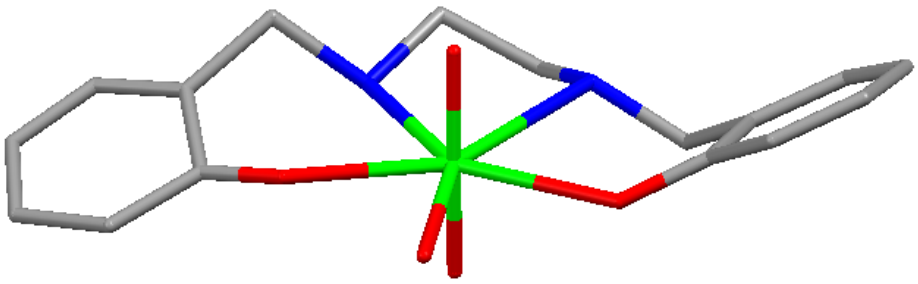

Figure 2.7. The molecular unit $UO_2(^t Bu_4\text{-}H_2\text{salen})(OH_2)$ (**5**).

Table 2.3. Selected metrical parameters for complexes **2, 3, 4, 6 and 7**.

	2 L = THF	**3** L = N_{apex}	**4** -----	**6** L = OAc^-/ NMe_2	**7** L = MeOH/ OMe^-
U=O (Å)	1.778(4)	1.791(6)	1.798(7)	1.775(2)	1.776(11)
O=U=O (º)	176.5(3)	173.3(3)	180.0(2)	176.8(2)	179.5(5)
υ_{as} (cm^{-1})	896	892	859	891	890
U-O_{Ar} (Å)	2.256(4)	2.255(6)	2.257(8)	2.229(2)	2.252(11)
O_{Ar}-U-O_{Ar} (º)	159.42(2)	91.5(2)	89.94(7)	--------	136.6(3)
U-N_{im} (Å)	2.586(4)	2.551(8)	--------	2.497(6)	2.540(11)
U-L (Å)	2.466(6)	2.704(8)	--------	2.399(4) / 2.684(4)	2.436(9) / 2.366(7)

Category 3. The final category contains two homobimetallic uranyl(VI) Schiff base-phenolate complexes prepared in methanol by protonolysis of the respective ligand with a stoichiometric amount of $UO_2(OAc)_2(H_2O)_2$ shown in reaction **Scheme 2.2**. The monoanionic Schiff base derivative ^{t}Bu$_2$-salNMe$_2$H (**HL^6**) contains the ethylenediamine backbone, which provides a crescent shaped N_2O tridentate coordination mode in complex **6**. Each uranium site adopts the expected pentagonal bipyramidal geometry and pertinent structural parameters are unexceptional. Two UO_2(^{t}Bu$_4$-salNMe$_2$) units are bridged via two acetates with U(1)-O(4)$_{carbonato}$ bond lengths (2.399(5) Å) close in value to those observed in other uranyl(VI)-carbonate structures.[32] The centrosymmetric dimer supports the dioxouranium(VI) ions at a distance of ~6 Å apart.

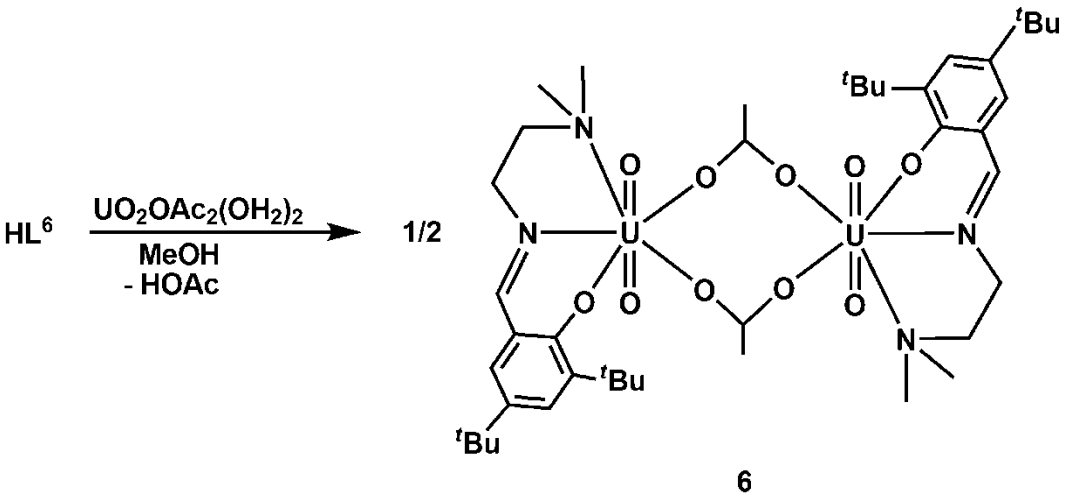

Scheme 2.2. Benchtop synthesis of the acetate bridged bimetallic complex **6**.

In contrast, $^{t}Bu_4$-salhpnH_3 (**H_3L^7**) bridges two uranyl(VI) ions within the N_2O_3 cavity in complex **7** revealed in **Figure 2.8**. The dimer is bridged by the alkoxide appendage contained in the ligand backbone and a methoxide capping linkage. The bridging U(1)-O(6,3)$_{alkoxo}$ bond distances of 2.366(7) Å are comparable to those observed in other alkoxide bridged uranyl(VI) complexes,[33] and elongated in comparison to the U(1)-O(5)$_{Ar}$ bonds of 2.252(11) Å. UO_2^{2+} units reside at identical pentagonal sites with U(1)---U(1A) related by a mirror plane, and held at a distance of 3.905 Å apart. The uranyl units are slightly tilted towards one another with U=O bonds and O=U=O angles within the expected range. As seen in UO_2($^{t}Bu_4$-saloph), this chelate bends to encompass both uranyl(VI) ions within its boat shaped cavity. The UO_2^{2+} unit is capped by a methanol, with a U(1)-O(4) distance of 2.436(9) Å equivalent to those reported for other neutral oxygen donor capping ligands encountered in this investigation, and within the range expected for uranyl(VI)-methanol adducts.[34] A number of homo- and hetero-

multimetallic uranyl(VI) Schiff base complexes have been reported,[35] though the paucity of attempts to examine metal-metal electronic communication is surprising.

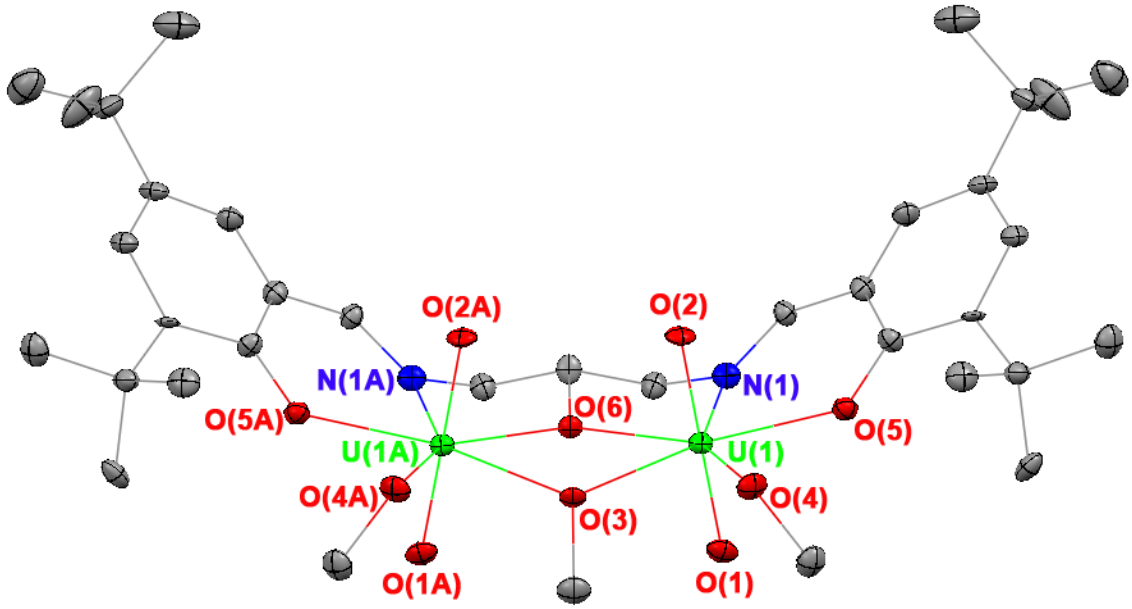

Figure 2.8. Molecular structure of (^{t}Bu$_4$-salhpn)(UO$_2$)$_2$(μ^2-OMe)(MeOH)$_2$ (**7**) with thermal ellipsoids depicted at the 50% probability level.

Table 2.4. Selected crystallographic parameters for **2-7**.

	2	**3**	**4**	**6**	**7**
formula	$C_{54}H_{58}N_2O_5U$	$C_{51}H_{76}N_4O_5U$	$C_{68}H_{110}N_4O_6U$	$C_{42}H_{68}N_4O_{10}U_2$	$C_{36}H_{58}N_2O_{10}U_2$
color	red	red	dark red-orange	dark red	red
a (Å)	23.734(3)	21.1662(3)	11.3879(17)	10.177(2)	10.1314(14)
b (Å)	19.718(3)	21.1662(3)	16.694(2)	10.694(2)	37.633(5)
c (Å)	16.228(2)	27.7896(7)	19.135(3)	13.372(3)	11.8382(16)
α (º)	90	90	90	91.036(4)	90
β (º)	133.097(2)	90	91.199(2)	96.058(4)	90
γ (º)	90	90	90	111.885(4)	90
V (Å ^{3})	5545.4(12)	12450.0(4)	3636.8(9)	1340.3(5)	4513.6(11)
Z	4	8	4	2	4
FW	1053.09	1063.22	1317.67	1265.08	1152.92
crystal system	monoclinic	tetragonal	monoclinic	triclinic	orthorhombic
space group	C*2/c*	P*4(2)/n*	P$2_1/n$	P-*1*	P*nma*
T (K)	173(2)	173(2)	173(2)	173(2)	173(2)
λ (Å)	0.71073	0.71073	0.71073	0.71073	0.71073
F(000)	2100	4336	1456	632	2196
ρ_{calc} (g•cm^{-1})	1.1872	1.134	1.276	1.707	1.695
μ (mm^{-1})	2.968	2.646	2.283	6.285	7.215
θ range (º)	1.56-27.14	1.21-27.12	1.62-27.12	1.53-27.13	1.08-27.10
total reflections	19314	89253	25666	8241	30080
unique reflections	6098	13761	8036	5701	5026
parameters	304	569	400	333	240
R_1	0.0463	0.0646	0.0274	0.0512	0.0759
wR_2 (all data)	0.1142	0.2438	0.1137	0.1376	0.2638
max, min peaks eÅ^{-3}	2.050, -2.322	1.855, -0.890	1.467, -1.104	3.717, -3.739	4.630, -8.704
GOF on F^2	1.069	1.373	0.897	1.001	1.961

Electrochemistry

Category 1. Complete cyclic voltammetric data for the full suite of complexes reported here are collected in **Table 2.5**. The electrochemical characteristics for the $U^{VI}O_2^{2+}/U^{V}O_2^{+}$ redox couple for the $UO_2(^{t}Bu_4\text{-saloph})L$ series are dependent on two factors: the formal charge on the complex and participation of the capping ligand. Neutral complexes **1a** and **1b** each display a reversible reduction wave centered near -1.5 V that spans the scan rate range of 0.50 to 2.5 V/s. These redox energetics are within the scope reported for the same process in other neutral uranyl(VI) complexes, including uranyl-saloph compounds.[6,36] The cyclic voltammogram for complex **1a** in $[Bu_4N][PF_6]$/MeCN is presented in **Figure 2.9a**. The anionic derivatives **1c** and **1d** display irreversible reduction process near -2.1 V and -2.4 V, respectively. There is not a voluminous body of work reported on the redox dynamics for structurally characterized anionic uranyl(VI) species, however these values are shifted to more negative reducing potentials than neutral derivatives due to the monoanionic ligand at the uranyl(VI)-saloph capping site.

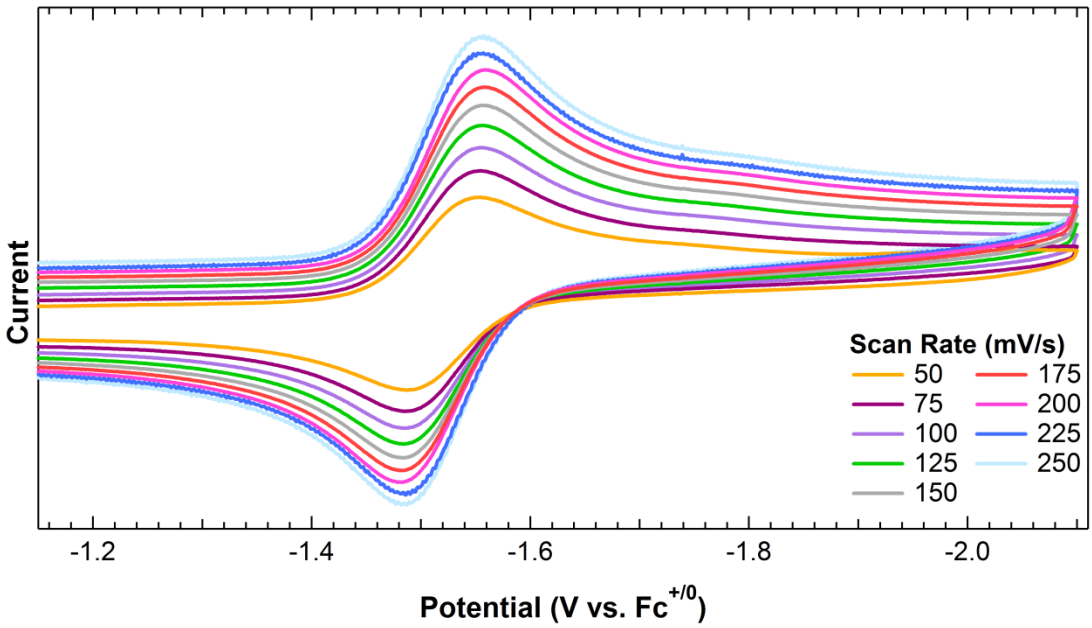

Figure 2.9a. Cyclic Voltammogram for $UO_2(^tBu_4\text{-saloph})THF$ (**1a**) in ~0.1 M $[Bu_4N][PF_6]$/MeCN solution at room temperature within a scan rate range of 50-250 mV/s.

The U^{VI} to U^{V} reduction process for **1a** is reversible in THF and MeCN, yet irreversible in methylene chloride over the entire range of scan rate trials. This solvent influence on electron transfer kinetics can be accredited to the availability and binding ability of the capping species. A mechanism has been postulated, where upon reduction the electro-generated anion $U^VO_2(saloph)^-$ has a decreased affinity for the neutral THF cap causing dissociation. Reoxidation is sluggish in non-coordinating solvents since the capping position cannot resolvate quickly, in turn causing the irreversible redox wave in methylene chloride.[6] On the other hand, when conducted in the presence of coordinating solvent (i.e., THF, MeCN) reoxidation is facile at both slow and fast scan rates due to constant occupancy of the capping site, which generates the reversible uranyl(VI/V) wave portrayed in Figure 2.9. In further support of this mechanism, voltammetric experiments conducted on **1a** in a methylene chloride/THF mixture display a redox rate dependence

on methylene chloride concentration. Illustrated in **Figure 2.9b**, redox in methylene chloride exhibits limited electron transfer behavior whereas the anodic peak slowly grows in when THF is administered in sequential dropwise steps. In contrast, for complex **1b** this same process remains reversible regardless of solvent and capping ligand effects. This difference indicates that the phosphine oxide cap in **1b** remains bound upon reduction, which is reflected by the shorter U-O_{TMPO} bond length versus U-O_{THF} in the solid state structures. One final observation about electrochemistry performed in methylene chloride is the appearance of an additional feature near -1.9 V for complexes reported in each of the three categories. This wave is not likely a second metal based reduction ($U^{V/IV}$) due to the relatively small separation from the $U^{VI}O_2^{2+}/U^{V}O_2^{+}$ process, and may be due to reduction of the salicylidene moieties.

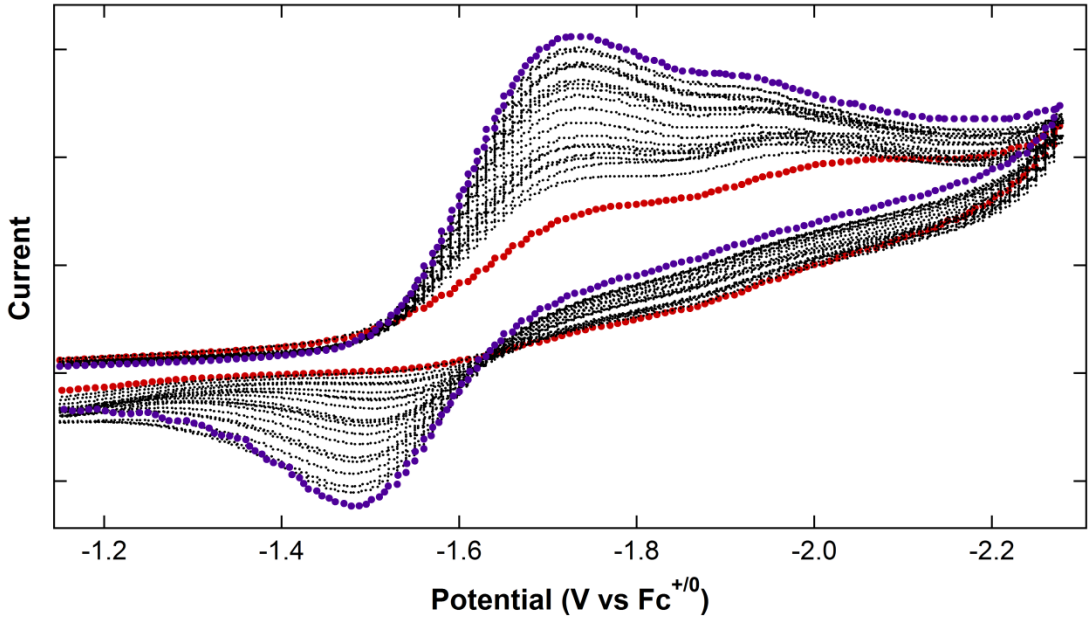

Figure 2.9b. Cyclic Voltammogram for UO_2(^{t}Bu$_4$-saloph)THF (**1a**) in 2 mL of ~0.1 M [Bu_4N][PF_6]/CH_2Cl_2 solution (red) with THF administered dropwise until a total of 3 mL solution (blue) with a constant scan rate of 250 mV/s.

Sluggish uranyl(VI/V) electron transfer kinetics for the anionic UO_2(saloph) derivatives **1c** and **1d** are attributed to the inability of the electro-generated $U^VO_2(saloph)^{2-}$ species to retain the coordination sphere. Similar to the solvent dependence observed in the reduction of the neutral uranyl-saloph species, this process for anionic derivatives is irreversible in methylene chloride, yet displays a slight quasi-reversibility in THF or MeCN as shown in **Figure 2.10** for **1d**. The limited kinetics for electron transfer in non-coordinating solvents for the full suite of UO_2(saloph) complexes in category 1 are suggestive of dissociation of the donor at the capping site upon reduction, whereas in coordinating solvent reoccupation occurs prior to reoxidation allowing for a facile redox process. Similar redox waves indicative of sluggish electron transfer behavior have been observed for the uranyl(VI)-triscarbanato anion in aqueous media at a similar potential.[37] Finally, within the available polarographic window an additional reversible reduction wave observed for **1d** at -1.3 V arises from the presence of the cobaltocenium cation (Figure 2.10), and this process interferes with the ferrocene internal standard.

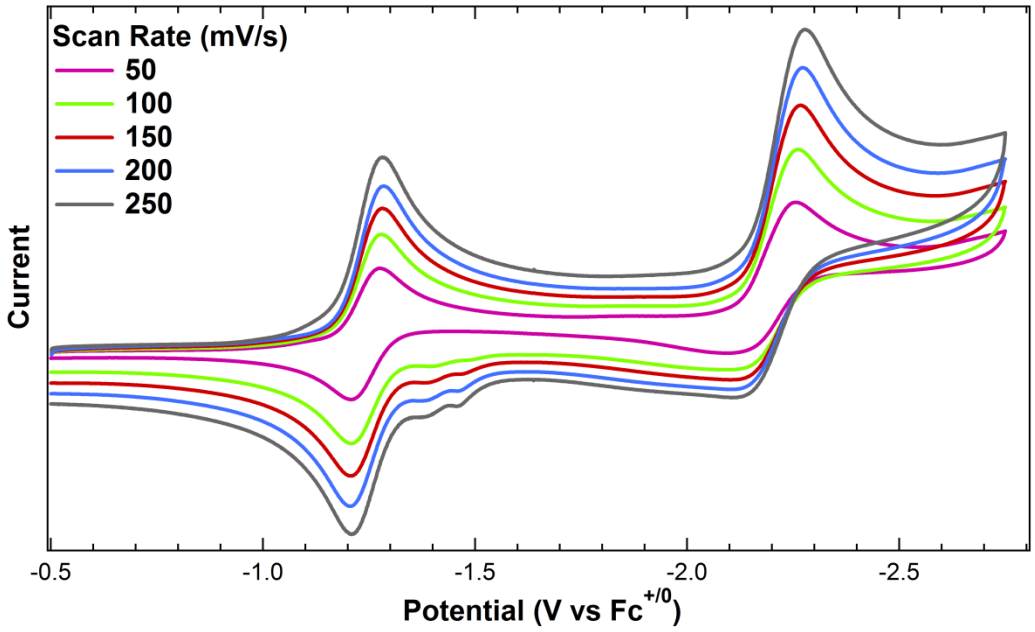

Figure 2.10. Cyclic Voltammogram for [UO_2(^{t}Bu_4-saloph)OH][$CoCp_2$] (**1d**) in ~0.1 M [*n*-Bu_4N][PF_6]/MeCN solution with a scan rate range of 50-250 mV/s. $CoCp_2$ based process (left) and uranyl process (right) are shown.

Category 2. UO_2(^{t}Bu_4-salbinap)THF **(2)** displays a reversible one electron reduction wave centered at -1.5 V versus ferrocene in MeCN and THF. The redox behavior observed for **2** is indistinguishable from that for the uranyl-saloph congener **1a**, even though **2** is not as chemically robust as **1a** as mentioned in the structural discussion. In contrast, for complex **3** the uranyl(VI) equatorial plane is completely surrounded by the chelate compartment of the saltren ligand and lacks a monodentate capping equatorial functionality. Therefore, it is not surprising that the facile nature of the $U^{VI}O_2^{2+}/U^{V}O_2^{+}$ redox couple is not influenced by capping ligand effects, except for trivial solvent dependent shifts in thermodynamic data. Complex **3** displays a reversible redox wave centered at -1.7 V versus ferrocene in THF, -1.5 V in MeCN, and -1.3 V in CH_2Cl_2. This reduction potential is on par with other neutral uranyl(VI)-Schiff base phenolate species, for example complexes **1a**, **1b**, and **2** are adequate references. The reversibility

characterized for these systems indicates the robust uranyl-Schiff base unit remains intact upon uranyl(VI) reduction with insignificant ligand reorganization effects and no sign of disproportionation.

Complexes **4** and **5** each exhibit an irreversible uranyl(VI/V) redox wave that does not experience any noticeable solvent dependence. For complex **4**, the irreversible wave appears at -2.59 V and this potential is comparable to the category 1 anionic derivatives **1c** and **1d**, however since **4** contains a dianionic uranyl site harsher energetics by ~0.5 V are required to achieve reduction. The irreversibility observed for this couple is not dependent on capping ligand effects since the equatorial environment in **4** does not include any capping ligand or solvent molecule, and can be ascribed to the dibasic character of the complex since reduction to form a trianionic uranyl(V) site likely results in decomposition via ligand dissociation. For **5** the uranyl(VI/V) process is observed at -1.72 V, and this value is on mark with redox energetics reported for neutral uranyl(VI) complexes. The sluggishness of this process cannot exclusively be attributed to capping ligand effects since there is no evident solvent dependence. However, since **5** contains a capping aqua ligand, these traits are not fully understood in comparison to **1a** but may be a consequence of the flexible ethylenediamine backbone.

Category 3. The bimetallic complexes **6** and **7** exhibit similar electrochemical behavior, exhibiting irreversible uranyl(VI/V) reductions at -1.4 V and -1.6 V, respectively. These values are on par with reduction potentials observed in other neutral uranyl complexes, and the lack of multiple redox waves are a sign that the metal ions are not in communication. In other words, the UO_2^{2+} centers are reduced simultaneously unaware of the electroactivity of the other, presumably due to the distance between the

uranyl units in adjoined compartments. **6** does not contain a capping monodentate ligand whereas **7** possesses a single coordinated methanol cap per uranyl(VI) ion and a methoxide bridge, though neither complex portrays marked solvent dependent behavior indicative of capping ligand participation.

Table 2.5. Summary of redox potential data for uranyl(VI) Schiff base-phenolate complexes **1-7** in ~0.1 M $[Bu_4N][PF_6]$/MeCN, THF, or CH_2Cl_2. $E_{1/2}$ values are referenced to $Fc^{+/0}$ and were determined from the average of the cathodic and anodic peaks. R = reversible; QR = *quasi*-reversible; I = irreversible.

$U^{VI}O_2^{2+}$ Complexes	$E_{1/2}$ ($U^{VI}O_2^{+2}/U^{V}O_2^{+}$) (V)		
	MeCN	THF	CH_2Cl_2
1a	-1.62 R	-1.55 QR	-1.78 IR
1b	-1.53 R	-1.71 QR	-1.77 QR
1c	-2.32 IR	----------	----------
1d	-2.31 IR	----------	----------
2	-1.62 R	-1.55 QR	-1.78 IR
3	-1.52 R	-1.73 R	-1.77 QR
4	-2.59 IR	----------	----------
5	-1.72 IR	----------	----------
6	-1.41 IR	----------	----------
7	-1.56 IR	----------	----------

Photochemistry

Category 1. The electronic absorption spectra for ligands $\mathbf{H_2L^1}$-$\mathbf{H_2L^7}$ and their respective uranyl(VI) complexes **1-7** display intense broad absorption features that span the UV and high energy portion of the visible spectrum. These transitions are responsible for the hallmark brilliant red and orange colors for species in all three categories. A representative absorption spectrum shown in **Figure 2.11a** depicts the absorption for $\mathbf{H_2L^1}$ versus the corresponding uranyl(VI) complex **1a** in THF solution. The complex

contains two intense intraligand $\pi \rightarrow \pi^*$ transitions for the phenylene and salicylidene moieties that coincide with the corresponding transitions for the free ligands at 295 and 423 nm. A spectral band at 368 nm falls in between the intraligand peaks and has been attributed to charge transfer from aryloxide to uranyl(VI).[11a] The more faint oxo-uranium ligand-to-metal-charge-transfer (LMCT) commonly observed for uranyl complexes in the visible region is presumably masked by intense $UO_2(^tBu_4$-saloph) absorptions.[38] The UV-visible electronic absorption characteristics for complex **1a** are consistent among category 1 derivatives regardless of solvent.

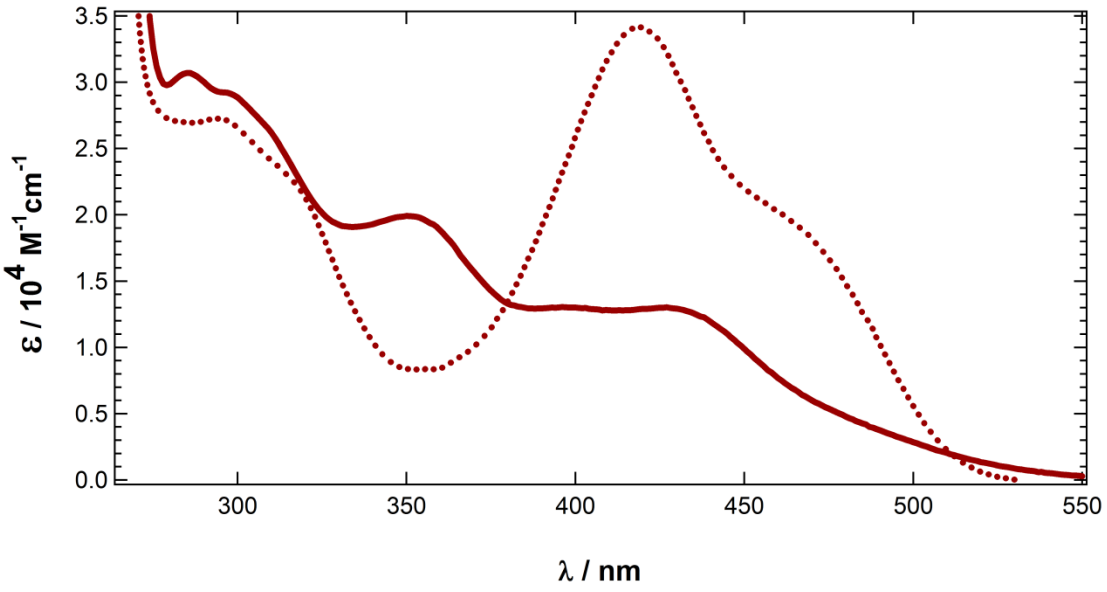

Figure 2.11a. UV-visible absorption spectra for $\mathbf{H_2L^1}$ (dashed) vs. **1a** (solid) in THF.

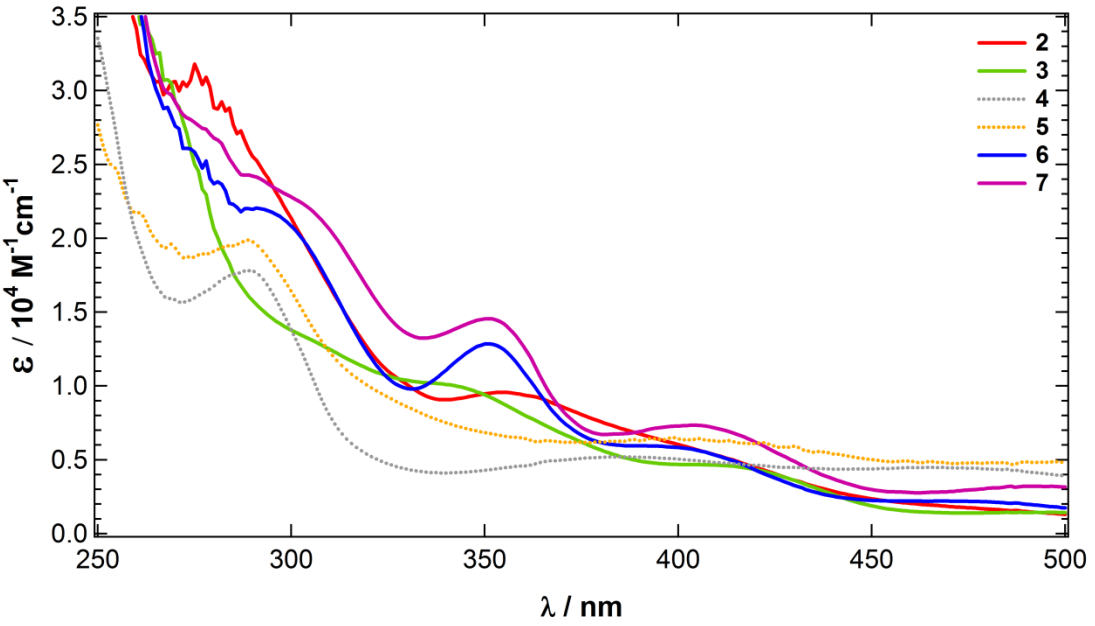

Figure 2.11b. UV-visible absorption spectra for uranyl(VI) Schiff base-phenolate complexes (solid) and amino-phenolate complexes (dashed).

Luminescent properties for complex **1a** are dominated by the saloph ligand since no fluorescence features for uranyl(VI) are detectable. It has been postulated that uranyl(VI) emission is quenched by localized charge transfer from the aryloxide attachments,[39] however this trend does not hold true for simple homoleptic uranyl aryloxide species.[44] A number of ligands have been utilized to markedly reduce the fluorescence timescale (ms or μs) common for uranyl ion complexes, however only a few ligands are capable of absolutely extinguishing uranyl emission and these cases are often accompanied by photolytic activation.[40] A solution of **1a** in toluene (or methylene chloride) displays an excitation/emission profile similar to that of the free ligand.[10a,41] As show in **Figure 2.12**, excitation at 295 nm is followed by a large Stokes shift (~9100 cm^{-1}) and a relatively intense emission at 510 nm, which is slightly red shifted with respect to $\mathbf{H_2L^1}$. In contrast, the luminescent spectral features in THF or MeCN solution

lack the large Stokes shift, and excitation at 295 nm is immediately followed by an emission at 356 nm. These corresponding excitation and emission spectra for **1a** in THF and toluene are portrayed in Figure 2.12.

Large Stokes shifts between excitation and emission in Schiff base-phenolate compounds has been attributed to the photochromic keto-enol type tautomerism.[41] The tendency to undergo a photoexcited state isomerism is caused by the low energy barrier between keto and enol tautomers. In order to emit after excitation, the structure must first convert back into the ground configuration. The solvent based phenomenon for **1a** in THF versus toluene solution in Figure 2.12 is caused by the ability of the capping ligand to block any ligand based photochromic rearrangement. Excitation via $\pi \rightarrow \pi^*$ transitions within the salicylidene molecular orbitals induce an internal repulsion along the uranyl-aryloxide connection. A possible mechanism for the structural alteration, shown in **Scheme 2.3**, might be initiated by cleavage of the capping THF ligand upon excitation. In toluene, the Schiff base is allowed to reorganize around the uranyl equatorial region following dissociation. In THF the photo-induced isomerism is obstructed by steric interactions associated with constant solvation at the equatorial site.

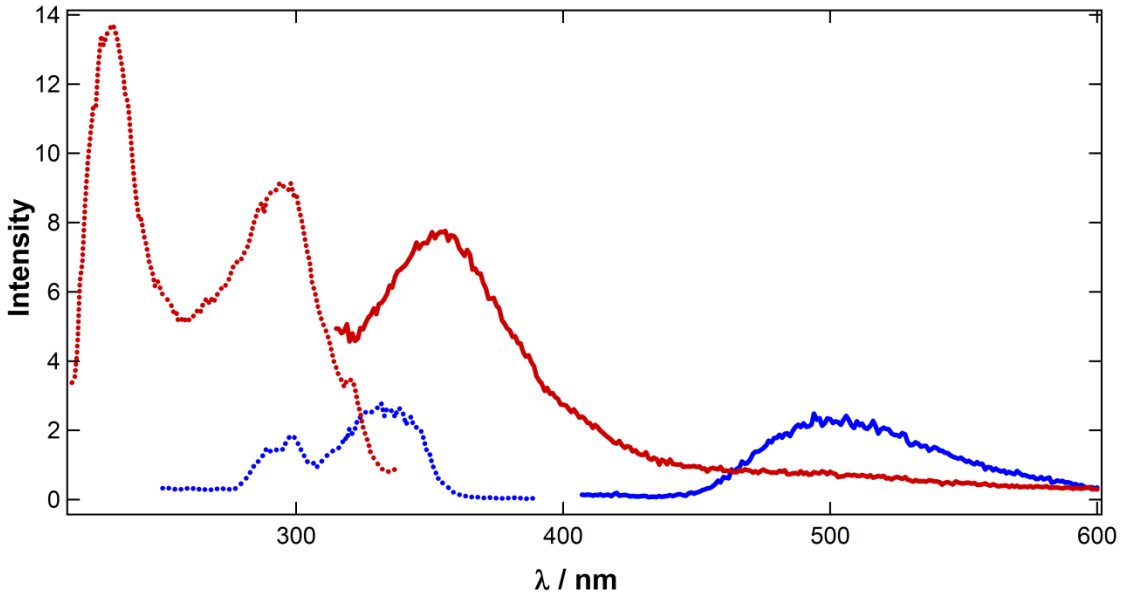

Figure 2.12. Excitation (dashed) and emission (solid) spectra for **1a** in toluene (blue) versus THF (red).

The broad emission at 356 nm for complex **1a** in THF coincides with the saloph → UO_2 charge transfer band in the absorption spectrum. Therefore, continuous occupancy of the capping equatorial site by THF prevents photochromism and redirects the luminescence away from an exclusive uranyl(VI) or ligand based process. Instead excitation energy is transferred to a local emission pathway that involves the entire UO_2(^{t}Bu$_4$-saloph) framework.[42] Analogous fluorescence near 356 nm is observed for category 1 derivatives **1b**-**1d** regardless of solvent conditions. In these cases the monodentate capping ligands (TMPO, Cl, OH) are securely bound and do not dissociate upon exposure to UV radiation to allow any structural transformation. Accordingly, **1b**-**d** do not exhibit solvent influenced fluorescence properties and the luminescence spectra in THF and methylene chloride solutions for category 1 complexes are close in appearance. The luminescent lifetime for this process is much shorter than typical uranyl(VI)

fluorescence, and the measured lifetime of ~ 3 ns for **1a** in THF or toluene lies closer in value to reported lifetimes for salicylideneiminato fluorescence.[43]

Categories 2 & 3. Absorption spectra for complexes **2-7** are similar to those observed for the category **1** series (**Figure 2.11b**), however when compared to their respective ligands, any intraligand and aryloxide → uranyl(VI) charge transfer bands cannot be deconvoluted as clearly as for **1**. The photophysical trends inherent to complexes in category 1 are conserved only for complexes **2** and **3** in the remainder of the discussion. Luminescence for **2** (**Figure 2.13**) is analogous to **1**, where a Stokes shift of ~7900 cm^{-1} is observed for $\mathbf{H_2L^2}$ and for complex **2** in non-coordinating solvent (i.e., toluene or methylene chloride). When fluorescence measurements are conducted on **2** in THF or MeCN, however, the capping site remains solvated, blocking the photochromism observed in toluene, and a salbinap → uranyl energy transfer process takes place resulting in emission at 409 nm from excitation at 360 nm. Recall from the structural and electrochemical discussions that **3** does not contain a monodentate capping ligand functionality since the Schiff base chelate serves to completely surround the uranyl(VI) equatorial region. Therefore, luminescence is not dependent on the presence of coordinating solvent to interfere in a photo-induced structural rearrangement. Accordingly, the excitation and emission spectrum contains no Stokes shift regardless of the solvent conditions. For **3** a broad emission band is observed at 477 nm following excitation at 396 nm depicted in **Figure 2.14**. The free ligand ($\mathbf{H_3L^3}$) on the other hand, displays emissive properties indicative of Schiff base-phenolate photochromism with excitation at 379 nm and emission at 538 nm separated by a Stokes shift of ~7900 cm^{-1}, which is comparable to the Stokes shift separations observed for $\mathbf{H_2L^1}$, **1a**, $\mathbf{H_2L^2}$, and **2**.

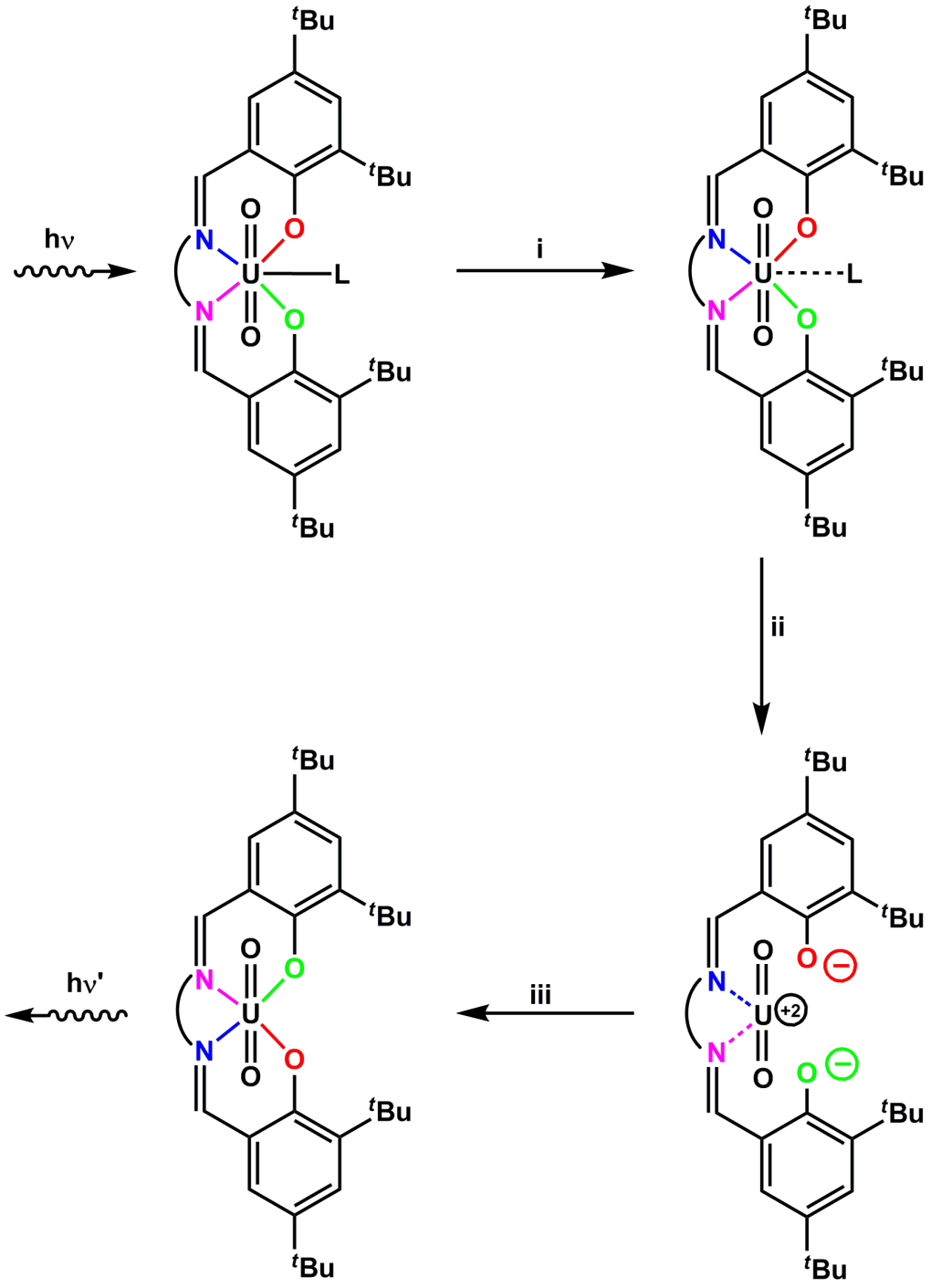

Scheme 2.3. Color-coded mechanism monitoring the tentative photochromic rearrangement for uranyl(VI) Schiff base-phenolate complexes. The steps following photoexcitation include, i) dissociation of the capping ligand, ii) Schiff base aryloxide donors dissociate from UO_2^{2+}, and iii) reorganization around the equatorial plane and recoordinate. Following this three step process, the complex displays a red shifted luminescence (hv').

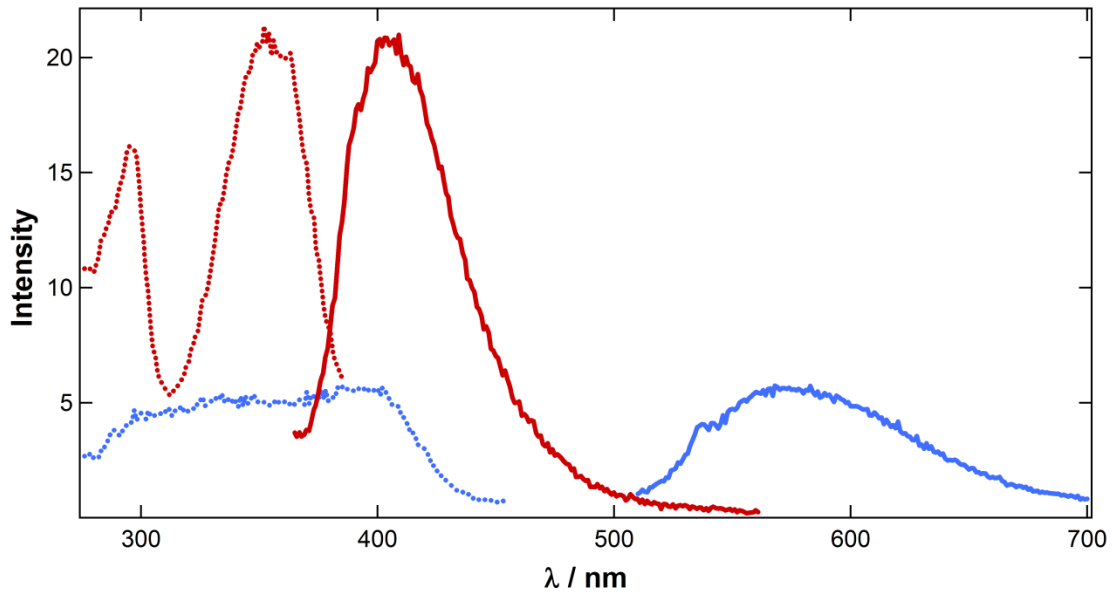

Figure 2.13. Excitation (dashed) and emission (solid) spectra for complex **2** in toluene (blue) versus THF (red).

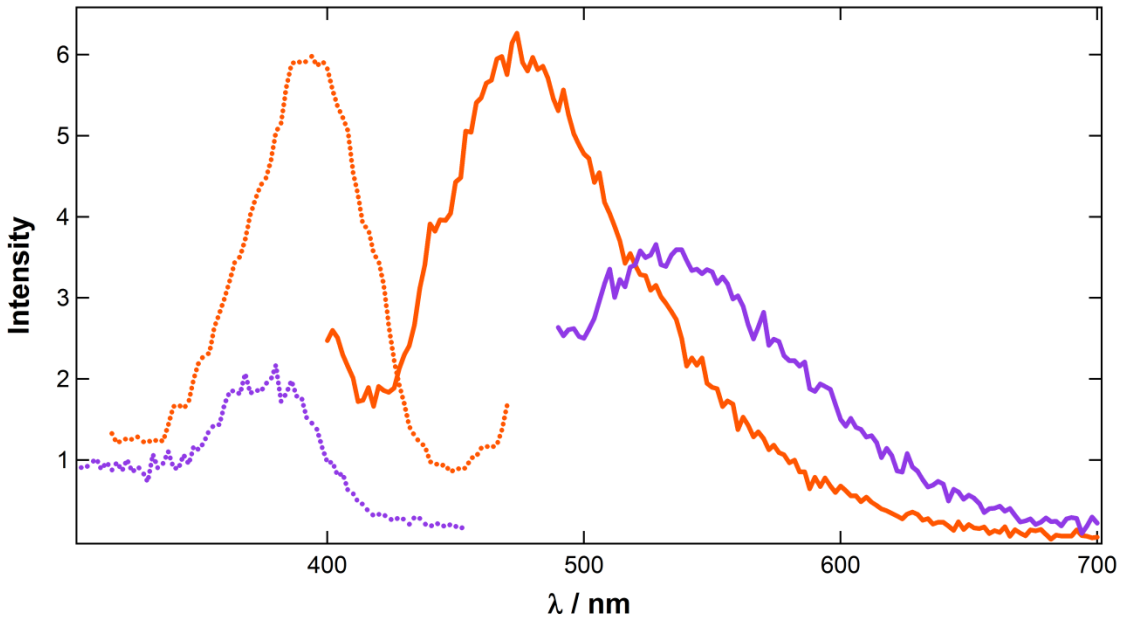

Figure 2.14. Excitation (dashed) and emission (solid) spectra for ligand $\mathbf{H_3L^3}$ (purple) versus complex **3** in toluene or THF (orange).

The intense broad width emission bands at 409 nm for **2** and 477 nm for **3** vaguely coincide with a faint peak in the absorption spectra of each that might be attributed to salbinap → uranyl and saltren → uranyl charge transfer, respectively. Thus luminescence likely arises from energy transfer character much like the description for **1** above. Unfortunately this connection is not evident as in category 1 since the absorption spectra for ligands $\mathbf{H_2L^2}$ and $\mathbf{H_3L^3}$ and complexes **2** and **3** display more peaks than expected. The luminescence spectra for **1-3** provide one additional interesting result. Illustrated in Figures 2.12-2.14, the energy transfer processes for the uranyl-Schiff base phenolate complexes is considerably more intense than the ligand based photochromism for each and this could be a measure of energy loss during photochromic structural rearrangement. Notably, for complexes **2** and **3** luminescence appears at lower energy than for **1**. It bears mention that this energy transfer luminescence has not previously been observed in simple uranyl-aryloxide species, which exhibit identifiable uranyl(VI) based electronic absorption and emission processes.[44]

The remainder of the complexes in these final two categories display ligand based luminescent characteristics indicative of a photochromic structural rearrangement regardless of solvent and capping ligand influences, varied chelate design, or multiple uranyl ions present. These traits are not yet fully understood, and a more detailed treatment of the electronic absorption and excitation/emission behavior is required to flesh out the systematic factors that account for this inconsistency.

2.3 Photosynthetic production of 1d

During the course of investigating the nature of the $U^{VI}O_2^{2+}/U^{V}O_2^{+}$ redox couple it was realized that complexes **1a, 1b, 2,** and **3** would respond favorably to one electron chemical reductants. An extensive review on organometallic redox reagents exists,[45] though the scope is limited here by the relatively large reduction potential (-1.6 V) for neutral uranyl(VI) Schiff base-phenolate complexes. Cobaltocene (-1.3 V) or permethylated cobaltocene (-1.6 V) are applicable, and offer the cobaltocenium countercation for appropriate size stabilization of the resultant $U^{V}O_2(saloph)^{-}$. However, neither provides ample redox energetics suited to sustain chemical reduction. A similar reduction methodology using $CoCp_2$ was performed to successfully generate the first $Mo^{V}O_2^{+}$ complex from $Mo^{VI}O_2^{2+}$.[46]

Exposure to an intense UV light source is required to drive the photochemical conversion of complex **1a** with cobaltocene in THF into **1d** as shown in **Scheme 2.4**. The steps in the reaction involve oxidation of $CoCp_2$ by the excited state of **1a** and reduction of the coordinated THF ligand. Together these processes are responsible for the formation of the cobaltocenium cation and the hydroxide capping anion in **1d**, and this formulation is consistent with the uranium hexavalent oxidation state assignment. It should be noted that the uranyl(V)-saloph species is not capable of activating THF since electrochemical experiments conducted on **1a** in THF display reversible redox waves, however, activation of coordinated THF has been observed in uranium chemistry.[47] Adventitious moisture may seem the likely source of the hydroxide ligand, however **1d** is reproducibly isolated in high yield, and when trace water is added the reaction mixture decomposes readily. When the reaction in Scheme 2.4 is carried out in THF-d_8 the

presence of a singlet at 2.49 ppm in the ^{2}H NMR spectrum of the product confirms that reductive activation of THF produces the hydroxide cap in **1d**. The slower reaction rate in deuterated versus non-deuterated THF is indicative of a kinetic isotope effect, but this rate dependence has not been quantified. GC-MS headspace gas analysis failed to identify any THF activation products, most likely small hydrocarbons fragments, even when the reaction was scaled to half-gram.

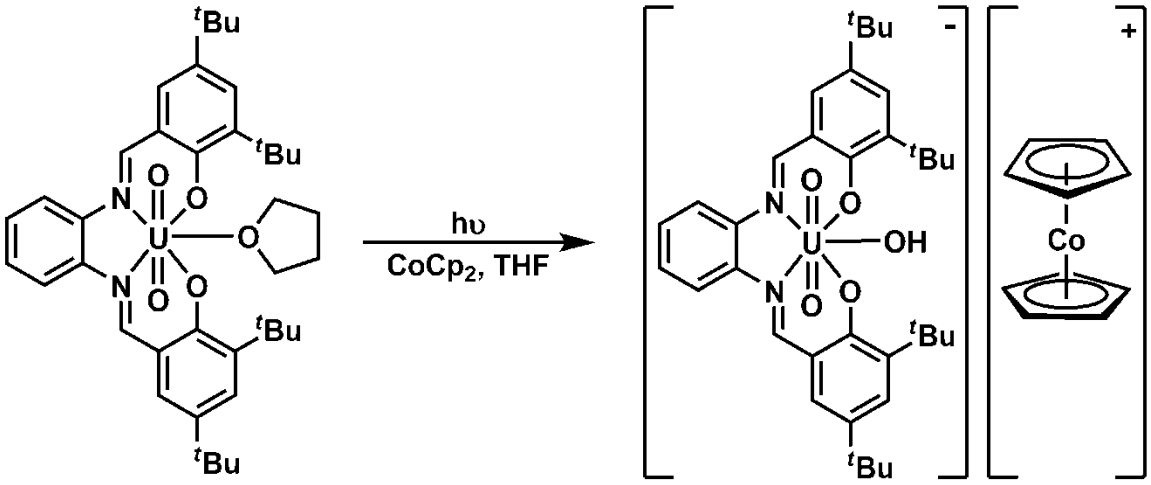

1a **1d**

Scheme 2.4. Photosynthesis of **1d**.

Photoexcitation of **1a** in THF with $CoCp_2$ produces **1d** in good yield (69 %) for a photosynthetic process, yet no reaction takes place in toluene. Likewise no reaction occurs for any other category 1 derivative with cobaltocene regardless of solvent conditions. Clarification for these differences is explained by the two-fold activity of the capping THF functionality to both control the photoactivation pathway and to undergo a one electron reduction process. Photooxidation of cobaltocene is only achieved by **1a** in

THF, and it is clear that the $UO_2(^tBu_4$-saloph) excited state (which in the absence of $CoCp_2$ luminesces near 365 nm) is responsible for this transformation.[48] Although **1b-1d** display analogous capping ligand directed photoexcited behavior as **1a** in THF, these derivatives do not photolyze $CoCp_2$ since the fate of the single electron transfer is reliant on the reduction of THF, which is absent in these derivatives.

A variety photochemical reactions for uranyl(VI) complexes have been attributed to the long lived and highly oxidizing fluorescent excited state.[49] However, it is clear that this process is quenched in **1** and excitation energy is channeled to the aryloxide-uranyl-THF arrangement, which produces a higher energy excited state than that observed in uranyl(VI) photochemistry. It is well established that photochemical reduction reactions are accompanied by reorganization of the uranyl(VI) coordination environment, however in this case the robust $UO_2(^tBu_4$-saloph) framework stays intact. There are only a few examples where advances have been made to secure a large portion of uranyl(VI) equatorial ligation to remain fixed during photosynthesis.[49] The photodeoxygenation of ethereal species has been reported for uranyl systems,[50] and a similar mechanism may be in place to activate THF in this instance guided by coordination at the capping equatorial position. This realization is supported by the fact that none of the derivatives **1b-1d**, **2**, or **3** react significantly with $CoCp_2$ in THF, even though they display analogous luminescent properties. Additional information was obtained from photochemical investigations on **1-7** conducted in methanol. Given that the large majority of uranyl complexes in our lab react significantly with methanol and ethers when illuminated by an intense UV source, it is surprising that no reaction proceeds

under these conditions for any of the complexes reported here. This is presumably due to the quenched uranyl(VI) excited state, and the robust uranyl-Schiff base framework.

2.4 Conclusion

The uranyl(VI) Schiff base-phenolate complexes and related derivatives presented here are structurally related. In each case the U^{VI} center is surrounded in a pentagonal bipyramidal geometry, with the exception of the square bipyramidal complex **4**. The chelates $\mathbf{H_2L^1}$-$\mathbf{H_2L^7}$ bind in the equatorial plane through phenolate and imino/amino donors whereas the O=U=O unit occupies the axial position, and all bond length and angle parameters are all within the expected ranges. In category 1 the presence of the capping ligand that saturates the site left available by the saloph chelate has a dramatic influence on $U^{VI}O_2^{2+}/U^{V}O_2^{+}$ redox energetics and kinetics. A similar process also controls the photoexcited state behavior, where vacancy at the capping site allows for a large Stokes shift reminiscent of the photochromism reminiscent of the free ligand. A tentative mechanism for this process is postulated, where excitation induces chelate dissociation followed by recombination and emission. This isomerism is effectively blocked by constant sovlation of the capping site (**1a**) and when the capping ligand is securely bound (**1b-1d**). This competitive photolytic pathway is responsible for the generation of complex **1d** in good isolated yield, where inadvertent redox activation of the capping THF ligand results in the formation of the UO_2(saloph)-hydroxide adduct confirmed by deuterium labeling studies.

Category 2 complexes are constructed from an assortment of more flexible ligand backbones than the *o*-phenylenediimine backbone in category 1. The salbinap, saltren,

and BAP ligands are not specifically designed for plannar equatorial coordination around uranyl(VI), however in these cases the essentially linear O=U=O moiety accomodates each within the equatorial plane. For complex **2**, the flexible binapthylene backbone creates a significantly puckered equatorial region that has not previously been incorporated into a chelate cavity for uranyl(VI) chemistry. For complex **3** a pendant arm of the saltren ligand remains uncoordinated, whereas for the square bipyramidal complex **4**, each of the two BAP ligands leaves a dimethylamino pendant sidearm. The electrochemical energetics and kinetics for **2** and **3** follow the expected trends. The uranyl(VI/V) redox couple for **2** displays the same solvent dependence as that observed for **1a,** whereas for **3** the capping functionality is provided by the apical nitrogen of the tren backbone and results in a facile redox process regardless of solvent conditions. Within this category, complexes **2** and **3** display solvatochromatic fluorescent properties similar to **1a**, where complex **3** does not exhibit any Stokes shifted emission regardless of solvent effects. In contrast, for complexes **4**, **5** and the bimetallic derivatives **6** and **7** the uranyl(VI/V) redox couple is sluggish on the voltammetric timescale, and the bimetallics show no sign of any communication between the metal ions. For these species, luminescence is dominated by the respective ligand, indicative of a photochromic isomerism regardless of varied capping ligand, solvent, and chelate backbone conditions.

The lack of photochemical reactivity for **1**-**7** further substantiates the supposition that uranyl-Schiff base complexes have the ability to remain intact during photolysis even though Schiff bases are prone to undergo a photochromic redistribution both on their own and when coordinated around uranyl(VI). This observation arises from quenching of a predominant uranyl(VI) photoactive excited state, and will lead to the use of more

aggressive reducing media to formulate a constructive hypothesis. One final observation on the structural data, the IR absorptions for the asymmetric $O=U=O^{2+}$ stretch for the anionic derivative seen here (**1c**, **1d**, and **4**) appear at significantly lower energy (865-880 cm^{-1}) than the neutral derivatives (~900 cm^{-1}), is indicative of attenuated central oxide bonds in the former. However, no deviation is observed in the solid state structural metrical parameters and this trend is not conserved for all reported anionic uranyl(VI) complexes, and is a common anomaly among actinyl An=O bonds.

Acknowledgment. The author thanks Drs. S. Tucker, D. Bassil, and L. Morgan (University of Missouri-Columbia) for collaboration on fluorescent lifetime measurements. This research was performed at the University of Missouri-Columbia Chemistry Department under the auspices of the ACS Petroleum Research Fund and the University of Missouri Research Board.

Supporting Information Available: Crystallographic information in Appendix 1 on CD-ROM.

2.5 Experimental

General Considerations

Unless otherwise stated all laboratory manipulations were carried under an inert atmosphere of dry, oxygen-free dinitrogen in a MBraun Labmaster 130 drybox equipped with a MB 20G purification system or in standard Schlenk-type glassware on a dual vacuum/dinitrogen line. Depleted uranium (^{238}U) is a weak α-emitter (4.197 MeV) with a half-life of 4.47×10^9 y, and should be handled in fume hoods or in a drybox contained in

an area regularly monitored for radioactivite isotope management. Complexes **5-7** were prepared on the bench top in undried organic solvents. Toluene, diethyl ether and hexanes were dried by passage through an MBraun purification system (MB-SPS) consisting of consecutive passage thru one column of activated alumina followed by one column of activated copper catalyst (toluene, hexanes), or two columns of alumina (diethyl ether). Tetrahydrofuran (THF) was distilled over sodium and benzophenone. Acetonitrile (MeCN) was dried over CaH_2 and methylene chloride was distilled from anhydrous $CaCl_3$. Dry solvents were tested for moisture with Zn/titanocene dichloride prior to use. Glassware was dried at 150 ºC overnight and subsequently exposed to vacuum for 12 h. Tris(aminoethyl)amine (tren) was distilled, Celite® was heated to 150 °C and dried under vacuum overnight, and NaH was washed with hexanes. All other reagents were purchased from reputable commercial sources and used without further purification. $[UO_2Cl_2(THF)_2]_2$ and ligands $\mathbf{H_2L^1}$-$\mathbf{H_3L^7}$ were prepared in accordance with previously documented accounts.[51,52] The formal and common ligand nomenclature used herein and hitherto: ^{t}Bu$_4$-H$_2$saloph ($\mathbf{H_2L^1}$) = N,N'-bis(3,5-di-*t*-butylsalicylideneiminato)-*o*-phenylene; ^{t}Bu$_4$-H$_2$salbinap ($\mathbf{H_2L^2}$) = N,N'-bis(3,5-di-*t*-butylsalicylideneiminato)-1,1'-binapthyl; ^{t}Bu$_6$-H$_3$saltren ($\mathbf{H_3L^3}$) = N,N',N''-tris((3,5-di-*t*-butylsalicylideneiminato)ethyl)amine; ^{t}Bu$_4$-H$_2$BAP ($\mathbf{H_2L^4}$) = N'N'-bis(3,5-di-*t*-butylsalicylidene)-N,N-dimethylethylenediamine; ^{t}Bu$_4$-H$_4$salen ($\mathbf{H_4L^5}$) = N,N'-bis(3,5-di-*t*-butylsalicylidene)ethylenediamine; ^{t}Bu$_4$-HsalNMe$_2$ ($\mathbf{HL^6}$) = N-(3,5-di-*t*-butylsalicylideneiminato)-N',N'-dimethylethyleneamine; ^{t}Bu$_4$-H$_3$salhpn ($\mathbf{H_3L^7}$) = N,N'-bis(3,5-di-*t*-butylsalicylideneiminato)-2-propanol. To extend these formal nomenclature

to the complexes **1**-**5**, add a dioxouranium(VI), and for the bimetallics **6** and **7** use bis(dioxouranium(VI))

Instrumentation and Sample Protocols

^{1}H NMR (referenced to protio impurity in deuterated solvent) and ^{31}P NMR spectra (referenced to 85% H_3PO_4) were recorded on Bruker AMX-250, -300, or -500MHz spectrometers. ^{2}H spectra (referenced to THF-d_8) were recorded at 46.05 MHz on the same instrument. Radioactive samples were handled in sealed Teflon inserts. Chemicals shifts are reported in ppm and all coupling constants are reported in hertz unless otherwise noted. Infrared spectra were obtained as nujol mulls in a mixture of type NVH and type B immersion oil pressed between KBr plates on a Thermo Nicolet Nexus 670 FT-IR spectrometer. Elemental analysis was performed by Desert Analytics (Tuscon, Az).

Cyclic voltammetric studies were performed with a Bioanalytic Systems Epsilon EC-2000-Xp C3 model potentiostat/galvanostat under computer control using BAS software. Samples were run in the drybox in 0.1 M [*n*-Bu_4][PF_6] solution at a ~3 mm platinum or graphite working electrode with a Ag/Ag^+ quasi-reference electrode (0.01 M $AgNO_3$) contained in a Teflon-sealed Vycor bridge and a Pt wire auxiliary electrode. Measured potentials were calibrated using the ferrocene/ferrocenium couple ($E_{1/2}$ ~ 0.55 V vs SCE).[53] Compensation for solvent resistance was not employed, but did not display any noticeable differences in potential or current values.

Photochemical reactions were conducted with an Ace Glass reactor assembly outfitted with a 450 W Hg vapor lamp in a quartz immersion well contained within a

photochemical safety cabinet, and samples were contained in scintillation vials with a stir bar, and parafilm was used to exclude moisture. UV-visible spectra were taken in solution on an HP 8453 with diode-array deuterium (UV) and tungsten (Vis) lamps and Chemstation analysis software. Luminescence data was obtained on a Varian Fluorescence Fluorometer with quartz solution cuvets using the Cary Eclipse Scan Application. The excitation source was a 15 W Xenon arc lamp pulsed at 80 Hz. The excitation and emission monochromators were set to a step size of 10 and 2 nm, respectively, with a bandpass of 5 nm, collecting from 250 – 600 and 300 – 700 nm, respectively. Fluorescence lifetimes were collected in the frequency domain, on a SLM 48000 DSCF/MHF spectrofluorometer. The excitation source was a Coherent Innova 307C argon ion laser operating at 351 nm and 260 mW. A base frequency of 4.0 MHz and a cross-correlation frequency of 7.000 Hz were used in all measurements. Ten pairs of sample/reference measurements were collected in triplicate for each sample, and each measurement contained 50 internal averages. POPOP (1,4-bis[5-phenyl-2-oxazolyl]benzene) in ethanol was used as the lifetime reference (τ_{ref} = 1.4 ns), and a 370 long-pass/610 short-pass filter combination defined the emission window. The lifetimes and fractional intensities were obtained from the phase and modulation data using the maximum entropy method (MEM). The three replicate phase and modulation data sets collected for each sample were analyzed both individually and as a combined file. The lifetime window consisted of 500 discrete, equally spaced cells from 0.01 to 10 ns. In all photophysical measurements, samples and solvents were run separately to ensure the observed spectra were attributable to complexes and not solvent or solvent impurities. All

electronic spectrophotometry measurements were obtained at ambient temperature and referenced to the respective solvent.

Single crystals, as determined by polarized optical microscopy, were immersed in degassed hydrocarbon oil and mounted on a thin glass fiber using silicon grease. Full hemispheres of data were then collected at -100 ^{o}C on a Bruker SMART system equipped with a CCD Area Detector system using ω scan technique with K_{α} radiation from molybdenum (λ = 0.7073 Å) from a graphite monochromator. Intensities were corrected for Lorentz and polarization effects, equivalent reflections were merged, and absorption corrections were applied using the multi-scan application. Structures were solved using direct methods with the SHELX package and then refined using a full least squares treatment of F^2.[54] All non-hydrogen atoms were refined with anisotropic thermal parameters. Hydrogen atoms were placed at the calculated positions and included in refinement using a riding model, with fixed isotropic *U*. The final difference map contained no features of chemical significance. SQUEEZE was applied to **1d** on anomalous electron density peaks to allow for complete structural refinement. Disordered *t*-butyl substituents were modeled for disorder, and various solvents of crystallization are excluded from the discussion. Complete crystallographic data collection and refinement details are provided as supplementary information in Appendix 1.

Synthetic Details

Synthesis of UO_2(^{t}Bu_4-saloph)(THF) (1a): To a solution of **H_2L^1** (250 mg, 0.462 mmol) in 100 mL THF was added an excess of sodium hydride. The orange solution was allowed to stir overnight, after which it was filtered to remove unreacted sodium hydride.

The filtrate was added to a solution of $[UO_2Cl_2(THF)_2]_2$ (224.6 mg, 0.231 mmol) in THF, and turned red immediately. After stirring for 8 h the solvent was removed under vacuum and the remaining red crude product was dissolved in toluene and filtered thru Celite. X-ray quality single crystals of the dark red complex were grown upon slow evaporation of a concentrated toluene solution (156.7 mg, 0.179 mmol, 77%). ^{1}H NMR δ (THF-*d*$_8$) 9.54 (s, 2H, N=C*H*), 7.79 (d, 2H, Ar*H*), 7.59 (dd, 2H, Ar*H*), 7.57 (d, 2H, Ar*H*), 7.39 (dd, 2H, Ar*H*), 3.92 (br, 4H, THF) 1.85 (br, 2H, THF) 1.77 (s, 18H, C(C*H*$_3$)$_3$), 1.37 (s, 18H, C(C*H*$_3$)$_3$). IR (Nujol, cm^{-1}) 1607$\nu_{C=N}$, 903$\nu_{U=O}$. U(VI/V) $E_{1/2}$ = -1.55 V (THF, QR), -1.62 V (MeCN, R), -1.78 V (CH_2Cl_2, IR).

Synthesis of UO_2(^{t}Bu$_4$-saloph)(TMPO) (1b): To a solution of **1a** (100 mg, 0.114 mmol) in benzene/MeCN was added trimethylphosphineoxide (10.5 mg, 0.114 mmol) and stirred overnight. The resulting solution was filtered and allowed to evaporate to afford **1b** as single red crystals (48.2 mg, 0.0536 mmol, 47%). ^{1}H NMR δ (C_6D_6) 9.00 (s, 2H, N=C*H*), 7.99 (s, 2H, Ar*H*), 7.36 (s, 2H, Ar*H*), 6.97 (dd, 2H, Ar*H*), 6.82 (dd, 2H, Ar*H*), 2.00 (s, 18H, C(C*H*$_3$)$_3$), 1.29 (d, 9H, J_{PH} = 9Hz, P(CH$_3$)$_3$), 1.36 (s, 18H, C(CH$_3$)$_3$). ^{31}P{^{1}H} NMR δ (MeCN) 63.8. IR (Nujol, cm^{-1}) 1613$\nu_{C=N}$, 907$\nu_{U=O}$. U(VI/V) $E_{1/2}$ = -1.71 V (THF, QR), -1.53 V (MeCN, R), -1.77 V (CH_2Cl_2, QR).

Synthesis of [UO_2(^{t}Bu$_4$-saloph)(Cl)][PPh$_4$] (1c): To a solution of **1a** (100 mg, 0.114 mmol) in THF was added tetraphenylphosphonium chloride (40.2 mg, 0.114 mmol). After stirring overnight, the orange precipitate was collected and redisolved in benzene and acetonitrile for recrystallization (111.6 mg, 0.0946 mmol, 83%). ^{1}H NMR δ (MeCN-*d*$_3$) 9.44(s, 1H, HC=N), 7.35-7.9 (m, 28H, Ar*H*/Ph*H*), 1.8 (s, 18H, C(C*H*$_3$)$_3$), 1.40 (s, 18H, C(C*H*$_3$)$_3$). ^{31}P NMR δ (MeCN) 24.3. IR (Nujol, cm^{-1}) 1607$\nu_{C=N}$, 886$\nu_{U=O}$. U(VI/V)

$E_{1/2}$ = -2.32V (MeCN, IR). Anal. (%) cald for $C_{60}H_{62}N_2O_4ClPU$: C, 60.88; H, 5.62; N, 2.37. found: C, 61.45; H, 5.62; N, 1.99.

Synthesis of [UO_2(^{t}Bu_4-saloph)(OH)][$CoCp_2$] (1d): A THF solution containing equimolar quantities of **1a** (206 mg, 0.234 mmol) and cobaltocene (44.0 mg, 0.234 mmol) was photo irradiated for 6 hr. The resulting brown mixture was filtered, and the orange precipitate washed with minimal cold THF, dried under vacuum, and recrystallized from acetonitrile to give orange crystals of **1d** (163.5 mg, 0.161 mmol, 69%). ^{1}H NMR δ (MeCN-d_3): 9.33 (s, 2H, N=C*H*), 7.62 (s, 2H, Ar*H*), 7.40 (s, 2H, Ar*H*), 7.35 (m, 2H, Ar*H*), 7.23 (t, 2H, Ar*H*), 5.66 (s, 10H, Co(C_5H_5)$_2$), 1.73 (s, 18H, C(CH_3)$_3$), 1.32 (s, 18H, C(CH_3)$_3$), 1.11 (br, 1H, O*H*). IR (Nujol, cm^{-1}) 1606$\nu_{C=N}$, 865$\nu_{U=O}$. U(VI/V) $E_{1/2}$ = -1.33 V ($CoCp_2^+$/$CoCp_2$), -2.31 (MeCN, IR). Anal. (%) calcd for $C_{46}H_{57}CoN_2O_5U$: C, 54.44; H, 5.66; N, 2.67. found: C, 52.13; H, 4.97; N 2.71.

Synthesis of UO_2(^{t}Bu_4-salbinap)(THF) (2): H_2L^2 (428 mg, 0.597 mmol) was dissolved in THF and stirred overnight with excess sodium hydride. The solution was filtered, and [$UO_2Cl_2(THF)_2$]$_2$ (289.6 mg, 0.298 mmol) was added. After stirring overnight, the red solution was filtered through a thick pad of celite. An analytically pure sample of 2 was obtained from slow evaporation of toluene (471.5 mg, 0.448 mmol, 75%). ^{1}H NMR δ (Tol-d_8) 9.21 (s, 2H, C=N*H*), 7.80 (s, 2H, Ar*H*), 7.51 (d, 4H, Ar*H*), 7.23-7.11 (m, 4H, Ar*H*), 7.05 (d, 4H, Ar*H*), 6.59 (s, 2H, Ar*H*), 4.04 (br, 4H, THF), 1.82 (s, 18H, C(CH_3)$_3$), 1.49 (br, 4H, THF), 1.16 (s, 18H, C(CH_3)$_3$). IR (Nujol, cm^{-1}) 1603$\nu_{C=N}$, 896$\nu_{U=O}$. U(VI/V) $E_{1/2}$ = -1.55 V (THF, QR), -1.62 V (MeCN, R), -1.78 V (CH_2Cl_2, IR). Anal. (%) cald for $C_{54}H_{58}N_2O_5U$: C, 61.35; H, 5.91; N, 2.65. found: C, 61.48; H, 6.27; N, 2.55.

Synthesis of UO_2(^{t}Bu_6-saltrenH) (3): H_3L^3 (250 mg, 0.314 mmol) was dissolved in THF and stirred with NaH overnight. Excess NaH was removed by filtration after which $[UO_2Cl_2THF_2]_2$ (153 mg, 0.158 mmol) was added while stirring. The red solution was dried, and the residue dissolved in toluene and filtered thru Celite. Solvent was again removed and the solid material redissolved in hexanes to give x-ray quality single crystals at -38 ^{o}C (287.1 mg, 0.270, 86%). ^{1}H NMR δ (C_6D_6) 13.88 (s, 1H, O*H*), 8.99 (s, 2H, N=C*H*), 8.01 (s, 1H, N=C*H*), 7.65 (s, 1H, Ar*H*), 7.61 (s, 1H, Ar*H*), 7.31 (s, 2H, Ar*H*), 7.04 (s, 2H, Ar*H*), 4.09 (br, 2H, CH_2), 3.72 (d, 2H, CH_2) 3.57 (br, 2H, CH_2), 3.43 (br, 2H, CH_2), 3.22 (m, 4H, CH_2), 2.06 (s, 18H, C(CH_3)$_3$), 1.67 (s, 9H, C(CH_3)$_3$), 1.44 (s, 18H, C(CH_3)$_3$), 1.33 (s, 9H, C(CH_3)$_3$. IR (Nujol, cm^{-1}) 1624$\nu_{C=N}$, 892$\nu_{U=O}$. U(VI/V) $E_{1/2}$ = -1.52 V (MeCN, R), -1.73 V (THF, R), -1.77 V ($MeCl_2$, R). Anal. (%) cald for $C_{51}H_{76}N_4O_5U$: C, 57.61; H, 7.20; N, 5.27. found: C, 57.47; H, 6.87; N, 4.76.

Synthesis of UO_2(^{t}Bu_4-BAP)$_2$ (4): H_2L^5 (185 mg, 0.354 mmol) was dissolved in THF and stirred with an excess of NaH overnight. The solution was filtered and $[UO_2Cl_2THF_2]_2$ (88.3 mg, 0.091 mmol) was added. The resulting red solution stirred overnight and was filtered over celite and concentrated. Single crystals suitable for x-ray crystallography were grown from THF/acetonitrile (172.6 mg, 0.131 mmol, 74%). ^{1}H NMR δ (THF-d_8) 7.47 (br, 4H, Ar*H*), 7.27 (br, 4H, Ar*H*), 5.10 (d, 4H, CH_2), 4.07 (d, 4H, CH_2), 3.24 (t, 4H, CH_2), 2.48 (t, 4H, CH_2), 2.33 (s, 1H, O*H*), 1.97 (s, 1H, O*H*), 1.74 (s, 12H, N(CH_3)$_2$), 1.71 (s, 36H, C(CH_3)$_3$), 1.41 (s, 36H, C(CH_3)$_3$). IR (Nujol, cm^{-1}) 859$\nu_{U=O}$. U(VI/V) $E_{1/2}$ = -2.59 V (MeCN, IR), -2.516 V (THF, IR).

Synthesis of UO_2(^{t}Bu_4-H_2salen)(H_2O) (5): H_4L^4 (200 mg, 0.426 mmol) and $UO_2(OAc)_2{\cdot}2H_2O$ (180.5 mg, 0.426 mmol) were stirred in methanol overnight. Crystals

of **5** were obtained by concentrating the reaction mixture, adding an excess of methylene chloride, and allowing the solution to evaporate (203.3 mg, 0.268 mmol, 63%). ^{1}H NMR δ ($CDCl_3$) 10.79 (br, 2H, N*H*), 7.27 (d, 2H, Ar*H*), 6.87 (d, 2H, Ar*H*), 5.26 (br, 2H, H_2O), 3.98 (s, 4H, CH_2), 2.88 (s, 4H, CH_2), 1.42 (s, 18H, C(CH_3)$_3$), 1.29 (s, 18H, C(CH_3)$_3$). IR (Nujol, cm^{-1}) 890$\nu_{U=O}$. U(VI/V) $E_{1/2}$ = -1.72 (MeCN, IR).

Synthesis of [UO_2(^{t}Bu$_2$-salNMe$_2$)(μ^2-OAc)]$_2$ (6): HL^6 (250 mg, 0.822 mmol) and $UO_2(OAc)_2{\cdot}2H_2O$ (349 mg, 0.822 mmol) were stirred overnight in methanol and methylene chloride. **6** was afforded upon evaporation of the reaction solution (426.4 mg, 0.337 mmol, 82%). ^{1}H NMR δ (C_6D_6) 8.62 (s, 2H, N=C*H*), 8.00 (s, 2H, Ar*H*), 7.27 (s, 2H, Ar*H*), 3.59 (br, 4H, CH_2), 3.05 (s, 12H, N(CH_3)$_2$), 2.67 (br, 4H, CH_2), 2.38 (s, 6H, O_2CCH_3), 2.01 (s, 18H, C(CH_3)$_3$), 1.43 (s, 18H, C(CH_3)$_3$). IR (Nujol, cm^{-1}) 1623$\nu_{C=N}$, 903$\nu_{U=O}$. U(VI/V) $E_{1/2}$ = -1.41V (MeCN, IR). Anal. (%) calcd for $C_{42}H_{68}N_4O_{10}U_2$: C, 39.87; H, 5.37; N, 4.43. found: C, 39.82; H, 5.31; N, 4.40.

Synthesis of (UO_2)$_2$(^{t}Bu$_4$-salhpn)(μ^2-OMe)(MeOH)$_2$ (7): H$_3$L^7 (100 mg, 0.191 mmol) and $UO_2(OAc)_2{\cdot}2H_2O$ (163 mg, 0.383 mmol) were stirred in methanol and methylene chloride overnight. X-ray quality crystals were obtained from slow evaporation of the reaction mixture (167.4 mg, 0.145 mmol, 76%). ^{1}H NMR δ (CD_3CN) 9.418 (s, 2H, N=C*H*), 7.80 (s, 2H, Ar*H*), 7.50 (s, 2H, Ar*H*), 5.43 (s, 1H, C*H*), 3.27 (s, 9H, CH_3), 2.16 (br, 4H, CH_2) 1.84 (s, 18H, C(CH_3)$_3$), 1.37 (s, 18H, C(CH_3)$_3$). IR (Nujol, cm^{-1}) 1623$\nu_{C=N}$, 890$\nu_{U=O}$. U(VI/V) $E_{1/2}$ = -1.56 V (MeCN, IR). Anal. (%) calcd for $C_{36}H_{58}N_2O_{10}U_2$: C, 36.71; H, 4.19; N, 2.38. found: C, 36.70; H, 4.77; N, 2.45.

References

[1] For an extensive review on Schiff base complexes, refer to; Vigato, P. A.; Tamburini, S. *Coord. Chem. Rev*. **2004**, *248*, 1217-2128, and references therein.

[2] For representative examples of uranyl(VI) sal-type complexes, see (a) Bandolini, G.; Clemente, D.; Croatto, U.; Vidali, M.; Vigato, P. A. *J. Chem. Soc., Chem. Commun.* **1971**, 1330-1331. (b) Benetollow, F.; Bombieri, G. *Acta Cryst.* **1979**, *B35*, 3091-3093. (c) Bandolini, G.; Clemente, D. A.; *J. Chem. Soc., Dalton Trans.* **1974**, 612-615. (d) Brock, A. M.; Cook, D. H.; Fenton, D. E.; Bombieri, G.; Forsellini, E.; Benetollo, F. *J. Inorg. and Nucl. Chem.* **1978**, *40*, 1551-1559.

[3] (a) Rudkevich, D. M.; Verboom, W.; Brzozka, Z.; Palys, M. J.; Stauthamer, W. P. R. V.; Hummel, G. J.; Franken, S. M.; Harkema, S. M.; Engbersen, J. F. J.; Reinhoudt, D. N. *J. Am. Chem. Soc.* **1994**, *116*, 4341-4351. (b) Cort, A. D.; Mandolini, L.; Schiaffino, L.; *J. Chem. Soc., Chem. Commun.* **2005**, 3867-3869 and references therein.

[4] Kannappan, R.; Tanase, S.; Tooke, D. M.; Spek, A. L.; Mutikainenc, I.; Turpeinen, U.; Reedijk, J. *Polyhedron* **2004**, *23*, 2285-2291, and references therein.

[5] Choppin, G. R.; Jensen, M. P. Actinides in Solution: Complexation and Kinetics. In *The Chemistry of the Actinide and Transactinide Elements*, 3rd ed.; Morss, L. R., Edelstein, N. M., Fuger, J., The Netherlands, 2006; Vol. 5, pp 2524-2608, and references therein.

[6] (a) Mizuoka, K.; Kim, S.-Y.; Hasegawa, M.; Hoshi, T.; Uchiyama, G.; Ikeda, Y. *Inorg. Chem*. **2003**, *42*, 1031-1038. (b) Mizuoka, K.; Ikeda, Y. *Inorg. Chem.* **2003**, *42*, 3396-2298. (c) Mizuoka, K; et al *Inorg. Chem.* **2005**, *44*, 6211-6218.

[7] Bakac, A.; Espenson, J. H. *Inorg. Chem.* **1995**, *34*, 1730-1735.

[8] McClesky, T. M.; Foreman, T. M.; Hallman, E. E.; Burns, C. J.; Sauer, N. N. *Environ. Sci. Technol.* **2001**, *35*, 547-551.

[9] For a review on uranyl photochemistry, see: Burrows, H. D.; Kemp, T. J. *J. Chem. Soc., Chem. Rev.* **1974**, *3*,139-165.

[10] For reports on Schiff base fluorescence and photochromism, see (a) Huisen, Y.; Xinfu, X. *Chem. J. Internet.*, **2003**, 5, 17-25. (b) Hadjoidis, E.; Mavridis, I. M. *Chem. Soc. Rev*., **2004**, *33*, 579-588.

[11] For uranyl-Schiff base photochemistry, refer to (a) Kunkely, H.; Vogler, A. *Z. Naturforsch* **2002**, *57b*, 301-304. (b) Nour, E. M.; Alnaimi, I. S.; Alem, N. A. *J. Phys. Chem. Solids* **1992**, *53*, 197-201.

[12] (a) Hayton, T. W.; Wu, G. *J. Am. Chem. Soc.* **2008**, *130*, 2005-2014. (b) Arnold, P. L.; Patel, D.; Wilson, C.; Love, J. B. Nature **2008**, 451, 315-317. (c) Berthet, J. C.; Nierlich, M.; Ephritikhine, M. *Agnew. Chem. Int. Ed.* **2003**, *42*, 1952-1954. (d) Burdet, F.; Pecaut, J.; Mazzanti, M. *J. Am. Chem. Soc.* **2006**, *128*, 16512-16513. (e) Natrajan, L.; Burdet, F.; Pecaut, J.; Mazzanti, M. *J. Am. Chem. Soc.* **2006**, *128*, 7152-7153. (f) Berthet, J. C.; Siffredi, G.; Thuery, P.; Ephritikhine, M. *Chem. Commun.* **2006**, 3184-3186.

[13] For uranyl(VI)-saloph complexes, see (a) Evans, D. J.; Junk, P. C.; Smith, M. K. *Polyhedron* **2002**, *21*, 2421-2431. (b) Takao, K.; Ikeda, Y. *Inorg. Chem.* **2007**, *46*, 1550-1562.

[14] (a) see reference 2a (b) Cort, A. D.; Mandolini, L.; Pasquini, C.; Schiaffino, L. *Org. Leters* **2004**, *6*, 1697-1700 and references therein.

[15] $UO_2(O\text{-}2,6\text{-}^{i}Pr_2\text{-}C_6H_3)_2(py)_3$ dispalys U-O_{Ar} distances of 2.179(5) and 2.215(5) Å in reference; Barnhart, D. M.; Burns, C. J.; Sauer, N. N.; Watkin, J. G. *Inorg. Chem.* **1995**, *34*, 4079-4084.

[16] Thousands of uranyl(VI) complexes have been structurally characterized and all but one reported in the literature contain short U=O bonds (~1.78 Å) with nearly linear O=U=O angles (~176º) indicative of an axial bond order greater than two.

[17] (a) $UO_2(O\text{-}2,6\text{-}^{t}Bu_2\text{-}C_6H_3)_2(THF)_2$ diplays U-O_{THF} distances of 2.450(8) and 2.466(8) Å in reference;Wilkerson, M. P.; Burns, C. J.; Morris, D. E.; Paine, R. T.; Scott, B. L. *Inorg. Chem.* **2002**, *41*, 3110-3120. (b) also see reference 44.

[18] Uranyl(VI)-phosphine oxide within the range 2.342(2)-2.455(2) Å in reference; Kannan, S.; Moody, M. A.; Barnes, C. L.; Duval, P. B. *Inorg. Chem.* **2006**, *45*, 9206-9212 and references therein.

[19] Representative P=O (1.518(8) Å) coordinated to uranyl(VI) see, Bombieri, G.; Forsellini, E.; Day, J. P.; Azeez, W. I. *J. Chem. Soc., Datlton Trans.* **1978**, 677-680.

[20] Haller, L. J. L; Kaltsoyannis, N.; Sarsfield, M. J.; May, I.; Cornet, S. M.; Redmond, M. P.; Helliwell, M. *Inorg. Chem.* **2007**, *46*, 4868-4875.

[21] Uranyl(VI)-chloride distances of 2.6898(8) and 2.6679(8) Å were reported in the cis-dihalide starting materials in reference; Duval, P. B.; Kannan, S.; Barnes, C. L. *Inorg. Chem. Commun.* **2006**, *9*, 426-428.

[22] PPh_4^+ ^{31}P NMR siganl at 24.9 ppm for $[UO_2I_4][PPh_4]$ in, Margaret-Jane, C.; Mayer, P. *Inorg. Chem.* **2004**, *44*, 5547-5549.

[23] Braga, D.; Polito, M.; Grepioni, F. *Cryst. Growth Des.* **2004**, *4*, 769-774.

[24] Average U-OH distance of 2.26(2) Å in $UO_2(OH)_4^{-2}$: Clark, D. L.; Conradson, S. D.; Donohoe, R. J.; Keogh, D. W.; Morris, D. E.; Palmer, P. D.; Rogers, R. D.; Tait, C. D. *Inorg. Chem.* **1999**, *38*, 1456-1466 and references therein.

[25] (a) Woodman, P. R.; Munslow, I. J.; Hitchcock, P. B.; Scott, P. *J. Chem. Soc., Dalton Trans.* **1999**, 4069-4076. (b) Che, C. M.; Huang, J. S. *Coord. Chem. Rev.* **2003**, *242*, 97-113.

[26] For a recent example of distorted uranyl equatorial complexation, see; Sarsfield, M. J.; Helliwell, M.; Raftery, J. *Inorg. Chem.* **2004**, *43*, 3170-3179.

[27] (a) see reference 3 (b) Cametti, M.; Nissinen, M.; Dalla Cort, A.; Mandolini, L.; Rissanen, K. *J. Am. Chem. Soc.* **2005**, *127*, 3831-3837. (c) Cort, A. D.; et al *Chem. Eur. J.* **2004**, *10*, 3301-3307. (d) Cozzi, P. G. *J. Chem. Soc., Chem. Rev.* **2004**, *33*, 410-421 is a good general reference on the topic.

[28] Azenha, M. E.; Burrows, H. D.; Formosinho, S. J.; Leitae, M. L. P.; Miguel, M. G. *J. Chem. Soc., Dalton Trans.* **1988**, 2893-2895.

[29] Liu, S.; Gelmini, L.; Rettig, S. J.; Thompson, R. C.; Orvig, C. *J. Am. Chem. Soc.* **1992**, *114*, 6081-6087.

[30] An unpublished result: Treatment of $\mathbf{H_2L^5}$ with excess $KN(SiMe_3)_2$ affords the structurally characterized dimer $[HLK(THF)]_2$ upon recrystallization from THF.

[31] For lanthanide complexes, refer to (a) Yao, Y.; et al *Organomet.* **2005**, *24*, 4014-4020, and (b) Ma, M.; Xu, X.; Yao, Y.; Zhang, Y.; Shen, Q. *J. Mol. Struct.* **2005**, *740*, 69-74. For early transition metal complexes, see to (c) Sarazin, Y.; Howard, R. H.; Hughes, D. L.; Humphrey, S. M.; Bochmann, M. *J. Chem. Soc., Dalton Trans.* **2006**, 340-350 and references therein.

[32] $U\text{-}O_{carboxylate}$ average bond distances of ~2.36 Å in reference; Frisch, M.; Cahill, C. L. *J. Chem. Soc., Dalton Trans.* **2006**, 4679-4690.

[33] Terminal uranyl alkoxide distances between 2.015(6) and 2.162(6) Å are observed in a variety of complexes in; Wilkerson, M. P.; Burns, C. J.; Dewey, H. J.; Martin, J. M.; Morris, D. E.; Paine, R. T.; Scott, B. L. *Inorg. Chem.* **2000**, *39*, 5277-5285.

[34] A uranyl-ethanol distance of 2.46 Å is observed for UO_2(saloph)EtOH in reference 2a.

[35] For polynuclear uranyl(VI) Schiff base complexes refer to (a) Salmon, L.; Thuery, P.; Ephritikhine, M. *Polyhedron* **2003**, *22*, 2683-2688. (b) Casellato, U.; Guerriero, P.; Tamburini, S.; Vigato, P. A.; Graziani, R. *J. Chem. Soc., Dalton Trans.* **1990**, 1533-1541. (c) Khalil, S. M. *Chem. Papers* **2000**, *54*, 12-18. (d) Mohan, S. B.; Strawbridge, K.; Vilsek, J. Z.; Bray, T. H.; Borden, A. V. *Inorg. Chem.* **2007**, *46*, 8309-8315.

[36] (a) Ikeda, A.; Hennig, C.; Tsushima, S.; Takao, K.; Ikeda, Y.; Scheinost, A. C.; Bernhard, G. *Inorg. Chem.* **2007**, *46*, 4212-4219. (b) Yamamura, T.; Shirasaki, K.; Sato, H.; Nakamura, Y.; Tomiyasu, H.; Satoh, I.; Shiokawa, Y. *J. Phys. Chem. C.* **2007**, *111*, 18812-18820.

[37] Morris, D. E. *Inorg. Chem*. **2002**, 41, 3542-3547. Also see reference 6.

[38] Denning, R. G. *Structure and Bonding* **1992**, *79*, 215-275. Also see reference 11.

[39] For a comprehensive review on uranyl fluorescence quenching mechanisms refer to; Baird, C. P.; Kemp, T. J. *Prog. React. Kinet.* **1997**, *22*, 87-139.

[40] (a) Wang, W. D.; Bakac, A.; Espenson, J. H. *Inorg. Chem.* **1995**, *34*, 6034-6039 and references therein. (b) McClesky, T. M.; Burns, C. J.; Tumas, W. *Inorg. Chem.* **1999**, *38*, 5924-5925.

[41] (a) Evangelio, E.; Ruiz-Molina, D. *Eur. J. Inorg. Chem.* **2005**, 2957-2971. (b) Khudyakov, I. V.; Turro, N. J.; Yakushenko, I. K. *J. Photochem. Photobiol. A: Chem.* **1992**, *63*, 25-31. (c) see reference 10.

[42] For a recent communication on this topic released from our lab, refer to: Vaughn, A. E.; Bassil, D. B.; Barnes, C. L.; Tucker, S. A.; Duval, P. B. *J. Am. Chem. Soc.* **2006**, 128, 10656.

[43] Barbara, P. F.; Rentzepis, P. M.; Brus, L. E. *J. Am. Chem. Soc.* **1980**, *102*, 2786-2791.

[44] Wilkerson, M. P.; Burns, C. J.; Morris, D. E.; Paine, R. T.; Scott, B. L. Inorg. Chem. 2002, 41, 3110-3120.

[45] Connelly, N. G.; Geiger, W. E. *Chem. Rev*. **1996**, 96, 877.

[46] Xiao, Z.; Gable, R. W.; Wedd, A. G.; Young, C. G. *J. Am. Chem. Soc*. **1996**, 118, 2912-2921.

[47] (a) Avens, L. R.; Barnhart, D. M.; Burns, C. J.; McKee, S. D. *Inorg. Chem.* **1996**, *35*, 537-539. (b) Boisson, C.; Berthet, J. C.; Lance, M.; Nierlich, M.; Ephirtikhine, M. *Chem. Commun.* **1996**, 2129-2130.

[49] Kannan, S.; Vaughn, A. E.; Weis, E. M.; Barnes, C. L.; Duval, P. B. *J. Am. Chem. Soc.* **2006**, *128*, 14024-14025.

[50] Suib, S. L.; Tanguay, J. F.; Occelli, M. L. *J. Am. Chem. Soc.* **1986**, *108*, 6972-6977.

[51] Synthesis of $[UO_2Cl_2(THF)_2]_2$: Wilkerson, M. P.; Burns, C. J.; Paine, R. T.; Scott, B. L. *Inorg. Chem*. **1999**, 38, 4156-4158.

[52] For ligand synthesis refer to: ($\mathbf{H_2L^1}$) see reference 4. ($\mathbf{H_2L^2}$) Bernardo, K. S.; Robert, A.; Dahan, F.; Meunier, B. *New J. Chem*. **1995**, 19, 129. ($\mathbf{H_3L^3}$) Liu, S.; Gelmini, L.; Rettig, S. J.; Thompson, R. C.; Orvig, C. *J. Am. Chem. Soc*. **1992**, 114, 6081. ($\mathbf{H_4L^4}$) Higham, C. S.; Dowling, D. P.; Shaw, J. L.; Cetin, A.; Ziegler, C. J.; Farrell, J. R. *Tetrahedron Letters* **2006**, 47, 4419. ($\mathbf{H_2L^5}$) Tshuva, E. Y.; Goldberg, I.; Kol, M.; Goldschmidt, Z. *Inorg. Chem*. **2001**, 40, 4256. ($\mathbf{HL^6}$) Cameron, P. A.; Gibson, V. C.; Redshaw, C.; Segal, J. A.; White, A. J. P.; Willioms, D. J. *J. Chem. Soc. Dalton Trans*. **2002**, 415. ($\mathbf{H_3L^7}$) Lukov, V. V.; Kogan, V. A.; Novotortsev, V. M.; Tupolova, Yu. P.; Gevorkyan, I. E. *Russian J. Coord. Chem*. **2005**, 31, 353.

[53] Gange, R. R.; Koval, C. A.; Lisensky, G. C. *Inorg. Chem*. **1980**, 19, 2854-2855.

[54] (a) SMART V5.051 and SAINT V5.00, Area Detector Control and Integration Software, Bruker AXS Inc., Madison, WI-53719, **1998**. (b) G. M. Sheldrick, SADABS, Bruker AXS Inc., Madison, WI-53719, **1997**. (c) Sheldrick, G. M.; *SHELXS-97: Program for Structural Solution*; University of Götten, Germany, **1997**. (d) Sheldrick, G. M.; *SHELXTL-97: Program for Structural Refinement (version 5.10)*; University of Götten, Germany, **1997**. (e) Barbour, L.; *X-SEED: Graphical interface for SHELXL*; University of Missouri-Columbia, **2001**.

Chapter 3

Structure and Bending in the Uranyl Ion: A Terminal *cis*-Dioxo Uranyl(VI) Moiety Supported in a Reversible Coordination Polymer

Abstract

A simple benchtop reaction between uranyl acetate and ferrocenemonocarboxylic acid (FCA) affords the reversible carboxylate bridged coordination polymers $[UO_2(fcdc)(THF)\bullet(Fc)]_n$ (**1a**) and $[UO_2(fcdc)(2\text{-Me-THF})\bullet(Fc)]_n$ (**1b**) in good isolated yield. These compounds contain the *cis*-dioxo uranyl(VI) moiety, a species whose existence has been speculated and sought since the conception of the actinide series. The polymer **1** has been characterized by a combination of single-crystal and powder X-ray diffraction, ^1H and ^{13}C NMR spectroscopies, solid and solution state FTIR spectroscopy, elemental analysis, thermogravimetric analysis, Mössbauer spectroscopy, cyclic voltammetry, and solid state and solution UV-visible absorption and fluorescence spectroscopies. The *cis*-dioxo unit contains short terminal U=O bonds (1.745(9) Å) with a dramatically acute O=U=O angle (69.5(6)º). Infrared active symmetric and asymmetric stretches for the C_{2v} dioxo unit appear at 915 and 936 cm^{-1}. Variable temperature NMR analysis reveals a fluxional carboxylate abstraction mechanism that accounts for the formation and reversible solubility of **1**, and describes a sterically demanding situation responsible for bending the dioxo unit. TGA provides

evidence for the interstitial ferrocene units that hold the polymer chains in a network through C-H···π and C-H···O=U contacts, however, Mossbauer spectroscopy fails to resolve the two ferrocene environments. Cyclic voltammetric experiments portray sluggish ferrocene/ferrocenium and uranyl(VI/V) redox waves within the expected potential ranges. Photophysical measurements performed at ambient temperature are dominated by absorption and fluorescence assigned to ferrocene. Preliminary reactivity studies imply that **1** is unreactive towards a variety of photolytic reducing media and oxide abstraction reagents that commonly activate oxide substituents in -yl type ions. Information garnered from interpretation of these data suggest that the bent dioxo uranyl(VI) moiety is constructed from considerably altered electronic structure and multiple bonding properties in comparison to conventional linear actinyl complexes. This revelation could lead to surprising and unparalleled insights regarding the nature of 5f versus 6d σ- and π-bonding in actinide ion complexes.

3.1 Introduction

A foremost theme in f-element chemistry is the elucidation of the nature of multiple bonding in actinide ion complexes.[1] This subject is highlighted by the dioxouranium(VI) (UO_2^{2+}) and uranium-imido ($U{=}NR^{n+}$; n = 2,3,4) units, which bear isoelectronic ligands with short bonds that render them chemically robust. The chemistry of multiply bound high-valent uranium-oxide and -imide fragments has been well established as a platform to shed light on electronic structure, and multiple bonding qualities can be traced to covalent contributions from an admixture of uranium based 5f and 6d valence orbitals that accommodate filled ligand 2p electron density. These molecular units have been extensively exploited as a foundation to host a wide variety of ligands that bind with variable denticity and bridging modes.[2]

Covalent bonding in actinide ion complexes is clearly manifested in the geometry of the dioxo uranyl moiety and encompass the entire actinyl series, which adopt an essentially linear (*trans*) geometry independent of metal ion electronic configuration ($f^{1\text{-}4}$). This invariant directional preference is in peculiar contrast to dioxo transition metal congeners' ability to take on *trans* or *cis* (bent) geometries as a function of valence electrons housed in d-orbitals. In both instances the geometric disposition of the MO_2^{n+} moiety is determined by the intrinsic ability to maximize metal ion-ligand interactions.[3] A contrasting factor that defines the structure of the actinyl ion, however, is possession of the 5f manifold that participates in covalent overlap with the surrounding ligand field. When the potent oxophilic affinity is taken into account, it is curious that actinyl ions are not capable of adopting coordination geometries outside the typical bipyramidal group. This is especially true in light

of the fact that the isoelectronic U^{VI} bis-imido and oxo-imido units can adopt either *cis* or *trans* geometries.[2]

A number of researchers have sought out the possibility to deviate from the fixed trans $O=An=O^{n+}$ configuration. Theoretical and chemical treatments involve manipulation of electronic and sterically demanding ligand sets geared towards effectively bending the dioxo unit. For example, the central UO_2^{2+} entity in the complexes $UO_2(NCN)_2(THF)$ (**i**) and $[Cp^*UO_2(CN)_3][N(Et)_4]_2$ (**ii**) display subtle perturbations of 169.7(2)º and 168.40(9)º respectively, and retain short terminal U=O bonds.[4,5] Attempts to construct the dioxo unit via two electron oxidation of tetravalent precursors outfitted with an ancillary framework designed to direct oxide ligands to assemble *cis* to one another are exemplified in the synthetic routes reported for the production of (**ii**) and (**iii**). The U^V isopolyoxometallate $(Cp^{\ddagger})_4U_6O_{13}(bpy)_2$ (**iii**) bridges a gap between actinide and transition metal –yl ion behavior since it is well established that dioxotransition metal ions form isopolyoxometallate anions.[6] Complex (**iii**) was the earliest example of such a molecule representing the f-elements, and contains structurally significant O=U=O bending between 20º and 30º with elongated bonds.[6] On the other hand, theoretical methodologies have modeled environmentally relevant situations that saturate the actinyl equatorial region with powerful π-donor hydroxide ligands capable of influencing valence orbitals to support the bent geometry.[7] This speculative method compliments classic experiments that probe the basicity of the oxide ligands as a function of equatorial coordination. Theoreticians have obtained computational evidence that the bent dioxo unit would possess elongated U=O bonds with a dioxo angle near 113º that would favor bridging oxide modes, and a low energy barrier for the *cis-trans* isomerism.[7,8]

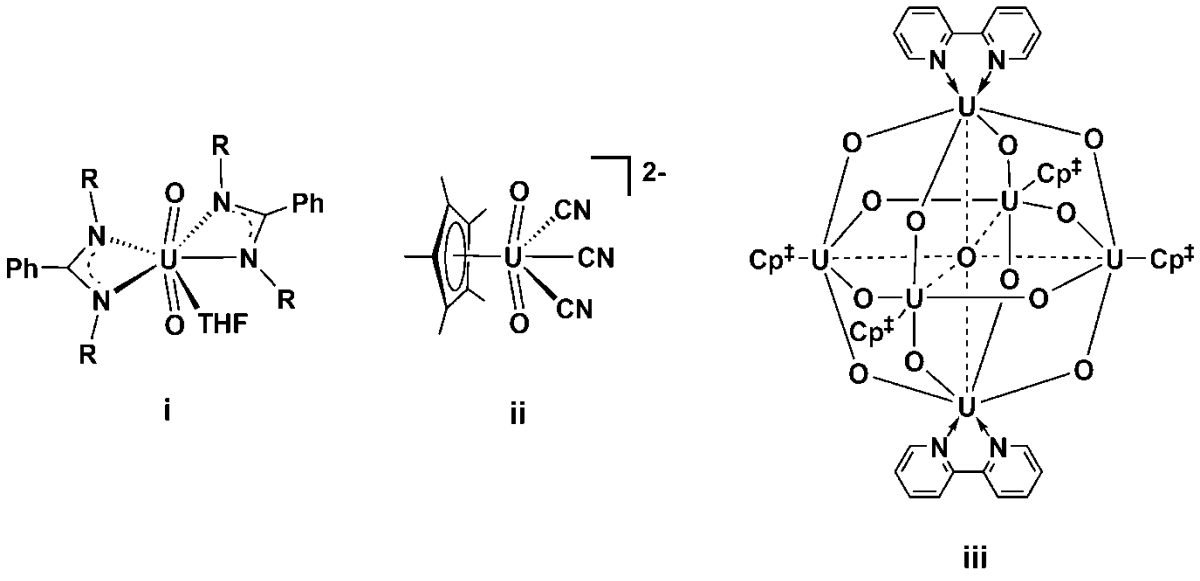

Figure 3.1. The molecular structures of $UO_2(NCN)_2(THF)$ (**i**), $[Cp^*UO_2(CN)_3][NEt_4]_2$ (**ii**), and $(Cp^‡)_4U_6O_{13}(bpy)_2$ (**iii**).

Information gleaned from this collection infers that isolation of a well defined *cis*-actinyl complex is an achievable objective and the species would possess considerably altered molecular and electronic structural properties in comparison to the conventional *trans* geometry.[9] A breakthrough of this sort would reveal new insights into the factors that govern multiple bonding in actinide complexes and could lead to the rational pursuit of marketable separation technologies vital to spent nuclear fuel recycling and remediation practices. This account focuses on the synthesis and structural characterization of a *cis*-dioxo uranyl(VI) unit, the first of its kind in actinide sciences, contained within a reversible coordination polymer constructed from a carboxylate bridged scaffold. The influential ligand that supports this behavior is founded on the ferrocene unit endowed with carboxylate substituents (FCA and fcdc). The unique product is obtained from a simple bentchtop recipe and the solid state and solution characteristics clarified by a variety of diagnostic techniques that account for structure, formation, and solubility. These studies are followed by a brief

examination of the electronic properties in comparison and contrast to *trans*-uranyl(VI) properties.

3.2 Results and Discussion

Synthesis and Structural Characterization

The synthetic procedure employed to generate the coordination polymer **1** entails protonolysis between uranyl acetate dihydrate and two equivalents of FCA to eliminate acetic acid and water as shown in **Scheme 3.1**. The reaction was conducted in undried organic solvents on the benchtop, and the red-orange heterobimetallic coordination polymers crystallized directly from their respective reaction mixture in reproducible high yield (~83%). **1** is constructed from carboxylate bridged polymeric chains containing unexpected *cis*-dioxo uranyl(VI) units. It should be noted that the mild synthetic approach described here contrasts the hydrothermal techniques commonly used in the preparation of uranyl coordination polymers.[10] **1a** and **1b** are isostructural in the solid state except for the prescence of a THF (**1a**) or 2-methyl-THF (**1b**), however the poor quality of x-ray data collected on single crystals of **1b** precluded exact structural refinement beyond molecular connectivity. The molecular structure for **1a** contains a disordered THF cap whereas attempts to use a 2-methyl-THF cap did not resolve any disorder. The data collection and refinement details for **1a** are collected in **Table 3.1**, whereas complete crystallographic details are provided in appendix 2. Powder XRD performed on the bulk solid material matched the diffraction pattern calculated from single crystal data (**Figure S3.1**).

1 does not contain the expected FCA ligand, but instead consists of coordinated 1,2-ferrocenedicarboxylate (fcdc) bridging ligands and a stoichiometric amount of ferrocene (Fc)

embedded in the lattice organized between the polymer chains. The details that account for the rearrangement that engenders Fc and fcdc from FCA are described below. The average Fe-$Cp_{centroid}$ length of 1.651 Å and (Cp)C-C distances between 1.333 and 1.491 Å in the Fc and fcdc moieties are consistent with the formal oxidation state assignment of Fe^{II} for ferrocene species.[11] The Cp-CO_2 length C(4)-C(7) of 1.574(18) Å in fcdc is considerably elongated in comparison to the Cp-CO_2 distance of 1.46(2) Å in FCA.[12] Although $fcdcH_2$ has been reported in a single document, no solid state structural information was revealed,[13] and the material could not be reproduced in our laboratory.

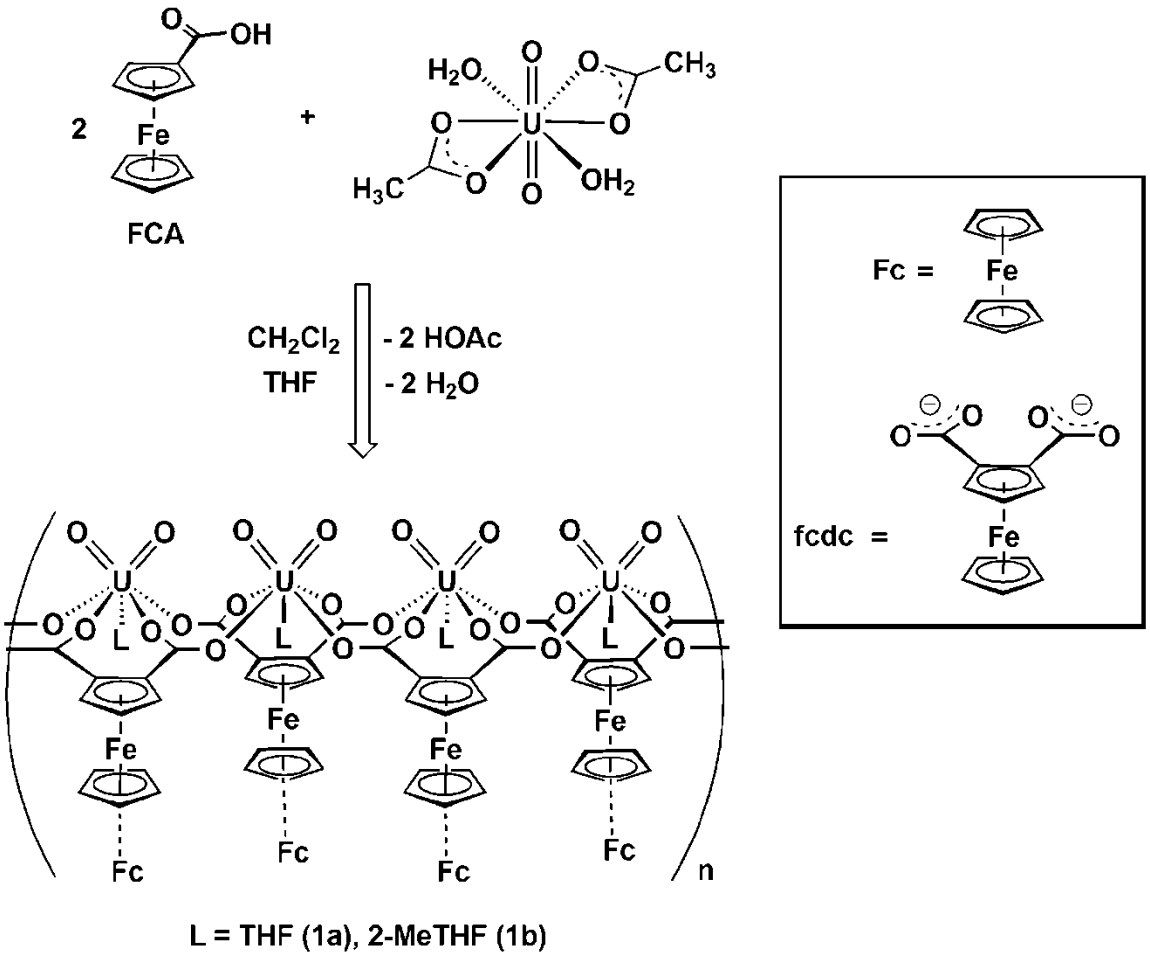

Scheme 3.1. Benchtop synthesis of the coordination polymers **1a** and **1b.**

Table 3.1. Selected crystallographic data for **1a**.

	$[UO_2(fcdc)(THF)\bullet(Fc)]_n$ **(1a)**
formula	$C_{26}H_{26}Fe_2O_7U$
color	red-orange
a (Å)	9.5227(13)
b (Å)	11.6414(16)
c (Å)	22.268(3)
α (º)	90
β (º)	90
γ (º)	90
V ($Å^3$)	2468.6(6)
Z	4
FW	800.2
crystal system	orthorhombic
space group	A*ma*2
T (K)	173
λ (Å)	0.71073
F(000)	1528
ρ_{calc} ($g\bullet cm^{-1}$)	2.153
μ (mm^{-1})	7.749
θ range (º)	1.83-27.11
total reflections	8614
unique reflections	2867
parameters	158
R_1	0.0499
wR_2 (all data)	0.1313
max, min peaks, e $Å^{-3}$	3.607, -1.752
GOF	1.066

The repeating unit for the polymer **1** shown in **Figure 3.2** contains a *cis*-uranyl unit bound to three fcdc ligands through a total of four carboxylate oxygen donors. The fcdc ligands adopt an η^2-μ^3 coordination mode which bichelates one uranium and bridges two others. This is repeated along the polymer chain in an alternating front-back fashion as portrayed in **Figure 3.3**. Each U^{VI} ion is nestled in a slightly distorted seven coordinate monocapped trigonal prismatic geometry in which the faces of the prism are comprised of one oxide O(3) ligand and two carboxylate oxygens O(1) and O(2), and capped by a facial THF donor O(4). Although seven coordinate arrangements are common for uranyl(VI)

coordination complexes, the pentagonal bipyramidal geometry is usually adopted due to the linear UO_2^{2+} moiety occupying the axial positions.[14] In the case of **1**, the lack of a linear uranyl unit to restrict ligands to bind only around the equator allows for the atypical prismatic geometry.

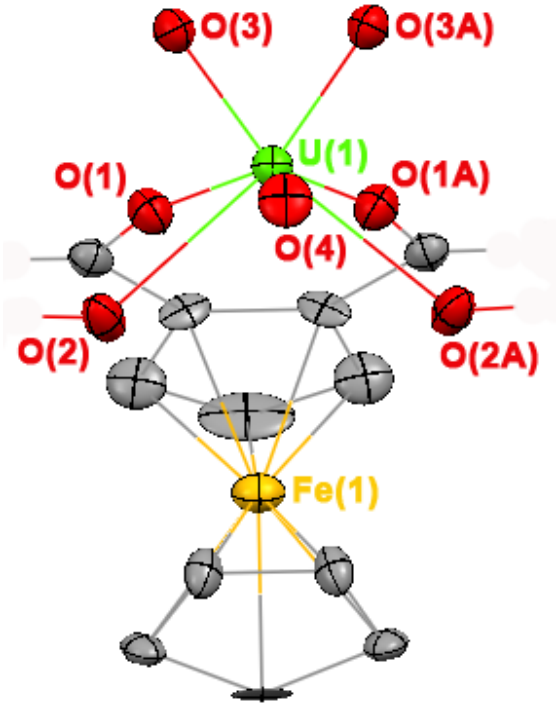

Figure 3.2. Molecular structure of the repeating unit in **1** with thermal ellipsoids depicted at the 50% probability level. Disordered THF carbon atoms omitted for clarity.

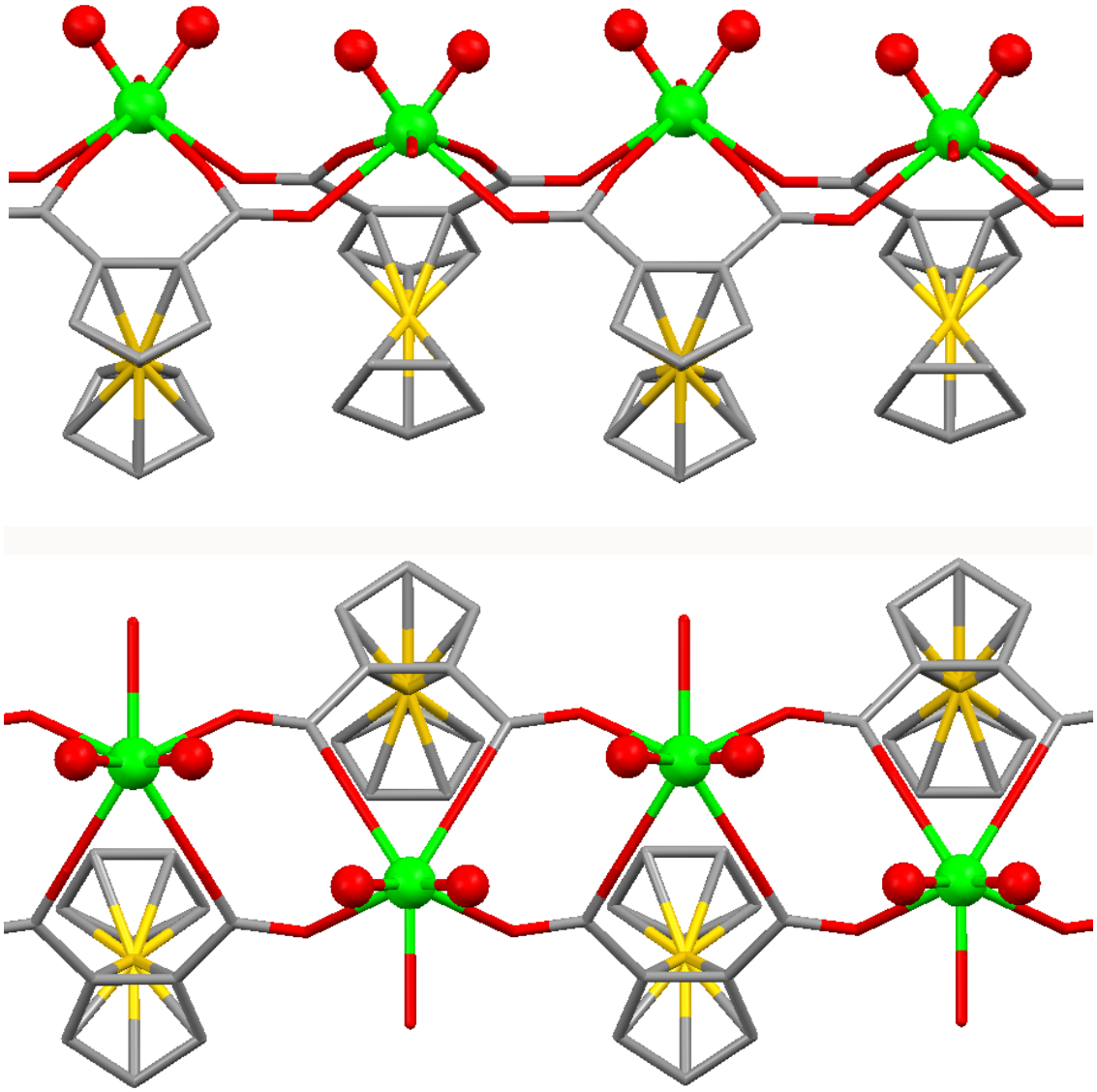

Figure 3.3. Top: A ball and stick model of the one-dimensional polymer chain along the a-axis. Bottom: Viewing down the c-axis illustrating the alternating UO_2-fcdc arrangement. Disordered THF carbon atoms omitted for clarity.

The U-O bond lengths in **1** are characteristic of uranyl(VI) ion complexes. U^{VI}-carboxylate distances U(1)-O(1) 2.298(9) Å and U(1)-O(2) 2.415(8) Å are comparable those found in other structurally characterized uranyl(VI)-carboxylate species.[15] Likewise the U-O(4) length of 2.425(8) Å is representative of a uranyl(VI)-THF linkage.[16] The U(1)=O(3) contacts are short and terminal as observed in the majority of uranyl(VI) complexes, however

the distance of 1.745(9) Å is modestly shorter than the range recorded for uranyl(VI) ions (1.77-1.83 Å).[17] The shorter bonds in this case are an indication of a greater degree of multiple bonding than in linear uranyl(VI), where a bond order between two and three has been proposed.[17,18]

Prior to this point in actinyl chemistry, the most significant deviation from linearity among AnO_2^{n+} ions is ~12º observed in complexes (**i**) and (**ii**) with respective O=U=O angles of 168.40(9)º and 169.7(2)º.[4,5] Although these angles reside outside the archetypal range (173º -180º), they are nearly linear when compared to the severely bent dioxo angle of 69.5(6)º observed in **1**. This angle is considerably more acute than those observed in *cis*-dioxo transition metal complexes where angles between 95º and 110º are encountered.[19] This disparity can be attributed to the crowded seven coordinate geometry in **1,** whereas transition metal analogues possess coordination numbers that generally do not exceed six.[20] It has been speculated that the dioxoactinide geometry might be persuaded to bend by the use of π-donor ligands that influence metal valence orbitals, however the extremely acute dioxo angle in the case of **1** can be attributed to the high coordination number and geometric constraint imposed by the sterically demanding fcdc scaffold.

The *cis*-uranyl units in **1** are situated along the linear polymeric chain in a zigzag fashion that forces the fcdc ligands into a staggered arrangement (**Figure 3.3**), whereas for typical uranyl polymers equatorial coordination extends oligomerization into planar sheets or chains.[21] The tilted orientation of the fcdc ligands are positioned such that the interstitial Fc molecules reside below the polymer chains. The Fc units give rise to a network of C-H···π interactions (2.88 Å) that knit the polymeric chains together in layers. The Fc cyclopentadienyl rings are involved in two of these contacts that interpenetrate the layer as

shown in **Figure 3.4**. Each 11 Å thick layer is stacked on top of the next and held in place by weak C-H···O=U interactions (2.56 Å, 3.33 Å) between the *cis* uranyl units and Fc units from the layer above it to form an extensive hydrogen bonded 3-D network.

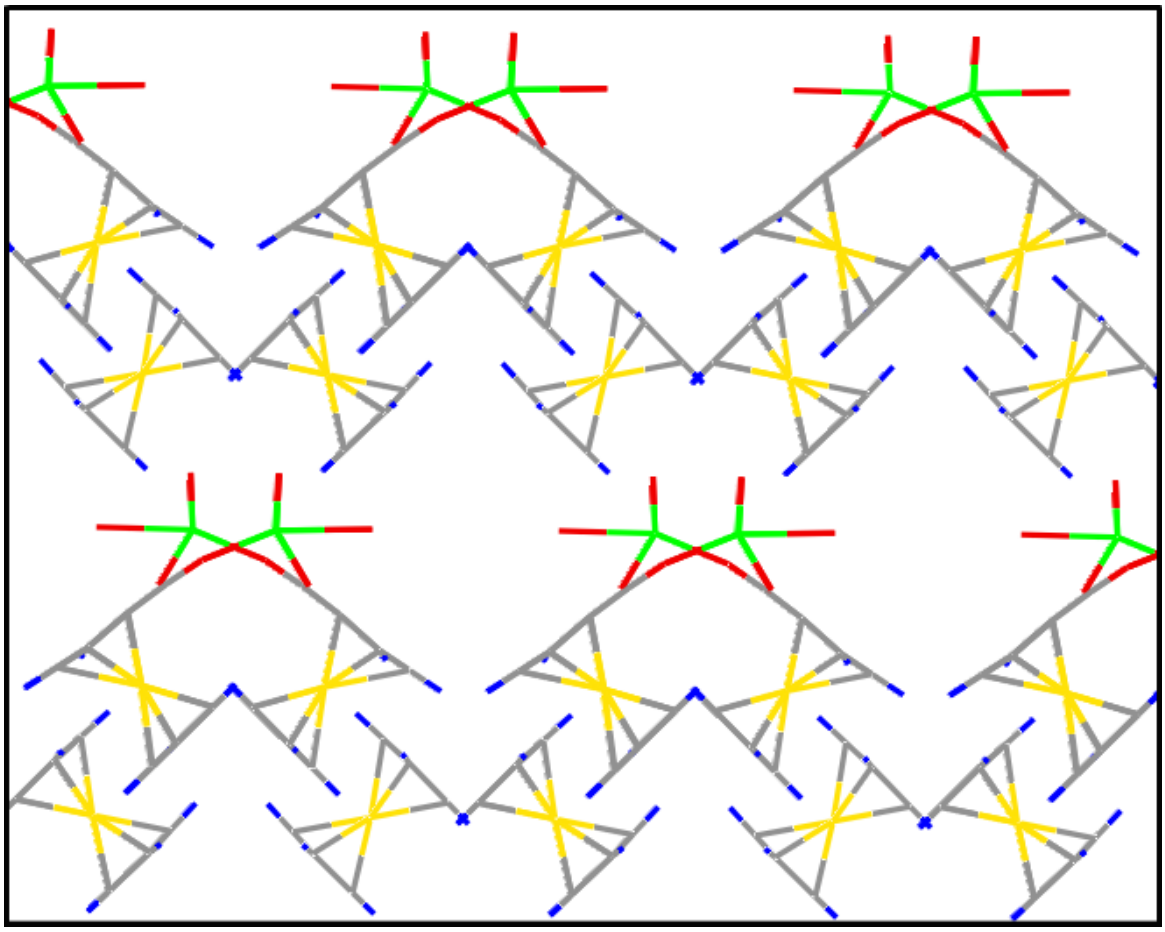

Figure 3.4. Two-dimensional cross-section of the network viewed down the polymer chains (a-axis) showing interstitial ferrocene units. Hydrogen atoms (blue) are involved in an extensive array of C-H···π and C-H···O=U interactions that hold the polymer chains together layers along the b-axis and support the stacked layers along the c-direction. Disordered THF carbon atoms omitted for clarity.

The strength of the short U=O bonds in **1** are reflected in the infrared absorptions at 915 and 934 cm^{-1} shown in **Figure 3.5**. These peaks are attributed to the symmetric and antisymmetric stretches for the C_{2v} *cis*-UO_2^{2+} moiety, and these vibrational modes appear in

the region expected for M=O stretches for –yl type ions.[22] Both of these stretches are observed in IR spectra of *cis*-$Mo^{VI}O_2^{+2}$ species and other bent dioxo transition metal ion complexes, whereas for uranyl ions of higher symmetry ($D_{\infty h}$) only the antisymmetric stretch is IR active and falls within the range 890-960 cm^{-1}.[23,24] In comparison, the symmetric stretch for the *trans*-uranyl(VI) moiety is active in Raman spectra and appears at lower energy (790-900 cm^{-1}).[25] Furthermore, an isotopic labeled oxo study is required to conclusively assign these stretches to the *cis*-dioxo moiety. Additionally, broad intense carboxylate vibrations observed at higher energy (1400-1520 cm^{-1}) are red shifted with respect to FCA.

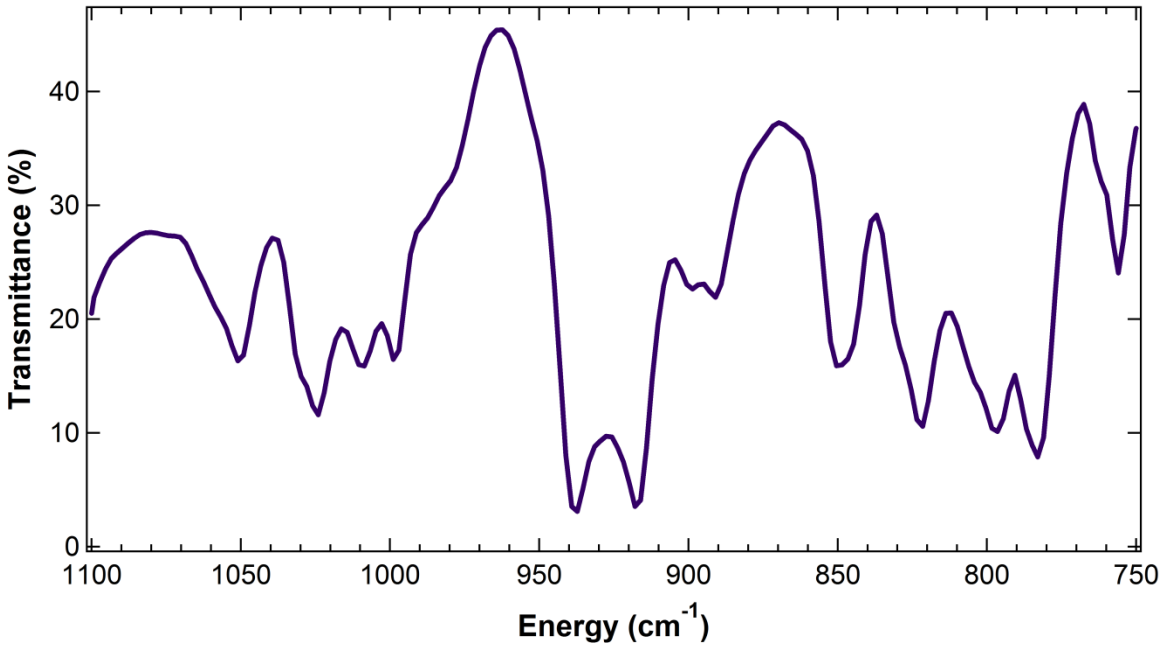

Figure 3.5. Solid-state infrared spectrum of **1b**.

Evidence for the presence of the interstitial ferrocene molecules is revealed in the thermogravimetric analysis (TGA) plot for **1a** in **Figure 3.6**. The TGA curve depicts initial

loss of coordinated THF up to 200 ºC, whereas mass loss equivalent to the calculated ferrocene percentage occurs between 200 ºC and 435 ºC. The double humped structure of the plot in this region (200-320 ºC, 320-435 ºC) might indicate a high temperature structural morphism during the volatilization of ferrocene. The fact that coordinated THF completely volatilizes prior to Fc reflects the strength of the extensive hydrogen bonding in **1**. Once the Fc is removed, an intractable black solid remains that shows no spectroscopic evidence for the presence of the dioxo unit, and **Figure S3.2** shows alterations in the IR spectrum of **1** upon progressive thermolysis monitored by TGA. Once coordinated THF is volatilized, a red material remains that displays infrared and ^{1}H NMR spectral features similar to **1**. Likewise, upon THF loss the remaining red material displays a powder XRD pattern similar to **1**, however the black material absent of interstitial Fc is amorphous.

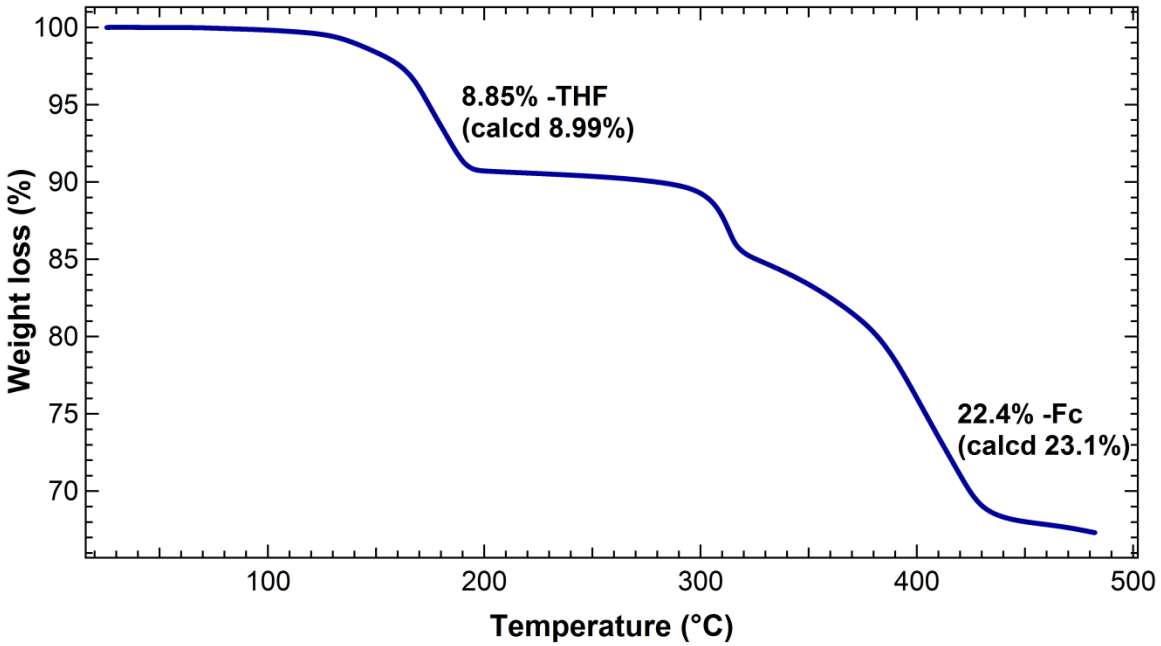

Figure 3.6. Thermogravimetric analysis (TGA) curve for **1a** conducted with a thermal ramp of 5 ºC/min to 500 ºC under a constant N_2 stream.

^{57}Fe Mössbauer spectroscopy was employed to distinguish between the two ferrocene environments in the solid material. Mössbauer data collected on a bulk solid sample of **1a** is shown in **Figure 3.7** and **Table 3.2** and displays a single doublet feature centered near 0.442 mms^{-1} with a quadrupolar splitting of 2.29 mms^{-1} at 250 K indicative of Fe^{II}. This spectral signature is similar to that of ferrocene, and it is common for Cp ring substituents to have few noticeable effects on Fc Mössbauer partial isomer shifts and quadrupolar splitting values.[26] The only significant differences between **1a** and free ferrocene is a slightly smaller quadrupolar splitting (E_Q) and a somewhat larger line width (Γ). The larger line width indicates the small distribution of local environments around the Fc and fcdc units that would be expected for a polymeric material. The different quadrupolar splitting could be evidence of subtle effects on the electric field gradient at the Fe^{II} center in fcdc that arise from the electron withdrawing *ortho*-carboxylate substituents (and the U^{VI} attachment). However, Mössbauer data reported for FCA displays chemical shift, quadrupolar splitting, and line width parameters comparable to ferrocene and **1a**.[27]

This nuclear spectroscopic study is inconclusive in assigning two distinct iron environments in the crystal structure, persumably due to the similar bis-Cp coordination sites. Ferrocene Mössbauer has been extensively studied, however, to the best of our knowledge only one report has examined the behavior of a structurally characterized compound containing two distinct ferrocene environments that differ in the ring substituents but could not be resolved spectroscopically.[28] This fact makes it difficult to establish any structural exchange for **1a** in the solid state on the Mössbauer timescale between 85 and 250 K. One final important observation about the Mössbauer spectroscopic study is the absence of any

spectral features indicative of a cationic ferrocenium species over the entire temperature range employed, since Fe^{III} would be expected to have a negative isomer shift and a larger magnitude of closely spaced bands relative to Fe^{II}.[29]

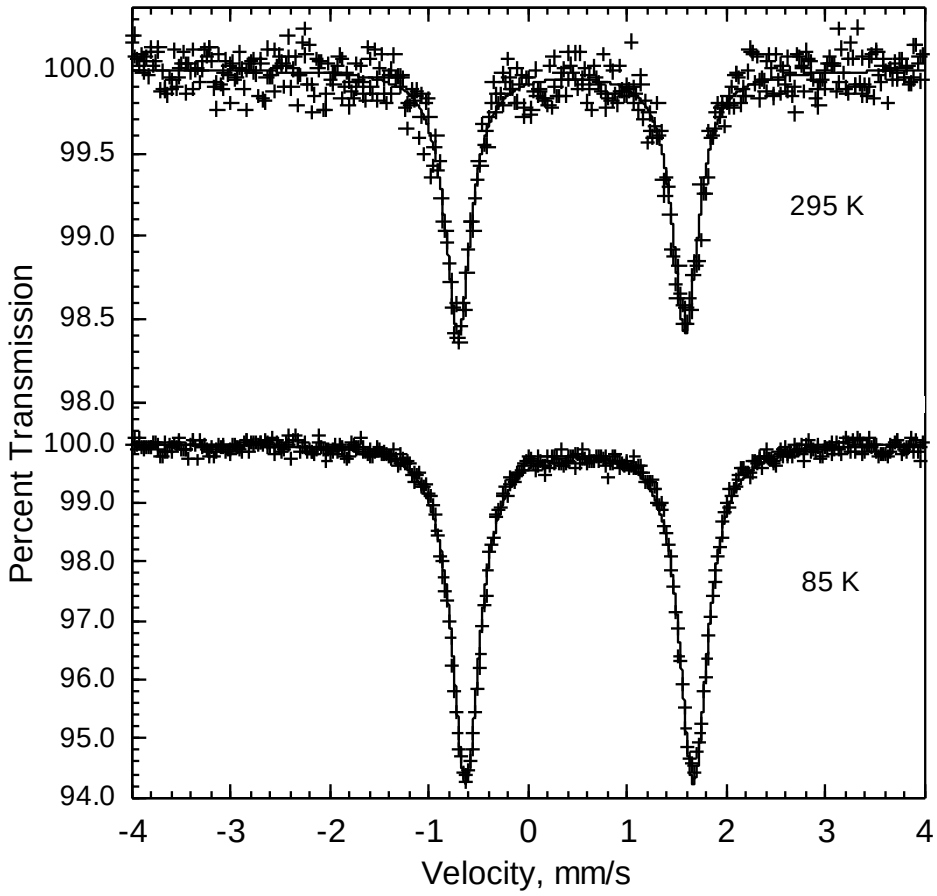

Figure 3.7. ^{57}Fe Mössbauer spectrum for **1a** at 295K and 85K referenced to metallic Fe.

Table 3.2. Mössbauer spectral hyperfine parameters for **1a**, Fc, and FCA

Compound	*T*, K	δ, mm/s[a]	E_Q, mm/s	Γ mm/s	*Area*, (%ε)(mm/s)
1a	295	0.442	2.29	0.32	1.539
	225	0.470	2.29	0.33	2.653
	155	0.497	2.29	0.33	3.837
	85	0.521	2.30	0.34	5.972
FCA[26]	80	0.450	2.21	0.34	-
Fc[b]	295	0.447	2.40	0.23	-
	85	0.533	2.40	0.26	-

[a] Isomer shifts relative to room temperature α-iron foil.
[b] Fc spectrum measured here is comparable to reference [27].

The coordination polymer **1** is soluble in methanol (MeOH), methylene chloride, chloroform, acetonitrile (MeCN), dimethylsulfoxide (DMSO), dimethylformamide (DMF), and considerably less soluble in THF and benzene. When the reaction mixture is dried to completeness, a small amount of ferrocene can be extracted using low polarity solvents, however, interstitial ferrocene cannot be extracted nor sublimed from the analytically pure polymer. Addition of THF or 2-methyl-THF to a solution of **1** in methanol or methylene chloride induces recrystallization. Thus, **1** is a reversibly soluble coordination polymer that disassembles upon dissolution and recombines via recrystallization in the presence of capping THF ligand. The molar mass of **1** in solution is unknown, however interpretation of variable temperature (VT) NMR and solution IR data below ascertain the structural characteristics and account for the formation of **1**.

The ^{1}H NMR spectrum of **1** at ambient temperature in solution displays broadened peaks in the ferrocene chemical shift region (4-6 ppm) that cannot be strictly assigned to fcdc, FCA, nor Fc,[30] suggestive of facile exchange on the NMR timescale. Interpretation of variable temperature (VT) NMR spectra reveals a solvent dependent fluxional interconversion between these species that produces the fcdc and Fc units observed in the solid state structure. The concerted mechanism for this transformation is identified in **Scheme 3.2**, in which initial coordination of an FCA ligand to uranyl(VI) is followed by exchange of a carboxylate for an α-hydrogen atom with a neighboring FCA.

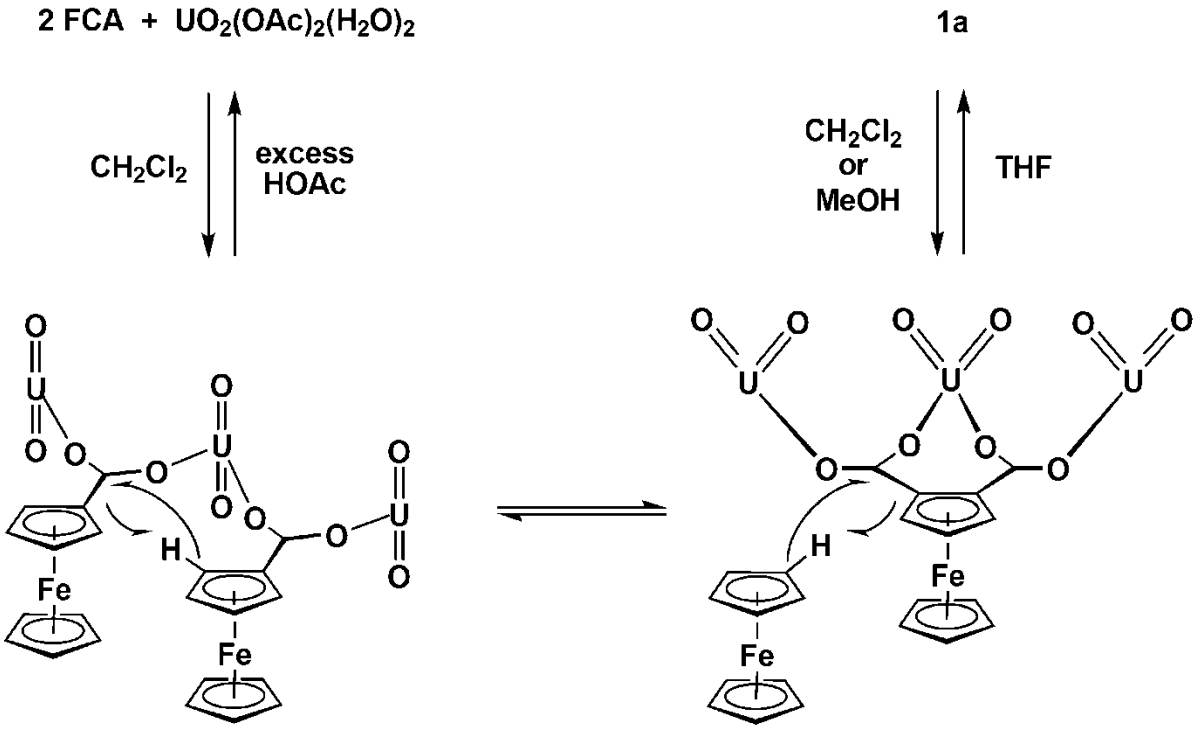

Scheme 3.2. Solvent-dependent mechanism describing the carboxylate abstraction responsible for the formation and reversible solubility of **1**.

Seven distinct types of Cp ring proton resonances in three chemical shift regions would designate the three ferrocene derivatives in equilibrium. The fcdc ligand should

display a 5:2:1 integration ratio, whereas FCA would give rise to a 5:2:2 (10:4:4 for two equivalents) integration ratio, and Fc would display an intense singlet due to the ten equivalent ring protons.[30] In methanol-d_4, three broadened peaks (~5.2, ~4.7, ~4.2 ppm) observed at room temperature signify a rapid exchange rate on the NMR timescale and averaged resonances. When heated to 55 ºC the three peaks sharpen, as is commonplace for coalescence features.[31] Upon cooling to -70 ºC, the slow exchange limit is approached and these three broadened peaks divide into seven more narrow overlapping resonances as discerned in **Figure 3.8**.

The considerable degree of peak overlap at low temperatures and the lack of a single coalescence point at elevated temperature hinder spectral line shape analysis (i.e., width, integration, coupling constants) and precludes measurement of rate and equilibrium constants to extract accurate quantitative kinetic and thermodynamic characteristics. In accordance with Le Chatelier's principle, when additional ferrocene is administered the peak integrations in the 4.7 and 5.2 ppm substituted Cp ring chemical shift regimes are perturbed, presumably favoring the left side of the equilibrium in Scheme 3.2 and the growth of FCA. Moreover, when **1** is dissolved in glacial acetic acid, FCA and uranyl acetate are recovered, further supporting the viability for the concerted fluctuation in solution.

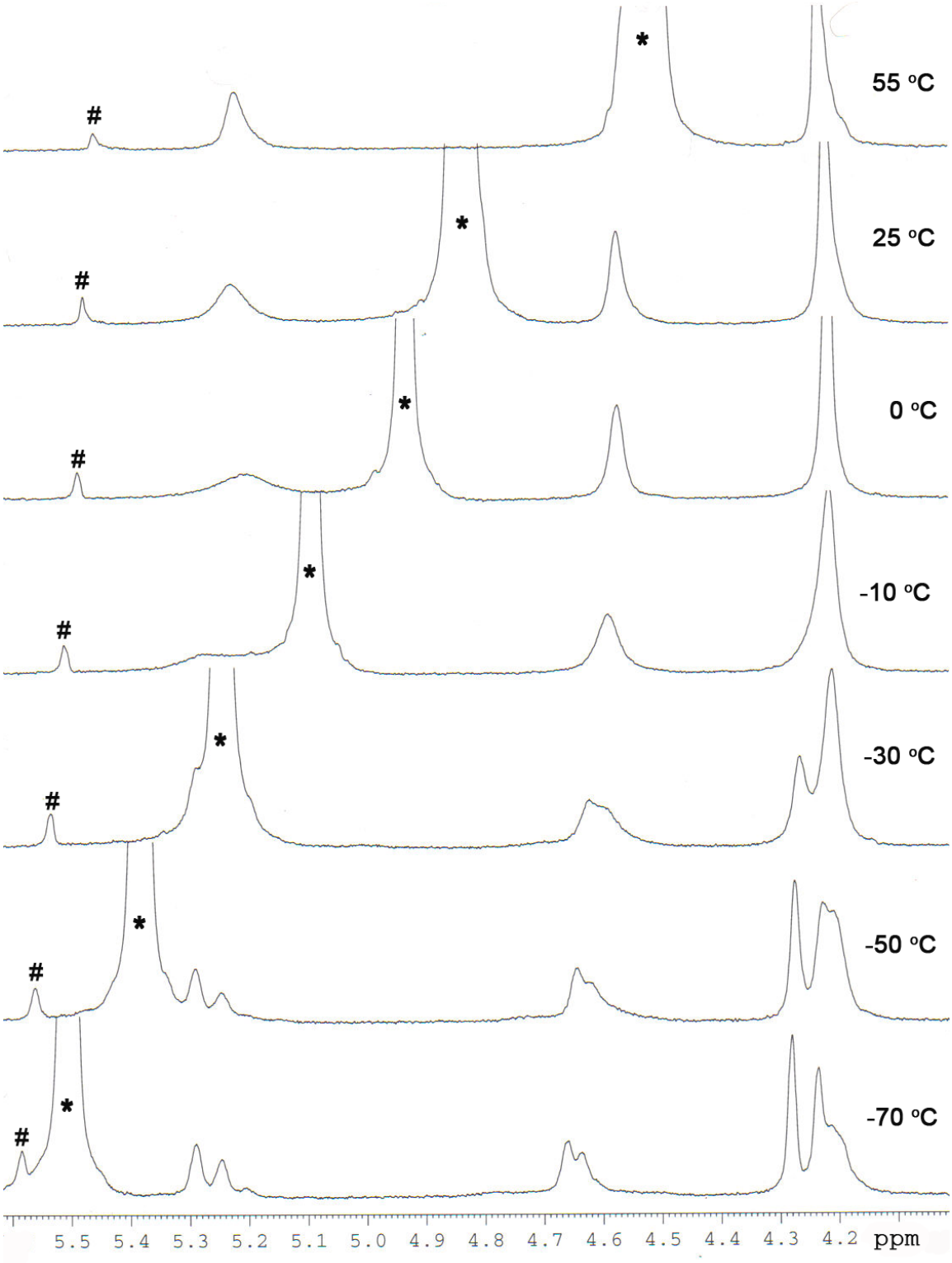

Figure 3.8. VT-^{1}H NMR of **1a** in MeOH-d_4. Asterisks (*) denote coordinated protic MeOH whereas hash (#) marks are attributed to an impurity of unknown composition.

Methanol is an adequate donor solvent for actinyl ions, and the intense peak at 4.9 ppm at 25 ºC is indicative of coordinated MeOH. Upon heating, this peak shifts upfield towards coalescence with free methanol. Methanol inhibits the fluxional process outlined in Scheme 3.2, and slow conversion is observed at low temperatures. Likewise, DMSO is a potent donor solvent and the slow exchange is detected at ambient temperature, however the presence of additional peaks implies that DMSO coordination might obstruct the process to create multiple species (**Figure S3.3**). When a solution of **1** in DMSO-d_6 is heated these peaks broaden, characteristic of facile exchange. In contrast, when conducted in methylene chloride or chloroform (**Figure S3.4**) fast exchange is observed across the entire range of temperature trials since these solvents lack the ability to coordinate to uranyl and interfere with exchange. In theory, carboxylate fluctuation should be easily followed by VT ^{13}C NMR using the carboxylate spectroscopic handle. However, preliminary studies using a ^{13}C-labeled version of FCA are unable to clarify any exchange in the carboxylate chemical shift region ~180 ppm (**Figure S3.5**).[32]

Scheme 3.2 outlines a process that involves substantial steric congestion at the uranium center that would be most easily be accommodated if the small oxide ligands bend out of the way rather than having the fluctuation restricted around the *trans* uranyl equator. The low energy barrier of rotation about the (Cp)C-C(CO_2) single bond provides a measure of overcrowding directed parallel to the linear uranyl, and may assist in repelling the oxide ligands. This rotational ability prompted us to utilize the FCA ligand initially, to serve as a bulky redox active functionality to shield the uranyl ion. The reversible carboxylate abstraction that transforms the fcdc ligand is instrumental in driving the severe bend in the

uranyl unit and this concerted mechanism is also the template that strings the polymer together.

While the fluxional carboxylate migration in Scheme 3.2 has not been described previously, there is precedence for photolytic cleavage of ferrocene ring substituents when appended with electron withdrawing functionalities (i.e., $–CO_2^-$), and FCA complexes are commonly synthesized in the dark to avoid decomposition pathways.[33,34] This conjecture is further evidenced by the elongated Cp-CO_2 (1.574(18) Å) bond distance in the solid state, indicating the susceptibility of this site. This bond elongation is also suggestive of a degree of electronic delocalization involved in the carboxylate-U^{VI} interaction. On the other hand, uranyl(VI)-carboxylate complexes are also photolytically sensitive,[35] however, compound **1** is produced regardless of whether or not the reaction mixture is exposed to a light source. The C-C and C-H bond cleavage responsible for the generation of the fcdc ligand is likely driven by the extensive C-H$^{\cdots}\pi$ bonding network observed in the solid state network.

The infrared spectrum of **1** in methanol (**Figure S3.6**) shows two strong absorptions at 915 and 896 cm^{-1} that suggests the *cis* isomer is present in solution while the reversible carboxylate fluctuation is ongoing. These peaks are slightly shifted with respect to the solid material, which accounts for the methanol adduct observed in NMR spectra. This behavior is analogous to the *trans*-uranyl isomer, where the linear geometry is retained in solution and the solid state with no sign of isomerization.[36] In methylene chloride one absorption at 910 cm^{-1} is observed and the peak-shape appears to be a convolution of two overlapping bands.

1 was prepared on the benchtop in the presence of trace amounts of moisture, and the material does not appreciably decay in air in the solid state nor in solution, though the addition of excessive water decomposes the polymer into an unidentified brown intractable

material. The fact that the solid material is indefinitely stable in air is curious since all uranium containing materials react in air to afford *trans*-uranyl(VI) species. **1** can be prepared from anhydrous uranyl acetate, which excludes hydration as a significant participant in the formation of the coordination polymer. The ferrocene species decompose in the prescence of acids, whereas the addition of strong bases afford intractable yellow material suggestive of a uranyl(VI) hydroxide oligomer. Preliminary reactivity studies suggest that **1** is remarkably unreactive with reagents that typically abstract oxo ligands from *cis*-dioxo complexes (i.e., primary amines and phosphines), highlighting the strength and inert tendencies of the multiply bound *cis*-UO_2^{2+} unit and its carboxylate attachments. The reactivity trends for the *cis*-uranyl unit deserve extensive exploration, especially in light of the chemical activity observed for transition metal –yl type ions (i.e., oxide nucleophilicity and redox coupled oxide abstraction).[37]

Electrochemistry

Cyclic voltammetric data acquired for **1** portrays two electroactive species in solution. A *quasi*-reversible oxidative wave present at 0.05 V with respect to the $Ag^{+/0}$ couple is attributed to the ferrocene/ferrocenium couple (**Figure S3.7**). This signal is broad owing to the interconversion of three ferrocene derivatives in solution, and additional Fc obstructs the shape of this wave. In contrast, it is common for Fc compounds to display facile electron transfer kinetics within a similar potential range.[38] The uranyl(VI/V) redox couple for **1** is irreversible in methylene chloride at -1.74 V in **Figure 3.9**, yet displays a slight *quasi*-reversibility in methanol near the same potential. It should be noted that the reduction of the *cis*-uranyl(VI) unit in **1** requires energetics comparable to neutral *trans*-uranyl(VI)

complexes, for example the neutral uranyl(VI) Schiff base-phenolate complexes in Chapter 2 display a uranyl(VI/V) redox couple near -1.6 V. However, **1** is not well-behaved on the voltammetric timescale in reference to discrete molecular uranyl(VI) carboxylate compounds.[39] Uranyl reduction in **1** hinders the ferrocene wave, and vice-versa, when the two species are electrolyzed consecutively, which expresses some extent of redox interplay between the two metal units. The use of chemical redox agents to activate the processes observed in voltammetric studies have been hampered by decomposition.

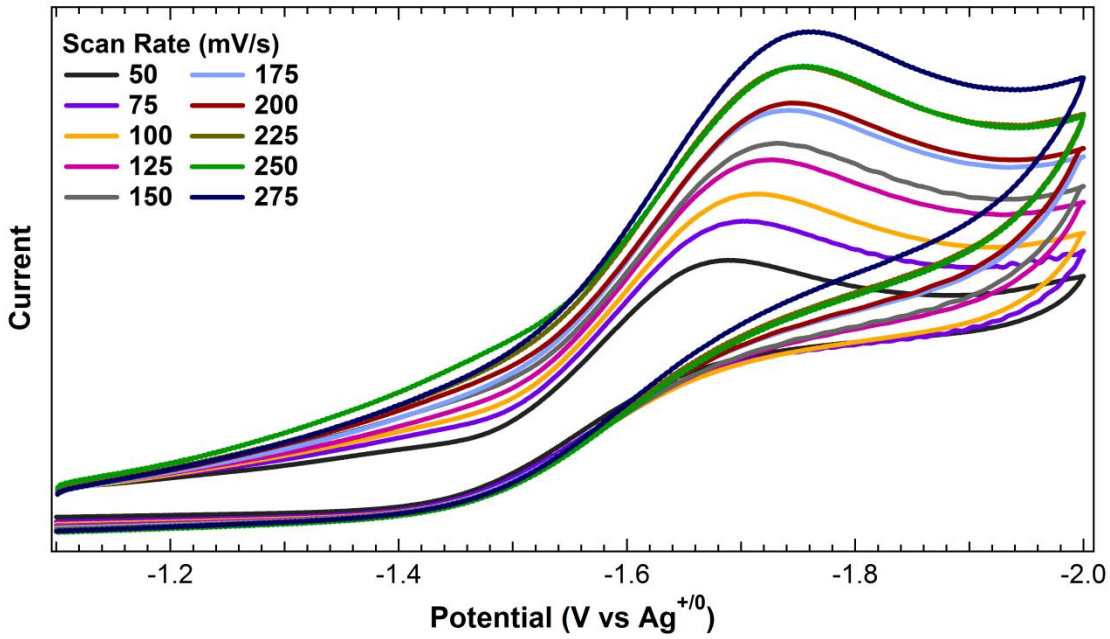

Figure 3.9. Cyclic Voltammogram for **1a** in ~0.1 M $[Bu_4N][PF_6]/MeCl_2$ solution at room temperature with a scan rate range of 50-275 mV/s.

Electronic Spectroscopy

Electronic absorption and emission spectroscopies are often employed to evaluate electronic structure and bonding in uranyl(VI) ion complexes.[8,18] We intended to probe **1** accordingly to gain insight on the nature of the metal based valence orbitals involved in

covalent bonding in the *cis*-uranyl(VI) geometry. However, the UV-visible photophysical behavior is evidently overwhelmed by the presence of ferrocene units. The absorption spectrum of **1a** is virtually indistinguishable from that of free FCA in solution and in the solid state as portrayed **Figure 3.10**, and is also on par with literature reports of complexes that contain the FCA ligand.[40] The only difference between the two spectra in Figure 3.11 is the more intense broad peaks for **1** than FCA that tail further into the visible region. This may account for the red-orange color of **1**, whereas ferrocene species display hallmark orange colors. Ligand-to-metal charge transfer (LMCT) inherent to the UV and visible regions for uranyl(VI) and other U-O bound species are masked by the broad and intense FCA based absorption features.

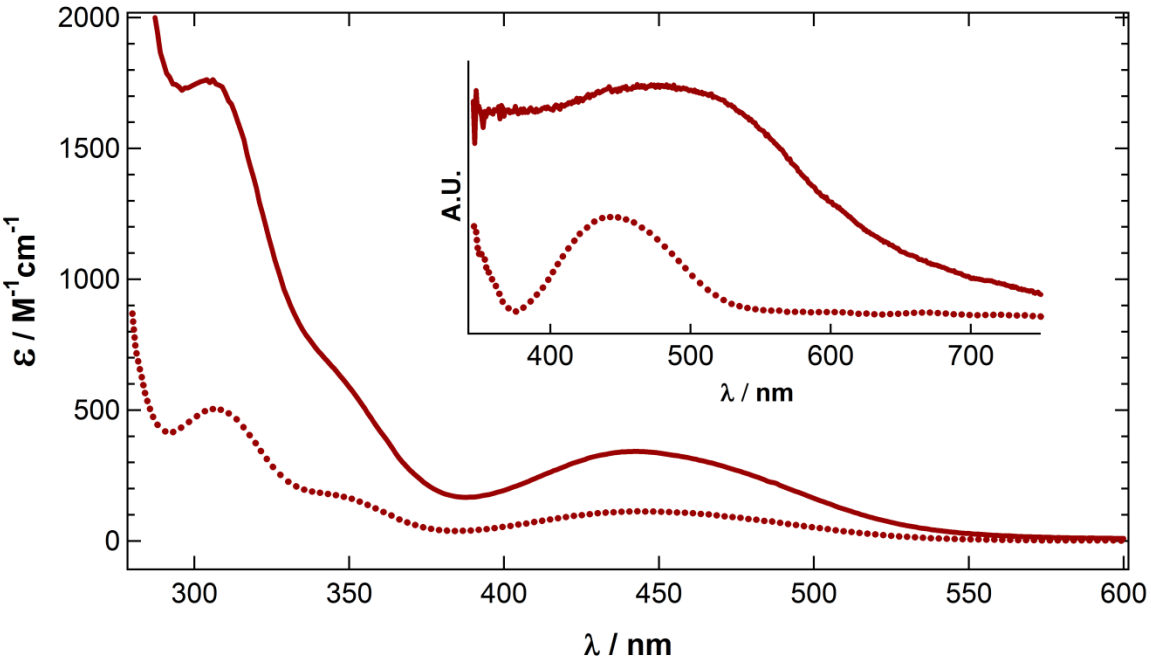

Figure 3.10. UV-visible absorption spectra for **FCA** (dashed) and **1a** (solid) in MeOH. Inlay (top right) depicts the respective solid state diffuse reflectance absorption profiles.

1 exhibits two luminescent features in solution. When excited at 245 nm a broad intense emission band is detected at 365 nm that is characteristic of ferrocene carboxylate species.[41] When excited at 345 nm in methanol a broad lower energy luminescence centered at 480 nm is observed in **Figure 3.11**, whereas in methylene chloride only the ferrocene based fluorescence prevails. The source of the emission at 480 nm is unknown at this juncture, however, *trans*-uranyl(VI) species commonly display long-lived green fluorescence.[42] In comparison, this process is slightly blue shifted with respect to that of *trans*-uranyl, but the excitation profile resembles the LMCT observed in uranyl chemistry. Solid state luminescence experiments carried out at ambient temperature exhibit only ferrocene based emission at variable excitation wavelength (**Figure S3.8)**, with no sign of lower energy fluorescence of uranyl(VI) origin.

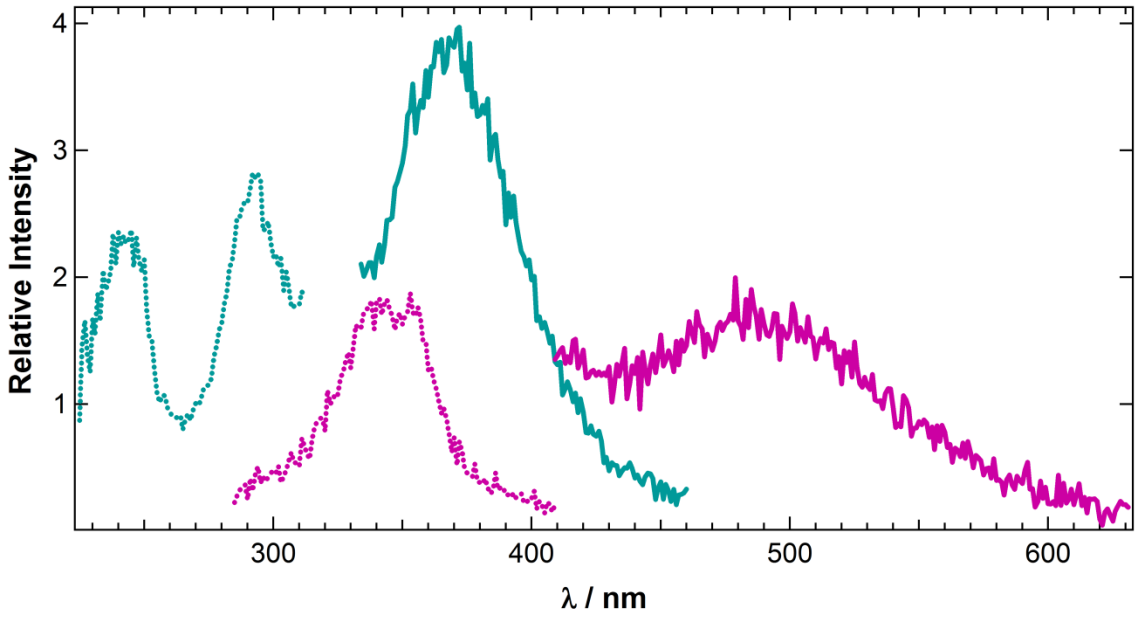

Figure 3.11. Excitation (dashed) and emission (solid) spectra for **1a** in MeOH. Fc based luminescence (blue), and emission of possible *cis*-uranyl (pink).

Non-radiative energy transfer markedly decreases UO_2^{2+} photolytic efficiency, yet it is well established that uranyl carboxylate species are photoactive under a variety of aerobic and nonaqueous conditions.[35,43,44] With regard to extensive reports on fluorescent uranyl(VI)-carboxylate polymers, our attempts at identifying room temperature solid state uranyl(VI) emission were met with unanticipated hindrance from the overwhelming Fc based signal. Since **1** contains three potential sources for uranyl reduction (i.e., Fc, fcdc, and RCO_2) one might expect an opportunity for synthetic photo-reductive interplay in this new uranyl coordination polymer. On the contrary, it seems counterintuitive that a solution of **1** in methanol does not photolyze over a period of four days to at least yield intractable material, in contrast to most *trans*-uranyl(VI) complexes. It should be noted that the lack any distinguishable *cis*-uranyl(VI) luminescence and photoreactivity could perhaps be caused by either a redox quenching mechanism from the Fc metallocene unit, which is known to quench uranyl(VI) fluorescence,[45] or an excited state manifold that lacks predominant 5f nonbonding character that is intrinsic to uranyl ion luminescence.[46] The analogous transition metal congener $Mo^{VI}O_2^{2+}$ is not a luminescent nor photoreactive moiety due to non-radiative decay of the photoexcited state.[47] This connection reveals the nature of the valence orbital bonding for *cis*-actinyl species might be in large part comprised of 6d orbital character to maximize bonding. Further studies to unravel these details are ongoing in our lab.

3.3 Conclusion

In summary, **1** is the first reported complex containing a severely bent uranyl(VI) unit that was synthesized on the benchtop and crystallized directly from the reaction mixture. The bent uranyl(VI) units are supported within a carboxylate bridged coordination polymer that

displays reversible solubility. The short terminal oxo groups observed in the solid structure are reflected in the υ_s and υ_{as} stretches in the IR spectrum, and solution IR provides evidence that the bent geometry is retained upon dissolution. The proposed mechanism that leads to the solid state characteristics entails bending of the *trans*-UO_2^{2+} group by the bulky Fc units coupled with an FCA transformation. The fluxional carboxylate migration abstraction process that accounts for the reversible solubility and formation of the fcdc and Fc from FCA is borne out of VT-^{1}H NMR spectroscopic measurements, however ^{13}C NMR experiments are inconclusive. TGA supports the extensive hydrogen bonding motif caused by the ability of Fc to hold the polymer chains into a 3-dimensional network, whereas ^{57}Fe Mössbauer spectroscopy is inconclusive in assigning two distinct ferrocene environments.

Sluggish electron transfer kinetics attributed to the ferrocene/ferrocenium and uranyl(VI/V) couples fall within the predicted potential window. Electronic absorption and emission spectroscopies are dominated by the ferrocene moieties and uranyl(VI) properties are masked. The unforeseen lack of photolytic activation is suggestive of excited state behavior that contrasts with traditional uranyl(VI) carboxylate complexes. The likely cause for this difference is enhanced covalent overlap between O(2p) and U(6d) versus U(5f) valence orbitals. Our current stance is aimed at further scrutinizing the physicochemical properties of this moiety, extending the *cis-trans* isomerism trend for other actinyl ions, and exploring potential chemical applications associated with the bent disposition.

Acknowledgment. The author thanks Drs. G. Long (University of Missouri-Rolla), F. Grandjean (University of Liège, Belgium), and C. Cahill and M. Frisch (George Washington University) for collaboration on Mössbauer and solid-state luminescence studies,

respectfully. This research, performed at the University of Missouri-Columbia Chemistry Department, was supported by the ACS Petroleum Research Fund and the University of Missouri Research Board.

Supporting Information Available: Crystallographic information for 1a, and **Figures S3.1-S3.8** are provided in appendix 2 on CD-ROM.

3.4 Experimental

General Considerations

Unless otherwise stated all synthetic manipulations were performed under ambient atmospheric conditions on the benchtop, and the samples stored in the drybox referenced in Chapter 2. Depleted uranium (^{238}U) is a weak α-emitter (4.197 MeV) with a half-life of 4.47 x 10^9 y, and should be handled in a fume hood or in a drybox contained in an area regularly monitored for radioactive isotope management. $UO_2(OAc)_2(H_2O)_2$, ferrocene, and all solvents were received from reputable commercial sources and used without further purification. Anhydrous-$UO_2(OAc)_2$, FCA, and ^{13}C-FCA were prepared in accordance with previously documented accounts.[34,51,52]

Sample and Instrumentation Protocol

VT ^{1}H and ^{13}C NMR spectra (referenced to protio impurity in deuterated solvent) were recorded on a Bruker AMX-250, -300, or -500MHz spectrometer and radioactive samples were handled in sealed Teflon inserts. Chemicals shifts are reported in ppm and all coupling constants and peak shapes are reported in Hertz unless otherwise noted. Infrared spectra were obtained as nujol mull in a mixture of type NVH and type B immersion oil or in

saturated solution pressed between KBr plates on a Thermo Nicolet Nexus 670 FT-IR spectrometer. Elemental analysis was performed by Desert Analytics (Tuscon, AZ). Thermogravimetric analysis was conducted using a Cahn TA-50 microbalance by heating the material at 5 ºC/min in a flowing dinitrogen atmosphere.

Mössbauer spectroscopy was performed at Fonds National de la Recherche Scientifique. Data was collected on 47 mg/cm^2 of powdered sample mixed with boron nitride. The spectra were obtained between 85 and 295 K on a constant-acceleration spectrometer that utilized a room temperature rhodium matrix cobalt-57 source and was calibrated at room temperature with α-iron foil. The estimated relative errors are ±0.005 mm/s for the isomer shifts, ±0.01 mm/s for the quadrupole splittings and line widths, and ±0.005 (% ε)(mm/s) for the spectral absorption area. The absolute errors are approximately twice as large. A linear fit of the temperature dependence of the isomer shift yields a slope of -3.77×10^{-4} (mm/s)/K and a corresponding iron effective vibrating mass of 110(5) g/mol. A linear fit of the temperature dependence of the logarithm of the spectral absorption area yields a slope of -6.34×10^{-3} 1/K and a corresponding Mössbauer temperature of 105(10) K. Both the effective vibrating mass and the Mössbauer temperature are similar to the values of 86 g/mol and 130 K observed for ferrocene

Cyclic voltammetric studies were performed with a Bioanalytic Systems Epsilon EC-2000-Xp C3 model potentiostat/galvanostat under computer control using BAS software. Samples were run in dry solvents in the drybox in ~0.1 M [*n*-Bu_4][PF_6] solution at a ~3 mm platinum or graphite working electrode with a Ag/Ag^+ reference electrode (0.01 M $AgNO_3$) contained in a Teflon-sealed Vycor bridge and a Pt wire auxiliary electrode.

UV-visible spectra were taken in solution on an HP 8453 with diode-array deuterium (UV) and tungsten (Vis) lamps and Chemstation analysis software. Solid state UV-visible spectra were recorded on a Cary 3 diode array spectrophotometer using the diffuse reflectance accessory with a barium sulfate reference. Luminescence data was obtained on a Varian Fluorescence Fluorometer with quartz solution cuvets with a 1.0 cm pathlength, using the Cary Eclipse Scan Application. The excitation source was a 15 W Xenon arc lamp pulsed at 80 Hz. The excitation and emission monochromators were set to a step size of 10 and 2 nm, respectively, with a bandpass of 5 nm, collecting from 250 – 600 and 300 – 700 nm, respectively. All photophysical measurements were obtained at ambient temperature and samples and solvents were run separately to ensure the observed spectrum were attributable to complexes and not solvent impurities. Solid state luminescence was performed at George Washington University on a Shimadzu RF-5301 PC spectrofluorophotometer. The excitation source was a Xenon lamp and emissions were collected from 400-800nm. Excitation and emission monochromators were set to a slit width of 1.5 nm and 3.0 nm, respectively. Data was collected on a pressed pellet of **1** with KBR. Trial photochemical reactions were conducted with an Ace Glass reactor assembly outfitted with a 450 W Hg vapor lamp in a quartz immersion well contained within a photochemical safety cabinet.

Powder XRD data was collected on a Scintag X_2 system at 40 kV and 30 mA for Cu ($K\alpha$ = 1.540562 Å). A continuous scan was taken over a 2θ range of 20-90° at 2.5°/min. The calculated powder XRD pattern was simulated using the Lazy Pulverix interface with SHELX. Single crystals, as determined by polarized optical microscopy, were immersed in degassed hydrocarbon oil and mounted on a thin glass fiber using silicon grease. Full hemispheres of data were then collected at -100 ^{o}C on a Bruker SMART system equipped

with a CCD Area Detector system using ω scan technique with K_α radiation from molybdenum (λ = 0.7073 Å) from a graphite monochromator. Intensities were corrected for Lorentz and polarization effects, equivalent reflections were merged, and absorption corrections were applied using the multi-scan application. Structures were solved using direct methods with the SHELX package and then refined using a full least squares treatment of F^2.[53] All non-hydrogen atoms were refined with anisotropic thermal parameters. Hydrogen atoms were placed at the calculated positions and included in refinement using a riding model, with fixed isotropic *U*. The final difference map contained no features of chemical significance. Complete crystallographic data collection and refinement details are provided in Appendix 2.

Synthetic Details

Synthesis of $[UO_2(fcdc)(THF)\bullet(Fc)]_n$ (1a): Uranyl acetate dihydrate (100 mg, 0.234 mmol) was added to a stirring suspension of ferrocenemonocarboxylic acid (108 mg, 0.471 mmol) in methylene chloride (5 mL). Tetrahydrofuran (5 mL) was added and the mixture stirred for 12 h. The resulting red solution evaporated to yield (155.4 mg, 0.194 mmol, 83%) tiny red-orange crystals of **1a** suitable for x-ray analysis. ^{1}H NMR δ (MeOD-d_8, 25ºC) 5.23br, 4.93br, 4.6br, 4.2br, 3.65 (t, 4H), 1.78 (t, 4H). IR (Nujol, cm^{-1}) 915 $\upsilon_{U=O}$, 934 $\upsilon_{U=O}$, 1472 υ_{C-O}, 1519 υ_{C-O} (MeOH, cm^{-1}) 917 $\upsilon_{U=O}$, 896 $\upsilon_{U=O,}$ ($MeCl_2$, cm^{-1}) 915(br) $\upsilon_{U=O.}$ Elemental analysis (%) calcd. C 39.02, H 3.28, found C 38.33, H 3.29. Eº ($MeCl_2$) = -1.75 V (I), 0.7 V (QR), Eº (MeOH) = -1.66 V (QR), -0.45 V (QR).

Synthesis of $[UO_2(fcdc)(2\text{-methyl-THF})\bullet(Fc)]_n$ (1b): **1b** was prepared analogous to **1a** with the exception that (5 mL) 2-methyl-tetrahydrofuran was used in place of tetrahydrofuran. **1b**

could not be obtained in an analytically pure form due to the high degree of solubility in the crystallization solution. IR (Nujol, cm^{-1}) 917 $\upsilon_{U\text{-}O}$, 936 $\upsilon_{U\text{-}O.}$ Voltammetric, NMR, solution IR, and photophysical data are analogous to **1a**.

References

[1] (a) Clark, D. L.; Gordon, J. C.; Hay, P. J.; Poli, R. *Organomet.* **2005**, *24*, 5747-5758. (b) Burns, C. J. *Science* **2005**, *309*, 1823-1824.

[2] (a) Arney, D. S. J.; Burns, C. J. *J. Am. Chem. Soc.* **1995**, *117*, 9448-9460. Also see reference [36]. (b) Hayton, T. W.; Boncella, J. M.; Scott, B. L.; Palmer, P. D.; Batista, E. R.; Hay, P. J. *Science*, **2005**, *310*, 1941-1943. (c) Hayton, T. W.; Boncella, J. M.; Scott, B. L.; Batista, E. R.; Hay, P. J. *J. Am. Chem. Soc.* **2006**, *128*, 10549-10559. (d) Hayton, T. W.; Boncella, J. M.; Scott, B. L.; Batista, E. R. *J. Am. Chem. Soc.* **2006**, *128*, 12622-12623.

[3] (a) Cotton, F. A.; Wing, R. M. *Inorg. Chem.* **1965**, *4*, 867-873. (b) Tatsumi, K.; Hoffman, R. *Inorg. Chem.* **1980**, *19*, 2656-2658.

[4] (a) Sarsfield, M. J.; Helliwell, M.; Raftery, J. *Inorg. Chem.* **2004**, *43*, 3170-3179. (b) Sarsfield, M. J.; Helliwell, M. *J. Am. Chem. Soc.* **2004**, *126*, 1036-1037.

[5] Maynadié, J.; Berthet, J. C.; Thuéry, P.; Ephritikhine, M. *Chem. Commun.*, **2007**, 486 – 488.

[6] Duval, P. B.; Burns, C. J.; Clark, D. L.; Morris, D. E.; Scott, B. L.; Thompson, J. D.; Werkema, E. L.; Jia, L.; Andersen, R. A. *Angew. Chem. Int. Ed.* **2001**, *40*, 3357-3361, and references therein.

[7] (a) Schreckenbach, G.; Hay, P. J.; Martin, R. L. *Inorg. Chem.* **1998**, *37*, 4442-4451. (b) Hratchian, H. P.; Sonnenberg, J. L.; Hay, P. J.; Martin, R. L.; Bursten, B. E.; Schlegel, H. B. *J. Phys. Chem. A* **2005**, *109*, 8579-8586. (c) Schreckenbach, G.; Hay, P. J.; Martin, R. L. *J. Comp. Chem.* **1999**, *20*, 70-90.

[8] (a) Wilkerson, M. P.; et al *Inorg. Chem.* **2000**, *39*, 5277-5285. (b) Clark, D. L.; Conradson, S. D.; Donohoe, R. J.; Keogh, D. W.; Morris, D. E.; Palmer, P. D.; Rogers, R. D.; Tait, C. D. *Inorg. Chem.* **1999**, *38*, 1456-1466. (c) Wilkerson, M. P.; Burns, C. J.; Morris, D. E.; Paine, R. T.; Scott, B. L. *Inorg. Chem.* **2002**, *41*, 3110-3120.

[9] (a) Ram, M. S.; Hupp, J. T. *Inorg. Chem.* **1991**, *30*, 130-131. (b) Dyall, K. G. *Mol. Physics* **1999**, *36*, 511-518. (b) Wadt, W. R. *J. Am. Chem. Soc.*, **1981**, *103*, 6053-6057. (c) DuMez, D. D.; Mayer, J. M. *Inorg. Chem.* **1998**, 37, 445-453.

[10] (a) Cahill, C. L.; Borkowski, L. A. *Inorg. Chem.* **2003**, *42*, 7041-7045 and references therein. (b) Hardiman, C. J.; Archer, R. D. *Macromolecules*, **1987**, *20*, 1527-1534.

[11] Dunitz, J. D.; Orgel, L. E.; Rich, A. *Acta Cryst.* **1956**, *9*, 373.

[12] (a) Cp-CO_2H bond distance in free FCA is 1.407(2) Å in (a) Cotton, F. A.; Reid, A. H. *Acta Cryst.* **1985**, *C41*, 686-688. (b) How, H.; Li, G.; Li, L.; Zhu, Y.; Meng, X.; Fan, X. *Inorg. Chem.* **2003**, *42*, 428-435.

[13] Roling, P. V.; Rausch, M. D. *J. Org. Chem.* **1974**, *39*, 1420-1424.

[14] Cotton, S. *Lanthanide and Actinide Chemistry*, England, 2006; pp 173-196. Also see references [17, 37, 41].

[15] Thuéry, P. *Chem. Commun.* **2006**, 853-855.

[16] Wilkerson, M. P.; Burns, C. J.; Paine, R. T.; Scott, B. L. *Inorg. Chem.* **1999**, *38*, 4156-4158.

[17] Kaltsoyannis, N.; Scott, P. *The f elements*, Oxford, **1999**, pp 52, and references therein

[18] For a comprehensive review on electronic structure of uranyl(VI) complexes, see; Denning, R. G. *Struct. Bonding* **1992**, *79*, 215-275.

[19] Ryan, R. R.; Mastin, S. H.; Reisfeld, M. J. *Acta Cryst.* **1971**, *B27*, 1270-1274.

[20] Stiefel, E. I.; Miller, K. F.; Bruce, A. E.; Corbin, J. L.; Berg, J. M.; Hodgson, K. O. *J. Am. Chem. Soc.* **1980**, *102*, 3624-3626.

[21] Borowski, L. A.; Cahill, C. L. *Crystal Growth & Design* **2006**, *6*, 2241-2247.

[22] Moore, F. W.; Rice, R. E. *Inorg. Chem*. **1968**, *7*, 2510-2514.

[23] Griffith, W. P. *J. Chem. Soc. A, Inorg. Phys. Theor.* **1969**, 211-217.

[24] (a) Quiles, F.; Burneau, A. *Vibrational Spec.* **1998**, *18*, 61-75.

[25] (a) Bullock, J. I. *J. Chem. Soc. A, Inorg. Phys. Theor.* **1969**, 781-784. (b) Nguyen-Trung, C.; Begun, G. M.; Palmer, D. A. *Inorg. Chem.* **1992**, *31*, 5280-5287.

[26] (a) Herber, R. H.; Nowik, I. *Solid State Sci*. **2002**, *4*, 691-694. (b) Bullita, E. *Inorg. Chim. Acta* **1999**, *287*, 117-133.

[27] Bickar, D.; Lukas, B.; Roberts, R.; Silver, J. *J. Organomet. Chem.* **1984**, *263*, 225-234.

[28] Tárraga, A.; Molina, P.; López, J. L.; Espinosa, A.; Evans, D. J. *Tet. Letters* **2002**, *43*, 4717–4720.

[29] Schnitzler, M. C.; Mangrich, A. S.; Macedo, W. A. A.; Ardisson, J. D.; Zarbin, A. J. G. *Inorg. Chem*. **2006**, *45*, 10642-10650.

[30] ^{1}H NMR data for Fc and substituted derivatives are evaluated in the reference; Pickett, T. E.; Richards, C. J. *Tet. Letters* **1999**, *40*, 5251-5254, and references therein.

[31] Drago, R. S. *Physical Methods for Chemists*, 2nd ed.; Saunders, Philidelphia, **1992**, pp 290-352.

[32] ^{13}C NMR for an FCA complex ($CDCl_3$, δ, ppm 180.5 CO_2) in reference; Bailey, A.; Shang, M.; Fehlner, T. P. Inorg. Chem. 2000, 39, 4374-4376. No ^{13}C NMR data is available for the fcdc ligand.

[33] Dong, G.; Yu-ting, L.; Chun-ying, D.; Hong, M.; Qing-jin, M. *Inorg. Chem.* **2003**, *42*, 2519-2530 and references therein.

[34] Benkeser, R. A.; Goggin, D.; Schroll, G. *J. Am. Chem. Soc.* **1954**, *76*, 4025 – 4026.

[35] McCleskey, T. M.; Foreman, T. M.; Hallman, E. E.; Burns, C. J.; Sauer, N. N. *Environ. Sci. & Technol.* **2001**, *35*, 547-551.

[36] Choppin, G. R.; Jensen, M. P. Actinides in Solution: Complexation and Kinetics. In *The Chemistry of the Actinide and Transactinide Elements*, 3rd ed.; Morss, L. R., Edelstein, N. M., Fuger, J., The Netherlands, **2006**; Vol. 5, pp 2524-2608, and references therein.

[37] Holm, R. H. *Chem. Rev.* **1987**, *87*, 1401-1449.

[38] Gange, R. R.; Koval, C. A.; Lisensky, G. C. *Inorg. Chem*. **1980**, 19, 2854-2855.

[39] Morris, D. E. *Inorg. Chem*. **2002**, 41, 3542-3547.

[40] Prokopuk, N.; Shriver, D. F. *Inorg. Chem.* **1997**, *36*, 5609-5613.

[41] Meng, X.; Li, G.; Hou, H.; Han, H.; Fan, Y.; Zhu, Y.; Du, C. *J. Organomet. Chem.* **2003**, *679*, 153-161.

[42] Burrows, H. D. *Chem. Soc. Rev.*, **1974**, 139-165.

[43] Baird, C. P.; Kemp, T. J. *Prog. React. Kin.* **1997**, *22*, 87-139.

[44] Frisch, M.; Cahill, C. L. *Dalton Trans.* **2006**, 4679-4690.

[45] Traverso, O.; Rossi, R.; Magon, L. *J. Chem. Soc., Datlon Trans.* **1978**, 569-572.

[46] Kaltsoyannis, N. *Chem. Soc. Rev.* **2003**, *32*, 9-16.

[47] Winkler, J. R. *Spectroscopy and Photochemistry of Metal-Oxo complexes*, **1983**, dissertation, Caltech.

[48] For the synthesis of anhydrous-uranyl acetate from commercial dihydrate, see; Grigor'ev, M. S.;Antpin, M. Y.; Krot, N. N. *Radiochem.* **2004**, *46*, 224-231.

[49] For an improved synthesis of FCA refer to; Neto, A. F.; et al. *Z. Anorg. Allg. Chem.* **2002**, *628*, 209-216.

[50] (a) SMART V5.051 and SAINT V5.00, Area Detector Control and Integration Software, Bruker AXS Inc., Madison, WI-53719, **1998**. (b) G. M. Sheldrick, SADABS, Bruker AXS Inc., Madison, WI-53719, **1997**. (c) Sheldrick, G. M.; *SHELXS-97: Program for Structural Solution*; University of Götten, Germany, **1997**. (d) Sheldrick, G. M.; *SHELXTL-97: Program for Structural Refinement (version 5.10)*; University of Götten, Germany, **1997**. (e) Barbour, L.; *X-SEED: Graphical interface for SHELXL*; University of Missouri-Columbia, **2001**.

Chapter 4

Uranium(V) Organometallic Imido Complexes Part I: Ligand Substitution Effects on the Electronic Structure of Organouranium(V)-Imido Complexes

Abstract

A series of organouranium(V)-imido complexes of the general formula $(C_5Me_5)_2U(=N\text{-}2,6\text{-}^{i}Pr_2\text{-}C_6H_3)L$ (L = NPh_2 (**13**), OPh (**14**), $N{=}CPh_2$ (**15**)) have been prepared from the combination of salt metathesis and protonolysis reactions with U^{V}-imido iodide precursor (**10**). This collection of complexes are based on the bent metallocene-imido framework, and substitution of unidentate monoanionic ligands (L) takes place within the metallocene wedge. Analytically pure samples of each complex have been isolated in high yield and characterized using ^{1}H NMR spectroscopy, elemental analysis, mass spectrometry, single crystal X-ray diffraction, cyclic and square wave voltammetry, UV-visible-NIR electronic absorption spectroscopy, and variable temperature magnetic susceptibility measurements. For the entire series of U^{V} derivatives both reversible $U^{VI/V}$ and $U^{V/IV}$ redox couples are observed with a constant potential separation of about 1.50 V. UV-visible electronic absorption features display a broad range of charge transfer bands, whereas narrow low intensity intra-5f transitions in the near-infrared region give a signature fingerprint of spectral bands similar to those reported for octahedral $5f^{1}$ systems. Variable temperature

magnetic susceptibility measurements illustrate subtle differences in magnetic behavior for all derivatives, and therefore the magnetically active 5f states in each complex are comparable to some extent. These studies collectively compare the structural and electronic properties for the entire assemblage, and offer interpretation that confirms that the single metal based valence electron housed within the 5f orbital manifold displays subtle sensitivity to the surrounding ligand field. In one instance, reaction between **10** and potassium phenylanalide generates the U^{VI} bis-imido species **16**.

4.1 Introduction

The early actinides have gained considerable stature in organometallic chemistry in large part due to participation of 5f valence orbitals in bonding and reactivity.[1,2] For almost four decades these traits have been most readily examined for the bent metallocene-uranium framework, which is known to host a range of formal oxidation states (III through VI) and support a variety of functionalities and chemical processes in the metallocene wedge.[2,3] This class of molecules have received substantial attention to the U^{III}, U^{IV} and U^{VI} valence states, whereas few accounts have probed pentavalent uranium species. Indeed, the literature on U^{V} chemistry is scant and little is known about reactivity and molecular and electronic structural properties due to the redox instability inherent to this oxidation state.[4,5] Accounts of fully characterized pentavalent uranium ion complexes have, however, recently begun to emerge on a frequent periodicity in the literature,[6] but collectively lack a distinct rational tactic to outline their methodical preparation. Thus, the synthesis of discrete U^{V} compounds has remained a challenge that requires a more rigorous and systematic approach to access this elusive oxidation state because it presents an appropriate platform to inspect stability, electronic structure, and chemical behavior.

Several rational objectives have motivated the launch of U^{V} chemistry into focus, including (i) elucidating the behavior of an important intermediate in uranium redox reactions, which hold the potential for facile control of one electron processes previously overlooked in the literature; (ii) further understanding the threat of pentavalent species towards environmental migration and remediation concerns;[7] and (iii) from a fundamental standpoint clarifying the extent to which populated 5f orbitals participate in covalent bonding and reactivity. It is the latter point that has remained a significantly complicated theme in

light actinide sciences since the conception of the 5f series. Relativistic and quantum heavy atom effects render the 5f orbitals shielded from the nucleus with a radial distribution and a multitude of orbital lobes susceptible to covalent overlap. High valent actinide ions possess a greater tendency to extract covalency from outlying ligands and consequently generate surmountable crystal field splittings relative to spin-orbit coupling in contrast to low valent ions.[8] A handful of reports have commented on the electronic structure of the $5f^1$ configuration, however, only a few detailed accounts of U^V-halide and organometallic amide and alkoxide complexes serve as the foundation of the current knowledge base on the subject.[5,9] These studies were prompted by the questionable the nature of the spin-orbit $^2F_{5/2}$ ground and $^2F_{7/2}$ excited states as to whether the molecular orbital manifold generated from metal based 5f orbitals is prone to the effects of the surrounding ligand field.[10] In this respect, U^V is an attractive avenue for exploration of the influence of high oxidation state on covalency in comparison to the breadth of work reported on other valencies. The benefit of the pentavalent uranium ion and other $5f^1$ species (i.e., Pa^{IV}, Np^{VI}), is the singly occupied valence shell, void of any intraelectronic repulsive interactions, that can be probed as an electrochemical, spectroscopic, and magnetic marker to interpret electronic structure and bonding under simplified criteria.

Towards these interests, Graves and co-workers recently communicated a convenient and versatile oxidative route to furnish a series of organouranium(V)-imido complexes of the general formula $(C_5Me_5)_2U(=N\text{-}2,4,6\text{-}^tBu_3\text{-}C_6H_2)X$ (X = F, Cl, Br, I) (**3**-**6**) and $(C_5Me_5)_2U(=N\text{-}2,6\text{-}^iPr_2\text{-}C_6H_3)X$ (X = F, Cl, Br, I, OTf, SPh) (**7**-**12**) that possess marked stability.[11] Their methodology involves oxidation of U^{IV}-imido species (**1** and **2**) that display redox energetics[12] favorably suited for use of Cu^I oxidants to access U^V, while

providing functional variation in the metallocene wedge as exemplified in **Scheme 4.1**. This structurally homologous assortment of complexes display both reversible $U^{VI/V}$ and $U^{V/IV}$ redox couples, broad UV-visible LMCT absortpions, low intensity NIR intra-5f transitions, and temperature dependent magnetic susceptibilties in reasonable agreement with theoretical findings. Interpretation gleaned from these data is suggestive of minimal deviation within the 5f orbital manifold that accompany changes in the identity of X, and are closely related to the data reported for the few other known $5f^1$ species.[11]

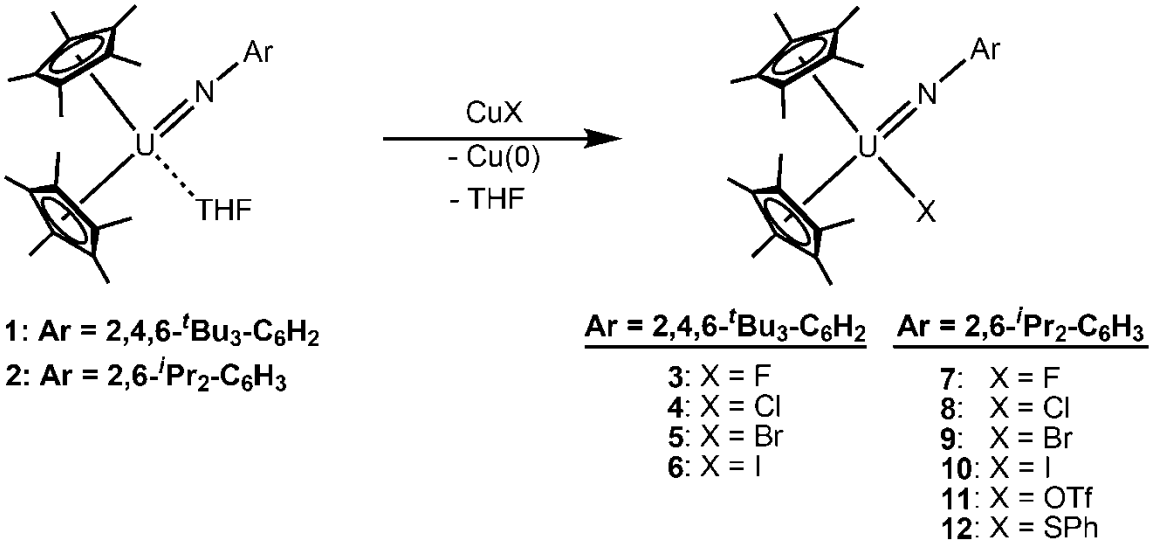

1: Ar = 2,4,6-^{t}Bu$_3$-C$_6$H$_2$
2: Ar = 2,6-^{i}Pr$_2$-C$_6$H$_3$

Ar = 2,4,6-^{t}Bu$_3$-C$_6$H$_2$	Ar = 2,6-^{i}Pr$_2$-C$_6$H$_3$
3: X = F	**7**: X = F
4: X = Cl	**8**: X = Cl
5: X = Br	**9**: X = Br
6: X = I	**10**: X = I
	11: X = OTf
	12: X = SPh

Scheme 4.1. Synthesis of U^V-imido complexes via Cu^I-based oxidation.[11]

This process contrasts reported procedures that produce quinquivalent uranium ion complexes that utilize silver or thallium ion oxidation of neutral tetravalent uranium complexes to form cationic U^V derivatives,[13] or require powerful two electron oxidation (i.e., azide, *N*-oxide) pathways capable of activating trivalent precursors with concurrent stabilization of the resultant U^V species by strong π-donor oxide or imide ligands (Scheme 1.2).[14] The use of mild one electron Cu(I) oxidants that also decorate the wedge vicinity

with monoanionic ligands (X) provides an economical and facile synthetic route applicable to access an array of neutral organouranium(V) derivatives stabilized by the multiply bound ancillary imido fragment. This work dispels the presupposition that U^V chemistry runs the risk of being inoperable due to instability, and herein presents suitable entry to extend synthetic functionality and reactivity, and to examine perturbations on the $5f^1$ electronic structure accompanying ligature modification within the metallocene wedge. Our aim is to develope the chemistry of this scarcely divulged oxidation state and at gaining clarification on the spin-orbit/crystal field continuum for the *pseudo*-tetrahedral coordination geometry by probing the $5f^1$ system using a combination of electrochemistry, electronic spectroscopy, and variable temperature magnetometry. Interpretation of these data suggest marginal differences in structural parameters, redox potentials and kinetics, charge transfer and f-f absorption profiles, and magnetic susceptibilities, which together are inferred as more significant ligand field perturbation trends within the 5f manifold than previously observed for the imido-halide suite.

4.2 Results and Discussion

Synthesis and Structural Characterization

Reaction **Scheme 4.2** portrays the general synthetic procedures used to prepare the substituted organouranium(V)-imido complexes **13** and **14**. Using the precursor $(C_5Me_5)_2U(=N\text{-}2,6\text{-}^{i}Pr_2\text{-}C_6H_3)I$ (**10**), salt metathesis reactions were used to produce the amide (**13**) and aryloxide (**14**) derivatives in 75% and 80% yield, respectively. The synthesis of triflate (**11**) and thiolate (**12**) analogues have been communicated elsewhere and are shown in Scheme 4.1.[11] Complex **12** could not be generated from salt metathesis between **10** and

sodium thiolate, however reaction between **11** and sodium thiolate allows for quantitative conversion to complex **12** and sodium triflate (evidenced by NMR) proving the utility of the triflate derivative (**11**) as a suitable starting material.

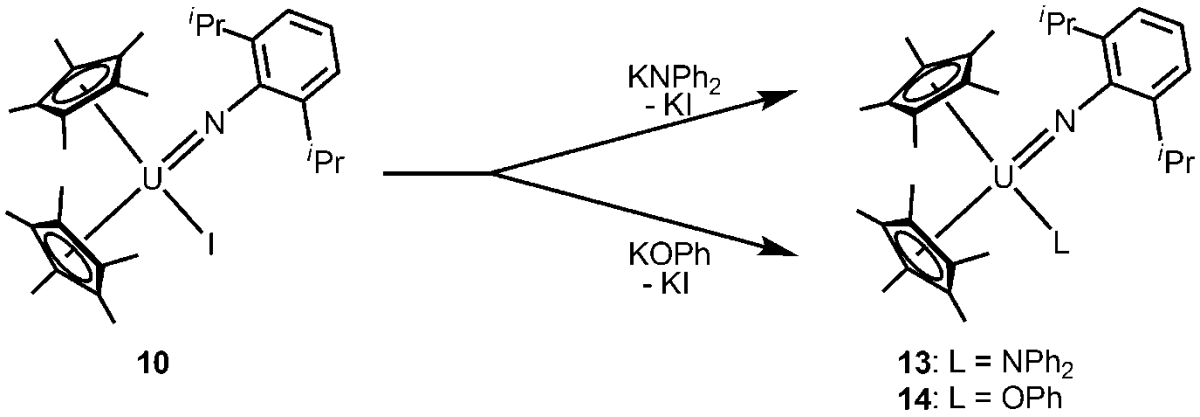

10

13: L = NPh_2
14: L = OPh

Scheme 4.2. Salt metathesis substitution preparation of **13** and **14**.

An indirect protonolysis methodology was employed to generate the ketimide species (**15**) shown in **Scheme 4.3**. Our selection of preparative route to furnish **15** that procedes through the *in-situ* $(C_5Me_5)_2U(=N\text{-}2,6\text{-}^{i}Pr_2\text{-}C_6H_3)(N(SiMe_3)_2$ species proved to be problematic and does not deliver a clean protonolysis reaction with diphenylimine, and there was evidence for a uranium(IV)-ketimide species in spectroscopic and electrochemical studies. Nonetheless, single crystals of **15** suitable for x-ray analysis was isolated from the mixture as the only clean species. However, progress has been made to overcome this synthetic hindrance by reverting to the more sophisticated phenylnitrile insertion with a novel imidouranium(V)-alkyl complex that has been recently isolated.[15] Nitrile coupling to metal-alkyl fragments has been employed in the past to afford a variety of tetravalent thorium and uranium ketimides as well as early transition metal congeners,[16,17] and in this case generates

the organouranium(V)-ketimide derivative (**15**) in reproducible high yield and analytically pure form, which will be described in more detail in a future chronicle.

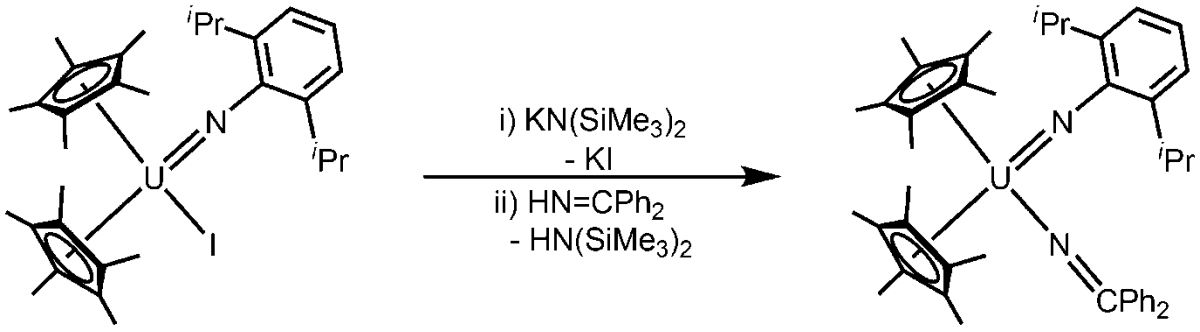

10 **15**

Scheme 4.3. Salt metathesis (i) followed by protonolysis (ii) to generate **15**.

The tri-*t*-butyl substituted arylimido U^V-halides (**3-6**) are not effective starting materials to explore simple ligand substitution reactions, and only the di-isopropyl derived arylimido complexes (**7-10**) permit clean substitution reactions to form **12-15**. This is an undoubted effect of greater steric crowding that arises from the *t*-butyl encumbrance proximal to the substitution site, whereas the di-isopropylaryl imido fragments are less sterically demanding and allow ligand exchange. Reactions were run in toluene, and following workup in hexanes **13** and **14** were obtained reproducibly from hexamethyldisiloxane in good isolated yield in analytically pure form and characterized by ^{1}H NMR, elemental analysis, mass spectrometry, UV-visible-NIR electronic absorption spectroscopy, cyclic and square wave voltammetry, variable temperature magnetic susceptibility, and single crystal X-ray crystallography.[18]

Variable temperature proton NMR experiments performed on **13** and **14** depict broadened resonances indicative of paramagnetic U^V complexes. $C_5Me_5^-$ ligand protons

display a broad signal near ~5 ppm and inequivalent 2,6-diisopropylarylimido signals. Single-crystal x-ray diffraction analysis performed on complexes **13-15** verified their molecular structures as a series of structurally homologous *pseudo*-tetrahedral bent-sandwich U^V-imido species. **Figure 4.1** portrays the structures of **13** and **15** and **Table 4.1** contains relevant metrical parameter comparisons for **11-15**, whereas complete structural data collection and refinement details are supplied in **Table 4.2** and in the supporting information. X-ray crystallographic data refinement for the aryloxide derivative (**14**) could not be resolved beyond molecular connectivity. The molecular structures for **13-15** are analogous to previously reported bent metallocene U^V species, including the imido-halides (**3-10),** -triflate (**11**), -thiolate (**12**) and the oxo-alkoxide complex $(C_5Me_5)_2U(O\text{-}2,6\text{-}^iPr_2\text{-}C_6H_3)(=O)$.[14e] Across the full series of complexes, the $U{=}N_{imido}$ bond distances and $U{=}N\text{-}C_{ipso}$ angles differ little, with short (1.958(6)-2.012(4) Å) and linear (169.6(4)-174.6(4)º) average binding modes that reside within the range of reported U^V imido units.[11,15] In comparison, minimal differences are observed in $U{=}N_{imido}$ bond distances and $U\text{-}N\text{-}C_{ipso}$ angles between tetra-, penta-, and hexavalent uranium-imido species.[13,19]

Table 4.1. Selected crystallographic data for **13, 15,** and **16**.

	13	**15**	**16**
formula	$C_{44}H_{57}N_2U$	$C_{45}H_{57}N_2U$	$C_{38}H_{52}N_2U$
a (Å)	13.328(3)	10.4240(9)	18.297(2)
b (Å)	16.963(4)	19.0426(17)	17.094(2)
c (Å)	32.855(8)	19.6998(18)	21.555(3)
α (º)	90	90	90
β (º)	90	98.9870(10)	90
γ (º)	90	90	90
V (Å^3)	7428(3)	3862.4(6)	6741.8(15)
Z	10	4	9
FW	851.98	863.96	774.87
crystal system	Orthorhombic	monoclinic	orthorhombic
space group	P*bca*	P$2_1/c$	P*bca*
T (K)	100(2)	120(1)	100(2)
λ (Å)	0.71073	0.71073	0.71073
ρ_{calc} (g•cm^{-1})	1.524	1.486	1.527
μ (mm^{-1})	4.403	4.235	4.843
F(000)	3416	1732	3088
θ range (º)	1.97 - 25.04	1.98 - 28.38	1.88 - 23.27
total reflections	84966	38983	7925
unique reflections	6560	9039	4449
parameters	438	447	384
R_1	0.0488	0.0416	0.0561
wR_2 (all data)	0.1513	0.0867	0.1591
max min peaks eÅ^{-3}	0.802, -1.934	1.275, -0.930	3.132, -1.581
GOF on F^2	1.099	0.956	0.899

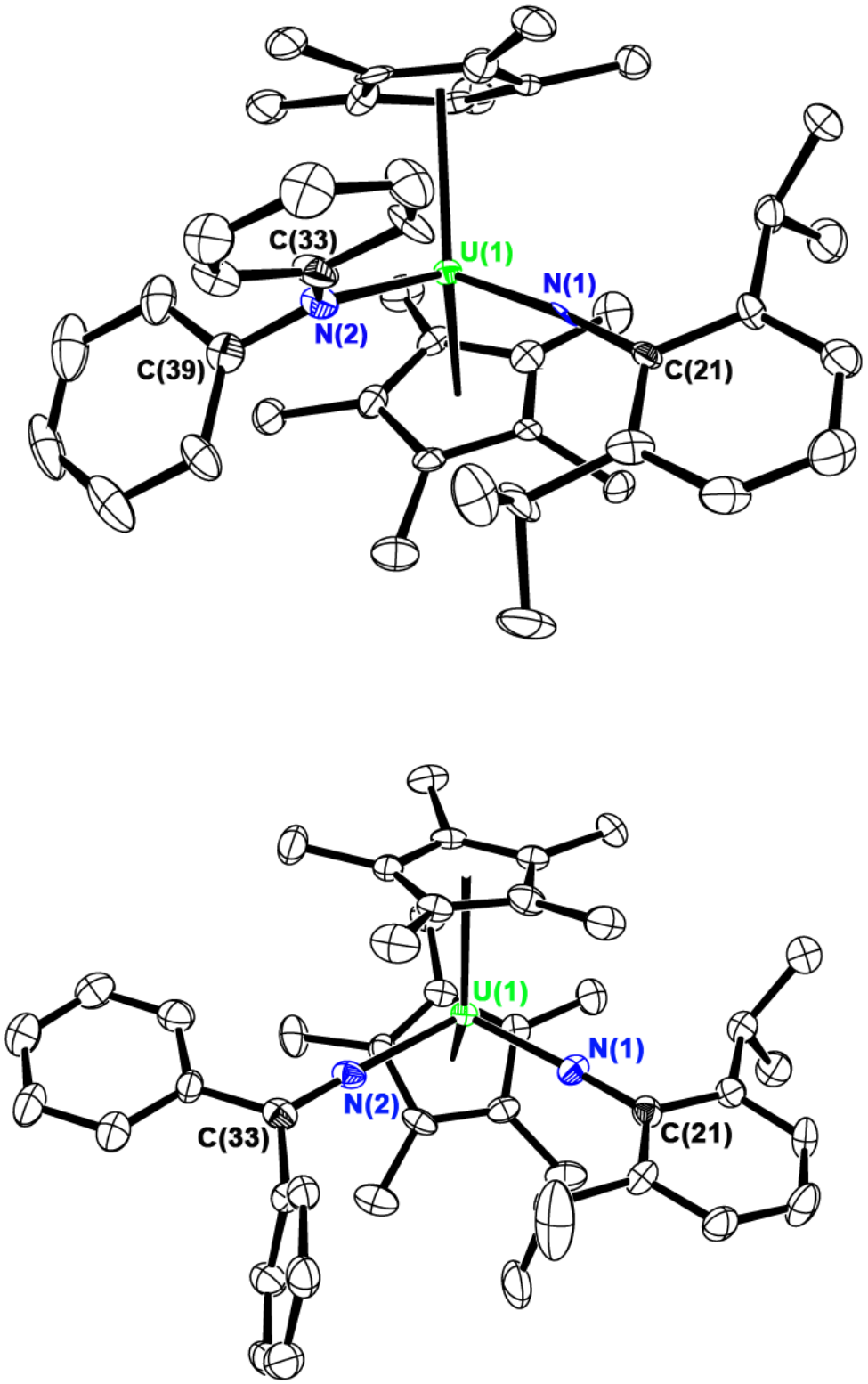

Figure 4.1. Molecular structures of complexes **13** (top) and **15** (bottom) with thermal ellipsoids represented at the 50% probability level.

The most significant structural differences between complexes **11-15** is are the U-L (L = OTf, SPh, NPh_2, OPh, $N=CPh_2$) contacts situated within the metallocene wedge, and a similar trend was reported for the halide derivatives (**3**-**10**).[11] The U-NPh_2 bond distance U(1)-N(2) 2.316(7) Å observed in **13** is consistent with other known U^V-amide complexes. For example, a uranium-amide distance of 2.295(10) Å was observed in $U(=NSiMe_3)[N(SiMe_3)_2]_3$[14a] and respective bond lengths of 2.25(2) Å and 2.31(5) Å were reported for the cationic organouranium(V) complexes $[(C_5Me_5)U(NSiMe_3)_2)_3(THF)]^+$ and $[(C_5Me_5)_2U(NEt_2)_2]^+$.[13a] Although these pentavalent uranium-amide bonds might be expected to be considerably shorter than tri- or tetravalent uranium-amide fragments yet longer than hexavalent analogues, they are in fact comparable in all cases, with related distances of 2.320(4) Å in $U[N(SiMe_3)_2]_3$,[20] 2.276(6) Å in $(C_5Me_5)_2U[NH(2,6\text{-}Me_2\text{-}C_6H_3)]_2$,[21] and 2.23 Å in $UF(=NR)[N(SiMe_3)_2]_3$.[22] This bond distance is also on par with the median uranyl(VI)-amide length of ~2.31 Å observed in $UO_2(N(SiMe_3)_2)_2(THF)_2$ and $[UO_2(N(SiMe_3)_2)_3][M(THF)_2]$ ($M = Na^+, K^+$).[23]

Table 4.2. Pertinent bond lengths and angles for complexes **10-15**.

	10[11] L = I	**11**[11] L = OTf	**12**[11] L = SPh	**13** L = NPh_2	**14**[a] L = OPh	**15** L = $NCPh_2$
U-L (Å)	3.0385(7)	2.379(6)	2.7230(1)	2.316(7)	2.127	2.199(4)
U-L-C (º)	-----	-----	131.08(2)	-----	173.54	177.8(4)
U=N (Å)	1.974(7)	1.958(2)	1.976(4)	1.990(6)	1.922	2.012(4)
N-C_{ipso} (Å)	1.406(10)	1.419(9)	1.398(6)	1.392(10)	1.507	1.288(7)
U=N-C (º)	170.7(6)	166.7(4)	171.6(3)	174.3(5)	170.45	174.6(4)
L-U=N (º)	107.0(2)	109.46(2)	103.35(1)	93.8(2)	112.02	111.99(2)

[a] Metrical parameters for **14** are approximate based on a poorly refined data set.

Despite the fact that single crystal data for **14** was of poor quality, informative structural assignments could be extracted. The approximate U-OPh distance U(1)-O(1) 2.127 Å and U-O-C_{ipso} angle (173.45º) are similar to the distance of 2.135 Å and the nearly linear angle (169.5º) reported in the pentavalent oxo-alkoxide $(C_5Me_5)_2U(O\text{-}2,6\text{-}^{i}Pr_2\text{-}C_6H_3)(=O)$,[14e] and is also within the range of 2.03-2.29(1) Å and 160-165º for bridging and terminal alkoxides in the uranium(V) dimer $U_2(OCHMe_2)_{10}$.[24] As expected, the U^{V}-OPh bond in **14** and other pentavalent derivatives is modestly shorter than those observed in U^{IV}-alkoxides/aryloxides. For example, 2.145(8) Å in $U(O\text{-}2,6\text{-}^{t}Bu_2\text{-}C_6H_3)[N(SiMe_3)_2]$[25] and 2.208(9) Å in $[U(N(CH_2CH_2N(SiMe_3))_3)(O\text{-}t\text{-}C_4F_9)]$,[26] which are also bound with nearly linear U-O-C_{ipso} angles of 158.6(8)º and 173.7(9)º , respectively. Likewise, the U-OPh bond parameters in **14** resemble those in the uranyl(VI)-aryloxide complex $UO_2(O\text{-}2,6\text{-}^{i}Pr_2\text{-}C_6H_3)(Py)_3$ with respective distances of 2.179(5) and 2.215(5) Å and U-O-C_{ipso} angles of 161.6(5) and 151.5(5)º.[27]

The synthesis and characterization information for the triflate (**11**) and thiolate (**12**) derivatives were developed by Graves and co-workers.[15] However, a few relevant structural and spectroscopic parameters bear mention in this account to compare and contrast with the recently reported imido-halide examples.[11] As expected the U-OTf (**11**) and U-SPh (**12**) bonds are long due to their weak coordinating ability with respect to other anionic ligands used. The uranium-thiolate bond distance U(1)-S(1) 2.684(2) Å in **12** is comparable to the reported U^{V}-dithiolene complex with an average U-S distance of 2.7230(13) Å.[28] The U^{V}-imido thiolate (**12**) and aryloxide (**14**) derivatives are structurally homologous with inequivalent U-E-Ph (E = S, O) bond angles of 131.08(17)º versus 173.54º respectively, and the U-SPh distance is comparably elongated in **12**. This large bond distance and angular

discrepancy are presumably a consequence of an enhanced covalent match between U^V and the aryloxide over the thiolate ligand, and the variation in donor ligand radius. The uranium-thiolate bond in **12** is similar to that reported for U(S-2,6-Me_2-C_6H_3)[$N(SiMe_3)_2$]$_3$ (2.696(3) Å, 114.9º)[29] and for the unsupported uranyl(VI)-thiolate $UO_2(SPh)_2(O=C(^iPr)(N^iPr_2))_2$ where long bonds of 2.7143(7)-2.7325(8) Å, and more acute U-S-C_{ipso} angles between 106.1(1)-111.2(1)º[30] are in contrast to uranium-alkoxide/aryloxide congeners due to enhanced π-bonding in the latter. The U-OTf bond length of U(1)-O(1) 2.379(6) Å in **11** is within the range of other reported uranium triflate complexes (for example, 2.395(14) Å in the hydrazonato-triflate complex $(C_5Me_5)_2U(N,N'\text{-}CH_3N\text{-}N=CPh_2)(OTf))$[31] however **11** represents the solitary example of a U^V-triflate reported to date.[32]

Complex **15** represents the first uranium-ketimide with a corresponding formal metal oxidation state other than four.[17,33] The short bond distance U(1)-N(2) 2.199(4) Å, nearly linear U(1)-N(2)-C(33) angle of 178.2(5)º and intraligand N(2)=C(33) length of 1.288(4) Å for **15** together suggest that filled ligand orbitals of both σ and π symmetry are involved in multiple covalent overlap with available metal based orbitals. For comparison, the uranium(IV)-N=CPh_2 distances in $(C_5Me_5)_2U(\text{-}N=CPh_2)_2$ between 2.179(6)-2.185(5) Å and the U-N=C_{ipso} angles of 173.4(6)-176.5(5)º are close in value to the parameters observed for **15** and other U^{IV}-ketimide derivatives.[17,33] These structural features are in contrast to related group four transition metal-ketimido complexes where nominally bent M-N=C_{ipso} angles (164.1(2)º) are observed (M = Zr, Ti).[17,33] This suggests that nitrogen 2p orbitals on the ketimide ligand donate considerable electron density to the metal center and afford a bond order greater than one. The favorable π-bonding in the uranium-ketimide contact is also

highlighted by comparison to terminal uranium-imido and alkoxide fragments bound in a linear fashion with short U-N and U-O bonds indicative of multiple bonding.

Synthesis of $(C_5Me_5)_2U(=N\text{-}2,6\text{-}^{i}Pr_2\text{-}C_6H_3)(=N\text{-}C_6H_5)$ (**16**)

Reaction between **10** and potassium analide (KNHPh) presents an interesting anomaly in comparison to the metathesis steps employed to furnish the pentavalent derivatives **13-15**. In contrast, the reaction shown in **Scheme 4.4** affords the U^{VI} bis-imido complex **16** in 62% isolated yield. In this case the product does not contain the expected U^{V}-NHPh attachment, but rather the analide has lost a proton to form the phenylimido substituent accompanied by electron loss from U^{V} resulting in a formal U^{VI} oxidation state assignment with dual imido donors situated in the wedge. The fate of the pilfered proton in Scheme 4.3 is uncertain at this juncture, however since it is required that potassium analide be administered in excess of two equivalents to maximize production yield, our preliminary proposition is that additional KNHPh might serve as a sacrificial proton acceptor. **16** is isolated with ease from a solution of hexamethyldisiloxane with few drops of pyridine, however the role of pyridine is unclear since there is no evidence for coordinated pyridine nor pyridinium species in ^{1}H NMR studies. Experiments that utilize established proton abstraction reagents to drive the formation of **16** are currently underway, as well as a deuterium labelling study.

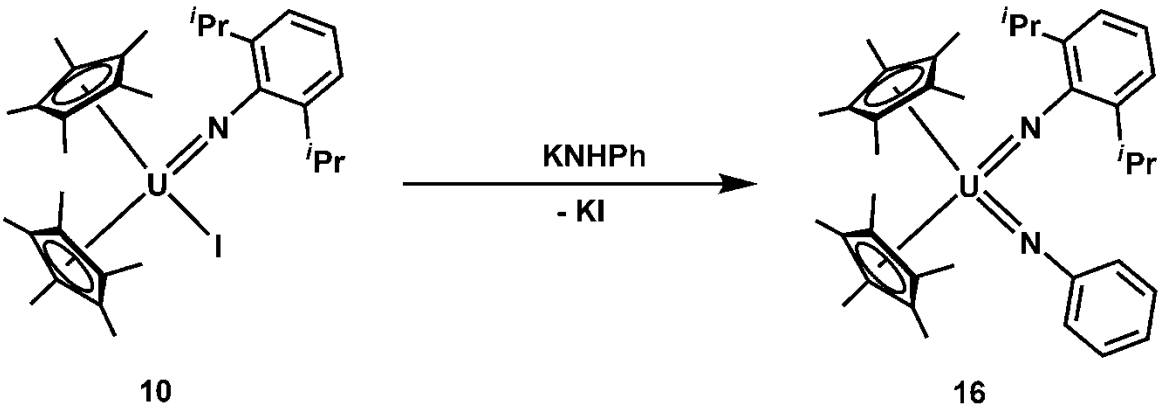

10 16

Scheme 4.4. Synthesis of U^{VI} bis-imido complex **16**.

Isolation of **16** is not all that astonishing in light of the bleak historical development of pentavalent uranium chemistry since complexes of this sort are prone to undergo facile oxidation and/or reduction to result in more stable tetravalent and hexavalent species.[5] During the course of our pursuits to establish the organouranium(V)-imido system we encountered redox decomposition under a few conditions. For example, recall that initial efforts to synthesize the ketimide derivative resulted in a U^{IV} contaminant, but furthermore when **3**-**10** were treated with a wide variety of alkali substrates the reactions frequently churned out **1** or **2**. A number of reported oxidative routes that led to U^{VI} bis-imido species, including azide and *N*-oxide oxidation of tetravalent precursors that bypass U^{V} altogether.[36] In this context, it is worth mentioning that H-atom abstraction has been observed for U^{VI} bis-imido species, which have been shown to consume dihydrogen and activate proximal alkyl fragments to form amide and tuck complexes respectively.[37] These reactions are a *pseudo*-reversal of the reaction postulated in Scheme 4.3, thus supporting relevant sensitivity of these species to H-atom abstraction pathways. Nonetheless, the resultant high-valent uranium ions are stabilized by multiply bound imido fragments that are enormously inert compared to

prolific reactivity observed for early transition metal imido species.[38] One final note about this discovery is that the salt metathesis, H-atom loss, and oxidative synthetic process outlined in Scheme 4.4 is reminiscent of transition metal-imido and –oxo species formation from respective amide and hydroxide species induced by proton-coupled-electron-transfer (PCET) mechanisms,[35] however no account of this sort of reaction has been demonstrated in f-element chemistry.

Proton and carbon NMR experiments performed on **16** at ambient temperature display narrow peaks in the chemical shift region expected for a formally diamagnetic hexavalent uranium ion species. An intense peak at 4.46 ppm displays the permethylated cyclopentadienyl ancillary ligands, whereas two doublets at 2.11 and 1.68 ppm are observed for the ^{i}Pr substituents on the aryl imido, and aryl protons are intermittent in the range 0-10 ppm. The structure of **16** was further evidence via single crystal x-ray diffraction study and the molecular structure is depicted in **Figure 4.2**, and pertinent crystallographic information is listed in Table 4.1. The metrical parameters extracted from crystallographic data are consistent with other reported U^{VI} imido species.[36] The average U-$(C_5Me_5)_{centroid}$ distance is 2.474 Å and C_5Me_5-U-C_5Me_5 angle is 137.79º. More importantly, the respective short U(1)-N(1) and U(1)-N(2) distances of 1.970(11) Å and 1.965(11) Å and nearly linear U(1)-N(1)-C(1) and U(1)-N(2)-C(13) angles of 171.2(9)º and 173.5(3)º fit the expected regime for U^{VI}-imido contacts.[39] Likewise, the N(1)-U(1)-N(2) angle of 108.1(4)º is on par with other bent metallocene complexes with bis-imido ligation in the wedge. It should be noted that these parameters in whole do not deviate far from the U=N, U=N-C_{ispo}, and N-C_{ipso} parameters observed for U^{V} organoimido species **1**-**15**.

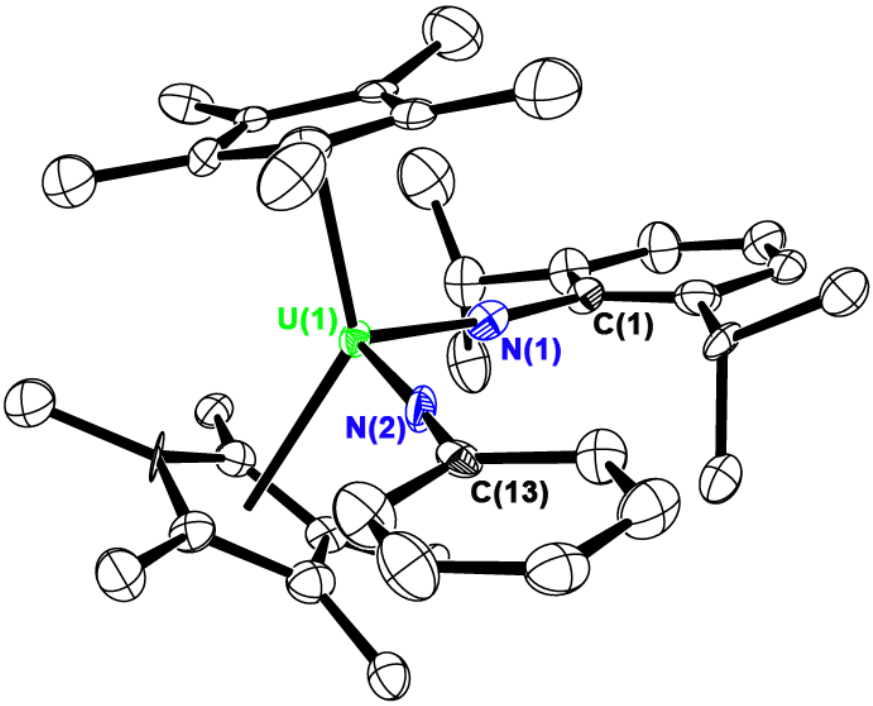

Figure 4.2. Molecular structure of **16** with thermal ellipsoids shown at 50% probability.

Electrochemistry

Complexes **13**, **14**, and **15** display $U^{VI/V}$ oxidation and $U^{V/IV}$ reduction waves with no sign of any disproportionation in the cyclic and square wave voltammetric plots. The properties of these redox couples rival the recently reported organouranium(V)-imido halides (**3**-**10**) and the thiolate (**11**) and triflate (**12**) counterparts.[11,15] Electrochemical characteristics are represented herein for complex **13** in **Figure 4.3** where both essentially reversible reductive and oxidative processes are centered near $E_{1/2}$ = - 0.30 V vs $E_{1/2}$ = -1.65 V with a rest potential of -1.0 V versus the $Fc^{+/0}$ couple respectively, and fall within the range comparable to those observed for other derivatives collected in **Table 4.3**. Notably, the large potential separation of about 1.5 V between oxidative and reductive waves is general for the full suite of halides, and extends to include the new derivatives **13** and **14**. In a similar vien,

Mo^{V} complexes have been shown to undergo two reversible redox processes for nominal $Mo^{VI/V}$ and $Mo^{V/IV}$ assignments with large potential separation between the peaks, similar to that observed here.[40] An additional irreversible oxidative process observed near 1 V (vs $Fc^{+/0}$) is likely due to the C_5Me_5 fragments (not shown). There is no additional reductive signature that might be suggestive of a progressive second metal based reduction (U^{IV}/U^{III}) within the available potential window allotted by the solvent and supporting electrolyte blend, although it should be mentioned that the $U^{IV/III}$ couple has been reasonably assigned for a variety of tetravalent uranium metallocene derivatives at more negative potential of -2.1 V.[12]

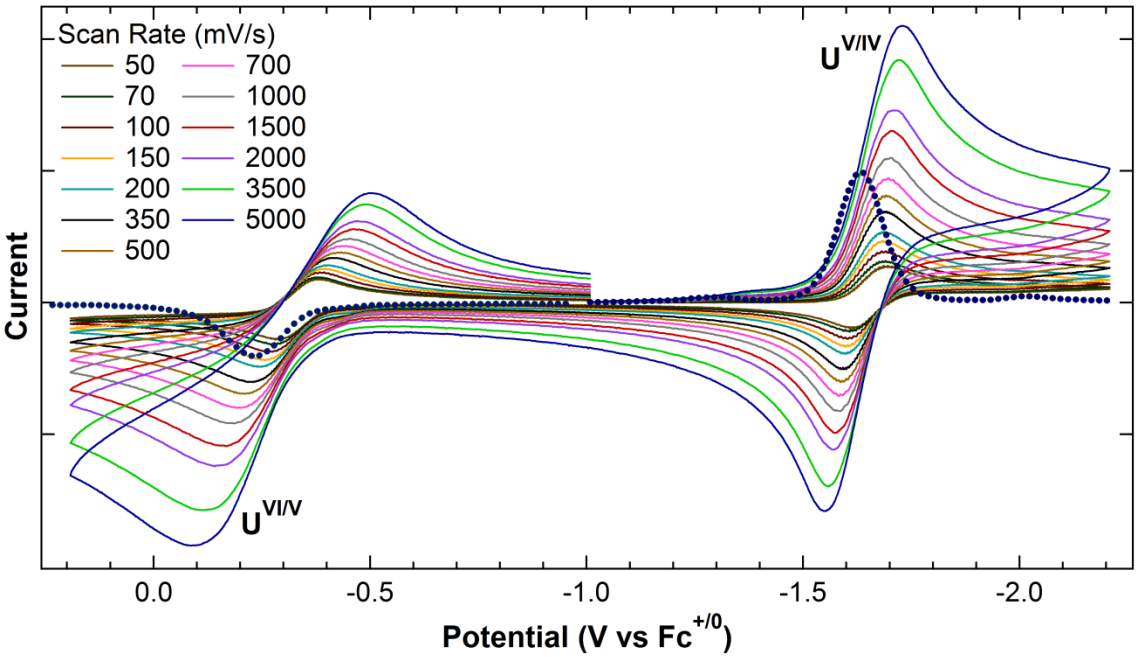

Figure 4.3. Cyclic (solid) and square wave (dashed) voltammetric curves for complex **13** in ~0.1 M [TBA][BAr_f]/THF solution obtained room temperature with variable scan rates between 0.50 and 5.0 V/s.

Table 4.3. Summary of redox potential data for U^V complexes **1-15**.

Complexes[a]	$E_{1/2}$ (U^{VI}/U^V) (V vs $Fc^{+/0}$)	$E_{1/2}$ (U^V/U^{IV}) (V vs $Fc^{+/0}$)	$\Delta E_{1/2}$ (V)
3	-0.19	-1.78	1.59
4	0.04	-1.50	1.54
5	0.04	-1.43	1.47
6	0.04	-1.25	1.29
7	-0.14	-1.81	1.67
8	0.03	-1.52	1.55
9	0.07	-1.44	1.51
10	0.11	-1.37	1.48
11	0.36	-1.21	1.57
12	0.00	-1.43	1.43
13	-0.30	-1.65	1.35
14	-0.22	-1.75	1.53
15	-0.34	-1.84	1.50
		$\Delta E_{1/2}$ (ave)	= 1.49

[a] Electrochemical data for **3-10** reported in ref. [11], and **11** and **12** in ref. [15].

There is not a large body of literature documenting the electrochemistry of well defined U^V derivatives, and information is often garnered from tetravalent and hexavalent uranium ion oxidation and reduction, respectively. The $U^{V/IV}$ reduction potentials for these organouranium(V) complexes are shifted by about -1.0 V with respect to the same process for $(C_5Me_5)_2U(=N\text{-}2,6\text{-}{}^{i}Pr_2\text{-}C_6H_3)THF$ (**2**),[12] and this difference is attributable to the electronic influence of the additional anionic ligand in the former. Similarly, the $U^{VI/V}$ couple for organouranium(VI) complexes require considerably more reducing potential than those seen here, for example the bis-imido complex **16** displays a reversible reduction at -1.65 V (*vide infra*).

A comparison of the voltammetric data for **3-14** is presented in **Table 4.3**. The trend illustrated by the redox energetics for the U^V-fluoride, -amide, -aryloxide, and -ketimide derivatives with more negative potentials signify these species are thermodynamically more

difficult to reduce and can be oxidized with less effort than thiolate, triflate, and heavier halide (Cl, Br, I) derivatives. This result is accounted for by increased electron density donated at the metal center from stronger π-donor ligands (i.e., F, OPh, NPh_2) resulting from a detracted metal ion core electron affinity in contrast to the remainder of the σ-donor ligands studied here.

The reversible behavior for both of these processes indicates minimal molecular reorganization during oxidation and/or reduction retained across the entire scan rate window of 0.5-5 V/s. However, it is obvious in Figure 4.3 that the oxidation process for these complexes is somewhat more sluggish in contrast to the ideal Nernstian reversibility of $U^{V/IV}$ reduction, which is manifested in the larger potential and current separation between cathodic and anodic peaks for the $U^{VI/V}$ oxidation in the forward and reverse scans. This subtle difference in the rate of heterogeneous electron transfer is a direct consequence of changes in metal ion size coupled with ligand affinities and geometric redistribution accompanying oxidation, although attaining an accurate quantitative kinetic comparison for systems in low polarity solvents (i.e. THF) is typically precluded by resistivity compensation.[11,41] It should be noted that the $U^{VI/V}$ couple for the reductive step for organouranium(VI) complexes displays a constant peak separation regardless of scan rate with no kinetic perturbation as described here for the same couple as an oxidative process for U^{V} derivatives.[42]

Electronic Absorption Spectroscopy

Complexes **13** and **14** exhibit a series of broad intense electronic absorption features that span the visible and ultraviolet regions, whereas comparably less intense and narrow f-f transition peaks appear at lower energy in the near-infrared spectral region. The higher

energy absorption bands shown in **Figure 4.4** give rise to the hallmark dark brown color for complexes of this design and are attributed to ligand to metal charge transfer (LMCT). This region is predominated by transitions within the $U{=}N_{imide}$ unit between a filled imido π-orbital ground state and an empty uranium based non-bonding excited state manifold derived from 5f orbital character. These absorption characteristics are, within experimental certainty, consistent in energy and molar absorptivity across the entire series (**3**-**14**), and trail into the visible and lower energy region with decreasing oscillator strength. A recent manuscript has deconvoluted the high energy spectral regime for the imido-halide derivatives (**3**-**10**) to reveal a series of consecutive bands assigned as electronic dipole allowed progressions comprised of charge transfer between the ground ligand based electronic states (i.e., imide, halide, C_5Me_5) and a variety of low lying 5f nonbonding states in agreement with projected theoretical models.[11] Similar LMCT bands have been described for high valent early transition metal imido complexes, with an excited state composed of a d^0 nonbonding manifold.[43] In fact, intense high energy charge transfer bands have been documented for a variety of hexa- and tetravalent organouranium complexes, including bent metallocene derived imide, ketimide, halide, and alkyl complexes.[12] The lack of contrast between the UV-visible spectra for the full suite of organouranium(V) imido complexes is not apparently clear, and predicted differences introduced by varied ligand substituents in the wedge are presumably masked by higher intensity charge transfer, or simply might not be obvious within the available spectral window. Orbitally allowed transitions between the f→d manifolds would be expected to appear at higher energy outside the spectral region available in toluene solution.[8] In summary, the appearance of these charge transfer bands are shielded from the influences of ligand substitution within the metallocene wedge.

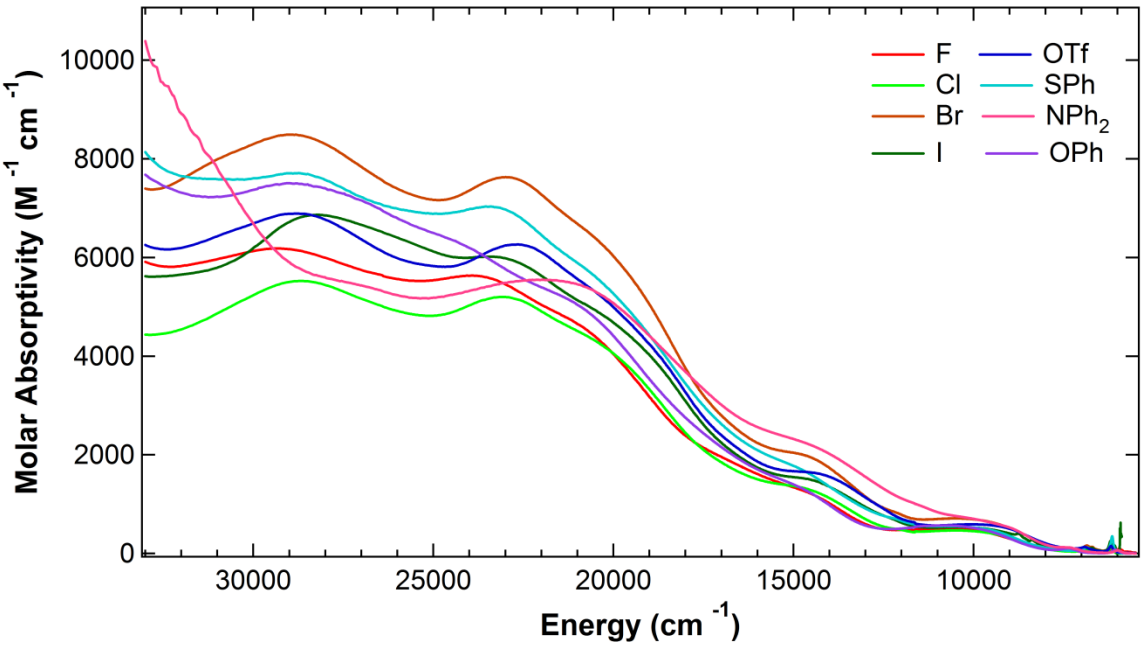

Figure 4.4. UV-visible absorption spectra for **7**-**14** obtained at room temperature in toluene-d_8 solution. The halide derivatives (**7**-**10**) and triflate and thiolate species (**11**, **12**) are reported elsewhere.[11,15]

Intra-5f transitions for the $5f^1$ electronic configuration arise from states split by spin-orbit coupling and symmetry induced ligand field effects discussed below. These peaks reside at low energy in the NIR region, where two structured bands display considerably weaker intensities and narrower bandwidths in comparison to higher energy LMCT progressions. All organouranium(V)-imido derivatives studied thus far (**3**-**14**) show a similar NIR spectral envelope. Illustrated in **Figure 4.5**, a sharp absorption near ~6000 cm^{-1} is adjacent to a lower intensity broadened band near ~7000 cm^{-1}. The lower energy feature originates from a pure electronic transition, whereas the higher energy NIR band shows fine structure indicatively coupled to vibronic modes. Spectral studies performed at liquid helium temperatures on the imido-halide, -thiolate, and -triflate derivatives did not show any noticeable difference with the room temperature profile,[11,15] however the new derivatives first reported herein (**13**-**15**) have not been examined under cryogenic conditions. Whereas

LMCT absorption features are not appreciably responsive to changes in ligand field effects, f→f transitions show subtle distinctions in energy and intensities interpreted as 5f orbital sensitivity to ligand substitution modification around the metallocene wedge

Dissimilarities in the energies where the two individual NIR peaks lie are significant for the F (**7**), NPh_2 (**13**), and OPh (**14**) derivatives compared to the remainder of the complexes that have been evaluated. For **13** and **14** the separation between these bands is nearly double (~1400 cm^{-1}) those for **3**-**12** (~700 cm^{-1}). It is likely that this deviation arises from ligand field perturbations experienced in the 5f ground and excited states by strong π-donor ligand sets, and this observation is supported by the redox potentials for **7**, **13** and **14** discussed above. A similar observation has been reported for the organouranium(V)-alkoxide derivative (COT)U(O-2,6-^{i}Pr-$C_6H_3)_3$ for which EPR studies revealed significant mixing of the ground and excited states interpreted as a strong ligand field approximation in comparison to other derivatives.[44] Notably, all complexes compared here display NIR absorptions with low intensities that remain roughly constant across the series and fall within the range expected for electronic dipole forbidden transitions (100-300 $M^{-1}cm^{-1}$).

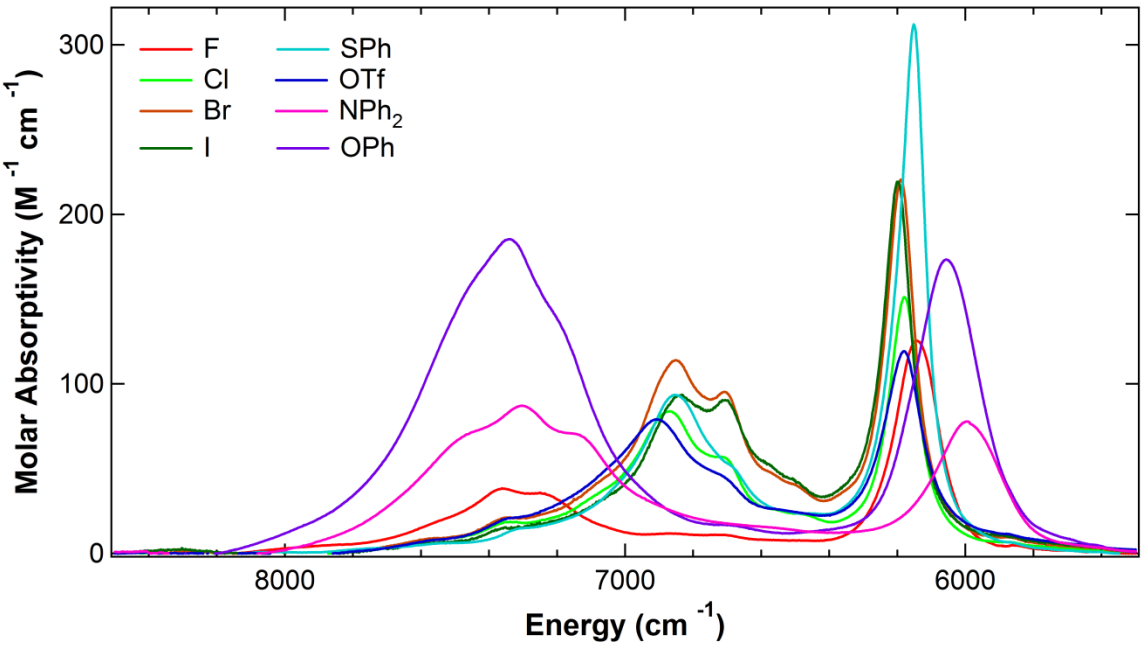

Figure 4.5. The NIR portion of the electronic absorption spectra overlying traces for complexes **7**-**14** obtained under ambient conditions in toluene-d_8 solution. The spectra for **7**-**12** are adapted from references [11] and [15].

In contrast, molar absorptivities reported for *pseudo*-octahedral $5f^1$ complexes are exceedingly low (5-25 $M^{-1}cm^{-1}$).[45] This discrepancy has been attributed to vibronic coupling and the lower symmetry environment which together induce relaxation of orbitally forbidden transitions in the present case.[11] Recent advances in the course of these pursuits include acetylide and a pure ketimide specimen that display remarkably more intense f→f transitions with molar absorptivity values an order of magnitude larger than those disclosed herein (~1500 cm^{-1}). These anomalous intensities reside outside the upper limit of the range expected for orbitally forbidden transitions, and presumably result from intra-5f absorptions gaining intensity from the chromophoric uranium-imido linkage in close proximity. A similar mechanism has been examined in depth for tetravalent uranium-ketimide species,[46] and these recent developments reveal that the imido substituents and monoanionic ligand (L)

ligated in the metallocene wedge are engaged in covalent overlap with the same 5f orbital that houses the single valence electron involved in excitation. However, this is in stark contrast to **3**-**14** and a more detailed spectroscopic and theoretical comparative treatment will be discussed in a forthcoming manuscript for the entire series of pentavalent organouranium imide complexes.[15]

In any case, the absorption profiles depicted in Figure 4.5 follow characteristic trends reported for *pseudo*-octahedral and tetragonal U^{V} halide complexes, as well as other $5f^1$ ions (i.e. Pa^{IV}, Np^{VI}) that also display two similar low intensity f→f peaks within a comparable scope of energies.[5,47,48] Negligible differences in the NIR band structure between high and low symmetry ligand field environments at the uranium (i.e. O_h vs D_4 vs *pseudo*-T_d) indicates a lack of sensitivity within the crystal-field parameters of the 5f molecular orbital manifold that accompany alterations in coordination geometries. The f^1 configuration gives rise to the formal Russel-Sanders spin-orbit doublet $F_{5/2}$ (L = 3, S = ½, J = 5/2) ground and $F_{7/2}$ excited state terms. The symmetry of the ligand field environment serves to lift spin-orbit degeneracy according to double point group symmetry operations, resulting in a series of Kramer's doublets.[49] The molecular orbital scheme described for an O_h f^1 environment is depicted in **Figure 4.6**, and describes a total of four expected low energy intra 5f transitions among population of the Γ levels.

The bent-sandwich framework encountered here has approximate C_s symmetry that should in theory create a greater multitude of energy level splittings resulting in an increased number of transitions within the NIR window.[48] However, in all cases two absorptions are observed in the allotted spectral window whereas the remaining expected peaks should lie at higher and lower energy and might be masked by solvent based vibronic overtones or lower

energy LMCT bands that trail into the NIR region. The experimental finding of two peaks in this region are indicative of the splitting of the excited state manifold. The separation between the two observed peaks (average ~1000 cm^{-1}) gives a measure of energy level splitting between the ground Γ_7 and low lying excited state. These two transitions have previously been assigned to the nominal $\Gamma_7 \rightarrow \Gamma_7$' and $\Gamma_7 \rightarrow \Gamma_8$' transitions for the octahedral situation.[5,47,48] Although there are subtle differences in f→f band profiles for the derivatives that accompany ligand substitution, there is an obvious insensitivity to the 5f orbital manifold regardless of coordination geometry and crystal field strength. This is demonstrative that the 5f orbitals for this high oxidation state species follow an approximated ionic bonding status, and suggests covalent attributes might be accentuated by participation from empty outlying metal based 6d valence orbitals. However, the slight broad band widths arise from 5f orbital involvement in covalent bonding in contrast to the sharp f→f spectroscopic peaks associated with lanthanides and later actinide ions that possess contracted f-orbitals with predominant ionic bonding qualities.

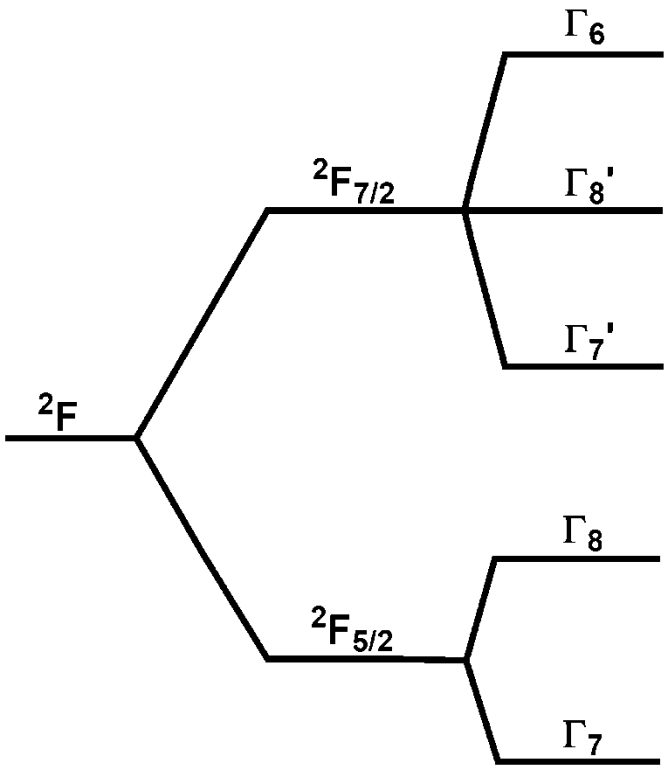

Figure 4.6. Generic energy level diagram depicting the $5f^1$ Russell-Sanders spin orbit and O_h ligand field splittings where each level represents a pair of Kramer's doublets. This description is dependent on the strength and geometry of the ligand field, the energy separation between states dictates thermal population, and the degree of admixture of excited and ground levels.

Magnetism

Magnetic susceptibility data obtained from bulk crystalline solid samples of the variety of organouranium(V)-imido complexes are summarized in **Table 4.4**. **Figure 4.7** portrays the variable temperature susceptibility curves for **13** and **14,** which are characteristic of temperature dependent Curie-Weiss paramagnetic behavior as expected for U^V ion complexes and do not exhibit any noticeable magnetic field strength dependence. Although these data fit the simplified f^1 paramagnetic properties that lack any electronic-electron repulsions, interpretation of comparably large spin-orbit and ligand field splittings for higher oxidation states are convoluted by an underlying temperature independent paramagnetic

(TIP) component that renders assessment difficult.[50] From the Russell-Sanders (RS) formalism, the $5f^1$ electronic configuration results in a $^2F_{5/2}$ ground state from which a calculated susceptibility of 2.54 μ_B (0.80 emu K mol^{-1}) is predicted.[11,50] At low temperature (2 - 40 K) the lone electron is confined to ligand field ground state derived from the RS splitting which results in a reduced χT product due to quenching of orbital contributions. Above 40 K, thermal population of the low lying excited state ligand field domains is induced ($\Delta E < kT$) and μ_{eff} does not quite reach the predicted RS value at 350 K.

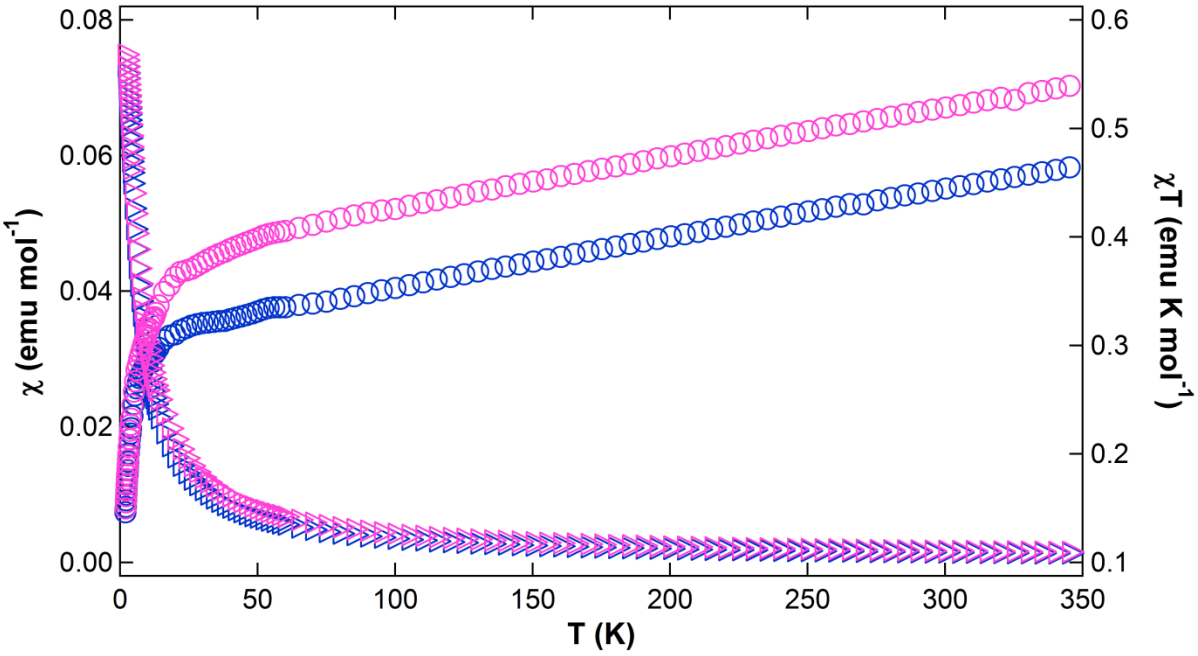

Figure 4.7. Variable temperature magnetic susceptibilities for **13** (blue) and **14** (pink). χ vs T (triangular markers) shows the gradual temperature variant, whereas χT vs T (circular markers) illustrates pronounced temperature regions.

Table 4.4. Summary of room temperature magnetic susceptibility data for **3-14** in comparison to reported U^V complexes.

U^V Complexes	μ_{eff} (μ_B/U^V)
UCl_5[a]	2.00
$UF(SO_3F)_4$[b]	2.8
$UO(SO_3F)_3$[b]	3.5
$(^RArO)_3U(=NSiMe_3)$[c]	2 – 2.24
3-10[d]	2.22 - 2.53
11	2.65
12	2.48
13	2.27
14	2.38
15	2.03

[a,b] see reference [52]. [c] see reference [53].
[d] see reference [11].

Magnetic moments (μ_{eff}) for **3-14** between 2.03-2.65 μ_B were extracted from a linear fit of the high temperature region obtained with the B = 5.0 T magnetic field. These values are in agreement with the range reported for U^V complexes,[52-54] however, are slightly lower than those predicted by the RS model (except for **11**). The difference between calculated and actual magnetic susceptibility values has been presumed to indicate a significant admixture of magnetically active ground and low lying excited states comingled by the ligand field. Deviations between observed and calculated magnetic data have been ascribed to a consequence of enhanced covalent interactions involving the 5f manifold to relieve the degeneracy predicted by the free ion term.[50,51] If this were an accurate assumption then significant differences between the room temperature magnetic moments for U^V complexes would be dependent on the symmetry and field strength of the donor atoms present. However, conspicuous similarities between the temperature dependent paramagnetic behavior of U^V complexes in octahedral versus lower-symmetry coordination geometries,

and π-donor imido versus predominant σ-bonding in UCl_5 imply insignificant differences in the ground state crystal field splitting parameters. Likewise, a comparison of the magnetic susceptibilities for the entire series of U^V-halides and new substituted derivatives reveal minor differences in magnetic behavior. Thus, there is no obvious disparity between the magnetically active 5f states regardless of substitution effects for this series of complexes.

The susceptibility values obtained experimentally for **3-14** are lower than those observed for $5f^2$ and $5f^3$ systems, not only as a result of increased spin contribution from the multiplet terms in the latter, but also indicative of the strong crystal field approximation customary for high-valent species where enhanced covalent attributes quench metal spin densities by lifting degeneracy from the RS scheme.[53] In contrast, tri- and tetravalent uranium complexes display susceptibilities closer in range to the calculated values. These discrepancies may in fact convey greater 5f covalent interactions for higher oxidation states.

4.3 Conclusion

In light of the scarcity of pentavalent uranium complexes reported in the literature, initial endeavors of Graves and co-workers pioneered a reliable systematic entry point to gain access to this elusive oxidation state. We have extended our studies on organouranium(V)-imido complexes to generate a variety of derivatives prepared via salt metathesis, protonolysis, or Cu^I oxidation methodologies. This collection of complexes with a rare metal oxidation state presents an ideal platform to study the effects of ligand substitution on the electronic properties of a structurally homologous series of complexes with the simplified $5f^1$ electronic configuration. Information garnered from complimentary electrochemical, electronic spectroscopic, and temperature dependent magnetic moment measurements

indicate nearly insignificant perturbations on the $5f^1$ system regardless of the surrounding ligand field.

The most noticeable differences are observed for the F (**7**), NPh_2 (**13**) and OPh (**14**) derivatives, where redox potentials and intra-5f absorption profiles signify minor orbital disturbances by π-donor ligand fields interpreted as ground and excited state splitting variation. The fact that the bent metallocene-imido complexes reported here exhibit magnetic susceptibilities and electronic absorptions nearly indistinguishable to those observed for other $5f^1$ complexes in higher symmetry coordination environments suggests that the 5f orbital manifold is remarkably insensitive to symmetry and subtle field strength alterations in the ligand field. However, indirect evidence of the effects of enhanced covalency with respect to ligand substitution are manifested in intra-5f absorption oscillator strengths an order of magnitude larger than those previously reported due to an intensity stealing mechanism. This dependence implies that ligation in the wedge is mediated through the same uranium based valence orbitals, both 5f and 6d, that bind the imido functionality.

Since there was an anomalous instance where the expected salt metathesis route turned out to generate a U^{VI} bis-imido species in a process reminiscent of PCET type reactivity, we are currently looking into the possibility of expanding upon novel reactivity pathways for these complexes. Furthermore, these rare complexes are more stable than previously reported, and the $5f^1$ system is among the simplest electron configuration to interpret for the actinide series. We are currently extending our interests to study the preparation of a multitude of new derivatives, and to probe electronic communication between multiple U^V centers tethered in close proximity through the prominent wedge substitution site.

Chapter 4

Part II: Exploring Electronic Communication in Homobimetallic High Valent Uranium Organo-Imido Complexes

Abstract

Two bimetallic organouranium(V)-imido complexes of the formula $[(C_5Me_5)_2U(=N\text{-}2,6\text{-}{}^{i}Pr_2\text{-}C_6H_3)]_2(\mu\text{-}N(Bz)\text{-}C_6H_4\text{-}N(Bz))$ (**18**) and $[(C_5Me_5)_2U(O\text{-}2,6\text{-}{}^{i}Pr_2\text{-}C_6H_3)]_2(\mu\text{-}N\text{-}C_6H_4\text{-}N]$ (**19**) have been prepared via salt metathesis and azide oxidation, respectively. The U^{VI} bimetallic analogue $[(C_5Me_5)_2U(=N\text{-}2,6\text{-}{}^{i}Pr_2\text{-}C_6H_3)]_2(\mu\text{-}N\text{-}C_6H_4\text{-}N]$ (**20**) was furnished from an azide oxidation reaction. Analytically pure samples of each complex have been isolated in high yield and characterized using ^{1}H NMR spectroscopy, elemental analysis, single crystal x-ray diffraction, cyclic and square wave voltammetry, UV-visible-NIR electronic absorption spectroscopy, and variable temperature magnetic susceptibility measurements. The series of bimetallic species documented herein are based on the bent metallocene-imido framework, and substitution of unidentate *p*-phenylene substituted bridging ligands takes place within the metallocene wedge. Structural parameters for these complexes are within the expected ranges predicted from mononuclear studies in Part I, and the uranium ions are supported at a distance of ~9 Å apart. Complex **18** is non-centrosymmetric, whereas centrosymmetric **19** and **20** are structurally homologous except for metal ion oxidation state and imide versus aryloxide ancillary ligands situated in the wedge. **18** and **19** each display reversible $U^{IV/V}$ and $U^{VI/V}$ redox couples,

along with a reversible process associated with the phenylene linkage. Similar to monometallic derivatives (**3**-**14**) the oxidative waves display limited electron transfer kinetics in comparison to facile reductive processes. **18** exhibits overlapping waves for the two metal based $1e^-$ step processes indicative of negligible electrochemical communication, whereas **19** displays separation between individual oxidative waves (200 mV) and reductive waves (160 mV) signifying intramolecular metal ion communication on the voltammetric timescale. In contrast, the hexavalent species (**20**) displays two reductive process, one of which corresponds to the $U^{VI/V}$ couple at -1.74 V, analogous to the monometallic bis-imido species **16**. UV-visible charge transfer absorption features for **18**-**20** are consistent with monometallic analogues, whereas low intensity intra-5f electronic transitions in the near-infrared region demonstrate significantly altered spectral signatures for **18** and **19** in comparison to monometallic derivatives. Variable temperature magnetic susceptibility measurements illustrate a small degree of $5f^1$-$5f^1$ spin exchange, and the additive magnetic moments of 3.38 μ_B indicate the two U^V ions in each complex behave as isolated paramagnets with weak ferromagnetic exchange in the elevated temperature region. Together these data suggest that the single f electron confined to the 5f orbital manifold at each metal site is only mildly sensitive to correlation with an identical U^V site tethered in close proximity.

4.4 Introduction

General interests in the isolation and diagnostics for discrete multimetallic assemblies have sparked fascination since the dawning of the Creutz-Taube ions.[55] Substantial attention has been devoted to d-block species and their prolific permutations, due to intramolecular metal ion communication that can be harnessed for key applications in the fields of mimetic bioinorganic design and molecular electronic devices.[56,57] In contrast to authoritative investigations on d transition metal homo- and heteropolynuclear iso- and mixed valent complexes, alternative f-element contributions within this arena have remained relatively under-represented.[58-60] Shortcomings for the lanthanide and actinide ion platforms are indeed a consequence of synthetic challenges presented by large ionic radii that impart flexible coordination modes where steric control must be implemented to render fixed structures. The shortage of light actinide multimetallic complexes is surprising since respective ions possess provocative electronic structural features due to 5f orbital complexities in housing valence electrons and participating in chemical bonding in reactivity. However, the multitude of valence 5f orbital lobes lack directional bonding requirements yet exhibit radial extension of electron density in contrast to contracted f orbitals for the lanthanide and late-actinide series.[61] Therefore, accentuated electronic communication could be expected from derivatives of the former.[60] Together, these rationale explain the overwhelming structural investigations on oligomeric actinyl coordination topologies, which are accustomed to restricted ligand binding in the equatorial plane due to steric requirements of the linear $[O=An=O]^{n+}$ moiety.[62] However, recent advances have sought to focus on organoactinide bent metallocene fragments, due to convenient access to a variety of available oxidation states, for use as directional building blocks to assemble discrete multimetallic species upon ligand substitution in the wedge area.[63]

Our interrogation of molecular and electronic structural aspects of an arsenal of monometallic uranium complexes in the neglected pentavalent oxidation state motivated exploration into bimetallic analogues since there are only three reports that pertain to well defined corresponding U^V multimetallic derivatives, all of which infer intramolecular metal-metal communication. The homoleptic U^V pentaethoxide dimer $[U(OC_2H_5)_5]_2$ displays a lower magnetic moment than expected, resulting from a weak antiferromagnetic interaction between two $5f^1$ spins.[64] The isopolyoxometallate $[U_6O_{13}Bpy_2Cp^{‡}_4]$ prepared by Duval and co-workers (Figure 3.1) contains a cluster of bent uranyl(V) ions supported by dative cation-cation type interactions with organic capping ligandds at the terminals (i.e., bpy, $Cp^{‡}$).[65] The six U^V ions act as individual paramagnets where weak antiferromagnetic coupling was observed at high temperatures, while electrochemical studies suggest that the cluster is not robust on the voltammetric timescale. The properties observed for this cluster complex are in contrast with early transition metal isopolyoxometallate congeners capable of multiple reversible reductions and display strong magnetic coupling between d^n ions.[66] Andersen and colleagues compared two para- and meta-substituted phenylenediimido bridged $(C_5H_4Me)_2U^V$ fragments, shown in **Figure 4.8**, where the *p*-substituted derivative (**i**) displayed pronounced antiferromagnetic exchange as a result of spin polarization that couples the U^V ions across the π-conjugated bridge.[67]

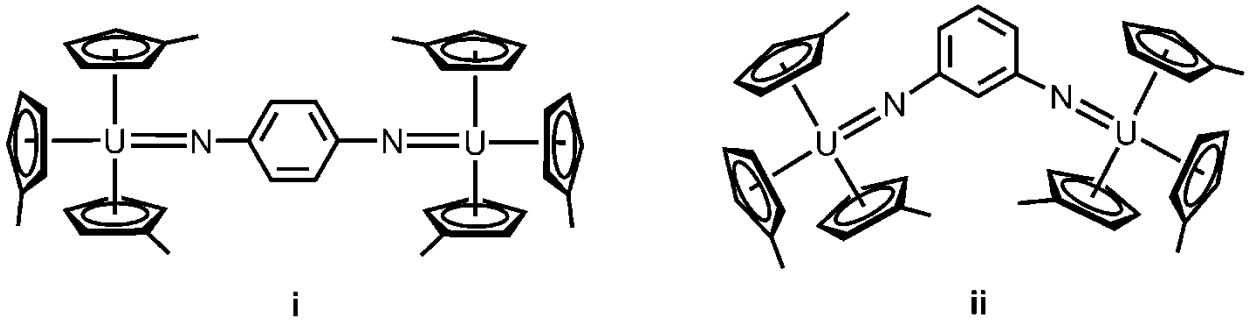

Figure 4.8. Organouranium(V)-imido bridged bimetallics reported by Andersen and co-workers.[67]

Andersen's exquisite U^{V}-U^{V} prototypes inspired us to investigate electronic communication phenomena in more depth for $5f^{1}$ electronic materials. This report questioned the presence of a U^{III} impurity in magnetic samples, and lacked conclusive structural, electrochemical, spectroscopic, and theoretical characterization data such that exact structure-property relationships deserve more a detailed systematic treatment. On the other hand, a series of symmetric Mo^{V} d^{1} bimetallic complexes established electronic communication in electrochemical, magnetic, and spectroscopic studies, and these studies serve as a cornerstone for comparison to $5f^{1}$ systems.[68] Together these d and f high-valent transition ion species possess simplified electronic structural properties in contrast to multiplet spin orbit states derived for low valent ions. For the actinides, interpretation of these data are complicated by spin-orbit coupling and the symmetry of ligand field perturbations, however, as it was shown in Part I for the monometallic comparison there are not large differences that accompany modification of the coordination environment.

The studies in this report are predicated on the rational design of structural and electronic criteria required to exert electronic communication as a function of the symmetry at each metal site, the mutual distance and symmetry between the metal ions, and relative energies and spatial arrangement of metal and ligand respective HOMO and LUMO manifolds.[69] However, in

examples where the metal ions are separated by a distance to large to mediate interactions directly through space, electronic communication can be transmitted across the bridging conduit (i.e., superexchange pathway) that is largely dependent on the ability of metal based valence orbitals to participate in covalent overlap to assist in delocalizing spin density across a π-conjugated bridge.[70] The electrochemical methodology to probe communication is based on the response of one metal to changes in electron density at the other metal site upon redox stimulation, where larger potential separations between redox waves are ascribed to a greater degree of communication.[71] Similarly, electronic spectral profiles are dependent on the presence of second metal ion to influence energies and intensities of transitions in relation to monometallic derivatives.[72] Variable temperature magnetic susceptibility measurements have been used to examine communication to a much greater extent than other diagnostic methods. In this case, magnetic coupling is manifested through space or by alignment of radical-like metal paramagnetic spin exchange via polarization concerted across the bridging link.[73] For actinides the questionable degree of admixtures of 5f and 6d spatial overlap that participate in multiple bonding is of extreme significance since the magnetically active electrons reside in states derived from 5f character. Depending on the orientation of orbitals interacting with those of the bridging ligand (i.e. orthogonal or parallel) it is generally much more difficult to acquire exact experimental assessment of bridging interactions as opposed to contacts through space.[74]

The investigation documented below reveals the results of synthetic and characterization developments in the pursuit to establish U^V-U^V electronic communication between U^V ions flanked by *p*-phenylene bridging components that separate the metal ions ~9 Å apart. The strategic crafting of discrete U^V bimetallics extends from well-founded monometallic endeavors, where the intent to probe electronic communication is predicated on a range of information

gleaned from individual metal ion fragments as benchmark to acquire predictable characteristics from structural-property associations when conjoined by bifunctional para-substituted phenylene-diimide and -diamide bridges. Two isovalent $5f^1$ bimetallic assemblies contain U^V-U^V ions tethered ~9 Å apart are stable with respect to disproportionation. Their syntheses utilize salt metathesis and oxidative routes known to produce pentavalent uranium complexes. The U^V ions within these complexes enable structural parameters, electrochemical signatures, spectral fingerprints, and variable temperature magnetic moments that compare and contrast with monometallic organouranium(V)-imido derivatives. This report also introduces a hexavalent uranium analogue with similar bimetallic structural properties to the pentavalent derivatives. The resulting molecular and electronic structural designs were characterized by the combination of NMR spectroscopy, X-ray crystallography, elemental analysis, cyclic and square wave voltammetries, UV-visible-NIR electronic absorption spectroscopy, and variable temperature magnetic susceptibility measurements.

4.5 Results and Discussion

Synthesis and Structural Characterization

Two preparative routes were employed to produce the discrete bimetallic complexes **18-20**. The synthetic procedure used to prepare **18** involves salt metathesis between two equivalents of **10** with the dipotassium salt of N,N'-bis(benzyl)-*p*-phenylenediamine shown in **Scheme 4.4**. This procedure is analogous to that used for the synthesis of the monometallic amide derivative (**13**) in Part I of this chapter, and following workup in hexanes the U^V-amido bridged bimetallic complex was afforded as a black crystalline solid in 42% yield based on uranium. Salt metathesis and protonolysis attempts failed to produce a *p*-phenolate analogue, whereas a series of Mo^V

derivatives with this ligand have been prepared successfully in the past.[68] The synthesis of **19** and **20** follow the azide oxidation pathway first developed for early transition metal complexes, and later extended to the actinides by Andersen and coworkers.[14,19,75] This procedure involves facile two electron oxidation of low valent uranium precursors with *p*-diazidobenzene shown in **Scheme 4.5**. Starting with two equivalents of the trivalent aryloxide precursor $(C_5Me_5)_2U(O\text{-}2,6\text{-}{}^{i}Pr_2\text{-}C_6H_3)THF$ (**17**),[14] this oxidative procedure generates the U^{V}-imido linked bimetallic (**19**), whereas starting from the tetravalent imido complex (**2**)[11,19] produces the U^{VI} bis-imido analogue (**20**). Similar oxidative routes have been developed in the past to produce high valent monometallic uranium complexes stabilized by multiply bound imide and oxide ligands and is reminiscent of the route used by Andersen to prepare the U^{V} bimetallics in Figure 4.7.[14,19,67] As shown in Scheme 4.5, the reaction liberates dinitrogen rapidly, and after stirring for 1 h the resultant mixture was pumped to dryness and the residue redissolved in hexanes, upon which single crystals suitable for xrd studies were isolated from solution at -30ºC in respective yields of 78% and 85% based on uranium. It should be mentioned that attempts to prepare a version of **19** starting from the U^{III}-amide precursor $(C_5Me_5)_2U(NPh_2)(THF)$ failed to produce the corresponding bimetallic species, and oxidation was accompanied by ligand redistribution to produce $(C5Me_5)_2U(NPh_2)_2$ (**21**) under a range of solvent and temperature controlled conditions.[76,77] It was gathered from this observation that the superior aryloxide ligand served as a more secure ancillary ligand than the diphenylamide, likely due to the shorter bonds commonly encountered for complexes of the former, and prevents the proclivity for any undesirable redistribution event during production of **19**.

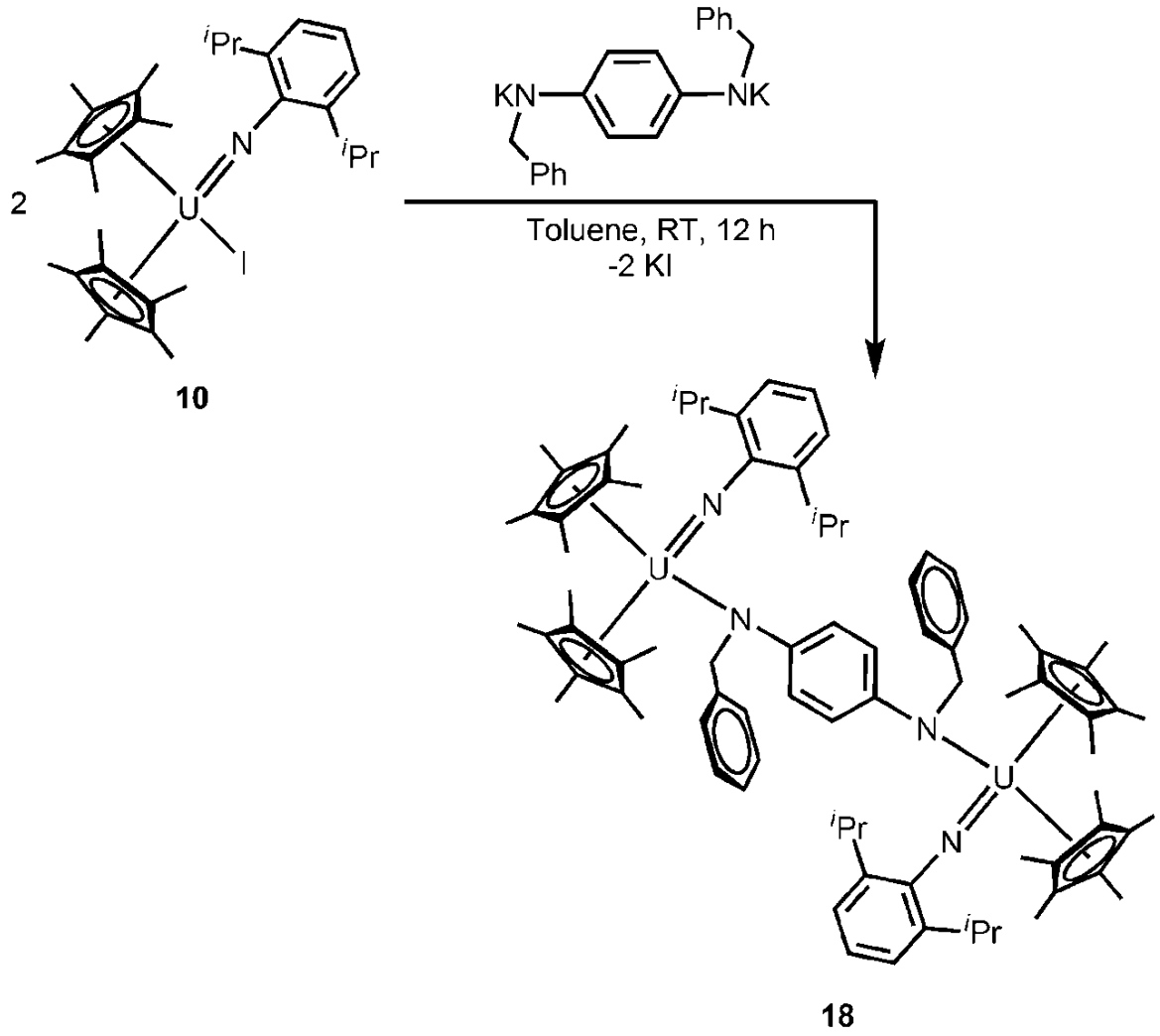

Scheme 4.5. Synthesis of the U^{V}-amide bridged bimetallic **18**.

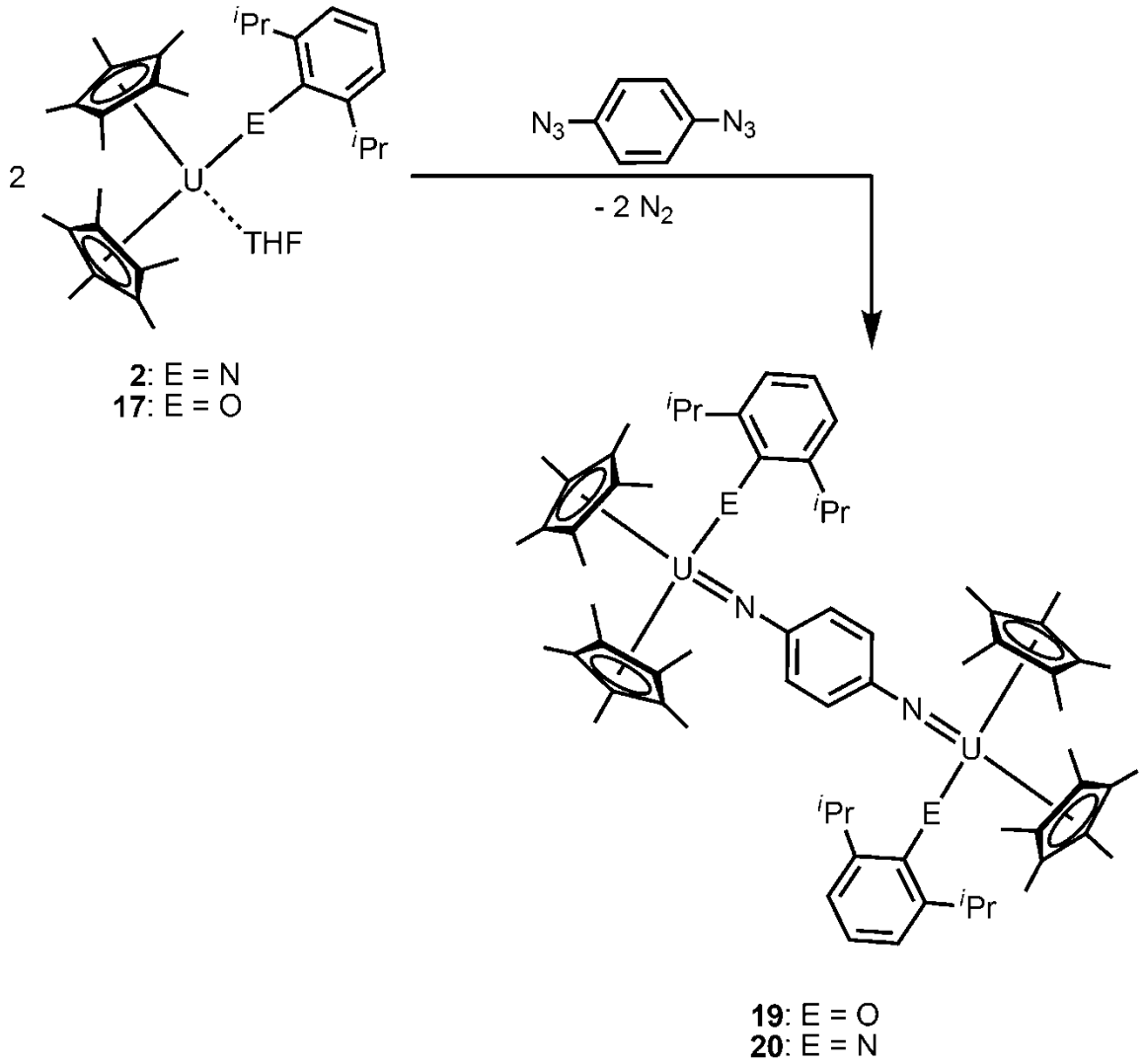

Scheme 4.6. Synthesis of U^{V} and U^{VI}-imide bridged bimetallics **19** and **20**.

^{1}H NMR spectroscopic characteristics for the two U^{V} bimetallic species are quite different by comparison. The ^{1}H NMR spectrum of **18** depicts two broadened resonances at 8.87 ppm and 5.18 ppm, thus any structural features are unidentifiable by NMR. This spectral profile is similar in both toluene-d_8 and THF-d_8 solvents, providing evidence that the complex retains the discrete bimetallic structure upon dissolution and does not dissociate into solvated monometallic fragments. These broadened spectral bands contrast the sharp well defined peaks

characterized for the monometallic pentavalent derivatives in Part I, and this difference might possibly signify an altered paramagnetic situation due to the presence of two $5f^1$ centers attached across the bridging unit. On the other hand, complex **19** displays an NMR spectrum indicative of a U^V ion complex with slightly broadened integratable peaks that fall within the expected paramagnetic chemical shift region comparable to monometallic derivatives. For example the presence of four C_5Me_5 ligands in similar chemical environments give rise to one intense peak observed at 4.98 ppm that integrates to 60 H. The phenylene protons on the bridging unit show a singlet at 0.21 ppm, and ^{i}Pr substituents on the aryloxide ancillary give rise to a set of broad singlets at 12.43 ppm and -8.64 ppm that indicate hindered rotational motion about the U-O-Ar^{i}Pr linkage. These identifiable NMR handles reflect the centrosymmetric structural arrangement discussed below.

The ^{1}H and ^{13}C NMR spectra for complex **20** are analogous to those found for the monometallic hexavalent bis-imido species **16** (from Part I). The spectroscopic peaks exhibited by this bimetallic complex are sharper than those observed for pentavalent analogues and fall within the typical chemical shift regime (0-10 ppm) indicative of the formal diamagnetic U^{VI} bis-imido bimetallic arrangement. The NMR spectrum in this case reflects striking molecular structural similarities to **19**, where an intense peak for the C_5Me_5 resonances at 4.31 ppm, a singlet for the phenylene protons on the bridged at 4.63 ppm, and two ^{i}Pr doublets at 2.23 ppm and 1.64 ppm are indicative of obstructed rotational motion about the uranium imido attachment. Due to the NMR spectroscopic differences between the pentavalent analogues **18** and **19**, and the similarities between the pentavalent and hexavalent derivatives **19** and **20**, X-ray crystallographic analyses were undertaken to conclusively assign molecular structural features for the bent-metallocene bimetallics with bond length and angle parameters that fall within the ranges

expected from the analogous monometallics discussed in part I. Pertinent crystallographic parameters are given in **Tables 4.5** and **4.6**.

The solid state molecular structures of **18**-**20** consist of bent-metallocene uranium units attached by para-substituted phenylene linkers. Complex **18** contains individual U^{V}-imide units $(C_5Me_5)_2U(=N\text{-}2,6\text{-}^{i}Pr_2\text{-}C_6H_3)$ bridged through amide donors from the N,N'-bis(benzyl)-*p*-phenylenediamide ligand shown in **Figure 4.9**. The geometry at each uranium center is *pseudo*-tetrahedral with amide and imide ligands situated in the wedge. The respective U^{V}-amide, -imide, and –permethylatedcyclopentadienyl bond parameters compiled in **Table 4.5** fall within the expected range comparable to the monometallic U^{V}-imide/amide derivative (**13**) exemplified in Part I and respective references therein. Due to the geometry about the *p*-phenylenediamide bridge, the top C_5Me_5 ancillaries fall roughly parallel to the C_6H_4 phenylene bridging moiety, whereas and the two bottom C_5Me_5 ligands are forced to tilt out of the way. The N,N'-benzyl substituents on the bridging functionality are oriented in the same direction with faces of the aryl planes parallel to one another. This arrangement forbids a center of symmetry, and the dual benzyl orientation likely arises from long range C-H$\cdots\pi$ interactions with proximal methyl and isopropyl protons. Complex **18** bears two symmetry elements including a C_2 rotation axis directed orthogonal to the centroid of the C_6H_4 linkage, and a mirror plane bisects the C_6H_4 phenylene bridge. Together these symmetry operations generate the bimetallic framework from the asymmetric repeating unit, where the two U^{V} ions are supported a distance of 9.226 Å apart.

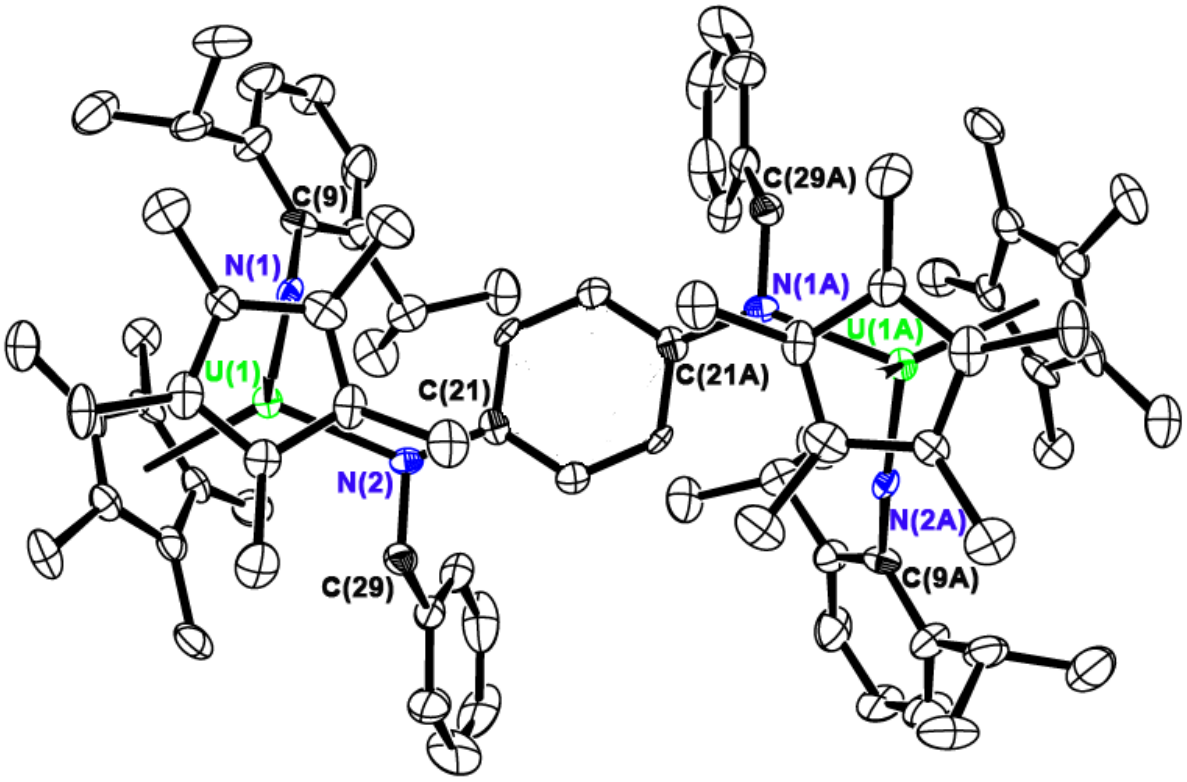

Figure 4.9. Molecular structure of **18** with thermal ellipsoids depicted at 50% probability.

Table 4.5. Selected metrical parameters for complexes **18-20,** where L represents the ancillary donor ligand present in the wedge. **19** is based on a poorly refined data set, and refinement of disorder in **20** is pending.

	18 L = N(Bz)(C_6H_4)N(Bz)	**19** L = (O^iPr_2Ar)	**20** L = N($^iPr_2Ar$)
U-L (Å)	2.257(7)	2.132	1.936(9)
U-L-C (º)	-----	165.77	175.9(8)
U=N (Å)	1.990(7)	1.956	1.972(9)
N-C_{ipso} (Å)	1.393(10)	1.461	1.367(14)
U=N-C (º)	173.1(6)	171.46	171.5(7)
L-U=N (º)	95.8(2)	108.96	108.7(4)
U···U (Å)	9.226	9.517	9.536

The slightly distorted centrosymmetric molecular frameworks in **19** and **20** are isostructural. Complex **19** contains two bent-sandwich U^V-aryloxide fragments $(C_5Me_5)_2U(O\text{-}2,6\text{-}^iPr_2\text{-}C_6H_3)$ bridged by the *p*-phenylenedimido unit. Exact metrical parameters for **19** could not be obtained due to the poor quality of x-ray data collected on single crystals, however the approximate bond parameters are within the range expected, comparable to those observed for the monometallic U^V-aryloxide analogue (**14**) discussed in Part I. More importantly, the uranium-arlyoxide and –imide attachments are short with nearly linear U-E-C_{ipso} (E = O, N) angles indicative of multiple bonding within the ample space provided in the metallocene wedge. The metal ions are held at a distance of ~9.516 Å apart, not all that much different from **18**, and consistent with the M···M distances in other characterized *p*-phenyleneimido bridged bimetallic complexes.[75] The most distinct structural disparity between the U^V bimetallic complexes is the presence of the amide (**18**) versus imide (**19**) donors presented at the *para* positions on the phenylene bridging units. These donors impart varied symmetries for the resultant bimetallic species, where **19** is centrosymmetric and **18** is not, due to the proximal benzyl substituents in the latter. Alongside this observation is the elongated U-N_{amide} contact in the former in comparison to the short U=N_{imide} for the latter. A final notable feature for both is the C_6H_4 phenylene ring atoms in the bridge are arranged in a coplanar orientation with U and N atoms situated in wedge.

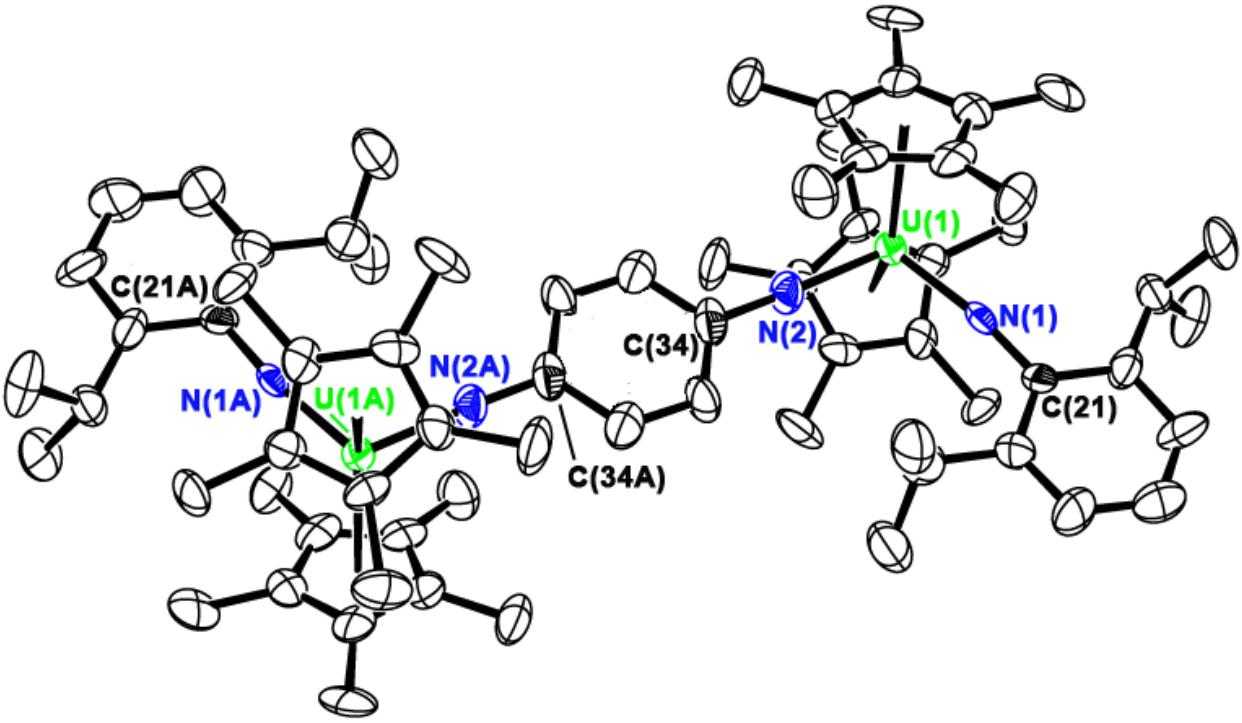

Figure 4.10. Molecular structure of **20** with thermal ellipsoids depicted at 50% probability. The structure of **19** is similar and provided in the supporting information.

Complex **20,** on the other hand, is a U^{VI} bis-imido complex that like **19** possesses the same *p*-diimidobenzene bridging linkage. However, for complex **20** the ancillary unit in the metallocene wedge is identified as a diisopropyl substituted arylimide ligand. The structural parameters for the U^{VI} bis-imido bimetallic complex (**20**) are comparable to those observed in other complexes reported of this construction, including the monometallic derivative **16** disclosed in Part I and references therein. Specifically the parameters for the two imido units situated in the wedge contain short average bonds (1.97 Å) with nearly linear U=N-C_{ipso} average angles (174º) indicative of multiple bonding for both imide units. Across the entire series of penta- and hexavalent species discussed here, the U-$(C_5Me_5)_{centroid}$ and U=N-C parameters are consistent, listed in Table 4.5.

Table 4.6. Selected crystallographic parameters for **18** and **20**.

	18	**20**
Formula	$C_{84}H_{122}N_4U_2$	$C_{75}H_{98}N_4U2$
a (Å)	34.745(5)	11.1290(15)
b (Å)	10.4755(14)	16.080(2)
c (Å)	23.027(3)	20.767(3)
α (º)	90	83.198(2)
β (º)	110.339(2)	79.802(2)
γ (º)	90	87.113(2)
V (A^3)	7858.6(18)	3630.3(8)
Z	8	2
FW	1663.98	1531.69
crystal system	monoclinic	Triclinic
space group	C*2/c*	P-*1*
T (K)	100(2)	120(1)
λ (Å)	0.71073	0.71073
ρ_{calc} ($g \cdot cm^{-1}$)	1.471	1.504
μ (mm^{-1})	4.163	4.501
F(000)	3512	1660
θ range (º)	1.87 - 25.13	1.86 - 24.76
total reflections	36361	33074
unique reflections	7007	12270
parameters	448	494
R_1	0.0421	0.0678
wR_2 (all data)	0.1197	0.1971
max min peaks e$Å^{-3}$	1.315, -1.027	1.722, -1.758
GOF on F^2	0.560	0.827

Electrochemistry

Cyclic and square wave voltammetric data was acquired for the bimetallic complexes **18-20** to assess the nature of the $U^{VI/V}$ and $U^{V/IV}$ redox couples as a function of intramolecular electronic interactions. Electrochemical experiments were carried out at room temperature in ~0.1 M [TBA][BAr_f]/THF solution in a drybox, and potentials determined by the average of the cathodic and anodic waves referenced to the ferrocene/ferrocinium internal standard and found to correspond with peaks in the respective square wave voltammograms. Intramolecular electronic communication between two metal ions supported across a bridging unit is borne out of

electrochemical data by the presence of multiple redox processes. In general, the larger separation observed between waves assigned to the same redox couple for each metal ion, the greater degree of interactive communication.[71] To clarify, if one metal is oxidized or reduced, the other metal ion is responsive to the electroactivity of the other. This description is simplified in assuming that the ligands are 'innocent' and do not convolute observation of the desired process or participate in any charge transfer.[78,79] In accord with studies on monometallic U^{V} organo-imido complexes, two separate oxidation and reduction waves were expected to result in a total of four individual $1e^{-}$ stepwise processes. Each species exhibits multiple redox waves including facile uranium based oxidation and reduction along with ligand based processes with no sign of any disproportionation as discussed below. Discerning the voltammetric assignments is informative of the extent of electronic communication between uranium ions, and thermodynamic and kinetic information for each is summarized in **Table 4.7**.

The amide bridged U^{V} bimetallic complex **18** exhibits three reversible redox processes, including well defined waves at -1.69 and -1.95 V and a broad process centered near -0.53 V in the cyclic and square wave voltammograms (**Figures 4.11** and **4.12**). The process at -0.53 V falls near the potential range expect for $U^{VI/V}$ oxidative couple, however it is shifted by 200 mV to a more negative potential than monometallic amide derivative (**13**) discussed in part I. The anodic half of this wave is considerably broadened, which is a sign of sluggish electron transfer kinetics characterized for monometallic $U^{VI/V}$ oxidative processes. However in this case, the broadness is also indicative of two simultaneous individual electron oxidations for both metal ions. As illustrated in the square wave plot the double humped peak shape analysis centered near -0.53 V yields a separation of about 110 mV with comparable current produced for each individual oxidation step (**Figure 4.12**). In contrast, the two low potential processes to the right of the rest

potential (~1.0 V) are clearly separated by ~260 mV. The first step at -1.69 V is on par with the $U^{V/IV}$ reduction reported for the monometallic amide species ($U^{V/IV}$ for **13** is -1.63 V), however the second process in this region (-1.95 V) requires greater energetics than any $U^{V/IV}$ couple is likely due to participation from low energy empty π* molecular orbital delocalized on the phenylene moiety in the bridging unit.

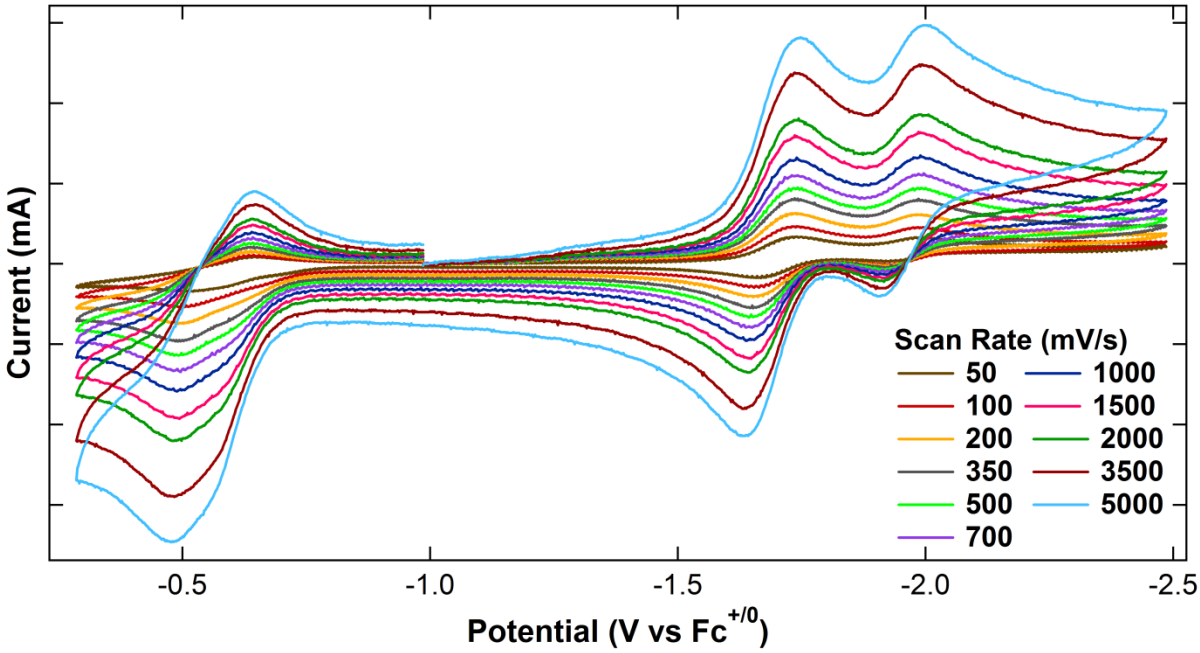

Figure 4.11. Cyclic voltammetric data for **18** with variable scan rates between 0.05 and 5.0 V/s.

These tentative electrochemical assignments are further supported by the current observed for the square wave voltammetric peaks, portrayed in **Figure 4.12,** as a direct measure of the type of process (i.e., oxidative or reductive) and the number of electrons participating in each. The broad oxidative wave centered near -0.53 V and the single reductive wave at -1.95 V each produce an equivalent (but opposite sign) current of ~6.5 μA, whereas the reductive wave at -1.64 V displays a current that is roughly double, 13.2 μA. These peak currents are an

informative first approximation of the number of electrons participating in each process. From left to right in the voltammograms, the first wave appears to be based on two one electron oxidations separated by a small potential (110 mV), the next is twice that indicating two $1e^-$ reductive process, and the most negative wave is ascribed to a one electron ligand based reduction. These approximations are more accurately confirmed by the relationship of the limiting peak current as a function of the square root of the scan rate from the cyclic voltammetric data.[41] Shown in **Figure 4.13**, using a least squares fit to simulate the ratio of electrons transferred, the total oxidation wave and the first reduction each arises from two coincident $1e^-$ electron process, whereas the more negative reduction is assigned to a single electron transfer. The oxidative wave, assigned to $U^{VI/V}$ oxidation of each metal ion, shows a slight separation between the two peaks indicative of a small degree of electrochemical interaction between the metal ions, where any lesser interaction would likely go unnoticed. The wave at -1.69 V is attributed to concerted $U^{V/IV}$ reduction of both metal ions, with no potential separation indicating a lack of electroactive communication. Finally, the process at the far right of the voltammogram is presumably a one electron ligand based ordeal, however voltammetric experiments must be performed on the free ligand (or the dipotassium salt) to give a more affirmative assignment for this process.

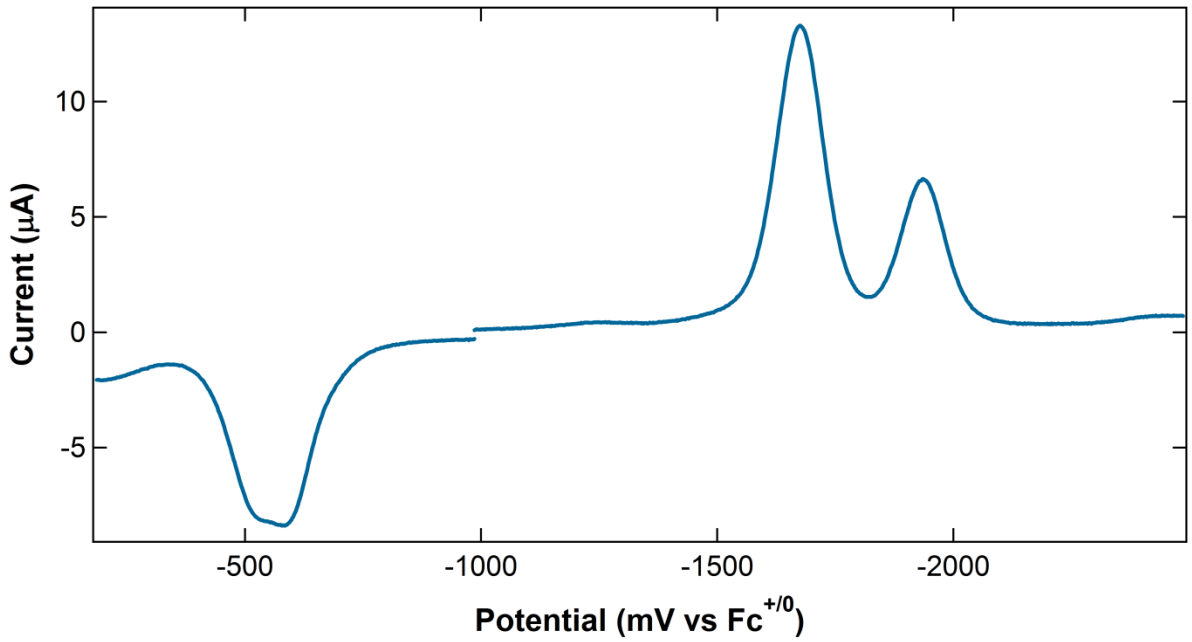

Figure 4.12. Square wave voltammogram for **18** obtained for the same solution used in cyclic voltammetric studies in figure 4.10.

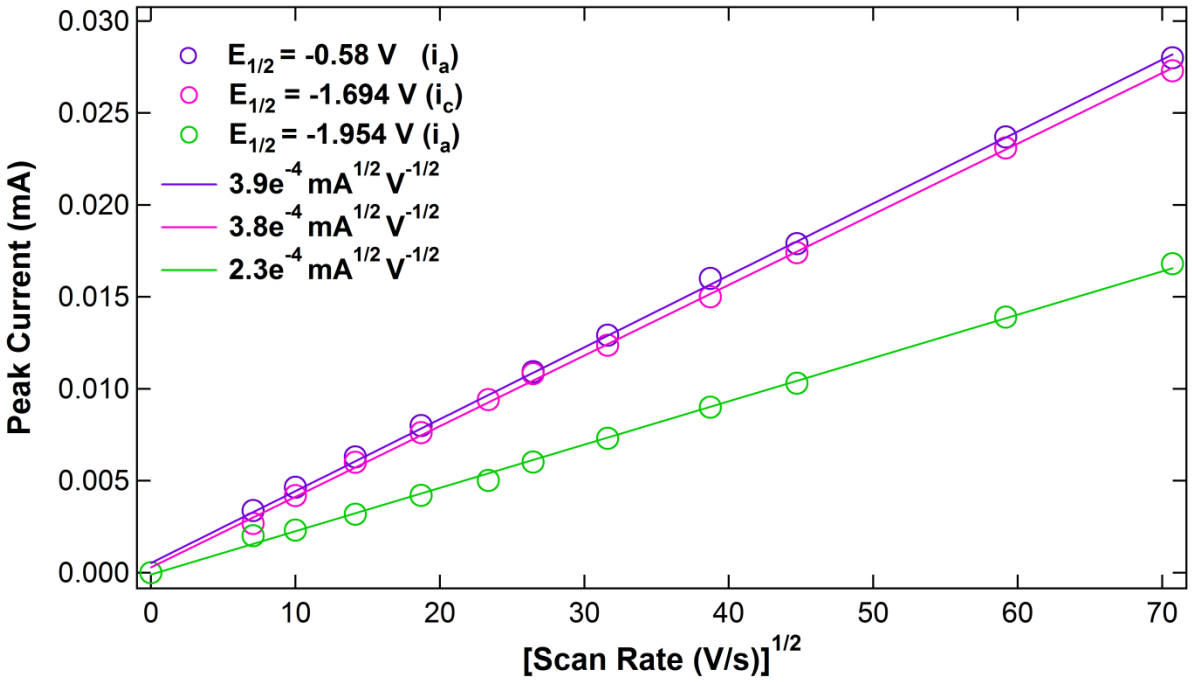

Figure 4.13. Peak current dependence on the scan-rate for **18**. U(VI/V) oxidation (purple), U(V/IV) reduction (pink) and ligand based reduction (green). The slopes for the lines were extracted from a linear least-squares fit for data points at each scan rate.

The U^{V}-imido bridged complex **19** displays metal-metal communication for both the $U^{VI/V}$ oxidation and $U^{V/IV}$ reduction, and these processes are more well resolved as individual one electron transfers than observed for the amide bridged congener **18**. Cyclic and square wave voltammetric data for **19** is shown in **Figure 4.14**. In the cyclic voltammogram a broad oxidative wave appears at -0.419 V, comparable to the potential for the $U^{VI/V}$ couple observed for monometallic U^{V} derivatives and **18**. The square wave plot in this region clearly shows a broad intense overlapping double-band and a low current peak separated by about 200 mV with negative peak currents indicative of oxidative processes. To the polarographic side of the rest potential, under more reducing energetics a series of three consecutive peaks appear at -1.56, -1.72, and -1.923 V that display variable scan rate dependent reversible electron transfer kinetics on the voltammetric timescale. Likewise these processes are present in the square wave sweep where the positive current produced for each is indicative of reduction. The more negative redox couple (-1.923 V) falls at a similar potential to that ascribed for the phenylene linkage in the bimetallic complex **18**, and appears to be conserved for the *p*-phenylenediimido unit here. To the best of my knowledge, no one has reported any redox associated with this phenylene linkage in any of its many bimetallic complexes, however it is not uncommon for phenyl rings to be reduced at a similar potential.[80] This leads to the deduction that the first two waves in this region are each attributable to one electron metal based $U^{V/IV}$ reductions separated by a potential of 160 mV. The separation between both oxidative and reductive metal based processes is a strong indication that the metal ions are in communication at a distance of ~9 Å across the bridging unit.

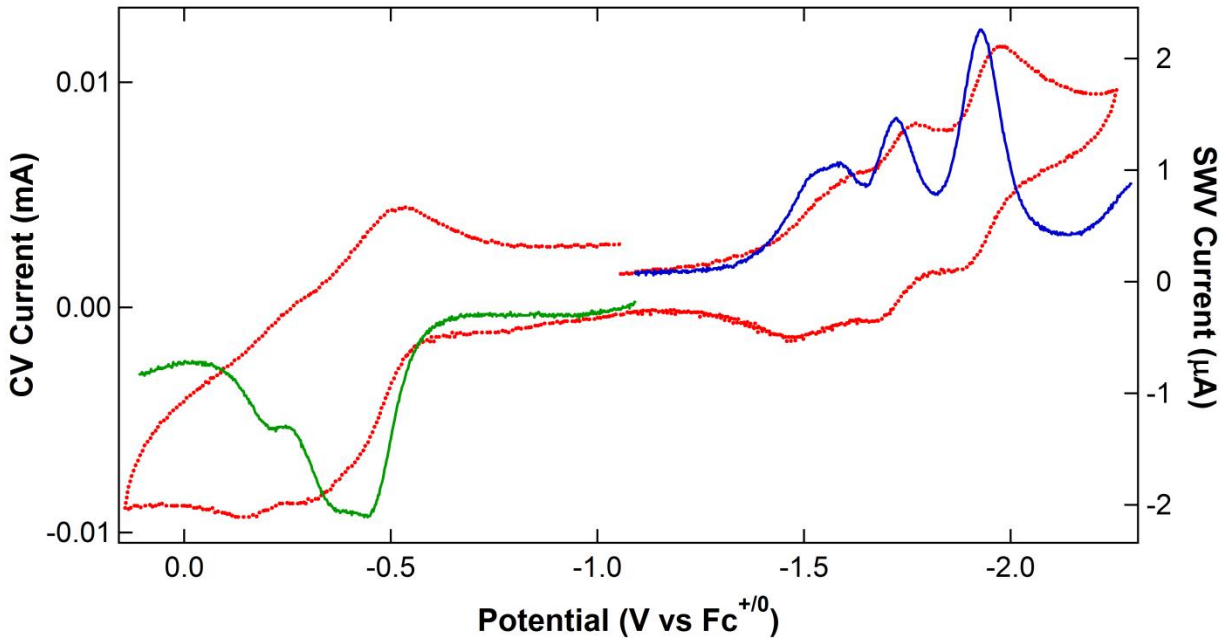

Figure 4.14. Cyclic (red) and square wave (green and blue) voltammetric plots for **19**.

The current produced in the area under each square wave voltammetric peak cannot be reasonably assigned to the relative number of electrons that take part in each process, and therefore to clarify this ambiguity the peak current dependence on scan rate variation was extracted to obtain a quantitative assessment for each of the observed waves. As shown in **Figure 4.15**, the slope for the linear least squares fit of the data approximates that each reduction arises from a one electron transfer, whereas the total peak current produced for the anodic scan of the oxidative wave is due to three single electron steps. The presence of three overlapping one electron oxidative waves was expected from the square wave data, and two of these are likely due to consecutive $U^{VI/V}$ processes whereas the third might be of ligand based origin, yet these tentative assignments require further inspection. A final observation on the electrochemical properties of the U^{V} bimetallics is the distinct separation between $U^{V/IV}$ couple versus the overlapping coincident oxidative waves. Whereas this might be a factor of sluggish electron

transfer kinetics inherent to oxidation of these U^V-imido species, a similar observation has been reported for Mo^V fragments tethered by *p*-substituted phenylene ligands into bimetallic assemblies. In these cases the energy levels of the metal based valence orbitals with respect to those of the ligand have been used to explain the anomalous peak separations. Specifically, oxidation of the metal based SOMO causes a cationic charge that lowers the energy of the metal orbitals to permit electronic delocalize via the LUMO of the bridge.[70] These accounts also commented that the ligand LUMO is too high in energy such that reductions are localized on the metal, and this is congruent with our observation of ligand based reduction that falls higher in energy than the U^V reduction. Further investigations will probe the substitution pattern (i.e., *p*-, *m*-, *o*-) and length variance of the bridge to assess if communication is a carried across the conduit bridge or simply a factor of metals in close proximity. We also plan to utilize the observed processes here to extend to synthetic chemical reductants or oxidants with the intent stabilize mixed valence species that appear to be accessible from these electrochemical studies.

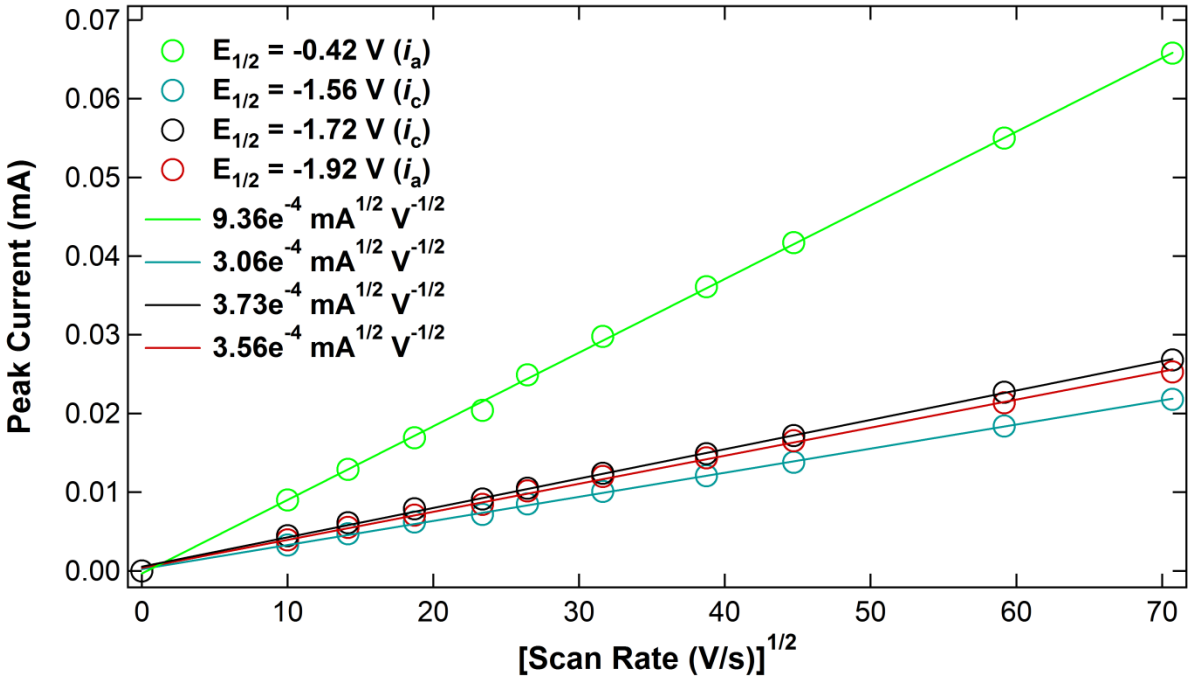

Figure 4.15. Peak current dependence on the scan-rate for **19**. U(VI/V) oxidation (green), U(V/IV) reductions (blue and black) and ligand based reduction (red). The slopes for the lines were extracted from a linear least-squares fit for data points at each scan rate.

The U^{VI}-imido bridged bimetallic complex **20** displays two well resolved reversible reduction waves at -1.75 and -2.14 V shown in **Figure 4.16**. Although this large potential separation (390 mV) would demonstrate considerable electrochemical communication for the $U^{VI/V}$ couple at each metal center, two reversible waves in the same potential region are also exhibited by the monometallic U^{VI} bis-imido species **16** and other reported monometallic analogues.[12] The square wave voltammograms for **16** and **20** (not shown) display two peaks in agreement with the cyclic voltammetric findings, each having roughly equivalent peak currents indicative of a one to one ratio for the number of electrons transferred in each step. Therefore, the potential for the first reduction is comparable to the $U^{VI/V}$ redox couple observed for neutral U^{VI} complexes, for example refer to the breadth of uranyl(VI/V) couples studied in Chapter 2 of this text and references therein. The second reduction that requires greater energetics might be a

second progressive $U^{V/IV}$ process. Although multiple progressive redox processes have been observed for organouranium species, this separation is considerably smaller than those reported, for example a separation of ~1.0 V was reported for $(C_5Me_5)_2U(N{=}CPh_2)_2$,[12] and this second peak is of uncertain origin. Notably, the $U^{VI/V}$ reduction observed in **16** and **20** require harsher energetics than the same process observed for oxidation of neutral U^{V} complexes, and this is an effect of the of the additional monoanionic charge present at the metal center.

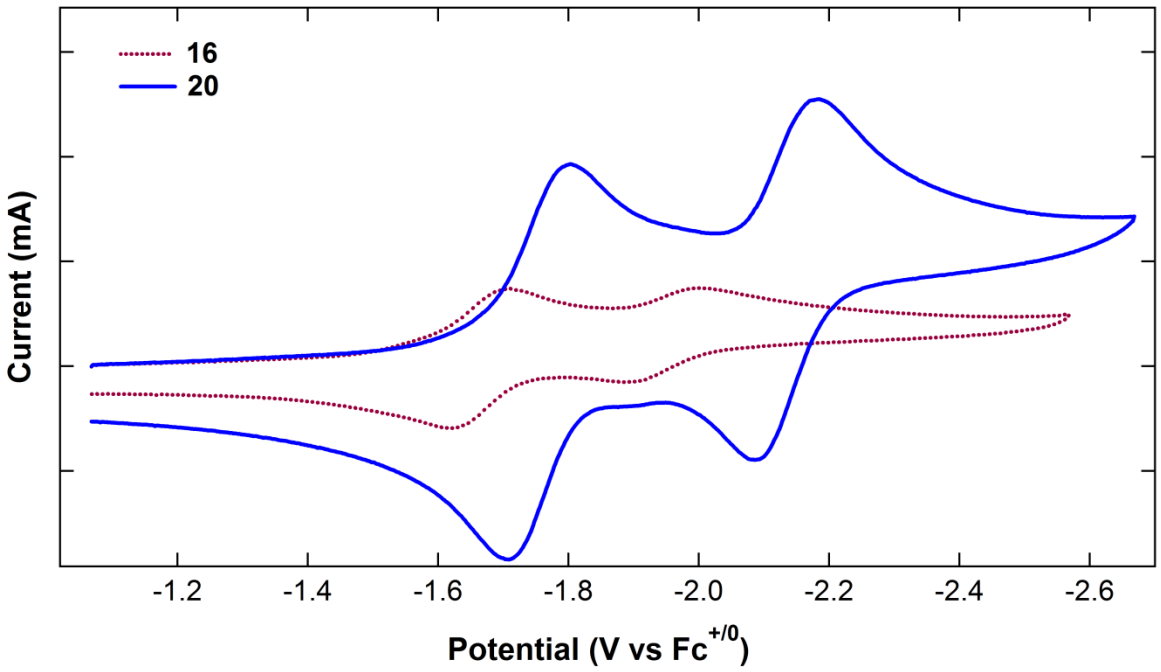

Figure 4.16. Cyclic voltammetric waves for uranium(VI) bis-imido complexes **16** (dashed) and **20** (solid).

Table 4.7. Summary of redox potential data for complexes **16-20** reported in V vs $Fc^{+/0}$.

Complexes	$E_{1/2}$ (U^{VI}/U^{V})	$\Delta E_{1/2}$	$E_{1/2}$ (U^{V}/U^{IV})	$\Delta E_{1/2}$	$E_{1/2}$ ($L^{0/-}$)
16	-1.72	-----	-----	-----	-1.97
18	-0.53,-0.62	0.11	-1.69	0	-1.95
19	-0.45,-0.37	0.08	-1.58,-1.74	0.24	-1.95
20	-1.76	-----	-----	-----	-2.14

Electronic Absorption Spectroscopy

Another diagnostic route to probe metal-metal communication would be the observation of differences in electronic transition energies and intensities in comparison to those observed for monometallic species, caused by field perturbations induced by a second metal ion in close proximity. Accordingly, the U^V bimetallic complexes **19** and **20** display slightly altered intra-5f absorption profiles in the NIR region with respect to the monometallic derivatives (**3-14**). As shown in **Figure 4.17**, each complex displays a broad peak near 6000 cm^{-1}, in the same region that f→f transitions ($\Gamma_7 \rightarrow \Gamma_{7'}$) were observed for the monometallic derivatives. In this case, the peak maxima display intensities comparable to the monometallic species, however the baseline is considerably more intense for each and convolutes the appearance of f→f bands. The origin of the intense baseline in the spectra for **18** and **19** is uncertain, although it is experimentally reproducible, and could presumably be a consequence of U^V ions in communication with one another. In each case the high energy UV-visible absorption progressions trail into the NIR region and convolute these narrow low intensity bands. The charge transfer absorptions for **18**-**20** present a nearly indistinguishable energy and intensities range in the UV-visible region in comparison to monometallic derivatives, however an additional peak near 10000 cm^{-1} is attributed to $\pi \rightarrow \pi^*$ transitions for the delocalized phenylene linkage. Finally, it should be mentioned that the hexavalent monometallic (**16**) and bimetallic (**20**) bis-imido derivatives also exhibit a broad series of UV-visible charge transfer absorptions comparable to previous reports,[12] with slightly more intense and featured band structure than the pentavalent derivatives shown in **Figure 4.18**. The nominal $5f^0$ electronic configuration for these hexavalent derivatives renders the NIR region vacant as expected. The imido bridged bimetallic complex **20** also

exhibits a $\pi \rightarrow \pi^*$ transition for the phenylene unit in the bridge near 10000 cm^{-1} comparable to that observed for **18** and **19**.

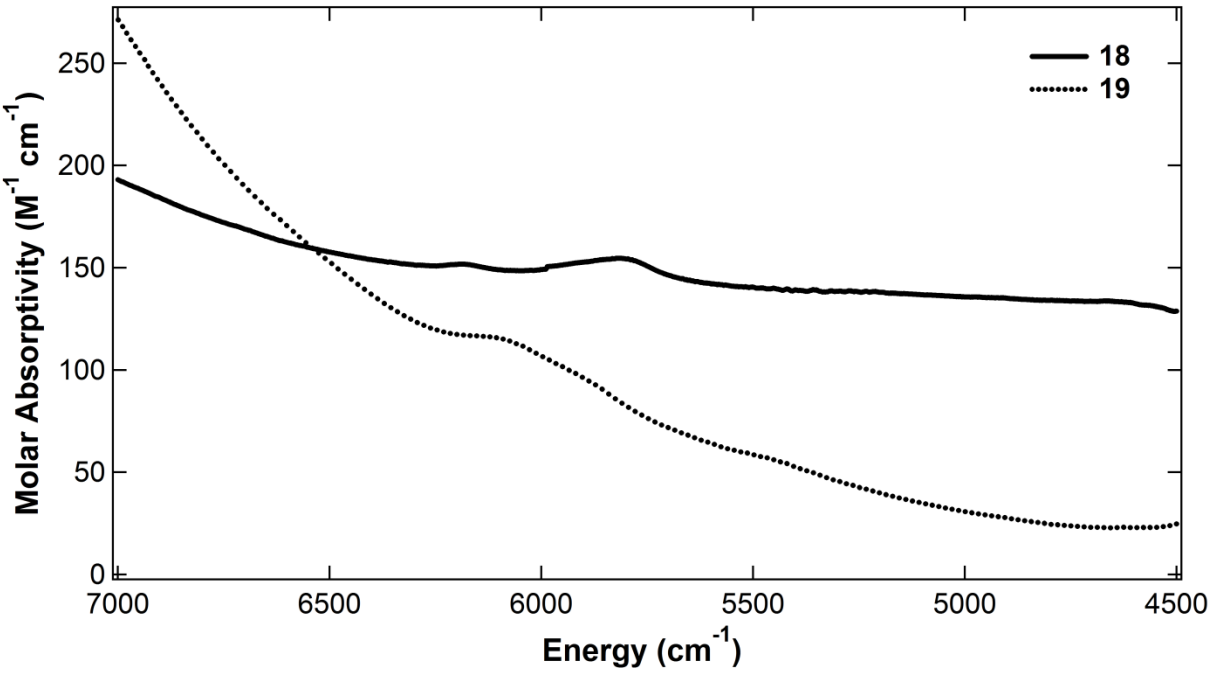

Figure 4.17. NIR portion of the electronic absorption spectra for uranium(V) bimetallic complexes **18** (solid) and **19** (dashed) obtained at room temperature in toluene-d_8 solution.

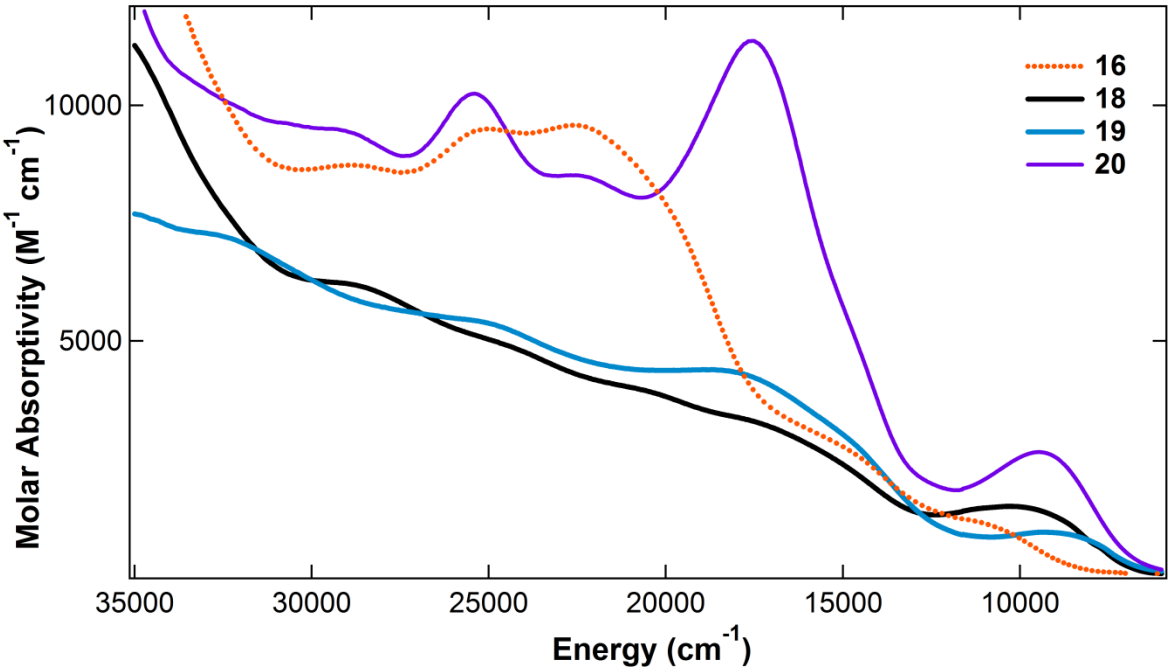

Figure 4.18. UV-visible spectra for the bimetallic complexes **18**, **19**, and **20** (solid) and the monometallic **16** (dashed) obtained at room temperature in toluene-d_8 solution.

Magnetism

Magnetic moments extracted from variable temperature magnetic susceptibility measurements for the U^V bimetallic complexes **18** and **19** do not display any direct evidence indicative of strong magnetic exchange (i.e., the curves lack any Curie or Neil low temperature transition) as shown in **Figure 4.19**. Rather, the U^V ions in each case consist of $5f^1$ spins confined to the respective f orbital states and each ion behaves, for the most part, as disconnected individual paramagnets. The respective magnetic moments extracted from a linear fit of the high temperature region are both 3.38 μ_B. This susceptibility value (per mole of U^V ions) is considerably larger than that calculated for an f^1 ion (2.54 μ_B) or for any of the monometallic derivatives discussed in Part I. This might indicate weak ferromagnetic coupling within the higher temperature regime. A similar magnetic interaction has been observed in the U^V pentaethoxide dimer $[U(OC_2H_5)_5]_2$[64] and the isopolyoxometallate $[U_6O_{13}(Bpy)_2(Cp)_4]$,[65] which

revealed substantially smaller magnetic susceptibilities than expected attributed to weak antiferromagnetic interactions for both. In the case of Andersen's discrete imido-bridged U^V bimetallics, the *meta* substituted derivative shown in **Figure 4.7** displays a typical U^V magnetic susceptibility of 2.12 μ_B, and the high temperature regime for the *para* substituted derivative of 2.08 μ_B is both closer in value to the calculated moment indicative of no net interaction.[67] In the same respect, it is interesting that the para substituted U^V bimetallics revealed here do not display any strong magnetic communication like Andersen's, and this could be an effect of the different coordination geometries and ligand field effects. A final observation worth mention is the appearance of the χT vs T plot shown in **Figure 4.20** where bimetallic derivatives display a more gradual transition than that accentuated for the monometallic derivatives near ~40 K. A possible explanation for this difference is that thermal population of the excited states are affected by the prescience of second U^V ion in close proximity attached through ligand. In other words, the bimetallic arrangement might have a pronounced effect on the excited state manifold derived from 5f character.

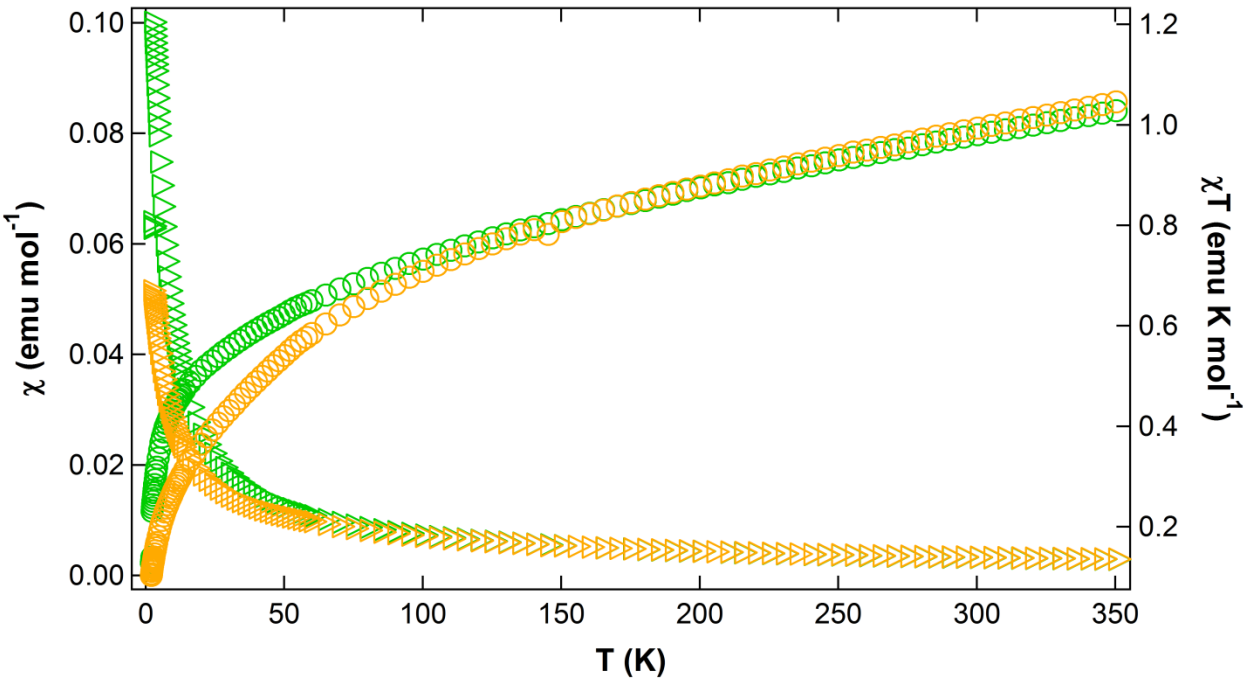

Figure 4.19. Variable temperature magnetic susceptibility for **18** (green) and **19** (orange) with χ vs T curve (triangular markers) and χT vs T plot (circular markers) from 2 K to 350 K.

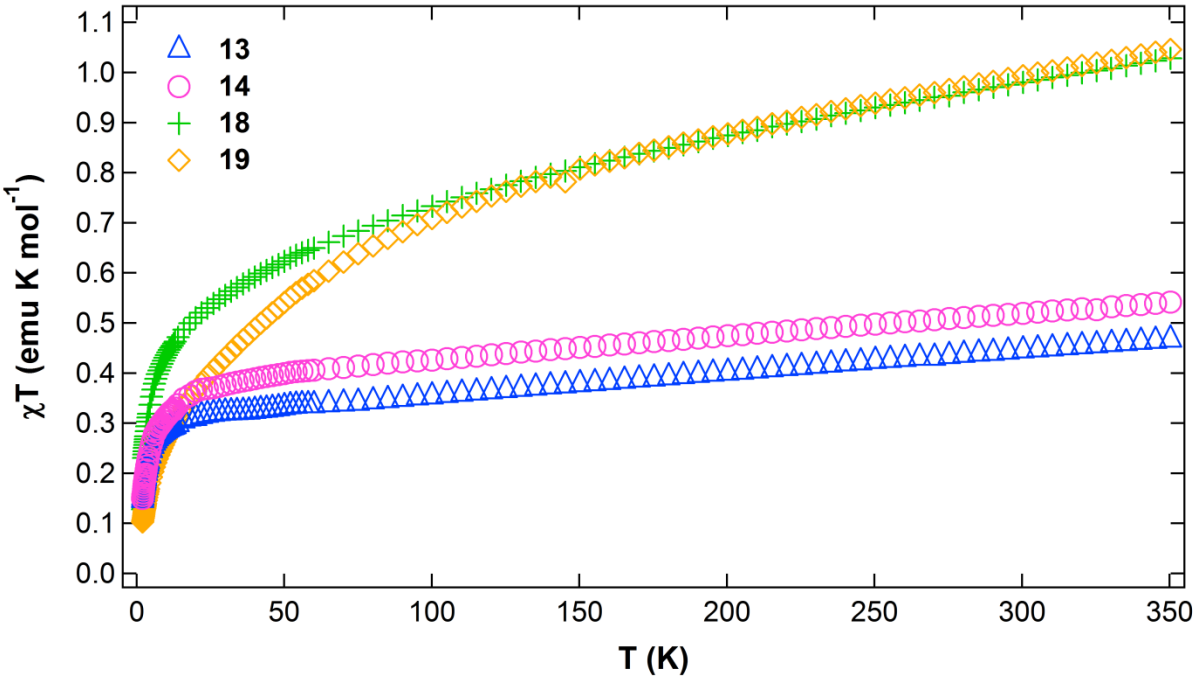

Figure 4.20. Variable temperature magnetic susceptibility for U(V) bimetallics with respect to monometallic analogues from 2 K to 350 K.

The fact that both **18** and **19** display similar variable temperature magnetic curves suggests that any weak electronic interaction occurs through space, and since for each the U^{V} ions are sterically encumbered by the ligand arrangement any intermolecular ordering would be negligible. Both structural arrangements support the metal ions ~9 Å apart, with the caveat that a superexchange mechanism would be mediated by each bridging ligand in a different manner. To clarify, the *p*-phenylenediimide (**19**) versus the *p*-phenylenediamide (**18**) ligands contain different conjugated delocalization pathways, and the multiply bound imide donors in **19** should be able to drain spin density from the paramagnetic center onto the bridging ligand more easily than the amide donor. Consider that the imido bridging donors in **19** might not be multiply bound through 5f state that houses the magnetically active spin, but rather fielded by 6d overlap. It should be mentioned that while 5f versus 6d covalent overlap is a complicated subject for the early actinides, many theoretical reports exist that attribute multiple bonding to a larger contribution of 6d (~70 %) rather than 5f (~30 %) orbitals.[81] These experimental findings are also comparable to preliminary theoretical results that indicate a small energy preference for the singlet verses triplet exchange states, whereas a calculated superconjugation pathway describes a more accentuated spin alignment across the imide bridged bimetallic than other *p*-phenylene linked models (i.e., amide or aryloxide).[82]

4.6 Conclusion

In summary, we have devised two reliable methods to prepare, isolate, and analyze well defined U^{V} and U^{VI} organo-imido bimetallic complexes that extend from routes previously developed for monometallic derivatives. The molecular structures are derived from bifunctional *p*-phenylene substituted diimide (**19**, **20**) and diamide (**18**) ligands that link bent metallocene

fragments together through wedge ligation. Whereas the U^{VI} bis-imido bimetallic analogue does not exhibit any proof of intramolecular metal ion communication, the pentavalent imide-amide and imide-aryloxide bimetallic assemblies exhibit subtle evidence for communication on the electrochemical, spectroscopic, and magnetic fronts in comparison to recent advances on characterization for monometallic organouranium(V)-imido system. These species posses the singly occupied 5f molecular orbital states that serve as a marker for f-orbital perturbations in the $5f^1$-$5f^1$ configuration.

Electrochemical experimentation performed on **18** and **19** uncovered communication between the two U^V ions manifested by the appearance of multiple redox waves in the general region expected for $U^{VI/V}$ and $U^{V/IV}$ processes. Assignments gleaned from cyclic and square wave voltammetric analysis confirmed the presence of metal based redox waves and ligand based waves. The imido-bridged bimetallic species **19** displayed larger peak separation for the $U^{V/IV}$ reduction, interpreted as an enhanced degree of electronic interaction in comparison to **18** which displayed coincident $1e^-$ step reductions. The $U^{VI/V}$ oxidative processes display a lesser extent of separation between the waves, and a similar observation for Mo^V bimetallics has been attributed to charge delocalization across the *p*-phenylene π-conjugated bridge. Whereas electrochemical communication is not difficult to attain or assess the response to electroactivity, it has never been reported for discrete actinide homobimetallic complexes until now. Similarly electronic spectroscopic analysis revealed stark alterations in the f→f NIR absorption profiles in relation to clearly defined bands for monometallic derivatives. These deviations are presumably attributed to the presence of a second paramagnetic U^V ion in close proximity to induce perturbations on the spin-orbit and crystal-field states of the other. Variable temperature magnetic susceptibility data does not exhibit strong ferro- or anitferromagnetic exchange as that observed for Andersen's

organometallic *p*-phenlenediimide bridged U^V bimetallic. Instead, the two U^V ions within each of the molecules reported here behave as isolated paramagnets, where the observation of increased magnetic moments in comparison to monometallic derivatives are suggestive of high temperature weakly additive magnetic coupling.

Future work in the multimetallic arena will adjust steric and electronic variables in these frameworks, including a variety of substituted phenylene bridges (i.e. *p*-, *m*-, *o*-) with a various donor atoms (i.e., aryloxide, acetylide) to tune the 5f versus 6d orbital energy match with respective ligand atomic orbitals to enhance the degree of multiple bonding and consequent superexchange delocalization. These attempts will be complimented by thorough computational studies to model structural dependence on electronic communication for a variety of bimetallic assemblies. Further studies currently underway include extending or shortening the distance between the metals to probe the effects of elongated superexchange or remote through space pathways, and possibly even vary the structural orientation of the phenylene linkage such that it is not coplanar to wedge ligation. Future endeavors are planned to construct architectures that support higher nuclearity that may present multicenter communication.

Acknowledgements. This work was performed at Los Alamos National Laboratory under the auspices of a G.T. Seaborg Graduate Summer Research Fellowship. The author is extremely grateful for guidance from the talented staff of scientists at LANL, especially Drs. Jaqueline L. Kiplinger, David E. Morris, Christopher R. Graves, Eric J. Schelter, Brian L. Scott, and Joseph D. Thompson.

Supporting Information Available: Crystallographic data in Appendix 3 on CD-ROM.

4.7 Experimental

General Considerations

All laboratory manipulations were performed at ambient conditions in a recirculating Vacuum Atmospheres NEXUS model drybox under dinitrogen outfitted with a 40CFM Dual Purifier NI-Train, or using standard Schlenk techniques on a dual nitrogen/vacuum line. Glassware was dried at 150 ^{o}C overnight before use. THF-d_8, toluene-d_8 and benzene-d_6 were obtained from Cambridge Isotope Laboratories and purified by passage through activated alumina and storage over activated 4Å molecular sieves 48 h prior to use. Anhydrous solvents (Aldrich) were dried over KH for 24 h, passed through a column of activated alumina, and stored over activated 4 Å molecular sieves prior to use. KH was washed with hexanes and dried thouroughly prior to use. Phenol, diphenylamine, phenylamine, benzophenone imine, trimethylphosphine oxide (TMPO), and potassium hexamethyldisilylamide were purchased (Aldrich) and used as received without further purification. KOAr, $KNPh_2$, KNHPh,[84] N,N'-bisbenzylidenebenzene-1,4-diamine,[85] *p*-diazidobenzene,[86] $(C_5Me_5)_2U(=N\text{-}2,6\text{-}^{i}Pr_2\text{-}C_6H_3)THF$ **(2)**,[19] $(C_5Me_5)_2U(=N\text{-}2,6\text{-}^{i}Pr_2\text{-}C_6H_3)I$ **(10)**, $(C_5Me_5)_2U(=N\text{-}2,6\text{-}^{i}Pr_2\text{-}C_6H_3)OTf$ **(11)**, $(C_5Me_5)_2U(=N\text{-}2,6\text{-}^{i}Pr_2\text{-}C_6H_3)SPh$ **(12)**,[11] $(C_5Me_5)_2UI(THF)$,[87] $(C_5Me_5)_2U(O\text{-}2,6\text{-}^{i}Pr_2\text{-}C_6H_3)THF$ **(17)**[14] were prepared and purified according to literature methods. Depleted uranium (^{238}U) is a weak α-emitter (4.197 MeV) with a half-life of 4.47 x 10^9 y, and should be handled in a fume hood or in a drybox contained in an area regularly monitored for radioactive isotope management.

Instrumentation and Sample Protocols

NMR spectra were recorded in C_6D_6 or toluene-d_8 on a Bruker Avance 300 MHz spectrometer and chemical shifts for ^{1}H NMR spectra were referenced to protio impurties. Mass spectrometric (MS) analyses were obtained at University of California, Berkly MS Facility, using a VG ProSpec (EI) mass spectrometer. Elemental analyses were performed at the University of California, Berkeley Microanalytical Facility on a Perkin-Elmer series II 2400 CHNS analyzer. X-ray data were collected on a Bruker APEX2 or on a Bruker SMART system equipped with a CCD Area Detector diffractometer. Structural solution and refinement was performed using the SHELXL97 program suite.[88] Details regarding the data collection and refinement are provided in the CIF files. The structures for **14**, **19**, and **20** are extensively disordered, and this will be resolved prior to publication.

Electronic absorption data were obtained at ambient temperature for toluene-d_8 solutions of complexes over the wavelength range 300-1600 nm on a Perkin-Elmer Model Lambda 950 UV-visible-NIR spectrophotometer. All data were collected in 1 cm path length cuvettes loaded in the drybox noted above and run versus a toluene-d8 solvent reference. Samples were run at two dilutions, ~0.1 and ~0.5 mM, to optimize absorbance in the UV-visible and near-infrared, respectively. Spectral resolution was typically 2 nm in the visible region and 4-6 nm in the near-infrared.

Cyclic wave voltammetric data were obtained in the drybox described above using a Perkin-Elmer Princeton Applied Research Corporation (PARC) Model 263 potentiostat under computer control with PARC Model 270 software. All samples solutions were prepared at a concentration of ~5mM in complex with 0.1 M $[Bu_4N][B(3,5\text{-}(CF_3)_2\text{-}(C_6H_3)_4]$. Data were collected with the positive-feedback IR compensation feature of the software/potentiostat

activated to ensure minimal contribution to the voltammetric waves from uncompensated resistance from the solution (typically ~1 kΩ under the conditions employed). Solutions were contained in PARC Model K0264 microcells consisting of a ~3 mm diameter Pt disk working electrode, a Pt wire counter electrode, and a silver wire quasi-reference electrode. Scan rates from 20-5000 mV/s were employed in the cyclic voltammetry scans to investigate the chemical and electrochemical reversibility of the observed redox processes. Half-wave potentials were determined from the peak maxima in the square-wave voltammograms or from the average of the anodic and cathodic peak potentials for reversible cyclic waves. Calibrations were preformed after each data collection cycle using the internal standard ferrocenium/ferrocene couple. Electronic absorption and cyclic voltammetric data were analyzed using Wavemetrics IGOR Pro (Version 4.0) software on a PC platform.

Temperature dependent magnetic susceptibility data were collected using a Quantum Design Superconducting Interference Device (SQUID) magnetometer at 5 T from 2-350 K. Samples were sealed in 5 mm Wilmad 505-PS NMR tube along with a small plug of quartz wool to hold the sample near the center of the tube. Magnetic contributions from the quartz wool and NMR tube were measured independently and subtracted from the sample measurement. Diamagnetic corrections were made using Pascal's constants.

Synthetic Details

Synthesis of $(C_5Me_5)_2U(=N\text{-}^{i}Pr_2\text{-}C_6H_3)(NPh_2)$ (13): A 125 mL side-arm Erlenmeyer flask equipped with a stir bar was charged with $(C_5Me_5)_2U(=N\text{-}^{i}Pr_2\text{-}C_6H_3)$(I) (0.250g, 0.308 mmol) and $KNPh_2$ (0.0767mg, 0.370 mmol) and ~50 mL toluene. The resulting black slurry was stirred at room temperature for 12 h. The black reaction mixture was then filtered through a Celite-padded

coarse frit to remove the insoluble salts. The filtrate was collected and the volatiles removed under reduced pressure. The residue was extracted into hexanes (50 mL) and filtered through a Celite-padded coarse porosity frit. The filtrate was collected and the volatiles were removed under reduced pressure to give crude **$(C_5Me_5)_2U(=N\text{-}^{i}Pr_2\text{-}C_6H_3)(NPh_2)$** as a black solid. Analytically pure samples of **$(C_5Me_5)_2U(=N\text{-}^{i}Pr_2\text{-}C_6H_3)(NPh_2)$** were obtained by recrystallization from toluene (2 ml) and hexamethyldisiloxane (2 ml) at -30 ºC (0.209 g, 0.245 mmol, 80%). ^{1}H NMR (C_6D_6, 300 MHz, 398 K): δ 30.12 (br, 1H, C*H*$(CH_3)_2$), 21.34 (s, 1H, Ar*H*), 20.078 (s, 1H, Ar*H*), 7.41 (br, 30H, $C_5(CH_3)_5$), 7.29 (s, 4H, NPh-*H*), 4.54 (s, 6H, $CH(CH_3)_2$), 2.88 (s, 6H, $CH(CH_3)_2$), 1.78 (s, 2H, NPh-*H*), 1.72 (s, 2H, NPh-*H*), -0.37 (s, 2H, NPh-*H*), -5.06 (s, 1H, Ar*H*), -14.96 (br, 1H, $CH(CH_3)_2$). Mp = 206 °C. MS (EI, 70 eV): *m/z* 851 (M^+). U(VI/V) $E_{1/2}$ = -0.30 V, U(V/IV) $E_{1/2}$ = -1.65 V (vs. $[(C_5H_5)_2Fe]^{+/0}$ in THF/0.1 M $[Bu_4N][B(C_6F_5)_4]$). Anal. Calcd for $C_{44}H_{57}N_2U$ (851.97 g/mol): C, 62.03, H, 6.74; N, 3.29. Found: C, 61.94; H, 6.37; N, 3.54.

Synthesis of $(C_5Me_5)_2U(=N\text{-}^{i}Pr_2\text{-}C_6H_3)(OPh)$ (14): A 100 mL Schlenk tube sealed with a Teflon valve was loaded with $(C_5Me_5)_2U(=N\text{-}^{i}Pr_2\text{-}C_6H_3)$(I) (0.250 g, 0.308 mmol) and toluene (50 mL). To this solution was added solid KOPh (0.0489 g, 0.3701 mmol) and the resulting mixture was placed in a 75 ºC oil bath for 12 h to yield a black solution. The reaction mixture was filtered through a Celite-padded coarse porosity frit and the volatiles were removed from the filtrate under reduced pressure to afford a dark solid. The solid was extracted into hexanes (50 mL) and filtered through a Celite-padded coarse porosity frit and the volatiles were removed under reduced pressure to give crude **$(C_5Me_5)_2U(=N\text{-}^{i}Pr_2\text{-}C_6H_3)(OPh)$** as a black solid. Analytically pure samples of **$(C_5Me_5)_2U(=N\text{-}^{i}Pr_2\text{-}C_6H_3)(OPh)$** were obtained by recrystallization from a concentrated hexamethyldisiloxane solution at -30 ºC (0.179 g, 0.230 mmol, 75%). ^{1}H

NMR (C_6D_6, 300 MHz, 298 K): δ 50.05 (br, 1H, C*H*$(CH_3)_2$), 26.07 (s, 1H, Ar*H*), 17.79 (s, 1H, Ar*H*), 14.56 (s, 6H, CH(C*H*$_3)_2$), 11.31 (s, 2H, OAr*H*), 9.12 (s, 1H, OAr*H*), 3.56 (br, 30H, C_5(C*H*$_3)_5$), 2.98 (s, 2H, OAr*H*), -8.47 (s, 6H, CH(C*H*$_3)_2$), -13.37 (s, 1H, Ar*H*), -20.3 (br, 1H, C*H*$(CH_3)_2$). Mp = 198 °C. MS (EI, 70 eV): *m/z* 776 (M^+). U(VI/V) $E_{1/2}$ = -0.22 V, U(V/IV) $E_{1/2}$ = -1.75 V (vs. $[(C_5H_5)_2Fe]^{+/0}$ in THF/0.1 M $[Bu_4N][B(C_6F_5)_4]$). Anal. Calcd for $C_{38}H_{52}NOU$ (776.85 g/mol): C, 58.75; H, 6.75; N, 1.80. Found: C, 58.74; H, 6.96; N, 2.04.

Synthesis of $(C_5Me_5)_2U(=N\text{-}^iPr_2\text{-}C_6H_3)(\text{-}N=CPh_2)$ (15): A 125 mL side-arm flask equipped with a stir bar was charged with $(C_5Me_5)_2U(=N\text{-}^iPr_2\text{-}C_6H_3)$(I) (0.250 g, 0.308 mmol), $KN(TMS)_2$ (0.0738 g, 0.370 mmol), and toluene (50 mL). The resulting mixture was stirred at room temperature for 20 min at which time $HN=CPh_2$ (0.067 g, 0.370 mmol) in toluene (20 mL) was added dropwise with stirring. The resulting mixure was stirred at room temperature for 12 h and filtered through a Celite-padded coarse porosity frit. The filtrate was collected and the volatiles were removed under reduced pressure to afford a black tarry residue. Hexanes (50 mL) was added to dissolve the black tar and the resulting solution was filtered through a Celite-padded coarse frit and the volatiles were removed under reduced pressure to give crude **$(C_5Me_5)_2U(=N\text{-}^iPr_2\text{-}C_6H_3)(\text{-}N=CPh_2)$** as a black solid. The solid was taken up in 15 mL hexamethyldisiloxane and slow evaporation of this solution at room temperature afforded single crystals of x-ray quality. This reaction produced a mixture of uranium containing products such that further analytical data is for 15 is unavailable at this time but will be described in a forthcoming publication.[15]

Synthesis of $(C_5Me_5)_2U(=N\text{-}^iPr_2\text{-}C_6H_3)(=NPh)$ (16): A 125 mL side-arm flask equipped with a stir bar was charged with $(C_5Me_5)_2U(=N\text{-}^iPr_2\text{-}C_6H_3)$(I) (0.250 g, 0.308 mmol), KNHPh (0.0485 g, 0.370 mol) and toluene (50 ml). The resulting reaction mixture was stirred at room temperature

for 12 h, filtered through a Celite-padded coarse frit, and the volatile were removed under reduced pressure to give a black residue. The residue was extracted with hexanes (50 mL) and filtered through a Celite-padded coarse porosity frit. The filtrate was collected, 10 drops of pyridine was added, and the volatiles were removed under reduced pressure to afford a black solid. The solid was taken up in hexamethyldisiloxane (2 mL) and stored at -30 ºC for 12 h to give **$(C_5Me_5)_2U(=N\text{-}^{i}Pr_2\text{-}C_6H_3)(=NPh)$** as an analytically pure black crystalline solid (0.148 g, 0.191 mmol, 62%). ^{1}H NMR (C_6D_6, 300 MHz, 298 K): δ 9.62 (d, 1H, p-NPh), 9.41 (t, 2H, m-NPh), 9.18 (d, 2H, o-NPh), 7.21 (b, 1H, CH(CH_3)$_2$) 4.46 (s, 30H, C_5(CH_3)$_5$)$_2$), 2.84 (d, 2H, m-Ar-*H*), 2.68 (b, 1H, C*H*(CH_3)$_2$) 2.11 (d, 6H, CH(CH_3)$_2$), 1.68 (d, 6H, CH(CH_3)$_2$), 0.52 (t, 1H, p-Ar-*H*). Mp = 199 °C MS (EI, 70 eV): *m/z* 774.5 (M^+). U(VI/V) $E_{1/2}$ = -1.67 V, U(V/IV) $E_{1/2}$ = -1.94 V (vs. $[(C_5H_5)_2Fe]^{+/0}$ in THF/0.1 M $[Bu_4N][B(C_6F_5)_4]$). Anal. Calcd for $C_{38}H_{52}N_2U$ (774.86 g/mol): C, 58.90; H, 6.76; N, 3.62. Found: C, 58.59; H, 6.99, N, 3.51.

Synthesis of dipotasium N,N'-bis(benzyl)phenyldiamide: A 125 mL side-arm flask equipped with a stir bar was charged with N,N'-bisbenzylidenebenzene-1,4-diamine (0.250 g, 0.308 mmol) and THF (50 mL). To this solution was added a substiochiometric amount of KH (0.054 g, 0.154 mmol). The resulting reaction slurry was stirred at room temperature for 12 h over which time the color changed drastically from yellow to pink. The solid product was collected by filtration and washed with THF and hexanes. The product is not soluble in any solvent.

Synthesis of $[(\eta^5\text{-}C_5Me_5)_2U(=N\text{-}^{i}Pr_2\text{-}C_6H_3)]_2[\mu\text{-}N(Bz)\text{-}C_6H_4\text{-}(Bz)N\text{-}]$ (18): A 125 mL side-arm flask equipped with a stir bar was charged with $(C_5Me_5)_2U(=N\text{-}^{i}Pr_2\text{-}C_6H_3)$(I) (0.250 g, 0.308 mmol) and toluene (50 mL). To this solution was added dipotassium p-phenylbis(benzylidene)diamide (0.054 g, 0.154 mmol). The resulting reaction mixture was stirred at room temperature for 12 h, then filtered through a Celite-padded coarse frit, and the

volatiles were removed under reduced pressure. The remaining solid was extracted with hexanes (30 mL), filtered through a Celite-padded coarse frit, and concentrated to a volume of 2 ml. Diethyl ether (2 mL) was added and the solution was allowed to evaporate to afford analytically pure **[(η^5-C_5Me_5)$_2$U(=N-^{i}Pr$_2$-C_6H_3)]$_2$[μ-N(Bz)-C_6H_4-(Bz)N-]** (0.107 g, 0.065 mmol, 42 %). ^{1}H NMR (C_6D_6, 300 MHz, 298 K): δ 8.97 broad, 5.18 broad. Mp 232 °C. U(VI/V) $E_{1/2}$ = -0.53 V, -0.62 V, U(V/IV) $E_{1/2}$ = -1.694 V (vs. $[(C_5H_5)_2Fe]^{+/0}$ in THF/0.1 M $[Bu_4N][B(C_6F_5)_4]$). Anal. Calcd for $C_{84}H_{112}N_4U_2$ (1653.9 g/mol): C, 61.20; H, 6.48; N, 3.40. Found: C, 61.35; H, 6.98; N, 3.47.

Synthesis of [(η^5-C_5Me_5)$_2$U(O-^{i}Pr$_2$-C_6H_3)]$_2$[μ-(=N-C_6H_4-N=)] (19): A 125 mL side-arm flask equipped with a stir bar was charged with (C_5Me_5)$_2$U(O-^{i}Pr$_2$-C_6H_3)(THF) (0.250 g, 0.330 mmol) and toluene (50 mL). To this solution was added *p*-diazidobenzene (0.026 g, 0.165 mmol). The resulting reaction mixture immediately evolved gas and was stirred at room temperature for 1 h, and the volatiles were removed under reduced pressure. The remaining solid was extracted with diethylether (10 mL), and hexamethyldisiloxane (5 mL) was added and the solution was allowed to evaporate to afford analytically pure **[(η^5-C_5Me_5)$_2$U(O-^{i}Pr$_2$-C_6H_3)]$_2$[μ-(=N-C_6H_4-N=)]** (0.189 g, 0.128 mmol, 78 %). ^{1}H NMR (C_6D_6, 300 MHz, 298 K): δ 53.89 (br, 2H, C*H*(CH_3)$_2$), 19.49 (s, 2H, Ar*H*), 14.61 (d, 2H, Ar*H*), 12.43 (s, 12H, CH(C*H*$_3$)$_2$), 4.98 (s, 60H, $C_5(CH_3)_5$), 0.21 (s, 4H, C_6H_4), -1.08 (s, 2H, Ar*H*), -8.62 (s, 12H, CH(C*H*$_3$)$_2$), -37.41 (br, 2H, C*H*(CH_3)$_2$). Mp 236 °C. U(VI/V) $E_{1/2}$ = -0.45, -0.37, U(V/IV) $E_{1/2}$ = -1.56, -1.72 (V vs. $[(C_5H_5)_2Fe]^{+/0}$ in THF/0.1 M $[Bu_4N][B(C_6F_5)_4]$). Anal. Calcd for $C_{70}H_{98}N_2O_2U_2$ (1475.60 g/mol): C, 56.98; H, 6.69; N, 1.90. Found: C, 55.11; H, 6.71; N, 1.95.

Synthesis of [(η^5-C_5Me_5)$_2$U(=N-^{i}Pr$_2$-C_6H_3)]$_2$[μ-(=N-C_6H_4-N=)] (20): A 125 mL side-arm flask equipped with a stir bar was charged with (C_5Me_5)$_2$U(=N-^{i}Pr$_2$-C_6H_3)(THF) (0.250 g, 0.331

mmol) and toluene (50 mL). To this solution was added *p*-diazidobenzene (0.026 g, 0.165 mmol). The resulting reaction mixture immediately evolved gas and was stirred at room temperature for 1 h, and the volatiles were removed under reduced pressure. The remaining solid was exctracted with hexanes (10 mL) and the solution was stored at -30 ºC for 12 h to afford analytically pure **$[(\eta^5\text{-}C_5Me_5)_2U(=N\text{-}^iPr_2\text{-}C_6H_3)]_2[\mu\text{-}(=N\text{-}C_6H_4\text{-}N=)]$** (0.207 g, 0.141 mmol, 85 %). ^{1}H NMR (C_6D_6, 300 MHz, 298 K): δ 9.68 (d, 2H, m-Ar-*H*), 9.17 (d, 2H, m-Ar-*H*), 4.63 (s, 4H, C_6H_4), 4.31 (s, 60H, $C_5(CH_3)_5)_2$), 2.23 (d, 12H, $CH(CH_3)_2$), 2.09 (septet, 2H, $CH(CH_3)_2$), 1.64 (d, 12H, $CH(CH_3)_2$), 1.48 (septet, 2H, $CH(CH_3)_2$), 0.37 (m, 2H, p-Ar-*H*). Mp 253 °C . U(VI/V) $E_{1/2}$ = -1.76 V, U(V/IV) $E_{1/2}$ = -2.13 V, (vs. $[(C_5H_5)_2Fe]^{+/0}$ in THF/0.1 M $[Bu_4N][B(C_6F_5)_4]$). Anal. Calcd for $C_{70}H_{98}N_4U_2$ (1471.61 g/mol): C, 57.13; H, 6.71; N, 3.81. Found: C, 56.78; H, 6.74; N, 4.10.

Synthesis of $[(\eta^5\text{-}C_5Me_5)_2U(NPh_2)_2$ (21): 21 has been reported before without any crystllographic information.[77] This complex was isolated from an attempted bimetallic reaction mixture, and single crystals of x-ray quality was obtained from evaporation of a diethyl ether solution of the reaction mixture. However, **21** could not be prepared from direct salt methathesis (which led only to the mixed chloro-amido species).

References

[1] (a) Burns, C. J.; Bursten, B. E. *Comments Inorg. Chem.* **1989**, *9*, 61-93. (b) Burns, C. J. *Science* **2005**, *309*, 1823-1824. (c) Choppin, G. R. *J. All. Com.* **2002**, *344*, 55-59. (c) Eisenstein, J. C. *J. Chem. Phys.* **1956**, *25*, 142-146.

[2] Burns, C. J.; Eisen, M. S. Organoactinide Chemistry: Synthesis and Characterization. In *The Chemistry of the Actinide and Transactinide Elements*, 3rd ed.; Morss, L. R., Edelstein, N. M., Fuger, J., The Netherlands, **2006**; Vol. 5, pp 2799-2910, and references therein.

[3] Ephritikhine, M. *Dalton Trans*, **2006**, 2501-2516.

[4] Bagnal, K. W. *Comprehensive Coordination Chemistry*; Wilkinson, G., Gillard, R. D., McCleverty, J. A.; Pergamon: Oxford, 1987; Vol. 3, p1129.

[5] For a review on the synthesis, stability and properties of uranium(V) complexes, refer to: Selbin, J.; Ortego, J. D. *Chem. Rev.* **1969**, 69, 657-671.

[6] For examples of U^V complexes, refer to: (a) Chen, C. S.; Lee, S. F.; Lii, K. H. *J. Am. Chem. Soc.* **2005**, *127*, 12208-12209. (b) Gray, D. L.; Backus, L. A.; Krug von Nidda, H.-A.; Skanthakumar, S.; Loidl, A.; Soderholm, L.; Ibers, J. A. *Inorg. Chem.*, **2007**, *46*, 6992-6996. (c) Salmon, P.; Thuery, P.; Ephritikhine, M. *Polyhedron* **2007**, *26*, 631-636. (d) Boisson, C.; Berthet, J. C.; Lance, M.; Nierlich, M.; Vigner, J.; Ephritikhine, M *J. Chem. Soc., Chem. Commun.* **1995**, 543-544. (e) Gourier, D.; Caurant, D. *Inorg. Chem.* **1997**, *36*, 5931-5936. (f) Ephritikhine, M.; Berthet, J. C.; Boisson, C.; Lance, M.; Nierlich, M. *J. Alloys Compd*. **1998**, *271-273*, 144-149. (g) Boaretto, R.; Roussel, P.; Alcock, N. W.. ;. Kingsley, A. J.; Munslow, I. J.; Sanders,. C. J.; Scott, P. **J**.*J. Organomet. Chem.* **1999**, *591*, 174-184. (h) Arliguie, T.; Rourmigue, M.; Ephritikhine, M. *Organometallics* **2000**, *19*, 109-111. (i) Levard, P. C.; Nierlich, M. *Eur. J. Inorg. Chem*. **2000**, 1733-1738.

[7] For recent reports on the chemistry of uranyl(V) complexes, refer to: (a) Berthet, J. C.; Nerlich, M.; Ephritikhine, M *Agnew. Chem. Int. Ed.* **2003**, 42, 1952-1954. (b) Renshaw, J. C.; Butchins, L. J. C.; Livens, F. R.; May, I.; Charnock, J. M.; Lloyd, J. R. *Environ. Sci. Technol*. **2005**, *39*, 5657-5660. (c) Burdet, F.; Pecaut, J.; Mazzanti, M *J. Am. Chem. Soc.*, **2006**, *128*, 16512-16513. (d) Natrajan, L.; Burdet, F.; Pecaut, J.; Mazzanti, M. *J. Am. Chem. Soc.* **2006**, *128*, 7152-7153. (e) Berthet, J. C.; Siffredi, G.; Thuery, P.; Ephritikhine, M *Chem. Comm*. **2006**, 3184-3186.

[8] Kaltsoyannis, N.; Scott, P. *The f elements*, Oxford, **1999**, and references therein

[9] Edelstein, N.; Brown, D.; Whittaker, B. *Inorg. Chem.* **1974**, *13*, 563-567.

[10] (a) Bowmaker, G. A.; Goerling, A.; Haeberlen, O.; Roesch, N.; Goodman, G. L.; Ellis, D. E. *Inorg. Chem.* **1992**, *31*, 577-581. (b) Warren, K. D. *Inorg. Chem.* **1975**, *14*, 3095-3103.

[11] (a) Graves, C. R.; Scott, B. L.; Morris, D. E.; Kiplinger, J. L. *J. Am. Chem. Soc.* **2007**, *129*, 11914-11915. (b) Graves, C. R.; Yang, P.; Kozimoir, S. A.; Vaughn, A. E.; Clark, D. L.; Conradson, S. D.; Schelter, E. J.; Scott, B. L.; Thompson, J. D.; Hay, P. J.; Morris, D. E.; Kiplinger, J. L. *J. Am. Chem. Soc*. **2008**, *130*, 5272-5285.

[12] Morris, D. E.; Da Re, R. E.; Jantunen, K C.; Castro-Rodriguez, I.; Kiplinger, J. L. *Organometallics* **2004**, *23*, 5142-5153.

[13] For examples of Ag^{I} salt oxidation of uranium(IV), refer to (a) Boisson, C.; Berthet, J. C.; Lance, M.; Nierlich, M.; Vignerb, J.; Ephritikhine, M. *J. Chem. Soc., Chem. Commun*. **1995**, 543-544. (b) Berthet, J. C.; Ephritikhine, M. *J. Chem. Soc., Chem. Commun.* **1993**, 1566-1567.

[14] (a) Zalkin, A.; Brennan, J. G.; Andersen, R. A. Acta Cryst. **1998**, *C44*, 1553-1554. (b) Brenan,, J. G.; Andersen, R. A. *J. Am. Chem. Soc.* **1985**, *107*, 514-516. (c) Meyer, K.; Nakai, H.; Castro-Rodriguez, I. *Angew. Chem*. **2006**, *118*, 2449-2452. (d) Roussel, P.; Boaretto, R.; Kingsley, A. J.; Alcock, N. W.; Scott, P *J. Chem. Soc., Dalton Trans.* **2002**, 1423-1428. (e) Arney, D. S. J.; Burns, C. J. *J. Am. Chem. Soc.* **1993**, *115*, 9840-9841.

[15] Graves and coworkers (LANL) recent unpublished result.

[16] (a) Evans, W. J.; Meadows, J. H.; Hunter, W. E.; Atwood, J. L. J. Am. Chem. Soc. 1984, 106, 1291-1300. (b) Boring, E.; Sabat, M.; Finn, M. G.; Grimes, R. *Organomet.* **1997**, *16*, 3993-4000. (c) Erker, G.; Fromberg, W.; Atwood, J. L.; Hunter, W. E. *Agnew. Chem. Int. Ed. Engl.* **1984**, *23*, 68-69. (d) Bercaw, J. E.; Davies, D. L.; Wolzanski, P. T. *Organomet.* **1986**, *5*, 443-450.

[17] (a) Jantunen, K. C.; Burns, C. J.; Castro-Rodriguez, I.; Da Re, R. E.; Golden, J. T.; Morris, D. E.; Scott, B. L.; Taw, F. L.; Kiplinger, J. L. *Organometallics* **2004**, *23*, 4682-4692. (b) Schelter, E. J.; Morris, D. E.; Scott, B. L.; Kiplinger, J. L. *Chem. Commun.* **2007**, 1029-1031. (c) Schelter, E. J.; Yang, P.; Scott, B. L.; Thompson, J. D.; Martin, R. L.; Hay, P. J.; Morris, D. E.; Kiplinger, J. L. *Inorg. Chem.* **2007**, *46*, 7477-7488. (d) Schelter, E. J.; Yang, P.; Scott, B. L.; Da Re, R. E.; Jantunen, K. C.; Martin, R. L.; Hay, P. J.; Morris, D. E.; Kiplinger, J. L. *J. Am. Chem. Soc.* **2007**, *129*, 5139-5152.

[18] For complete characterization data for complexes **11** and **12** please refer to reference [11] and [15].

[19] Arney, D. S. J.; Burns, C. J. *J. Am. Chem. Soc.* **1995**, *117*, 9448-9460.

[20] Stewart, J. L.; Andersen, R. A. *Polyhedron* **1998**, *17*, 953.

[21] Straub, T.; Frank, W.; Reis, G. J.; Moris, E. S. *J. Chem. Soc., Dalton Trans.* **1996**, 2541-2546.

[22] Burns, C. J.; Smith, W. H.; Huffman, J. C.; Sattelberger, A. P. *J. Am. Chem. Soc.* **1990**, *112*, 3237-3238.

[23] (a) Vaughn, A. E.; Barnes, C. E.: Duval, P. B. *J. Chem. Crystalogr.* **2007**, *37*, 779-782. (b) Burns, C. J.; Clark, D. L.; Donohoe, R. J.; Duval, P. B.; Scott, B. L.; Tait, C. D. *Inorg. Chem.* **2000**, *39*, 5464-5468.

[24] Cotton, F. A.; Marler, D.; Schwotzer, W. *Inorg. Chem.* **1984**, *23*, 4211-4215.

[25] Berg, J. M.; Clark, D. L.; Huffman, J. C.; Morris, D. E.; Sattelberger, A. P.; Streib, W. E.; Van der Sluys, W. G.; Watkin, J. G. *J. Am. Chem. Soc.* **1992**, *114*, 10811-10821.

[26] Roussel, P.; Hitchcock, P. B.; Tinker, N. D.; Scott, P. *Inorg. Chem.* **1997**, *36*, 5716-5721.

[27] Barnhart, D. M.; Burns, C. J.; Sauer, N. N.; Watkin, J. G. *Inorg. Chem.* **1995**, *34*, 4079-4084.

[28] Arliguie, T.; Fourmigue M.; Ephritikhine, M. *Organomet.* **2000**, *19*, 109-111.

[29] Clark, D. L.; Miller, M. M.; Watkin, J. G. *Inorg. Chem.* **1993**, *32*, 772-774.

[30] Kannan, S.; Barnes, C. L.; Duval, P. B. *Inorg. Chem.* **2005**, *44*, 9137-9139.

[31] Kiplinger, J. L.; John, K. D.; Morris, D. E.; Scott, B. L.; Burns, C. J. *Organometallics* **2002**, *21*, 4306-4308.

[32] To the best of our knowledge complex **11** represents the sole example of a U(V)-triflate currently on the market.

[33] Kiplinger, J. L.; Morris, D. E.; Scott, B. L.; Burns, C. J. *Organometallics* **2002**, *21*, 3073-3075.

[34] Da Re, R. E.; Jantunen, K. C.; Golden, J. T.; Kiplinger, J. L.; Morris, D. E. J. *Am. Chem. Soc.* **2005**, *127*, 682-689 and references therein.

[35] (a) Soper, J. D.; Mayer, J. M *J. Am. Chem. Soc.* **2003**, *125*, 12217-12229. (b) Huynh, M. H. V.; Meyer, T. J.; White, P. J. *J. Am. Chem. Soc.* **1999**, *121*, 4530-4531. (c) Eckert, N. A.; Vaddadi, S.; Stoian, S.; Lachicotte, R. J.; Cundari, T. R.; Holland, P. L. *Angew. Chem. Int. Ed. Engl.* **2006**, *45*, 6868-6871. (d) Mindiola, D. J.; Hillhouse, G. L. *J. Am. Chem. Soc.* **2001**, *123*, 4623-4624.(e) Lucas, R. L.; Powell, D. R.; Borovik, A. S. *J. Am. Chem. Soc.* **2005**, *127*, 11596-11597. (f) Kogut, E.; Wiencko, H. L.; Zhang, L.; Cordeau, D. E.; Warren, T. H. *J. Am. Chem. Soc.* **2005**, *127*, 11248-11249. (g) Cowley, R. E.; Bontchev, R. P.; Sorrell, J.; Sarracino, O.; Feng, Y.; Wang, H.; Smith, J. M. *J. Am. Chem. Soc.* **2007**, *129*, 2424-2425.

[36] (a) Arney, D. S. J.; Burns, C. J.; Smith, D. C. *J. Am. Chem. Soc.* **1992**, *114*, 10068-10069. (b) Burns, C. J.; Smith, W. H.; Huffman, J. C.; Sattelberger, A. P. *J. Am. Chem. Soc.* **1990**, *112*, 3237-3239. (c) Schnabel, R. C.; Scott, B. L.; Smith, W. H.; Burns, C. J. *J. Organomet. Chem.* **1999**, *591*, 14-23. (d) Warner, B. P.; Scott, B. L.; Burns, C. J. *Agnew. Chem. Int. Ed.* **1998**, *37*, 959-960. (e) Also see references [14e] and [19].

[37] (a) Peters, R. G.; Warner, B. P.; Scott, B. L.; Burns, C. *J. Organomet. Chem.* **1999**, *18*, 2587-2589. (b) Peters, R. G.; Warner, B. P.; Burns, C. J. *J. Am. Chem. Soc.* **1999**, *121*, 5585-5586.

[38] (a) Wigley, D. E. *Prog. Inorg. Chem.* **1994**, *42*, 289-482, and references therein. (b) Duncan, A. P.; Bergman, R. G. *Chem. Rec.* **2002**, *2*, 431-445.

[39] For $U^{VI}=N_{imido}$ bond lenghts are on average ~2 Å in references (a) Hayton, T. W.; Boncella, J. M.; Scott, B. L.; Palmer, P. D.; Batista, E. R.; Hay, P. J. *Science*, **2005**, *310*, 1941-1943. (b) Hayton, T. W.; Boncella, J. M.; Scott, B. L.; Batista, E. R.; Hay, P. J. *J. Am. Chem. Soc.* **2006**, *128*, 10549-10559. (c) Hayton, T. W.; Boncella, J. M.; Scott, B. L.; Batista, E. R. *J. Am. Chem. Soc.* **2006**, *128*, 12622-12623. (d) also see reference [36].

[40] For Mo^{V} redox properties see: Ung, V. A.; Bardwell, D. A.; Jeffery, J. C.; Maher, J. P.; McCleverty, J. A.; Ward, M. D.; Williamson, A.*Inorg. Chem.* **1996**, *35*, 5290-5299.

[41] Bard, A. J.; Faulkner, L. R. *Electrochemical Methods: Fundamentals and Applications*, 2nd ed.; Wiley & Sons; U.S.A.; **2001**.

[42] For electrochemistry of the organouranium(VI) bis-imide complex **16** refer to Part II of this chapter, and see reference [12].

[43] For LMCT in d^0 transition metal imido complexes see; (a) Heinselman, K. S.; Hopkins, M. D. *J. Am. Chem. Soc.* **1995**, *117*, 12340-12431. (b) Williams, D. S.; Korolev, A. V.; *Inorg. Chem.* **1998**, *37*, 3809-3819.

[44] Gourier, D.; Caurant, D.; Berthet, J. C.; Boisson, C.; Ephritikhine, M. *Inorg. Chem.* **1997**, *36*, 5931-5936.

[45] Ryan, J. L. *J. Inorg. Nucl. Chem.* **1971**, *33*, 153-177, and references therein.

[46] (a) Da Re, R. E.; Jantunen, K. C.; Golden, J. T.; Kiplinger, J. L.; Morris, D. E. *J. Am. Chem. Soc.* **2005**, 127, 682-689. (b) Clark, A. E.; Martin, R. L.; Hay, P. J.; Green, J. C.; Jantunen, K. C.; Kiplinger, J. L. *J. Phys. Chem. A* **2005**, 109, 5481-5491. (c) Schelter, E. J.; Yange, P.; Scott, B. L.; Thompson, J. D.; Martin, R. L.; Hay, P. J.; Morris, D. E.; Kiplinger, J. L. *Inorg. Chem*. **2007**, *46*, 7477-7488. (d) Also see reference [17].

[47] Liu, G.; Beitz, J. V. Optical Spectra and Electronic Structure. In *The Chemistry of the Actinide and Transactinide Elements*, 3rd ed.; Morss, L. R., Edelstein, N. M., Fuger, J., Eds; Springer: The Netherlands, 2006; Vol. 3, pp 2013-2111 and references therin.

[48] (a) Masson, J. P.; Naulin, C.; Charpin, P.; Bougon, R. *Inorg. Chem*. **1978**, *17*, 1878-1861. (b) Karraker, D. G. *Inorg. Chem.* **1964**, *3*, 1618-1622. (c) Reisfeld, M. J.; Crosby, G. A. *Inorg. Chem.* **1965**, *4*, 65-70. (d) Penneman, R. A.; Sturgeon, G. D.; Asprey, L. B. *Inorg. Chem*. **1964**, *3*, 126-129. (e) Reisfeld, M. J.; Crosby, G. A. *J. Mol. Spec*. **1963**, *10*, 232-234. (e) Selbin, J.; Ortego, J. D.; Gritzner, G. *Inorg. Chem*. **1968**, *7*, 976-982. (f) Ryan, J. L *J. Inorg. Nucl. Chem.* **1971**, *33*, 153-177. (g) Bagnall, K. W.; Brown, D.; Du Preez, J. G. H. *J. Chem. Soc.* **1965**, 5217-5221. (h) Selbin, J.; Ballhausen, C. J.; Durret, D. G. *Inorg. Chem.* **1972**, *11*, 510-515. (i) Arnaudet, L.; Bougon, R.; Buu, B.; Lance, M.; Nierlich, M.; Vigner, J. *Inorg. Chem.* **1994**, *33*, 4510-4516.

[49] Cotton, F. A. *Chemical Applications of Group Theory*, 3rd ed.; Wiley & Sons, Canada, **1990**.

[50] (a) Boudreax, W. A.; Mulay, L. N. *Theory and Applications of Molecular Paramagnetism*, Wiley & Sons, New York, **1976**. (b) Drago, R. S. *Physical Methods for Chemists*, 2nd ed.; Saunders, Philidelphia, **1992**, pp 290-352.

[51] (a) Edelstein, N. M.; Lander, G. H. Magnetic Properties. In *The Chemistry of the Actinide and Transactinide Elements*, 3rd ed.; Morss, L. R., Edelstein, N. M., Fuger, J., Eds.; Springer: The Netherlands, 2006; Vol. 4, pp 2241-2247, and references therein.

[52] (a) Masson, J. P.; Naulin, C.; Charpin, P.; Bougon, R. *Inorg. Chem.* **1978**, *17*, 1858-1861. (b) Selbin, J.; Ahmad, N.; Pribble, M. J. *J. Chem. Soc., Chem. Commun.* **1969**, 759-760.

[53] Castro-Rodriguez, I.; Meyer, K. *Chem. Commun.* **2006**, 1353-1368.

[54] (a) Selbin, J.; Ahmad, N.; Pribble, M. J. *J. Inorg. Nucl. Chem.* **1970**, *32*, 3249-3258. (b) Handler, P.; Hutchison, C. A. *J. Chem. Phys.* **1956**, *25*, 1210-1213.

[55] (a) Creutz, C.; Taube, H. *J. Am. Chem. Soc.* **1973**, *95*, 1086-1094.

[56] (a) Creutz, C. *Prog. Inorg. Chem.* **1983**, *30*, 1-73. (b) Kaim, W.; Klein, A.; Glockle, M. *Acc. Chem. Res.* **2000**, *33*, 755-763. (c) Richardson, D. E.; Taube, H. *Coord. Chem. Rev.* **1984**, *60*, 107-129.

[57] (a) Vigato, P. A.; Tamburini, **S.;** Fenton, D. E. *Coord. Chem. Rev.* **1990**, *106*, 1897-1928. (b) Ward, M. D. Chem. Ind. 1996, 568-573. (c) Ward, M. D. Chem. Ind. 1997, 640-645. (d) Gamelin, D. R.; Bominaar, E. L.; Kirk, M. L.; Wieghardt, K.; Solomon, E. I. *J. Am. Chem. Soc.* **1996**, *118*, 8085-8097.(e) Astruc, D. *Acc. Chem. Res.* **1997**, *30*, 383-391. (f) Blondin, G.; Girerd, J. *J. Chem. Rev.* **1990**, *90*, 1359-1376.

[58] For representative discrete Ln multimetallic comlexes, refer to: (a) Bunzli, J.-C. G.; Piguet, C. *Chem. Rev.* **2002**, *102*, 1897-1928. (b) Imbert, D.; Cantuel, M.; Bunzli, J.-C. G.; Bernardinelli, G.; Piguet, C. *J. Am. Chem. Soc.* **2003**, *125*, 15698-15699. (c) Furphy, B. M.; et al. *Inorg. Chem*. **1987**, *26*, 4231-4236. (d) Dalla-Favera, N.; Hamacek, J.; Borkovec, M.; Jeannerat, D.; Ercolani, G.; Piguet, C. *Inorg. Chem.* **2007**, *46*, 9312-9322. (e) Chen, Q.-Y.; Luo, Q.-H.; Zheng, L.-M.; Wang, Z.-L.; Chen, J.-T. *Inorg. Chem.* **2002**, *41*, 605-609. (f) Carlson, C. N.; Kuehl, C. J.; Ogallo, L.; Shultz, D. A.; Thompson, J. D.; Kirk, M. L.; Martin, R. L.; John, K. D.; Morris, D. E. *Organomet.* **2007**, *26*, 4234. (g) also see references [72].

[59] For representative actinide homomultimetallics refer to; (a) Schelter, E. J.; Morris, D. E.; Scott, B. L.; Thompson, J. D.; Kiplinger, J. L. *Inorg. Chem.* **2007**, *46*, 5528 -5536. (b) Brennan, J. G.; Andersen, R. A.; Zalkin, A. *J. Am. Chem. Soc.* **1988**, *110*, 4554-4558. (c) Diaconescu, P. L.; Cummins, C. C. *J. Am. Chem. Soc.* **2002**, *124*, 7660-7661. (d) Diaconescu, P. L.; Arnold, P. L.; Baker, T. A.; Mindiola, D. J.; Cummins, C. C. *J. Am. Chem. Soc.* **2000** *122*, 6108-6109. For mixed valent species see; (e) Roussel, P.; Hitchcock, P. B.; Tinker, N.; Scott, P. *Chem. Commun.*, **1996**, 2053-2054. (f) Duval, P. B.; Burns, C. J.; Buschmann, W. E.; Clark, D. L.; Morris, D. E.; Scott, B. L. *Inorg. Chem.* **2001**, *40*, 5491-5496. (g) Burns, C. J.; Sattelberger, A. P. *Inorg. Chem.* **1988**, *27*, 3692-3693. (h) Lukens, W. W., Jr.; Beshouri, S. M.; Blosch, L. L.; Andersen, R. A. *J. Am. Chem. Soc.* **1996**, *118*, 901-902. (i) Also see reference [64-66].

[60] For actinide heterobimetallic complexes see; (a) Schelter, E. J.; Veauthier, J. M.; Thompson, J. D.; Scott, B. L.; John, K. D.; Morris, D. E.; Kiplinger, J. L. *J. Am. Chem. Soc.* **2006**, *128*, 2198-2199. (b) Kozimor, S. A.; Bartlett, B. M.; Rineheart, J. D.; Long, J. R. *J. Am. Chem. Soc.* **2007**, *129*, 10672-10674. (c) Arnold, P. L.; Patel, D.; Blake, A. J.; Wilson, C.; Love, J. B. *J. Am. Chem. Soc.* **2006**, *128*, 9610-9611. (d) Tsutsui, M.; Ely, N.; Gebala, A. *Inorg. Chem.* **1975**, *14*, 78-81. (e) Evans, W. J.; Nyce, G. W.; Greci, M. A.; Ziller, J. W. *Inorg. Chem.* **2001**, *40*, 6725-6730. (e) Odom, A. L.; Arnold, P. L.; Cummins, C. C. *J. Am. Chem. Soc.* **1998**, *120*, 5836-5837. (f) Monreal, M. J.; Carver, C. T.; Diaconescu, P. L. *Inorg. Chem.* **2007**, *46*, 7226-7228. (g) Paine, R. T.; Duesler, E. N.; Moody, D. C. *Organomet.* **1982**, *1*, 1097-1098. (g) Sternal, R. S; Brock, C. P.; Marks, T. J. *J. Am. Chem. Soc.* **1985**, *107*, 8270-8272.

[61] (a) Clark, D. L. *Los Alamos Science* **2000**, *26*, 364-381. (b) *The Chemistry of the Actinide and Transactinide Elements*, 3rd ed.; Morss, L. R., Edelstein, N. M., Fuger, J., The Netherlands, **2006**; Vol. 1-5, and references therein.

[62] For representative examples of uranyl oligomeric topologies see: (a) Thuery, P. *J. Am. Chem. Soc.* **2004**, *126*, 6838-6839. (b) Frisch, M.; Cahill, C. L. J. Chem. Soc., *Dalton Trans.* **2006**, 4679-4690, and references therein.

[63] For recent advances in organouranium bimetallic complexes refer to: (a) Kiplinger, J. L.; Pool, J. A.; Schelter, E. J.; Thompson, J. D.; Scott, B. L.; Morris, D. E. *Angew. Chem. Int. Ed. Engl.* **2006**, *45*, 2036-2041. (b) Evans, W. J.; Kozimor, S. A.; Ziller, J. W. *Science* **2005**, *309*, 1835-1838.

[64] (a) Karraker, D. G.; Siddall, T. H.; Stewart, W. E. *J. Inorg. Nuc. Chem.* **1969**, *31*, 711-714. (b) Cotton, F. A.; Marler, D. O.; Schwotzer, W. *Inorg. Chem.* **1984**, *23*, 4211-4215.

[65] Duval, P. B.; Burns, C. J.; Clark, D. L.; Morris, D. E.; Scott, B. L.; Thompson, J. D.; Werkema, E. L.; Jia, L.; Andersen, R. A. *Angew. Chem. Int. Ed. Engl.* **2001**, *40*, 3357-3361.

[66] (a) Spivack, B.; Dori, Z. *Coord. Chem. Rev.* **1975**, *17*, 99. (b) Steifel, E. I. *Prog. Inorg. Chem.* **1977**, *22*, 1. (c) Pope, M. T. *Prog. Inorg. Chem.* **1991**, *39*, 181.

[67] Rosen, R. K.; Andersen, R. A.; Edelstein, N. M. *J. Am. Chem. Soc.* **1990**, *112*, 4588-4590.

[68] (a) Ung, V. A.; Bardwell, D. A.; Jeffery, J. C.; Maher, J. P.; McCleverty, J. A.; Ward, M. D.; Williamson, A. *Inorg. Chem.* **1996**, *35*, 5290-5299. (b) Cleland, W. E.; Barhhart, K. M.; Yamanouchi, K.; Collison, D.; Mabbs, F. E.; Ortega, R. B.; Enemark, J. H. *Inorg. Chem.* **1987**, *26*, 1017-1025.

[69] (a) Ward, M. D. *Chem. Soc. Rev.* **1995**, 121-134. (b) Cotton, F. A.; Li, Z.; Liu, C. Y.; Murillo, C. A.; Villagran, D. *Inorg. Chem.* **2006**, *45*, 767-778.

[70] McCleverty, J. A.; Ward, M. D. *Acc. Chem. Res.* **1998**, *31*, 842-851.

[71] (a) Hogarth, G.; Humphrey, D. G.; Kaltsoyannis, N.; Kim, W.; Lee, M. V.; Norman, T.; Redmond, S. P. *J. Chem. Soc., Dalton Trans*. **1999**, 2705-2723. (b) Carlson, C. N.; Kuehl, C. J.; Da Re, R. E.; Veauthier, J. M.; Schelter, E. J.; Milligan, A. E.; Scott, B. L.; Bauer, E. D.; Thompson, J. D.; Morris, D. E.; John, K. D. *J. Am. Chem. Soc.* **2006**, *128*, 7230-7241.

[72] Carlson, C. N.; Scott, B. L.; Martin, R. L.; Thompson, J. D.; Morris, D. E.; John, K. D. *Inorg. Chem.* **2007**, *46*, 5013-5022.

[73] See references [67, 69, 74, 78] and references therein.

[74] McCleverty, J. A.; Ward, M. D. *Acc. Chem. Res.* **1998**, *31*, 842-851.

[75] (a) Antinolo, A. *J. Organomet. Chem.* **2006**, *691*, 1361-1368. (b) Liang, M.; Maatta, E. A. *Inorg. Chem.* **1992**, *31*, 953-956. (c) Wheeler, D. E.; Wu, J. F.; Maatta, E. J. *Polyhedron* **1998**, *17*, 969-977. (d) Clegg, W.; Errington, R. J.; Hockless, D. C. R.; Kirk, J. M.; Redshaw, C. *Polyhedron* **1992**, *11*, 381-384. (e) Maatta, E. A.; Kim, C. *Inorg. Chem.* **1989**, *28*, 624-625. (f) Hogarth, G.; Norman, T.; Redmond, S. P. *Polyhedron* **1999**, *18*, 1221-1227.

[76] $(C_5Me_5)_2U(NPh_2)$ was prepared using an inhouse procedure based on references [87] and [14].

[77] $(C_5Me_5)_2U(NPh_2)_2$ (**21**) has been prepared previously, and the crystal structure reported here for the first time. Arduini, A. L; Edelstein, N. M.; Jamerson, J. D.; Reynolds, J. G.; Schmid, K.; Takats, J. *Inorg. Chem.* **1981**, *20*, 2470-2474.

[78] Pierpont, C. G. *Coord. Chem. Rev.* **2001**, *216*, 99-125 and references therein.

[79] Ward, M. D.; McCleverty, J. A. *J. Chem. Soc., Dalton Trans.* **2002**, 275-288 and references therein. Also refer to [74] and [75].

[81] Pappenfus, T. M.; Mann, K. R. *Inorg. Chem.* **2001**, *40*, 6301-6307.

[82] Hay, P. J.; Martin, R. L *Los Alamos Science*, **2000**, *26*, 382-391 and references therein.

[83] Preliminary theoretical calculations performed by; Henson, N. J. and Hay, P. J.

[84] KOAr, $KNPh_2$, KNHPH were prepared according to a slight modification of the literature procedure using an excess of KH in THF with the respective phenol or amine, and following filtration over a thick pad of celite the resultant solution was dried and washed with hexanes. Nelson, J. E.; Clark, D. L.; Burns, C. J.; Sattelberger, A. P. *Inorg. Chem.* **1992**, *31*, 1973-1976.

[85] Krebs, F. C.; Jorgensen, M. *J. Org. Chem.* **2002** *67*, 7511 -7518.

[86] Herring, D. L. *J. Org. Chem.* **1961**, *26*, 3998-3999.

[87] Avens, L. R.; Burns, C. J.; Butcher, R. J.; Clark, D. L.; Gordon, J. C.; Schake, A. R.; Scott, B. L.; Watkin, J. G.; Zwick, B. D. *Organomet.* **2000**, *19*, 451-457.

[88] (a) SMART V5.051 and SAINT V5.00, Area Detector Control and Integration Software, Bruker AXS Inc., Madison, WI-53719, **1998**. (b) G. M. Sheldrick, SADABS, Bruker AXS Inc., Madison, WI-53719, **1997**. (c) Sheldrick, G. M.; *SHELXS-97: Program for Structural Solution*; University of Götten, Germany, **1997**. (d) Sheldrick, G. M.; *SHELXTL-97: Program for Structural Refinement (version 5.10)*; University of Götten, Germany, **1997**. (e) Barbour, L.; *X-SEED: Graphical interface for SHELXL*; University of Missouri-Columbia, **2001**.

Chapter 6

Concluding Remarks

In summary, the research developed in this dissertation covers the design, synthesis, and characterization of a three types of high-valent uranium ion complexes stabilized by multiply bound oxo and imido ligands. Together, these new species provide insight on the factors that govern 5f molecular and electronic structure, bonding, and reactivity trends that have an influential impact on cutting-edge research. This work builds upon previous endeavors while at the same time overturns new perspectives that implicate prospective key applications in the fields of fundamental actinide chemistry, nuclear waste separations and environmental remediation, and organoactinide activity. It is not the intent of this chapter to rehash the summaries from each previous study, but rather to highlight the most profound discoveries herein, and to set the landscape for future endeavors for the course of this research.

5.1 Uranyl(VI) Schiff base-Phenolate Chemistry

The study in Chapter 2 applies a group of salicylidene derived Schiff base ligands and related derivative with a range of different backbone architectures to the uranyl(VI) ion, and all result in bipyramidal coordination geometries with the chelate ligated around the equatorial plane. The variety of backbones exemplified here is one mere aspect of the

versatility of the Schiff base-phenolate chelates, and could extend to include a redox active transition metal unit within the backbone as shown in **Figure 5.1** to promote intramolecular electron transfer (i.e., $M^{n+}/U^{VI}O_2^{2+} \rightarrow M^{n+1}/U^{V}O_2^{+}$). Another viable alternative for future work includes reduction of the imino nitrogens on the sal-type pro-ligands to form amino-phenolate chelates to generate the corresponding uranyl(VI)-amide derivatives. A plausible pronotolysis route to gain entry to these systems is shown in **Scheme 5.1**, where the secondary amine donors disrupt the inherent planarity of the Schiff base parent species, and present the opportunity to deviate from exclusive equatorial uranyl coordination by saturating the coordination sphere with both steric and electronic excess.

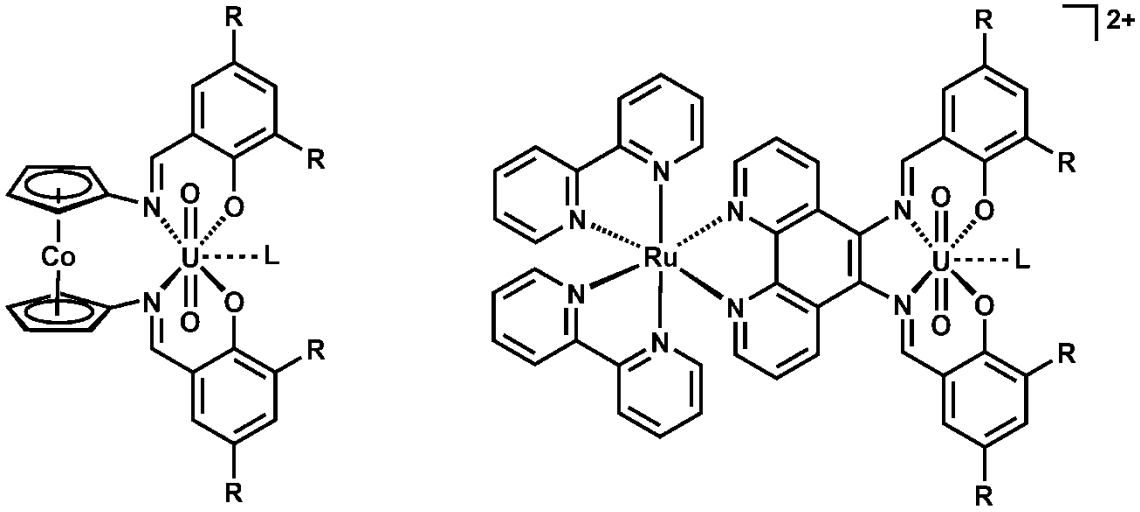

Figure 5.1. Heterobimetallic uranyl(VI) Schiff base-phenolate complexes with redox active transition metal units contained within the chelate backbone. R = ^{t}Bu, ^{i}Pr, CF_3, C_6F_5, adamantyl, $^{t}Bu_3Ar$, mesityl, or *p*-tolyl.

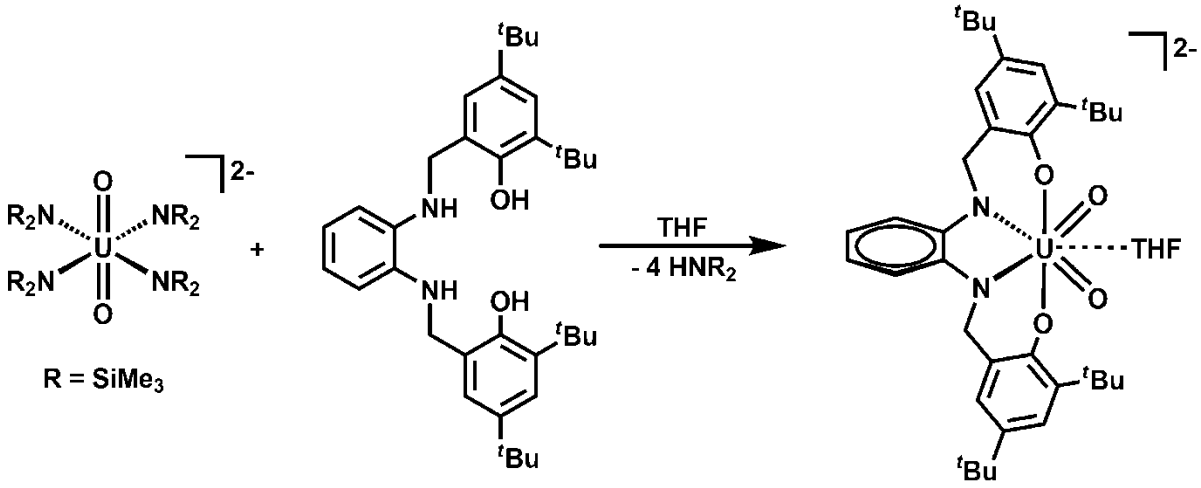

Scheme 5.1. A synthetic route to access a uranyl(VI) amido-phenolate complex.

Another aspect of the versatility of this set of ligands is alteration of the functionalities at the 3,5-positions on the phenolate sidearms. For instance, replacement of *t*-butyl substituents with functional groups suited to tune specific steric or electronic properties. The use of bulkier adamantyl or supermesityl substituted salicylidene sidearms would provide an additional measure of steric encapsulation to prevent the uranyl(V) proclivity for disproportionation. This would also block the region around the capping position to result in avoiding undesirable THF activation, and may redirect electron transfer to the uranyl(VI) moiety directly. These studies might also support our conjecture about capping ligand influences on electro- and photochemical behavior since easy access to the capping site would be lost by additional steric encumbrance. The electron withdrawing $–CF_3$ or $–C_6F_5$ units should be employed to adjust the electronic properties at the aryloxide-uranyl attachment and consequently result in modification of reduction potentials and photophysical properties. Overall, changing substituents on salicylidene moieties has the likelihood for a two-fold return: to provide steric protection against uranyl(V) disproportionation and to tune

the reduction potentials of the uranyl(VI/V) couple to gain entry to uranyl(V) by deploying a broader scope of applicable chemical reductants.

Future pursuits to generalize this behavior should focus on the use of alternative one electron chemical reductants with more powerful reducing strenth, for example the iron FiB dimer, or KC_8 or Na combined with a crown ether or PPh_4Cl would provide sufficient reducing strength and also offer a countercation for ionic stabilization of the resultant uranyl(V) anionic species. In this respect, preliminary studies with permethylatedcobaltocene in THF and Et_2O do not require photolysis to drive reduction of **1a** in THF. One final variation on this theme would be to design cationic uranyl(VI) chelate complexes to tune the uranyl(VI/V) couple to require low redox energetics to sustain reduction.

An interesting discovery during the course of this work was the dominant ligand based photophysical and photochemical properties that are complimented by occupation of the equatorial capping site. The long-lived uranyl(VI) excited state is quenched since no luminescence nor photoreactivity of uranyl(VI) origin is observed, thus proving the resilience of these complexes in conditions that would normally prompt uranyl(VI) photoreduction (i.e., methanol, $CoCp_2$). Resonance enhanced Raman spectroscopy could be employed to uncover the uranyl(VI) based LMCT excited state that is masked by higher oscillator strength ligand based absorptions. In the instance where photochemical reduction does occur, the UO_2(saloph) site remains intact whereas it is common for such reactions for uranyl(VI) to result in marked scrambling of the coordination sphere. This reaction progresses in the presence of THF to generate an excited state energy transfer process by blocking Schiff base-phenolate photochromic rearrangement, however when the capping equatorial site is not occupied the ligand based photoexcitation is unreactive towards $CoCp_2$, MeOH. Future work

on the reaction between **1a** and $CoCp_2$ will include quantifying the isotopic rate difference between THF and THF-d_8 activation.

A final notable feature, and possibly the most profound discovery during the course of the study of these uranyl(VI) Schiff base complexes, is the electrochemical and photochemical dependence on the availability of the capping site occupancy that introduces dramatic influences on redox kinetics and fluorescent properties. This behavior could be harnessed for use as a suitable sensor for species that bind at the equatorial site. The uranyl-saloph capping position has been utilized extensively as a platform to host neutral and anionic guest molecules like oxygenated solvents, phosphates, carbonates, and other oxyanions, and now this behavior is complimented by redox and photophysical sensor behavior.

5.2 A Bent Uranyl(VI) Moiety

In the second segment, the *cis*-dioxo uranyl(VI) unit contained within a ferrocenecarboxylate bridged coordination polymer presents an unparalleled discovery in actinide sciences that has been speculated and sought for years. The synthesis and structural properties of uranyl(VI) carboxylate complexes have been studied in extensive detail, however this is the sole example that displays a uranyl(VI) species that contains an $O=U=O^{2+}$ unit with an enormous deviation from the linear geometry (~110º). This remarkable deviation is presumably a result of the bulky ferrocene functionality tethered in close proximity to the carboxylate binding site coupled with the *in-situ* transformation between ferrocenemonocarboxylate, ferrocene, and 1,2-dicarboxylate ferrocene that generates the coordination polymer and allows for reversible solubility. Future endeavors ought to explore

the carboxylate migration in greater detail, and the first step should focus on discovering a facile synthetic route to access the free fcdcH2 ligand for direct application to the uranyl(VI) ion. Another direction prompted from this unusual discover should attempt to prevent carboxylate migration by blocking the Cp α-positions, however only recently have advances been made to cleanly activate the α-position on ferrocene Cp rings. Another possibility would be to alter the unsubstituted Cp rings, for example replacement with a permethylatedcyclopentadienyl to dislocate the extensive C-H···π contacts that support the polymer chains in a 3-D network. In a similar regard, attempts to replace the interstitial ferrocene units with other metallocene units (i.e., $RuCp_2$, $[Fc][PF_6]$, $CoCp_2$) have thus far proven unsuccessful.

The employment of a variety of sterically demanding carboxylate ligands, in contrast to the aliphatic and phthalic carboxylates familiar in uranyl chemistry, like those shown in **Figure 5.2** should be inspected further. Preliminary studies with mono- and 1,1'-disubstituted ruthenocenecarboxylate and 1,1'-ferrocenedicarboxylate have produced intractable products with no spectroscopic signature of any *cis*-dioxo unit. Likewise, the use of tritylcarboxylate has also resulted in an intractable product, and future workers might resort to the use of hydrothermal techniques for solubility and crystallinity. Additional studies should be carried out that design more sophisticated sterically hindered frameworks suited to push the oxo ligands out of the way. For instance, rigid cavitands with sufficient compartment size to accommodate the large uranium ion or other sterically encumbering chelates that present a steric mismatch for uranyl(VI) equatorial coordination. For example, the use of tripodal chelates like the pendant arm species in Chapter 2 have shown some promise upon deprotonation of the aryloxide pendant arm.

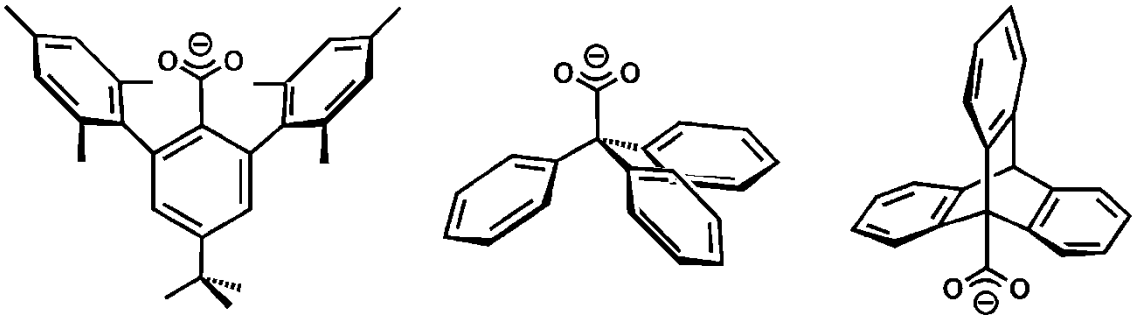

Figure 5.2. Sterically hindered carboxylate ligands.

The new *cis*-dioxo uranyl geometry presents an opportunity to examine the possibility for oxo atom abstraction reactions that are commonplace in *cis*-MoO_2^{2+} chemistry due to oxo lability and Mo^{VI} reduction. Preliminary attempts to remove the oxide ligands have not yet shown any sign of success with $PhNH_2$ or Ph_3P. This lack of immediate reactivity might be a consequence of the short strong U=O bonds that are conserved for both *cis* and *trans* uranyl species. Future endeavors should focus on the use of more aggressive oxophilic reagents for oxide extraction, for example using a coordinatively unsaturated U^{IV} species. Studies are currently being planned to promote oxo coordination to electrophilic species (i.e., metal cation, silyl groups, borates), however, again the short U=O bonds are a sign that the oxo ligands lack any obvious nucleophilic character. However, under certain circumstances *trans*-uranyl oxo ligands have been known to coordinate cations and other acidic groups when the oxide ligands are sufficiently basic. Furthermore, since the polymer displayed uncommon reversible solubility where the *cis*-UO_2^{2+} geometry is retained in solution (evidenced by IR), plans to harvest the *cis*-uranyl units by transplanting them into other chelate ligands with greater metallicity than the carboxylate manifold (for example 4-*t*-butylcalixarene) have been hampered by lack of exchange (evidenced by NMR).

Preliminary photolytic and electrochemical reactions with the *cis*-dioxo polymer have also turned out to be unfruitful. Attempts to oxidize the Fc units using silver salts and to reduce the uranyl(VI) units using cobaltocene, with the intent to support long range Fe^{III}/U^{V} paramagnetic ordering in the extended solid structure, have resulted in decomposition. Photophysical studies did not reveal any trace of *cis*-uranyl(VI) ground or excited state electronic or vibronic information to compare and contrast to well known *trans*-dioxo properties. This was obscured by overwhelming ferrocene absorption and emission, however one is inclined to believe that the *cis*-geometry should exhibit oxo-to-uranium LMCT. Similarly, the coordination polymer did not photolyze appreciably when dissolved methanol. In this case, the lack of photochemical reactivity may in part be due to altered excited state properties in contrast to the long lived photoexcited *trans*-uranyl(VI) excited state, or it could be quenched by proximal Fc units. In other words, the excited state may not be composed of a nonbonding 5f manifold as it is well known for traditional uranyl complexes.

In light of the short bonds, air stability, extremely acute dioxo angle, and lack of a predominant uranyl(VI) photoactive center, inspection of the bonding situation in comparison and contrast to extensive reviews on *trans* species might reveal electronic structure and bonding traits unparalleled in actinide chemistry. An isotopic ^{18}O or ^{17}O oxide labeling study would provide conclusive IR, Raman, or NMR spectroscopic assignments for the *cis*-uranyl unit. Similarly the C_{2v} symmetric and asymmetric U=O stretching vibrational modes should be Raman active, and resonance enhanced Raman spectroscopy might also be useful to pinpoint any LMCT for the *cis*-uranyl unit that is hidden under more intense ferrocene based absorptions. The use of other sterically hindered ligands (mentioned above) that do not contain any photoactive moieties might help to alleviate this dilemma in the

future. Luminescent lifetime measurements would provide more conclusive evidence of the nature of fluorescence observed in solution and the solid state, and determine if any can be assigned to uranyl origin with a long lived excited state.

EXAFS studies designed to tune into the uranium or ligand (carboxylate) edge would confirm structural parameters, and gain a measure of the electron density perturbed by the presence of U=O multiple bonding. Preliminary theoretical results carried out by Martin and Batastia at LANL indicate that both 5f (~65%) and 6d (~35%) valence orbitals participate in multiple bonding. However, it should be noted that a different 5f orbital bonding regime would be required to support the *cis*-dioxo C_{2v} geometry, especially since the $5f_z3$ and $6p_z$ orbitals cannot contribute to give strong σ-bonding as they do to lock the *trans* configuration in place. We tend to harbor the belief that these short U=O bonds are accommodated through d-orbital π-type bonding much like their *cis*-dioxo transition metals counterparts.

Future plans are in the works to generalize the dioxo bending method to other actinyl ions and the isoelectronic bis-imido and mixed oxo-imido species. Results from these studies will be interesting since the imido analogues also display a complicated admixture of 6d and 5f uranium based valence orbitals that facilitate U=NR multiple covalent bonding. These studies will be especially interesting for neptunyl and plutonyl species, since linear actinyl O=An=O bonds follow the expected trend and get shorter across the series, yet the shorter bonds display anomalously lower energy vibrational stretches in both IR and Raman spectroscopies. These new properties imparted by the *cis* geometry could in the future be harnessed for key applications for solvent based separations of the mixture of actinyl ions from spent nuclear fuel streams. This idea is founded on the net dipole moment for the C_{2v} geometry that leads to solubility in (and stabilization from) higher dielectric solvents than the

trans actinyl species, not to mention the advantage of reversible polymers in recycling scenarios.

5.3 Mono- and Homobimetallic Organouranium(V)-Imido Complexes

In the third topic in this text, the thorough interrogation of the synthesis and molecular and electronic structural aspects of a series of pentavalent uranium organometallic imido complexes revealed (i) that this oxidation state is not as unstable as past workers have assumed, and (ii) the electronic structure of these complexes do not reveal large perturbations within the 5f orbital manifold manifested from ligand substitution in the wedge site. Since U^{V} chemistry has rarely been exploited under such rigorous and systematic scrutiny, work is currently underway to extend ligand substitution to include a variety of derivatives that are known for other oxidation states but not yet for the pentavalent ion, including; silyl, alkyl, aryl, acetylide, and phosphide to uranium contacts. Also, since a U^{IV}-phosphinidene complex is known, plans have been made to replace the imido functionality with the multiply bound phosphinidene and reinvent all of this starting from Cu^{I} oxidation (**Scheme 5.2**).

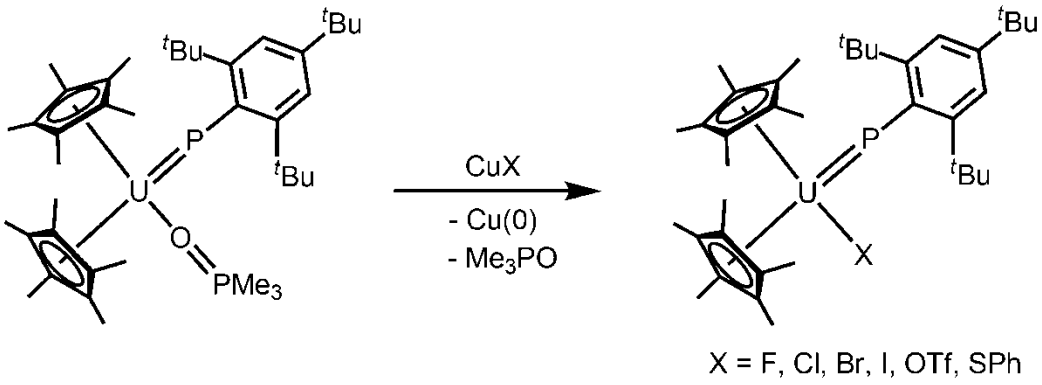

Scheme 5.2. Prospective synthesis of organouranium(V)-phosphinidene complexes.

The observation of a reaction reminiscent of PCET discovered for the generation of a U^{VI} bis-imido complex requires further elucidation. For example, by using known hydrogen abstraction reagents (i.e., tri-*t*-butylphenoxy radical) or monitoring reaction progress using deuterated phenylanalide. This potentially useful type of reaction might find application in future strategies to gain synthetic access to other multiply bound uranium species, for example the highly sought after unsupported uranium alkylidene fragment, or as a route to access U^{VI}-phosphinidene species. This ideology parallels hydrogen atom abstraction routes used in the preparation of an high valent early transition metal alkylidene complexes.

Future directions for this work also include a variety of spectroscopic endeavors. For example, uranium edge EXAFS has recently confirmed the solid state structural parameters for the U^{V} imido-halide series, and could extended to the new substitution complexes to determine structural differences that accompany substitution within the metallocene wedge. The studies in chapter 4 suggest that there are nearly negligible differences within the 5f manifold for all derivatives examined thus far, and covalent bonding is likely accommodated by 6d orbitals. Theoretical findings will compliment this speculation and elucidate the nature of Russel-Sander and ligand-field ground and excited states participating in redox chemistry, electronic spectroscopy, and magnetism. Since a novel NIR fluorescence was recently reported for neptunyl(VI) complexes, these U^{V} $5f^{1}$ congeners may also have the ability to intra-5f luminescence with comparably short lifetimes. Albeit excitation relies on forbidden f→f transitions, intensity could be siphoned from the imido functionality as it was in electronic absorption studies. Also, the U=N unit might participate in photolytic pathways to activate the inert U=N bond, as there is the possibility that these multiply bound high valent

species possess the unique combination of luminescence and excited state reactivity similar to that observed in uranyl(VI) systems.

A number of questions arose from the studies on U^{V} bimetallic complexes, which logically prompts the desire to vary synthetic design and formulate hypotheses from known monometallic properties and the information made available from bimetallic studies here. These complexes displayed a degree of metal-metal communication, albeit relatively weak, in electrochemical, spectroscopic, magnetic, and preliminary theoretical studies. Future studies will focus on adjusting the tunable properties to enhance $5f^{1}$-$5f^{1}$ interactions. Specific examples includes decreasing the space between the metal ions via modifying the length or substitution pattern of the bridge (**Figure 5.3**) based on the pretense that if the metals are closer together they can *talk* to one another in an easier manner. The use of different conjugated bridges is another attractive variable to adjust superconjugation by presenting different donor atoms tethered through a phenylene ring For example aryloxide or acetylide donors offer the ability tune the orbital overlap energy and spatial match with the 5f orbital that houses the valence electron involved in communication. Another promising option would be to adjust the planarity of the phenylene ring in the bridge such that any conjugation pathway might be twisted perpendicular to the metallocene wedge as in Figure 5.3.

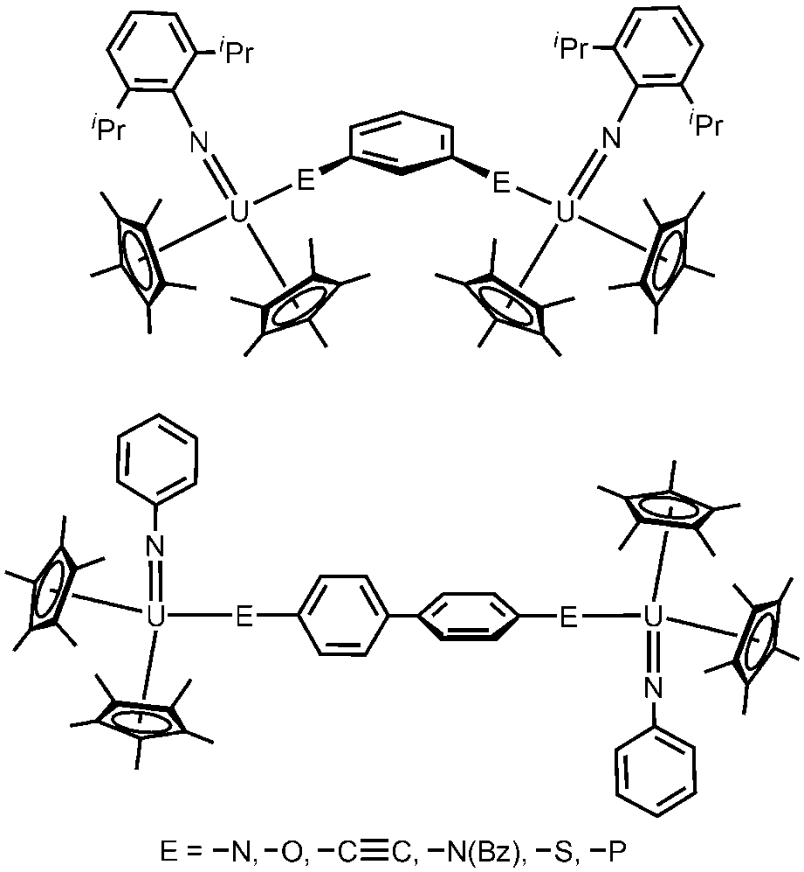

Figure 5.3. Bridging ligand variation for the high-valent bimetallic complexes.

Since the bimetallic complexes displayed a well-behaved electrochemical response to oxidation and reduction, future endeavors will put this into practice by using chemical reductants or oxidants capable of stabilizing mixed valent species. This will result in electronic delocalization that might lead to valence ambiguity or charge transfer to the noninnocent phenylene bridge. In the distant future, we plan to use this knowledge to synthesize higher nuclearity polymetallics, for example starting from the trivalent amide bridged bimetallic to form a molecular square (or higher order polygonal architecture) containing multiple pentavalent ions in close proximity, as demonstrated in **Scheme 5.3**.

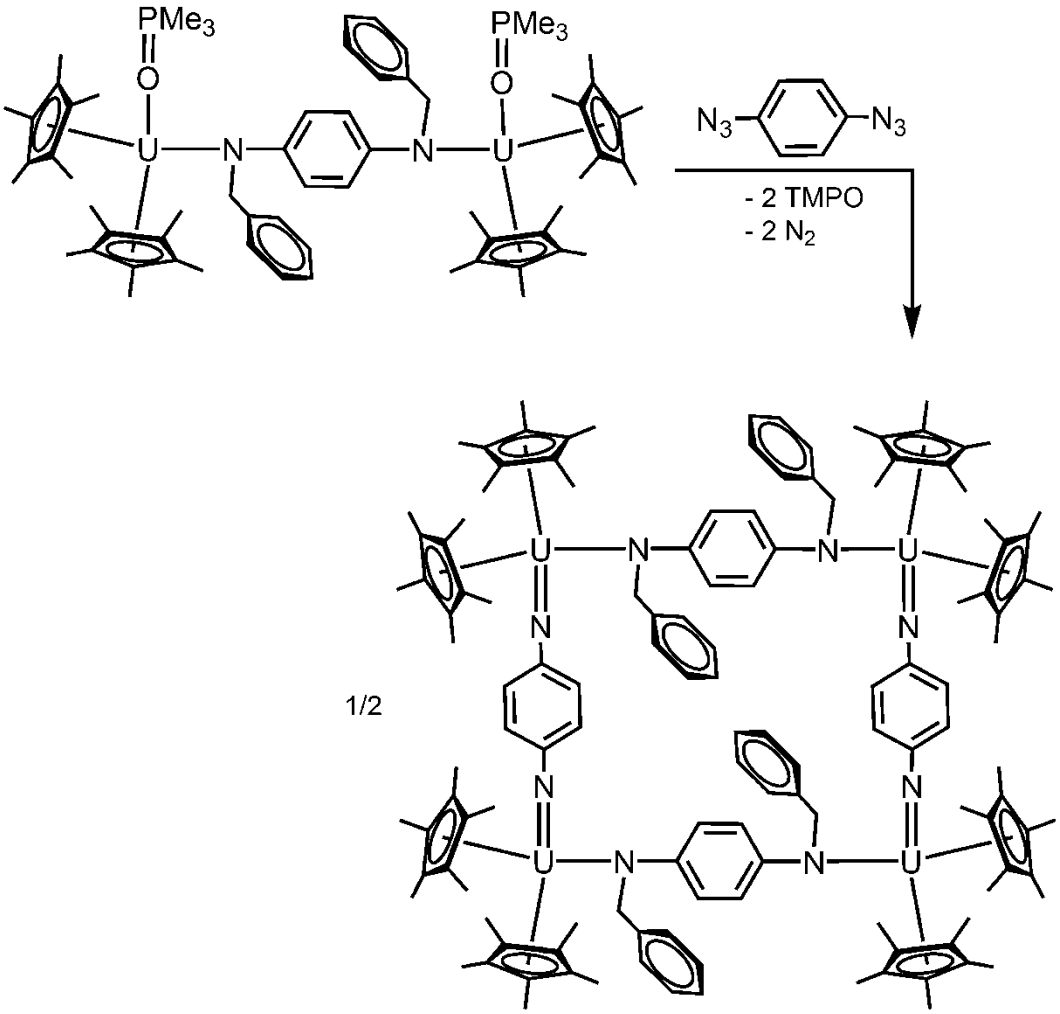

Scheme 5.3. Potential synthesis of a multimetallic U^{V} cluster.

VITA

Anthony E. Vaughn was born on March 15, 1981 in Florissant, Missouri. After graduating from McCluer North High School in 1999, he obtained a B.S. from Quincy University in 2002 majoring in chemistry with minors in mathematics and physics under the guidance of Professor Scott Luaders. After completing undergraduate work, he spent a year in St. Louis employed in a petrochemical quality control laboratory. He received his Ph.D. from the University of Missouri-Columbia in 2008 under the guidance of Professor Paul B. Duval with emphasis on inorganic aspects of f-element chemistry. He spent the summer of 2007 studying organometallic actinide chemistry at Los Alamos National Laboratory (LANL) as a G.T. Seaborg Graduate Summer Research fellow in the laboratory of Dr. Jaqueline L. Kiplinger. Anthony is planning to attend a postdoctoral appointment in the Chemistry and Materials Science division at LANL under the guidance of Drs. David E. Morris and Jaqueline L. Kiplinger, where he will continue f-element endeavors concentrating on electronic structure and bonding in multimetallic lanthanide and actinide organometallics. He plans to pursue a career as a synthetic inorganic chemist, electrochemist, spectroscopist, and crystallographer.

Appendix 1

Supporting Information for:

Structural, Electrochemical, and Photochemical Trends

Among Three Types of Uranyl(VI) Schiff Base-Phenolate Complexes

and Related Derivatives (Chapter 2)

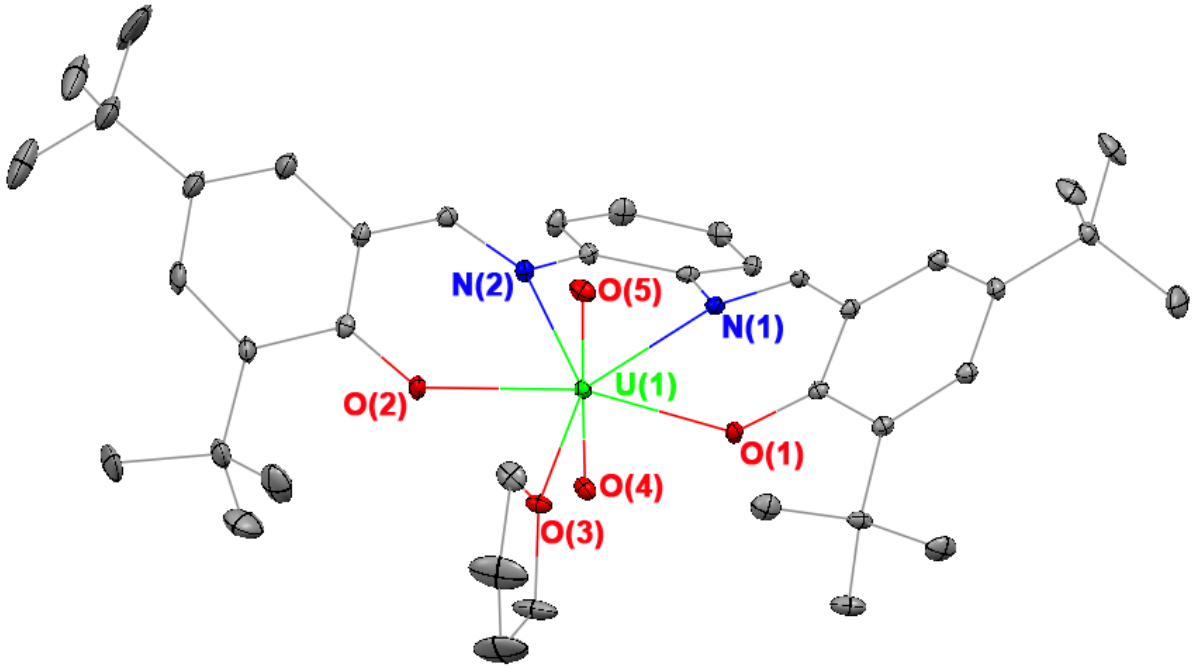

Figure S2.1. Molecular structure for **1a** with ellipsoids at the 50% probability level.

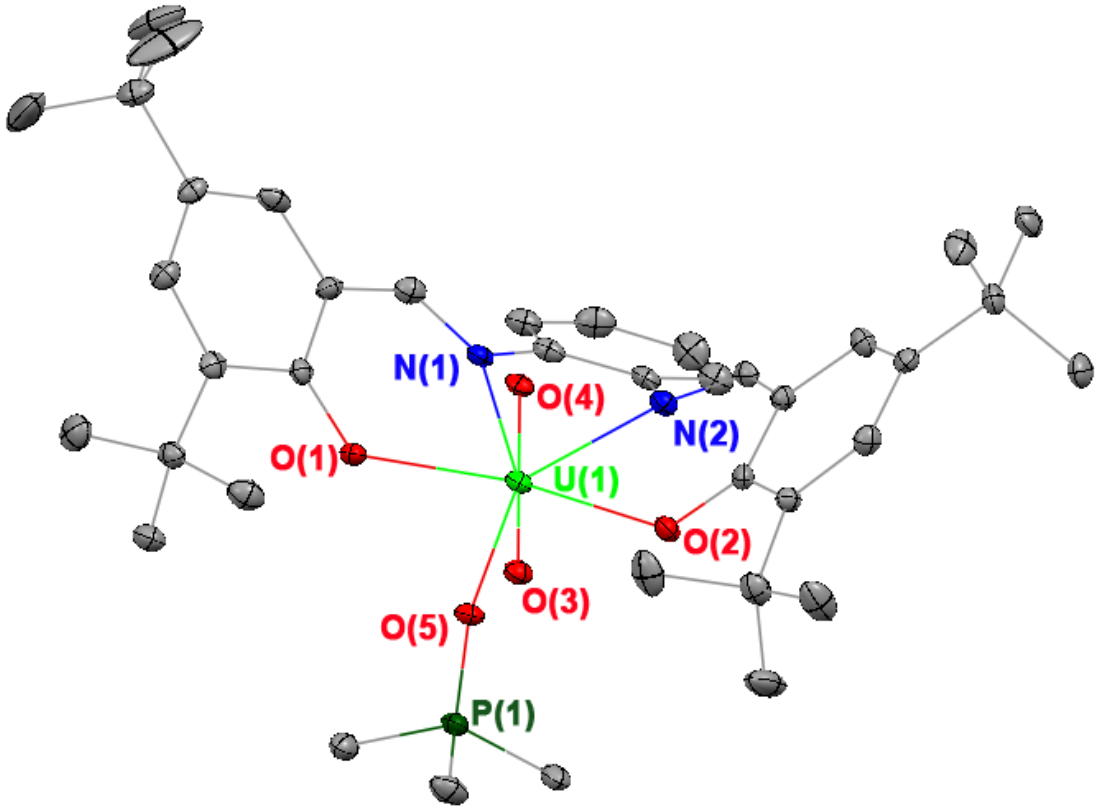

Figure S2.2. Molecular structure for **1b** with ellipsoids at the 50% probability level.

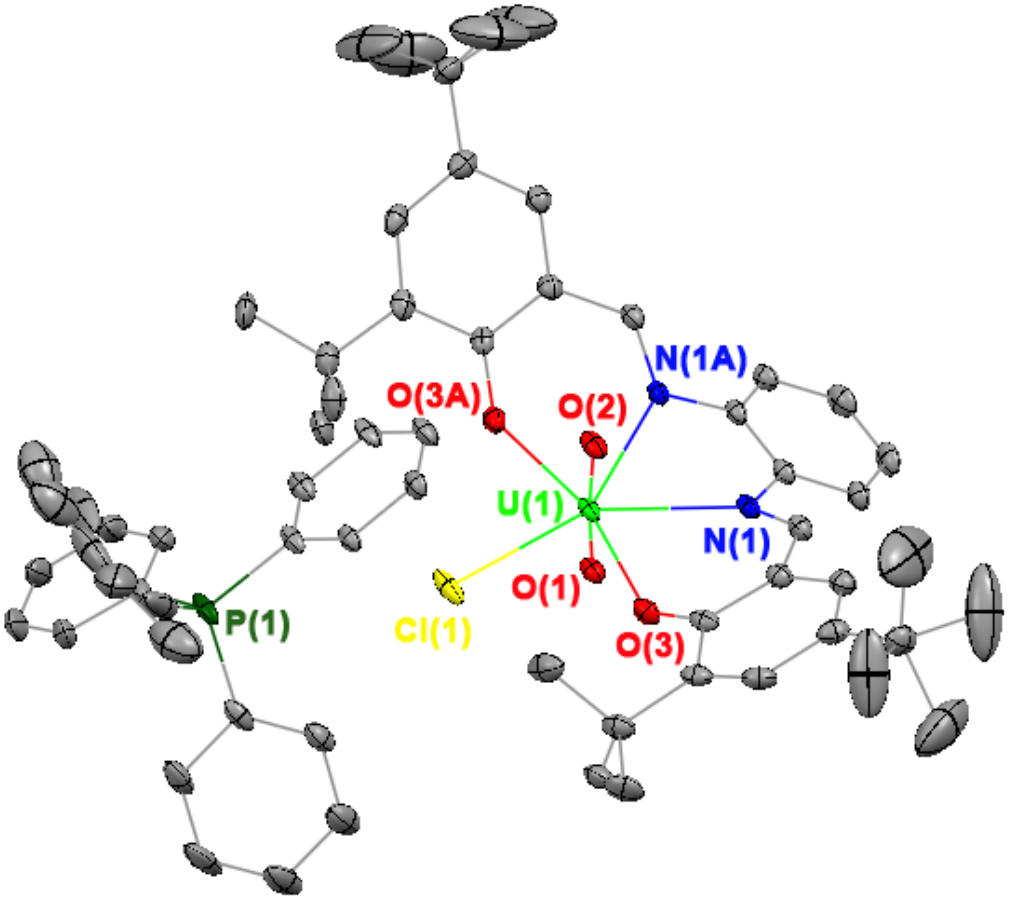

Figure S2.3. Molecular structure for **1c** with ellipsoids at the 50% probability level. Note one of the phenyl groups on the PPh_4^+ unit is disordered across a crystollographic mirror plane, and the disorder could not be resolved in P*nma*.

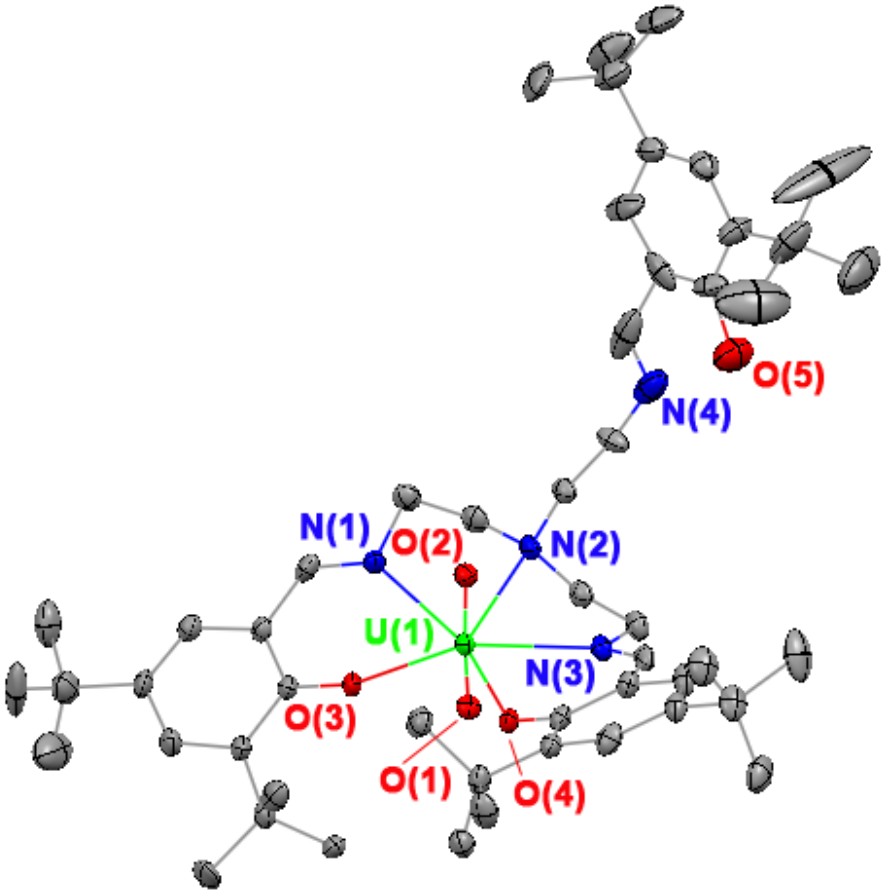

Figure S2.3. Molecular structure for **3** with ellipsoids at the 50% probability level.

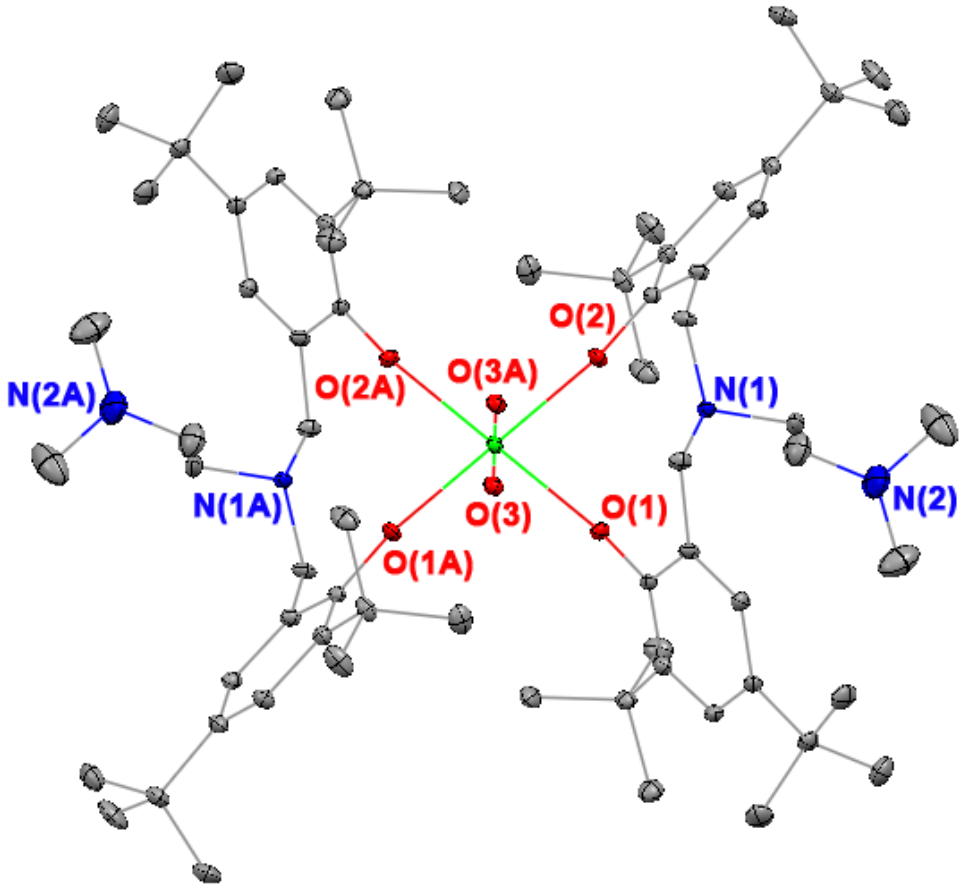

Figure S2.4. Molecular structure for **4** with ellipsoids at the 50% probability level.

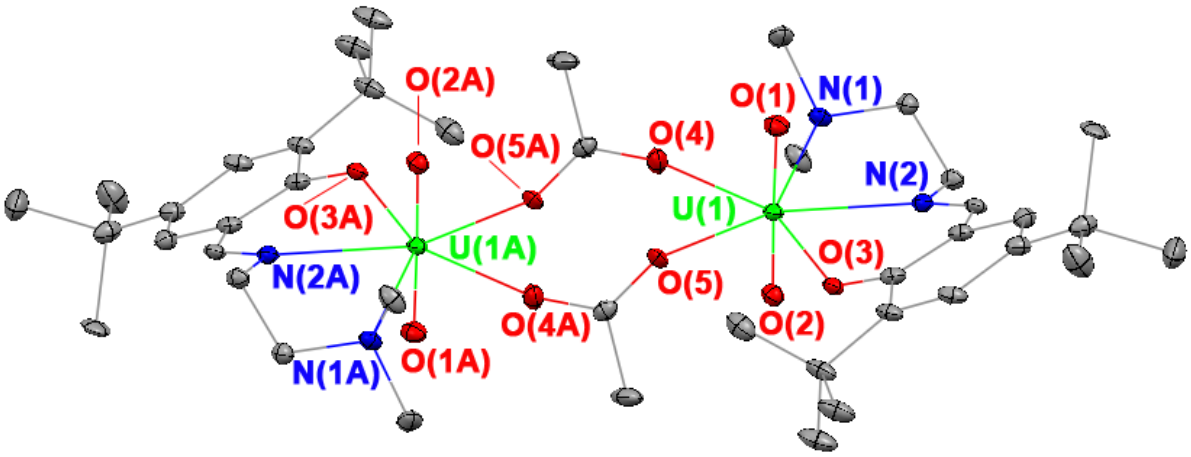

Figure S2.5. Molecular structure for **6** with ellipsoids at the 50% probability level.

Table S2.1. Atomic coordinates and equivalent isotropic displacement parameters (A^2) for **1a**. U(eq) is defined as one third of the trace of the orthogonalized U^{ij} tensor.

	X	*Y*	*Z*	U_{iso}*/U_{eq}
U1	0.110005 (9)	0.344573 (6)	0.890389 (12)	0.01150 (5)
O1	−0.01808 (17)	0.34089 (12)	0.7887 (3)	0.0156 (6)
N1	0.0556 (2)	0.44892 (15)	0.8446 (3)	0.0132 (7)
C1	−0.0636 (2)	0.36746 (18)	0.6992 (4)	0.0136 (8)
O2	0.22909 (18)	0.31065 (13)	0.9890 (3)	0.0197 (7)
N2	0.2061 (2)	0.42916 (15)	0.9517 (3)	0.0149 (7)
C2	−0.1287 (3)	0.33771 (18)	0.6257 (4)	0.0155 (9)
O3	0.08785 (19)	0.23585 (13)	0.8803 (3)	0.0189 (7)
C3	−0.1700 (3)	0.3677 (2)	0.5285 (4)	0.0171 (9)
H3	−0.2116	0.3470	0.4781	0.021*
O4	0.07797 (19)	0.34728 (13)	1.0242 (3)	0.0188 (6)
C4	−0.1551 (3)	0.4265 (2)	0.4984 (4)	0.0175 (9)
O5	0.1406 (2)	0.34282 (13)	0.7561 (3)	0.0212 (7)
C5	−0.0972 (2)	0.45595 (19)	0.5752 (4)	0.0167 (9)
H5	−0.0877	0.4965	0.5612	0.020*
C6	−0.0512 (2)	0.42802 (18)	0.6746 (4)	0.0145 (9)
C7	0.0031 (2)	0.46468 (18)	0.7545 (4)	0.0138 (8)
H7	−0.0003	0.5060	0.7388	0.017*
C8	0.0942 (3)	0.49501 (18)	0.9176 (4)	0.0140 (8)
C9	0.0576 (3)	0.54717 (18)	0.9404 (4)	0.0162 (9)
H9	0.0034	0.5534	0.9066	0.019*
C10	0.0999 (3)	0.59003 (19)	1.0122 (4)	0.0202 (10)
H10	0.0750	0.6259	1.0265	0.024*
C11	0.1787 (3)	0.5807 (2)	1.0631 (4)	0.0238 (10)
H11	0.2078	0.6104	1.1113	0.029*
C12	0.2152 (3)	0.5283 (2)	1.0441 (4)	0.0207 (9)

H12	0.2688	0.5218	1.0809	0.025*
C13	0.1735 (3)	0.48523 (18)	0.9710 (4)	0.0140 (8)
C14	0.2809 (3)	0.42727 (19)	0.9547 (4)	0.0179 (9)
H14	0.3055	0.4642	0.9474	0.021*
C15	0.3309 (3)	0.3762 (2)	0.9678 (4)	0.0187 (9)
C16	0.4107 (3)	0.3867 (2)	0.9713 (5)	0.0282 (11)
H16	0.4262	0.4243	0.9478	0.034*
C17	0.4667 (3)	0.3443 (2)	1.0077 (5)	0.0313 (12)
C18	0.4399 (3)	0.2898 (2)	1.0434 (5)	0.0298 (12)
H18	0.4780	0.2597	1.0684	0.036*
C19	0.3627 (3)	0.2766 (2)	1.0450 (4)	0.0221 (10)
C20	0.3041 (3)	0.3202 (2)	0.9979 (4)	0.0175 (9)
C21	−0.1522 (3)	0.27463 (19)	0.6537 (4)	0.0175 (9)
C22	−0.1703 (3)	0.2734 (2)	0.7760 (4)	0.0274 (11)
H22A	−0.1241	0.2870	0.8336	0.041*
H22B	−0.1833	0.2328	0.7948	0.041*
H22C	−0.2150	0.2995	0.7775	0.041*
C23	−0.0851 (3)	0.2313 (2)	0.6487 (4)	0.0274 (11)
H23A	−0.0774	0.2293	0.5687	0.041*
H23B	−0.0985	0.1919	0.6733	0.041*
H23C	−0.0365	0.2451	0.7008	0.041*
C24	−0.2259 (3)	0.2519 (2)	0.5676 (4)	0.0290 (11)
H24A	−0.2707	0.2775	0.5711	0.043*
H24B	−0.2373	0.2113	0.5883	0.043*
H24C	−0.2166	0.2525	0.4884	0.043*
C25	−0.2025 (3)	0.45385 (19)	0.3850 (4)	0.0191 (9)
C26	−0.1827 (3)	0.4199 (2)	0.2822 (4)	0.0302 (12)
H26A	−0.1263	0.4236	0.2847	0.045*

H26B	−0.2129	0.4363	0.2088	0.045*
H26C	−0.1961	0.3779	0.2876	0.045*
C27	−0.2916 (3)	0.4494 (3)	0.3781 (5)	0.0391 (14)
H27A	−0.3066	0.4077	0.3805	0.059*
H27B	−0.3203	0.4673	0.3051	0.059*
H27C	−0.3046	0.4705	0.4442	0.059*
C28	−0.1822 (3)	0.5193 (2)	0.3732 (4)	0.0331 (13)
H28A	−0.1929	0.5416	0.4395	0.050*
H28B	−0.2144	0.5353	0.3006	0.050*
H28C	−0.1263	0.5230	0.3719	0.050*
C29	0.5558 (3)	0.3539 (3)	1.0185 (7)	0.0500 (17)
C30	0.5740 (4)	0.4188 (4)	1.0006 (12)	0.129 (5)
H30A	0.5411	0.4440	1.0383	0.193*
H30B	0.5629	0.4276	0.9170	0.193*
H30C	0.6296	0.4267	1.0349	0.193*
C31	0.6011 (3)	0.3378 (3)	1.1398 (6)	0.059 (2)
H31A	0.5955	0.2953	1.1528	0.089*
H31B	0.5801	0.3602	1.1975	0.089*
H31C	0.6568	0.3475	1.1477	0.089*
C32	0.5842 (4)	0.3147 (4)	0.9300 (6)	0.070 (2)
H32A	0.6395	0.3236	0.9315	0.105*
H32B	0.5522	0.3224	0.8519	0.105*
H32C	0.5791	0.2729	0.9500	0.105*
C33	0.3401 (3)	0.2198 (2)	1.1014 (5)	0.0323 (12)
C34	0.3044 (4)	0.2372 (3)	1.2042 (5)	0.0550 (18)
H34A	0.3435	0.2590	1.2618	0.083*
H34B	0.2886	0.2014	1.2403	0.083*
H34C	0.2582	0.2624	1.1765	0.083*

C35	0.4121 (4)	0.1798 (3)	1.1475 (7)	0.068 (2)
H35A	0.4351	0.1675	1.0824	0.102*
H35B	0.3956	0.1447	1.1851	0.102*
H35C	0.4514	0.2019	1.2043	0.102*
C36	0.2817 (4)	0.1827 (3)	1.0143 (6)	0.0502 (17)
H36A	0.2340	0.2060	0.9844	0.075*
H36B	0.2681	0.1470	1.0529	0.075*
H36C	0.3056	0.1713	0.9495	0.075*
C37	0.0516 (4)	0.2023 (2)	0.9599 (5)	0.0416 (15)
H37A	0.0808	0.2087	1.0413	0.050*
H37B	−0.0035	0.2154	0.9531	0.050*
C38	0.0536 (5)	0.1405 (3)	0.9297 (7)	0.067 (2)
H38A	0.0007	0.1228	0.9217	0.080*
H38B	0.0907	0.1189	0.9919	0.080*
C39	0.0785 (5)	0.1355 (3)	0.8211 (6)	0.066 (2)
H39A	0.0336	0.1236	0.7578	0.079*
H39B	0.1203	0.1051	0.8277	0.079*
C40	0.1095 (3)	0.1955 (2)	0.7945 (4)	0.0254 (11)
H40A	0.1673	0.1943	0.8033	0.030*
H40B	0.0849	0.2081	0.7141	0.030*
C1S	0.3833 (8)	0.5896 (4)	1.3752 (10)	0.200*
H1S1	0.3814	0.5904	1.4578	0.200*
H1S2	0.3366	0.6094	1.3292	0.200*
H1S3	0.4307	0.6101	1.3645	0.200*
C2S	0.3847 (5)	0.5356 (4)	1.3415 (6)	0.200*
C3S	0.4561 (4)	0.5106 (5)	1.3323 (8)	0.200*
H3S	0.5025	0.5341	1.3475	0.200*
C4S	0.4596 (6)	0.4514 (5)	1.3010 (9)	0.200*

H4S	0.5084	0.4344	1.2947	0.200*
C5S	0.3917 (8)	0.4172 (4)	1.2788 (8)	0.200*
H5S	0.3941	0.3767	1.2575	0.200*
C6S	0.3202 (6)	0.4420 (5)	1.2877 (9)	0.200*
H6S	0.2738	0.4185	1.2723	0.200*
C7S	0.3167 (4)	0.5012 (5)	1.3190 (8)	0.200*
H7S	0.2678	0.5181	1.3251	0.200*

Table S2.2. Anisotropic displacement parameters (A^2) for **1a**. The anisotropic displacement factor exponent takes the form: $-2\pi^2$ [$h^2 a^2 U^{11}$ + ... + 2 h k a* b* U^{12}].

	U^{11}	U^{22}	U^{33}	U^{12}	U^{13}	U^{23}
U1	0.01222 (9)	0.00959 (8)	0.01214 (8)	0.00001 (6)	0.00153 (5)	0.00011 (6)
O1	0.0127 (15)	0.0131 (14)	0.0181 (15)	−0.0021 (12)	−0.0026 (12)	0.0005 (12)
N1	0.0135 (18)	0.0115 (17)	0.0147 (17)	−0.0007 (14)	0.0034 (14)	0.0001 (13)
C1	0.014 (2)	0.0137 (19)	0.014 (2)	−0.0005 (17)	0.0049 (16)	−0.0017 (16)
O2	0.0131 (16)	0.0170 (16)	0.0273 (17)	0.0039 (12)	0.0012 (13)	0.0035 (13)
N2	0.0143 (19)	0.0122 (17)	0.0164 (18)	0.0003 (14)	−0.0001 (14)	−0.0016 (14)
C2	0.016 (2)	0.015 (2)	0.015 (2)	−0.0029 (17)	0.0037 (17)	−0.0028 (16)
O3	0.0263 (18)	0.0134 (15)	0.0185 (16)	−0.0018 (13)	0.0085 (13)	0.0009 (12)
C3	0.016 (2)	0.020 (2)	0.015 (2)	−0.0040 (18)	0.0018 (17)	−0.0016 (17)
O4	0.0224 (17)	0.0171 (15)	0.0164 (15)	0.0039 (13)	0.0031 (12)	0.0029 (12)
C4	0.015 (2)	0.021 (2)	0.015 (2)	0.0017 (18)	0.0012 (17)	0.0024 (17)
O5	0.0288 (19)	0.0165 (15)	0.0186 (15)	0.0005 (14)	0.0062 (13)	−0.0004 (13)
C5	0.015 (2)	0.017 (2)	0.017 (2)	−0.0026 (17)	0.0026 (17)	−0.0002 (17)
C6	0.011 (2)	0.017 (2)	0.014 (2)	−0.0037 (17)	0.0001 (16)	−0.0022 (16)
C7	0.012 (2)	0.0107 (19)	0.019 (2)	−0.0009 (16)	0.0043 (16)	0.0020 (17)
C8	0.017 (2)	0.013 (2)	0.013 (2)	−0.0045 (17)	0.0036 (16)	−0.0014 (16)
C9	0.014 (2)	0.016 (2)	0.019 (2)	0.0023 (17)	0.0052 (17)	0.0027 (17)
C10	0.024 (3)	0.014 (2)	0.023 (2)	0.0023 (18)	0.0072 (19)	−0.0026 (18)

C11	0.025 (3)	0.017 (2)	0.027 (3)	−0.0063 (19)	0.001 (2)	−0.0087 (19)
C12	0.015 (2)	0.021 (2)	0.024 (2)	−0.0017 (18)	−0.0015 (18)	−0.0046 (19)
C13	0.015 (2)	0.014 (2)	0.012 (2)	−0.0008 (16)	0.0005 (16)	−0.0019 (16)
C14	0.015 (2)	0.017 (2)	0.021 (2)	−0.0015 (17)	0.0024 (18)	0.0004 (17)
C15	0.012 (2)	0.020 (2)	0.022 (2)	0.0013 (18)	0.0005 (17)	−0.0009 (18)
C16	0.016 (2)	0.026 (3)	0.042 (3)	0.001 (2)	0.005 (2)	0.003 (2)
C17	0.014 (2)	0.035 (3)	0.046 (3)	0.001 (2)	0.008 (2)	0.003 (2)
C18	0.018 (3)	0.030 (3)	0.039 (3)	0.013 (2)	−0.001 (2)	0.005 (2)
C19	0.016 (2)	0.027 (2)	0.021 (2)	0.0060 (19)	−0.0018 (18)	0.0039 (19)
C20	0.016 (2)	0.018 (2)	0.018 (2)	0.0014 (18)	0.0035 (17)	−0.0026 (17)
C21	0.021 (2)	0.016 (2)	0.016 (2)	−0.0065 (18)	0.0050 (17)	0.0003 (17)
C22	0.043 (3)	0.023 (2)	0.019 (2)	−0.013 (2)	0.013 (2)	−0.0014 (19)
C23	0.032 (3)	0.021 (2)	0.029 (3)	−0.006 (2)	0.005 (2)	−0.005 (2)
C24	0.028 (3)	0.028 (3)	0.028 (3)	−0.017 (2)	0.001 (2)	−0.003 (2)
C25	0.019 (2)	0.020 (2)	0.014 (2)	−0.0009 (18)	−0.0032 (17)	0.0014 (17)
C26	0.042 (3)	0.033 (3)	0.013 (2)	0.000 (2)	0.002 (2)	0.004 (2)
C27	0.023 (3)	0.059 (4)	0.029 (3)	0.002 (3)	−0.006 (2)	0.010 (3)
C28	0.047 (3)	0.024 (3)	0.020 (2)	0.002 (2)	−0.010 (2)	0.007 (2)
C29	0.017 (3)	0.052 (4)	0.082 (5)	0.006 (3)	0.014 (3)	0.013 (3)
C30	0.020 (4)	0.084 (7)	0.286 (16)	0.005 (4)	0.043 (6)	0.073 (8)
C31	0.017 (3)	0.085 (5)	0.072 (5)	0.004 (3)	0.002 (3)	−0.031 (4)
C32	0.022 (3)	0.153 (8)	0.036 (4)	0.020 (4)	0.006 (3)	0.003 (4)
C33	0.024 (3)	0.026 (3)	0.041 (3)	0.005 (2)	−0.004 (2)	0.013 (2)
C34	0.068 (5)	0.066 (5)	0.033 (3)	−0.002 (4)	0.016 (3)	0.019 (3)
C35	0.037 (4)	0.060 (5)	0.099 (6)	0.019 (3)	−0.002 (4)	0.051 (4)
C36	0.053 (4)	0.022 (3)	0.066 (4)	0.000 (3)	−0.007 (3)	0.009 (3)
C37	0.074 (5)	0.022 (3)	0.040 (3)	−0.008 (3)	0.037 (3)	0.004 (2)
C38	0.100 (6)	0.020 (3)	0.096 (6)	−0.020 (3)	0.053 (5)	0.002 (3)

C39	0.130 (7)	0.017 (3)	0.064 (5)	−0.020 (4)	0.049 (5)	−0.015 (3)
C40	0.037 (3)	0.019 (2)	0.020 (2)	0.003 (2)	0.008 (2)	−0.0072 (19)

Table S2.3. Bond lengths [Å], bond angles [º], and torsion angles [º] for **1a.**

U1—O5	1.776 (3)	C15—C16	1.401 (6)
U1—O4	1.784 (3)	C15—C20	1.419 (6)
U1—O2	2.274 (3)	C16—C17	1.366 (7)
U1—O1	2.288 (3)	C17—C18	1.412 (7)
U1—O3	2.481 (3)	C17—C29	1.544 (7)
U1—N2	2.535 (3)	C18—C19	1.381 (7)
U1—N1	2.550 (3)	C19—C20	1.438 (6)
O1—C1	1.314 (5)	C19—C33	1.534 (7)
N1—C7	1.287 (5)	C21—C23	1.534 (7)
N1—C8	1.420 (5)	C21—C24	1.537 (6)
C1—C6	1.423 (6)	C21—C22	1.540 (6)
C1—C2	1.432 (6)	C25—C28	1.532 (6)
O2—C20	1.305 (5)	C25—C26	1.535 (6)
N2—C14	1.296 (6)	C25—C27	1.539 (7)
N2—C13	1.425 (5)	C29—C31	1.514 (10)
C2—C3	1.385 (6)	C29—C30	1.521 (10)
C2—C21	1.536 (6)	C29—C32	1.530 (10)
O3—C37	1.454 (5)	C33—C36	1.524 (8)
O3—C40	1.469 (5)	C33—C34	1.529 (8)
C3—C4	1.411 (6)	C33—C35	1.542 (7)
C4—C5	1.368 (6)	C37—C38	1.441 (8)
C4—C25	1.535 (6)	C38—C39	1.443 (9)
C5—C6	1.411 (6)	C39—C40	1.515 (7)
C6—C7	1.439 (6)	C1S—C2S	1.2830
C8—C9	1.392 (6)	C2S—C3S	1.3911

C8—C13	1.402 (6)	C2S—C7S	1.3916
C9—C10	1.384 (6)	C3S—C4S	1.3901
C10—C11	1.386 (6)	C4S—C5S	1.3882
C11—C12	1.383 (6)	C5S—C6S	1.3903
C12—C13	1.391 (6)	C6S—C7S	1.3903
C14—C15	1.431 (6)		
O5—U1—O4	178.98 (14)	C12—C13—C8	119.7 (4)
O5—U1—O2	91.55 (13)	C12—C13—N2	123.1 (4)
O4—U1—O2	89.39 (13)	C8—C13—N2	117.1 (4)
O5—U1—O1	89.09 (13)	N2—C14—C15	127.9 (4)
O4—U1—O1	90.19 (13)	C16—C15—C20	121.4 (4)
O2—U1—O1	158.22 (10)	C16—C15—C14	116.4 (4)
O5—U1—O3	90.53 (12)	C20—C15—C14	121.1 (4)
O4—U1—O3	90.03 (11)	C17—C16—C15	121.8 (5)
O2—U1—O3	78.85 (11)	C16—C17—C18	116.2 (5)
O1—U1—O3	79.38 (10)	C16—C17—C29	124.2 (5)
O5—U1—N2	87.74 (13)	C18—C17—C29	119.5 (5)
O4—U1—N2	92.23 (13)	C19—C18—C17	125.4 (4)
O2—U1—N2	68.75 (11)	C18—C19—C20	117.2 (4)
O1—U1—N2	133.01 (10)	C18—C19—C33	122.0 (4)
O3—U1—N2	147.49 (11)	C20—C19—C33	120.7 (4)
O5—U1—N1	90.18 (12)	O2—C20—C15	120.4 (4)
O4—U1—N1	88.90 (12)	O2—C20—C19	122.0 (4)
O2—U1—N1	132.30 (11)	C15—C20—C19	117.4 (4)
O1—U1—N1	69.46 (10)	C23—C21—C2	109.9 (4)
O3—U1—N1	148.81 (11)	C23—C21—C24	107.1 (4)
N2—U1—N1	63.69 (11)	C2—C21—C24	113.0 (4)
C1—O1—U1	138.4 (3)	C23—C21—C22	109.8 (4)

C7—N1—C8	116.8	(3)	C2—C21—C22	109.6	(3)
C7—N1—U1	126.3	(3)	C24—C21—C22	107.2	(4)
C8—N1—U1	116.3	(3)	C28—C25—C26	108.2	(4)
O1—C1—C6	120.6	(4)	C28—C25—C4	112.1	(4)
O1—C1—C2	121.8	(4)	C26—C25—C4	108.2	(4)
C6—C1—C2	117.6	(4)	C28—C25—C27	108.0	(4)
C20—O2—U1	140.3	(3)	C26—C25—C27	109.1	(4)
C14—N2—C13	117.3	(4)	C4—C25—C27	111.2	(4)
C14—N2—U1	125.4	(3)	C31—C29—C30	106.3	(7)
C13—N2—U1	116.8	(3)	C31—C29—C32	108.9	(5)
C3—C2—C1	117.8	(4)	C30—C29—C32	110.7	(7)
C3—C2—C21	121.0	(4)	C31—C29—C17	110.3	(5)
C1—C2—C21	121.2	(4)	C30—C29—C17	111.1	(5)
C37—O3—C40	109.5	(4)	C32—C29—C17	109.4	(6)
C37—O3—U1	124.7	(3)	C36—C33—C34	110.3	(5)
C40—O3—U1	125.8	(3)	C36—C33—C19	111.4	(4)
C2—C3—C4	125.1	(4)	C34—C33—C19	108.4	(5)
C5—C4—C3	116.1	(4)	C36—C33—C35	106.6	(5)
C5—C4—C25	123.7	(4)	C34—C33—C35	108.3	(5)
C3—C4—C25	120.2	(4)	C19—C33—C35	111.9	(5)
C4—C5—C6	122.0	(4)	C38—C37—O3	107.9	(5)
C5—C6—C1	120.9	(4)	C37—C38—C39	108.8	(5)
C5—C6—C7	117.1	(4)	C38—C39—C40	107.7	(5)
C1—C6—C7	121.7	(4)	O3—C40—C39	104.8	(4)
N1—C7—C6	128.6	(4)	C1S—C2S—C3S	119.2	
C9—C8—C13	119.6	(4)	C1S—C2S—C7S	121.0	
C9—C8—N1	124.0	(4)	C3S—C2S—C7S	119.8	
C13—C8—N1	116.3	(4)	C4S—C3S—C2S	120.1	

C10—C9—C8	120.2 (4)	C5S—C4S—C3S	119.9
C9—C10—C11	120.0 (4)	C4S—C5S—C6S	120.2
C12—C11—C10	120.5 (4)	C5S—C6S—C7S	119.9
C11—C12—C13	120.0 (4)	C6S—C7S—C2S	120.0

Table S2.4. Atomic coordinates and equivalent isotropic displacement parameters (A^2) for **1b**. U(eq) is defined as one third of the trace of the orthogonalized U^{ij} tensor.

	X	*Y*	*Z*	U_{iso}*/U_{eq}
U1	0.728425 (18)	0.216706 (8)	0.233734 (14)	0.02208 (7)
P1	0.61694 (13)	0.26209 (6)	−0.00127 (10)	0.0275 (4)
O1	0.7886 (3)	0.14780 (14)	0.1696 (2)	0.0259 (9)
N1	0.7339 (4)	0.13792 (17)	0.3353 (3)	0.0242 (11)
C1	0.8727 (5)	0.1155 (2)	0.2049 (4)	0.0240 (13)
C26	1.2622 (6)	0.0416 (3)	0.3646 (8)	0.128 (5)
H26A	1.2577	0.0617	0.4188	0.192*
H26B	1.2696	0.0645	0.3147	0.192*
H26C	1.3290	0.0192	0.3836	0.192*
C27	1.1403 (6)	−0.0205 (3)	0.4092 (6)	0.081 (3)
H27A	1.2079	−0.0419	0.4351	0.121*
H27B	1.0723	−0.0420	0.3865	0.121*
H27C	1.1306	0.0023	0.4583	0.121*
C28	1.1699 (8)	−0.0268 (3)	0.2561 (6)	0.114 (4)
H28A	1.1759	−0.0083	0.2007	0.172*
H28B	1.1034	−0.0495	0.2379	0.172*
H28C	1.2395	−0.0469	0.2825	0.172*
C2S	1.2328 (8)	0.2340 (3)	0.2247 (5)	0.060 (2)
H2S	1.2006	0.2010	0.2219	0.072*
C5S	1.3285 (9)	0.3285 (4)	0.2351 (6)	0.086 (3)
H5S	1.3614	0.3613	0.2373	0.103*

C6S	1.2112 (8)	0.3235 (4)	0.2163 (6)	0.085 (3)
H6S	1.1640	0.3528	0.2082	0.102*
O2	0.7011 (3)	0.30007 (13)	0.2636 (2)	0.0276 (9)
N2	0.6788 (4)	0.22697 (16)	0.3880 (3)	0.0258 (11)
C2	0.9492 (5)	0.1005 (2)	0.1522 (4)	0.0273 (14)
O3	0.5810 (3)	0.20268 (13)	0.1817 (2)	0.0278 (9)
C3	1.0366 (5)	0.0674 (2)	0.1963 (4)	0.0324 (15)
H3	1.0895	0.0587	0.1631	0.039*
O4	0.8771 (3)	0.22793 (13)	0.2922 (2)	0.0244 (9)
C4	1.0543 (5)	0.0457 (2)	0.2853 (4)	0.0288 (14)
O5	0.7168 (3)	0.25418 (13)	0.0869 (2)	0.0259 (9)
C5	0.9772 (5)	0.0589 (2)	0.3318 (4)	0.0313 (15)
H5	0.9842	0.0441	0.3915	0.038*
C6	0.8879 (5)	0.0937 (2)	0.2940 (4)	0.0258 (13)
C7	0.8099 (5)	0.1023 (2)	0.3476 (4)	0.0297 (14)
H7	0.8144	0.0793	0.3977	0.036*
C8	0.6567 (4)	0.1374 (2)	0.3907 (4)	0.0268 (14)
C9	0.6112 (5)	0.0935 (2)	0.4166 (4)	0.0337 (15)
H9	0.6330	0.0612	0.3992	0.040*
C10	0.5338 (5)	0.0970 (2)	0.4677 (4)	0.0398 (17)
H10	0.5027	0.0671	0.4863	0.048*
C11	0.5018 (5)	0.1445 (3)	0.4917 (4)	0.0433 (17)
H11	0.4479	0.1470	0.5262	0.052*
C12	0.5473 (5)	0.1879 (2)	0.4662 (4)	0.0379 (16)
H12	0.5248	0.2201	0.4831	0.045*
C13	0.6251 (5)	0.1848 (2)	0.4165 (4)	0.0258 (13)
C14	0.7089 (4)	0.2643 (2)	0.4465 (4)	0.0232 (13)
H14	0.6988	0.2597	0.5068	0.028*

C15	0.7562 (4)	0.3122 (2)	0.4299 (4)	0.0233 (13)
C16	0.8063 (4)	0.3427 (2)	0.5082 (4)	0.0279 (14)
H16	0.8104	0.3303	0.5690	0.033*
C17	0.8494 (4)	0.3896 (2)	0.5006 (4)	0.0258 (13)
C18	0.8387 (5)	0.4061 (2)	0.4085 (4)	0.0302 (14)
H18	0.8674	0.4389	0.4014	0.036*
C19	0.7897 (4)	0.3784 (2)	0.3270 (4)	0.0242 (13)
C20	0.7482 (4)	0.3290 (2)	0.3377 (4)	0.0241 (13)
C21	0.9313 (5)	0.1184 (2)	0.0515 (4)	0.0283 (14)
C22	1.0197 (5)	0.0965 (2)	0.0072 (4)	0.0468 (18)
H22A	1.0965	0.1078	0.0431	0.070*
H22B	1.0025	0.1083	−0.0580	0.070*
H22C	1.0165	0.0593	0.0081	0.070*
C23	0.8112 (5)	0.1008 (2)	−0.0103 (4)	0.0373 (16)
H23A	0.8084	0.0636	−0.0121	0.056*
H23B	0.7970	0.1139	−0.0743	0.056*
H23C	0.7525	0.1136	0.0165	0.056*
C24	0.9391 (5)	0.1763 (2)	0.0460 (4)	0.0412 (17)
H24A	0.8853	0.1919	0.0752	0.062*
H24B	0.9199	0.1868	−0.0200	0.062*
H24C	1.0172	0.1873	0.0794	0.062*
C25	1.1559 (5)	0.0104 (2)	0.3289 (5)	0.0393 (16)
C29	0.9068 (5)	0.4235 (2)	0.5859 (4)	0.0302 (14)
C30	0.8438 (5)	0.4753 (2)	0.5729 (4)	0.0398 (17)
H30A	0.7628	0.4699	0.5676	0.060*
H30B	0.8500	0.4918	0.5156	0.060*
H30C	0.8786	0.4971	0.6272	0.060*
C31	1.0327 (5)	0.4321 (2)	0.5905 (5)	0.0444 (18)

H31A	1.0693	0.4542	0.6439	0.067*
H31B	1.0364	0.4482	0.5321	0.067*
H31C	1.0727	0.3994	0.5983	0.067*
C32	0.9030 (5)	0.4001 (2)	0.6777 (4)	0.0397 (16)
H32A	0.8232	0.3941	0.6756	0.060*
H32B	0.9388	0.4233	0.7297	0.060*
H32C	0.9447	0.3678	0.6874	0.060*
C33	0.7772 (5)	0.4019 (2)	0.2295 (4)	0.0372 (16)
C34	0.6501 (6)	0.4030 (2)	0.1732 (5)	0.057 (2)
H34A	0.6419	0.4142	0.1088	0.085*
H34B	0.6094	0.4265	0.2030	0.085*
H34C	0.6176	0.3689	0.1719	0.085*
C35	0.8234 (6)	0.4561 (2)	0.2356 (4)	0.052 (2)
H35A	0.8050	0.4707	0.1723	0.078*
H35B	0.9067	0.4557	0.2640	0.078*
H35C	0.7882	0.4767	0.2743	0.078*
C36	0.8451 (6)	0.3699 (2)	0.1786 (4)	0.0517 (19)
H36A	0.8155	0.3350	0.1715	0.078*
H36B	0.9261	0.3696	0.2155	0.078*
H36C	0.8370	0.3844	0.1164	0.078*
C37	0.5769 (5)	0.2043 (2)	−0.0644 (4)	0.0373 (16)
H37A	0.6414	0.1914	−0.0840	0.056*
H37B	0.5114	0.2104	−0.1200	0.056*
H37C	0.5558	0.1792	−0.0238	0.056*
C38	0.6563 (5)	0.3071 (2)	−0.0764 (4)	0.0431 (17)
H38A	0.6795	0.3390	−0.0422	0.065*
H38B	0.5908	0.3133	−0.1320	0.065*
H38C	0.7203	0.2936	−0.0961	0.065*

C39	0.4943 (4)	0.2876 (2)	0.0231 (4)	0.0369 (15)
H39A	0.4710	0.2651	0.0666	0.055*
H39B	0.4315	0.2906	−0.0356	0.055*
H39C	0.5125	0.3212	0.0517	0.055*
C1S	1.1639 (7)	0.2767 (4)	0.2096 (5)	0.070 (2)
H1S	1.0832	0.2731	0.1945	0.084*
C3S	1.3479 (8)	0.2404 (4)	0.2438 (5)	0.066 (2)
H3S	1.3956	0.2113	0.2529	0.080*
C4S	1.3965 (7)	0.2870 (4)	0.2502 (5)	0.068 (2)
H4S	1.4773	0.2905	0.2652	0.081*

Table S2.5. Anisotropic displacement parameters (A^2) for **1b**. The anisotropic displacement factor exponent takes the form: $-2\pi^2$ [$h^2 a^2 * U^{11}$ + ... + 2 h k a* b*U^{12}].

	U^{11}	U^{22}	U^{33}	U^{12}	U^{13}	U^{23}
U1	0.02259 (11)	0.02557 (12)	0.01569 (10)	−0.00255 (12)	0.00198 (8)	−0.00042 (12)
P1	0.0311 (9)	0.0305 (9)	0.0177 (8)	0.0011 (7)	0.0021 (7)	0.0010 (7)
O1	0.027 (2)	0.027 (2)	0.020 (2)	0.0036 (18)	0.0014 (18)	0.0014 (18)
N1	0.029 (3)	0.022 (3)	0.017 (3)	−0.004 (2)	0.000 (2)	0.000 (2)
C1	0.027 (3)	0.020 (3)	0.023 (3)	−0.002 (3)	0.004 (3)	−0.004 (3)
C26	0.026 (5)	0.081 (7)	0.238 (14)	0.001 (5)	−0.021 (6)	0.046 (7)
C27	0.057 (5)	0.092 (7)	0.097 (7)	0.036 (5)	0.029 (5)	0.062 (6)
C28	0.158 (10)	0.114 (8)	0.075 (7)	0.106 (7)	0.041 (7)	0.028 (6)
C2S	0.073 (6)	0.067 (6)	0.040 (5)	0.000 (5)	0.015 (4)	0.000 (4)
C5S	0.092 (8)	0.059 (7)	0.096 (8)	−0.006 (6)	0.011 (6)	0.013 (5)
C6S	0.080 (8)	0.068 (7)	0.092 (8)	0.030 (6)	0.003 (6)	−0.009 (5)
O2	0.035 (2)	0.028 (2)	0.019 (2)	−0.0025 (18)	0.0062 (18)	−0.0026 (17)
N2	0.029 (3)	0.026 (3)	0.022 (3)	−0.004 (2)	0.006 (2)	−0.001 (2)
C2	0.026 (3)	0.021 (3)	0.031 (4)	−0.006 (3)	0.003 (3)	−0.004 (3)

O3	0.029 (2)	0.027 (2)	0.023 (2)	−0.0037 (17)	0.0014 (18)	−0.0016 (17)
C3	0.030 (4)	0.029 (4)	0.039 (4)	0.001 (3)	0.011 (3)	0.002 (3)
O4	0.019 (2)	0.033 (3)	0.019 (2)	−0.0055 (16)	0.0015 (17)	−0.0001 (17)
C4	0.022 (3)	0.027 (4)	0.037 (4)	0.000 (3)	0.008 (3)	0.004 (3)
O5	0.025 (2)	0.030 (2)	0.019 (2)	−0.0011 (18)	−0.0004 (18)	0.0027 (17)
C5	0.041 (4)	0.029 (4)	0.020 (3)	−0.006 (3)	0.004 (3)	0.008 (3)
C6	0.025 (3)	0.025 (3)	0.025 (3)	0.007 (3)	0.005 (3)	0.005 (3)
C7	0.032 (4)	0.028 (4)	0.027 (4)	−0.006 (3)	0.006 (3)	0.004 (3)
C8	0.024 (3)	0.037 (4)	0.018 (3)	−0.008 (3)	0.004 (3)	0.003 (3)
C9	0.031 (4)	0.040 (4)	0.027 (4)	−0.007 (3)	0.003 (3)	0.006 (3)
C10	0.039 (4)	0.041 (4)	0.039 (4)	−0.010 (3)	0.012 (3)	0.014 (3)
C11	0.039 (4)	0.051 (5)	0.046 (4)	−0.010 (3)	0.024 (3)	0.003 (4)
C12	0.037 (4)	0.042 (4)	0.036 (4)	−0.007 (3)	0.011 (3)	0.002 (3)
C13	0.026 (3)	0.033 (4)	0.016 (3)	−0.004 (3)	0.002 (3)	0.000 (3)
C14	0.022 (3)	0.030 (3)	0.020 (3)	0.001 (3)	0.011 (3)	0.003 (3)
C15	0.026 (3)	0.022 (3)	0.023 (3)	0.000 (3)	0.008 (3)	0.000 (3)
C16	0.030 (3)	0.031 (4)	0.025 (3)	−0.002 (3)	0.011 (3)	−0.003 (3)
C17	0.023 (3)	0.026 (4)	0.028 (3)	0.005 (3)	0.006 (3)	−0.001 (3)
C18	0.034 (4)	0.024 (3)	0.034 (4)	−0.002 (3)	0.013 (3)	0.002 (3)
C19	0.026 (3)	0.021 (3)	0.023 (3)	−0.002 (3)	0.004 (3)	0.000 (3)
C20	0.025 (3)	0.025 (3)	0.023 (3)	0.004 (3)	0.007 (3)	−0.005 (3)
C21	0.027 (3)	0.036 (4)	0.023 (3)	0.002 (3)	0.010 (3)	0.003 (3)
C22	0.052 (4)	0.053 (5)	0.045 (4)	0.013 (4)	0.029 (4)	0.007 (4)
C23	0.038 (4)	0.045 (4)	0.025 (4)	0.002 (3)	0.002 (3)	0.001 (3)
C24	0.045 (4)	0.042 (4)	0.034 (4)	−0.008 (3)	0.009 (3)	0.006 (3)
C25	0.027 (4)	0.045 (4)	0.044 (4)	0.006 (3)	0.008 (3)	0.010 (3)
C29	0.035 (4)	0.028 (4)	0.028 (3)	−0.002 (3)	0.011 (3)	−0.009 (3)

C30	0.048 (4)	0.029 (4)	0.040 (4)	0.001 (3)	0.008 (3)	−0.012 (3)
C31	0.032 (4)	0.040 (4)	0.055 (5)	−0.009 (3)	0.004 (3)	−0.016 (3)
C32	0.053 (4)	0.033 (4)	0.028 (4)	−0.003 (3)	0.003 (3)	−0.010 (3)
C33	0.051 (4)	0.033 (4)	0.030 (4)	−0.005 (3)	0.015 (3)	0.002 (3)
C34	0.072 (5)	0.047 (5)	0.035 (4)	0.004 (4)	−0.009 (4)	0.010 (4)
C35	0.091 (6)	0.032 (4)	0.037 (4)	−0.018 (4)	0.024 (4)	0.003 (3)
C36	0.079 (5)	0.047 (5)	0.045 (4)	−0.014 (4)	0.043 (4)	−0.004 (4)
C37	0.039 (4)	0.033 (4)	0.031 (4)	0.004 (3)	−0.002 (3)	−0.004 (3)
C38	0.056 (4)	0.043 (4)	0.027 (4)	−0.009 (3)	0.006 (3)	0.009 (3)
C39	0.032 (3)	0.050 (4)	0.023 (3)	0.003 (3)	0.000 (3)	−0.007 (3)
C1S	0.051 (5)	0.106 (8)	0.052 (5)	0.009 (6)	0.015 (4)	−0.018 (5)
C3S	0.072 (7)	0.084 (7)	0.042 (5)	0.028 (5)	0.015 (5)	−0.011 (5)
C4S	0.058 (5)	0.089 (7)	0.054 (5)	0.005 (6)	0.014 (4)	−0.018 (5)

Table S2.6. Bond lengths [Å], bond angles [º], and torsion angles [º] for **1b.**

U1—O3	1.778 (3)	C4—C5	1.369 (7)
U1—O4	1.792 (3)	C4—C25	1.533 (8)
U1—O1	2.272 (4)	C5—C6	1.410 (7)
U1—O2	2.284 (4)	C6—C7	1.430 (7)
U1—O5	2.364 (3)	C8—C9	1.386 (7)
U1—N1	2.557 (4)	C8—C13	1.395 (7)
U1—N2	2.557 (4)	C9—C10	1.383 (8)
P1—O5	1.519 (4)	C10—C11	1.389 (8)
P1—C39	1.777 (5)	C11—C12	1.373 (8)
P1—C37	1.780 (5)	C12—C13	1.370 (7)
P1—C38	1.791 (6)	C14—C15	1.438 (7)
O1—C1	1.319 (6)	C15—C16	1.400 (7)
N1—C7	1.295 (6)	C15—C20	1.417 (7)
N1—C8	1.425 (6)	C16—C17	1.361 (7)

C1—C6	1.406 (7)	C17—C18	1.406 (7)
C1—C2	1.443 (7)	C17—C29	1.540 (7)
C26—C25	1.496 (9)	C18—C19	1.389 (7)
C27—C25	1.505 (9)	C19—C20	1.423 (7)
C28—C25	1.508 (10)	C19—C33	1.544 (8)
C2S—C3S	1.361 (10)	C21—C24	1.533 (8)
C2S—C1S	1.382 (10)	C21—C22	1.536 (7)
C5S—C4S	1.350 (10)	C21—C23	1.555 (7)
C5S—C6S	1.384 (11)	C29—C32	1.512 (8)
C6S—C1S	1.353 (11)	C29—C31	1.538 (7)
O2—C20	1.324 (6)	C29—C30	1.552 (7)
N2—C14	1.293 (6)	C33—C35	1.529 (8)
N2—C13	1.417 (6)	C33—C36	1.531 (8)
C2—C3	1.384 (7)	C33—C34	1.532 (8)
C2—C21	1.524 (7)	C3S—C4S	1.356 (10)
C3—C4	1.400 (8)		
O3—U1—O4	176.26 (16)	N1—C7—C6	127.3 (5)
O3—U1—O1	93.65 (14)	C9—C8—C13	120.2 (5)
O4—U1—O1	85.85 (14)	C9—C8—N1	123.9 (5)
O3—U1—O2	95.53 (14)	C13—C8—N1	115.8 (5)
O4—U1—O2	86.16 (14)	C10—C9—C8	119.7 (6)
O1—U1—O2	159.03 (13)	C9—C10—C11	119.5 (6)
O3—U1—O5	84.74 (14)	C12—C11—C10	120.7 (6)
O4—U1—O5	98.87 (14)	C13—C12—C11	120.3 (6)
O1—U1—O5	83.28 (12)	C12—C13—C8	119.6 (5)
O2—U1—O5	78.84 (12)	C12—C13—N2	125.0 (5)
O3—U1—N1	86.25 (15)	C8—C13—N2	115.4 (5)
O4—U1—N1	90.10 (14)	N2—C14—C15	126.9 (5)

O1—U1—N1	69.23 (13)	C16—C15—C20	121.0 (5)
O2—U1—N1	130.15 (13)	C16—C15—C14	117.3 (5)
O5—U1—N1	150.41 (13)	C20—C15—C14	121.6 (5)
O3—U1—N2	86.20 (15)	C17—C16—C15	122.5 (5)
O4—U1—N2	91.32 (15)	C16—C17—C18	115.8 (5)
O1—U1—N2	130.87 (13)	C16—C17—C29	123.3 (5)
O2—U1—N2	68.67 (13)	C18—C17—C29	120.9 (5)
O5—U1—N2	145.18 (13)	C19—C18—C17	125.5 (5)
N1—U1—N2	61.73 (14)	C18—C19—C20	117.3 (5)
O5—P1—C39	112.8 (2)	C18—C19—C33	120.5 (5)
O5—P1—C37	111.3 (2)	C20—C19—C33	122.1 (5)
C39—P1—C37	108.3 (3)	O2—C20—C15	121.0 (5)
O5—P1—C38	109.5 (2)	O2—C20—C19	121.0 (5)
C39—P1—C38	106.1 (3)	C15—C20—C19	118.0 (5)
C37—P1—C38	108.6 (3)	C2—C21—C24	111.6 (5)
C1—O1—U1	131.2 (3)	C2—C21—C22	113.1 (5)
C7—N1—C8	118.8 (5)	C24—C21—C22	106.8 (5)
C7—N1—U1	124.3 (4)	C2—C21—C23	108.9 (4)
C8—N1—U1	116.4 (3)	C24—C21—C23	109.2 (5)
O1—C1—C6	120.6 (5)	C22—C21—C23	107.2 (5)
O1—C1—C2	121.0 (5)	C26—C25—C27	108.4 (7)
C6—C1—C2	118.4 (5)	C26—C25—C28	109.9 (7)
C3S—C2S—C1S	118.4 (8)	C27—C25—C28	106.7 (6)
C4S—C5S—C6S	120.4 (8)	C26—C25—C4	109.1 (6)
C1S—C6S—C5S	119.8 (8)	C27—C25—C4	112.7 (5)
C20—O2—U1	131.5 (3)	C28—C25—C4	109.9 (6)
C14—N2—C13	117.4 (4)	C32—C29—C31	108.6 (5)
C14—N2—U1	126.1 (3)	C32—C29—C17	112.4 (5)

C13—N2—U1	116.1 (3)	C31—C29—C17	109.1 (4)
C3—C2—C1	116.7 (5)	C32—C29—C30	108.9 (5)
C3—C2—C21	121.8 (5)	C31—C29—C30	109.2 (5)
C1—C2—C21	121.5 (5)	C17—C29—C30	108.6 (5)
C2—C3—C4	125.9 (6)	C35—C33—C36	107.4 (5)
C5—C4—C3	116.0 (5)	C35—C33—C34	108.2 (5)
C5—C4—C25	122.2 (5)	C36—C33—C34	110.5 (5)
C3—C4—C25	121.7 (5)	C35—C33—C19	112.7 (5)
P1—O5—U1	132.0 (2)	C36—C33—C19	109.1 (5)
C4—C5—C6	122.1 (5)	C34—C33—C19	108.8 (5)
C1—C6—C5	120.8 (5)	C6S—C1S—C2S	120.2 (8)
C1—C6—C7	122.5 (5)	C4S—C3S—C2S	122.1 (8)
C5—C6—C7	116.5 (5)	C5S—C4S—C3S	119.0 (8)

Table S2.7. Atomic coordinates and equivalent isotropic displacement parameters (A^2) for **1c**. U(eq) is defined as one third of the trace of the orthogonalized U^{ij} tensor.

	X	*Y*	*Z*	U_{iso}*/U_{eq}
U1	0.197675 (11)	0.2500	0.844423 (18)	0.02757 (12)
C30	0.1747 (4)	0.2500	1.4293 (6)	0.0429 (18)
H30	0.2067	0.2500	1.4882	0.051*
Cl1	0.08170 (9)	0.2500	0.96588 (15)	0.0551 (6)
P1	−0.02904 (9)	0.2500	1.39819 (14)	0.0414 (5)
O3	0.18554 (19)	0.34957 (18)	0.8690 (3)	0.0374 (8)
N1	0.28930 (19)	0.30914 (18)	0.7395 (3)	0.0300 (8)
C5	0.2891 (3)	0.3999 (3)	0.8513 (4)	0.0349 (11)
C9	0.1983 (2)	0.4423 (2)	0.9610 (5)	0.0388 (12)
C4	0.3164 (2)	0.3595 (2)	0.7690 (4)	0.0353 (10)
C6	0.3314 (3)	0.4487 (2)	0.8809 (5)	0.0385 (11)
H6	0.3760	0.4509	0.8514	0.046*

C10	0.2227 (3)	0.3950 (2)	0.8946 (4)	0.0334 (10)
C7	0.3094 (3)	0.4924 (2)	0.9505 (5)	0.0433 (13)
C8	0.2419 (3)	0.4877 (2)	0.9871 (5)	0.0436 (13)
H8	0.2251	0.5183	1.0336	0.052*
C1	0.3176 (3)	0.2811 (2)	0.6441 (4)	0.0303 (10)
C27	0.0825 (3)	0.2500	1.2559 (5)	0.0333 (14)
H27	0.0507	0.2500	1.1966	0.040*
C20	−0.0702 (3)	0.3147 (3)	1.3434 (4)	0.0429 (14)
C29	0.1970 (3)	0.2500	1.3190 (8)	0.0435 (19)
H29	0.2441	0.2500	1.3031	0.052*
C28	0.1509 (3)	0.2500	1.2337 (5)	0.0346 (15)
H28	0.1663	0.2500	1.1590	0.042*
C31	0.1060 (4)	0.2500	1.4526 (6)	0.0407 (17)
H31	0.0906	0.2500	1.5273	0.049*
C26	0.0600 (3)	0.2500	1.3658 (5)	0.0351 (16)
C21	−0.0385 (3)	0.3531 (3)	1.2729 (5)	0.0497 (14)
H21	0.0079	0.3470	1.2550	0.060*
C25	−0.1384 (3)	0.3247 (3)	1.3721 (7)	0.0633 (19)
H25	−0.1609	0.2995	1.4236	0.076*
O2	0.2512 (2)	0.2500	0.9640 (4)	0.0379 (11)
O1	0.1506 (2)	0.2500	0.7184 (4)	0.0336 (10)
C3	0.3673 (3)	0.2802 (3)	0.4628 (4)	0.0473 (13)
H3	0.3849	0.3012	0.4008	0.057*
C2	0.3417 (3)	0.3111 (2)	0.5527 (4)	0.0371 (11)
H2	0.3408	0.3532	0.5515	0.044*
C11	0.1264 (3)	0.4406 (3)	1.0058 (5)	0.0462 (13)
C12	0.0744 (3)	0.4312 (3)	0.9129 (5)	0.0506 (14)
H12A	0.0786	0.4631	0.8580	0.076*

H12B	0.0286	0.4315	0.9444	0.076*
H12C	0.0827	0.3929	0.8768	0.076*
C15	0.3536 (3)	0.5455 (2)	0.9831 (6)	0.0536 (15)
C14	0.1065 (3)	0.4975 (3)	1.0674 (6)	0.0599 (17)
H14A	0.1386	0.5046	1.1281	0.090*
H14B	0.0608	0.4931	1.0978	0.090*
H14C	0.1075	0.5310	1.0158	0.090*
C13	0.1213 (4)	0.3893 (3)	1.0906 (5)	0.0615 (18)
H13A	0.1409	0.3533	1.0586	0.092*
H13B	0.0736	0.3822	1.1088	0.092*
H13C	0.1460	0.4000	1.1583	0.092*
C24	−0.1719 (4)	0.3718 (4)	1.3238 (8)	0.083 (3)
H24	−0.2185	0.3778	1.3398	0.100*
C22	−0.0724 (3)	0.4008 (3)	1.2269 (8)	0.075 (2)
H22	−0.0499	0.4270	1.1774	0.090*
C23	−0.1398 (3)	0.4097 (3)	1.2543 (9)	0.085 (3)
H23	−0.1636	0.4425	1.2240	0.102*
C32	−0.0342 (4)	0.2702 (3)	1.5676 (13)	0.123 (5)
C33	−0.0319 (4)	0.3211 (7)	1.5907 (8)	0.141 (6)
C16	0.4129 (11)	0.5551 (10)	0.9082 (12)	0.223 (12)
C19	0.3255 (11)	0.5996 (7)	0.9139 (18)	0.188 (8)
C17	0.4112 (9)	0.5218 (7)	1.059 (2)	0.213 (10)
C18	0.3302 (10)	0.5767 (8)	1.0864 (10)	0.185 (9)
C36	−0.0269 (9)	0.2500	1.7343 (14)	0.111 (10)
C35	−0.0213 (7)	0.2902 (6)	1.7685 (14)	0.124 (6)
C34	−0.0235 (6)	0.3392 (7)	1.6967 (11)	0.129 (4)

Table S2.8. Anisotropic displacement parameters (A^2) for **1c**. The anisotropic displacement factor exponent takes the form: $-2\pi^2$ [$h^2 a^2 * U^{11}$ + ... + 2 h k a* b* U^{12}].

	U^{11}	U^{22}	U^{33}	U^{12}	U^{13}	U^{23}
U1	0.01725 (16)	0.04806 (18)	0.01739 (16)	0.000	0.00013 (8)	0.000
C30	0.019 (3)	0.077 (5)	0.033 (4)	0.000	−0.008 (3)	0.000
Cl1	0.0224 (8)	0.1177 (18)	0.0251 (9)	0.000	0.0026 (7)	0.000
P1	0.0199 (8)	0.0885 (15)	0.0158 (8)	0.000	0.0011 (6)	0.000
O3	0.0308 (18)	0.050 (2)	0.0318 (18)	0.0037 (16)	0.0035 (15)	−0.0093 (16)
N1	0.0229 (18)	0.043 (2)	0.024 (2)	0.0014 (16)	0.0037 (15)	−0.0024 (17)
C5	0.032 (3)	0.041 (3)	0.032 (3)	0.002 (2)	−0.0033 (19)	−0.001 (2)
C9	0.038 (3)	0.045 (3)	0.033 (3)	0.015 (2)	−0.008 (2)	0.000 (2)
C4	0.026 (2)	0.048 (3)	0.032 (3)	0.000 (2)	0.000 (2)	−0.002 (2)
C6	0.034 (3)	0.042 (3)	0.039 (3)	0.003 (2)	−0.002 (2)	0.001 (2)
C10	0.032 (3)	0.046 (3)	0.022 (2)	0.010 (2)	−0.0047 (19)	−0.002 (2)
C7	0.051 (3)	0.037 (3)	0.042 (3)	0.007 (2)	−0.014 (2)	−0.002 (2)
C8	0.046 (3)	0.041 (3)	0.043 (3)	0.017 (2)	−0.010 (2)	−0.006 (2)
C1	0.024 (2)	0.046 (3)	0.021 (2)	0.000 (2)	0.0020 (17)	−0.0025 (19)
C27	0.024 (3)	0.055 (4)	0.021 (3)	0.000	0.004 (2)	0.000
C20	0.026 (3)	0.053 (3)	0.049 (3)	−0.001 (2)	0.004 (2)	−0.029 (3)
C29	0.021 (4)	0.068 (6)	0.041 (4)	0.000	−0.001 (3)	0.000
C28	0.033 (4)	0.051 (4)	0.020 (3)	0.000	0.007 (3)	0.000
C31	0.028 (4)	0.070 (5)	0.023 (3)	0.000	−0.002 (3)	0.000
C26	0.020 (3)	0.069 (5)	0.017 (3)	0.000	0.000 (2)	0.000
C21	0.029 (3)	0.049 (3)	0.071 (4)	−0.003 (2)	0.002 (3)	−0.017 (3)
C25	0.034 (3)	0.060 (4)	0.097 (5)	−0.001 (3)	0.024 (3)	−0.023 (4)
O2	0.026 (2)	0.064 (3)	0.024 (2)	0.000	−0.0023 (19)	0.000
O1	0.024 (2)	0.053 (3)	0.023 (2)	0.000	−0.0007 (18)	0.000
C3	0.044 (3)	0.072 (3)	0.027 (3)	−0.006 (3)	0.009 (2)	0.006 (2)
C2	0.034 (3)	0.048 (3)	0.029 (3)	−0.005 (2)	0.005 (2)	0.000 (2)
C11	0.044 (3)	0.054 (3)	0.041 (3)	0.016 (2)	0.002 (2)	−0.005 (2)

C12	0.032 (3)	0.061 (4)	0.059 (4)	0.015 (2)	0.005 (3)	0.001 (3)
C15	0.056 (4)	0.035 (3)	0.070 (4)	−0.001 (2)	−0.004 (3)	−0.009 (3)
C14	0.055 (4)	0.061 (4)	0.063 (4)	0.027 (3)	0.006 (3)	−0.020 (3)
C13	0.072 (4)	0.072 (4)	0.041 (3)	0.031 (3)	0.019 (3)	0.009 (3)
C24	0.030 (4)	0.063 (4)	0.156 (9)	0.012 (3)	0.013 (4)	−0.035 (5)
C22	0.046 (4)	0.038 (3)	0.141 (8)	−0.002 (3)	0.006 (4)	−0.016 (4)
C23	0.043 (4)	0.035 (3)	0.177 (10)	0.006 (3)	0.007 (5)	−0.027 (4)
C32	0.041 (4)	0.034 (3)	0.295 (16)	0.006 (3)	0.008 (7)	0.020 (5)
C33	0.054 (5)	0.289 (17)	0.080 (7)	−0.003 (8)	0.002 (5)	−0.122 (9)
C16	0.28 (2)	0.30 (2)	0.096 (9)	−0.21 (2)	0.057 (12)	−0.064 (12)
C19	0.233 (19)	0.108 (11)	0.225 (19)	−0.064 (12)	−0.085 (17)	0.072 (12)
C17	0.154 (15)	0.178 (15)	0.31 (3)	−0.086 (12)	−0.115 (16)	0.047 (16)
C18	0.253 (17)	0.225 (16)	0.077 (7)	−0.160 (15)	0.064 (10)	−0.089 (9)
C36	0.044 (8)	0.23 (3)	0.055 (8)	0.000	0.013 (6)	0.000
C35	0.072 (7)	0.125 (12)	0.176 (16)	0.011 (7)	−0.013 (8)	0.055 (11)
C34	0.094 (8)	0.196 (13)	0.096 (8)	0.036 (8)	−0.010 (7)	0.002 (9)

Table S2.9. Bond lengths [Å], bond angles [º], and torsion angles [º] for **1c** using the symmetry codes: (i) x, −y+1/2, z.

U1—O1	1.780 (5)	C31—C26	1.386 (9)
U1—O2	1.787 (5)	C31—H31	0.9500
U1—O3	2.279 (4)	C21—C22	1.383 (10)
U1—O3^{i}	2.279 (4)	C21—H21	0.9500
U1—N1	2.579 (4)	C25—C24	1.382 (11)
U1—N1^{i}	2.579 (4)	C25—H25	0.9500
U1—Cl1	2.7183 (19)	C3—C3^{i}	1.365 (12)
C30—C31	1.386 (10)	C3—C2	1.384 (7)
C30—C29	1.401 (11)	C3—H3	0.9500
C30—H30	0.9500	C2—H2	0.9500

P1—C20^{i}	1.797 (6)	C11—C12	1.534 (8)
P1—C20	1.797 (6)	C11—C14	1.533 (8)
P1—C26	1.801 (7)	C11—C13	1.547 (8)
P1—C32	2.094 (16)	C12—H12A	0.9800
P1—C32^{i}	2.094 (16)	C12—H12B	0.9800
O3—C10	1.298 (7)	C12—H12C	0.9800
N1—C4	1.305 (7)	C15—C16	1.494 (16)
N1—C1	1.426 (6)	C15—C18	1.503 (13)
C5—C10	1.415 (8)	C15—C17	1.551 (17)
C5—C6	1.429 (8)	C15—C19	1.578 (16)
C5—C4	1.451 (7)	C14—H14A	0.9800
C9—C8	1.373 (8)	C14—H14B	0.9800
C9—C10	1.418 (7)	C14—H14C	0.9800
C9—C11	1.520 (8)	C13—H13A	0.9800
C6—C7	1.365 (8)	C13—H13B	0.9800
C6—H6	0.9500	C13—H13C	0.9800
C7—C8	1.410 (8)	C24—C23	1.355 (12)
C7—C15	1.532 (8)	C24—H24	0.9500
C8—H8	0.9500	C22—C23	1.386 (9)
C1—C2	1.378 (7)	C22—H22	0.9500
C1—C1^{i}	1.402 (11)	C23—H23	0.9500
C27—C28	1.377 (9)	C32—C32^{i}	0.912 (13)
C27—C26	1.397 (8)	C32—C33	1.183 (14)
C27—H27	0.9500	C33—C34	1.351 (15)
C20—C21	1.367 (8)	C16—C17	1.96 (2)
C20—C25	1.409 (8)	C16—C19	2.00 (3)
C29—C28	1.373 (10)	C36—C35	1.003 (16)
C29—H29	0.9500	C36—C35^{i}	1.003 (16)

C28—H28	0.9500	C35—C34	1.40 (2)
O1—U1—O2	175.2 (2)	C26—C31—H31	120.4
O1—U1—O3	93.21 (10)	C30—C31—H31	120.4
O2—U1—O3	87.55 (10)	C31—C26—C27	120.5 (7)
O1—U1—O3^{i}	93.21 (10)	C31—C26—P1	118.4 (5)
O2—U1—O3^{i}	87.55 (10)	C27—C26—P1	121.1 (5)
O3—U1—O3^{i}	160.7 (2)	C20—C21—C22	121.3 (6)
O1—U1—N1	87.05 (15)	C20—C21—H21	119.4
O2—U1—N1	88.85 (16)	C22—C21—H21	119.4
O3—U1—N1	68.13 (13)	C24—C25—C20	118.5 (7)
O3^{i}—U1—N1	130.36 (13)	C24—C25—H25	120.7
O1—U1—N1^{i}	87.05 (15)	C20—C25—H25	120.7
O2—U1—N1^{i}	88.85 (16)	C3^{i}—C3—C2	120.2 (3)
O3—U1—N1^{i}	130.36 (13)	C3^{i}—C3—H3	119.9
O3^{i}—U1—N1^{i}	68.13 (13)	C2—C3—H3	119.9
N1—U1—N1^{i}	62.31 (18)	C1—C2—C3	120.3 (5)
O1—U1—Cl1	91.10 (15)	C1—C2—H2	119.9
O2—U1—Cl1	93.70 (16)	C3—C2—H2	119.9
O3—U1—Cl1	80.87 (10)	C9—C11—C12	111.8 (5)
O3^{i}—U1—Cl1	80.87 (10)	C9—C11—C14	113.0 (5)
N1—U1—Cl1	148.76 (9)	C12—C11—C14	107.4 (5)
N1^{i}—U1—Cl1	148.76 (9)	C9—C11—C13	108.3 (5)
C31—C30—C29	120.0 (7)	C12—C11—C13	109.5 (5)
C31—C30—H30	120.0	C14—C11—C13	106.8 (5)
C29—C30—H30	120.0	C11—C12—H12A	109.5
C20^{i}—P1—C20	108.6 (3)	C11—C12—H12B	109.5
C20^{i}—P1—C26	111.3 (2)	H12A—C12—H12B	109.5
C20—P1—C26	111.3 (2)	C11—C12—H12C	109.5

C20^{i}—P1—C32	120.9 (3)	H12A—C12—H12C	109.5
C20—P1—C32	99.2 (2)	H12B—C12—H12C	109.5
C26—P1—C32	105.0 (3)	C16—C15—C18	132.3 (8)
C20^{i}—P1—C32^{i}	99.2 (2)	C16—C15—C7	113.9 (7)
C20—P1—C32^{i}	120.9 (3)	C18—C15—C7	113.8 (7)
C26—P1—C32^{i}	105.0 (3)	C16—C15—C17	80.1 (12)
C32—P1—C32^{i}	25.2 (4)	C18—C15—C17	84.3 (12)
C10—O3—U1	138.6 (3)	C7—C15—C17	107.3 (7)
C4—N1—C1	116.4 (4)	C16—C15—C19	81.2 (12)
C4—N1—U1	127.2 (3)	C18—C15—C19	88.1 (13)
C1—N1—U1	116.1 (3)	C7—C15—C19	105.6 (7)
C10—C5—C6	120.6 (5)	C17—C15—C19	146.5 (9)
C10—C5—C4	123.2 (5)	C11—C14—H14A	109.5
C6—C5—C4	116.0 (5)	C11—C14—H14B	109.5
C8—C9—C10	118.5 (5)	H14A—C14—H14B	109.5
C8—C9—C11	121.5 (5)	C11—C14—H14C	109.5
C10—C9—C11	120.0 (5)	H14A—C14—H14C	109.5
N1—C4—C5	125.5 (5)	H14B—C14—H14C	109.5
C7—C6—C5	121.6 (5)	C11—C13—H13A	109.5
C7—C6—H6	119.2	C11—C13—H13B	109.5
C5—C6—H6	119.2	H13A—C13—H13B	109.5
O3—C10—C5	119.8 (5)	C11—C13—H13C	109.5
O3—C10—C9	122.4 (5)	H13A—C13—H13C	109.5
C5—C10—C9	117.7 (5)	H13B—C13—H13C	109.5
C6—C7—C8	116.0 (5)	C23—C24—C25	121.5 (6)
C6—C7—C15	122.7 (5)	C23—C24—H24	119.3
C8—C7—C15	121.2 (5)	C25—C24—H24	119.3
C9—C8—C7	125.3 (5)	C21—C22—C23	119.0 (7)

C9—C8—H8	117.3	C21—C22—H22	120.5
C7—C8—H8	117.3	C23—C22—H22	120.5
C2—C1—C1^{i}	119.5 (3)	C24—C23—C22	120.3 (7)
C2—C1—N1	124.1 (5)	C24—C23—H23	119.8
C1^{i}—C1—N1	116.4 (3)	C22—C23—H23	119.8
C28—C27—C26	119.7 (6)	C32^{i}—C32—C33	166.2 (11)
C28—C27—H27	120.1	C32^{i}—C32—P1	77.41 (18)
C26—C27—H27	120.1	C33—C32—P1	116.1 (11)
C21—C20—C25	119.4 (6)	C32—C33—C34	121.4 (18)
C21—C20—P1	122.4 (4)	C15—C16—C17	51.2 (7)
C25—C20—P1	118.2 (5)	C15—C16—C19	51.3 (9)
C28—C29—C30	120.1 (6)	C17—C16—C19	98.4 (11)
C28—C29—H29	119.9	C15—C19—C16	47.6 (7)
C30—C29—H29	119.9	C15—C17—C16	48.7 (9)
C29—C28—C27	120.4 (7)	C35—C36—C35^{i}	130 (3)
C29—C28—H28	119.8	C36—C35—C34	117 (2)
C27—C28—H28	119.8	C33—C34—C35	110.4 (15)
C26—C31—C30	119.3 (7)		

Table S2.10. Atomic coordinates and equivalent isotropic displacement parameters (A^2) for **1d**. U(eq) is defined as one third of the trace of the orthogonalized U^{ij} tensor.

	x	*Y*	*Z*	U_{iso}*/U_{eq}
U1	0.035977 (13)	0.664203 (10)	0.689790 (12)	0.03104 (8)
Co1	−0.00927 (5)	0.88819 (4)	0.86480 (5)	0.0389 (2)
O1	−0.0964 (2)	0.6296 (2)	0.6520 (2)	0.0404 (10)
N1	0.0117 (3)	0.5883 (2)	0.8018 (3)	0.0332 (11)
C1	−0.1518 (4)	0.6332 (3)	0.6814 (3)	0.0375 (14)
O2	0.1513 (2)	0.72187 (19)	0.6966 (2)	0.0360 (9)
N2	0.1593 (3)	0.6406 (2)	0.8252 (3)	0.0357 (11)

C2	−0.2326 (4)	0.6555 (3)	0.6349 (4)	0.0449 (16)
O3	0.0126 (2)	0.74081 (19)	0.7346 (2)	0.0382 (10)
C3	−0.2885 (4)	0.6574 (3)	0.6710 (4)	0.0461 (16)
H3	−0.3421	0.6734	0.6394	0.055*
O4	0.0625 (3)	0.58479 (19)	0.6518 (2)	0.0421 (10)
C4	−0.2706 (4)	0.6372 (3)	0.7517 (4)	0.0451 (16)
O5	−0.0123 (3)	0.7094 (2)	0.5646 (2)	0.0515 (12)
C5	−0.1935 (4)	0.6147 (3)	0.7969 (4)	0.0395 (15)
H5	−0.1799	0.5999	0.8511	0.047*
C6	−0.1330 (4)	0.6131 (3)	0.7642 (3)	0.0393 (14)
C7	−0.0543 (4)	0.5871 (3)	0.8153 (3)	0.0349 (14)
H7	−0.0500	0.5666	0.8650	0.042*
C8	0.0810 (4)	0.5497 (3)	0.8537 (3)	0.0317 (13)
C9	0.0764 (4)	0.4851 (3)	0.8886 (3)	0.0422 (15)
H9	0.0249	0.4665	0.8821	0.051*
C10	0.1467 (5)	0.4483 (3)	0.9325 (4)	0.0505 (18)
H10	0.1431	0.4047	0.9564	0.061*
C11	0.2213 (4)	0.4740 (3)	0.9420 (4)	0.0500 (17)
H11	0.2691	0.4479	0.9718	0.060*
C12	0.2275 (4)	0.5375 (3)	0.9085 (3)	0.0441 (16)
H12	0.2796	0.5551	0.9156	0.053*
C13	0.1581 (4)	0.5758 (3)	0.8644 (3)	0.0361 (14)
C14	0.2191 (4)	0.6831 (3)	0.8629 (4)	0.0400 (15)
H14	0.2547	0.6702	0.9163	0.048*
C15	0.2367 (4)	0.7473 (3)	0.8324 (4)	0.0394 (14)
C16	0.2939 (4)	0.7930 (3)	0.8874 (4)	0.0574 (19)
H16	0.3176	0.7804	0.9430	0.069*
C17	0.3168 (5)	0.8551 (4)	0.8636 (5)	0.066 (2)

C18	0.2819 (4)	0.8709 (3)	0.7826 (4)	0.0520 (18)
H18	0.2977	0.9136	0.7657	0.062*
C19	0.2260 (4)	0.8300 (3)	0.7238 (4)	0.0390 (14)
C20	0.2017 (3)	0.7641 (3)	0.7483 (3)	0.0332 (13)
C21	−0.2568 (4)	0.6797 (4)	0.5474 (4)	0.057 (2)
C22	−0.2084 (5)	0.7468 (4)	0.5469 (5)	0.083 (3)
H22A	−0.2236	0.7627	0.4910	0.124*
H22B	−0.1500	0.7366	0.5713	0.124*
H22C	−0.2210	0.7837	0.5781	0.124*
C23	−0.2374 (5)	0.6227 (5)	0.4969 (4)	0.082 (3)
H23A	−0.2532	0.6392	0.4411	0.123*
H23B	−0.2677	0.5799	0.4969	0.123*
H23C	−0.1789	0.6126	0.5205	0.123*
C24	−0.3473 (5)	0.6969 (6)	0.5054 (5)	0.086 (3)
H24A	−0.3596	0.7121	0.4497	0.130*
H24B	−0.3610	0.7346	0.5349	0.130*
H24C	−0.3794	0.6551	0.5046	0.130*
C25	−0.3388 (4)	0.6423 (4)	0.7845 (4)	0.0551 (18)
C26	−0.3608 (7)	0.7209 (5)	0.7858 (6)	0.107 (4)
H26A	−0.3125	0.7468	0.8211	0.160*
H26B	−0.4037	0.7254	0.8065	0.160*
H26C	−0.3802	0.7400	0.7308	0.160*
C27	−0.4139 (5)	0.6024 (6)	0.7302 (5)	0.105 (4)
H27A	−0.4315	0.6196	0.6745	0.157*
H27B	−0.4576	0.6094	0.7492	0.157*
H27C	−0.4011	0.5523	0.7317	0.157*
C28	−0.3109 (5)	0.6159 (4)	0.8707 (4)	0.061 (2)
H28A	−0.2621	0.6416	0.9053	0.091*

H28B	−0.2982	0.5658	0.8723	0.091*
H28C	−0.3542	0.6231	0.8902	0.091*
C29	0.3793 (7)	0.9056 (5)	0.9218 (6)	0.116 (4)
C30	0.4182 (11)	0.8764 (7)	1.0045 (7)	0.248 (12)
H30A	0.4421	0.8306	1.0022	0.372*
H30B	0.3773	0.8709	1.0276	0.372*
H30C	0.4610	0.9083	1.0385	0.372*
C31	0.4521 (6)	0.9168 (6)	0.8919 (9)	0.149 (6)
H31A	0.4305	0.9377	0.8377	0.223*
H31B	0.4771	0.8714	0.8902	0.223*
H31C	0.4931	0.9480	0.9297	0.223*
C32	0.3396 (6)	0.9773 (5)	0.9169 (6)	0.101 (3)
H32A	0.3141	0.9922	0.8602	0.151*
H32B	0.3811	1.0115	0.9479	0.151*
H32C	0.2980	0.9741	0.9396	0.151*
C33	0.1873 (5)	0.8534 (4)	0.6345 (4)	0.0541 (19)
C34	0.1957 (6)	0.7977 (4)	0.5764 (5)	0.086 (3)
H34A	0.1700	0.8147	0.5206	0.129*
H34B	0.1688	0.7543	0.5818	0.129*
H34C	0.2534	0.7884	0.5899	0.129*
C35	0.2255 (6)	0.9215 (4)	0.6211 (5)	0.094 (3)
H35A	0.2200	0.9580	0.6571	0.141*
H35B	0.1975	0.9365	0.5647	0.141*
H35C	0.2832	0.9138	0.6332	0.141*
C36	0.0976 (5)	0.8692 (4)	0.6135 (5)	0.081 (3)
H36A	0.0930	0.9046	0.6509	0.121*
H36B	0.0699	0.8262	0.6183	0.121*
H36C	0.0724	0.8868	0.5579	0.121*

C37	−0.0941 (4)	0.8107 (4)	0.8258 (4)	0.0507 (17)
H37	−0.0847	0.7616	0.8280	0.061*
C38	−0.1003 (4)	0.8533 (3)	0.7623 (4)	0.0494 (17)
H38	−0.0942	0.8394	0.7142	0.059*
C39	−0.1176 (4)	0.9222 (3)	0.7816 (4)	0.0452 (16)
H39	−0.1264	0.9623	0.7479	0.054*
C40	−0.1195 (4)	0.9211 (4)	0.8579 (4)	0.0510 (17)
H40	−0.1294	0.9600	0.8856	0.061*
C41	−0.1039 (4)	0.8506 (4)	0.8877 (4)	0.0536 (18)
H41	−0.1007	0.8340	0.9387	0.064*
C42	0.1027 (5)	0.8409 (4)	0.9163 (5)	0.068 (2)
H42	0.1141	0.7922	0.9232	0.082*
C43	0.0976 (4)	0.8833 (3)	0.8494 (4)	0.0483 (16)
H43	0.1047	0.8671	0.8027	0.058*
C44	0.0806 (4)	0.9522 (4)	0.8628 (4)	0.0550 (18)
H44	0.0740	0.9904	0.8269	0.066*
C45	0.0747 (4)	0.9558 (5)	0.9378 (5)	0.068 (2)
H45	0.0643	0.9967	0.9623	0.081*
C46	0.0871 (4)	0.8871 (6)	0.9704 (4)	0.076 (3)
H46	0.0853	0.8740	1.0206	0.091*

Table S2.11. Anisotropic displacement parameters (A^2) for **1d**. The anisotropic displacement factor exponent takes the form: $-2\pi^2$ [$h^2 a^2 U^{11}$ + ... + 2 h k a* b* U^{12}].

	U^{11}	U^{22}	U^{33}	U^{12}	U^{13}	U^{23}
U1	0.04376 (14)	0.02233 (11)	0.02415 (11)	−0.00649 (10)	0.01038 (9)	0.00046 (9)
Co1	0.0522 (5)	0.0349 (5)	0.0322 (4)	0.0077 (4)	0.0196 (4)	0.0023 (3)
O1	0.042 (3)	0.046 (3)	0.034 (2)	−0.011 (2)	0.015 (2)	0.0010 (19)
N1	0.044 (3)	0.024 (2)	0.028 (2)	−0.010 (2)	0.009 (2)	0.0005 (19)
C1	0.050 (4)	0.027 (3)	0.028 (3)	−0.009 (3)	0.007 (3)	−0.001 (2)

O2	0.046 (2)	0.029 (2)	0.032 (2)	−0.0112 (18)	0.0144 (19)	−0.0025 (17)
N2	0.042 (3)	0.028 (2)	0.034 (3)	−0.002 (2)	0.013 (2)	0.003 (2)
C2	0.046 (4)	0.052 (4)	0.030 (3)	−0.016 (3)	0.008 (3)	0.002 (3)
O3	0.051 (3)	0.030 (2)	0.037 (2)	0.0014 (18)	0.021 (2)	0.0023 (17)
C3	0.042 (4)	0.046 (4)	0.041 (4)	−0.001 (3)	0.007 (3)	−0.001 (3)
O4	0.064 (3)	0.026 (2)	0.038 (2)	−0.0064 (19)	0.022 (2)	−0.0061 (17)
C4	0.053 (4)	0.041 (4)	0.038 (3)	−0.003 (3)	0.014 (3)	−0.009 (3)
O5	0.059 (3)	0.069 (3)	0.024 (2)	−0.018 (2)	0.013 (2)	−0.003 (2)
C5	0.055 (4)	0.028 (3)	0.036 (3)	−0.011 (3)	0.019 (3)	−0.006 (3)
C6	0.053 (4)	0.027 (3)	0.034 (3)	−0.011 (3)	0.014 (3)	−0.003 (3)
C7	0.046 (4)	0.027 (3)	0.029 (3)	−0.002 (3)	0.012 (3)	0.000 (2)
C8	0.047 (4)	0.021 (3)	0.024 (3)	−0.003 (3)	0.011 (3)	0.001 (2)
C9	0.058 (4)	0.031 (3)	0.037 (3)	−0.004 (3)	0.019 (3)	0.000 (3)
C10	0.084 (5)	0.029 (3)	0.038 (3)	0.009 (4)	0.024 (4)	0.014 (3)
C11	0.062 (5)	0.046 (4)	0.035 (3)	0.006 (3)	0.011 (3)	0.006 (3)
C12	0.055 (4)	0.033 (3)	0.034 (3)	0.000 (3)	0.006 (3)	0.003 (3)
C13	0.054 (4)	0.025 (3)	0.026 (3)	−0.003 (3)	0.013 (3)	0.001 (2)
C14	0.045 (4)	0.032 (3)	0.030 (3)	0.002 (3)	0.001 (3)	0.002 (2)
C15	0.043 (4)	0.028 (3)	0.040 (3)	−0.005 (3)	0.009 (3)	−0.002 (3)
C16	0.065 (5)	0.041 (4)	0.038 (4)	−0.013 (3)	−0.010 (3)	0.002 (3)
C17	0.072 (5)	0.035 (4)	0.059 (5)	−0.019 (4)	−0.009 (4)	−0.004 (3)
C18	0.053 (4)	0.022 (3)	0.073 (5)	−0.010 (3)	0.017 (4)	−0.008 (3)
C19	0.042 (4)	0.031 (3)	0.048 (4)	−0.002 (3)	0.023 (3)	0.000 (3)
C20	0.036 (3)	0.024 (3)	0.040 (3)	−0.002 (2)	0.016 (3)	−0.005 (3)
C21	0.034 (4)	0.093 (6)	0.033 (4)	−0.012 (4)	0.000 (3)	0.016 (4)
C22	0.068 (6)	0.086 (6)	0.075 (6)	−0.009 (5)	0.010 (5)	0.047 (5)
C23	0.074 (6)	0.143 (9)	0.027 (4)	−0.031 (6)	0.017 (4)	0.001 (4)
C24	0.059 (5)	0.141 (8)	0.045 (4)	−0.004 (5)	0.005 (4)	0.026 (5)

C25	0.061 (5)	0.064 (5)	0.040 (4)	0.012 (4)	0.019 (4)	−0.008 (3)
C26	0.160 (10)	0.095 (7)	0.085 (6)	0.073 (7)	0.071 (7)	0.028 (6)
C27	0.060 (6)	0.193 (11)	0.073 (6)	−0.038 (6)	0.038 (5)	−0.053 (7)
C28	0.068 (5)	0.068 (5)	0.057 (4)	0.011 (4)	0.036 (4)	0.002 (4)
C29	0.140 (10)	0.049 (5)	0.085 (7)	−0.052 (6)	−0.035 (7)	0.004 (5)
C30	0.35 (2)	0.129 (11)	0.083 (8)	−0.149 (13)	−0.113 (11)	0.011 (8)
C31	0.076 (7)	0.082 (8)	0.220 (15)	−0.026 (6)	−0.015 (8)	−0.023 (8)
C32	0.130 (8)	0.073 (6)	0.085 (6)	−0.043 (6)	0.027 (6)	−0.041 (5)
C33	0.077 (5)	0.043 (4)	0.043 (4)	−0.019 (4)	0.024 (4)	0.001 (3)
C34	0.159 (9)	0.058 (5)	0.066 (5)	−0.042 (6)	0.071 (6)	−0.021 (4)
C35	0.171 (10)	0.048 (5)	0.074 (6)	−0.047 (6)	0.059 (6)	0.000 (4)
C36	0.072 (6)	0.063 (5)	0.083 (6)	0.011 (4)	0.005 (5)	0.036 (5)
C37	0.056 (4)	0.034 (3)	0.062 (5)	0.000 (3)	0.023 (4)	0.004 (3)
C38	0.058 (4)	0.048 (4)	0.041 (4)	0.003 (3)	0.018 (3)	−0.006 (3)
C39	0.051 (4)	0.039 (4)	0.038 (3)	0.007 (3)	0.010 (3)	0.003 (3)
C40	0.047 (4)	0.059 (5)	0.054 (4)	0.009 (3)	0.027 (4)	−0.003 (3)
C41	0.057 (5)	0.057 (5)	0.050 (4)	0.003 (3)	0.025 (4)	0.015 (3)
C42	0.073 (6)	0.058 (5)	0.075 (5)	0.020 (4)	0.031 (5)	0.033 (4)
C43	0.053 (4)	0.047 (4)	0.053 (4)	0.005 (3)	0.030 (4)	0.001 (3)
C44	0.059 (5)	0.042 (4)	0.060 (4)	−0.002 (3)	0.019 (4)	0.008 (3)
C45	0.056 (5)	0.080 (6)	0.060 (5)	0.000 (4)	0.015 (4)	−0.031 (5)
C46	0.049 (5)	0.147 (9)	0.028 (4)	0.004 (5)	0.012 (4)	0.019 (5)

Table S2.12. Bond lengths [Å], bond angles [º], and torsion angles [º] for **1d.**

U1—O3	1.797 (4)	C23—H23A	0.9800
U1—O4	1.801 (4)	C23—H23B	0.9800
U1—O5	2.240 (4)	C23—H23C	0.9800
U1—O1	2.288 (4)	C24—H24A	0.9800
U1—O2	2.300 (4)	C24—H24B	0.9800

U1—N2	2.597 (5)	C24—H24C	0.9800
U1—N1	2.653 (4)	C25—C28	1.514 (9)
Co1—C46	1.997 (7)	C25—C27	1.516 (10)
Co1—C45	2.020 (7)	C25—C26	1.554 (11)
Co1—C41	2.026 (7)	C26—H26A	0.9800
Co1—C40	2.027 (6)	C26—H26B	0.9800
Co1—C38	2.029 (7)	C26—H26C	0.9800
Co1—C39	2.030 (6)	C27—H27A	0.9800
Co1—C44	2.031 (7)	C27—H27B	0.9800
Co1—C37	2.035 (7)	C27—H27C	0.9800
Co1—C43	2.040 (6)	C28—H28A	0.9800
Co1—C42	2.054 (8)	C28—H28B	0.9800
O1—C1	1.297 (7)	C28—H28C	0.9800
N1—C7	1.297 (7)	C29—C30	1.479 (13)
N1—C8	1.427 (7)	C29—C32	1.528 (13)
C1—C2	1.418 (9)	C29—C31	1.609 (17)
C1—C6	1.443 (8)	C30—H30A	0.9800
O2—C20	1.289 (6)	C30—H30B	0.9800
N2—C14	1.299 (7)	C30—H30C	0.9800
N2—C13	1.428 (7)	C31—H31A	0.9800
C2—C3	1.393 (9)	C31—H31B	0.9800
C2—C21	1.529 (8)	C31—H31C	0.9800
C3—C4	1.410 (9)	C32—H32A	0.9800
C3—H3	0.9500	C32—H32B	0.9800
C4—C5	1.363 (9)	C32—H32C	0.9800
C4—C25	1.555 (9)	C33—C36	1.527 (11)
C5—C6	1.421 (8)	C33—C35	1.531 (9)
C5—H5	0.9500	C33—C34	1.538 (10)

C6—C7	1.430 (8)	C34—H34A	0.9800
C7—H7	0.9500	C34—H34B	0.9800
C8—C9	1.400 (7)	C34—H34C	0.9800
C8—C13	1.406 (8)	C35—H35A	0.9800
C9—C10	1.382 (9)	C35—H35B	0.9800
C9—H9	0.9500	C35—H35C	0.9800
C10—C11	1.369 (9)	C36—H36A	0.9800
C10—H10	0.9500	C36—H36B	0.9800
C11—C12	1.376 (8)	C36—H36C	0.9800
C11—H11	0.9500	C37—C38	1.370 (9)
C12—C13	1.389 (8)	C37—C41	1.415 (9)
C12—H12	0.9500	C37—H37	0.9500
C14—C15	1.427 (8)	C38—C39	1.427 (8)
C14—H14	0.9500	C38—H38	0.9500
C15—C16	1.408 (8)	C39—C40	1.385 (9)
C15—C20	1.425 (8)	C39—H39	0.9500
C16—C17	1.377 (9)	C40—C41	1.433 (9)
C16—H16	0.9500	C40—H40	0.9500
C17—C18	1.372 (10)	C41—H41	0.9500
C17—C29	1.532 (10)	C42—C46	1.421 (11)
C18—C19	1.375 (9)	C42—C43	1.421 (9)
C18—H18	0.9500	C42—H42	0.9500
C19—C20	1.455 (7)	C43—C44	1.393 (9)
C19—C33	1.542 (9)	C43—H43	0.9500
C21—C24	1.527 (10)	C44—C45	1.394 (10)
C21—C23	1.543 (11)	C44—H44	0.9500
C21—C22	1.548 (10)	C45—C46	1.418 (11)
C22—H22A	0.9800	C45—H45	0.9500

C22—H22B	0.9800	C46—H46	0.9500
C22—H22C	0.9800		
O3—U1—O4	175.99 (17)	H22B—C22—H22C	109.5
O3—U1—O5	94.12 (17)	C21—C23—H23A	109.5
O4—U1—O5	89.88 (17)	C21—C23—H23B	109.5
O3—U1—O1	88.32 (17)	H23A—C23—H23B	109.5
O4—U1—O1	92.42 (17)	C21—C23—H23C	109.5
O5—U1—O1	82.60 (14)	H23A—C23—H23C	109.5
O3—U1—O2	87.14 (15)	H23B—C23—H23C	109.5
O4—U1—O2	93.25 (16)	C21—C24—H24A	109.5
O5—U1—O2	81.36 (14)	C21—C24—H24B	109.5
O1—U1—O2	162.96 (14)	H24A—C24—H24B	109.5
O3—U1—N2	89.01 (16)	C21—C24—H24C	109.5
O4—U1—N2	87.45 (17)	H24A—C24—H24C	109.5
O5—U1—N2	148.77 (15)	H24B—C24—H24C	109.5
O1—U1—N2	128.58 (14)	C28—C25—C27	109.9 (7)
O2—U1—N2	67.76 (14)	C28—C25—C26	106.7 (6)
O3—U1—N1	88.09 (15)	C27—C25—C26	109.2 (7)
O4—U1—N1	88.58 (15)	C28—C25—C4	112.1 (6)
O5—U1—N1	149.26 (15)	C27—C25—C4	110.7 (5)
O1—U1—N1	66.80 (14)	C26—C25—C4	108.0 (7)
O2—U1—N1	129.38 (14)	C25—C26—H26A	109.5
N2—U1—N1	61.79 (14)	C25—C26—H26B	109.5
C46—Co1—C45	41.3 (3)	H26A—C26—H26B	109.5
C46—Co1—C41	106.3 (3)	C25—C26—H26C	109.5
C45—Co1—C41	124.1 (3)	H26A—C26—H26C	109.5
C46—Co1—C40	121.0 (3)	H26B—C26—H26C	109.5
C45—Co1—C40	107.3 (3)	C25—C27—H27A	109.5

C41—Co1—C40	41.4 (3)	C25—C27—H27B	109.5
C46—Co1—C38	160.2 (4)	H27A—C27—H27B	109.5
C45—Co1—C38	157.3 (3)	C25—C27—H27C	109.5
C41—Co1—C38	68.5 (3)	H27A—C27—H27C	109.5
C40—Co1—C38	68.5 (3)	H27B—C27—H27C	109.5
C46—Co1—C39	156.5 (3)	C25—C28—H28A	109.5
C45—Co1—C39	121.4 (3)	C25—C28—H28B	109.5
C41—Co1—C39	68.4 (3)	H28A—C28—H28B	109.5
C40—Co1—C39	39.9 (2)	C25—C28—H28C	109.5
C38—Co1—C39	41.1 (2)	H28A—C28—H28C	109.5
C46—Co1—C44	68.4 (3)	H28B—C28—H28C	109.5
C45—Co1—C44	40.3 (3)	C30—C29—C32	114.7 (12)
C41—Co1—C44	161.4 (3)	C30—C29—C17	112.0 (7)
C40—Co1—C44	124.8 (3)	C32—C29—C17	109.1 (8)
C38—Co1—C44	122.5 (3)	C30—C29—C31	105.3 (12)
C39—Co1—C44	109.0 (3)	C32—C29—C31	106.4 (8)
C46—Co1—C37	124.4 (3)	C17—C29—C31	108.9 (10)
C45—Co1—C37	161.7 (3)	C29—C30—H30A	109.5
C41—Co1—C37	40.8 (3)	C29—C30—H30B	109.5
C40—Co1—C37	68.2 (3)	H30A—C30—H30B	109.5
C38—Co1—C37	39.4 (3)	C29—C30—H30C	109.5
C39—Co1—C37	67.3 (3)	H30A—C30—H30C	109.5
C44—Co1—C37	156.8 (3)	H30B—C30—H30C	109.5
C46—Co1—C43	68.0 (3)	C29—C31—H31A	109.5
C45—Co1—C43	67.8 (3)	C29—C31—H31B	109.5
C41—Co1—C43	156.3 (3)	H31A—C31—H31B	109.5
C40—Co1—C43	161.4 (3)	C29—C31—H31C	109.5
C38—Co1—C43	108.7 (3)	H31A—C31—H31C	109.5

C39—Co1—C43	126.0	(3)	H31B—C31—H31C	109.5	
C44—Co1—C43	40.0	(3)	C29—C32—H32A	109.5	
C37—Co1—C43	122.1	(3)	C29—C32—H32B	109.5	
C46—Co1—C42	41.0	(3)	H32A—C32—H32B	109.5	
C45—Co1—C42	69.3	(3)	C29—C32—H32C	109.5	
C41—Co1—C42	119.9	(3)	H32A—C32—H32C	109.5	
C40—Co1—C42	156.4	(3)	H32B—C32—H32C	109.5	
C38—Co1—C42	123.6	(3)	C36—C33—C35	106.5	(7)
C39—Co1—C42	161.7	(3)	C36—C33—C34	110.1	(7)
C44—Co1—C42	68.5	(3)	C35—C33—C34	108.2	(6)
C37—Co1—C42	107.3	(3)	C36—C33—C19	108.0	(6)
C43—Co1—C42	40.6	(3)	C35—C33—C19	111.4	(6)
C1—O1—U1	137.1	(4)	C34—C33—C19	112.4	(6)
C7—N1—C8	119.3	(5)	C33—C34—H34A	109.5	
C7—N1—U1	125.9	(4)	C33—C34—H34B	109.5	
C8—N1—U1	114.6	(3)	H34A—C34—H34B	109.5	
O1—C1—C2	122.8	(5)	C33—C34—H34C	109.5	
O1—C1—C6	120.2	(6)	H34A—C34—H34C	109.5	
C2—C1—C6	117.1	(6)	H34B—C34—H34C	109.5	
C20—O2—U1	134.0	(3)	C33—C35—H35A	109.5	
C14—N2—C13	117.0	(5)	C33—C35—H35B	109.5	
C14—N2—U1	126.8	(4)	H35A—C35—H35B	109.5	
C13—N2—U1	116.1	(3)	C33—C35—H35C	109.5	
C3—C2—C1	119.1	(6)	H35A—C35—H35C	109.5	
C3—C2—C21	120.5	(6)	H35B—C35—H35C	109.5	
C1—C2—C21	120.3	(6)	C33—C36—H36A	109.5	
C2—C3—C4	124.0	(6)	C33—C36—H36B	109.5	
C2—C3—H3	118.0		H36A—C36—H36B	109.5	

C4—C3—H3	118.0		C33—C36—H36C	109.5	
C5—C4—C3	117.6	(6)	H36A—C36—H36C	109.5	
C5—C4—C25	123.8	(6)	H36B—C36—H36C	109.5	
C3—C4—C25	118.6	(6)	C38—C37—C41	110.0	(6)
C4—C5—C6	121.2	(6)	C38—C37—Co1	70.1	(4)
C4—C5—H5	119.4		C41—C37—Co1	69.2	(4)
C6—C5—H5	119.4		C38—C37—H37	125.0	
C5—C6—C7	117.3	(5)	C41—C37—H37	125.0	
C5—C6—C1	121.0	(6)	Co1—C37—H37	127.3	
C7—C6—C1	121.6	(6)	C37—C38—C39	107.3	(6)
N1—C7—C6	127.7	(5)	C37—C38—Co1	70.5	(4)
N1—C7—H7	116.2		C39—C38—Co1	69.5	(4)
C6—C7—H7	116.2		C37—C38—H38	126.4	
C9—C8—C13	118.7	(5)	C39—C38—H38	126.4	
C9—C8—N1	123.8	(5)	Co1—C38—H38	125.3	
C13—C8—N1	117.3	(5)	C40—C39—C38	108.6	(6)
C10—C9—C8	120.0	(6)	C40—C39—Co1	69.9	(4)
C10—C9—H9	120.0		C38—C39—Co1	69.4	(4)
C8—C9—H9	120.0		C40—C39—H39	125.7	
C11—C10—C9	120.8	(6)	C38—C39—H39	125.7	
C11—C10—H10	119.6		Co1—C39—H39	126.6	
C9—C10—H10	119.6		C39—C40—C41	107.9	(6)
C10—C11—C12	120.3	(6)	C39—C40—Co1	70.2	(4)
C10—C11—H11	119.9		C41—C40—Co1	69.3	(4)
C12—C11—H11	119.9		C39—C40—H40	126.0	
C11—C12—C13	120.3	(6)	C41—C40—H40	126.0	
C11—C12—H12	119.8		Co1—C40—H40	126.1	
C13—C12—H12	119.8		C37—C41—C40	106.1	(6)

C12—C13—C8	119.9 (5)	C37—C41—Co1	70.0 (4)
C12—C13—N2	123.6 (5)	C40—C41—Co1	69.3 (4)
C8—C13—N2	116.5 (5)	C37—C41—H41	126.9
N2—C14—C15	126.7 (5)	C40—C41—H41	126.9
N2—C14—H14	116.7	Co1—C41—H41	125.4
C15—C14—H14	116.7	C46—C42—C43	105.2 (6)
C16—C15—C20	119.8 (5)	C46—C42—Co1	67.3 (4)
C16—C15—C14	118.1 (5)	C43—C42—Co1	69.2 (4)
C20—C15—C14	122.0 (5)	C46—C42—H42	127.4
C17—C16—C15	122.5 (6)	C43—C42—H42	127.4
C17—C16—H16	118.7	Co1—C42—H42	127.6
C15—C16—H16	118.7	C44—C43—C42	109.6 (6)
C18—C17—C16	116.9 (6)	C44—C43—Co1	69.6 (4)
C18—C17—C29	119.3 (7)	C42—C43—Co1	70.2 (4)
C16—C17—C29	123.8 (7)	C44—C43—H43	125.2
C17—C18—C19	125.3 (6)	C42—C43—H43	125.2
C17—C18—H18	117.3	Co1—C43—H43	126.6
C19—C18—H18	117.3	C43—C44—C45	108.6 (7)
C18—C19—C20	118.1 (6)	C43—C44—Co1	70.4 (4)
C18—C19—C33	121.7 (6)	C45—C44—Co1	69.5 (4)
C20—C19—C33	120.1 (5)	C43—C44—H44	125.7
O2—C20—C15	120.8 (5)	C45—C44—H44	125.7
O2—C20—C19	122.0 (5)	Co1—C44—H44	126.1
C15—C20—C19	117.2 (5)	C44—C45—C46	107.2 (7)
C24—C21—C2	112.8 (6)	C44—C45—Co1	70.3 (4)
C24—C21—C23	107.6 (6)	C46—C45—Co1	68.4 (4)
C2—C21—C23	110.7 (6)	C44—C45—H45	126.4
C24—C21—C22	107.8 (7)	C46—C45—H45	126.4

C2—C21—C22	108.9 (6)	Co1—C45—H45	126.4
C23—C21—C22	108.9 (6)	C45—C46—C42	109.3 (6)
C21—C22—H22A	109.5	C45—C46—Co1	70.2 (4)
C21—C22—H22B	109.5	C42—C46—Co1	71.6 (4)
H22A—C22—H22B	109.5	C45—C46—H46	125.3
C21—C22—H22C	109.5	C42—C46—H46	125.3
H22A—C22—H22C	109.5	Co1—C46—H46	124.4

Table S2.13. Atomic coordinates and equivalent isotropic displacement parameters (A^2) for **2**. U(eq) is defined as one third of the trace of the orthogonalized U^{ij} tensor.

	X	*Y*	*Z*	U_{iso}*/U_{eq}	Occ. (<1)
U1	0.5000	0.070054 (14)	0.7500	0.01938 (10)	
O1	0.4453 (2)	0.04962 (19)	0.5716 (3)	0.0271 (8)	
N1	0.4996 (2)	0.1775 (2)	0.6582 (4)	0.0216 (9)	
C1	0.5566 (3)	0.2287 (3)	0.7337 (4)	0.0222 (11)	
O2	0.5000	−0.0550 (3)	0.7500	0.0504 (19)	
C2	0.6308 (3)	0.2215 (3)	0.7741 (5)	0.0301 (12)	
H2	0.6423	0.1834	0.7519	0.036*	
O3	0.4047 (2)	0.0673 (2)	0.6952 (3)	0.0293 (8)	
C3	0.6866 (3)	0.2689 (3)	0.8453 (5)	0.0303 (13)	
H3	0.7362	0.2644	0.8708	0.036*	
C4	0.6703 (3)	0.3249 (3)	0.8811 (4)	0.0245 (11)	
C5	0.7268 (3)	0.3753 (3)	0.9535 (5)	0.0326 (13)	
H5	0.7760	0.3723	0.9770	0.039*	
C6	0.7115 (4)	0.4278 (3)	0.9896 (5)	0.0369 (14)	
H6	0.7497	0.4614	1.0374	0.044*	
C7	0.6394 (4)	0.4329 (3)	0.9567 (5)	0.0371 (14)	
H7	0.6294	0.4696	0.9832	0.044*	
C8	0.5827 (3)	0.3847 (3)	0.8856 (5)	0.0292 (12)	

H8	0.5343	0.3881	0.8646	0.035*	
C9	0.5964 (3)	0.3305 (3)	0.8444 (4)	0.0229 (11)	
C10	0.5389 (3)	0.2805 (3)	0.7690 (4)	0.0206 (10)	
C11	0.4545 (3)	0.1914 (3)	0.5515 (4)	0.0258 (12)	
H11	0.4597	0.2353	0.5332	0.031*	
C12	0.3975 (3)	0.1479 (3)	0.4582 (4)	0.0250 (11)	
C13	0.3956 (3)	0.0774 (3)	0.4707 (5)	0.0252 (11)	
C14	0.3402 (3)	0.0371 (3)	0.3718 (5)	0.0284 (12)	
C15	0.2903 (4)	0.0706 (3)	0.2688 (5)	0.0375 (14)	
H15	0.2528	0.0442	0.2031	0.045*	
C16	0.2912 (4)	0.1407 (3)	0.2547 (5)	0.0417 (16)	
C17	0.3460 (4)	0.1780 (3)	0.3506 (5)	0.0341 (14)	
H17	0.3491	0.2255	0.3440	0.041*	
C18	0.3350 (3)	−0.0396 (3)	0.3798 (5)	0.0304 (13)	
C19	0.3137 (4)	−0.0543 (3)	0.4493 (6)	0.0414 (16)	
H19A	0.3104	−0.1034	0.4546	0.062*	
H19B	0.2637	−0.0335	0.4122	0.062*	
H19C	0.3534	−0.0353	0.5253	0.062*	
C20	0.2721 (4)	−0.0725 (3)	0.2629 (5)	0.0445 (16)	
H20A	0.2709	−0.1215	0.2719	0.067*	
H20B	0.2837	−0.0641	0.2163	0.067*	
H20C	0.2218	−0.0528	0.2262	0.067*	
C21	0.4117 (4)	−0.0727 (3)	0.4336 (6)	0.0385 (14)	
H21A	0.4082	−0.1218	0.4385	0.058*	
H21B	0.4528	−0.0541	0.5095	0.058*	
H21C	0.4234	−0.0633	0.3874	0.058*	
C22	0.2248 (3)	0.1690 (3)	0.1365 (4)	0.074 (3)	
C23	0.1447 (5)	0.1528 (5)	0.0942 (9)	0.074 (4)*	0.757 (13)

C24	0.2270 (5)	0.1374 (4)	0.0523 (7)	0.048 (3)*	0.757 (13)
C25	0.2309 (6)	0.2464 (3)	0.1348 (8)	0.067 (3)*	0.757 (13)
H23A	0.1414	0.1724	0.1463	0.100*	0.757 (13)
H24A	0.2231	0.0880	0.0530	0.100*	0.757 (13)
H25A	0.2296	0.2669	0.1885	0.100*	0.757 (13)
H23B	0.1379	0.1036	0.0907	0.100*	0.757 (13)
H24B	0.2757	0.1494	0.0738	0.100*	0.757 (13)
H25B	0.1876	0.2635	0.0588	0.100*	0.757 (13)
H23C	0.1042	0.1723	0.0189	0.100*	0.757 (13)
H24C	0.1836	0.1547	−0.0236	0.100*	0.757 (13)
H25C	0.2796	0.2583	0.1562	0.100*	0.757 (13)
C23'	0.2584 (5)	0.2056 (4)	0.0933 (8)	0.23 (4)*	0.243 (13)
C24'	0.1761 (5)	0.2210 (4)	0.1353 (8)	0.076 (12)*	0.243 (13)
C25'	0.1722 (5)	0.1120 (3)	0.0527 (7)	0.24 (5)*	0.243 (13)
H23D	0.2924	0.2425	0.1452	0.100*	0.243 (13)
H24D	0.2094	0.2576	0.1886	0.100*	0.243 (13)
H25D	0.2030	0.0786	0.0531	0.100*	0.243 (13)
H23E	0.2161	0.2242	0.0180	0.100*	0.243 (13)
H24E	0.1511	0.1986	0.1572	0.100*	0.243 (13)
H25E	0.1327	0.1310	−0.0232	0.100*	0.243 (13)
H23F	0.2878	0.1731	0.0895	0.100*	0.243 (13)
H24F	0.1366	0.2399	0.0592	0.100*	0.243 (13)
H25F	0.1472	0.0898	0.0748	0.100*	0.243 (13)
C26	0.4520 (6)	−0.0972 (5)	0.7548 (8)	0.093 (4)	
H26A	0.3973	−0.0964	0.6826	0.111*	
H26B	0.4556	−0.0831	0.8168	0.111*	
C27	0.4897 (17)	−0.1685 (5)	0.7780 (13)	0.224 (15)	
H27A	0.5350	−0.1749	0.8596	0.268*	

H27B	0.4521	−0.2052	0.7513	0.268*		
C1S	0.058 (11)	0.171 (12)	−0.21 (2)	1.9 (3)*	0.76	(16)
C2S	−0.058 (2)	0.070 (2)	−0.219 (4)	0.36 (4)*	1.00	(11)
C3S	−0.068 (2)	0.010 (2)	−0.154 (4)	0.29 (3)*	1.00	(9)
C4S	−0.016 (2)	−0.007 (2)	−0.046 (3)	0.08 (2)*	0.26	(5)
C5S	0.018 (3)	0.065 (4)	0.022 (5)	0.34 (4)*	0.86	(10)
C6S	0.001 (4)	0.123 (4)	−0.031 (7)	0.13 (4)*	0.27	(7)
C7S	−0.065 (3)	0.119 (2)	−0.135 (5)	0.24 (3)*	0.77	(11)
C8S	−0.048 (6)	0.149 (8)	−0.180 (11)	0.07 (10)*	0.30	(15)

Table S2.14. Anisotropic displacement parameters (A^2) for **2**. The anisotropic displacement factor exponent takes the form: $-2\pi^2$ [$h^2 a^{2}*U^{11}$ + ... + 2 h k a* b* U^{12}].

	U^{11}	U^{22}	U^{33}	U^{12}	U^{13}	U^{23}
U1	0.01803 (15)	0.02096 (15)	0.01847 (14)	0.000	0.01220 (12)	0.000
O1	0.031 (2)	0.026 (2)	0.025 (2)	−0.0026 (16)	0.0194 (18)	−0.0027 (15)
N1	0.022 (2)	0.023 (2)	0.024 (2)	−0.0034 (17)	0.017 (2)	−0.0043 (17)
C1	0.021 (3)	0.023 (3)	0.022 (3)	−0.005 (2)	0.015 (2)	−0.002 (2)
O2	0.051 (4)	0.026 (3)	0.041 (4)	0.000	0.018 (3)	0.000
C2	0.029 (3)	0.035 (3)	0.035 (3)	−0.001 (2)	0.025 (3)	−0.006 (2)
O3	0.0236 (19)	0.035 (2)	0.029 (2)	0.0020 (17)	0.0177 (17)	0.0027 (17)
C3	0.022 (3)	0.033 (3)	0.037 (3)	−0.008 (2)	0.021 (3)	−0.007 (2)
C4	0.022 (3)	0.025 (3)	0.023 (3)	−0.005 (2)	0.015 (2)	−0.002 (2)
C5	0.024 (3)	0.042 (3)	0.026 (3)	−0.010 (2)	0.015 (3)	−0.005 (2)
C6	0.035 (3)	0.035 (3)	0.029 (3)	−0.015 (3)	0.017 (3)	−0.007 (3)
C7	0.036 (3)	0.031 (3)	0.031 (3)	0.000 (3)	0.017 (3)	−0.006 (3)
C8	0.027 (3)	0.026 (3)	0.027 (3)	−0.001 (2)	0.015 (3)	−0.003 (2)
C9	0.021 (3)	0.020 (3)	0.020 (3)	−0.004 (2)	0.010 (2)	0.0001 (19)
C10	0.020 (3)	0.017 (2)	0.020 (2)	0.003 (2)	0.012 (2)	0.0042 (19)
C11	0.030 (3)	0.023 (3)	0.029 (3)	0.001 (2)	0.022 (3)	−0.001 (2)

C12	0.026 (3)	0.027 (3)	0.022 (3)	0.000 (2)	0.016 (2)	−0.006 (2)
C13	0.022 (3)	0.031 (3)	0.026 (3)	−0.001 (2)	0.018 (2)	−0.006 (2)
C14	0.029 (3)	0.031 (3)	0.026 (3)	0.000 (2)	0.019 (3)	−0.007 (2)
C15	0.034 (3)	0.037 (3)	0.022 (3)	0.004 (3)	0.011 (3)	−0.010 (3)
C16	0.047 (4)	0.035 (3)	0.025 (3)	0.013 (3)	0.018 (3)	−0.001 (2)
C17	0.043 (4)	0.026 (3)	0.026 (3)	0.007 (3)	0.020 (3)	0.001 (2)
C18	0.036 (3)	0.032 (3)	0.027 (3)	−0.009 (3)	0.023 (3)	−0.011 (2)
C19	0.052 (4)	0.040 (4)	0.050 (4)	−0.019 (3)	0.042 (4)	−0.016 (3)
C20	0.053 (4)	0.038 (4)	0.037 (3)	−0.016 (3)	0.028 (3)	−0.017 (3)
C21	0.048 (4)	0.031 (3)	0.042 (3)	0.000 (3)	0.033 (3)	−0.006 (3)
C22	0.096 (7)	0.041 (4)	0.028 (4)	0.024 (4)	0.020 (4)	−0.002 (3)
C26	0.101 (8)	0.056 (5)	0.049 (5)	−0.042 (5)	0.024 (5)	0.002 (4)
C27	0.40 (3)	0.024 (5)	0.101 (13)	−0.038 (11)	0.117 (16)	0.000 (5)

Table S2.15. Bond lengths [Å], bond angles [º], and torsion angles [º] for **2** using the symmetry codes: (i) −*x*+1, *y*, −*z*+3/2; (ii) −*x*, −*y*, −*z*.

U1—O3^{i}	1.778 (4)	C16—C17	1.374 (8)
U1—O3	1.778 (4)	C16—C22	1.531 (7)
U1—O1	2.256 (4)	C18—C21	1.527 (9)
U1—O1^{i}	2.256 (4)	C18—C20	1.543 (8)
U1—O2	2.466 (6)	C18—C19	1.546 (8)
U1—N1^{i}	2.586 (4)	C22—C24	1.5344
U1—N1	2.586 (4)	C22—C25	1.5345
O1—C13	1.317 (7)	C22—C25'	1.5345
N1—C11	1.298 (7)	C22—C24'	1.5348
N1—C1	1.444 (6)	C22—C23'	1.5508
C1—C10	1.368 (7)	C22—C23	1.5512
C1—C2	1.405 (7)	C26—C27	1.57 (2)
O2—C26^{i}	1.455 (10)	C27—C27^{i}	1.29 (4)

O2—C26	1.455 (10)	C1S—C7S	4.0 (2)
C2—C3	1.369 (8)	C1S—C8S	2.9 (3)
C3—C4	1.417 (8)	C1S—C2S	3.4 (2)
C4—C9	1.420 (8)	C1S—C6S	4.1 (3)
C4—C5	1.420 (7)	C2S—C3S	1.70 (5)
C5—C6	1.355 (9)	C2S—C7S	1.76 (6)
C6—C7	1.405 (9)	C2S—C8S	1.63 (12)
C7—C8	1.388 (8)	C3S—C4S	1.32 (5)
C8—C9	1.412 (8)	C4S—C4S^{ii}	1.15 (8)
C9—C10	1.432 (7)	C4S—C5S^{ii}	1.21 (8)
C10—C10^{i}	1.496 (10)	C4S—C5S	1.63 (9)
C11—C12	1.435 (7)	C5S—C6S	1.32 (8)
C12—C17	1.407 (8)	C5S—C4S^{ii}	1.21 (8)
C12—C13	1.410 (8)	C5S—C7S	2.15 (9)
C13—C14	1.434 (7)	C6S—C7S	1.30 (7)
C14—C15	1.388 (8)	C6S—C8S	1.90 (17)
C14—C18	1.529 (8)	C7S—C8S	1.20 (14)
C15—C16	1.403 (9)		
O3^{i}—U1—O3	176.5 (3)	C25—C22—C25'	138.0
O3^{i}—U1—O1	93.26 (16)	C24—C22—C24'	138.0
O3—U1—O1	86.12 (16)	C25—C22—C24'	54.3
O3^{i}—U1—O1^{i}	86.12 (16)	C25'—C22—C24'	109.1
O3—U1—O1^{i}	93.26 (16)	C24—C22—C16	109.6 (5)
O1—U1—O1^{i}	159.42 (19)	C25—C22—C16	110.9 (5)
O3^{i}—U1—O2	88.26 (12)	C25'—C22—C16	111.1 (5)
O3—U1—O2	88.26 (12)	C24'—C22—C16	112.4 (5)
O1—U1—O2	79.71 (10)	C24—C22—C23'	56.4
O1^{i}—U1—O2	79.71 (10)	C25—C22—C23'	56.4

O3^{i}—U1—N1^{i}	103.52 (16)	C25'—C22—C23'	107.4
O3—U1—N1^{i}	79.39 (16)	C24'—C22—C23'	107.4
O1—U1—N1^{i}	131.12 (13)	C16—C22—C23'	109.2 (6)
O1^{i}—U1—N1^{i}	68.59 (13)	C24—C22—C23	107.4
O2—U1—N1^{i}	145.01 (9)	C25—C22—C23	107.4
O3^{i}—U1—N1	79.39 (16)	C25'—C22—C23	56.4
O3—U1—N1	103.52 (16)	C24'—C22—C23	56.4
O1—U1—N1	68.59 (13)	C16—C22—C23	112.3 (6)
O1^{i}—U1—N1	131.12 (13)	C23'—C22—C23	138.5
O2—U1—N1	145.01 (9)	O2—C26—C27	100.7 (13)
N1^{i}—U1—N1	69.98 (18)	C27^{i}—C27—C26	105.0 (8)
C13—O1—U1	139.7 (3)	C7S—C1S—C8S	8(3)
C11—N1—C1	115.1 (4)	C7S—C1S—C2S	26 (2)
C11—N1—U1	128.0 (4)	C8S—C1S—C2S	29 (3)
C1—N1—U1	116.8 (3)	C7S—C1S—C6S	18.3 (15)
C10—C1—C2	121.7 (5)	C8S—C1S—C6S	25 (4)
C10—C1—N1	119.9 (5)	C2S—C1S—C6S	38 (3)
C2—C1—N1	118.3 (5)	C1S—C2S—C3S	148 (4)
C26^{i}—O2—C26	110.3 (11)	C1S—C2S—C7S	99 (6)
C26^{i}—O2—U1	124.9 (6)	C3S—C2S—C7S	78 (3)
C26—O2—U1	124.9 (5)	C1S—C2S—C8S	61 (8)
C3—C2—C1	120.4 (5)	C3S—C2S—C8S	118 (7)
C2—C3—C4	120.1 (5)	C7S—C2S—C8S	41 (5)
C3—C4—C9	119.5 (5)	C4S—C3S—C2S	127 (4)
C3—C4—C5	121.1 (5)	C4S^{ii}—C4S—C5S^{ii}	87 (5)
C9—C4—C5	119.3 (5)	C4S^{ii}—C4S—C3S	148 (7)
C6—C5—C4	120.8 (6)	C5S^{ii}—C4S—C3S	117 (5)
C5—C6—C7	120.5 (5)	C4S^{ii}—C4S—C5S	48 (4)

C8—C7—C6	120.3 (6)	C5S^{ii}—C4S—C5S	135 (4)
C7—C8—C9	120.3 (6)	C3S—C4S—C5S	105 (5)
C8—C9—C4	118.7 (5)	C6S—C5S—C4S^{ii}	164 (7)
C8—C9—C10	122.2 (5)	C6S—C5S—C4S	122 (6)
C4—C9—C10	119.2 (5)	C4S^{ii}—C5S—C4S	45 (4)
C1—C10—C9	119.1 (5)	C6S—C5S—C7S	34 (4)
C1—C10—C10^{i}	118.2 (4)	C4S^{ii}—C5S—C7S	130 (5)
C9—C10—C10^{i}	122.6 (4)	C4S—C5S—C7S	90 (3)
N1—C11—C12	127.3 (5)	C7S—C6S—C5S	111 (6)
C17—C12—C13	120.6 (5)	C7S—C6S—C1S	77 (5)
C17—C12—C11	116.8 (5)	C5S—C6S—C1S	125 (5)
C13—C12—C11	122.5 (5)	C7S—C6S—C8S	39 (4)
O1—C13—C12	120.0 (5)	C5S—C6S—C8S	136 (7)
O1—C13—C14	121.3 (5)	C1S—C6S—C8S	41 (4)
C12—C13—C14	118.7 (5)	C1S—C7S—C6S	84 (5)
C15—C14—C13	117.3 (5)	C1S—C7S—C8S	21 (6)
C15—C14—C18	121.4 (5)	C6S—C7S—C8S	99 (8)
C13—C14—C18	121.2 (5)	C1S—C7S—C2S	55 (4)
C14—C15—C16	124.7 (5)	C6S—C7S—C2S	111 (5)
C17—C16—C15	116.8 (5)	C8S—C7S—C2S	63 (6)
C17—C16—C22	126.2 (6)	C1S—C7S—C5S	103 (4)
C15—C16—C22	116.5 (5)	C6S—C7S—C5S	35 (4)
C16—C17—C12	121.8 (6)	C8S—C7S—C5S	123 (7)
C21—C18—C14	109.7 (5)	C2S—C7S—C5S	99 (3)
C21—C18—C20	107.3 (5)	C1S—C8S—C7S	150 (9)
C14—C18—C20	112.2 (5)	C1S—C8S—C2S	90 (8)
C21—C18—C19	111.1 (5)	C7S—C8S—C2S	75 (9)
C14—C18—C19	109.5 (5)	C1S—C8S—C6S	115 (7)

C20—C18—C19	107.1 (5)	C7S—C8S—C6S	43 (5)
C24—C22—C25	109.1	C2S—C8S—C6S	92 (8)
C24—C22—C25'	54.3		

Table S2.16. Atomic coordinates and equivalent isotropic displacement parameters (A^2) for **3**. U(eq) is defined as one third of the trace of the orthogonalized U^{ij} tensor.

	X	*Y*	*Z*	U_{iso}*/U_{eq}
U1	0.725337 (16)	0.606645 (17)	0.133724 (12)	0.03593 (15)
O4	0.7692 (3)	0.5362 (3)	0.1846 (2)	0.0387 (15)
N1	0.6973 (4)	0.6618 (4)	0.0540 (3)	0.044 (2)
O3	0.8046 (3)	0.5940 (3)	0.0805 (2)	0.0411 (16)
C9	0.6619 (5)	0.5653 (5)	0.2434 (4)	0.047 (3)
H9	0.6317	0.5711	0.2683	0.057*
C35	0.8150 (6)	0.4142 (6)	0.1332 (4)	0.061 (3)
H35A	0.7762	0.3896	0.1290	0.091*
H35B	0.8490	0.3952	0.1141	0.091*
H35C	0.8079	0.4577	0.1224	0.091*
C13	0.8325 (4)	0.6213 (4)	0.0438 (3)	0.038 (2)
C12	0.8995 (5)	0.6145 (5)	0.0360 (3)	0.046 (3)
C36	0.8872 (5)	0.4632 (5)	0.1965 (4)	0.057 (3)
H36A	0.8764	0.5034	0.1810	0.086*
H36B	0.9271	0.4474	0.1833	0.086*
H36C	0.8916	0.4697	0.2312	0.086*
C34	0.8339 (5)	0.4142 (5)	0.1868 (4)	0.054 (3)
C10	0.8880 (5)	0.6724 (5)	−0.0422 (4)	0.053 (3)
C23	0.2622 (6)	0.4971 (6)	0.1202 (5)	0.063 (3)
H23	0.2275	0.4689	0.1173	0.076*
C19	0.7474 (5)	0.4924 (5)	0.2138 (3)	0.041 (2)
C1	0.7299 (5)	0.6684 (5)	0.0164 (3)	0.049 (3)

H1	0.7083	0.6846	−0.0109	0.058*
C39	0.7151 (7)	0.3358 (6)	0.3491 (4)	0.079 (4)
H39A	0.6943	0.3110	0.3743	0.118*
H39B	0.7294	0.3761	0.3625	0.118*
H39C	0.7515	0.3123	0.3366	0.118*
C14	0.6927 (5)	0.5044 (5)	0.2426 (3)	0.044 (2)
N3	0.6697 (4)	0.6130 (4)	0.2150 (3)	0.0396 (19)
C11	0.9233 (5)	0.6406 (6)	−0.0073 (4)	0.057 (3)
H11	0.9672	0.6360	−0.0132	0.068*
C48	0.1691 (8)	0.5004 (8)	0.0471 (6)	0.115 (6)
H48A	0.1379	0.5075	0.0216	0.172*
H48B	0.1507	0.5118	0.0783	0.172*
H48C	0.1814	0.4558	0.0475	0.172*
C15	0.6684 (5)	0.4589 (5)	0.2740 (4)	0.053 (3)
H15	0.6322	0.4688	0.2928	0.063*
C20	0.3574 (6)	0.5789 (6)	0.1287 (6)	0.076 (4)
C46	0.2287 (7)	0.5423 (7)	0.0375 (5)	0.087 (4)
C16	0.6957 (5)	0.4001 (5)	0.2784 (4)	0.052 (3)
C8	0.7971 (5)	0.6542 (4)	0.0098 (3)	0.040 (2)
C22	0.2700 (6)	0.5412 (6)	0.0841 (4)	0.064 (3)
C26	0.9226 (7)	0.6962 (7)	−0.0866 (5)	0.077 (4)
O5	0.3931 (5)	0.5342 (5)	0.1978 (4)	0.105 (3)
H5	0.4136	0.5002	0.1970	0.127*
C18	0.7760 (5)	0.4321 (5)	0.2175 (3)	0.042 (2)
C25	0.3495 (6)	0.5340 (6)	0.1624 (5)	0.067 (3)
C50	0.8252 (5)	0.6761 (5)	−0.0331 (4)	0.049 (3)
H50	0.7986	0.6944	−0.0569	0.059*
C24	0.2996 (7)	0.4903 (6)	0.1595 (4)	0.072 (4)

C17	0.7490 (6)	0.3889 (5)	0.2496 (4)	0.059 (3)
H17	0.7684	0.3486	0.2521	0.071*
C40	0.6712 (6)	0.3475 (5)	0.3106 (5)	0.064 (3)
C30	0.9430 (5)	0.5797 (5)	0.0714 (4)	0.052 (3)
C21	0.3225 (7)	0.5874 (8)	0.0868 (5)	0.099 (6)
H21	0.3312	0.6186	0.0631	0.119*
C47	0.2068 (9)	0.6161 (7)	0.0283 (6)	0.124 (7)
H47A	0.2436	0.6440	0.0315	0.186*
H47B	0.1748	0.6280	0.0521	0.186*
H47C	0.1891	0.6202	−0.0041	0.186*
O2	0.6751 (3)	0.5461 (3)	0.1121 (2)	0.0441 (16)
O1	0.7681 (3)	0.6737 (3)	0.1556 (2)	0.0414 (16)
N2	0.6194 (4)	0.6776 (4)	0.1402 (3)	0.045 (2)
C6	0.5632 (5)	0.6393 (5)	0.1423 (4)	0.049 (3)
H6A	0.5694	0.6060	0.1669	0.059*
H6B	0.5577	0.6179	0.1108	0.059*
C4	0.6312 (5)	0.7142 (5)	0.1851 (4)	0.049 (3)
H4A	0.5969	0.7454	0.1898	0.059*
H4B	0.6715	0.7376	0.1821	0.059*
C7	0.5017 (5)	0.6757 (5)	0.1542 (5)	0.060 (3)
H7A	0.4915	0.7058	0.1280	0.072*
H7B	0.5069	0.6999	0.1844	0.072*
C2	0.6324 (5)	0.6863 (5)	0.0519 (4)	0.057 (3)
H2A	0.6022	0.6510	0.0478	0.069*
H2B	0.6278	0.7152	0.0241	0.069*
C31	0.9363 (5)	0.6078 (5)	0.1221 (3)	0.048 (3)
H31A	0.8918	0.6072	0.1317	0.072*
H31B	0.9518	0.6514	0.1221	0.072*

H31C	0.9611	0.5826	0.1449	0.072*
N4	0.4475 (6)	0.6259 (7)	0.1598 (4)	0.098 (5)
C3	0.6185 (5)	0.7218 (5)	0.0988 (4)	0.054 (3)
H3A	0.6506	0.7552	0.1037	0.065*
H3B	0.5765	0.7422	0.0967	0.065*
C5	0.6343 (5)	0.6704 (5)	0.2280 (4)	0.053 (3)
H5A	0.6554	0.6920	0.2552	0.063*
H5B	0.5910	0.6588	0.2383	0.063*
C33	0.9274 (5)	0.5115 (5)	0.0717 (4)	0.063 (3)
H33A	0.8839	0.5057	0.0827	0.094*
H33B	0.9563	0.4893	0.0934	0.094*
H33C	0.9319	0.4945	0.0391	0.094*
C38	0.6592 (6)	0.2887 (6)	0.2813 (5)	0.080 (4)
H38A	0.6994	0.2669	0.2753	0.120*
H38B	0.6398	0.3003	0.2505	0.120*
H38C	0.6307	0.2605	0.2990	0.120*
C37	0.8591 (6)	0.3476 (5)	0.1995 (5)	0.072 (4)
H37A	0.8640	0.3440	0.2344	0.108*
H37B	0.9001	0.3410	0.1839	0.108*
H37C	0.8291	0.3157	0.1882	0.108*
C32	1.0125 (5)	0.5855 (7)	0.0567 (5)	0.082 (4)
H32A	1.0392	0.5658	0.0813	0.124*
H32B	1.0238	0.6302	0.0536	0.124*
H32C	1.0191	0.5641	0.0258	0.124*
C27	0.8787 (8)	0.7336 (7)	−0.1177 (6)	0.102 (6)
H27A	0.8648	0.7714	−0.1002	0.153*
H27B	0.8419	0.7077	−0.1260	0.153*
H27C	0.9007	0.7463	−0.1472	0.153*

C41	0.6061 (8)	0.3681 (6)	0.3333 (6)	0.106 (6)
H41A	0.5915	0.3354	0.3557	0.159*
H41B	0.5748	0.3736	0.3077	0.159*
H41C	0.6115	0.4080	0.3507	0.159*
C51	0.4173 (10)	0.6317 (8)	0.1281 (5)	0.117 (8)
H51	0.4238	0.6623	0.1037	0.140*
C28	0.9477 (9)	0.6412 (8)	−0.1148 (5)	0.129 (8)
H28A	0.9734	0.6568	−0.1416	0.193*
H28B	0.9124	0.6163	−0.1273	0.193*
H28C	0.9738	0.6147	−0.0937	0.193*
C42	0.2876 (11)	0.4401 (10)	0.1956 (6)	0.125 (7)
C49	0.2668 (7)	0.5170 (7)	−0.0042 (4)	0.100 (5)
H49A	0.3050	0.5426	−0.0083	0.150*
H49B	0.2414	0.5190	−0.0337	0.150*
H49C	0.2787	0.4731	0.0022	0.150*
C44	0.2789 (11)	0.4694 (11)	0.2446 (6)	0.185 (12)
H44A	0.2339	0.4702	0.2527	0.278*
H44B	0.2955	0.5126	0.2443	0.278*
H44C	0.3018	0.4444	0.2686	0.278*
C45	0.2247 (19)	0.4046 (15)	0.1925 (11)	0.46 (4)
H45A	0.2048	0.4037	0.2244	0.683*
H45B	0.2323	0.3613	0.1815	0.683*
H45C	0.1967	0.4262	0.1697	0.683*
C29	0.9749 (9)	0.7389 (10)	−0.0741 (7)	0.146 (8)
H29A	1.0137	0.7143	−0.0696	0.219*
H29B	0.9647	0.7614	−0.0443	0.219*
H29C	0.9812	0.7695	−0.1002	0.219*
C43	0.3518 (13)	0.3991 (12)	0.1929 (12)	0.243 (17)

H43A	0.3677	0.3916	0.2255	0.365*
H43B	0.3836	0.4222	0.1743	0.365*
H43C	0.3431	0.3585	0.1773	0.365*

Table S2.17. Anisotropic displacement parameters (A^2) for **3**. The anisotropic displacement factor exponent takes the form: $-2\pi^2$ [$h^2 a^{2*}U^{11}$ + ... + 2 h k a* b* U^{12}].

	U^{11}	U^{22}	U^{33}	U^{12}	U^{13}	U^{23}
U1	0.0345 (2)	0.0412 (2)	0.0321 (2)	0.00217 (16)	0.00319 (16)	−0.00354 (16)
O4	0.044 (4)	0.045 (4)	0.028 (3)	−0.001 (3)	0.006 (3)	0.006 (3)
N1	0.038 (5)	0.057 (6)	0.036 (5)	0.008 (4)	0.002 (4)	0.005 (4)
O3	0.039 (4)	0.057 (4)	0.028 (3)	0.000 (3)	0.007 (3)	0.002 (3)
C9	0.045 (6)	0.057 (7)	0.039 (6)	−0.004 (5)	0.010 (5)	−0.022 (5)
C35	0.070 (8)	0.066 (8)	0.046 (6)	0.010 (6)	0.005 (6)	−0.012 (6)
C13	0.039 (6)	0.047 (6)	0.029 (5)	0.000 (5)	0.002 (4)	−0.004 (4)
C12	0.041 (6)	0.066 (7)	0.030 (5)	−0.001 (5)	0.004 (4)	−0.003 (5)
C36	0.052 (7)	0.064 (8)	0.057 (7)	0.004 (6)	0.010 (6)	0.009 (6)
C34	0.065 (8)	0.059 (7)	0.040 (6)	0.007 (6)	0.012 (5)	0.009 (5)
C10	0.063 (8)	0.069 (8)	0.027 (5)	0.005 (6)	0.007 (5)	−0.001 (5)
C23	0.057 (8)	0.061 (8)	0.071 (8)	−0.011 (6)	0.005 (6)	−0.007 (7)
C19	0.052 (6)	0.041 (6)	0.029 (5)	−0.002 (5)	−0.002 (4)	−0.003 (4)
C1	0.070 (8)	0.048 (6)	0.028 (5)	0.014 (5)	−0.005 (5)	−0.001 (5)
C39	0.106 (11)	0.079 (10)	0.051 (7)	−0.029 (8)	0.010 (8)	0.011 (7)
C14	0.057 (7)	0.042 (6)	0.033 (5)	0.000 (5)	0.005 (5)	−0.001 (5)
N3	0.042 (5)	0.037 (5)	0.040 (5)	−0.001 (4)	0.008 (4)	−0.005 (4)
C11	0.050 (7)	0.080 (8)	0.040 (6)	0.009 (6)	0.010 (5)	−0.002 (6)
C48	0.121 (14)	0.124 (14)	0.100 (12)	0.026 (11)	−0.063 (11)	−0.050 (11)
C15	0.065 (7)	0.047 (7)	0.046 (6)	−0.010 (5)	0.022 (5)	−0.010 (5)
C20	0.056 (8)	0.053 (8)	0.121 (13)	0.005 (6)	0.044 (9)	−0.020 (8)
C46	0.095 (11)	0.099 (12)	0.067 (9)	0.019 (9)	−0.027 (8)	−0.017 (8)

C16	0.063 (7)	0.053 (7)	0.040 (6)	−0.013 (6)	0.014 (5)	−0.005 (5)
C8	0.045 (6)	0.042 (6)	0.034 (5)	0.013 (4)	0.004 (4)	−0.006 (4)
C22	0.053 (7)	0.076 (9)	0.063 (8)	0.007 (6)	−0.009 (6)	−0.016 (7)
C26	0.072 (9)	0.095 (11)	0.062 (9)	0.008 (8)	0.009 (7)	0.027 (8)
O5	0.112 (9)	0.115 (9)	0.089 (7)	0.002 (7)	−0.025 (7)	0.011 (7)
C18	0.048 (6)	0.046 (6)	0.031 (5)	−0.001 (5)	0.000 (4)	0.000 (4)
C25	0.062 (8)	0.068 (9)	0.069 (9)	0.008 (7)	−0.028 (7)	−0.022 (7)
C50	0.058 (7)	0.052 (7)	0.037 (6)	0.008 (5)	0.002 (5)	−0.002 (5)
C24	0.091 (10)	0.069 (9)	0.055 (8)	−0.011 (7)	−0.025 (7)	0.008 (7)
C17	0.087 (9)	0.045 (7)	0.046 (7)	−0.001 (6)	0.001 (6)	−0.007 (5)
C40	0.086 (9)	0.041 (7)	0.065 (8)	−0.019 (6)	0.017 (7)	0.001 (6)
C30	0.048 (6)	0.065 (8)	0.041 (6)	0.011 (5)	0.010 (5)	−0.003 (5)
C21	0.087 (11)	0.132 (14)	0.080 (10)	0.048 (10)	−0.034 (9)	−0.071 (10)
C47	0.166 (17)	0.107 (13)	0.099 (13)	0.058 (12)	−0.047 (12)	−0.021 (10)
O2	0.040 (4)	0.049 (4)	0.043 (4)	0.002 (3)	0.000 (3)	−0.005 (3)
O1	0.044 (4)	0.036 (4)	0.044 (4)	−0.004 (3)	0.001 (3)	0.000 (3)
N2	0.036 (5)	0.054 (5)	0.044 (5)	0.008 (4)	0.008 (4)	−0.012 (4)
C6	0.039 (6)	0.054 (7)	0.053 (7)	0.004 (5)	0.003 (5)	−0.017 (5)
C4	0.044 (6)	0.050 (7)	0.053 (7)	0.006 (5)	0.007 (5)	−0.013 (5)
C7	0.037 (6)	0.052 (7)	0.091 (9)	−0.005 (5)	0.001 (6)	−0.018 (6)
C2	0.048 (7)	0.060 (7)	0.064 (7)	0.007 (5)	0.000 (6)	0.014 (6)
C31	0.043 (6)	0.067 (7)	0.034 (5)	0.004 (5)	−0.005 (4)	−0.001 (5)
N4	0.104 (10)	0.131 (11)	0.059 (8)	0.063 (9)	−0.018 (7)	−0.026 (8)
C3	0.049 (7)	0.055 (7)	0.059 (7)	0.018 (5)	0.004 (6)	0.000 (6)
C5	0.052 (7)	0.053 (7)	0.053 (7)	0.003 (5)	0.016 (5)	−0.013 (6)
C33	0.073 (8)	0.064 (8)	0.051 (7)	0.036 (6)	−0.002 (6)	−0.012 (6)
C38	0.102 (11)	0.058 (8)	0.079 (9)	−0.014 (7)	0.016 (8)	0.006 (7)
C37	0.075 (9)	0.064 (8)	0.078 (9)	0.028 (7)	0.022 (7)	0.012 (7)

C32	0.038 (7)	0.136 (13)	0.074 (9)	0.028 (7)	0.014 (6)	0.018 (8)
C27	0.132 (14)	0.100 (12)	0.075 (10)	0.002 (10)	0.043 (10)	0.020 (9)
C41	0.152 (15)	0.058 (9)	0.108 (12)	−0.021 (9)	0.070 (11)	0.011 (8)
C51	0.19 (2)	0.110 (14)	0.051 (9)	0.106 (15)	0.011 (10)	−0.004 (9)
C28	0.170 (18)	0.148 (16)	0.068 (9)	0.089 (14)	0.072 (11)	0.045 (10)
C42	0.19 (2)	0.122 (16)	0.065 (11)	0.029 (15)	−0.039 (12)	0.007 (10)
C49	0.135 (14)	0.124 (13)	0.040 (7)	0.006 (11)	0.001 (8)	−0.028 (8)
C44	0.23 (3)	0.25 (3)	0.079 (14)	−0.11 (2)	−0.016 (15)	0.048 (16)
C45	0.68 (7)	0.38 (4)	0.31 (4)	−0.46 (5)	−0.38 (5)	0.26 (4)
C29	0.127 (16)	0.20 (2)	0.111 (14)	−0.076 (15)	−0.013 (12)	0.058 (14)
C43	0.22 (3)	0.15 (2)	0.36 (5)	−0.08 (2)	−0.11 (3)	0.08 (3)

Table S2.18. Bond lengths [Å], bond angles [º], and torsion angles [º] for **3.**

U1—O2	1.770 (6)	C20—C25	1.345 (18)
U1—O1	1.791 (6)	C20—C21	1.390 (19)
U1—O3	2.253 (6)	C20—C51	1.69 (3)
U1—O4	2.255 (6)	C46—C49	1.510 (18)
U1—N3	2.551 (8)	C46—C22	1.562 (17)
U1—N1	2.574 (8)	C46—C47	1.648 (19)
U1—N2	2.704 (8)	C16—C17	1.404 (14)
O4—C19	1.317 (10)	C16—C40	1.520 (14)
N1—C1	1.258 (12)	C8—C50	1.408 (13)
N1—C2	1.470 (12)	C22—C21	1.484 (19)
O3—C13	1.313 (10)	C26—C29	1.470 (19)
C9—N3	1.291 (12)	C26—C27	1.50 (2)
C9—C14	1.447 (13)	C26—C28	1.50 (2)
C35—C34	1.544 (14)	O5—C25	1.347 (13)
C13—C8	1.393 (13)	C18—C17	1.399 (14)
C13—C12	1.441 (13)	C25—C24	1.406 (17)

C12—C11	1.417 (14)	C24—C42	1.48 (2)
C12—C30	1.536 (14)	C40—C38	1.509 (16)
C36—C34	1.554 (15)	C40—C41	1.578 (18)
C34—C18	1.540 (14)	C30—C33	1.480 (15)
C34—C37	1.547 (14)	C30—C32	1.534 (14)
C10—C50	1.357 (14)	C30—C31	1.534 (13)
C10—C11	1.395 (14)	N2—C6	1.441 (13)
C10—C26	1.522 (15)	N2—C3	1.482 (13)
C23—C24	1.355 (16)	N2—C4	1.490 (12)
C23—C22	1.380 (16)	C6—C7	1.549 (14)
C19—C18	1.417 (13)	C4—C5	1.513 (14)
C19—C14	1.429 (13)	C7—N4	1.566 (18)
C1—C8	1.467 (13)	C2—C3	1.534 (14)
C39—C40	1.437 (17)	N4—C51	1.093 (16)
C14—C15	1.399 (13)	C42—C44	1.51 (2)
N3—C5	1.472 (12)	C42—C45	1.53 (3)
C48—C46	1.57 (2)	C42—C43	1.61 (3)
C15—C16	1.377 (14)		
O2—U1—O1	173.3 (3)	C22—C46—C47	107.4 (11)
O2—U1—O3	98.0 (3)	C48—C46—C47	109.7 (13)
O1—U1—O3	86.6 (3)	C15—C16—C17	116.0 (10)
O2—U1—O4	88.9 (3)	C15—C16—C40	124.8 (10)
O1—U1—O4	95.9 (3)	C17—C16—C40	119.1 (10)
O3—U1—O4	91.5 (2)	C13—C8—C50	120.8 (9)
O2—U1—N3	93.5 (3)	C13—C8—C1	122.6 (9)
O1—U1—N3	83.8 (3)	C50—C8—C1	116.6 (9)
O3—U1—N3	158.7 (2)	C23—C22—C21	119.9 (12)
O4—U1—N3	70.7 (2)	C23—C22—C46	123.2 (12)

O2—U1—N1	84.1 (3)	C21—C22—C46	116.8 (13)
O1—U1—N1	92.8 (3)	C29—C26—C27	106.2 (14)
O3—U1—N1	70.1 (2)	C29—C26—C28	109.5 (15)
O4—U1—N1	159.1 (2)	C27—C26—C28	109.3 (13)
N3—U1—N1	129.2 (3)	C29—C26—C10	111.9 (12)
O2—U1—N2	85.8 (3)	C27—C26—C10	110.1 (11)
O1—U1—N2	87.5 (3)	C28—C26—C10	109.7 (11)
O3—U1—N2	136.6 (2)	C17—C18—C19	117.3 (9)
O4—U1—N2	131.9 (2)	C17—C18—C34	121.2 (9)
N3—U1—N2	61.9 (2)	C19—C18—C34	121.4 (9)
N1—U1—N2	67.3 (2)	C20—C25—O5	114.9 (14)
C19—O4—U1	135.1 (6)	C20—C25—C24	121.0 (12)
C1—N1—C2	116.1 (9)	O5—C25—C24	124.0 (14)
C1—N1—U1	129.7 (7)	C10—C50—C8	123.5 (10)
C2—N1—U1	114.2 (6)	C23—C24—C25	114.6 (12)
C13—O3—U1	142.5 (6)	C23—C24—C42	121.4 (14)
N3—C9—C14	129.0 (9)	C25—C24—C42	124.0 (13)
O3—C13—C8	120.4 (9)	C18—C17—C16	125.6 (11)
O3—C13—C12	121.0 (8)	C39—C40—C38	111.6 (11)
C8—C13—C12	118.5 (9)	C39—C40—C16	110.1 (10)
C11—C12—C13	116.0 (9)	C38—C40—C16	110.1 (10)
C11—C12—C30	121.2 (9)	C39—C40—C41	108.4 (11)
C13—C12—C30	122.7 (8)	C38—C40—C41	107.3 (11)
C18—C34—C35	109.2 (9)	C16—C40—C41	109.3 (10)
C18—C34—C37	111.8 (9)	C33—C30—C32	106.9 (10)
C35—C34—C37	108.0 (10)	C33—C30—C31	110.7 (9)
C18—C34—C36	108.5 (9)	C32—C30—C31	107.6 (10)
C35—C34—C36	110.8 (9)	C33—C30—C12	109.7 (9)

C37—C34—C36	108.6 (10)	C32—C30—C12	111.5 (9)
C50—C10—C11	115.0 (10)	C31—C30—C12	110.3 (8)
C50—C10—C26	127.2 (11)	C20—C21—C22	110.7 (15)
C11—C10—C26	117.8 (10)	C6—N2—C3	112.1 (8)
C24—C23—C22	126.0 (12)	C6—N2—C4	113.4 (8)
O4—C19—C18	121.9 (9)	C3—N2—C4	108.8 (8)
O4—C19—C14	120.3 (9)	C6—N2—U1	112.0 (6)
C18—C19—C14	117.7 (9)	C3—N2—U1	108.1 (5)
N1—C1—C8	127.8 (9)	C4—N2—U1	101.9 (6)
C15—C14—C19	121.8 (9)	N2—C6—C7	115.0 (9)
C15—C14—C9	116.0 (9)	N2—C4—C5	110.4 (8)
C19—C14—C9	122.2 (9)	C6—C7—N4	107.6 (9)
C9—N3—C5	115.4 (8)	N1—C2—C3	108.6 (9)
C9—N3—U1	124.0 (6)	C51—N4—C7	105.9 (18)
C5—N3—U1	119.7 (6)	N2—C3—C2	110.4 (8)
C10—C11—C12	126.0 (10)	N3—C5—C4	109.6 (8)
C16—C15—C14	121.5 (10)	N4—C51—C20	110.9 (18)
C25—C20—C21	127.7 (15)	C24—C42—C44	109.6 (16)
C25—C20—C51	124.5 (14)	C24—C42—C45	117.5 (15)
C21—C20—C51	107.7 (14)	C44—C42—C45	98 (2)
C49—C46—C22	109.5 (11)	C24—C42—C43	102.2 (18)
C49—C46—C48	111.1 (13)	C44—C42—C43	111.4 (18)
C22—C46—C48	107.5 (12)	C45—C42—C43	118 (2)
C49—C46—C47	111.5 (13)		

Table S2.19. Atomic coordinates and equivalent isotropic displacement parameters (A^2) for **4**. U(eq) is defined as one third of the trace of the orthogonalized U^{ij} tensor.

	X	*Y*	*Z*	U_{iso}*/U_{eq}
U1	0.5000	0.0000	0.0000	0.01583 (8)

O1	0.58891 (15)	0.03573 (12)	0.10221 (9)	0.0195 (4)
N1	0.5434 (2)	0.19959 (13)	0.09028 (11)	0.0193 (5)
C1	0.6039 (2)	0.05300 (15)	0.17026 (13)	0.0177 (5)
O2	0.57486 (16)	0.11679 (11)	−0.03853 (9)	0.0200 (4)
N2	0.8718 (3)	0.2443 (2)	0.1167 (2)	0.0686 (11)
C2	0.6827 (3)	0.00921 (15)	0.2144 (2)	0.0197 (7)
O3	0.36832 (16)	0.05102 (11)	0.02512 (9)	0.0206 (4)
N3	1.1993 (4)	0.2544 (3)	0.1070 (2)	0.0886 (15)
C3	0.6900 (2)	0.03210 (19)	0.28454 (14)	0.0205 (6)
H3	0.7408	0.0023	0.3148	0.025*
C4	0.6277 (2)	0.09592 (16)	0.31325 (14)	0.0207 (6)
C5	0.5561 (2)	0.13942 (16)	0.26795 (14)	0.0213 (6)
H5	0.5147	0.1845	0.2851	0.026*
C6	0.5436 (2)	0.11852 (16)	0.19790 (13)	0.0198 (6)
C7	0.4695 (2)	0.16910 (17)	0.14940 (14)	0.0220 (6)
H7A	0.4367	0.2149	0.1754	0.026*
H7B	0.4033	0.1369	0.1303	0.026*
C8	0.4686 (3)	0.2391 (2)	0.03380 (16)	0.0215 (7)
H8A	0.4025	0.2034	0.0203	0.026*
H8B	0.4356	0.2898	0.0518	0.026*
C9	0.5420 (3)	0.25616 (19)	−0.02908 (16)	0.0201 (6)
C10	0.5937 (2)	0.19104 (16)	−0.06315 (14)	0.0175 (5)
C11	0.6670 (2)	0.20629 (16)	−0.12086 (15)	0.0206 (6)
C12	0.6806 (2)	0.28559 (16)	−0.14144 (15)	0.0234 (6)
H12	0.7288	0.2960	−0.1803	0.028*
C13	0.6281 (2)	0.35104 (16)	−0.10882 (15)	0.0219 (6)
C14	0.5600 (2)	0.33472 (16)	−0.05121 (14)	0.0212 (6)
H14	0.5252	0.3777	−0.0265	0.025*

C15	0.7590 (2)	−0.05799 (16)	0.18488 (15)	0.0224 (6)
C16	0.8380 (3)	−0.0241 (2)	0.1285 (2)	0.0331 (7)
H16A	0.7894	−0.0044	0.0893	0.050*
H16B	0.8906	−0.0662	0.1121	0.050*
H16C	0.8847	0.0202	0.1480	0.050*
C17	0.6816 (3)	−0.12563 (17)	0.15421 (17)	0.0322 (7)
H17A	0.6382	−0.1512	0.1918	0.048*
H17B	0.7315	−0.1655	0.1316	0.048*
H17C	0.6261	−0.1032	0.1196	0.048*
C18	0.8393 (3)	−0.09625 (19)	0.24162 (16)	0.0322 (7)
H18A	0.8926	−0.0555	0.2611	0.048*
H18B	0.8854	−0.1394	0.2209	0.048*
H18C	0.7911	−0.1181	0.2789	0.048*
C19	0.6424 (3)	0.11687 (18)	0.39166 (14)	0.0244 (6)
C20	0.6106 (3)	0.0446 (2)	0.43600 (16)	0.0393 (8)
H20A	0.6635	0.0000	0.4256	0.059*
H20B	0.5293	0.0286	0.4253	0.059*
H20C	0.6183	0.0585	0.4856	0.059*
C21	0.7710 (3)	0.1396 (2)	0.40741 (18)	0.0400 (8)
H21A	0.7810	0.1519	0.4573	0.060*
H21B	0.7919	0.1867	0.3797	0.060*
H21C	0.8222	0.0947	0.3953	0.060*
C22	0.5646 (4)	0.1874 (2)	0.41236 (18)	0.0354 (9)
H22A	0.4827	0.1755	0.3995	0.053*
H22B	0.5898	0.2358	0.3879	0.053*
H22C	0.5715	0.1960	0.4629	0.053*
C23	0.6464 (3)	0.43578 (16)	−0.13798 (15)	0.0250 (6)
C24	0.5828 (6)	0.49977 (14)	−0.0955 (4)	0.0418 (13)

H24A	0.5960	0.5526	−0.1163	0.063*
H24B	0.6134	0.4994	−0.0472	0.063*
H24C	0.4984	0.4882	−0.0958	0.063*
C25	0.7773 (3)	0.4562 (2)	−0.1369 (2)	0.0382 (8)
H25A	0.8181	0.4213	−0.1696	0.057*
H25B	0.8099	0.4483	−0.0896	0.057*
H25C	0.7878	0.5123	−0.1508	0.057*
C26	0.5976 (3)	0.4379 (2)	−0.21288 (18)	0.0403 (8)
H26A	0.6090	0.4914	−0.2326	0.060*
H26B	0.5135	0.4252	−0.2130	0.060*
H26C	0.6389	0.3983	−0.2411	0.060*
C27	0.7337 (2)	0.13825 (16)	−0.15709 (16)	0.0246 (6)
C28	0.6464 (3)	0.07745 (19)	−0.18873 (16)	0.0343 (7)
H28A	0.5984	0.1036	−0.2252	0.051*
H28B	0.5955	0.0572	−0.1520	0.051*
H28C	0.6898	0.0328	−0.2092	0.051*
C29	0.8098 (3)	0.1697 (2)	−0.21641 (18)	0.0382 (8)
H29A	0.7601	0.1981	−0.2507	0.057*
H29B	0.8487	0.1247	−0.2392	0.057*
H29C	0.8692	0.2066	−0.1972	0.057*
C30	0.8154 (3)	0.0971 (2)	−0.10343 (19)	0.0368 (8)
H30A	0.8588	0.0541	−0.1264	0.055*
H30B	0.7687	0.0744	−0.0658	0.055*
H30C	0.8710	0.1364	−0.0839	0.055*
C31	0.6465 (3)	0.25034 (19)	0.11507 (16)	0.0338 (7)
H31A	0.6503	0.2514	0.1668	0.041*
H31B	0.6368	0.3060	0.0980	0.041*
C32	0.7633 (3)	0.2131 (2)	0.0858 (2)	0.0515 (10)

H32A	0.7615	0.1544	0.0934	0.062*
H32B	0.7645	0.2223	0.0347	0.062*
C33	0.8936 (4)	0.2238 (3)	0.1884 (2)	0.0699 (14)
H33A	0.9712	0.2436	0.2032	0.105*
H33B	0.8911	0.1654	0.1937	0.105*
H33C	0.8334	0.2482	0.2174	0.105*
C34	0.8959 (5)	0.3227 (3)	0.0999 (4)	0.0793 (19)
H34A	0.8814	0.3311	0.0498	0.119*
H34B	0.9783	0.3345	0.1115	0.119*
H34C	0.8451	0.3583	0.1266	0.119*
C35	1.1025 (5)	0.1265 (3)	0.0547 (3)	0.0804 (16)
H35A	1.0493	0.1425	0.0162	0.121*
H35B	1.0581	0.0978	0.0901	0.121*
H35C	1.1638	0.0914	0.0366	0.121*
C36	1.1559 (4)	0.1969 (4)	0.0856 (2)	0.0646 (13)

Table S2.20. Anisotropic displacement parameters (A^2) for **4**. The anisotropic displacement factor exponent takes the form: $-2\pi^2$ [$h^2 a^2 * U^{11}$ + ... + 2 h k a* b* U^{12}].

	U^{11}	U^{22}	U^{33}	U^{12}	U^{13}	U^{23}
U1	0.02086 (11)	0.01270 (11)	0.01397 (11)	0.00035 (4)	0.00102 (7)	−0.00101 (4)
O1	0.0267 (10)	0.0185 (11)	0.0131 (9)	0.0036 (8)	−0.0010 (7)	−0.0021 (8)
N1	0.0285 (12)	0.0167 (12)	0.0125 (11)	−0.0014 (9)	−0.0006 (9)	0.0018 (9)
C1	0.0243 (13)	0.0157 (13)	0.0131 (12)	−0.0028 (10)	−0.0003 (10)	0.0018 (10)
O2	0.0275 (10)	0.0140 (10)	0.0187 (10)	−0.0016 (8)	0.0038 (8)	0.0021 (8)
N2	0.053 (2)	0.078 (3)	0.074 (3)	−0.0347 (19)	−0.0223 (19)	0.018 (2)
C2	0.0220 (16)	0.0181 (16)	0.0192 (17)	0.0001 (10)	0.0013 (13)	0.0019 (11)
O3	0.0238 (10)	0.0178 (10)	0.0204 (10)	0.0020 (8)	0.0023 (8)	−0.0007 (8)
N3	0.051 (2)	0.136 (5)	0.078 (3)	0.017 (3)	−0.002 (2)	−0.027 (3)
C3	0.0229 (14)	0.0195 (15)	0.0188 (14)	−0.0009 (12)	−0.0043 (11)	0.0042 (12)

C4	0.0255 (14)	0.0206 (14)	0.0157 (13)	−0.0043 (11)	−0.0011 (11)	0.0023 (11)
C5	0.0285 (14)	0.0191 (14)	0.0163 (14)	0.0009 (11)	−0.0001 (11)	−0.0023 (11)
C6	0.0257 (14)	0.0204 (14)	0.0132 (13)	0.0018 (11)	0.0005 (11)	0.0043 (11)
C7	0.0287 (15)	0.0232 (15)	0.0142 (13)	0.0059 (11)	0.0033 (11)	0.0003 (11)
C8	0.0290 (15)	0.0207 (16)	0.0150 (14)	0.0070 (13)	0.0039 (12)	0.0048 (12)
C9	0.0249 (15)	0.0200 (16)	0.0154 (14)	0.0016 (12)	0.0017 (12)	0.0015 (12)
C10	0.0188 (12)	0.0165 (14)	0.0170 (13)	0.0016 (10)	−0.0013 (10)	0.0032 (11)
C11	0.0227 (14)	0.0187 (14)	0.0205 (14)	−0.0005 (11)	−0.0002 (11)	0.0002 (11)
C12	0.0255 (14)	0.0213 (15)	0.0236 (15)	0.0004 (11)	0.0053 (12)	0.0043 (12)
C13	0.0229 (14)	0.0177 (14)	0.0250 (15)	0.0000 (11)	0.0007 (11)	0.0032 (11)
C14	0.0269 (14)	0.0179 (14)	0.0187 (14)	0.0041 (11)	−0.0013 (11)	0.0003 (11)
C15	0.0234 (14)	0.0206 (15)	0.0230 (14)	0.0052 (11)	−0.0020 (11)	0.0003 (11)
C16	0.0281 (17)	0.0365 (17)	0.035 (2)	0.0087 (17)	0.0086 (14)	0.0039 (18)
C17	0.0414 (18)	0.0181 (15)	0.0367 (18)	0.0045 (13)	−0.0069 (14)	−0.0038 (13)
C18	0.0327 (16)	0.0311 (18)	0.0327 (18)	0.0089 (13)	−0.0055 (14)	−0.0027 (14)
C19	0.0343 (16)	0.0249 (16)	0.0138 (14)	0.0014 (13)	−0.0018 (12)	−0.0021 (12)
C20	0.057 (2)	0.042 (2)	0.0199 (16)	−0.0045 (17)	0.0011 (15)	0.0046 (15)
C21	0.0409 (19)	0.048 (2)	0.0304 (18)	−0.0054 (16)	−0.0083 (15)	−0.0097 (16)
C22	0.050 (2)	0.039 (2)	0.0175 (16)	0.0048 (17)	−0.0028 (15)	−0.0090 (14)
C23	0.0316 (15)	0.0167 (14)	0.0268 (15)	0.0010 (11)	0.0047 (12)	0.0043 (12)
C24	0.052 (3)	0.016 (2)	0.058 (4)	0.0033 (11)	0.020 (3)	0.0048 (12)
C25	0.0337 (17)	0.0282 (19)	0.053 (2)	−0.0073 (14)	0.0045 (15)	0.0058 (16)
C26	0.053 (2)	0.0269 (18)	0.041 (2)	0.0006 (15)	−0.0038 (17)	0.0168 (15)
C27	0.0274 (14)	0.0175 (14)	0.0294 (16)	−0.0007 (11)	0.0114 (12)	−0.0023 (12)
C28	0.0421 (18)	0.0339 (18)	0.0274 (17)	−0.0049 (14)	0.0134 (14)	−0.0085 (14)
C29	0.0460 (19)	0.0265 (17)	0.043 (2)	0.0005 (14)	0.0273 (16)	−0.0011 (15)
C30	0.0301 (16)	0.0297 (18)	0.051 (2)	0.0093 (13)	0.0079 (15)	0.0060 (16)
C31	0.0498 (19)	0.0251 (17)	0.0261 (16)	−0.0138 (14)	−0.0108 (14)	0.0000 (13)

C32	0.037 (2)	0.056 (3)	0.061 (3)	−0.0033 (17)	−0.0036 (18)	−0.009 (2)
C33	0.066 (3)	0.090 (4)	0.053 (3)	0.033 (3)	−0.012 (2)	−0.012 (2)
C34	0.053 (3)	0.048 (3)	0.138 (6)	0.002 (2)	0.023 (3)	0.010 (3)
C35	0.070 (3)	0.070 (4)	0.102 (4)	0.024 (3)	0.027 (3)	0.002 (3)
C36	0.043 (2)	0.099 (4)	0.051 (3)	0.028 (2)	0.003 (2)	−0.007 (3)

Table S2.21. Bond lengths [Å], bond angles [º], and torsion angles [º] for **4** using the symmetry codes: (i) −*x*+1, −*y*, −*z*.

U1—O3^{i}	1.7987 (18)	C8—C9	1.506 (5)
U1—O3	1.7987 (18)	C9—C14	1.395 (4)
U1—O2^{i}	2.2578 (18)	C9—C10	1.403 (4)
U1—O2	2.2578 (18)	C10—C11	1.421 (4)
U1—O1^{i}	2.2634 (17)	C11—C12	1.391 (4)
U1—O1	2.2635 (17)	C11—C27	1.539 (4)
O1—C1	1.341 (3)	C12—C13	1.399 (4)
N1—C7	1.512 (3)	C13—C14	1.388 (4)
N1—C8	1.513 (4)	C13—C23	1.537 (4)
N1—C31	1.515 (4)	C15—C16	1.528 (5)
C1—C6	1.401 (4)	C15—C17	1.541 (4)
C1—C2	1.422 (4)	C15—C18	1.544 (4)
O2—C10	1.345 (3)	C19—C20	1.524 (4)
N2—C34	1.375 (6)	C19—C22	1.530 (5)
N2—C33	1.432 (6)	C19—C21	1.536 (4)
N2—C32	1.455 (5)	C23—C26	1.527 (4)
C2—C3	1.396 (5)	C23—C25	1.529 (4)
C2—C15	1.534 (4)	C23—C24	1.533 (5)
N3—C36	1.152 (6)	C27—C30	1.534 (4)

C3—C4	1.399 (4)	C27—C28	1.536 (4)
C4—C5	1.383 (4)	C27—C29	1.536 (4)
C4—C19	1.546 (4)	C31—C32	1.582 (5)
C5—C6	1.389 (4)	C35—C36	1.445 (7)
C6—C7	1.501 (4)		
O3^{i}—U1—O3	180.00 (16)	C14—C9—C8	120.5 (3)
O3^{i}—U1—O2^{i}	90.06 (7)	C10—C9—C8	118.0 (2)
O3—U1—O2^{i}	89.94 (7)	O2—C10—C9	118.7 (2)
O3^{i}—U1—O2	89.94 (7)	O2—C10—C11	122.5 (2)
O3—U1—O2	90.06 (7)	C9—C10—C11	118.8 (2)
O2^{i}—U1—O2	180.00 (10)	C12—C11—C10	117.5 (2)
O3^{i}—U1—O1^{i}	90.27 (7)	C12—C11—C27	121.1 (2)
O3—U1—O1^{i}	89.73 (7)	C10—C11—C27	121.4 (2)
O2^{i}—U1—O1^{i}	83.65 (7)	C11—C12—C13	124.5 (3)
O2—U1—O1^{i}	96.35 (7)	C14—C13—C12	116.9 (3)
O3^{i}—U1—O1	89.73 (7)	C14—C13—C23	123.5 (2)
O3—U1—O1	90.27 (7)	C12—C13—C23	119.6 (3)
O2^{i}—U1—O1	96.35 (7)	C13—C14—C9	120.9 (3)
O2—U1—O1	83.65 (7)	C16—C15—C2	109.6 (3)
O1^{i}—U1—O1	180.00 (11)	C16—C15—C17	110.1 (3)
C1—O1—U1	160.24 (17)	C2—C15—C17	110.7 (2)
C7—N1—C8	111.5 (2)	C16—C15—C18	107.5 (2)
C7—N1—C31	113.2 (2)	C2—C15—C18	112.1 (3)
C8—N1—C31	113.6 (2)	C17—C15—C18	106.9 (2)
O1—C1—C6	118.8 (2)	C20—C19—C22	108.6 (3)
O1—C1—C2	122.1 (3)	C20—C19—C21	108.9 (3)
C6—C1—C2	119.0 (2)	C22—C19—C21	108.3 (3)
C10—O2—U1	166.99 (16)	C20—C19—C4	109.8 (2)

C34—N2—C33	114.8 (4)	C22—C19—C4	111.9 (2)
C34—N2—C32	114.7 (4)	C21—C19—C4	109.3 (2)
C33—N2—C32	115.6 (4)	C26—C23—C25	110.1 (3)
C3—C2—C1	117.0 (3)	C26—C23—C24	108.4 (3)
C3—C2—C15	122.1 (3)	C25—C23—C24	107.9 (3)
C1—C2—C15	120.8 (3)	C26—C23—C13	108.2 (2)
C2—C3—C4	124.4 (3)	C25—C23—C13	109.9 (2)
C5—C4—C3	116.8 (2)	C24—C23—C13	112.3 (3)
C5—C4—C19	122.7 (3)	C30—C27—C28	110.3 (3)
C3—C4—C19	120.5 (2)	C30—C27—C29	107.7 (3)
C4—C5—C6	121.3 (3)	C28—C27—C29	107.8 (3)
C5—C6—C1	121.3 (2)	C30—C27—C11	109.1 (2)
C5—C6—C7	120.0 (2)	C28—C27—C11	110.1 (2)
C1—C6—C7	118.6 (2)	C29—C27—C11	111.8 (2)
C6—C7—N1	109.7 (2)	N1—C31—C32	108.7 (3)
C9—C8—N1	109.8 (3)	N2—C32—C31	115.4 (3)
C14—C9—C10	121.4 (3)	N3—C36—C35	176.7 (6)

Table S2.22. Atomic coordinates and equivalent isotropic displacement parameters (A^2) for **6**. U(eq) is defined as one third of the trace of the orthogonalized U^{ij} tensor.

	x	*Y*	*Z*	U_{iso}*/U_{eq}	Occ. (<1)
U1	−0.17263 (2)	−0.29381 (2)	0.009027 (17)	0.02270 (12)	
Cl1	0.2903 (9)	0.0396 (10)	0.3034 (4)	0.079 (3)	0.627 (18)
Cl2	0.2413 (10)	−0.073 (2)	0.2842 (7)	0.095 (7)	0.378 (18)
Cl3	0.4309 (3)	−0.0233 (3)	0.1384 (3)	0.0657 (7)	
O1	−0.0230 (6)	−0.3331 (6)	0.0522 (4)	0.0323 (12)	
O2	−0.3246 (6)	−0.2608 (6)	−0.0401 (4)	0.0287 (11)	
O3	−0.2553 (5)	−0.3331 (5)	0.1579 (4)	0.0253 (10)	
O4	−0.0413 (6)	−0.1481 (6)	−0.1105 (4)	0.0348 (12)	

O5	−0.0568 (5)	−0.0734 (5)	0.0900 (4)	0.0287 (11)		
N1	−0.1968 (6)	−0.4388 (6)	−0.1626 (4)	0.0263 (12)		
N2	−0.3271 (6)	−0.5374 (6)	0.0133 (4)	0.0248 (12)		
C1	−0.0548 (9)	−0.4182 (9)	−0.1947 (7)	0.0397 (19)		
C2	−0.2828 (10)	−0.3962 (9)	−0.2429 (6)	0.0395 (19)		
C3	−0.2702 (8)	−0.5842 (8)	−0.1508 (5)	0.0282 (14)		
C4	−0.3900 (8)	−0.6115 (8)	−0.0859 (5)	0.0268 (14)		
C5	−0.3432 (7)	−0.6100 (7)	0.0906 (5)	0.0247 (14)		
C6	−0.2985 (7)	−0.5579 (8)	0.1956 (5)	0.0260 (14)		
C7	−0.3045 (7)	−0.6573 (8)	0.2665 (5)	0.0274 (14)		
C8	−0.2736 (8)	−0.6188 (9)	0.3688 (5)	0.0316 (16)		
C9	−0.2509 (8)	−0.4852 (9)	0.3986 (5)	0.0309 (16)		
C10	−0.2479 (8)	−0.3860 (8)	0.3307 (5)	0.0289 (15)		
C11	−0.2651 (7)	−0.4238 (8)	0.2258 (5)	0.0269 (14)		
C12	−0.2678 (9)	−0.7210 (10)	0.4484 (6)	0.0357 (18)		
C13	−0.160 (2)	−0.7891 (19)	0.4183 (14)	0.041 (6)	0.52	(4)
C14	−0.245 (2)	−0.6802 (18)	0.5545 (12)	0.057 (7)	0.65	(4)
C15	−0.4223 (18)	−0.8573 (19)	0.4306 (16)	0.060 (7)	0.61	(4)
C16	−0.2303 (9)	−0.2426 (9)	0.3678 (6)	0.0353 (17)		
C17	−0.0910 (10)	−0.1378 (10)	0.3427 (7)	0.044 (2)		
C18	−0.2330 (11)	−0.2313 (11)	0.4844 (7)	0.048 (2)		
C19	−0.3594 (11)	−0.2119 (12)	0.3189 (7)	0.051 (2)		
C20	−0.0663 (8)	0.0372 (8)	0.1019 (5)	0.0290 (15)		
C21	−0.2093 (10)	0.0445 (11)	0.1143 (8)	0.048 (2)		
C22	0.2711 (12)	−0.0145 (15)	0.1742 (9)	0.065 (3)		
C13'	−0.1147 (19)	−0.6418 (19)	0.5210 (14)	0.060 (7)	0.62	(4)
C14'	−0.383 (2)	−0.726 (2)	0.5173 (14)	0.071 (8)	0.74	(5)
C15'	−0.271 (2)	−0.8437 (17)	0.4062 (13)	0.040 (7)	0.51	(4)

Table S2.23. Anisotropic displacement parameters (A^2) for **6**. The anisotropic displacement factor exponent takes the form: $-2\pi^2$ [$h^2 a^{2*}U^{11}$ + ... + 2 h k a* b* U^{12}].

	U^{11}	U^{22}	U^{33}	U^{12}	U^{13}	U^{23}
U1	0.02001 (16)	0.02313 (16)	0.02766 (16)	0.01151 (10)	0.00225 (9)	−0.00111 (10)
Cl1	0.097 (5)	0.092 (6)	0.058 (3)	0.043 (5)	0.025 (3)	0.015 (3)
Cl2	0.056 (5)	0.144 (17)	0.061 (5)	0.008 (6)	0.011 (4)	0.043 (7)
Cl3	0.0458 (13)	0.0636 (17)	0.095 (2)	0.0299 (12)	0.0082 (13)	−0.0146 (15)
O1	0.026 (3)	0.034 (3)	0.037 (3)	0.014 (2)	−0.003 (2)	−0.007 (2)
O2	0.029 (3)	0.027 (3)	0.031 (2)	0.013 (2)	0.001 (2)	0.001 (2)
O3	0.027 (2)	0.024 (2)	0.030 (2)	0.015 (2)	0.0049 (19)	−0.002 (2)
O4	0.041 (3)	0.023 (3)	0.036 (3)	0.006 (2)	0.012 (2)	0.000 (2)
O5	0.033 (3)	0.018 (2)	0.036 (3)	0.010 (2)	0.009 (2)	−0.006 (2)
N1	0.031 (3)	0.027 (3)	0.024 (3)	0.014 (2)	0.006 (2)	−0.003 (2)
N2	0.021 (3)	0.025 (3)	0.028 (3)	0.010 (2)	0.004 (2)	−0.005 (2)
C1	0.039 (4)	0.035 (4)	0.046 (5)	0.011 (3)	0.022 (4)	−0.007 (4)
C2	0.059 (5)	0.034 (4)	0.029 (4)	0.024 (4)	−0.002 (3)	0.000 (3)
C3	0.028 (3)	0.029 (4)	0.030 (3)	0.012 (3)	0.005 (3)	0.002 (3)
C4	0.027 (3)	0.027 (4)	0.026 (3)	0.011 (3)	0.002 (3)	−0.005 (3)
C5	0.026 (3)	0.025 (3)	0.029 (3)	0.016 (3)	0.006 (3)	−0.003 (3)
C6	0.022 (3)	0.035 (4)	0.026 (3)	0.016 (3)	0.005 (2)	0.000 (3)
C7	0.026 (3)	0.032 (4)	0.027 (3)	0.013 (3)	0.006 (3)	0.005 (3)
C8	0.033 (4)	0.039 (4)	0.031 (4)	0.022 (3)	0.009 (3)	0.006 (3)
C9	0.035 (4)	0.043 (5)	0.025 (3)	0.027 (3)	−0.001 (3)	−0.002 (3)
C10	0.028 (3)	0.035 (4)	0.031 (3)	0.022 (3)	−0.001 (3)	−0.006 (3)
C11	0.023 (3)	0.036 (4)	0.026 (3)	0.016 (3)	0.004 (3)	−0.001 (3)
C12	0.034 (4)	0.051 (5)	0.030 (4)	0.023 (4)	0.010 (3)	0.015 (4)
C13	0.044 (13)	0.042 (11)	0.056 (11)	0.037 (10)	0.008 (8)	0.006 (8)

C14	0.093 (17)	0.046 (10)	0.038 (8)	0.031 (9)	0.015 (8)	0.005 (7)
C15	0.044 (10)	0.042 (10)	0.090 (14)	0.008 (7)	0.021 (9)	0.020 (9)
C16	0.043 (4)	0.038 (4)	0.033 (4)	0.029 (4)	−0.008 (3)	−0.012 (3)
C17	0.051 (5)	0.038 (5)	0.045 (5)	0.025 (4)	−0.010 (4)	−0.007 (4)
C18	0.063 (6)	0.059 (6)	0.038 (4)	0.045 (5)	−0.006 (4)	−0.014 (4)
C19	0.062 (6)	0.067 (7)	0.043 (5)	0.052 (5)	−0.009 (4)	−0.012 (4)
C20	0.028 (4)	0.037 (4)	0.023 (3)	0.012 (3)	0.006 (3)	0.000 (3)
C21	0.038 (5)	0.056 (6)	0.062 (6)	0.031 (4)	0.009 (4)	−0.009 (5)
C22	0.047 (6)	0.092 (10)	0.076 (7)	0.044 (6)	0.016 (5)	0.027 (7)
C13'	0.055 (11)	0.048 (11)	0.069 (12)	0.014 (8)	−0.010 (8)	0.026 (9)
C14'	0.088 (16)	0.069 (13)	0.072 (12)	0.038 (10)	0.044 (10)	0.029 (9)
C15'	0.057 (16)	0.026 (9)	0.046 (10)	0.026 (9)	0.007 (8)	0.002 (7)

Table S2.24. Bond lengths [Å], bond angles [º], and torsion angles [º] for **6** using the symmetry codes: (i) −*x*, −*y*, −*z*.

U1—O1	1.769 (5)	C7—C8	1.390 (10)
U1—O2	1.775 (5)	C8—C9	1.403 (12)
U1—O3	2.229 (5)	C8—C12	1.553 (11)
U1—O5	2.384 (5)	C9—C10	1.402 (11)
U1—O4	2.399 (5)	C10—C11	1.428 (10)
U1—N2	2.497 (6)	C10—C16	1.543 (11)
U1—N1	2.684 (6)	C12—C15'	1.405 (19)
Cl1—Cl2	1.127 (17)	C12—C14	1.446 (18)
Cl1—C22	1.779 (15)	C12—C14'	1.551 (19)
Cl2—C22	1.621 (14)	C12—C13	1.605 (17)
Cl3—C22	1.778 (11)	C12—C13'	1.660 (19)
O3—C11	1.324 (9)	C12—C15	1.688 (19)
O4—C20^{i}	1.272 (9)	C13—C15'	1.06 (2)
O5—C20	1.232 (10)	C13—C13'	1.96 (3)

N1—C3	1.472 (10)	C14—C14'	1.34 (3)
N1—C1	1.489 (10)	C14—C13'	1.36 (3)
N1—C2	1.497 (10)	C15—C15'	1.56 (3)
N2—C5	1.291 (9)	C15—C14'	1.70 (3)
N2—C4	1.484 (9)	C16—C17	1.519 (13)
C3—C4	1.514 (10)	C16—C19	1.553 (11)
C5—C6	1.461 (10)	C16—C18	1.566 (12)
C6—C11	1.387 (11)	C20—O4^{i}	1.272 (9)
C6—C7	1.426 (10)	C20—C21	1.512 (11)
O1—U1—O2	176.8 (2)	C15'—C12—C14	126.4 (11)
O1—U1—O3	91.4 (2)	C15'—C12—C14'	118.1 (13)
O2—U1—O3	90.5 (2)	C14—C12—C14'	52.8 (11)
O1—U1—O5	89.8 (2)	C15'—C12—C8	113.5 (9)
O2—U1—O5	93.0 (2)	C14—C12—C8	119.8 (10)
O3—U1—O5	80.59 (18)	C14'—C12—C8	105.4 (9)
O1—U1—O4	90.9 (2)	C15'—C12—C13	40.4 (10)
O2—U1—O4	88.5 (2)	C14—C12—C13	112.4 (12)
O3—U1—O4	152.73 (19)	C14'—C12—C13	145.8 (12)
O5—U1—O4	72.25 (18)	C8—C12—C13	108.3 (8)
O1—U1—N2	88.9 (2)	C15'—C12—C13'	110.4 (12)
O2—U1—N2	89.4 (2)	C14—C12—C13'	51.5 (11)
O3—U1—N2	70.06 (19)	C14'—C12—C13'	103.9 (13)
O5—U1—N2	150.58 (18)	C8—C12—C13'	104.3 (8)
O4—U1—N2	137.16 (19)	C13—C12—C13'	73.6 (11)
O1—U1—N1	87.8 (2)	C15'—C12—C15	59.7 (12)
O2—U1—N1	89.0 (2)	C14—C12—C15	106.1 (12)
O3—U1—N1	136.65 (19)	C14'—C12—C15	63.3 (11)
O5—U1—N1	142.71 (18)	C8—C12—C15	108.7 (9)

O4—U1—N1	70.59 (19)	C13—C12—C15	99.6 (12)
N2—U1—N1	66.60 (19)	C13'—C12—C15	146.7 (10)
Cl2—Cl1—C22	63.2 (7)	C15'—C13—C12	59.6 (12)
Cl1—Cl2—C22	78.4 (9)	C15'—C13—C13'	110.0 (15)
C11—O3—U1	136.0 (4)	C12—C13—C13'	54.5 (8)
C20^{i}—O4—U1	133.5 (5)	C14'—C14—C13'	139.2 (16)
C20—O5—U1	144.0 (5)	C14'—C14—C12	67.6 (11)
C3—N1—C1	107.6 (6)	C13'—C14—C12	72.4 (12)
C3—N1—C2	108.7 (6)	C15'—C15—C12	51.1 (8)
C1—N1—C2	109.5 (6)	C15'—C15—C14'	102.0 (14)
C3—N1—U1	111.0 (4)	C12—C15—C14'	54.4 (9)
C1—N1—U1	111.7 (5)	C17—C16—C10	111.3 (7)
C2—N1—U1	108.2 (4)	C17—C16—C19	110.7 (8)
C5—N2—C4	116.1 (6)	C10—C16—C19	108.7 (7)
C5—N2—U1	127.2 (5)	C17—C16—C18	108.2 (7)
C4—N2—U1	116.1 (4)	C10—C16—C18	111.6 (7)
N1—C3—C4	111.8 (6)	C19—C16—C18	106.2 (7)
N2—C4—C3	107.5 (6)	O5—C20—O4^{i}	122.9 (7)
N2—C5—C6	125.4 (7)	O5—C20—C21	119.8 (7)
C11—C6—C7	121.9 (7)	O4^{i}—C20—C21	117.1 (8)
C11—C6—C5	122.7 (7)	Cl2—C22—Cl1	38.4 (7)
C7—C6—C5	115.1 (7)	Cl2—C22—Cl3	111.2 (8)
C8—C7—C6	119.3 (7)	Cl1—C22—Cl3	112.0 (7)
C7—C8—C9	118.2 (7)	C14—C13'—C12	56.1 (10)
C7—C8—C12	121.2 (8)	C14—C13'—C13	98.1 (14)
C9—C8—C12	120.6 (7)	C12—C13'—C13	51.9 (8)
C10—C9—C8	123.6 (7)	C14—C14'—C12	59.6 (11)
C9—C10—C11	117.5 (7)	C14—C14'—C15	110.7 (15)

C9—C10—C16	121.3 (7)	C12—C14'—C15	62.3 (10)
C11—C10—C16	121.2 (7)	C13—C15'—C12	80.0 (14)
O3—C11—C6	120.3 (6)	C13—C15'—C15	147.8 (19)
O3—C11—C10	120.5 (7)	C12—C15'—C15	69.2 (12)
C6—C11—C10	119.1 (7)		

Table S2.25. Atomic coordinates and equivalent isotropic displacement parameters (A^2) for **7**. U(eq) is defined as one third of the trace of the orthogonalized U^{ij} tensor.

	x	*Y*	*Z*	U_{iso}*/U_{eq}	Occ. (<1)
U1	0.17721 (5)	0.301883 (13)	0.01425 (4)	0.0209 (2)	
O5	0.1265 (10)	0.3600 (3)	−0.0006 (8)	0.029 (2)	
O1	0.3321 (9)	0.3103 (3)	−0.0508 (11)	0.035 (2)	
O2	0.0235 (9)	0.2938 (3)	0.0798 (8)	0.028 (2)	
O6	0.1413 (11)	0.2500	−0.0928 (10)	0.022 (3)	
C7	0.0222 (14)	0.3784 (4)	−0.0267 (11)	0.026 (3)	
N1	0.0590 (11)	0.3131 (3)	−0.1715 (9)	0.026 (3)	
C8	−0.0075 (11)	0.4116 (4)	0.0266 (11)	0.021 (3)	
C11	−0.1772 (13)	0.3856 (4)	−0.1431 (14)	0.033 (3)	
H12	−0.2318	0.3770	−0.2023	0.039*	
C9	−0.1299 (15)	0.4286 (4)	−0.0029 (11)	0.028 (3)	
H13	−0.1536	0.4496	0.0365	0.034*	
C3	0.047 (2)	0.2500	−0.1833 (14)	0.025 (4)	
C5	−0.0350 (14)	0.3369 (4)	−0.1884 (11)	0.026 (3)	
H16	−0.0891	0.3336	−0.2531	0.031*	
C10	−0.2144 (12)	0.4162 (4)	−0.0844 (12)	0.028 (3)	
C4	0.0653 (14)	0.2844 (4)	−0.2511 (12)	0.030 (3)	
H18A	0.1518	0.2842	−0.2900	0.036*	
H18B	−0.0051	0.2868	−0.3086	0.036*	
C6	−0.0644 (13)	0.3679 (4)	−0.1173 (11)	0.028 (3)	

C12	0.0862 (13)	0.4287 (4)	0.1114 (13)	0.031 (3)
C15	0.2207 (15)	0.4333 (4)	0.0593 (13)	0.035 (4)
H6A	0.2842	0.4400	0.1180	0.053*
H6B	0.2171	0.4520	0.0018	0.053*
H6C	0.2483	0.4109	0.0243	0.053*
C14	0.1009 (15)	0.4060 (4)	0.2173 (12)	0.038 (4)
H7A	0.1750	0.4149	0.2625	0.058*
H7B	0.1175	0.3813	0.1957	0.058*
H7C	0.0195	0.4074	0.2620	0.058*
C16	−0.3433 (14)	0.4341 (4)	−0.1116 (15)	0.037 (4)
C13	0.0433 (16)	0.4654 (4)	0.1480 (14)	0.043 (4)
H10A	−0.0409	0.4638	0.1885	0.064*
H10B	0.0325	0.4806	0.0814	0.064*
H10C	0.1103	0.4757	0.1980	0.064*
C17	−0.368 (2)	0.4673 (6)	−0.046 (2)	0.065 (6)
H1A	−0.3865	0.4612	0.0333	0.097*
H1B	−0.4445	0.4798	−0.0777	0.097*
H1C	−0.2903	0.4827	−0.0495	0.097*
C19	−0.4626 (17)	0.4066 (6)	−0.0968 (17)	0.062 (5)
H2A	−0.5065	0.4108	−0.0243	0.093*
H2B	−0.4283	0.3823	−0.0988	0.093*
H2C	−0.5261	0.4099	−0.1584	0.093*
C18	−0.356 (2)	0.4443 (6)	−0.2352 (17)	0.072 (7)
H3A	−0.4459	0.4525	−0.2503	0.107*
H3B	−0.3360	0.4237	−0.2826	0.107*
H3C	−0.2934	0.4635	−0.2523	0.107*
O3	0.2648 (12)	0.2500	0.0987 (10)	0.024 (3)
C1	0.407 (2)	0.2500	0.1338 (19)	0.040 (5)

H4A	0.4128	0.2545	0.2151	0.060*	0.50
H4B	0.4541	0.2686	0.0926	0.060*	0.50
H4C	0.4461	0.2268	0.1165	0.060*	0.50
O4	0.2599 (10)	0.3215 (3)	0.1971 (8)	0.034 (2)	
C2	0.3741 (15)	0.3450 (4)	0.2135 (14)	0.040 (4)	
H15A	0.4100	0.3518	0.1398	0.061*	
H15B	0.4420	0.3324	0.2569	0.061*	
H15C	0.3466	0.3663	0.2547	0.061*	

Table S2.26. Anisotropic displacement parameters (A^2) for **7**. The anisotropic displacement factor exponent takes the form: $-2\pi^2$ [$h^2 a^2 * U^{11}$ + ... + 2 h k a* b* U^{12}].

	U^{11}	U^{22}	U^{33}	U^{12}	U^{13}	U^{23}
U1	0.0203 (3)	0.0268 (4)	0.0156 (3)	0.00028 (19)	−0.00108 (17)	−0.00190 (17)
O5	0.024 (5)	0.031 (6)	0.032 (6)	0.000 (5)	−0.004 (4)	−0.005 (4)
O1	0.025 (5)	0.047 (6)	0.033 (6)	0.004 (4)	−0.010 (5)	−0.001 (5)
O2	0.019 (5)	0.043 (6)	0.022 (5)	0.001 (4)	0.007 (4)	−0.006 (4)
O6	0.023 (7)	0.027 (7)	0.016 (6)	0.000	−0.006 (5)	0.000
C7	0.026 (7)	0.029 (8)	0.022 (7)	0.004 (6)	−0.006 (5)	−0.001 (5)
N1	0.030 (6)	0.036 (7)	0.013 (5)	0.000 (5)	−0.001 (5)	0.001 (5)
C8	0.005 (5)	0.029 (8)	0.028 (7)	−0.003 (5)	−0.001 (4)	−0.005 (5)
C11	0.026 (7)	0.033 (8)	0.039 (9)	−0.002 (6)	−0.008 (6)	−0.001 (7)
C9	0.020 (7)	0.037 (9)	0.027 (8)	−0.001 (6)	0.002 (5)	−0.004 (6)
C3	0.038 (11)	0.028 (10)	0.009 (8)	0.000	−0.003 (8)	0.000
C5	0.028 (7)	0.026 (7)	0.024 (7)	0.003 (6)	−0.002 (6)	−0.003 (5)
C10	0.015 (6)	0.041 (9)	0.029 (8)	−0.004 (6)	0.000 (5)	−0.004 (6)
C4	0.035 (8)	0.030 (8)	0.025 (7)	−0.003 (6)	0.003 (6)	−0.001 (6)
C6	0.029 (7)	0.030 (8)	0.024 (7)	−0.001 (6)	0.003 (6)	−0.003 (6)
C12	0.022 (7)	0.034 (8)	0.037 (8)	0.000 (6)	0.000 (6)	−0.006 (6)
C15	0.035 (8)	0.038 (9)	0.034 (9)	−0.018 (7)	−0.010 (7)	0.005 (7)

C14	0.041 (9)	0.048 (10)	0.026 (8)	0.000 (8)	0.002 (6)	−0.005 (7)
C16	0.025 (8)	0.043 (9)	0.044 (10)	0.013 (7)	−0.001 (6)	−0.006 (7)
C13	0.051 (10)	0.038 (9)	0.038 (9)	−0.005 (8)	−0.013 (8)	−0.005 (7)
C17	0.059 (13)	0.064 (14)	0.072 (14)	0.015 (11)	−0.021 (11)	−0.020 (12)
C19	0.034 (9)	0.099 (16)	0.054 (12)	−0.004 (10)	0.000 (9)	0.008 (11)
C18	0.085 (15)	0.080 (15)	0.050 (13)	0.046 (12)	−0.008 (11)	0.012 (11)
O3	0.018 (6)	0.032 (8)	0.022 (7)	0.000	−0.010 (5)	0.000
C1	0.033 (12)	0.054 (15)	0.034 (12)	0.000	−0.012 (10)	0.000
O4	0.032 (5)	0.042 (6)	0.028 (6)	−0.006 (5)	−0.009 (4)	−0.008 (5)
C2	0.043 (9)	0.040 (9)	0.039 (9)	−0.007 (8)	−0.015 (7)	−0.002 (7)

Table S2.27. Bond lengths [Å], bond angles [º], and torsion angles [º] for **7** using the symmetry codes: (i) *x*, −*y*+1/2, *z*.

U1—O2	1.767 (9)	C11—C6	1.358 (19)
U1—O1	1.776 (11)	C11—C10	1.398 (19)
U1—O5	2.252 (11)	C9—C10	1.371 (19)
U1—O6	2.356 (7)	C3—C4	1.534 (16)
U1—O3	2.366 (7)	C3—C4^{i}	1.534 (16)
U1—O4	2.436 (9)	C5—C6	1.469 (18)
U1—N1	2.540 (11)	C10—C16	1.503 (18)
U1—U1^{i}	3.9050 (11)	C12—C15	1.505 (19)
O5—C7	1.302 (17)	C12—C13	1.51 (2)
O6—C3	1.44 (2)	C12—C14	1.52 (2)
O6—U1^{i}	2.356 (7)	C16—C17	1.50 (2)
C7—C8	1.430 (19)	C16—C18	1.52 (2)
C7—C6	1.441 (18)	C16—C19	1.60 (2)
N1—C5	1.322 (17)	O3—C1	1.50 (2)
N1—C4	1.437 (17)	O3—U1^{i}	2.366 (7)
C8—C9	1.438 (19)	O4—C2	1.468 (17)

C8—C12	1.525 (18)		
O2—U1—O1	179.5 (5)	C5—N1—C4	116.3 (12)
O2—U1—O5	90.0 (4)	C5—N1—U1	125.7 (9)
O1—U1—O5	89.7 (4)	C4—N1—U1	114.9 (9)
O2—U1—O6	87.6 (4)	C7—C8—C9	117.5 (12)
O1—U1—O6	93.0 (5)	C7—C8—C12	121.9 (11)
O5—U1—O6	136.6 (3)	C9—C8—C12	120.6 (12)
O2—U1—O3	90.2 (4)	C6—C11—C10	121.3 (14)
O1—U1—O3	90.0 (5)	C10—C9—C8	124.0 (14)
O5—U1—O3	156.8 (3)	O6—C3—C4	107.9 (10)
O6—U1—O3	66.5 (3)	O6—C3—C4^{i}	107.9 (10)
O2—U1—O4	88.0 (4)	C4—C3—C4^{i}	114.9 (15)
O1—U1—O4	91.6 (4)	N1—C5—C6	126.6 (13)
O5—U1—O4	81.6 (3)	C9—C10—C11	117.4 (13)
O6—U1—O4	141.5 (3)	C9—C10—C16	122.9 (14)
O3—U1—O4	75.3 (3)	C11—C10—C16	119.7 (13)
O2—U1—N1	89.6 (4)	N1—C4—C3	106.6 (11)
O1—U1—N1	90.6 (5)	C11—C6—C7	123.0 (13)
O5—U1—N1	70.3 (4)	C11—C6—C5	115.6 (13)
O6—U1—N1	66.4 (4)	C7—C6—C5	121.5 (13)
O3—U1—N1	132.9 (4)	C15—C12—C13	105.9 (12)
O4—U1—N1	151.8 (4)	C15—C12—C14	108.3 (12)
O2—U1—U1^{i}	80.1 (3)	C13—C12—C14	107.7 (13)
O1—U1—U1^{i}	100.3 (4)	C15—C12—C8	110.0 (12)
O5—U1—U1^{i}	166.0 (3)	C13—C12—C8	113.3 (12)
O6—U1—U1^{i}	34.0 (2)	C14—C12—C8	111.4 (12)
O3—U1—U1^{i}	34.4 (2)	C17—C16—C10	114.1 (14)
O4—U1—U1^{i}	107.7 (2)	C17—C16—C18	106.0 (16)

N1—U1—U1^{i}	99.6 (3)	C10—C16—C18	113.1 (14)
C7—O5—U1	136.3 (10)	C17—C16—C19	110.8 (15)
C3—O6—U1	120.2 (4)	C10—C16—C19	110.1 (13)
C3—O6—U1^{i}	120.2 (4)	C18—C16—C19	101.9 (15)
U1—O6—U1^{i}	111.9 (5)	C1—O3—U1^{i}	118.5 (4)
O5—C7—C8	122.1 (12)	C1—O3—U1	118.5 (4)
O5—C7—C6	121.5 (13)	U1^{i}—O3—U1	111.2 (5)
C8—C7—C6	116.2 (12)	C2—O4—U1	124.8 (8)

Appendix 2

Supporting Information for:

Structure and Bending in the Uranyl Ion:

A Terminal *cis*-Dioxo Uranyl(VI) Moiety Supported in a

Reversible Coordination Polymer (Chapter 3)

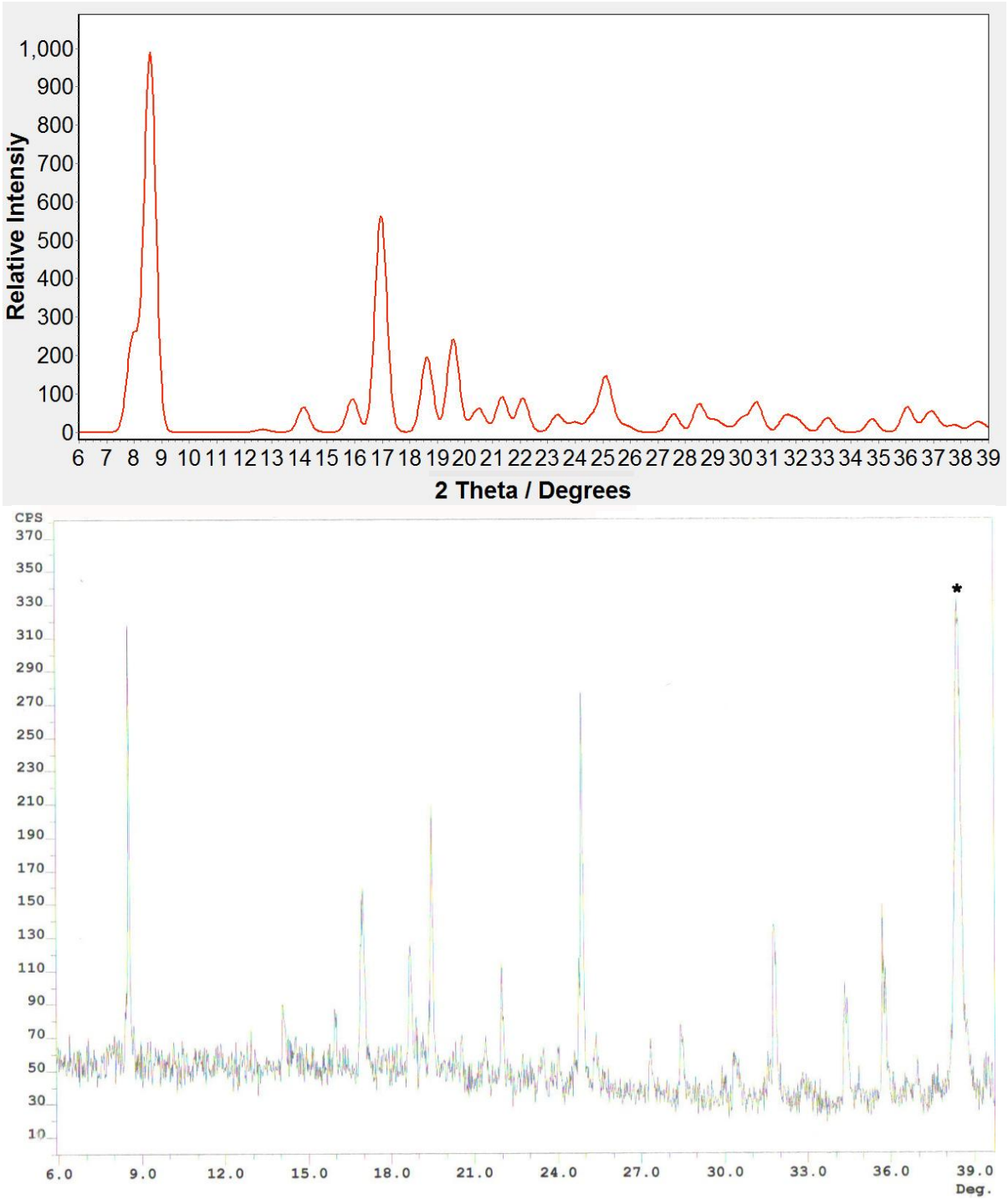

Figure S3.1. Calculated powder XRD pattern (top) for **1a**. Acquired XRD pattern (bottom) for **1a**. Asterisk (*) denotes background peak.

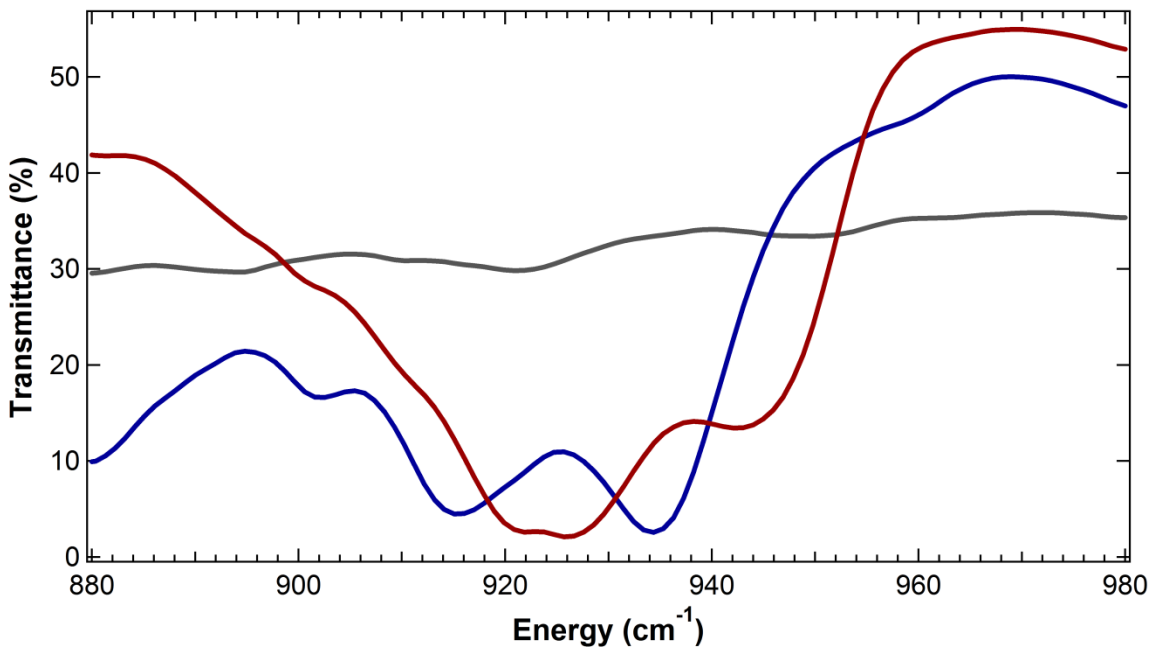

Figure S3.2. Infrared profile for **1a** (blue), after THF loss (red), and following Fc loss (gray). Samples monitored by thermogravimetric analysis and powder XRD.

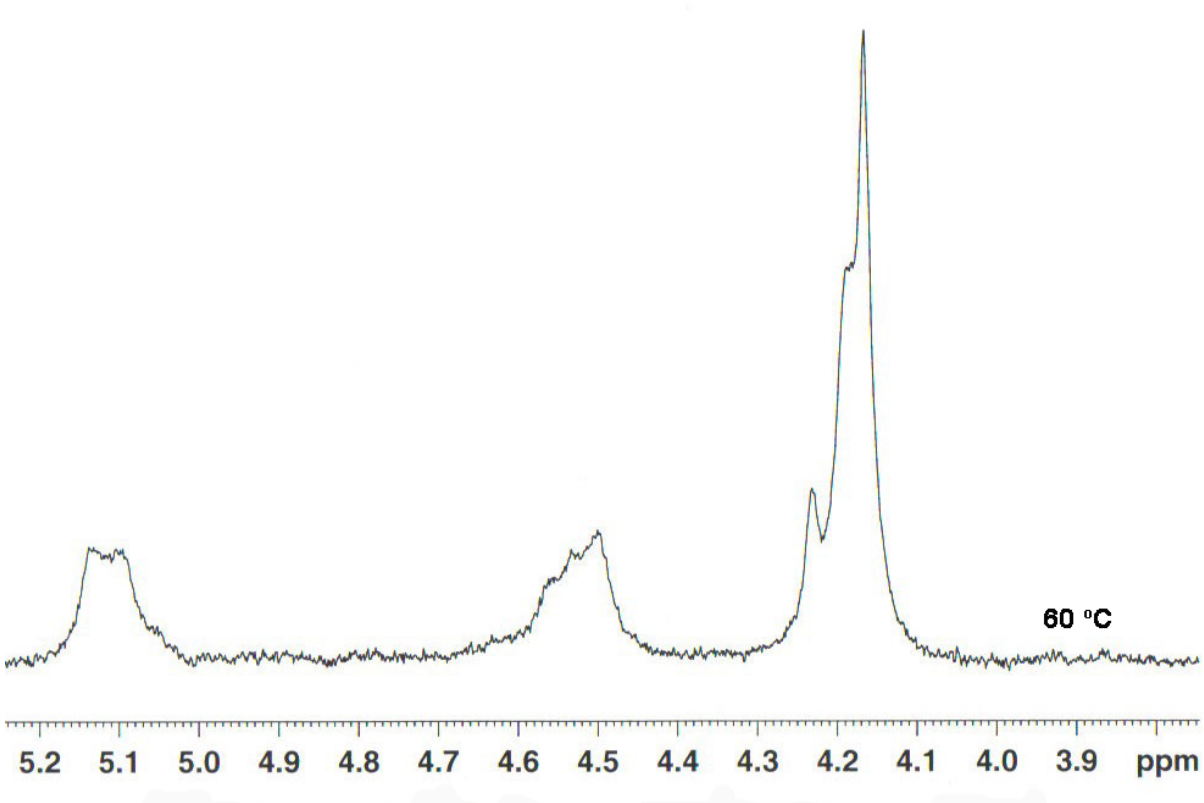

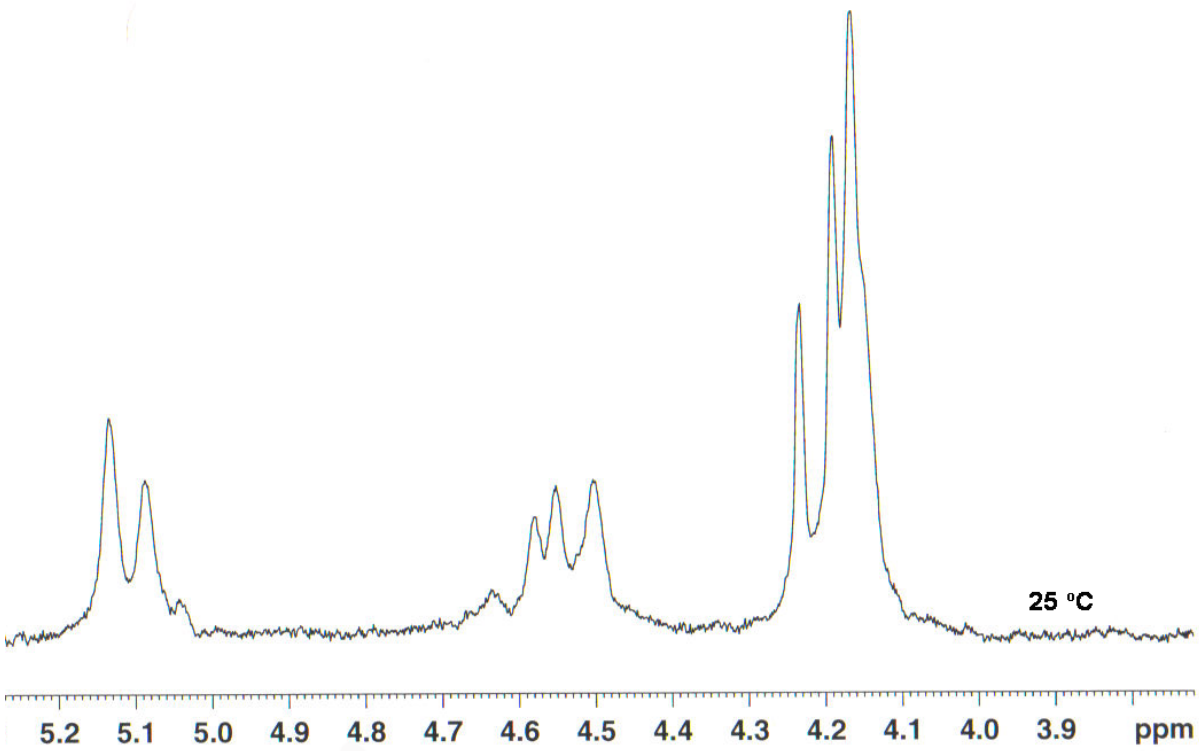

Figure S3.3. VT-^{1}H NMR for **1a** in DMSO-*d6*.

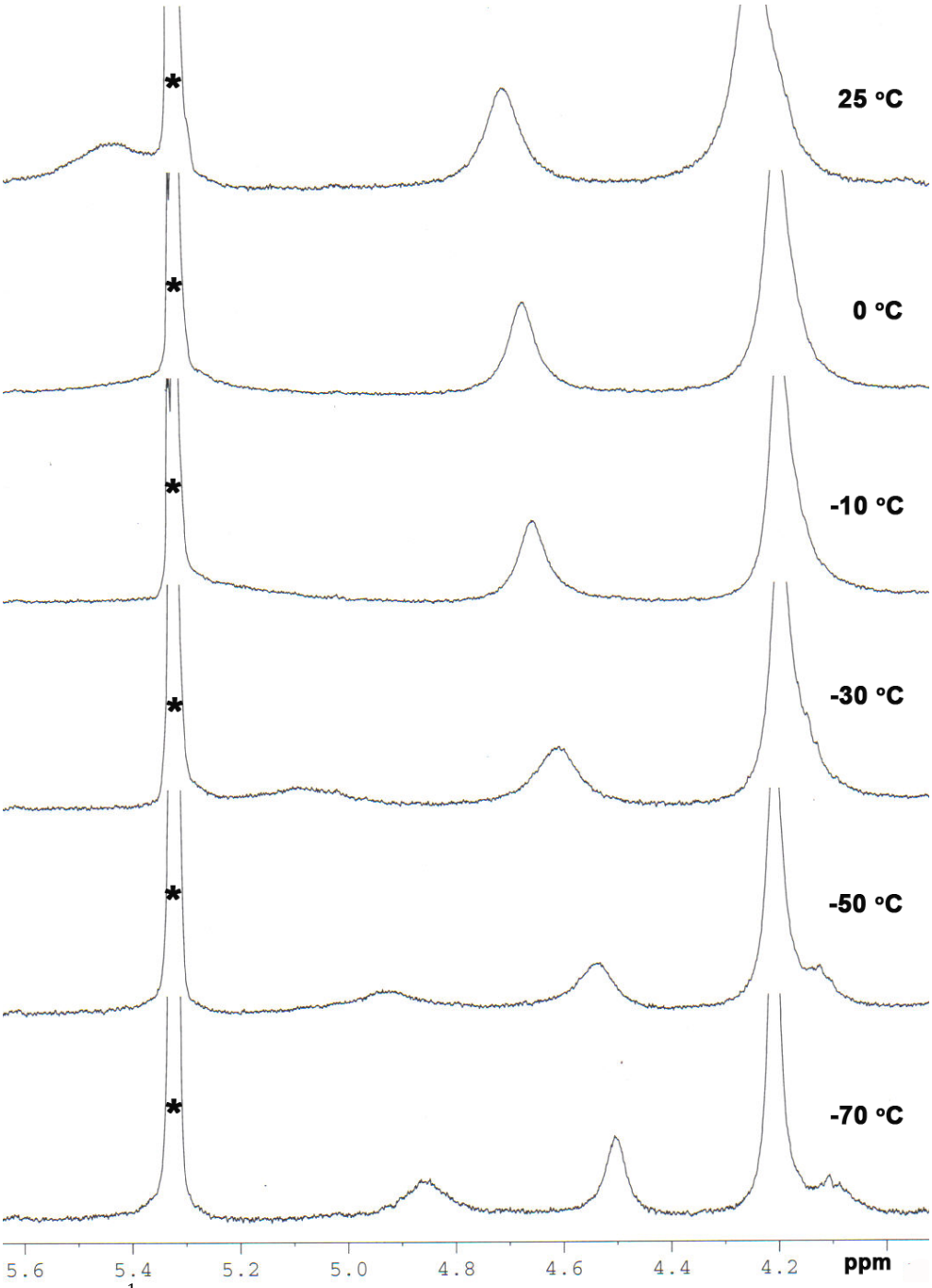

Figure S3.4. VT-^{1}H NMR for **1a** in CD_2Cl_2. Asterisks (*) denote solvent peaks.

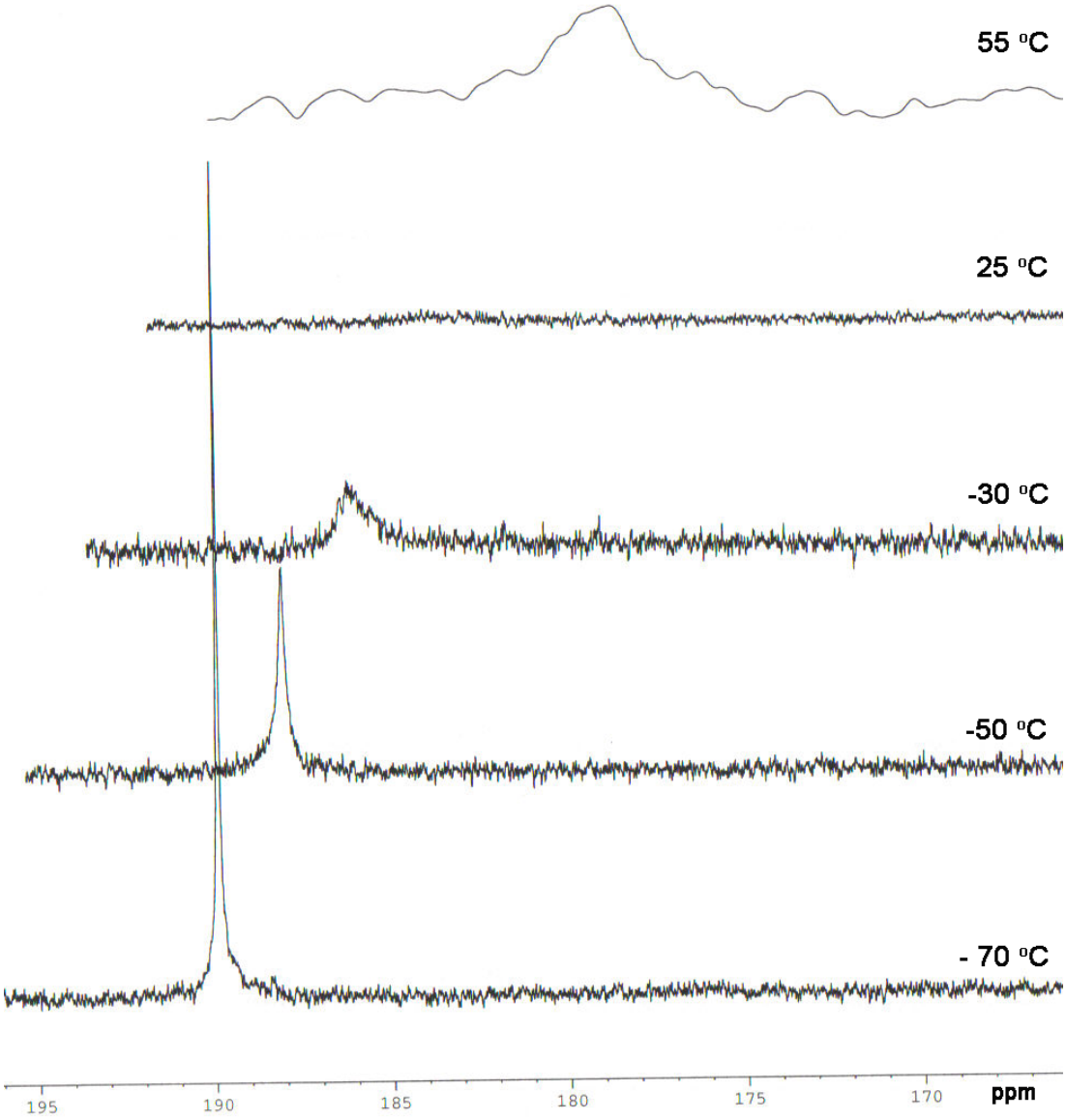

Figure S3.5. VT-^{13}C NMR for ^{13}C-labeled **1a** in MeOH-d_4. Each spectra was collected with a 1 h pulse sequence. Spectra offset for clarity.

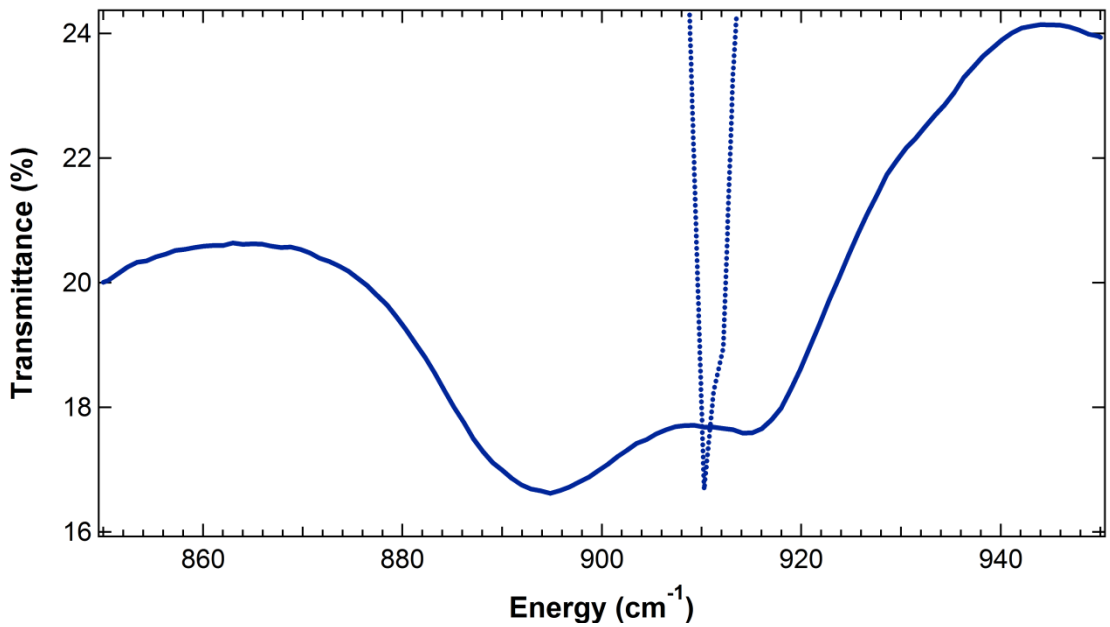

Figure S3.6. Solution infrared spectra for **1a** in MeOH (solid) vs. CH_2Cl_2 (dashed).

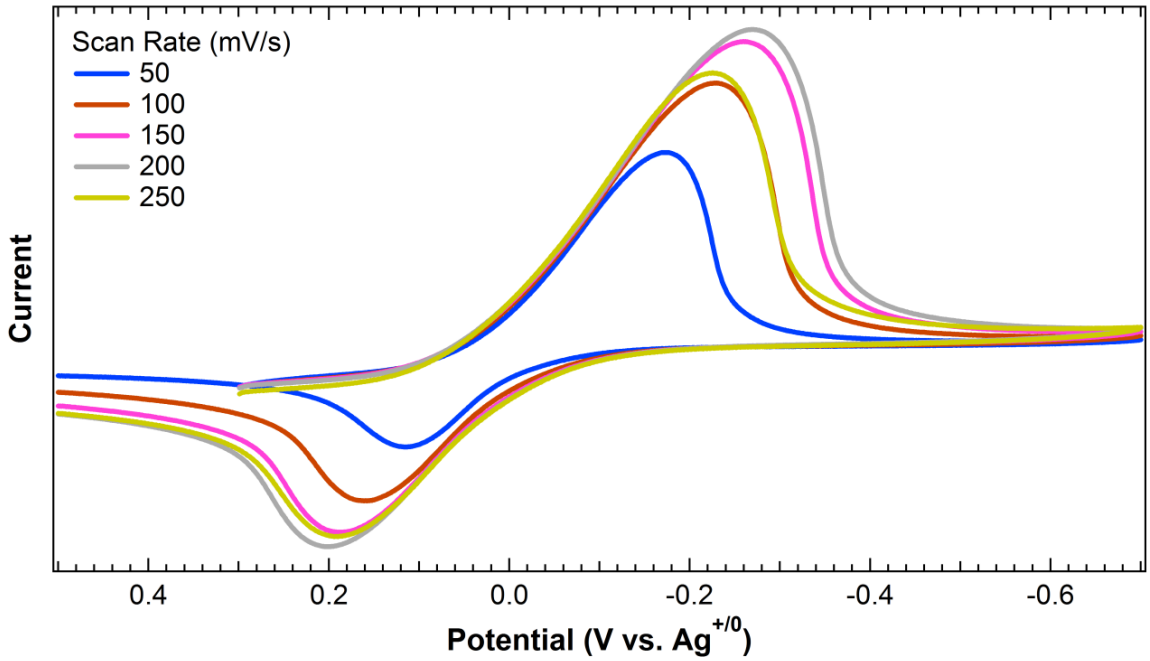

Figure S3.7. Cyclic voltammetric data for **1a** in ~0.1 M $[Bu_4N][PF_6]/MeCl_2$ solution at room temperature with a scan rate range of 50-250 mV/s. Fc/fcdc based oxidative wave shown.

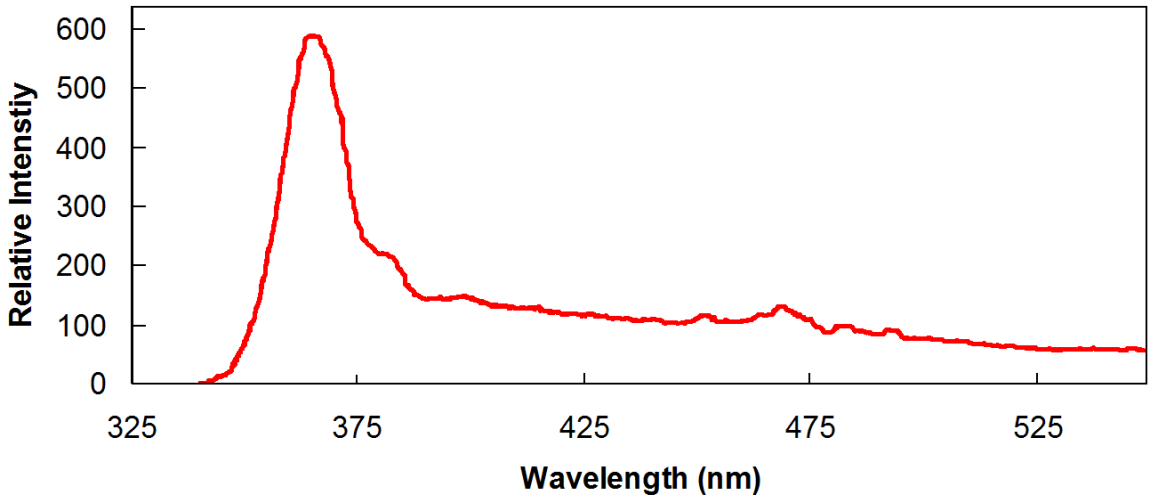

Figure S3.8. Solid State luminescence spectrum for **1a** from variable excitation between 245 and 365 nm.

Crystallographic Information

Table S3.1. Atomic coordinates and equivalent isotropic displacement parameters (A^2) for **1a**. U(eq) is defined as one third of the trace of the orthogonalized U^{ij} tensor.

	X	*Y*	*Z*	U_{iso}*/U_{eq}
U1	0.2500	0.58985 (3)	0.29417 (12)	0.03189 (17)
Fe1	0.2500	0.3020 (5)	0.47077 (11)	0.0460 (13)
O1	0.1286 (9)	0.4319 (7)	0.3279 (4)	0.0461 (19)
C1	0.1800 (19)	0.4572 (17)	0.4942 (8)	0.040 (4)
H1	0.1254	0.5056	0.4690	0.048*
Fe2	0.2500	0.3011 (4)	0.11773 (9)	0.0383 (11)
O2	−0.0626 (9)	0.3384 (8)	0.3568 (4)	0.049 (2)
C2	0.120 (2)	0.3771 (17)	0.5359 (7)	0.038 (4)
H2	0.0241	0.3607	0.5443	0.046*
O3	0.1455 (10)	0.5954 (6)	0.2299 (4)	0.0424 (18)
C3	0.2500	0.3268 (19)	0.5622 (8)	0.038 (7)
H3	0.2500	0.2691	0.5924	0.046*
O4	0.2500	0.7981 (7)	0.2921 (11)	0.049 (3)
C4	0.1751 (19)	0.2704 (10)	0.3887 (6)	0.035 (4)
C5	0.128 (2)	0.1832 (15)	0.4290 (8)	0.051 (6)
H5	0.0331	0.1692	0.4398	0.061*
C6	0.2500	0.119 (3)	0.4511 (14)	0.095 (17)
H6	0.2500	0.0502	0.4745	0.114*
C7	0.0698 (12)	0.3536 (9)	0.3559 (4)	0.036 (2)
C8	0.173 (2)	0.4676 (17)	0.1004 (8)	0.047 (5)
H8	0.1112	0.5124	0.1242	0.056*
C9	0.139 (3)	0.384 (2)	0.0557 (11)	0.057 (6)
H9	0.0449	0.3671	0.0451	0.069*
C10	0.2500	0.328 (3)	0.0290 (14)	0.070 (11)

H10	0.2500	0.2676	0.0001	0.085*
C11	0.174 (3)	0.2636 (17)	0.2031 (10)	0.078 (9)
H11	0.1130	0.3101	0.2265	0.093*
C12	0.135 (3)	0.1763 (17)	0.1589 (7)	0.071 (9)
H12	0.0413	0.1539	0.1493	0.086*
C13	0.2500	0.133 (2)	0.1346 (14)	0.053 (8)
H13	0.2500	0.0781	0.1032	0.063*
C18	0.1842	0.9918	0.2957	0.100*
C14	0.2500	0.8749	0.2439	0.100*
C15	0.1593	0.8736	0.2648	0.100*
C16	0.1563	0.8728	0.3251	0.100*
C17	0.2500	0.8755	0.3480	0.100*

Table S3.2. Anisotropic displacement parameters (A^2) for **1a**. The anisotropic displacement factor exponent takes the form: $-2\pi^2$ [$h^2 a^2 * U^{11}$ + ... + 2 h k a* b* U^{12}].

	U^{11}	U^{22}	U^{33}	U^{12}	U^{13}	U^{23}
U1	0.0351 (2)	0.0275 (2)	0.0331 (2)	0.000	0.000	0.0020 (5)
Fe1	0.059 (3)	0.046 (3)	0.033 (2)	0.000	0.000	0.002 (2)
O1	0.043 (5)	0.048 (5)	0.048 (4)	0.004 (4)	0.006 (4)	0.003 (4)
C1	0.033 (7)	0.040 (8)	0.048 (9)	−0.008 (7)	−0.005 (6)	0.019 (7)
Fe2	0.050 (3)	0.039 (2)	0.0259 (19)	0.000	0.000	−0.001 (2)
O2	0.042 (5)	0.049 (5)	0.057 (4)	−0.012 (4)	−0.013 (4)	0.018 (4)
C2	0.044 (10)	0.051 (8)	0.019 (6)	0.006 (8)	0.005 (6)	0.007 (6)
O3	0.039 (4)	0.045 (5)	0.044 (4)	0.005 (3)	0.002 (4)	−0.003 (3)
C3	0.077 (18)	0.030 (11)	0.007 (7)	0.000	0.000	−0.014 (7)
O4	0.062 (6)	0.030 (4)	0.055 (6)	0.000	0.000	0.026 (10)
C4	0.059 (11)	0.023 (6)	0.023 (6)	−0.015 (6)	−0.008 (6)	0.018 (5)
C5	0.075 (14)	0.026 (8)	0.051 (11)	0.007 (9)	0.000 (11)	0.018 (7)
C6	0.20 (5)	0.049 (14)	0.037 (16)	0.000	0.000	0.037 (13)

C7	0.042 (6)	0.031 (5)	0.035 (4)	0.000 (4)	0.003 (4)	−0.004 (4)
C8	0.059 (10)	0.051 (11)	0.031 (6)	0.022 (8)	−0.005 (7)	0.020 (7)
C9	0.038 (9)	0.078 (12)	0.056 (12)	−0.024 (8)	−0.017 (8)	0.023 (9)
C10	0.054 (19)	0.08 (2)	0.08 (2)	0.000	0.000	−0.044 (16)
C11	0.087 (18)	0.075 (12)	0.072 (13)	0.001 (11)	−0.008 (10)	0.059 (11)
C12	0.14 (2)	0.053 (12)	0.025 (9)	−0.049 (15)	0.010 (12)	−0.002 (8)
C13	0.09 (2)	0.029 (11)	0.039 (14)	0.000	0.000	0.015 (10)

Table S3.3. Bond lengths [Å], bond angles [º], and torsion angles [º] for **1a** using the symmetry codes: (i) −*x*+1/2, *y*, *z*; (ii) *x*+1/2, −*y*+1, *z*; (iii) −*x*, −*y*+1, *z*.

U1—O3	1.745 (9)	O4—C16^{i}	1.446 (15)
U1—O3^{i}	1.745 (9)	O4—C16	1.446 (15)
U1—O1^{i}	2.298 (9)	O4—C17	1.54 (2)
U1—O1	2.298 (9)	C4—C5	1.426 (19)
U1—O2^{ii}	2.415 (8)	C4—C4^{i}	1.43 (4)
U1—O2^{iii}	2.415 (8)	C4—C7	1.574 (18)
U1—O4	2.425 (8)	C5—C6	1.47 (2)
Fe1—C4^{i}	1.995 (15)	C5—H5	0.9500
Fe1—C4	1.995 (15)	C6—C5^{i}	1.47 (2)
Fe1—C1^{i}	2.00 (2)	C6—H6	0.9500
Fe1—C1	2.00 (2)	C8—C9	1.43 (3)
Fe1—C5	2.03 (2)	C8—C8^{i}	1.46 (4)
Fe1—C5^{i}	2.03 (2)	C8—H8	0.9500
Fe1—C3	2.056 (17)	C9—C10	1.37 (3)
Fe1—C2^{i}	2.10 (2)	C9—H9	0.9500
Fe1—C2	2.10 (2)	C10—C9^{i}	1.37 (3)
Fe1—C6	2.18 (4)	C10—H10	0.9500
O1—C7	1.238 (14)	C11—C11^{i}	1.45 (6)
C1—C1^{i}	1.33 (4)	C11—C12	1.46 (3)

C1—C2	1.44 (2)	C11—H11	0.9500
C1—H1	0.9500	C12—C13	1.32 (3)
Fe2—C9	1.98 (3)	C12—H12	0.9500
Fe2—C9^{i}	1.98 (3)	C13—C12^{i}	1.32 (3)
Fe2—C13	1.99 (3)	C13—H13	0.9500
Fe2—C10	2.00 (3)	C18—C18^{i}	1.2532
Fe2—C12	2.040 (18)	C18—C16	1.5551
Fe2—C12^{i}	2.040 (18)	C18—C15	1.5566
Fe2—C11^{i}	2.08 (2)	C18—C14	1.8908
Fe2—C11	2.08 (2)	C18—C17	1.8926
Fe2—C8^{i}	2.107 (18)	C14—C15^{i}	0.9812
Fe2—C8	2.107 (18)	C14—C15	0.9812
O2—C7	1.273 (14)	C14—C18^{i}	1.8908
O2—U1^{iii}	2.415 (8)	C14—C16^{i}	2.0165
C2—C3	1.49 (2)	C14—C16	2.0165
C2—H2	0.9500	C15—C16	1.3431
C3—C2^{i}	1.49 (2)	C15—C15^{i}	1.7274
C3—H3	0.9500	C16—C17	1.0282
O4—C15^{i}	1.374 (10)	C16—C16^{i}	1.7846
O4—C15	1.374 (10)	C17—C16^{i}	1.0282
O4—C14	1.397 (17)	C17—C18^{i}	1.8926
O3—U1—O3^{i}	69.5 (6)	C15—O4—C16	56.8 (3)
O3—U1—O1^{i}	125.8 (3)	C14—O4—C16	90.3 (4)
O3^{i}—U1—O1^{i}	90.6 (3)	C16^{i}—O4—C16	76.2 (9)
O3—U1—O1	90.6 (3)	C15^{i}—O4—C17	89.1 (7)
O3^{i}—U1—O1	125.8 (3)	C15—O4—C17	89.1 (7)
O1^{i}—U1—O1	60.4 (4)	C14—O4—C17	104.3 (6)
O3—U1—O2^{ii}	152.0 (4)	C16^{i}—O4—C17	40.2 (5)

O3^{i}—U1—O2^{ii}	92.3 (4)	C16—O4—C17	40.2 (5)
O1^{i}—U1—O2^{ii}	73.5 (3)	C15^{i}—O4—U1	130.4 (8)
O1—U1—O2^{ii}	117.4 (3)	C15—O4—U1	130.4 (8)
O3—U1—O2^{iii}	92.3 (4)	C14—O4—U1	130.9 (13)
O3^{i}—U1—O2^{iii}	152.0 (4)	C16^{i}—O4—U1	126.3 (7)
O1^{i}—U1—O2^{iii}	117.4 (3)	C16—O4—U1	126.3 (7)
O1—U1—O2^{iii}	73.5 (3)	C17—O4—U1	124.8 (10)
O2^{ii}—U1—O2^{iii}	95.3 (4)	C5—C4—C4^{i}	108.3 (11)
O3—U1—O4	87.0 (5)	C5—C4—C7	122.0 (15)
O3^{i}—U1—O4	87.0 (5)	C4^{i}—C4—C7	129.6 (7)
O1^{i}—U1—O4	143.7 (4)	C5—C4—Fe1	70.6 (9)
O1—U1—O4	143.7 (4)	C4^{i}—C4—Fe1	69.1 (5)
O2^{ii}—U1—O4	70.4 (4)	C7—C4—Fe1	122.6 (9)
O2^{iii}—U1—O4	70.4 (4)	C4—C5—C6	109.1 (18)
C4^{i}—Fe1—C4	41.9 (10)	C4—C5—Fe1	67.9 (10)
C4^{i}—Fe1—C1^{i}	106.6 (7)	C6—C5—Fe1	75.2 (17)
C4—Fe1—C1^{i}	121.7 (6)	C4—C5—H5	125.4
C4^{i}—Fe1—C1	121.7 (6)	C6—C5—H5	125.4
C4—Fe1—C1	106.6 (7)	Fe1—C5—H5	123.0
C1^{i}—Fe1—C1	39.0 (10)	C5^{i}—C6—C5	104 (2)
C4^{i}—Fe1—C5	70.1 (8)	C5^{i}—C6—Fe1	64.2 (15)
C4—Fe1—C5	41.5 (6)	C5—C6—Fe1	64.2 (15)
C1^{i}—Fe1—C5	158.0 (8)	C5^{i}—C6—H6	127.8
C1—Fe1—C5	123.0 (7)	C5—C6—H6	127.8
C4^{i}—Fe1—C5^{i}	41.5 (5)	Fe1—C6—H6	135.2
C4—Fe1—C5^{i}	70.1 (8)	O1—C7—O2	123.9 (10)
C1^{i}—Fe1—C5^{i}	123.0 (7)	O1—C7—C4	113.5 (10)
C1—Fe1—C5^{i}	158.0 (8)	O2—C7—C4	122.5 (10)

C5—Fe1—C5^{i}	69.7 (11)	C9—C8—C8^{i}	103.0 (13)
C4^{i}—Fe1—C3	158.8 (5)	C9—C8—Fe2	64.9 (13)
C4—Fe1—C3	158.8 (5)	C8^{i}—C8—Fe2	69.7 (6)
C1^{i}—Fe1—C3	67.3 (8)	C9—C8—H8	128.5
C1—Fe1—C3	67.3 (8)	C8^{i}—C8—H8	128.5
C5—Fe1—C3	123.3 (7)	Fe2—C8—H8	128.2
C5^{i}—Fe1—C3	123.3 (7)	C10—C9—C8	117 (2)
C4^{i}—Fe1—C2^{i}	119.9 (8)	C10—C9—Fe2	70.5 (19)
C4—Fe1—C2^{i}	157.0 (6)	C8—C9—Fe2	74.2 (13)
C1^{i}—Fe1—C2^{i}	41.0 (6)	C10—C9—H9	121.6
C1—Fe1—C2^{i}	68.9 (8)	C8—C9—H9	121.6
C5—Fe1—C2^{i}	159.7 (7)	Fe2—C9—H9	125.4
C5^{i}—Fe1—C2^{i}	105.2 (9)	C9^{i}—C10—C9	100 (3)
C3—Fe1—C2^{i}	42.0 (6)	C9^{i}—C10—Fe2	69.2 (17)
C4^{i}—Fe1—C2	157.0 (6)	C9—C10—Fe2	69.2 (17)
C4—Fe1—C2	119.9 (8)	C9^{i}—C10—H10	129.9
C1^{i}—Fe1—C2	68.9 (8)	C9—C10—H10	129.9
C1—Fe1—C2	41.0 (6)	Fe2—C10—H10	123.6
C5—Fe1—C2	105.2 (9)	C11^{i}—C11—C12	104.8 (16)
C5^{i}—Fe1—C2	159.7 (7)	C11^{i}—C11—Fe2	69.6 (8)
C3—Fe1—C2	42.0 (6)	C12—C11—Fe2	67.8 (11)
C2^{i}—Fe1—C2	72.4 (12)	C11^{i}—C11—H11	127.6
C4^{i}—Fe1—C6	68.6 (8)	C12—C11—H11	127.6
C4—Fe1—C6	68.6 (8)	Fe2—C11—H11	126.6
C1^{i}—Fe1—C6	160.0 (5)	C13—C12—C11	109 (3)
C1—Fe1—C6	160.0 (5)	C13—C12—Fe2	68.7 (15)
C5—Fe1—C6	40.6 (6)	C11—C12—Fe2	70.7 (11)
C5^{i}—Fe1—C6	40.6 (6)	C13—C12—H12	125.5

C3—Fe1—C6	109.7 (10)	C11—C12—H12	125.5
C2^{i}—Fe1—C6	123.2 (8)	Fe2—C12—H12	126.7
C2—Fe1—C6	123.2 (8)	C12^{i}—C13—C12	112 (3)
C7—O1—U1	168.9 (8)	C12^{i}—C13—Fe2	73.0 (14)
C1^{i}—C1—C2	113.5 (11)	C12—C13—Fe2	73.0 (14)
C1^{i}—C1—Fe1	70.5 (5)	C12^{i}—C13—H13	123.8
C2—C1—Fe1	73.4 (13)	C12—C13—H13	123.8
C1^{i}—C1—H1	123.2	Fe2—C13—H13	121.8
C2—C1—H1	123.2	C18^{i}—C18—C16	99.8
Fe1—C1—H1	124.5	C18^{i}—C18—C15	98.8
C9—Fe2—C9^{i}	64.1 (15)	C16—C18—C15	51.1
C9—Fe2—C13	127.3 (11)	C18^{i}—C18—C14	70.6
C9^{i}—Fe2—C13	127.3 (11)	C16—C18—C14	70.9
C9—Fe2—C10	40.3 (10)	C15—C18—C14	31.2
C9^{i}—Fe2—C10	40.3 (10)	C18^{i}—C18—C17	70.7
C13—Fe2—C10	109.8 (14)	C16—C18—C17	32.9
C9—Fe2—C12	111.8 (11)	C15—C18—C17	71.9
C9^{i}—Fe2—C12	160.6 (9)	C14—C18—C17	75.6
C13—Fe2—C12	38.3 (7)	C15^{i}—C14—C15	123.3
C10—Fe2—C12	123.7 (10)	C15^{i}—C14—O4	68.0 (2)
C9—Fe2—C12^{i}	160.6 (9)	C15—C14—O4	68.0 (2)
C9^{i}—Fe2—C12^{i}	111.8 (11)	C15^{i}—C14—C18^{i}	55.3
C13—Fe2—C12^{i}	38.3 (7)	C15—C14—C18^{i}	90.8
C10—Fe2—C12^{i}	123.7 (10)	O4—C14—C18^{i}	89.5 (7)
C12—Fe2—C12^{i}	65.2 (15)	C15^{i}—C14—C18	90.8
C9—Fe2—C11^{i}	157.3 (11)	C15—C14—C18	55.3
C9^{i}—Fe2—C11^{i}	123.5 (11)	O4—C14—C18	89.5 (7)
C13—Fe2—C11^{i}	67.7 (10)	C18^{i}—C14—C18	38.7

C10—Fe2—C11^{i}	159.2 (8)	C15^{i}—C14—C16^{i}	35.4
C12—Fe2—C11^{i}	68.1 (9)	C15—C14—C16^{i}	87.9
C12^{i}—Fe2—C11^{i}	41.6 (7)	O4—C14—C16^{i}	45.8 (6)
C9—Fe2—C11	123.5 (11)	C18^{i}—C14—C16^{i}	46.8
C9^{i}—Fe2—C11	157.3 (11)	C18—C14—C16^{i}	66.9
C13—Fe2—C11	67.7 (10)	C15^{i}—C14—C16	87.9
C10—Fe2—C11	159.2 (8)	C15—C14—C16	35.4
C12—Fe2—C11	41.6 (7)	O4—C14—C16	45.8 (6)
C12^{i}—Fe2—C11	68.1 (9)	C18^{i}—C14—C16	66.9
C11^{i}—Fe2—C11	40.8 (15)	C18—C14—C16	46.8
C9—Fe2—C8^{i}	67.2 (9)	C16^{i}—C14—C16	52.5
C9^{i}—Fe2—C8^{i}	40.9 (8)	C14—C15—C16	119.5
C13—Fe2—C8^{i}	159.7 (6)	C14—C15—O4	70.5 (6)
C10—Fe2—C8^{i}	71.1 (11)	C16—C15—O4	64.3 (9)
C12—Fe2—C8^{i}	157.6 (9)	C14—C15—C18	93.6
C12^{i}—Fe2—C8^{i}	123.4 (8)	C16—C15—C18	64.4
C11^{i}—Fe2—C8^{i}	103.9 (8)	O4—C15—C18	105.9 (7)
C11—Fe2—C8^{i}	118.8 (9)	C14—C15—C15^{i}	28.3
C9—Fe2—C8	40.9 (8)	C16—C15—C15^{i}	91.2
C9^{i}—Fe2—C8	67.2 (9)	O4—C15—C15^{i}	51.1 (3)
C13—Fe2—C8	159.7 (6)	C18—C15—C15^{i}	81.2
C10—Fe2—C8	71.1 (11)	C17—C16—C15	118.5
C12—Fe2—C8	123.4 (8)	C17—C16—O4	74.6 (7)
C12^{i}—Fe2—C8	157.6 (9)	C15—C16—O4	58.9 (8)
C11^{i}—Fe2—C8	118.8 (9)	C17—C16—C18	91.9
C11—Fe2—C8	103.9 (8)	C15—C16—C18	64.5
C8^{i}—Fe2—C8	40.6 (12)	O4—C16—C18	102.5 (5)
C7—O2—U1^{iii}	132.4 (7)	C17—C16—C16^{i}	29.8

C1—C2—C3	100.2 (17)	C15—C16—C16^{i}	88.8
C1—C2—Fe1	65.6 (12)	O4—C16—C16^{i}	51.9 (5)
C3—C2—Fe1	67.5 (10)	C18—C16—C16^{i}	80.2
C1—C2—H2	129.9	C17—C16—C14	93.5
C3—C2—H2	129.9	C15—C16—C14	25.0
Fe1—C2—H2	128.3	O4—C16—C14	43.9 (7)
C2^{i}—C3—C2	113 (2)	C18—C16—C14	62.4
C2^{i}—C3—Fe1	70.5 (10)	C16^{i}—C16—C14	63.7
C2—C3—Fe1	70.5 (10)	C16—C17—C16^{i}	120.4
C2^{i}—C3—H3	123.7	C16—C17—O4	65.19 (14)
C2—C3—H3	123.7	C16^{i}—C17—O4	65.19 (14)
Fe1—C3—H3	126.9	C16—C17—C18	55.2
C15^{i}—O4—C15	77.9 (7)	C16^{i}—C17—C18	90.2
C15^{i}—O4—C14	41.5 (4)	O4—C17—C18	85.5 (5)
C15—O4—C14	41.5 (4)	C16—C17—C18^{i}	90.2
C15^{i}—O4—C16^{i}	56.8 (3)	C16^{i}—C17—C18^{i}	55.2
C15—O4—C16^{i}	103.2 (6)	O4—C17—C18^{i}	85.5 (5)
C14—O4—C16^{i}	90.3 (4)	C18—C17—C18^{i}	38.7
C15^{i}—O4—C16	103.2 (6)		

Appendix 3

Supporting Information for:

Organouranium(V)-Imido Complexes

(Chapter 4, Parts I & II)

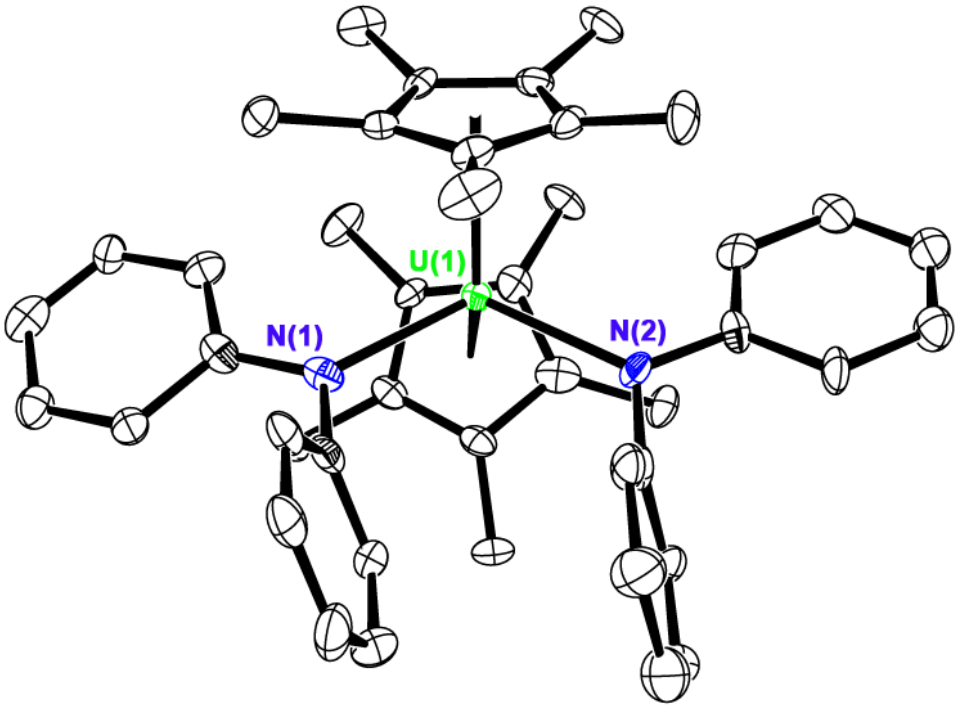

Figure S4.1. Molecular structure of **21** with thermal ellipsoids depicted at 50% probability.

Table S4.1. Atomic coordinates and equivalent isotropic displacement parameters (A^2) for **13**. U(eq) is defined as one third of the trace of the orthogonalized U^{ij} tensor.

	X	*Y*	*Z*	U_{iso}*/U_{eq}
U1	0.467067 (16)	0.239959 (12)	0.629193 (6)	0.01275 (8)
N1	0.4939 (4)	0.3501 (3)	0.64685 (15)	0.0126 (12)
N2	0.6124 (4)	0.2322 (3)	0.59051 (15)	0.0192 (12)
C21	0.5120 (5)	0.4297 (4)	0.6551 (2)	0.0160 (15)
C26	0.4853 (5)	0.4622 (4)	0.6938 (2)	0.0192 (15)
C25	0.4958 (6)	0.5423 (4)	0.7007 (2)	0.0281 (18)
H25	0.4755	0.5636	0.7262	0.034*
C24	0.5350 (6)	0.5916 (4)	0.6714 (2)	0.0323 (18)
H24	0.5412	0.6465	0.6765	0.039*
C23	0.5650 (5)	0.5603 (4)	0.6349 (2)	0.0287 (18)

H23	0.5928	0.5946	0.6150	0.034*
C22	0.5564 (5)	0.4802 (4)	0.6256 (2)	0.0220 (16)
C27	0.4454 (5)	0.4106 (4)	0.7277 (2)	0.0220 (16)
H27	0.4503	0.3546	0.7183	0.026*
C29	0.5088 (6)	0.4177 (4)	0.7663 (2)	0.0282 (18)
H29A	0.4966	0.4691	0.7790	0.042*
H29B	0.5800	0.4130	0.7593	0.042*
H29C	0.4903	0.3757	0.7854	0.042*
C28	0.3360 (6)	0.4269 (5)	0.7368 (2)	0.0318 (19)
H28A	0.3273	0.4830	0.7431	0.048*
H28B	0.3146	0.3951	0.7601	0.048*
H28C	0.2952	0.4132	0.7130	0.048*
C30	0.5931 (6)	0.4532 (4)	0.5843 (2)	0.0274 (17)
H30	0.5758	0.3962	0.5809	0.033*
C31	0.5425 (7)	0.4997 (5)	0.5501 (2)	0.039 (2)
H31A	0.4695	0.4960	0.5530	0.058*
H31B	0.5626	0.4779	0.5237	0.058*
H31C	0.5631	0.5551	0.5517	0.058*
C32	0.7066 (6)	0.4625 (5)	0.5797 (2)	0.036 (2)
H32A	0.7238	0.5186	0.5792	0.053*
H32B	0.7285	0.4376	0.5543	0.053*
H32C	0.7403	0.4371	0.6028	0.053*
C39	0.6077 (5)	0.1954 (4)	0.5513 (2)	0.0218 (16)
C44	0.6168 (5)	0.2406 (5)	0.5157 (2)	0.0283 (17)
H44	0.6250	0.2961	0.5175	0.034*
C43	0.6140 (5)	0.2045 (6)	0.4782 (2)	0.042 (2)
H43	0.6199	0.2354	0.4542	0.050*
C42	0.6028 (6)	0.1239 (6)	0.4750 (3)	0.048 (3)

H42	0.6000	0.0996	0.4490	0.057*
C41	0.5957 (6)	0.0790 (6)	0.5097 (3)	0.046 (2)
H41	0.5895	0.0233	0.5077	0.055*
C40	0.5973 (5)	0.1147 (4)	0.5476 (2)	0.0305 (18)
H40	0.5913	0.0833	0.5714	0.037*
C33	0.7105 (5)	0.2563 (4)	0.6015 (2)	0.0239 (16)
C38	0.7262 (5)	0.2990 (4)	0.6377 (2)	0.0256 (17)
H38	0.6705	0.3137	0.6540	0.031*
C37	0.8219 (5)	0.3196 (5)	0.6495 (2)	0.0302 (18)
H37	0.8309	0.3481	0.6742	0.036*
C36	0.9042 (6)	0.3003 (4)	0.6267 (2)	0.0326 (18)
H36	0.9696	0.3155	0.6351	0.039*
C35	0.8901 (5)	0.2584 (5)	0.5915 (2)	0.0313 (17)
H35	0.9466	0.2444	0.5755	0.038*
C34	0.7956 (5)	0.2361 (4)	0.5791 (2)	0.0265 (16)
H34	0.7882	0.2064	0.5547	0.032*
C11	0.5764 (5)	0.1260 (4)	0.6715 (2)	0.0218 (16)
C15	0.4841 (5)	0.0875 (4)	0.6611 (2)	0.0222 (16)
C14	0.4075 (5)	0.1212 (4)	0.6846 (2)	0.0217 (16)
C13	0.4487 (5)	0.1806 (4)	0.70861 (19)	0.0174 (15)
C12	0.5539 (5)	0.1836 (4)	0.7010 (2)	0.0192 (15)
C16	0.6792 (5)	0.0990 (5)	0.6595 (2)	0.0280 (18)
H16A	0.7280	0.1406	0.6655	0.042*
H16B	0.6803	0.0873	0.6303	0.042*
H16C	0.6966	0.0513	0.6748	0.042*
C20	0.4735 (6)	0.0170 (4)	0.6329 (2)	0.0322 (17)
H20A	0.4306	−0.0228	0.6457	0.048*
H20B	0.5399	−0.0056	0.6275	0.048*

H20C	0.4432	0.0340	0.6071	0.048*
C19	0.3064 (6)	0.0851 (4)	0.6932 (2)	0.0305 (18)
H19A	0.3080	0.0589	0.7198	0.046*
H19B	0.2903	0.0465	0.6720	0.046*
H19C	0.2552	0.1266	0.6935	0.046*
C18	0.3944 (5)	0.2185 (4)	0.7440 (2)	0.0225 (16)
H18A	0.3420	0.2536	0.7337	0.034*
H18B	0.4423	0.2489	0.7603	0.034*
H18C	0.3639	0.1774	0.7609	0.034*
C17	0.6273 (5)	0.2285 (5)	0.7252 (2)	0.0263 (17)
H17A	0.6295	0.2074	0.7529	0.039*
H17B	0.6072	0.2841	0.7261	0.039*
H17C	0.6938	0.2241	0.7127	0.039*
C5	0.2622 (5)	0.2647 (4)	0.62068 (19)	0.0179 (14)
C4	0.2751 (5)	0.1931 (4)	0.5994 (2)	0.0188 (15)
C3	0.3342 (5)	0.2089 (4)	0.5646 (2)	0.0201 (16)
C2	0.3545 (5)	0.2902 (4)	0.5633 (2)	0.0159 (14)
C1	0.3104 (4)	0.3246 (4)	0.59859 (19)	0.0124 (14)
C10	0.1985 (5)	0.2773 (5)	0.6580 (2)	0.0295 (18)
H10A	0.2419	0.2830	0.6819	0.044*
H10B	0.1539	0.2320	0.6618	0.044*
H10C	0.1583	0.3253	0.6546	0.044*
C9	0.2182 (6)	0.1175 (4)	0.6048 (3)	0.0323 (19)
H9A	0.1761	0.1210	0.6292	0.049*
H9B	0.2656	0.0737	0.6078	0.049*
H9C	0.1758	0.1083	0.5809	0.049*
C8	0.3512 (6)	0.1504 (4)	0.5305 (2)	0.0263 (17)
H8A	0.2911	0.1476	0.5134	0.039*

H8B	0.3652	0.0983	0.5421	0.039*
H8C	0.4084	0.1674	0.5140	0.039*
C7	0.3960 (6)	0.3347 (4)	0.5273 (2)	0.0268 (17)
H7A	0.4112	0.2976	0.5053	0.040*
H7B	0.4575	0.3622	0.5354	0.040*
H7C	0.3464	0.3731	0.5179	0.040*
C6	0.3000 (5)	0.4126 (4)	0.6056 (2)	0.0202 (15)
H6A	0.2421	0.4325	0.5903	0.030*
H6B	0.3609	0.4394	0.5963	0.030*
H6C	0.2901	0.4227	0.6347	0.030*

Table S4.2. Anisotropic displacement parameters (A^2) for **13**. The anisotropic displacement factor exponent takes the form: $-2\pi^2$ [h^2 a^2*U^{11} + ... + 2 h k a* b* U^{12}].

	U^{11}	U^{22}	U^{33}	U^{12}	U^{13}	U^{23}
U1	0.01213 (1)	0.01251 (1)	0.01360 (1)	−0.0001 (1)	−.00008 (1)	0.00122 (1)
N1	0.011 (3)	0.021 (3)	0.006 (3)	−0.001 (2)	0.000 (2)	0.001 (2)
N2	0.019 (3)	0.025 (3)	0.014 (3)	0.002 (3)	0.000 (2)	0.001 (2)
C21	0.014 (4)	0.020 (3)	0.014 (4)	−0.002 (3)	−0.002 (3)	0.000 (3)
C26	0.020 (4)	0.019 (3)	0.019 (4)	−0.003 (3)	−0.003 (3)	−0.003 (3)
C25	0.039 (5)	0.023 (4)	0.022 (4)	−0.001 (3)	−0.004 (3)	−0.004 (3)
C24	0.039 (5)	0.020 (4)	0.038 (5)	−0.006 (4)	−0.010 (4)	−0.006 (3)
C23	0.033 (4)	0.024 (4)	0.030 (4)	−0.009 (3)	−0.011 (3)	0.003 (3)
C22	0.015 (4)	0.026 (4)	0.024 (4)	−0.006 (3)	−0.012 (3)	0.004 (3)
C27	0.026 (4)	0.020 (4)	0.020 (4)	0.000 (3)	0.007 (3)	−0.004 (3)
C29	0.036 (5)	0.033 (4)	0.015 (4)	0.002 (3)	−0.006 (3)	−0.003 (3)
C28	0.030 (4)	0.039 (5)	0.027 (5)	0.006 (4)	−0.001 (4)	−0.003 (4)
C30	0.041 (5)	0.029 (4)	0.012 (4)	−0.007 (4)	−0.003 (3)	−0.001 (3)
C31	0.059 (6)	0.034 (4)	0.023 (4)	−0.015 (4)	−0.006 (4)	0.009 (3)
C32	0.036 (5)	0.041 (5)	0.031 (5)	−0.017 (4)	0.005 (4)	−0.007 (4)

C39	0.008 (3)	0.034 (4)	0.023 (4)	0.002 (3)	0.003 (3)	0.001 (3)
C44	0.015 (4)	0.047 (5)	0.023 (4)	0.000 (3)	0.003 (3)	−0.002 (4)
C43	0.012 (4)	0.093 (8)	0.020 (4)	0.001 (4)	0.001 (3)	−0.007 (4)
C42	0.023 (4)	0.092 (8)	0.028 (5)	0.006 (5)	−0.004 (4)	−0.037 (5)
C41	0.027 (5)	0.055 (6)	0.056 (6)	0.005 (4)	−0.006 (4)	−0.032 (5)
C40	0.019 (4)	0.034 (5)	0.039 (5)	0.006 (3)	0.003 (4)	−0.010 (4)
C33	0.016 (3)	0.037 (4)	0.018 (3)	0.003 (3)	0.000 (3)	0.008 (3)
C38	0.024 (4)	0.041 (4)	0.012 (4)	−0.003 (3)	0.000 (3)	−0.001 (3)
C37	0.022 (4)	0.046 (5)	0.023 (4)	−0.002 (3)	−0.006 (3)	−0.008 (4)
C36	0.019 (4)	0.039 (4)	0.040 (5)	−0.005 (3)	−0.009 (4)	−0.002 (4)
C35	0.015 (3)	0.042 (5)	0.037 (4)	0.004 (3)	0.006 (3)	0.009 (4)
C34	0.028 (4)	0.030 (4)	0.021 (4)	−0.003 (3)	0.000 (3)	0.003 (3)
C11	0.024 (4)	0.022 (4)	0.019 (4)	0.011 (3)	−0.002 (3)	0.011 (3)
C15	0.020 (4)	0.016 (3)	0.031 (4)	0.003 (3)	0.001 (3)	0.004 (3)
C14	0.021 (4)	0.018 (4)	0.025 (4)	−0.002 (3)	−0.001 (3)	0.014 (3)
C13	0.025 (4)	0.016 (3)	0.012 (3)	0.007 (3)	0.003 (3)	0.007 (3)
C12	0.020 (4)	0.019 (4)	0.018 (4)	0.001 (3)	0.001 (3)	0.004 (3)
C16	0.023 (4)	0.039 (5)	0.022 (4)	0.017 (3)	−0.001 (3)	0.004 (3)
C20	0.048 (5)	0.017 (3)	0.032 (4)	−0.002 (4)	−0.004 (4)	0.002 (3)
C19	0.028 (4)	0.029 (4)	0.034 (5)	−0.005 (3)	0.003 (4)	0.009 (4)
C18	0.023 (4)	0.025 (4)	0.019 (4)	0.003 (3)	0.004 (3)	0.003 (3)
C17	0.017 (4)	0.041 (4)	0.021 (4)	0.003 (3)	−0.003 (3)	0.003 (3)
C5	0.015 (3)	0.018 (3)	0.021 (4)	−0.001 (3)	−0.003 (3)	0.001 (3)
C4	0.014 (4)	0.016 (4)	0.027 (4)	0.000 (3)	−0.005 (3)	0.001 (3)
C3	0.020 (4)	0.016 (3)	0.025 (4)	0.004 (3)	−0.009 (3)	−0.005 (3)
C2	0.016 (3)	0.017 (3)	0.014 (4)	0.002 (3)	−0.007 (3)	0.001 (3)
C1	0.007 (3)	0.018 (3)	0.012 (3)	0.003 (2)	−0.009 (3)	0.001 (3)
C10	0.020 (4)	0.036 (5)	0.033 (4)	−0.001 (3)	0.004 (3)	0.001 (3)

C9	0.033 (5)	0.025 (4)	0.039 (5)	−0.008 (3)	−0.008 (4)	0.001 (4)
C8	0.030 (4)	0.023 (4)	0.026 (4)	0.004 (3)	−0.006 (4)	−0.008 (3)
C7	0.025 (4)	0.034 (4)	0.021 (4)	−0.006 (3)	−0.006 (3)	0.006 (3)
C6	0.025 (4)	0.014 (3)	0.022 (4)	0.000 (3)	−0.006 (3)	−0.004 (3)

Table S4.3. Bond lengths [Å], bond angles [º], and torsion angles [º] for **13**.

U1—N1	1.990 (6)	C15—C16	1.378 (14)
U1—N2	2.316 (7)	C16—C17	1.368 (15)
U1—C39	2.724 (6)	C17—C18	1.397 (12)
U1—C38	2.766 (7)	C19—C24	1.396 (12)
U1—C35	2.782 (8)	C19—C20	1.408 (12)
U1—C25	2.787 (7)	C20—C21	1.383 (11)
U1—C29	2.800 (8)	C21—C22	1.374 (12)
U1—C28	2.807 (8)	C22—C23	1.365 (12)
U1—C26	2.810 (8)	C23—C24	1.377 (12)
U1—C37	2.818 (8)	C25—C29	1.401 (11)
U1—C27	2.823 (7)	C25—C26	1.434 (11)
U1—C36	2.850 (7)	C25—C30	1.508 (10)
N1—C1	1.392 (10)	C26—C27	1.400 (11)
N2—C19	1.422 (10)	C26—C31	1.523 (12)
N2—C13	1.438 (10)	C27—C28	1.386 (11)
C1—C2	1.425 (10)	C27—C32	1.504 (11)
C1—C6	1.432 (11)	C28—C29	1.425 (10)
C2—C3	1.378 (11)	C28—C33	1.511 (11)
C2—C7	1.516 (11)	C29—C34	1.463 (11)
C3—C4	1.381 (12)	C35—C39	1.405 (11)
C4—C5	1.374 (12)	C35—C36	1.406 (10)
C5—C6	1.399 (12)	C35—C40	1.512 (11)
C6—C10	1.511 (11)	C36—C37	1.421 (11)

C7—C9	1.510 (11)	C36—C41	1.508 (10)
C7—C8	1.525 (11)	C37—C38	1.401 (11)
C10—C12	1.530 (12)	C37—C42	1.510 (10)
C10—C11	1.534 (11)	C38—C39	1.421 (10)
C13—C18	1.386 (12)	C38—C43	1.511 (11)
C13—C14	1.397 (12)	C39—C44	1.535 (9)
C14—C15	1.381 (12)		
N1—U1—N2	93.8 (2)	C9—C7—C2	112.4 (7)
N1—U1—C39	75.6 (2)	C9—C7—C8	111.3 (7)
N2—U1—C39	117.9 (2)	C2—C7—C8	111.8 (7)
N1—U1—C38	92.2 (2)	C6—C10—C12	111.6 (7)
N2—U1—C38	92.5 (2)	C6—C10—C11	110.4 (8)
C39—U1—C38	30.0 (2)	C12—C10—C11	108.6 (8)
N1—U1—C35	93.6 (2)	C18—C13—C14	118.8 (8)
N2—U1—C35	140.8 (2)	C18—C13—N2	120.5 (7)
C39—U1—C35	29.5 (2)	C14—C13—N2	120.7 (7)
C38—U1—C35	48.8 (2)	C15—C14—C13	120.7 (9)
N1—U1—C25	114.1 (2)	C16—C15—C14	120.0 (10)
N2—U1—C25	78.4 (2)	C17—C16—C15	120.1 (9)
C39—U1—C25	161.4 (2)	C16—C17—C18	120.6 (10)
C38—U1—C25	152.4 (2)	C13—C18—C17	119.8 (9)
C35—U1—C25	131.9 (2)	C24—C19—C20	117.5 (8)
N1—U1—C29	90.0 (2)	C24—C19—N2	122.6 (8)
N2—U1—C29	95.6 (2)	C20—C19—N2	119.8 (7)
C39—U1—C29	143.9 (2)	C21—C20—C19	119.8 (8)
C38—U1—C29	171.5 (2)	C22—C21—C20	121.4 (8)
C35—U1—C29	122.8 (2)	C23—C22—C21	119.3 (8)
C25—U1—C29	29.1 (2)	C22—C23—C24	120.7 (8)

N1—U1—C28	94.5 (2)	C23—C24—C19	121.3 (8)
N2—U1—C28	124.2 (2)	C29—C25—C26	107.5 (7)
C39—U1—C28	117.7 (2)	C29—C25—C30	126.7 (8)
C38—U1—C28	142.0 (2)	C26—C25—C30	124.6 (8)
C35—U1—C28	93.5 (2)	C29—C25—U1	76.0 (5)
C25—U1—C28	48.2 (2)	C26—C25—U1	76.0 (4)
C29—U1—C28	29.4 (2)	C30—C25—U1	123.8 (5)
N1—U1—C26	137.8 (2)	C27—C26—C25	107.6 (7)
N2—U1—C26	95.0 (2)	C27—C26—C31	126.4 (8)
C39—U1—C26	133.4 (2)	C25—C26—C31	125.9 (7)
C38—U1—C26	128.5 (2)	C27—C26—U1	76.1 (4)
C35—U1—C26	104.9 (2)	C25—C26—U1	74.3 (4)
C25—U1—C26	29.7 (2)	C31—C26—U1	118.4 (6)
C29—U1—C26	48.1 (2)	C28—C27—C26	108.9 (7)
C28—U1—C26	47.6 (2)	C28—C27—C32	122.6 (8)
N1—U1—C37	120.6 (2)	C26—C27—C32	125.8 (8)
N2—U1—C37	95.8 (2)	C28—C27—U1	75.1 (4)
C39—U1—C37	48.5 (2)	C26—C27—U1	75.1 (5)
C38—U1—C37	29.0 (2)	C32—C27—U1	131.1 (5)
C35—U1—C37	48.3 (2)	C27—C28—C29	108.2 (7)
C25—U1—C37	125.2 (2)	C27—C28—C33	124.0 (7)
C29—U1—C37	146.4 (2)	C29—C28—C33	125.9 (7)
C28—U1—C37	125.4 (2)	C27—C28—U1	76.4 (4)
C26—U1—C37	99.4 (2)	C29—C28—U1	75.0 (4)
N1—U1—C27	121.9 (2)	C33—C28—U1	127.3 (5)
N2—U1—C27	123.1 (2)	C25—C29—C28	107.8 (7)
C39—U1—C27	113.4 (2)	C25—C29—C34	126.1 (7)
C38—U1—C27	124.7 (2)	C28—C29—C34	125.4 (7)

C35—U1—C27	84.1 (2)	C25—C29—U1	75.0 (5)
C25—U1—C27	48.1 (2)	C28—C29—U1	75.5 (4)
C29—U1—C27	47.8 (2)	C34—C29—U1	123.4 (5)
C28—U1—C27	28.5 (2)	C39—C35—C36	107.8 (7)
C26—U1—C27	28.8 (2)	C39—C35—C40	125.5 (7)
C37—U1—C27	100.2 (2)	C36—C35—C40	126.5 (8)
N1—U1—C36	121.4 (2)	C39—C35—U1	72.9 (4)
N2—U1—C36	123.2 (2)	C36—C35—U1	78.2 (5)
C39—U1—C36	48.0 (2)	C40—C35—U1	119.3 (5)
C38—U1—C36	47.9 (2)	C35—C36—C37	108.2 (7)
C35—U1—C36	28.9 (2)	C35—C36—C41	127.9 (8)
C25—U1—C36	116.6 (2)	C37—C36—C41	122.1 (7)
C29—U1—C36	124.4 (2)	C35—C36—U1	72.9 (4)
C28—U1—C36	98.0 (2)	C37—C36—U1	74.3 (4)
C26—U1—C36	86.9 (2)	C41—C36—U1	130.9 (5)
C37—U1—C36	29.0 (2)	C38—C37—C36	108.0 (7)
C27—U1—C36	76.8 (2)	C38—C37—C42	126.5 (7)
C1—N1—U1	174.3 (5)	C36—C37—C42	124.3 (7)
C19—N2—C13	113.1 (6)	C38—C37—U1	73.4 (4)
C19—N2—U1	127.9 (5)	C36—C37—U1	76.7 (4)
C13—N2—U1	118.9 (5)	C42—C37—U1	125.9 (5)
N1—C1—C2	120.6 (7)	C37—C38—C39	107.7 (7)
N1—C1—C6	121.3 (7)	C37—C38—C43	125.5 (7)
C2—C1—C6	118.2 (7)	C39—C38—C43	125.8 (7)
C3—C2—C1	120.4 (8)	C37—C38—U1	77.5 (4)
C3—C2—C7	118.7 (7)	C39—C38—U1	73.4 (4)
C1—C2—C7	121.0 (7)	C43—C38—U1	124.5 (5)
C2—C3—C4	121.8 (9)	C35—C39—C38	108.4 (7)

C5—C4—C3	118.3 (9)	C35—C39—C44	126.1 (7)
C4—C5—C6	123.5 (8)	C38—C39—C44	124.4 (7)
C5—C6—C1	117.8 (8)	C35—C39—U1	77.5 (4)
C5—C6—C10	117.9 (8)	C38—C39—U1	76.7 (4)
C1—C6—C10	124.3 (8)	C44—C39—U1	122.1 (4)

Table S4.4. Atomic coordinates and equivalent isotropic displacement parameters (A^2) for **15**. U(eq) is defined as one third of the trace of the orthogonalized U^{ij} tensor.

	X	*Y*	*Z*	U_{iso}*/U_{eq}
U1	0.166590 (19)	0.529616 (10)	0.286092 (10)	0.01614 (6)
N1	0.2860 (4)	0.6131 (2)	0.2912 (2)	0.0215 (11)
N2	0.0193 (4)	0.5316 (2)	0.1931 (2)	0.0213 (10)
C34	−0.1705 (5)	0.4810 (3)	0.1198 (3)	0.0235 (13)
C7	−0.1696 (5)	0.4699 (3)	0.3226 (3)	0.0338 (15)
H7A	−0.1400	0.4234	0.3146	0.051*
H7B	−0.2147	0.4890	0.2805	0.051*
H7C	−0.2273	0.4681	0.3561	0.051*
C20	0.4922 (5)	0.5258 (3)	0.2266 (3)	0.0326 (14)
H20A	0.5522	0.4990	0.2047	0.049*
H20B	0.5372	0.5465	0.2680	0.049*
H20C	0.4545	0.5622	0.1961	0.049*
C40	−0.0750 (5)	0.5971 (3)	0.0914 (3)	0.0227 (13)
C14	0.3811 (5)	0.4451 (3)	0.3080 (3)	0.0200 (12)
C33	−0.0679 (5)	0.5352 (3)	0.1391 (3)	0.0231 (12)
C12	0.2169 (5)	0.4007 (3)	0.2290 (3)	0.0210 (12)
C15	0.3864 (5)	0.4782 (3)	0.2439 (3)	0.0243 (13)
C13	0.2773 (5)	0.3965 (3)	0.2979 (3)	0.0204 (12)
C44	−0.0053 (6)	0.6570 (3)	−0.0046 (3)	0.0310 (15)
H44	0.0516	0.6603	−0.0364	0.037*

C21	0.3663 (5)	0.6710 (3)	0.2880 (3)	0.0224 (13)
C5	0.0690 (5)	0.6137 (3)	0.3789 (3)	0.0238 (13)
C2	−0.0548 (5)	0.5158 (3)	0.3489 (3)	0.0206 (13)
C39	−0.2614 (6)	0.4867 (3)	0.0591 (3)	0.0335 (16)
H39	−0.2581	0.5254	0.0306	0.040*
C10	0.1069 (6)	0.6901 (3)	0.3871 (3)	0.0346 (16)
H10A	0.0483	0.7179	0.3555	0.052*
H10B	0.1939	0.6961	0.3776	0.052*
H10C	0.1028	0.7049	0.4333	0.052*
C11	0.2847 (5)	0.4516 (3)	0.1947 (3)	0.0225 (13)
C4	0.1251 (5)	0.5564 (3)	0.4185 (3)	0.0231 (13)
C31	0.4675 (6)	0.6914 (3)	0.4720 (3)	0.0337 (15)
H31A	0.5257	0.7308	0.4774	0.051*
H31B	0.4819	0.6631	0.5127	0.051*
H31C	0.3794	0.7080	0.4645	0.051*
C9	0.2334 (5)	0.5606 (3)	0.4787 (3)	0.0316 (15)
H9A	0.2083	0.5363	0.5173	0.047*
H9B	0.2509	0.6089	0.4906	0.047*
H9C	0.3101	0.5392	0.4666	0.047*
C6	−0.1380 (6)	0.6318 (3)	0.2869 (3)	0.0362 (16)
H6A	−0.1858	0.6616	0.3133	0.054*
H6B	−0.1970	0.6013	0.2585	0.054*
H6C	−0.0921	0.6603	0.2583	0.054*
C25	0.4302 (6)	0.7722 (3)	0.2271 (3)	0.0311 (15)
H25	0.4184	0.8004	0.1881	0.037*
C45	0.0081 (5)	0.6020 (3)	0.0430 (3)	0.0257 (13)
H45	0.0730	0.5686	0.0423	0.031*
C22	0.4656 (5)	0.6889 (3)	0.3438 (3)	0.0214 (13)*

C27	0.2488 (6)	0.6978 (3)	0.1671 (3)	0.0287 (14)
H27	0.2236	0.6485	0.1702	0.034*
C23	0.5412 (5)	0.7483 (3)	0.3393 (3)	0.0271 (14)
H23	0.6049	0.7601	0.3760	0.032*
C16	0.2643 (6)	0.4675 (3)	0.1198 (3)	0.0375 (16)
H16A	0.2788	0.5167	0.1131	0.056*
H16B	0.1768	0.4557	0.1000	0.056*
H16C	0.3240	0.4405	0.0979	0.056*
C18	0.2552 (6)	0.3384 (3)	0.3467 (3)	0.0314 (15)
H18A	0.1636	0.3301	0.3438	0.047*
H18B	0.2908	0.3517	0.3927	0.047*
H18C	0.2970	0.2963	0.3345	0.047*
C41	−0.1720 (6)	0.6480 (3)	0.0904 (3)	0.0282 (14)
H41	−0.2292	0.6457	0.1222	0.034*
C8	0.0633 (5)	0.4276 (3)	0.4387 (3)	0.0290 (14)
H8A	0.0240	0.4315	0.4794	0.043*
H8B	0.1538	0.4166	0.4511	0.043*
H8C	0.0212	0.3910	0.4100	0.043*
C3	0.0491 (5)	0.4963 (3)	0.4000 (3)	0.0225 (13)
C19	0.4763 (5)	0.4524 (3)	0.3727 (3)	0.0303 (15)
H19A	0.4307	0.4525	0.4115	0.046*
H19B	0.5232	0.4957	0.3717	0.046*
H19C	0.5361	0.4138	0.3767	0.046*
C30	0.4925 (5)	0.6471 (3)	0.4096 (3)	0.0278 (14)
H30	0.4326	0.6071	0.4054	0.033*
C35	−0.1777 (6)	0.4208 (3)	0.1600 (3)	0.0303 (14)
H35	−0.1178	0.4150	0.1998	0.036*
C24	0.5238 (6)	0.7906 (3)	0.2811 (3)	0.0336 (15)

H24	0.5745	0.8305	0.2787	0.040*
C43	−0.1015 (6)	0.7061 (3)	−0.0048 (3)	0.0343 (16)
H43	−0.1110	0.7421	−0.0370	0.041*
C17	0.1193 (6)	0.3489 (3)	0.1947 (3)	0.0368 (16)
H17A	0.1634	0.3077	0.1824	0.055*
H17B	0.0714	0.3697	0.1540	0.055*
H17C	0.0606	0.3363	0.2256	0.055*
C32	0.6314 (6)	0.6182 (3)	0.4227 (3)	0.0389 (17)
H32A	0.6487	0.5932	0.3828	0.058*
H32B	0.6409	0.5869	0.4614	0.058*
H32C	0.6917	0.6564	0.4321	0.058*
C1	−0.0422 (5)	0.5885 (3)	0.3347 (3)	0.0238 (13)
C37	−0.3592 (6)	0.3781 (4)	0.0829 (4)	0.0410 (17)
H37	−0.4223	0.3439	0.0708	0.049*
C26	0.3521 (5)	0.7132 (3)	0.2282 (3)	0.0247 (14)
C36	−0.2716 (6)	0.3701 (3)	0.1420 (3)	0.0361 (16)
H36	−0.2753	0.3309	0.1697	0.043*
C42	−0.1835 (6)	0.7015 (3)	0.0430 (3)	0.0357 (16)
H42	−0.2481	0.7351	0.0433	0.043*
C38	−0.3555 (6)	0.4360 (3)	0.0412 (4)	0.0430 (18)
H38	−0.4156	0.4408	0.0013	0.052*
C28	0.1300 (6)	0.7419 (4)	0.1710 (4)	0.061 (2)
H28A	0.1523	0.7907	0.1696	0.092*
H28B	0.0981	0.7320	0.2132	0.092*
H28C	0.0640	0.7310	0.1328	0.092*
C29	0.3003 (8)	0.7070 (5)	0.0996 (3)	0.071 (3)
H29A	0.2530	0.6770	0.0654	0.107*
H29B	0.3908	0.6949	0.1059	0.107*

H29C	0.2896	0.7550	0.0849	0.107*

Table S4.5. Anisotropic displacement parameters (A^2) for **15**. The anisotropic displacement factor exponent takes the form: $-2\pi^2$ [$h^2 a^2 * U^{11}$ + ... + 2 h k a* b* U^{12}].

	U^{11}	U^{22}	U^{33}	U^{12}	U^{13}	U^{23}
U1	0.01654 (10)	0.01540 (10)	0.01669 (10)	0.00124 (10)	0.00329 (7)	0.00093 (11)
N1	0.021 (2)	0.020 (3)	0.026 (3)	−0.002 (2)	0.010 (2)	−0.001 (2)
N2	0.025 (2)	0.021 (2)	0.018 (2)	0.004 (2)	0.0023 (19)	0.001 (2)
C34	0.021 (3)	0.021 (3)	0.027 (3)	−0.002 (2)	0.001 (2)	−0.005 (3)
C7	0.023 (3)	0.048 (4)	0.033 (3)	−0.005 (3)	0.012 (3)	−0.004 (3)
C20	0.029 (3)	0.031 (4)	0.040 (4)	0.003 (3)	0.015 (3)	0.010 (3)
C40	0.022 (3)	0.020 (3)	0.025 (3)	0.001 (2)	−0.001 (3)	−0.003 (3)
C14	0.021 (3)	0.019 (3)	0.020 (3)	0.006 (2)	0.004 (2)	−0.001 (2)
C33	0.023 (3)	0.028 (3)	0.020 (3)	0.007 (3)	0.007 (2)	−0.003 (3)
C12	0.015 (3)	0.021 (3)	0.026 (3)	0.004 (2)	0.003 (2)	−0.003 (3)
C15	0.023 (3)	0.025 (3)	0.027 (3)	0.007 (3)	0.010 (3)	0.005 (3)
C13	0.019 (3)	0.017 (3)	0.026 (3)	0.010 (2)	0.008 (2)	0.004 (2)
C44	0.035 (4)	0.033 (4)	0.023 (3)	−0.008 (3)	0.000 (3)	0.002 (3)
C21	0.016 (3)	0.025 (3)	0.027 (3)	0.002 (2)	0.005 (2)	−0.001 (3)
C5	0.028 (3)	0.021 (3)	0.025 (3)	0.007 (3)	0.009 (3)	−0.003 (3)
C2	0.020 (3)	0.020 (3)	0.023 (3)	−0.001 (2)	0.006 (2)	−0.003 (2)
C39	0.036 (4)	0.030 (4)	0.035 (4)	−0.006 (3)	0.005 (3)	−0.004 (3)
C10	0.043 (4)	0.028 (4)	0.035 (4)	0.012 (3)	0.013 (3)	−0.002 (3)
C11	0.021 (3)	0.023 (3)	0.023 (3)	0.010 (2)	0.006 (2)	0.001 (2)
C4	0.024 (3)	0.030 (3)	0.017 (3)	0.000 (3)	0.008 (3)	−0.004 (2)
C31	0.039 (4)	0.036 (4)	0.024 (3)	−0.003 (3)	0.000 (3)	0.006 (3)
C9	0.029 (3)	0.037 (4)	0.029 (4)	−0.002 (3)	0.004 (3)	−0.003 (3)
C6	0.037 (4)	0.042 (4)	0.031 (4)	0.015 (3)	0.010 (3)	0.005 (3)
C25	0.037 (4)	0.027 (4)	0.028 (4)	−0.008 (3)	0.002 (3)	0.007 (3)

C45	0.026 (3)	0.026 (3)	0.023 (3)	−0.003 (3)	−0.002 (3)	0.002 (3)
C27	0.033 (4)	0.030 (4)	0.023 (3)	−0.012 (3)	0.003 (3)	0.002 (3)
C23	0.023 (3)	0.032 (4)	0.026 (3)	−0.010 (3)	0.001 (3)	−0.004 (3)
C16	0.046 (4)	0.039 (4)	0.029 (3)	0.013 (4)	0.009 (3)	0.001 (3)
C18	0.038 (4)	0.020 (3)	0.039 (4)	0.006 (3)	0.016 (3)	0.005 (3)
C41	0.029 (3)	0.030 (4)	0.024 (3)	0.007 (3)	0.000 (3)	0.000 (3)
C8	0.032 (3)	0.033 (4)	0.024 (3)	0.005 (3)	0.013 (3)	0.003 (3)
C3	0.023 (3)	0.026 (3)	0.020 (3)	0.005 (3)	0.010 (3)	0.004 (3)
C19	0.023 (3)	0.032 (4)	0.032 (4)	0.002 (3)	−0.005 (3)	0.002 (3)
C30	0.024 (3)	0.024 (3)	0.035 (4)	−0.004 (3)	0.001 (3)	0.003 (3)
C35	0.028 (3)	0.032 (4)	0.031 (4)	0.007 (3)	0.004 (3)	0.002 (3)
C24	0.039 (4)	0.028 (4)	0.035 (4)	−0.016 (3)	0.007 (3)	0.004 (3)
C43	0.046 (4)	0.024 (4)	0.029 (4)	−0.003 (3)	−0.006 (3)	0.000 (3)
C17	0.028 (3)	0.028 (4)	0.053 (4)	−0.002 (3)	0.001 (3)	−0.012 (3)
C32	0.034 (4)	0.035 (4)	0.045 (4)	0.000 (3)	0.000 (3)	0.000 (3)
C1	0.024 (3)	0.032 (3)	0.015 (3)	0.015 (3)	0.005 (2)	0.002 (3)
C37	0.039 (4)	0.034 (4)	0.050 (5)	−0.013 (3)	0.007 (4)	−0.007 (3)
C26	0.028 (3)	0.020 (3)	0.027 (4)	−0.007 (3)	0.007 (3)	0.000 (3)
C36	0.039 (4)	0.028 (4)	0.041 (4)	−0.003 (3)	0.007 (3)	0.005 (3)
C42	0.039 (4)	0.033 (4)	0.031 (4)	0.013 (3)	−0.011 (3)	−0.005 (3)
C38	0.044 (4)	0.035 (4)	0.046 (4)	−0.015 (3)	−0.005 (3)	−0.006 (3)
C28	0.040 (4)	0.046 (5)	0.087 (6)	0.005 (4)	−0.028 (4)	−0.031 (5)
C29	0.077 (6)	0.119 (8)	0.018 (4)	−0.057 (6)	0.003 (4)	0.002 (4)

Table S4.6. Bond lengths [Å], bond angles [º], and torsion angles [º] for **15**.

U1—N1	2.012 (4)	C44—C43	1.370 (8)
U1—N2	2.199 (4)	C44—C45	1.398 (8)
U1—C14	2.734 (5)	C21—C26	1.415 (7)

U1—C15	2.737 (5)	C21—C22	1.428 (7)
U1—C5	2.743 (5)	C5—C1	1.421 (8)
U1—C1	2.750 (5)	C5—C4	1.414 (8)
U1—C4	2.758 (5)	C5—C10	1.510 (8)
U1—C11	2.767 (5)	C2—C3	1.409 (8)
U1—C13	2.779 (5)	C2—C1	1.422 (8)
U1—C12	2.784 (5)	C39—C38	1.383 (8)
U1—C3	2.793 (5)	C11—C16	1.490 (8)
U1—C2	2.797 (5)	C4—C3	1.405 (8)
N1—C21	1.391 (7)	C4—C9	1.506 (8)
N2—C33	1.288 (7)	C31—C30	1.546 (8)
C34—C35	1.401 (8)	C6—C1	1.507 (7)
C34—C39	1.408 (8)	C25—C24	1.371 (8)
C34—C33	1.493 (8)	C25—C26	1.389 (7)
C7—C2	1.507 (7)	C22—C23	1.390 (7)
C20—C15	1.507 (7)	C22—C30	1.511 (7)
C40—C45	1.387 (7)	C27—C28	1.508 (8)
C40—C41	1.399 (7)	C27—C29	1.520 (8)
C40—C33	1.503 (8)	C27—C26	1.513 (8)
C14—C13	1.415 (7)	C23—C24	1.389 (8)
C14—C15	1.418 (7)	C41—C42	1.374 (8)
C14—C19	1.495 (7)	C8—C3	1.510 (8)
C12—C13	1.407 (7)	C30—C32	1.533 (8)
C12—C11	1.428 (7)	C35—C36	1.381 (8)
C12—C17	1.500 (7)	C43—C42	1.369 (8)
C15—C11	1.414 (8)	C37—C38	1.378 (9)
C13—C18	1.507 (7)	C37—C36	1.371 (8)
N1—U1—N2	111.99 (17)	C13—C12—C11	108.3 (5)

N1—U1—C14	88.41 (17)	C13—C12—C17	124.6 (5)
N2—U1—C14	126.07 (16)	C11—C12—C17	125.7 (5)
N1—U1—C15	75.93 (17)	C13—C12—U1	75.2 (3)
N2—U1—C15	105.18 (16)	C11—C12—U1	74.4 (3)
C14—U1—C15	30.05 (16)	C17—C12—U1	127.2 (4)
N1—U1—C5	78.27 (17)	C11—C15—C14	108.8 (5)
N2—U1—C5	105.21 (16)	C11—C15—C20	123.9 (5)
C14—U1—C5	128.15 (17)	C14—C15—C20	126.8 (5)
C15—U1—C5	145.71 (17)	C11—C15—U1	76.3 (3)
N1—U1—C1	100.26 (17)	C14—C15—U1	74.8 (3)
N2—U1—C1	78.21 (16)	C20—C15—U1	122.0 (4)
C14—U1—C1	149.02 (16)	C12—C13—C14	108.4 (5)
C15—U1—C1	175.59 (18)	C12—C13—C18	124.6 (5)
C5—U1—C1	29.98 (16)	C14—C13—C18	125.5 (5)
N1—U1—C4	89.67 (17)	C12—C13—U1	75.5 (3)
N2—U1—C4	126.35 (16)	C14—C13—U1	73.4 (3)
C14—U1—C4	101.82 (16)	C18—C13—U1	128.3 (3)
C15—U1—C4	127.99 (17)	C43—C44—C45	120.6 (6)
C5—U1—C4	29.79 (16)	N1—C21—C26	120.2 (5)
C1—U1—C4	49.13 (16)	N1—C21—C22	121.6 (5)
N1—U1—C11	97.01 (17)	C26—C21—C22	118.2 (5)
N2—U1—C11	77.93 (16)	C1—C5—C4	107.7 (5)
C14—U1—C11	49.49 (16)	C1—C5—C10	124.5 (5)
C15—U1—C11	29.77 (17)	C4—C5—C10	127.4 (5)
C5—U1—C11	175.02 (17)	C1—C5—U1	75.3 (3)
C1—U1—C11	154.45 (17)	C4—C5—U1	75.7 (3)
C4—U1—C11	150.00 (17)	C10—C5—U1	121.0 (4)
N1—U1—C13	118.07 (17)	C3—C2—C1	108.2 (5)

N2—U1—C13	108.17 (16)	C3—C2—C7	125.0 (5)
C14—U1—C13	29.72 (15)	C1—C2—C7	126.1 (5)
C15—U1—C13	48.92 (16)	C3—C2—U1	75.2 (3)
C5—U1—C13	131.98 (16)	C1—C2—U1	73.3 (3)
C1—U1—C13	133.10 (16)	C7—C2—U1	124.6 (4)
C4—U1—C13	102.34 (16)	C38—C39—C34	121.2 (6)
C11—U1—C13	48.97 (16)	C15—C11—C12	107.0 (5)
N1—U1—C12	124.23 (16)	C15—C11—C16	125.6 (5)
N2—U1—C12	80.16 (16)	C12—C11—C16	127.0 (5)
C14—U1—C12	49.00 (16)	C15—C11—U1	74.0 (3)
C15—U1—C12	48.89 (16)	C12—C11—U1	75.7 (3)
C5—U1—C12	153.77 (16)	C16—C11—U1	121.7 (4)
C1—U1—C12	135.18 (17)	C3—C4—C5	108.5 (5)
C4—U1—C12	127.77 (17)	C3—C4—C9	124.7 (5)
C11—U1—C12	29.82 (15)	C5—C4—C9	126.0 (5)
C13—U1—C12	29.30 (15)	C3—C4—U1	76.7 (3)
N1—U1—C3	118.99 (17)	C5—C4—U1	74.5 (3)
N2—U1—C3	109.69 (16)	C9—C4—U1	123.0 (4)
C14—U1—C3	100.97 (16)	C24—C25—C26	122.8 (6)
C15—U1—C3	130.96 (17)	C40—C45—C44	120.2 (6)
C5—U1—C3	48.82 (16)	C23—C22—C21	119.7 (5)
C1—U1—C3	48.87 (16)	C23—C22—C30	117.0 (5)
C4—U1—C3	29.32 (16)	C21—C22—C30	123.3 (5)
C11—U1—C3	134.15 (16)	C28—C27—C29	112.7 (6)
C13—U1—C3	87.38 (16)	C28—C27—C26	109.8 (5)
C12—U1—C3	105.01 (16)	C29—C27—C26	111.7 (5)
N1—U1—C2	126.83 (16)	C22—C23—C24	121.5 (5)
N2—U1—C2	81.57 (16)	C42—C41—C40	120.5 (6)

C14—U1—C2	125.88 (16)	C2—C3—C4	108.1 (5)
C15—U1—C2	152.67 (17)	C2—C3—C8	126.3 (5)
C5—U1—C2	48.87 (16)	C4—C3—C8	124.6 (5)
C1—U1—C2	29.70 (16)	C2—C3—U1	75.6 (3)
C4—U1—C2	48.42 (16)	C4—C3—U1	74.0 (3)
C11—U1—C2	135.98 (16)	C8—C3—U1	125.5 (3)
C13—U1—C2	103.75 (15)	C22—C30—C32	112.2 (5)
C12—U1—C2	108.45 (15)	C22—C30—C31	111.2 (5)
C3—U1—C2	29.20 (15)	C32—C30—C31	109.5 (5)
C21—N1—U1	174.6 (4)	C36—C35—C34	121.6 (6)
C33—N2—U1	177.8 (4)	C25—C24—C23	118.5 (5)
C35—C34—C39	117.1 (5)	C44—C43—C42	119.3 (6)
C35—C34—C33	121.3 (5)	C5—C1—C2	107.5 (5)
C39—C34—C33	121.5 (5)	C5—C1—C6	126.5 (6)
C45—C40—C41	118.2 (5)	C2—C1—C6	125.7 (5)
C45—C40—C33	120.5 (5)	C5—C1—U1	74.7 (3)
C41—C40—C33	121.1 (5)	C2—C1—U1	77.0 (3)
C13—C14—C15	107.5 (5)	C6—C1—U1	119.2 (3)
C13—C14—C19	124.9 (5)	C38—C37—C36	121.2 (6)
C15—C14—C19	127.2 (5)	C25—C26—C21	119.2 (5)
C13—C14—U1	76.9 (3)	C25—C26—C27	119.3 (5)
C15—C14—U1	75.1 (3)	C21—C26—C27	121.4 (5)
C19—C14—U1	119.8 (4)	C37—C36—C35	119.5 (6)
N2—C33—C34	124.0 (5)	C43—C42—C41	121.2 (6)
N2—C33—C40	121.2 (5)	C37—C38—C39	119.4 (7)
C34—C33—C40	114.8 (5)		

Table S4.7. Atomic coordinates and equivalent isotropic displacement parameters (A^2) for **16**. U(eq) is defined as one third of the trace of the orthogonalized U^{ij} tensor.

	X	*Y*	*X*	U_{iso}*/U_{eq}
U1	0.10513 (3)	0.21745 (3)	0.34221 (2)	0.0150 (2)
N1	0.0222 (6)	0.2654 (6)	0.3864 (5)	0.020 (3)
N2	0.1382 (6)	0.2912 (7)	0.2782 (5)	0.020 (3)
C1	−0.0301 (7)	0.3093 (8)	0.4210 (6)	0.018 (3)
C2	−0.0760 (7)	0.2719 (9)	0.4641 (6)	0.024 (4)
C3	−0.1246 (8)	0.3181 (9)	0.4981 (7)	0.033 (4)
H3	−0.1560	0.2940	0.5262	0.040*
C4	−0.1274 (8)	0.3981 (9)	0.4914 (6)	0.028 (4)
H4	−0.1590	0.4277	0.5157	0.034*
C5	−0.0826 (7)	0.4344 (8)	0.4478 (6)	0.020 (3)
H5	−0.0843	0.4885	0.4431	0.024*
C6	−0.0356 (8)	0.3905 (8)	0.4114 (6)	0.027 (4)
C7	0.0075 (8)	0.4289 (8)	0.3593 (5)	0.018 (3)
H7	0.0548	0.4023	0.3566	0.022*
C8	−0.0327 (8)	0.4149 (8)	0.2988 (6)	0.027 (4)
H8A	−0.0820	0.4336	0.3025	0.040*
H8B	−0.0331	0.3599	0.2898	0.040*
H8C	−0.0083	0.4424	0.2659	0.040*
C9	0.0223 (8)	0.5158 (9)	0.3696 (6)	0.028 (4)
H9A	−0.0230	0.5441	0.3687	0.042*
H9B	0.0539	0.5349	0.3374	0.042*
H9C	0.0454	0.5231	0.4092	0.042*
C10	−0.0811 (8)	0.1849 (9)	0.4719 (7)	0.029 (4)
H10	−0.0474	0.1618	0.4416	0.035*
C11	−0.1571 (8)	0.1511 (10)	0.4577 (7)	0.043 (4)
H11A	−0.1924	0.1737	0.4853	0.065*

H11B	−0.1563	0.0954	0.4632	0.065*
H11C	−0.1702	0.1631	0.4156	0.065*
C12	−0.0563 (10)	0.1571 (11)	0.5350 (7)	0.056 (5)
H12A	−0.0100	0.1804	0.5449	0.084*
H12B	−0.0514	0.1012	0.5347	0.084*
H12C	−0.0917	0.1721	0.5657	0.084*
C13	0.1692 (7)	0.3389 (8)	0.2328 (5)	0.018 (3)
C14	0.1527 (8)	0.4214 (9)	0.2319 (6)	0.026 (4)
H14	0.1207	0.4427	0.2608	0.031*
C15	0.1851 (8)	0.4684 (9)	0.1874 (6)	0.033 (4)
H15	0.1743	0.5215	0.1875	0.040*
C16	0.2330 (8)	0.4404 (9)	0.1427 (6)	0.029 (4)
H16	0.2526	0.4733	0.1127	0.035*
C17	0.2505 (9)	0.3614 (10)	0.1445 (6)	0.035 (4)
H17	0.2847	0.3419	0.1166	0.043*
C18	0.2180 (9)	0.3106 (10)	0.1871 (7)	0.036 (4)
H18	0.2287	0.2574	0.1854	0.043*
C19	0.0388 (8)	0.1643 (9)	0.2359 (6)	0.026 (4)
C20	0.1041 (8)	0.1141 (8)	0.2432 (6)	0.022 (3)
C21	0.0931 (7)	0.0691 (8)	0.2958 (6)	0.021 (3)
C22	0.0255 (8)	0.0830 (9)	0.3219 (6)	0.022 (3)
C23	−0.0083 (7)	0.1417 (8)	0.2839 (6)	0.020 (3)
C24	−0.0861 (7)	0.1745 (9)	0.2923 (7)	0.030 (4)
H24A	−0.0898	0.2242	0.2719	0.045*
H24B	−0.0962	0.1808	0.3357	0.045*
H24C	−0.1208	0.1388	0.2745	0.045*
C25	−0.0095 (7)	0.0344 (8)	0.3726 (6)	0.023 (4)
H25A	−0.0146	−0.0186	0.3586	0.034*

H25B	−0.0568	0.0554	0.3823	0.034*
H25C	0.0208	0.0357	0.4090	0.034*
C26	0.1420 (9)	−0.0021 (10)	0.3146 (7)	0.039 (4)
H26A	0.1840	−0.0042	0.2880	0.059*
H26B	0.1145	−0.0496	0.3104	0.059*
H26C	0.1576	0.0038	0.3568	0.059*
C27	0.1650 (8)	0.1110 (9)	0.1962 (6)	0.034 (4)
H27A	0.2110	0.1187	0.2167	0.050*
H27B	0.1579	0.1514	0.1659	0.050*
H27C	0.1648	0.0609	0.1761	0.050*
C28	0.0230 (8)	0.2204 (9)	0.1850 (6)	0.024 (3)
H28A	−0.0133	0.1985	0.1578	0.037*
H28B	0.0669	0.2304	0.1620	0.037*
H28C	0.0050	0.2685	0.2022	0.037*
C29	0.2017 (8)	0.3010 (8)	0.4137 (7)	0.027 (4)
C30	0.2481 (9)	0.2572 (9)	0.3753 (7)	0.032 (4)
C31	0.2361 (8)	0.1767 (8)	0.3898 (6)	0.020 (4)
C32	0.1878 (7)	0.1720 (8)	0.4399 (6)	0.017 (3)
C33	0.1665 (7)	0.2494 (9)	0.4560 (6)	0.022 (4)
C34	0.1962 (10)	0.3891 (10)	0.4168 (8)	0.053 (5)
H34A	0.2392	0.4099	0.4362	0.080*
H34B	0.1539	0.4035	0.4405	0.080*
H34C	0.1919	0.4098	0.3755	0.080*
C35	0.2997 (8)	0.2866 (10)	0.3272 (7)	0.046 (5)
H35A	0.2911	0.3413	0.3203	0.068*
H35B	0.2923	0.2584	0.2893	0.068*
H35C	0.3490	0.2791	0.3412	0.068*
C36	0.2804 (8)	0.1129 (9)	0.3621 (6)	0.035 (4)

H36A	0.3309	0.1203	0.3726	0.053*
H36B	0.2749	0.1136	0.3178	0.053*
H36C	0.2639	0.0634	0.3779	0.053*
C37	0.1642 (8)	0.1002 (9)	0.4750 (6)	0.032 (4)
H37A	0.1132	0.1042	0.4850	0.048*
H37B	0.1921	0.0958	0.5125	0.048*
H37C	0.1722	0.0547	0.4498	0.048*
C38	0.1250 (9)	0.2754 (11)	0.5123 (7)	0.048 (5)
H38A	0.1578	0.3001	0.5410	0.072*
H38B	0.1027	0.2309	0.5317	0.072*
H38C	0.0878	0.3120	0.5002	0.072*

Table S4.8. Anisotropic displacement parameters (A^2) for **16**. The anisotropic displacement factor exponent takes the form: $-2\pi^2$ [$h^2 a^2 * U^{11}$ + ... + 2 h k a* b* U^{12}].

	U^{11}	U^{22}	U^{33}	U^{12}	U^{13}	U^{23}
U1	0.0110 (3)	0.0136 (3)	0.0203 (3)	0.0004 (3)	−0.0017 (2)	0.0002 (3)
N1	0.016 (6)	0.021 (6)	0.024 (5)	−0.005 (5)	−0.001 (4)	0.005 (5)
N2	0.024 (6)	0.011 (6)	0.023 (5)	0.005 (5)	0.000 (4)	0.003 (5)
C1	0.014 (6)	0.026 (7)	0.013 (6)	0.005 (6)	0.005 (5)	0.001 (5)
C2	0.013 (6)	0.027 (7)	0.032 (7)	−0.004 (6)	0.010 (5)	0.001 (6)
C3	0.032 (8)	0.034 (7)	0.035 (7)	0.003 (6)	0.011 (6)	−0.001 (6)
C4	0.023 (7)	0.037 (8)	0.025 (6)	0.010 (6)	0.004 (5)	0.000 (6)
C5	0.016 (7)	0.018 (7)	0.026 (6)	−0.004 (6)	−0.007 (5)	0.001 (5)
C6	0.034 (7)	0.028 (7)	0.018 (6)	−0.003 (6)	−0.005 (6)	0.000 (6)
C7	0.019 (7)	0.017 (7)	0.019 (6)	−0.001 (6)	−0.004 (5)	0.011 (5)
C8	0.025 (7)	0.022 (7)	0.032 (7)	0.001 (6)	−0.002 (6)	0.007 (6)
C9	0.019 (7)	0.032 (7)	0.033 (6)	0.004 (6)	−0.002 (6)	0.002 (6)
C10	0.027 (7)	0.028 (7)	0.033 (7)	0.000 (6)	0.013 (6)	0.003 (6)
C11	0.039 (8)	0.033 (7)	0.059 (8)	−0.001 (7)	0.018 (6)	−0.004 (7)

C12	0.068 (9)	0.047 (8)	0.054 (8)	−0.006 (7)	0.009 (7)	0.001 (7)
C13	0.016 (6)	0.019 (7)	0.020 (6)	−0.006 (6)	−0.003 (5)	−0.006 (5)
C14	0.019 (7)	0.027 (7)	0.032 (7)	−0.001 (6)	0.002 (6)	0.000 (6)
C15	0.036 (7)	0.026 (7)	0.037 (7)	−0.009 (7)	−0.006 (6)	0.012 (6)
C16	0.033 (7)	0.028 (7)	0.028 (7)	−0.010 (6)	−0.007 (6)	0.004 (6)
C17	0.035 (7)	0.038 (8)	0.033 (7)	0.001 (7)	0.013 (6)	−0.009 (6)
C18	0.043 (8)	0.029 (7)	0.035 (7)	−0.009 (6)	0.007 (6)	0.000 (6)
C19	0.027 (7)	0.026 (7)	0.026 (6)	−0.005 (6)	−0.003 (6)	0.001 (6)
C20	0.015 (6)	0.028 (7)	0.023 (6)	−0.001 (6)	−0.001 (6)	0.001 (5)
C21	0.014 (7)	0.006 (6)	0.041 (7)	0.009 (6)	−0.004 (5)	0.001 (5)
C22	0.023 (7)	0.023 (7)	0.020 (6)	−0.001 (6)	−0.002 (5)	−0.002 (5)
C23	0.020 (7)	0.013 (7)	0.026 (6)	−0.012 (6)	−0.008 (5)	0.000 (5)
C24	0.011 (7)	0.032 (7)	0.046 (7)	−0.003 (6)	−0.015 (6)	0.005 (6)
C25	0.023 (7)	0.015 (7)	0.030 (6)	−0.004 (6)	−0.012 (6)	0.000 (5)
C26	0.038 (7)	0.035 (8)	0.045 (7)	0.004 (7)	−0.014 (6)	−0.006 (6)
C27	0.034 (8)	0.032 (8)	0.035 (7)	0.004 (6)	−0.002 (6)	−0.008 (6)
C28	0.021 (6)	0.023 (7)	0.030 (6)	0.000 (6)	0.000 (5)	−0.004 (6)
C29	0.025 (7)	0.024 (7)	0.033 (7)	−0.001 (6)	−0.020 (6)	−0.006 (6)
C30	0.025 (7)	0.035 (8)	0.035 (7)	0.000 (6)	−0.011 (6)	−0.004 (6)
C31	0.018 (7)	0.019 (7)	0.024 (6)	0.005 (6)	−0.006 (5)	−0.002 (5)
C32	0.020 (6)	0.016 (7)	0.017 (6)	0.001 (6)	−0.010 (5)	−0.002 (5)
C33	0.015 (7)	0.030 (7)	0.021 (6)	0.004 (6)	−0.013 (5)	−0.009 (5)
C34	0.052 (9)	0.049 (8)	0.058 (8)	−0.002 (7)	−0.015 (7)	−0.001 (7)
C35	0.034 (8)	0.050 (8)	0.053 (8)	0.003 (7)	−0.006 (6)	0.010 (7)
C36	0.034 (7)	0.033 (8)	0.039 (7)	0.002 (7)	−0.005 (6)	−0.002 (6)
C37	0.036 (7)	0.038 (7)	0.021 (6)	−0.006 (6)	−0.002 (6)	−0.003 (6)
C38	0.047 (8)	0.055 (8)	0.042 (7)	0.003 (7)	−0.001 (6)	−0.013 (7)

Table S4.9. Bond lengths [Å], bond angles [º], and torsion angles [º] for **16**.

U1—N2	1.965 (11)	C13—C18	1.416 (19)
U1—N1	1.970 (11)	C13—C14	1.44 (2)
U1—C31	2.698 (13)	C14—C15	1.384 (18)
U1—C32	2.707 (12)	C15—C16	1.39 (2)
U1—C21	2.735 (13)	C16—C17	1.39 (2)
U1—C29	2.746 (13)	C17—C18	1.396 (19)
U1—C19	2.748 (13)	C19—C23	1.400 (17)
U1—C23	2.750 (12)	C19—C20	1.48 (2)
U1—C33	2.753 (12)	C19—C28	1.486 (18)
U1—C22	2.756 (14)	C20—C21	1.385 (18)
U1—C20	2.770 (13)	C20—C27	1.507 (18)
U1—C30	2.795 (16)	C21—C22	1.378 (18)
N1—C1	1.428 (16)	C21—C26	1.56 (2)
N2—C13	1.394 (16)	C22—C23	1.437 (18)
C1—C6	1.406 (18)	C22—C25	1.514 (18)
C1—C2	1.406 (18)	C23—C24	1.540 (18)
C2—C3	1.397 (19)	C29—C30	1.40 (2)
C2—C10	1.50 (2)	C29—C33	1.423 (19)
C3—C4	1.38 (2)	C29—C34	1.51 (2)
C4—C5	1.392 (18)	C30—C31	1.430 (19)
C5—C6	1.386 (19)	C30—C35	1.49 (2)
C6—C7	1.521 (18)	C31—C32	1.397 (18)
C7—C8	1.516 (17)	C31—C36	1.485 (19)
C7—C9	1.526 (19)	C32—C33	1.422 (18)
C10—C12	1.51 (2)	C32—C37	1.505 (18)
C10—C11	1.54 (2)	C33—C38	1.499 (19)
N2—U1—N1	108.1 (4)	C5—C6—C1	119.7 (13)

N2—U1—C31	99.2 (4)	C5—C6—C7	120.4 (13)
N1—U1—C31	127.4 (4)	C1—C6—C7	119.9 (13)
N2—U1—C32	123.9 (4)	C8—C7—C6	108.3 (11)
N1—U1—C32	100.0 (4)	C8—C7—C9	111.4 (11)
C31—U1—C32	30.0 (4)	C6—C7—C9	114.0 (11)
N2—U1—C21	111.3 (4)	C2—C10—C12	113.1 (13)
N1—U1—C21	120.0 (4)	C2—C10—C11	114.0 (12)
C31—U1—C21	88.3 (4)	C12—C10—C11	109.5 (13)
C32—U1—C21	93.6 (4)	N2—C13—C18	123.0 (13)
N2—U1—C29	82.1 (4)	N2—C13—C14	119.7 (12)
N1—U1—C29	90.4 (4)	C18—C13—C14	117.2 (13)
C31—U1—C29	49.4 (4)	C15—C14—C13	119.1 (14)
C32—U1—C29	49.7 (4)	C14—C15—C16	123.5 (15)
C21—U1—C29	137.7 (4)	C15—C16—C17	117.5 (14)
N2—U1—C19	76.3 (4)	C16—C17—C18	121.7 (14)
N1—U1—C19	101.6 (4)	C17—C18—C13	120.9 (15)
C31—U1—C19	128.6 (4)	C23—C19—C20	105.0 (12)
C32—U1—C19	143.2 (4)	C23—C19—C28	127.2 (13)
C21—U1—C19	49.7 (4)	C20—C19—C28	127.6 (12)
C29—U1—C19	157.6 (4)	C23—C19—U1	75.3 (7)
N2—U1—C23	102.3 (4)	C20—C19—U1	75.3 (7)
N1—U1—C23	80.5 (4)	C28—C19—U1	119.2 (9)
C31—U1—C23	136.2 (4)	C21—C20—C19	106.9 (12)
C32—U1—C23	130.0 (4)	C21—C20—C27	129.7 (13)
C21—U1—C23	48.4 (4)	C19—C20—C27	123.1 (12)
C29—U1—C23	170.8 (4)	C21—C20—U1	74.0 (8)
C19—U1—C23	29.5 (4)	C19—C20—U1	73.6 (7)
N2—U1—C33	111.9 (4)	C27—C20—U1	122.4 (9)

N1—U1—C33	78.5 (4)	C22—C21—C20	111.7 (12)
C31—U1—C33	49.4 (4)	C22—C21—C26	122.8 (13)
C32—U1—C33	30.2 (4)	C20—C21—C26	124.1 (13)
C21—U1—C33	122.9 (4)	C22—C21—U1	76.3 (8)
C29—U1—C33	30.0 (4)	C20—C21—U1	76.8 (8)
C19—U1—C33	171.5 (4)	C26—C21—U1	125.5 (9)
C23—U1—C33	144.0 (4)	C21—C22—C23	105.9 (12)
N2—U1—C22	125.9 (4)	C21—C22—C25	125.4 (13)
N1—U1—C22	90.9 (4)	C23—C22—C25	127.8 (13)
C31—U1—C22	108.3 (4)	C21—C22—U1	74.6 (8)
C32—U1—C22	100.3 (4)	C23—C22—U1	74.7 (8)
C21—U1—C22	29.1 (4)	C25—C22—U1	124.5 (8)
C29—U1—C22	149.7 (4)	C19—C23—C22	110.4 (13)
C19—U1—C22	50.1 (4)	C19—C23—C24	123.7 (13)
C23—U1—C22	30.2 (4)	C22—C23—C24	125.8 (12)
C33—U1—C22	121.5 (4)	C19—C23—U1	75.2 (7)
N2—U1—C20	82.6 (4)	C22—C23—U1	75.1 (8)
N1—U1—C20	129.2 (4)	C24—C23—U1	118.2 (9)
C31—U1—C20	97.7 (4)	C30—C29—C33	108.7 (13)
C32—U1—C20	114.8 (4)	C30—C29—C34	126.8 (15)
C21—U1—C20	29.1 (4)	C33—C29—C34	124.1 (14)
C29—U1—C20	140.2 (4)	C30—C29—U1	77.3 (8)
C19—U1—C20	31.1 (4)	C33—C29—U1	75.3 (7)
C23—U1—C20	48.9 (4)	C34—C29—U1	120.0 (10)
C33—U1—C20	144.6 (4)	C29—C30—C31	107.0 (14)
C22—U1—C20	48.9 (4)	C29—C30—C35	127.9 (15)
N2—U1—C30	74.6 (5)	C31—C30—C35	125.1 (14)
N1—U1—C30	119.7 (4)	C29—C30—U1	73.4 (9)

C31—U1—C30	30.1 (4)	C31—C30—U1	71.2 (8)
C32—U1—C30	49.3 (4)	C35—C30—U1	119.9 (10)
C21—U1—C30	113.2 (4)	C32—C31—C30	108.8 (13)
C29—U1—C30	29.3 (4)	C32—C31—C36	127.9 (13)
C19—U1—C30	135.0 (4)	C30—C31—C36	122.4 (13)
C23—U1—C30	159.6 (4)	C32—C31—U1	75.4 (8)
C33—U1—C30	48.9 (4)	C30—C31—U1	78.7 (8)
C22—U1—C30	137.6 (5)	C36—C31—U1	121.4 (9)
C20—U1—C30	111.0 (4)	C31—C32—C33	108.0 (12)
C1—N1—U1	171.2 (9)	C31—C32—C37	128.0 (13)
C13—N2—U1	173.5 (10)	C33—C32—C37	123.9 (12)
C6—C1—C2	120.2 (13)	C31—C32—U1	74.6 (7)
C6—C1—N1	119.3 (12)	C33—C32—U1	76.7 (7)
C2—C1—N1	120.4 (12)	C37—C32—U1	117.6 (9)
C3—C2—C1	118.0 (14)	C32—C33—C29	107.3 (12)
C3—C2—C10	117.6 (12)	C32—C33—C38	127.8 (14)
C1—C2—C10	124.2 (13)	C29—C33—C38	124.3 (14)
C4—C3—C2	122.0 (14)	C32—C33—U1	73.1 (7)
C3—C4—C5	119.5 (14)	C29—C33—U1	74.7 (7)
C6—C5—C4	120.4 (14)	C38—C33—U1	124.9 (9)

Table S4.10. Atomic coordinates and equivalent isotropic displacement parameters (A^2) for **18**. U(eq) is defined as one third of the trace of the orthogonalized U^{ij} tensor.

	X	*Y*	*Z*	U_{iso}*/U_{eq}
U1	0.140960 (9)	0.09161 (3)	0.342845 (15)	0.01879 (11)
N1	0.13715 (19)	0.1898 (6)	0.2671 (3)	0.0187 (16)
N2	0.0786 (2)	0.1489 (6)	0.3441 (3)	0.0187 (16)
C1	0.0947 (3)	−0.1321 (8)	0.3236 (4)	0.024 (2)
C2	0.2134 (2)	0.0962 (8)	0.4492 (4)	0.024 (2)

C3	0.0354 (2)	0.1591 (7)	0.2359 (4)	0.0143 (18)
H3	0.0589	0.1643	0.2253	0.017*
C4	0.1302 (3)	−0.1601 (8)	0.3766 (4)	0.024 (2)
C5	0.1610 (3)	0.4131 (9)	0.4206 (4)	0.036 (2)
H5A	0.1738	0.4814	0.4062	0.053*
H5B	0.1629	0.4300	0.4625	0.053*
H5C	0.1327	0.4069	0.3947	0.053*
C6	0.1510 (3)	−0.1464 (8)	0.2934 (4)	0.021 (2)
C7	0.1154 (3)	0.3893 (8)	0.2081 (4)	0.026 (2)
C8	0.0517 (3)	−0.1427 (8)	0.3213 (4)	0.031 (2)
H8A	0.0346	−0.0862	0.2901	0.047*
H8B	0.0502	−0.1198	0.3608	0.047*
H8C	0.0423	−0.2289	0.3114	0.047*
C9	0.1376 (3)	0.2692 (8)	0.2188 (4)	0.022 (2)
C10	0.0814 (3)	−0.1097 (9)	0.2058 (4)	0.038 (3)
H10A	0.0794	−0.1912	0.1858	0.058*
H10B	0.0933	−0.0488	0.1858	0.058*
H10C	0.0545	−0.0816	0.2029	0.058*
C11	0.2049 (2)	−0.2348 (8)	0.3920 (4)	0.032 (2)
H11A	0.2075	−0.2466	0.4346	0.049*
H11B	0.2271	−0.1827	0.3898	0.049*
H11C	0.2057	−0.3163	0.3734	0.049*
C12	0.1645 (3)	−0.1698 (8)	0.3578 (4)	0.029 (2)
C13	0.0906 (3)	0.4352 (7)	0.2466 (4)	0.027 (2)
H13	0.0909	0.3689	0.2768	0.032*
C14	0.1757 (3)	−0.1758 (8)	0.2526 (4)	0.034 (2)
H14A	0.2014	−0.1309	0.2676	0.051*
H14B	0.1607	−0.1493	0.2109	0.051*

H14C	0.1808	−0.2660	0.2532	0.051*
C15	0.2538 (3)	0.0768 (9)	0.3723 (5)	0.038 (3)
H15A	0.2725	0.0228	0.4030	0.057*
H15B	0.2690	0.1415	0.3600	0.057*
H15C	0.2386	0.0265	0.3369	0.057*
C16	0.2057 (3)	0.2617 (8)	0.3801 (4)	0.026 (2)
C17	0.1824 (2)	0.2904 (8)	0.4183 (4)	0.021 (2)
C18	0.1292 (3)	−0.1926 (9)	0.4398 (4)	0.035 (2)
H18A	0.1567	−0.2040	0.4682	0.053*
H18B	0.1140	−0.2701	0.4374	0.053*
H18C	0.1163	−0.1245	0.4541	0.053*
C19	0.2152 (3)	0.3539 (8)	0.3371 (4)	0.029 (2)
H19A	0.1929	0.4128	0.3211	0.043*
H19B	0.2191	0.3079	0.3035	0.043*
H19C	0.2399	0.4000	0.3593	0.043*
C20	0.2242 (3)	0.1395 (9)	0.3993 (4)	0.030 (2)
C21	0.0394 (3)	0.1549 (8)	0.2992 (4)	0.019 (2)
C22	0.0031 (2)	0.1556 (8)	0.3109 (4)	0.021 (2)
H22	0.0043	0.1535	0.3519	0.025*
C23	0.1823 (3)	0.1126 (9)	0.1880 (4)	0.035 (2)
H23	0.1779	0.0663	0.2221	0.042*
C24	0.1873 (3)	0.1877 (9)	0.4606 (4)	0.026 (2)
C25	0.1751 (3)	0.1873 (9)	0.5167 (4)	0.035 (2)
H25A	0.1642	0.1051	0.5211	0.053*
H25B	0.1546	0.2515	0.5124	0.053*
H25C	0.1987	0.2051	0.5528	0.053*
C26	0.1079 (3)	−0.1217 (8)	0.2724 (4)	0.028 (2)
C27	0.1599 (3)	0.2370 (9)	0.1800 (4)	0.032 (2)

C28	0.2333 (3)	−0.0079 (9)	0.4940 (4)	0.038 (3)
H28A	0.2500	−0.0591	0.4777	0.057*
H28B	0.2125	−0.0604	0.5005	0.057*
H28C	0.2500	0.0289	0.5328	0.057*
C29	0.0792 (3)	0.1398 (8)	0.4072 (4)	0.026 (2)
H29A	0.1065	0.1125	0.4330	0.031*
H29B	0.0603	0.0729	0.4085	0.031*
C30	0.0686 (3)	0.2592 (9)	0.4365 (4)	0.029 (2)
C31	0.0457 (3)	0.4612 (9)	0.2056 (5)	0.038 (3)
H31A	0.0450	0.5250	0.1754	0.057*
H31B	0.0307	0.4909	0.2310	0.057*
H31C	0.0335	0.3839	0.1850	0.057*
C32	0.0599 (3)	0.3731 (9)	0.4055 (5)	0.033 (2)
H32	0.0604	0.3790	0.3654	0.040*
C33	0.0667 (3)	0.2510 (12)	0.4957 (4)	0.047 (3)
H33	0.0721	0.1734	0.5167	0.056*
C34	0.1183 (3)	0.4664 (10)	0.1610 (5)	0.042 (3)
H34	0.1038	0.5428	0.1531	0.051*
C35	0.1093 (3)	0.5564 (9)	0.2813 (5)	0.047 (3)
H35A	0.1378	0.5417	0.3050	0.070*
H35B	0.0950	0.5799	0.3087	0.070*
H35C	0.1071	0.6240	0.2522	0.070*
C36	0.2284 (3)	0.1316 (11)	0.2043 (5)	0.051 (3)
H36A	0.2337	0.1635	0.1687	0.077*
H36B	0.2422	0.0515	0.2167	0.077*
H36C	0.2382	0.1917	0.2376	0.077*
C37	0.1414 (3)	0.4369 (11)	0.1252 (5)	0.051 (3)
H37	0.1433	0.4932	0.0951	0.061*

C38	0.0503 (3)	0.4811 (11)	0.4339 (6)	0.055 (3)
H38	0.0449	0.5593	0.4135	0.066*
C39	0.0572 (4)	0.3550 (15)	0.5234 (6)	0.071 (4)
H39	0.0564	0.3480	0.5632	0.085*
C40	0.1655 (3)	0.0312 (11)	0.1299 (5)	0.053 (3)
H40A	0.1371	0.0128	0.1220	0.079*
H40B	0.1807	−0.0473	0.1357	0.079*
H40C	0.1682	0.0767	0.0953	0.079*
C41	0.1616 (3)	0.3219 (10)	0.1349 (5)	0.047 (3)
H41	0.1769	0.3004	0.1104	0.056*
C42	0.0490 (4)	0.4680 (15)	0.4937 (7)	0.067 (4)
H42	0.0424	0.5382	0.5131	0.080*
C43	−0.0073 (5)	0.0287 (11)	0.4746 (6)	0.073 (5)
H43A	−0.0224	−0.0290	0.4416	0.088*
H43B	0.0139	0.0711	0.4634	0.088*
C44	−0.0344 (10)	0.120 (2)	0.4883 (10)	0.175 (14)
H44A	−0.0560	0.0766	0.4981	0.210*
H44B	−0.0192	0.1739	0.5229	0.210*
C45	−0.0476 (7)	0.178 (2)	0.4436 (15)	0.235 (17)
H45A	−0.0304	0.2514	0.4457	0.353*
H45B	−0.0748	0.2063	0.4389	0.353*
H45C	−0.0485	0.1265	0.4087	0.353*

Table S4.11. Anisotropic displacement parameters (A^2) for **18**. The anisotropic displacement factor exponent takes the form: $-2\pi^2$ [$h^2 a^2 U^{11}$ + ... + 2 h k a* b* U^{12}].

	U^{11}	U^{22}	U^{33}	U^{12}	U^{13}	U^{23}
U1	0.01886 (18)	0.01492 (17)	0.02177 (18)	−0.00088 (17)	0.00600 (13)	0.00119 (18)
N1	0.014 (4)	0.021 (4)	0.023 (4)	−0.002 (3)	0.009 (3)	−0.001 (3)

N2	0.025 (4)	0.015 (4)	0.018 (4)	0.000 (3)	0.010 (3)	−0.001 (3)
C1	0.021 (5)	0.012 (5)	0.038 (6)	−0.004 (4)	0.008 (4)	−0.001 (4)
C2	0.021 (5)	0.022 (5)	0.025 (5)	−0.007 (4)	0.002 (4)	0.002 (5)
C3	0.013 (4)	0.012 (4)	0.023 (5)	0.000 (3)	0.013 (4)	0.002 (4)
C4	0.025 (5)	0.016 (5)	0.031 (6)	−0.006 (4)	0.010 (4)	0.000 (4)
C5	0.041 (6)	0.032 (6)	0.033 (6)	−0.003 (5)	0.012 (5)	−0.008 (5)
C6	0.026 (5)	0.013 (4)	0.022 (5)	0.004 (4)	0.006 (4)	−0.001 (4)
C7	0.028 (5)	0.023 (5)	0.028 (5)	0.003 (4)	0.013 (4)	0.002 (4)
C8	0.033 (6)	0.016 (5)	0.042 (6)	−0.007 (4)	0.009 (5)	−0.007 (4)
C9	0.032 (5)	0.018 (5)	0.017 (5)	−0.010 (4)	0.008 (4)	0.000 (4)
C10	0.048 (6)	0.028 (6)	0.032 (6)	0.011 (5)	0.006 (5)	−0.003 (5)
C11	0.018 (5)	0.020 (5)	0.052 (6)	0.006 (4)	0.003 (5)	0.003 (5)
C12	0.027 (5)	0.013 (5)	0.043 (6)	0.000 (4)	0.008 (5)	−0.009 (4)
C13	0.040 (6)	0.007 (5)	0.037 (6)	−0.001 (4)	0.018 (5)	0.003 (4)
C14	0.046 (6)	0.014 (5)	0.045 (6)	0.006 (4)	0.021 (5)	0.001 (4)
C15	0.025 (5)	0.031 (6)	0.054 (7)	−0.002 (5)	0.009 (5)	0.002 (5)
C16	0.029 (5)	0.023 (5)	0.016 (5)	−0.007 (4)	−0.004 (4)	−0.001 (4)
C17	0.019 (5)	0.015 (5)	0.024 (5)	−0.004 (4)	−0.001 (4)	0.000 (4)
C18	0.037 (6)	0.026 (5)	0.046 (6)	−0.003 (5)	0.019 (5)	0.012 (5)
C19	0.033 (6)	0.016 (5)	0.038 (6)	−0.010 (4)	0.012 (5)	−0.003 (4)
C20	0.016 (5)	0.029 (5)	0.032 (6)	−0.005 (4)	−0.008 (4)	−0.006 (4)
C21	0.021 (5)	0.009 (4)	0.025 (5)	0.001 (4)	0.004 (4)	0.006 (4)
C22	0.025 (5)	0.016 (5)	0.024 (5)	−0.004 (4)	0.010 (4)	0.002 (4)
C23	0.042 (6)	0.042 (7)	0.028 (5)	0.000 (5)	0.020 (5)	−0.007 (5)
C24	0.020 (5)	0.031 (6)	0.022 (5)	−0.005 (4)	0.001 (4)	−0.004 (4)
C25	0.033 (6)	0.044 (7)	0.021 (5)	−0.008 (5)	−0.001 (4)	0.000 (5)
C26	0.039 (6)	0.012 (5)	0.029 (5)	−0.002 (4)	0.008 (5)	−0.006 (4)
C27	0.033 (6)	0.033 (6)	0.037 (6)	0.003 (5)	0.022 (5)	0.001 (5)

C28	0.026 (6)	0.036 (6)	0.039 (6)	−0.003 (5)	−0.005 (5)	0.008 (5)
C29	0.024 (5)	0.030 (5)	0.021 (5)	−0.005 (4)	0.006 (4)	−0.002 (4)
C30	0.020 (5)	0.041 (6)	0.025 (5)	−0.006 (4)	0.007 (4)	−0.019 (5)
C31	0.033 (6)	0.028 (5)	0.050 (7)	0.005 (5)	0.009 (5)	0.014 (5)
C32	0.027 (5)	0.035 (6)	0.039 (6)	−0.001 (4)	0.013 (5)	−0.023 (5)
C33	0.041 (6)	0.071 (8)	0.030 (6)	−0.008 (6)	0.014 (5)	−0.020 (6)
C34	0.033 (6)	0.044 (6)	0.051 (7)	0.015 (5)	0.016 (5)	0.021 (6)
C35	0.053 (7)	0.026 (6)	0.055 (7)	−0.001 (5)	0.012 (6)	−0.003 (5)
C36	0.048 (7)	0.061 (8)	0.056 (8)	0.002 (6)	0.032 (6)	−0.003 (6)
C37	0.053 (7)	0.070 (9)	0.040 (6)	0.019 (6)	0.029 (6)	0.042 (6)
C38	0.033 (6)	0.035 (7)	0.085 (10)	0.003 (5)	0.007 (6)	−0.021 (7)
C39	0.072 (10)	0.099 (11)	0.033 (7)	0.002 (9)	0.008 (7)	−0.050 (8)
C40	0.078 (9)	0.057 (8)	0.032 (6)	0.005 (7)	0.030 (6)	−0.002 (6)
C41	0.055 (7)	0.055 (8)	0.042 (7)	0.006 (6)	0.032 (6)	0.020 (6)
C42	0.044 (8)	0.089 (11)	0.077 (11)	−0.009 (8)	0.032 (7)	−0.065 (9)
C43	0.131 (13)	0.033 (8)	0.105 (13)	0.002 (8)	0.104 (12)	0.004 (7)
C44	0.30 (4)	0.15 (2)	0.094 (16)	−0.02 (2)	0.09 (2)	0.069 (16)
C45	0.13 (2)	0.18 (3)	0.43 (5)	−0.03 (2)	0.15 (3)	−0.18 (3)

Table S4.12. Bond lengths [Å], bond angles [º], and torsion angles [º] for **18** using symmetry codes: (i) −*x*, *y*, −*z*+1/2; (ii) −*x*, −*y*, −*z*+1.

U1—N1	1.990	(7)	C7—C13	1.514	(12)
U1—N2	2.257	(7)	C9—C27	1.412	(11)
U1—C16	2.762	(8)	C10—C26	1.496	(12)
U1—C26	2.766	(8)	C11—C12	1.510	(11)
U1—C17	2.772	(8)	C13—C35	1.521	(12)
U1—C20	2.773	(8)	C13—C31	1.540	(12)
U1—C1	2.788	(8)	C15—C20	1.523	(13)
U1—C4	2.810	(8)	C16—C17	1.420	(12)

U1—C6	2.813 (8)	C16—C20	1.431 (12)
U1—C24	2.815 (8)	C16—C19	1.500 (11)
U1—C2	2.838 (8)	C17—C24	1.421 (11)
U1—C12	2.845 (8)	C21—C22	1.379 (11)
N1—C9	1.393 (10)	C22—C3^{i}	1.395 (11)
N2—C21	1.397 (10)	C23—C27	1.497 (12)
N2—C29	1.449 (10)	C23—C40	1.521 (13)
C1—C26	1.409 (12)	C23—C36	1.524 (13)
C1—C4	1.432 (12)	C24—C25	1.494 (12)
C1—C8	1.481 (12)	C27—C41	1.383 (12)
C2—C20	1.401 (12)	C29—C30	1.526 (12)
C2—C24	1.405 (12)	C30—C32	1.369 (13)
C2—C28	1.495 (12)	C30—C33	1.390 (12)
C3—C22^{i}	1.395 (11)	C32—C38	1.404 (13)
C3—C21	1.415 (11)	C33—C39	1.359 (15)
C4—C12	1.406 (12)	C34—C37	1.368 (13)
C4—C18	1.508 (12)	C37—C41	1.373 (14)
C5—C17	1.495 (12)	C38—C42	1.399 (16)
C6—C12	1.414 (12)	C39—C42	1.348 (18)
C6—C26	1.431 (12)	C43—C43^{ii}	1.26 (2)
C6—C14	1.508 (11)	C43—C44	1.45 (3)
C7—C34	1.386 (12)	C44—C45	1.15 (3)
C7—C9	1.451 (11)		
N1—U1—N2	95.8 (2)	C22^{i}—C3—C21	121.2 (7)
N1—U1—C16	74.8 (3)	C12—C4—C1	109.0 (8)
N2—U1—C16	120.4 (3)	C12—C4—C18	126.0 (8)
N1—U1—C26	90.9 (3)	C1—C4—C18	124.4 (8)
N2—U1—C26	91.0 (3)	C12—C4—U1	77.0 (5)

C16—U1—C26	146.2 (3)	C1—C4—U1	74.3 (5)
N1—U1—C17	91.3 (3)	C18—C4—U1	121.9 (6)
N2—U1—C17	94.8 (2)	C12—C6—C26	108.1 (8)
C16—U1—C17	29.7 (2)	C12—C6—C14	124.4 (8)
C26—U1—C17	173.6 (3)	C26—C6—C14	125.7 (8)
N1—U1—C20	93.3 (3)	C12—C6—U1	76.8 (5)
N2—U1—C20	142.6 (3)	C26—C6—U1	73.3 (5)
C16—U1—C20	30.0 (2)	C14—C6—U1	127.7 (6)
C26—U1—C20	125.1 (3)	C34—C7—C9	117.3 (8)
C17—U1—C20	48.8 (3)	C34—C7—C13	119.0 (8)
N1—U1—C1	115.9 (3)	C9—C7—C13	123.6 (7)
N2—U1—C1	73.9 (2)	N1—C9—C27	121.6 (8)
C16—U1—C1	162.5 (3)	N1—C9—C7	119.9 (7)
C26—U1—C1	29.4 (3)	C27—C9—C7	118.5 (8)
C17—U1—C1	151.1 (3)	C4—C12—C6	107.6 (8)
C20—U1—C1	132.5 (3)	C4—C12—C11	127.2 (9)
N1—U1—C4	138.8 (3)	C6—C12—C11	122.4 (8)
N2—U1—C4	91.5 (2)	C4—C12—U1	74.2 (5)
C16—U1—C4	133.7 (3)	C6—C12—U1	74.3 (5)
C26—U1—C4	48.4 (3)	C11—C12—U1	132.3 (6)
C17—U1—C4	128.4 (2)	C7—C13—C35	110.2 (8)
C20—U1—C4	104.9 (3)	C7—C13—C31	111.1 (8)
C1—U1—C4	29.6 (2)	C35—C13—C31	109.4 (7)
N1—U1—C6	94.7 (3)	C17—C16—C20	106.8 (8)
N2—U1—C6	119.7 (2)	C17—C16—C19	125.2 (8)
C16—U1—C6	119.7 (3)	C20—C16—C19	127.0 (9)
C26—U1—C6	29.7 (2)	C17—C16—U1	75.5 (5)
C17—U1—C6	144.0 (2)	C20—C16—U1	75.4 (5)

C20—U1—C6	95.4 (3)	C19—C16—U1	123.6 (5)
C1—U1—C6	48.5 (2)	C16—C17—C24	107.8 (8)
C4—U1—C6	47.7 (3)	C16—C17—C5	126.9 (8)
N1—U1—C24	120.1 (3)	C24—C17—C5	124.8 (8)
N2—U1—C24	97.1 (2)	C16—C17—U1	74.7 (5)
C16—U1—C24	48.6 (3)	C24—C17—U1	77.0 (5)
C26—U1—C24	146.7 (3)	C5—C17—U1	120.9 (5)
C17—U1—C24	29.5 (2)	C2—C20—C16	108.9 (8)
C20—U1—C24	47.9 (3)	C2—C20—C15	127.2 (9)
C1—U1—C24	124.0 (3)	C16—C20—C15	123.6 (9)
C4—U1—C24	99.0 (3)	C2—C20—U1	78.1 (5)
C6—U1—C24	126.6 (3)	C16—C20—U1	74.6 (5)
N1—U1—C2	121.1 (2)	C15—C20—U1	118.2 (6)
N2—U1—C2	123.5 (2)	C22—C21—N2	125.4 (8)
C16—U1—C2	48.6 (2)	C22—C21—C3	115.6 (7)
C26—U1—C2	125.7 (3)	N2—C21—C3	119.0 (7)
C17—U1—C2	48.3 (2)	C21—C22—C3^{i}	123.0 (8)
C20—U1—C2	28.9 (2)	C27—C23—C40	110.8 (8)
C1—U1—C2	116.2 (3)	C27—C23—C36	111.9 (8)
C4—U1—C2	86.6 (2)	C40—C23—C36	109.8 (8)
C6—U1—C2	99.6 (3)	C2—C24—C17	108.7 (8)
C24—U1—C2	28.8 (2)	C2—C24—C25	123.7 (8)
N1—U1—C12	122.2 (3)	C17—C24—C25	126.3 (8)
N2—U1—C12	119.5 (2)	C2—C24—U1	76.5 (5)
C16—U1—C12	114.5 (3)	C17—C24—U1	73.6 (5)
C26—U1—C12	48.5 (3)	C25—C24—U1	126.3 (6)
C17—U1—C12	125.6 (2)	C1—C26—C6	108.2 (8)
C20—U1—C12	84.7 (3)	C1—C26—C10	127.0 (9)

C1—U1—C12	48.4 (2)	C6—C26—C10	124.1 (8)
C4—U1—C12	28.8 (2)	C1—C26—U1	76.2 (5)
C6—U1—C12	28.9 (2)	C6—C26—U1	77.0 (5)
C24—U1—C12	100.5 (3)	C10—C26—U1	121.1 (6)
C2—U1—C12	77.3 (3)	C41—C27—C9	119.8 (9)
C9—N1—U1	173.1 (6)	C41—C27—C23	119.8 (8)
C21—N2—C29	114.6 (7)	C9—C27—C23	120.5 (8)
C21—N2—U1	134.1 (5)	N2—C29—C30	117.9 (7)
C29—N2—U1	108.4 (5)	C32—C30—C33	119.3 (9)
C26—C1—C4	107.0 (8)	C32—C30—C29	121.8 (8)
C26—C1—C8	126.3 (8)	C33—C30—C29	118.9 (9)
C4—C1—C8	125.2 (8)	C30—C32—C38	120.3 (10)
C26—C1—U1	74.4 (5)	C39—C33—C30	120.8 (12)
C4—C1—U1	76.0 (5)	C37—C34—C7	123.9 (9)
C8—C1—U1	126.0 (6)	C34—C37—C41	118.2 (9)
C20—C2—C24	107.8 (8)	C42—C38—C32	118.3 (12)
C20—C2—C28	127.7 (8)	C42—C39—C33	120.6 (12)
C24—C2—C28	122.8 (8)	C37—C41—C27	122.3 (9)
C20—C2—U1	73.0 (5)	C39—C42—C38	120.8 (11)
C24—C2—U1	74.7 (5)	$C43^{ii}$—C43—C44	101.3 (15)
C28—C2—U1	129.9 (6)	C45—C44—C43	104 (2)

Table S4.13. Atomic coordinates and equivalent isotropic displacement parameters (A^2) for **20**. U(eq) is defined as one third of the trace of the orthogonalized U^{ij} tensor.

	x	y	z	U(eq)
U(1)	3068(1)	8054(1)	4139(1)	33(1)
U(2)	3985(1)	2415(1)	701(1)	48(1)

U(3)	5438(1)	2393(1)	702(1)	47(1)
N(1)	2345(8)	7051(5)	3966(4)	32(2)
N(2)	1748(8)	8834(6)	4480(5)	42(2)
N(3)	4398(12)	2486(7)	1625(5)	74(4)
N(4)	12260(17)	2404(12)	720(9)	46(5)
N(5)	7169(19)	2385(13)	713(10)	56(6)
C(1)	3577(11)	8301(7)	5341(6)	44(3)
C(2)	4683(10)	8013(7)	4986(6)	40(3)
C(3)	4552(10)	7167(7)	4897(5)	40(3)
C(4)	3386(11)	6936(7)	5197(5)	39(3)
C(5)	2758(10)	7632(8)	5457(5)	40(3)
C(6)	3360(13)	9157(8)	5599(8)	70(4)
C(7)	5818(11)	8496(8)	4799(6)	52(3)
C(8)	5512(10)	6615(7)	4543(6)	44(3)
C(9)	2860(11)	6073(7)	5312(6)	42(3)
C(10)	1502(11)	7662(9)	5869(6)	64(4)
C(11)	4700(11)	8897(8)	3139(6)	48(3)
C(12)	3701(12)	9437(7)	3272(6)	48(3)
C(13)	2712(11)	9091(8)	3073(5)	45(3)
C(14)	3104(12)	8346(7)	2816(6)	45(3)
C(15)	4354(11)	8226(7)	2885(5)	39(3)
C(16)	6011(11)	9060(8)	3181(6)	58(4)
C(17)	3719(13)	10273(7)	3521(6)	59(4)
C(18)	1472(12)	9490(8)	3056(7)	67(4)
C(19)	2350(12)	7837(8)	2479(6)	55(3)
C(20)	5201(12)	7520(8)	2613(6)	58(4)
C(21)	1681(10)	6343(7)	3919(5)	36(3)

C(22)	406(11)	6333(8)	4106(6)	52(3)
C(23)	-217(13)	5644(9)	4050(9)	85(6)
C(24)	375(14)	4949(10)	3800(8)	84(5)
C(25)	1625(13)	4937(8)	3608(7)	62(4)
C(26)	2316(11)	5611(7)	3652(6)	44(3)
C(27)	-321(11)	7091(9)	4344(8)	64(4)
C(28)	-909(13)	7554(9)	3797(8)	72(4)
C(29)	-1212(13)	6907(9)	4969(7)	71(4)
C(30)	3627(11)	5573(7)	3409(5)	41(3)
C(31)	4259(14)	4899(8)	3802(7)	71(4)
C(32)	3935(13)	5444(8)	2700(6)	64(4)
C(33)	895(11)	9408(7)	4728(6)	46(3)
C(34)	1186(12)	10226(8)	4827(7)	57(4)
C(35)	-322(11)	9210(7)	4912(7)	52(3)
C(36)	4179(9)	2553(5)	2290(3)	49(3)
C(37)	5155(7)	2570(5)	2623(5)	57(4)
C(38)	4939(11)	2619(6)	3297(5)	88(6)
C(39)	3748(14)	2652(6)	3639(3)	123(9)
C(40)	2772(10)	2636(6)	3305(5)	92(6)
C(41)	2988(7)	2586(5)	2631(5)	58(4)
C(42)	6442(16)	2556(13)	2307(12)	118(8)
C(43)	7130(20)	3340(14)	2368(17)	190(14)
C(44)	7104(19)	1795(13)	2555(14)	138(9)
C(45)	1895(14)	2574(8)	2293(11)	99(7)
C(46)	1120(20)	3403(13)	2331(16)	172(12)
C(47)	1117(18)	1826(12)	2576(14)	147(10)
C(48)	4808(10)	3515(5)	-392(5)	90(3)

C(49)	6038(9)	3614(5)	-323(5)	90(3)
C(50)	6028(10)	3925(4)	290(6)	90(3)
C(51)	4792(11)	4017(4)	600(5)	90(3)
C(52)	4038(9)	3764(4)	179(5)	90(3)
C(53)	4392(12)	3200(7)	-970(4)	90(3)
C(54)	7158(10)	3424(7)	-815(6)	90(3)
C(55)	7136(12)	4122(6)	565(7)	90(3)
C(56)	4356(14)	4330(5)	1262(6)	90(3)
C(57)	2660(9)	3760(5)	313(7)	90(3)
C(58)	4663(11)	769(4)	1110(5)	109(4)
C(59)	5777(10)	928(4)	668(5)	109(4)
C(60)	5501(9)	1121(4)	24(5)	109(4)
C(61)	4217(10)	1081(4)	68(5)	109(4)
C(62)	3699(10)	864(4)	739(5)	109(4)
C(63)	4528(15)	540(6)	1845(5)	109(4)
C(64)	7033(11)	898(6)	851(7)	109(4)
C(65)	6413(10)	1331(6)	-597(5)	109(4)
C(66)	3524(11)	1242(6)	-499(6)	109(4)
C(67)	2359(10)	753(6)	1010(7)	109(4)
C(68)	4846(10)	1140(9)	-63(5)	159(7)
C(69)	5841(10)	998(8)	270(7)	159(7)
C(70)	5370(11)	761(9)	956(5)	159(7)
C(71)	4078(11)	751(9)	1028(5)	159(7)
C(72)	3753(9)	997(9)	399(6)	159(7)
C(73)	4934(12)	1386(9)	-793(5)	159(7)
C(74)	7174(10)	1090(9)	-26(7)	159(7)
C(75)	6107(13)	568(9)	1503(6)	159(7)

C(76)	3201(13)	546(10)	1663(6)	159(7)
C(77)	2475(10)	1063(10)	246(7)	159(7)
C(78)	3646(11)	4135(4)	612(7)	214(10)
C(79)	3084(10)	3945(5)	88(7)	214(10)
C(80)	4011(10)	3657(5)	-403(6)	214(10)
C(81)	5147(10)	3668(4)	-179(6)	214(10)
C(82)	4921(11)	3963(4)	447(7)	214(10)
C(83)	3001(14)	4464(5)	1234(7)	214(10)
C(84)	1737(10)	4034(7)	56(9)	214(10)
C(85)	3821(13)	3384(7)	-1050(6)	214(10)
C(86)	6377(10)	3412(5)	-545(7)	214(10)
C(87)	5869(13)	4076(5)	862(7)	214(10)
C(91)	8460(30)	2350(20)	640(20)	166(9)
C(92)	9270(40)	2300(20)	60(17)	166(9)
C(93)	10520(40)	2320(20)	51(17)	166(9)
C(94)	10950(30)	2410(20)	630(30)	166(9)
C(95)	10140(40)	2460(20)	1212(17)	166(9)
C(96)	8890(40)	2440(20)	1220(17)	166(9)
H(6A)	2534	9204	5827	106
H(6B)	3497	9591	5237	106
H(6C)	3912	9214	5897	106
H(7A)	6444	8166	4557	78
H(7B)	6082	8629	5189	78
H(7C)	5662	9004	4530	78
H(8A)	6236	6928	4377	66
H(8B)	5215	6419	4183	66
H(8C)	5701	6144	4842	66

H(9A)	2027	6106	5532	63
H(9B)	3327	5707	5580	63
H(9C)	2891	5858	4897	63
H(10A)	1307	8221	5979	96
H(10B)	1484	7286	6266	96
H(10C)	914	7497	5625	96
H(16A)	6041	9570	3375	87
H(16B)	6491	9110	2747	87
H(16C)	6331	8602	3447	87
H(17A)	2908	10519	3581	88
H(17B)	4252	10634	3207	88
H(17C)	4008	10203	3933	88
H(18A)	1402	9996	3265	101
H(18B)	860	9110	3286	101
H(18C)	1358	9619	2607	101
H(19A)	2818	7352	2342	82
H(19B)	2127	8172	2102	82
H(19C)	1625	7665	2780	82
H(20A)	4728	7123	2462	87
H(20B)	5607	7244	2954	87
H(20C)	5797	7751	2253	87
H(23)	-1059	5644	4185	102
H(24)	-69	4488	3761	101
H(25)	2014	4462	3444	75
H(27)	271	7470	4440	76
H(28A)	-299	7672	3412	108
H(28B)	-1281	8070	3935	108

H(28C)	-1522	7214	3697	108
H(29A)	-793	6628	5303	107
H(29B)	-1832	6553	4895	107
H(29C)	-1584	7422	5109	107
H(30)	3956	6111	3461	49
H(31A)	5120	4896	3633	106
H(31B)	3940	4365	3768	106
H(31C)	4121	5004	4255	106
H(32A)	4806	5434	2565	96
H(32B)	3578	5893	2442	96
H(32C)	3620	4921	2635	96
H(34)	1994	10386	4711	68
H(35)	-561	8680	4858	63

Table S4.14. Anisotropic displacement parameters (A^2) for **20**. The anisotropic displacement factor exponent takes the form: $-2\pi^2 [h^2 a^{2}*U^{11} + ... + 2 h k a* b* U^{12}]$.

	U^{11}	U^{22}	U^{33}	U^{23}	U^{13}	U^{12}
U(1)	36(1)	31(1)	30(1)	-6(1)	-2(1)	-1(1)
U(2)	67(1)	45(1)	30(1)	0(1)	-1(1)	-10(1)
U(3)	65(1)	45(1)	32(1)	-1(1)	-10(1)	-4(1)
N(1)	42(5)	29(5)	17(4)	0(4)	6(4)	8(4)
N(2)	40(6)	38(6)	51(6)	-8(5)	-15(5)	5(4)
N(3)	130(11)	45(7)	42(7)	-4(5)	1(7)	-17(7)
C(1)	54(8)	47(7)	34(7)	-16(6)	-5(6)	1(6)
C(2)	44(7)	39(7)	40(7)	0(5)	-13(6)	-15(6)

C(3)	34(7)	50(7)	35(7)	-1(6)	-9(5)	0(5)
C(4)	58(8)	37(7)	24(6)	-7(5)	-11(6)	-8(6)
C(5)	41(7)	57(8)	20(6)	0(5)	-1(5)	-14(6)
C(6)	83(11)	38(8)	98(12)	-31(8)	-19(9)	-5(7)
C(7)	51(8)	56(8)	50(8)	-3(6)	-10(6)	-15(6)
C(8)	36(7)	45(7)	51(8)	-10(6)	-3(6)	2(5)
C(9)	54(8)	38(7)	36(7)	2(5)	-14(6)	-7(6)
C(10)	44(8)	100(11)	47(8)	-32(8)	13(6)	-13(7)
C(11)	56(8)	46(8)	36(7)	0(6)	7(6)	-23(6)
C(12)	65(9)	31(7)	47(8)	-3(6)	-11(7)	-4(6)
C(13)	51(8)	53(8)	26(6)	20(6)	-4(6)	-12(6)
C(14)	67(9)	36(7)	34(7)	4(5)	-11(6)	-11(6)
C(15)	50(8)	41(7)	22(6)	-1(5)	2(5)	1(6)
C(16)	48(8)	75(9)	39(7)	15(7)	14(6)	-19(7)
C(17)	92(11)	31(7)	50(8)	4(6)	-9(7)	-1(7)
C(18)	71(10)	58(9)	70(10)	0(7)	-16(8)	13(8)
C(19)	73(9)	51(8)	49(8)	-16(6)	-21(7)	-11(7)
C(20)	68(9)	69(9)	34(7)	6(6)	-2(6)	-10(7)
C(21)	36(7)	39(7)	30(6)	-4(5)	8(5)	-15(5)
C(22)	50(8)	46(8)	58(8)	-14(6)	8(6)	-10(6)
C(23)	45(9)	67(10)	146(16)	-56(11)	8(9)	-15(8)
C(24)	60(10)	81(12)	112(14)	-25(10)	5(9)	-52(9)
C(25)	81(11)	31(7)	72(10)	-4(7)	-1(8)	-19(7)

C(26)	52(8)	27(6)	53(8)	-7(5)	-5(6)	-4(5)
C(27)	33(7)	62(9)	94(12)	-29(8)	7(8)	-9(6)
C(28)	72(10)	58(9)	81(11)	-18(8)	6(9)	-2(8)
C(29)	65(10)	82(11)	67(10)	-28(8)	3(8)	-6(8)
C(30)	53(8)	34(6)	34(7)	-6(5)	-3(6)	-2(5)
C(31)	90(11)	40(8)	93(12)	-22(8)	-41(9)	16(7)
C(32)	86(11)	58(9)	45(8)	-29(7)	8(7)	15(7)
C(33)	52(8)	28(6)	60(8)	-23(6)	-4(6)	0(6)
C(34)	44(8)	50(8)	78(10)	-9(7)	-8(7)	-12(6)
C(35)	49(8)	34(7)	79(10)	-31(7)	-9(7)	6(6)
C(36)	72(9)	39(7)	36(7)	0(6)	-10(7)	-18(6)
C(37)	82(11)	30(7)	63(9)	-14(6)	-13(8)	-13(7)
C(38)	152(18)	39(9)	87(13)	-13(9)	-59(12)	24(10)
C(39)	250(30)	56(11)	67(13)	-24(9)	-53(16)	68(15)
C(40)	155(18)	38(8)	57(10)	11(8)	36(11)	18(10)
C(41)	86(11)	28(7)	54(9)	1(6)	3(8)	-5(7)
C(42)	61(12)	101(15)	190(20)	23(14)	-33(13)	-19(11)
C(43)	110(18)	95(17)	380(40)	30(20)	-90(20)	-51(14)
C(44)	101(16)	85(14)	240(30)	-36(16)	-66(18)	16(12)
C(45)	69(11)	20(7)	210(20)	9(10)	-30(12)	-1(7)
C(46)	170(20)	76(15)	300(40)	-26(18)	-100(20)	1(14)
C(47)	90(15)	87(14)	250(30)	9(16)	-2(16)	-42(12)

Table S4.15. Bond lengths [Å], bond angles [º], and torsion angles [º] for **20**. Symmetry transformations used to generate equivalent atoms: (1) x-1,y,z (2) x+1,y,z (3) -x,-y+2,-z+1

U(1)-N(1)	1.936(9)
U(1)-N(2)	1.972(9)
U(1)-C(13)	2.684(11)
U(1)-C(5)	2.706(10)
U(1)-C(12)	2.727(12)
U(1)-C(3)	2.718(11)
U(1)-C(2)	2.721(11)
U(1)-C(14)	2.726(11)
U(1)-C(15)	2.731(10)
U(1)-C(4)	2.731(11)
U(1)-C(1)	2.732(11)
U(1)-C(11)	2.774(11)
U(2)-U(3)	1.6158(14)
U(2)-N(4)#1	1.914(19)
U(2)-N(3)	2.068(11)
U(2)-C(52)	2.307(6)
U(2)-C(72)	2.473(16)
U(2)-C(62)	2.520(6)
U(2)-C(61)	2.623(7)
U(2)-C(71)	2.681(15)
U(2)-C(57)	2.682(7)
U(2)-C(82)	2.706(7)
U(2)-C(48)	2.756(7)
U(2)-C(51)	2.744(7)
U(3)-N(5)	1.93(2)

U(3)-N(3)	2.074(11)
U(3)-C(59)	2.373(6)
U(3)-C(69)	2.503(10)
U(3)-C(70)	2.617(14)
U(3)-C(60)	2.608(7)
U(3)-C(50)	2.588(7)
U(3)-C(82)	2.576(7)
U(3)-C(81)	2.630(9)
U(3)-C(51)	2.669(6)
U(3)-C(49)	2.734(7)
N(1)-C(21)	1.411(13)
N(2)-C(33)	1.367(14)
N(3)-C(36)	1.374(12)
N(4)-C(94)	1.50(3)
N(4)-U(2)#2	1.914(19)
N(5)-C(91)	1.41(3)
C(1)-C(2)	1.404(16)
C(1)-C(5)	1.417(15)
C(1)-C(6)	1.529(16)
C(2)-C(3)	1.413(15)
C(2)-C(7)	1.484(15)
C(3)-C(4)	1.385(15)
C(3)-C(8)	1.501(15)
C(4)-C(5)	1.402(15)
C(4)-C(9)	1.509(14)
C(5)-C(10)	1.506(15)
C(11)-C(15)	1.356(15)

C(11)-C(12)	1.385(17)
C(11)-C(16)	1.514(16)
C(12)-C(13)	1.403(16)
C(12)-C(17)	1.499(16)
C(13)-C(14)	1.388(16)
C(13)-C(18)	1.497(17)
C(14)-C(15)	1.425(16)
C(14)-C(19)	1.508(15)
C(15)-C(20)	1.533(16)
C(21)-C(22)	1.404(15)
C(21)-C(26)	1.457(15)
C(22)-C(23)	1.362(17)
C(22)-C(27)	1.512(17)
C(23)-C(24)	1.38(2)
C(24)-C(25)	1.377(18)
C(25)-C(26)	1.381(16)
C(26)-C(30)	1.458(15)
C(27)-C(28)	1.51(2)
C(27)-C(29)	1.496(18)
C(30)-C(32)	1.489(15)
C(30)-C(31)	1.501(16)
C(33)-C(35)	1.384(16)
C(33)-C(34)	1.416(15)
C(34)-C(35)#3	1.374(16)
C(35)-C(34)#3	1.374(16)
C(36)-C(37)	1.3900
C(36)-C(41)	1.3900

C(37)-C(38)	1.3900
C(37)-C(42)	1.47(2)
C(38)-C(39)	1.3900
C(39)-C(40)	1.3900
C(40)-C(41)	1.3900
C(41)-C(45)	1.511(18)
C(42)-C(44)	1.48(3)
C(42)-C(43)	1.53(3)
C(45)-C(47)	1.52(2)
C(45)-C(46)	1.55(3)
C(48)-C(49)	1.4200
C(48)-C(52)	1.4200
C(48)-C(53)	1.5095
C(49)-C(50)	1.4200
C(49)-C(54)	1.5095
C(50)-C(51)	1.4200
C(50)-C(55)	1.5095
C(51)-C(52)	1.4200
C(51)-C(56)	1.5095
C(52)-C(57)	1.5095
C(58)-C(59)	1.4200
C(58)-C(62)	1.4201
C(58)-C(63)	1.5094
C(59)-C(60)	1.4201
C(59)-C(64)	1.5094
C(60)-C(61)	1.4200
C(60)-C(65)	1.5093

C(61)-C(62)	1.4199
C(61)-C(66)	1.5095
C(62)-C(67)	1.5095
C(68)-C(72)	1.4208
C(68)-C(69)	1.402(9)
C(68)-C(73)	1.5086
C(69)-C(70)	1.441(10)
C(69)-C(74)	1.5094
C(70)-C(71)	1.4201
C(70)-C(75)	1.5095
C(71)-C(72)	1.4210
C(71)-C(76)	1.5090
C(72)-C(77)	1.5080
C(78)-C(79)	1.4177
C(78)-C(82)	1.4207
C(78)-C(83)	1.5030(14)
C(79)-C(80)	1.4168
C(79)-C(84)	1.5113
C(80)-C(81)	1.4231
C(80)-C(85)	1.5144(11)
C(81)-C(82)	1.4135(15)
C(81)-C(86)	1.5070
C(82)-C(87)	1.5055
C(91)-C(92)	1.3900
C(91)-C(96)	1.3900
C(92)-C(93)	1.3900
C(93)-C(94)	1.3900

C(94)-C(95)	1.3900
C(95)-C(96)	1.3900

N(1)-U(1)-N(2)	108.7(4)
N(1)-U(1)-C(13)	100.2(4)
N(2)-U(1)-C(13)	75.9(4)
N(1)-U(1)-C(5)	94.5(3)
N(2)-U(1)-C(5)	76.8(4)
C(13)-U(1)-C(5)	151.9(4)
N(1)-U(1)-C(12)	127.2(3)
N(2)-U(1)-C(12)	81.1(4)
C(13)-U(1)-C(12)	30.0(3)
C(5)-U(1)-C(12)	137.3(4)
N(1)-U(1)-C(3)	92.6(3)
N(2)-U(1)-C(3)	123.8(4)
C(13)-U(1)-C(3)	151.6(4)
C(5)-U(1)-C(3)	49.4(3)
C(12)-U(1)-C(3)	125.6(4)
N(1)-U(1)-C(2)	122.3(3)
N(2)-U(1)-C(2)	104.4(4)
C(13)-U(1)-C(2)	133.5(4)
C(5)-U(1)-C(2)	49.6(3)
C(12)-U(1)-C(2)	103.4(4)
C(3)-U(1)-C(2)	30.1(3)
N(1)-U(1)-C(14)	78.3(3)
N(2)-U(1)-C(14)	101.8(4)
C(13)-U(1)-C(14)	29.7(3)

C(5)-U(1)-C(14)	172.0(3)
C(12)-U(1)-C(14)	49.2(3)
C(3)-U(1)-C(14)	133.8(4)
C(2)-U(1)-C(14)	137.8(4)
N(1)-U(1)-C(15)	90.3(3)
N(2)-U(1)-C(15)	124.3(4)
C(13)-U(1)-C(15)	49.0(4)
C(5)-U(1)-C(15)	155.3(4)
C(12)-U(1)-C(15)	48.3(3)
C(3)-U(1)-C(15)	106.3(3)
C(2)-U(1)-C(15)	108.1(4)
C(14)-U(1)-C(15)	30.3(3)
N(1)-U(1)-C(4)	77.0(3)
N(2)-U(1)-C(4)	105.3(4)
C(13)-U(1)-C(4)	177.1(3)
C(5)-U(1)-C(4)	29.9(3)
C(12)-U(1)-C(4)	152.4(4)
C(3)-U(1)-C(4)	29.4(3)
C(2)-U(1)-C(4)	49.1(3)
C(14)-U(1)-C(4)	147.9(3)
C(15)-U(1)-C(4)	130.2(3)
N(1)-U(1)-C(1)	123.8(3)
N(2)-U(1)-C(1)	76.4(4)
C(13)-U(1)-C(1)	133.6(4)
C(5)-U(1)-C(1)	30.2(3)
C(12)-U(1)-C(1)	109.0(4)
C(3)-U(1)-C(1)	49.5(3)

C(2)-U(1)-C(1)	29.9(3)
C(14)-U(1)-C(1)	157.5(4)
C(15)-U(1)-C(1)	134.3(4)
C(4)-U(1)-C(1)	49.2(3)
N(1)-U(1)-C(11)	118.8(3)
N(2)-U(1)-C(11)	109.8(4)
C(13)-U(1)-C(11)	48.5(4)
C(5)-U(1)-C(11)	139.5(4)
C(12)-U(1)-C(11)	29.1(4)
C(3)-U(1)-C(11)	103.2(4)
C(2)-U(1)-C(11)	91.2(4)
C(14)-U(1)-C(11)	48.5(4)
C(15)-U(1)-C(11)	28.5(3)
C(4)-U(1)-C(11)	132.6(4)
C(1)-U(1)-C(11)	110.4(4)
U(3)-U(2)-N(4)#1	178.0(6)
U(3)-U(2)-N(3)	67.2(4)
N(4)#1-U(2)-N(3)	111.8(7)
U(3)-U(2)-C(52)	91.7(3)
N(4)#1-U(2)-C(52)	90.2(6)
N(3)-U(2)-C(52)	106.4(4)
U(3)-U(2)-C(72)	100.1(3)
N(4)#1-U(2)-C(72)	78.6(6)
N(3)-U(2)-C(72)	116.8(4)
C(52)-U(2)-C(72)	136.6(4)
U(3)-U(2)-C(62)	98.6(3)
N(4)#1-U(2)-C(62)	79.8(6)

N(3)-U(2)-C(62)	101.2(4)
C(52)-U(2)-C(62)	152.4(4)
C(72)-U(2)-C(62)	16.2
U(3)-U(2)-C(61)	90.8(2)
N(4)#1-U(2)-C(61)	88.4(6)
N(3)-U(2)-C(61)	126.5(4)
C(52)-U(2)-C(61)	123.2(3)
C(72)-U(2)-C(61)	17.4
C(62)-U(2)-C(61)	31.97(8)
U(3)-U(2)-C(71)	86.9(3)
N(4)#1-U(2)-C(71)	91.2(6)
N(3)-U(2)-C(71)	85.1(4)
C(52)-U(2)-C(71)	166.9(4)
C(72)-U(2)-C(71)	31.68(11)
C(62)-U(2)-C(71)	17.13(11)
C(61)-U(2)-C(71)	43.85(18)
U(3)-U(2)-C(57)	125.4(2)
N(4)#1-U(2)-C(57)	56.5(6)
N(3)-U(2)-C(57)	111.4(4)
C(52)-U(2)-C(57)	34.19(10)
C(72)-U(2)-C(57)	123.4(4)
C(62)-U(2)-C(57)	132.4(4)
C(61)-U(2)-C(57)	120.7(4)
C(71)-U(2)-C(57)	147.1(4)
U(3)-U(2)-C(82)	67.8(3)
N(4)#1-U(2)-C(82)	114.0(6)
N(3)-U(2)-C(82)	83.0(4)

C(52)-U(2)-C(82)	28.3(3)
C(72)-U(2)-C(82)	151.9(4)
C(62)-U(2)-C(82)	163.3(4)
C(61)-U(2)-C(82)	134.5(4)
C(71)-U(2)-C(82)	154.6(4)
C(57)-U(2)-C(82)	58.2(2)
U(3)-U(2)-C(48)	78.1(2)
N(4)#1-U(2)-C(48)	103.8(6)
N(3)-U(2)-C(48)	124.0(4)
C(52)-U(2)-C(48)	30.98(9)
C(72)-U(2)-C(48)	111.5(3)
C(62)-U(2)-C(48)	127.2(3)
C(61)-U(2)-C(48)	95.3(3)
C(71)-U(2)-C(48)	136.5(3)
C(57)-U(2)-C(48)	57.36(14)
C(82)-U(2)-C(48)	42.7(3)
U(3)-U(2)-C(51)	70.1(2)
N(4)#1-U(2)-C(51)	111.6(6)
N(3)-U(2)-C(51)	77.4(4)
C(52)-U(2)-C(51)	31.14(9)
C(72)-U(2)-C(51)	159.1(3)
C(62)-U(2)-C(51)	168.4(4)
C(61)-U(2)-C(51)	141.7(3)
C(71)-U(2)-C(51)	155.1(4)
C(57)-U(2)-C(51)	57.50(12)
C(82)-U(2)-C(51)	7.2(2)
C(48)-U(2)-C(51)	49.38(11)

U(2)-U(3)-N(5)	178.9(6)
U(2)-U(3)-N(3)	66.8(4)
N(5)-U(3)-N(3)	112.5(7)
U(2)-U(3)-C(59)	97.2(3)
N(5)-U(3)-C(59)	83.8(7)
N(3)-U(3)-C(59)	103.8(4)
U(2)-U(3)-C(69)	95.2(3)
N(5)-U(3)-C(69)	85.9(7)
N(3)-U(3)-C(69)	120.4(4)
C(59)-U(3)-C(69)	18.9(3)
U(2)-U(3)-C(70)	88.7(3)
N(5)-U(3)-C(70)	92.1(7)
N(3)-U(3)-C(70)	88.5(4)
C(59)-U(3)-C(70)	15.55(12)
C(69)-U(3)-C(70)	32.60(17)
U(2)-U(3)-C(60)	84.8(2)
N(5)-U(3)-C(60)	96.3(7)
N(3)-U(3)-C(60)	125.5(4)
C(59)-U(3)-C(60)	32.70(9)
C(69)-U(3)-C(60)	15.4(3)
C(70)-U(3)-C(60)	43.49(17)
U(2)-U(3)-C(50)	102.9(3)
N(5)-U(3)-C(50)	76.4(7)
N(3)-U(3)-C(50)	103.2(4)
C(59)-U(3)-C(50)	151.0(4)
C(69)-U(3)-C(50)	136.4(5)
C(70)-U(3)-C(50)	166.0(4)

C(60)-U(3)-C(50)	128.8(3)
U(2)-U(3)-C(82)	76.6(3)
N(5)-U(3)-C(82)	102.6(7)
N(3)-U(3)-C(82)	86.2(4)
C(59)-U(3)-C(82)	165.3(4)
C(69)-U(3)-C(82)	146.9(3)
C(70)-U(3)-C(82)	165.3(4)
C(60)-U(3)-C(82)	132.6(4)
C(50)-U(3)-C(82)	27.26(7)
U(2)-U(3)-C(81)	77.1(2)
N(5)-U(3)-C(81)	102.6(7)
N(3)-U(3)-C(81)	114.4(4)
C(59)-U(3)-C(81)	134.4(4)
C(69)-U(3)-C(81)	115.6(3)
C(70)-U(3)-C(81)	144.4(3)
C(60)-U(3)-C(81)	102.1(4)
C(50)-U(3)-C(81)	35.7(3)
C(82)-U(3)-C(81)	31.49(8)
U(2)-U(3)-C(51)	75.2(3)
N(5)-U(3)-C(51)	103.9(7)
N(3)-U(3)-C(51)	79.1(4)
C(59)-U(3)-C(51)	170.2(4)
C(69)-U(3)-C(51)	153.4(5)
C(70)-U(3)-C(51)	162.6(4)
C(60)-U(3)-C(51)	138.6(3)
C(50)-U(3)-C(51)	31.30(7)
C(82)-U(3)-C(51)	7.3(3)

C(81)-U(3)-C(51)	38.5(3)
U(2)-U(3)-C(49)	97.3(2)
N(5)-U(3)-C(49)	82.5(7)
N(3)-U(3)-C(49)	129.4(4)
C(59)-U(3)-C(49)	126.3(3)
C(69)-U(3)-C(49)	108.3(4)
C(70)-U(3)-C(49)	140.9(4)
C(60)-U(3)-C(49)	98.4(3)
C(50)-U(3)-C(49)	30.79(8)
C(82)-U(3)-C(49)	43.3(2)
C(81)-U(3)-C(49)	21.07(6)
C(51)-U(3)-C(49)	50.32(12)
C(21)-N(1)-U(1)	171.5(7)
C(33)-N(2)-U(1)	175.9(8)
C(36)-N(3)-U(2)	157.4(10)
C(36)-N(3)-U(3)	156.7(10)
U(2)-N(3)-U(3)	45.9(2)
C(94)-N(4)-U(2)#2	172(2)
C(91)-N(5)-U(3)	173(3)
C(2)-C(1)-C(5)	107.4(10)
C(2)-C(1)-C(6)	125.3(11)
C(5)-C(1)-C(6)	127.1(11)
C(2)-C(1)-U(1)	74.6(6)
C(5)-C(1)-U(1)	73.9(6)
C(6)-C(1)-U(1)	121.2(9)
C(1)-C(2)-C(3)	108.0(10)
C(1)-C(2)-C(7)	125.3(11)

C(3)-C(2)-C(7)	126.4(11)
C(1)-C(2)-U(1)	75.5(7)
C(3)-C(2)-U(1)	74.8(6)
C(7)-C(2)-U(1)	120.3(8)
C(4)-C(3)-C(2)	108.0(10)
C(4)-C(3)-C(8)	126.1(10)
C(2)-C(3)-C(8)	125.9(10)
C(4)-C(3)-U(1)	75.8(7)
C(2)-C(3)-U(1)	75.0(6)
C(8)-C(3)-U(1)	115.7(7)
C(3)-C(4)-C(5)	108.8(10)
C(3)-C(4)-C(9)	128.3(11)
C(5)-C(4)-C(9)	122.6(10)
C(3)-C(4)-U(1)	74.8(6)
C(5)-C(4)-U(1)	74.1(6)
C(9)-C(4)-U(1)	122.5(7)
C(4)-C(5)-C(1)	107.7(10)
C(4)-C(5)-C(10)	127.7(11)
C(1)-C(5)-C(10)	124.1(11)
C(4)-C(5)-U(1)	76.0(6)
C(1)-C(5)-U(1)	75.9(6)
C(10)-C(5)-U(1)	120.3(8)
C(15)-C(11)-C(12)	109.1(11)
C(15)-C(11)-C(16)	123.8(12)
C(12)-C(11)-C(16)	126.6(11)
C(15)-C(11)-U(1)	74.0(6)
C(12)-C(11)-U(1)	73.5(7)

C(16)-C(11)-U(1)	124.6(8)
C(11)-C(12)-C(13)	107.2(11)
C(11)-C(12)-C(17)	125.7(12)
C(13)-C(12)-C(17)	126.8(12)
C(11)-C(12)-U(1)	77.3(7)
C(13)-C(12)-U(1)	73.3(6)
C(17)-C(12)-U(1)	119.8(8)
C(14)-C(13)-C(12)	108.8(11)
C(14)-C(13)-C(18)	124.0(12)
C(12)-C(13)-C(18)	126.8(12)
C(14)-C(13)-U(1)	76.8(7)
C(12)-C(13)-U(1)	76.7(7)
C(18)-C(13)-U(1)	118.8(8)
C(13)-C(14)-C(15)	106.0(10)
C(13)-C(14)-C(19)	124.9(12)
C(15)-C(14)-C(19)	128.9(11)
C(13)-C(14)-U(1)	73.5(7)
C(15)-C(14)-U(1)	75.0(6)
C(19)-C(14)-U(1)	120.9(8)
C(11)-C(15)-C(14)	108.7(10)
C(11)-C(15)-C(20)	126.1(12)
C(14)-C(15)-C(20)	124.6(11)
C(11)-C(15)-U(1)	77.5(6)
C(14)-C(15)-U(1)	74.7(6)
C(20)-C(15)-U(1)	121.6(7)
C(22)-C(21)-N(1)	121.4(10)
C(22)-C(21)-C(26)	118.6(10)

N(1)-C(21)-C(26)	119.9(9)
C(23)-C(22)-C(21)	120.3(12)
C(23)-C(22)-C(27)	118.1(12)
C(21)-C(22)-C(27)	121.5(10)
C(22)-C(23)-C(24)	121.4(13)
C(25)-C(24)-C(23)	119.9(12)
C(24)-C(25)-C(26)	121.9(13)
C(25)-C(26)-C(30)	119.0(11)
C(25)-C(26)-C(21)	117.8(11)
C(30)-C(26)-C(21)	123.1(10)
C(28)-C(27)-C(29)	112.6(12)
C(28)-C(27)-C(22)	110.2(12)
C(29)-C(27)-C(22)	114.4(12)
C(26)-C(30)-C(32)	113.1(11)
C(26)-C(30)-C(31)	111.6(10)
C(32)-C(30)-C(31)	108.9(10)
N(2)-C(33)-C(35)	121.0(10)
N(2)-C(33)-C(34)	123.3(11)
C(35)-C(33)-C(34)	115.7(10)
C(35)#3-C(34)-C(33)	122.6(11)
C(34)#3-C(35)-C(33)	121.7(11)
N(3)-C(36)-C(37)	119.8(9)
N(3)-C(36)-C(41)	120.2(9)
C(37)-C(36)-C(41)	120.0
C(36)-C(37)-C(38)	120.0
C(36)-C(37)-C(42)	124.3(12)
C(38)-C(37)-C(42)	115.7(12)

C(37)-C(38)-C(39)	120.0
C(40)-C(39)-C(38)	120.0
C(39)-C(40)-C(41)	120.0
C(40)-C(41)-C(36)	120.0
C(40)-C(41)-C(45)	117.8(11)
C(36)-C(41)-C(45)	122.2(11)
C(44)-C(42)-C(37)	111.4(16)
C(44)-C(42)-C(43)	109.9(17)
C(37)-C(42)-C(43)	114.0(19)
C(47)-C(45)-C(41)	110.9(15)
C(47)-C(45)-C(46)	110.9(17)
C(41)-C(45)-C(46)	111.6(14)
C(49)-C(48)-C(52)	108.0
C(49)-C(48)-C(53)	126.0
C(52)-C(48)-C(53)	126.0
C(49)-C(48)-U(2)	101.8(2)
C(52)-C(48)-U(2)	56.75(14)
C(53)-C(48)-U(2)	107.01(18)
C(49)-C(48)-U(3)	69.20(18)
C(52)-C(48)-U(3)	74.22(18)
C(53)-C(48)-U(3)	122.23(13)
U(2)-C(48)-U(3)	33.12(8)
C(48)-C(49)-C(50)	108.0
C(48)-C(49)-C(54)	126.0
C(50)-C(49)-C(54)	126.0
C(48)-C(49)-U(3)	81.75(19)
C(50)-C(49)-U(3)	68.92(15)

C(54)-C(49)-U(3)	115.34(18)
C(49)-C(50)-C(51)	108.0
C(49)-C(50)-C(55)	126.0
C(51)-C(50)-C(55)	126.0
C(49)-C(50)-U(3)	80.29(18)
C(51)-C(50)-U(3)	77.5(2)
C(55)-C(50)-U(3)	109.14(19)
C(52)-C(51)-C(50)	108.0
C(52)-C(51)-C(56)	126.0
C(50)-C(51)-C(56)	126.0
C(52)-C(51)-U(3)	82.58(17)
C(50)-C(51)-U(3)	71.2(2)
C(56)-C(51)-U(3)	112.56(18)
C(52)-C(51)-U(2)	57.16(19)
C(50)-C(51)-U(2)	102.03(17)
C(56)-C(51)-U(2)	106.49(17)
U(3)-C(51)-U(2)	34.70(8)
C(51)-C(52)-C(48)	108.0
C(51)-C(52)-C(57)	126.0
C(48)-C(52)-C(57)	126.0
C(51)-C(52)-U(2)	91.7(2)
C(48)-C(52)-U(2)	92.27(19)
C(57)-C(52)-U(2)	86.6(2)
C(51)-C(52)-U(3)	67.89(15)
C(48)-C(52)-U(3)	77.20(18)
C(57)-C(52)-U(3)	120.58(18)
U(2)-C(52)-U(3)	34.43(11)

C(52)-C(57)-U(2)	59.18(18)
C(59)-C(58)-C(62)	108.0
C(59)-C(58)-C(63)	126.0
C(62)-C(58)-C(63)	126.0
C(59)-C(58)-U(3)	58.67(19)
C(62)-C(58)-U(3)	93.20(17)
C(63)-C(58)-U(3)	113.25(16)
C(59)-C(58)-U(2)	85.68(17)
C(62)-C(58)-U(2)	64.18(19)
C(63)-C(58)-U(2)	115.75(17)
U(3)-C(58)-U(2)	33.74(7)
C(58)-C(59)-C(60)	108.0
C(58)-C(59)-C(64)	126.0
C(60)-C(59)-C(64)	126.0
C(58)-C(59)-U(3)	90.6(2)
C(60)-C(59)-U(3)	82.77(19)
C(64)-C(59)-U(3)	95.6(2)
C(58)-C(59)-U(2)	66.49(14)
C(60)-C(59)-U(2)	72.63(16)
C(64)-C(59)-U(2)	126.39(17)
U(3)-C(59)-U(2)	31.90(10)
C(61)-C(60)-C(59)	108.0
C(61)-C(60)-C(65)	126.0
C(59)-C(60)-C(65)	126.0
C(61)-C(60)-U(3)	96.1(2)
C(59)-C(60)-U(3)	64.53(16)
C(65)-C(60)-U(3)	105.95(19)

C(61)-C(60)-U(2)	63.08(18)
C(59)-C(60)-U(2)	79.93(17)
C(65)-C(60)-U(2)	122.27(14)
U(3)-C(60)-U(2)	33.18(9)
C(62)-C(61)-C(60)	108.0
C(62)-C(61)-C(66)	126.0
C(60)-C(61)-C(66)	126.0
C(62)-C(61)-U(2)	69.99(16)
C(60)-C(61)-U(2)	88.1(2)
C(66)-C(61)-U(2)	108.7(2)
C(61)-C(62)-C(58)	108.0
C(61)-C(62)-C(67)	126.0
C(58)-C(62)-C(67)	126.0
C(61)-C(62)-U(2)	78.04(18)
C(58)-C(62)-U(2)	85.3(2)
C(67)-C(62)-U(2)	104.2(2)
C(59)-C(64)-U(3)	53.58(16)
C(72)-C(68)-C(69)	108.6(3)
C(72)-C(68)-C(73)	126.1
C(69)-C(68)-C(73)	125.3(3)
C(72)-C(68)-U(2)	63.0(2)
C(69)-C(68)-U(2)	89.8(4)
C(73)-C(68)-U(2)	114.2(2)
C(72)-C(68)-U(3)	88.85(19)
C(69)-C(68)-U(3)	60.5(2)
C(73)-C(68)-U(3)	116.9(2)
U(2)-C(68)-U(3)	33.19(17)

C(70)-C(69)-C(68)	108.0
C(70)-C(69)-C(74)	125.3(3)
C(68)-C(69)-C(74)	126.7(3)
C(70)-C(69)-U(3)	78.0(7)
C(68)-C(69)-U(3)	90.4(2)
C(74)-C(69)-U(3)	98.9(2)
C(69)-C(70)-C(71)	107.4(3)
C(69)-C(70)-C(75)	126.6(3)
C(71)-C(70)-C(75)	126.0
C(69)-C(70)-U(3)	69.4(8)
C(71)-C(70)-U(3)	93.6(2)
C(75)-C(70)-U(3)	103.7(2)
C(69)-C(70)-U(2)	78.6(9)
C(71)-C(70)-U(2)	61.7(2)
C(75)-C(70)-U(2)	123.9(3)
U(3)-C(70)-U(2)	32.05(16)
C(70)-C(71)-C(72)	108.0
C(70)-C(71)-C(76)	126.0
C(72)-C(71)-C(76)	125.94(6)
C(70)-C(71)-U(2)	90.5(2)
C(72)-C(71)-U(2)	66.0(11)
C(76)-C(71)-U(2)	108.3(2)
C(70)-C(71)-U(3)	58.7(2)
C(72)-C(71)-U(3)	81.9(9)
C(76)-C(71)-U(3)	122.6(2)
U(2)-C(71)-U(3)	31.88(16)
C(68)-C(72)-C(71)	108.0

C(68)-C(72)-C(77)	126.0
C(71)-C(72)-C(77)	126.0
C(68)-C(72)-U(2)	86.20(19)
C(71)-C(72)-U(2)	82.3(11)
C(77)-C(72)-U(2)	101.4(2)
C(79)-C(78)-C(82)	108.24(5)
C(79)-C(78)-C(83)	125.72(6)
C(82)-C(78)-C(83)	126.0
C(79)-C(78)-U(2)	79.0(2)
C(82)-C(78)-U(2)	72.73(19)
C(83)-C(78)-U(2)	114.7(2)
C(80)-C(79)-C(78)	107.8
C(80)-C(79)-C(84)	125.9
C(78)-C(79)-C(84)	126.24(5)
C(80)-C(79)-U(2)	75.60(17)
C(78)-C(79)-U(2)	71.81(19)
C(84)-C(79)-U(2)	118.46(18)
C(79)-C(80)-C(81)	108.0
C(79)-C(80)-C(85)	125.8
C(81)-C(80)-C(85)	126.1
C(79)-C(80)-U(2)	75.66(16)
C(81)-C(80)-U(2)	71.78(19)
C(85)-C(80)-U(2)	118.42(18)
C(82)-C(81)-C(80)	108.1
C(82)-C(81)-C(86)	125.8
C(80)-C(81)-C(86)	126.1
C(82)-C(81)-U(3)	72.1(2)

C(80)-C(81)-U(3)	112.3(2)
C(86)-C(81)-U(3)	86.5(2)
C(82)-C(81)-U(2)	72.81(19)
C(80)-C(81)-U(2)	78.9(2)
C(86)-C(81)-U(2)	114.60(16)
U(3)-C(81)-U(2)	34.76(10)
C(81)-C(82)-C(78)	107.9
C(81)-C(82)-C(87)	125.8
C(78)-C(82)-C(87)	126.30(7)
C(81)-C(82)-U(3)	76.4(2)
C(78)-C(82)-U(3)	111.3(2)
C(87)-C(82)-U(3)	83.8(2)
C(81)-C(82)-U(2)	77.2(2)
C(78)-C(82)-U(2)	77.18(18)
C(87)-C(82)-U(2)	112.2(2)
U(3)-C(82)-U(2)	35.52(8)
C(81)-C(86)-U(3)	62.86(17)
C(82)-C(87)-U(3)	64.37(19)
C(92)-C(91)-C(96)	120.0
C(92)-C(91)-N(5)	126(4)
C(96)-C(91)-N(5)	114(4)
C(91)-C(92)-C(93)	120.0
C(92)-C(93)-C(94)	120.0
C(93)-C(94)-C(95)	120.0
C(93)-C(94)-N(4)	127(4)
C(95)-C(94)-N(4)	112(4)
C(96)-C(95)-C(94)	120.0

C(95)-C(96)-C(91)	120.0

Table S4.16. Crystallographic data and structure refinement details for **21**.

	21
Formula	$C_{44}H_{57}N_2U$
a (Å)	13.328(3)
b (Å)	16.963(4)
c (Å)	32.855(8)
α (º)	90
β (º)	90
γ (º)	90
V (Å^3)	7428(3)
Z	10
FW	851.98
crystal system	orthorhombic
space group	P*bca*
T (K)	100(2)
λ (Å)	0.71073
ρ_{calc} (g•cm^{-1})	1.524
μ (mm^{-1})	4.403
F(000)	3416
θ range (º)	1.97 - 25.04
total reflections	84966
unique reflections	6560
parameters	438
R_1	0.0488
wR_2 (all data)	0.1513
max min peaks eÅ^{-3}	0.802, -1.934
GOF on F^2	1.099

Table S4.17. Atomic coordinates and equivalent isotropic displacement parameters (A^2) for **21**. U(eq) is defined as one third of the trace of the orthogonalized U^{ij} tensor.

	X	*Y*	*Z*	U_{iso}*/U_{eq}
U1	0.961523 (15)	0.488110 (15)	0.051397 (14)	0.01164 (8)
N1	1.0971 (4)	0.5112 (4)	−0.0243 (3)	0.0173 (12)
N2	0.8388 (4)	0.5779 (4)	0.0116 (4)	0.0162 (12)
C1	1.0450 (5)	0.4852 (4)	0.2121 (4)	0.0157 (12)

C2	0.9475 (4)	0.5031 (5)	0.2269 (4)	0.0150 (13)
C3	1.2663 (5)	0.4928 (5)	−0.0496 (4)	0.0226 (14)
H3	1.2665	0.5372	−0.0898	0.027*
C4	1.1868 (5)	0.4023 (5)	0.0511 (5)	0.0201 (14)
H4	1.1330	0.3863	0.0797	0.024*
C5	0.7368 (5)	0.3891 (4)	−0.0511 (5)	0.0191 (13)
H5A	0.7363	0.4455	−0.0780	0.029*
H5B	0.6946	0.3895	−0.0042	0.029*
H5C	0.7180	0.3450	−0.0908	0.029*
C6	0.7250 (5)	0.5164 (5)	0.1080 (4)	0.0180 (14)
H6	0.7730	0.4897	0.1378	0.022*
C7	0.8579 (5)	0.3317 (4)	0.0592 (5)	0.0164 (13)
C8	0.7467 (5)	0.5705 (4)	0.0380 (4)	0.0156 (14)
C9	1.1844 (5)	0.5794 (5)	0.1613 (5)	0.0247 (17)
H9A	1.1939	0.6032	0.1059	0.037*
H9B	1.2201	0.5265	0.1674	0.037*
H9C	1.2039	0.6213	0.2028	0.037*
C10	0.8548 (4)	0.6469 (5)	−0.0468 (5)	0.0175 (14)
C11	1.0268 (6)	0.7137 (5)	0.1293 (5)	0.0241 (16)
H11A	1.0902	0.7310	0.1381	0.036*
H11B	0.9863	0.7527	0.1593	0.036*
H11C	1.0127	0.7160	0.0701	0.036*
C12	1.1077 (5)	0.6583 (5)	−0.0870 (5)	0.0200 (15)
H12	1.1087	0.6834	−0.0336	0.024*
C13	1.0701 (5)	0.2884 (5)	−0.0704 (5)	0.0208 (16)
H13A	1.1115	0.2657	−0.0283	0.031*
H13B	1.1005	0.3345	−0.1011	0.031*
H13C	1.0530	0.2422	−0.1085	0.031*

C14	0.9994 (6)	0.2456 (5)	0.1163 (5)	0.0234 (17)
H14A	0.9748	0.2565	0.1716	0.035*
H14B	1.0649	0.2572	0.1161	0.035*
H14C	0.9886	0.1854	0.1012	0.035*
C15	1.0997 (5)	0.5677 (5)	−0.0958 (5)	0.0191 (15)
C16	1.1006 (5)	0.5323 (5)	−0.1775 (4)	0.0213 (16)
H16	1.0960	0.4719	−0.1844	0.026*
C17	1.0829 (5)	0.5590 (5)	0.1734 (4)	0.0196 (16)
C18	0.9113 (5)	0.3671 (5)	−0.0721 (4)	0.0154 (15)
C19	1.0131 (5)	0.6211 (5)	0.1611 (4)	0.0169 (14)
C20	0.5601 (5)	0.5423 (5)	0.0905 (5)	0.0220 (16)
H20	0.4990	0.5334	0.1074	0.026*
C21	0.9522 (5)	0.3046 (4)	0.0537 (5)	0.0166 (12)
C22	0.9848 (5)	0.3239 (5)	−0.0288 (4)	0.0178 (15)
C23	0.6337 (5)	0.5021 (5)	0.1332 (4)	0.0217 (15)
H23	0.6215	0.4656	0.1788	0.026*
C24	1.1822 (5)	0.4694 (5)	−0.0089 (4)	0.0174 (14)
C25	0.9125 (5)	0.3893 (5)	−0.1645 (5)	0.0223 (16)
H25A	0.8520	0.3795	−0.1880	0.033*
H25B	0.9570	0.3527	−0.1928	0.033*
H25C	0.9295	0.4498	−0.1716	0.033*
C26	0.8460 (5)	0.6436 (5)	0.2142 (5)	0.0209 (16)
H26A	0.8630	0.6921	0.2496	0.031*
H26B	0.8001	0.6084	0.2423	0.031*
H26C	0.8209	0.6653	0.1621	0.031*
C27	0.8701 (5)	0.6302 (5)	−0.1319 (5)	0.0230 (17)
H27	0.8705	0.5724	−0.1507	0.028*
C28	0.8326 (5)	0.3693 (5)	−0.0202 (4)	0.0141 (14)

C29	0.5807 (5)	0.5960 (5)	0.0222 (5)	0.0215 (16)
H29	0.5324	0.6227	−0.0070	0.026*
C30	1.2683 (6)	0.3591 (5)	0.0691 (4)	0.0237 (16)
H30	1.2684	0.3139	0.1085	0.028*
C31	0.8822 (5)	0.7830 (5)	−0.1626 (5)	0.0289 (17)
H31	0.8918	0.8283	−0.2010	0.035*
C32	0.8848 (6)	0.6970 (6)	−0.1891 (5)	0.0288 (18)
H32	0.8964	0.6839	−0.2454	0.035*
C33	0.8652 (5)	0.8019 (5)	−0.0784 (5)	0.0219 (16)
H33	0.8633	0.8599	−0.0603	0.026*
C34	1.1081 (5)	0.5854 (5)	−0.2480 (5)	0.0236 (16)
H34	1.1094	0.5609	−0.3017	0.028*
C35	1.3499 (5)	0.3823 (5)	0.0292 (5)	0.0245 (17)
H35	1.4050	0.3531	0.0415	0.029*
C36	0.6718 (5)	0.6109 (5)	−0.0036 (5)	0.0191 (15)
C37	1.0975 (6)	0.4110 (5)	0.2528 (5)	0.0253 (17)
H37A	1.1623	0.4159	0.2393	0.038*
H37B	1.0740	0.3561	0.2322	0.038*
H37C	1.0895	0.4137	0.3128	0.038*
C38	1.1142 (6)	0.7115 (5)	−0.1583 (5)	0.0297 (17)
H38	1.1190	0.7720	−0.1521	0.036*
C39	0.8865 (6)	0.4497 (5)	0.2833 (4)	0.0232 (15)
H39A	0.9007	0.4627	0.3411	0.035*
H39B	0.8970	0.3885	0.2728	0.035*
H39C	0.8226	0.4636	0.2722	0.035*
C40	0.8510 (5)	0.7344 (5)	−0.0213 (5)	0.0171 (15)
H40	0.8388	0.7477	0.0349	0.020*
C41	1.3484 (5)	0.4496 (6)	−0.0295 (5)	0.030 (2)

H41	1.4033	0.4662	−0.0560	0.036*
C42	0.9297 (5)	0.5891 (5)	0.1963 (4)	0.0168 (14)
C43	0.7928 (5)	0.3027 (5)	0.1281 (5)	0.0222 (16)
H43A	0.7356	0.3348	0.1238	0.033*
H43B	0.8207	0.3136	0.1820	0.033*
H43C	0.7804	0.2411	0.1222	0.033*
C44	1.1134 (6)	0.6752 (6)	−0.2378 (5)	0.0285 (18)
H44	1.1166	0.7114	−0.2849	0.034*

Table S4.18. Anisotropic displacement parameters (A^2) for **21**. The anisotropic displacement factor exponent takes the form: $-2\pi^2$ [$h^2 a^{2*}U^{11}$ + ... + 2 h k a* b* U^{12}].

	U^{11}	U^{22}	U^{33}	U^{12}	U^{13}	U^{23}
U1	0.01129 (11)	0.01231 (11)	0.01132 (11)	−0.00043 (9)	−0.00001 (9)	0.00019 (8)
N1	0.016 (3)	0.017 (3)	0.018 (3)	−0.001 (2)	0.000 (2)	0.001 (2)
N2	0.018 (3)	0.018 (3)	0.013 (3)	0.002 (2)	−0.002 (2)	0.001 (2)
C1	0.017 (3)	0.019 (3)	0.011 (3)	−0.003 (3)	0.002 (2)	−0.005 (2)
C2	0.014 (3)	0.025 (3)	0.006 (3)	−0.002 (3)	−0.001 (2)	0.000 (2)
C3	0.017 (3)	0.028 (4)	0.022 (3)	−0.001 (3)	0.001 (3)	0.003 (4)
C4	0.021 (3)	0.024 (3)	0.015 (3)	−0.002 (3)	0.000 (3)	−0.006 (3)
C5	0.023 (3)	0.016 (3)	0.018 (3)	0.001 (3)	−0.003 (3)	−0.006 (3)
C6	0.020 (3)	0.013 (3)	0.020 (3)	0.001 (3)	0.000 (3)	0.001 (3)
C7	0.021 (3)	0.014 (3)	0.015 (3)	−0.004 (2)	0.001 (3)	0.002 (3)
C8	0.017 (3)	0.014 (3)	0.016 (4)	0.002 (3)	−0.005 (3)	−0.003 (3)
C9	0.018 (4)	0.029 (4)	0.027 (4)	−0.007 (3)	0.000 (3)	−0.008 (3)
C10	0.008 (3)	0.028 (4)	0.017 (3)	0.002 (2)	0.001 (3)	0.001 (3)
C11	0.035 (4)	0.015 (3)	0.022 (4)	−0.005 (3)	0.000 (3)	−0.003 (3)
C12	0.021 (4)	0.023 (4)	0.016 (3)	0.007 (3)	0.003 (3)	−0.002 (3)
C13	0.021 (4)	0.021 (4)	0.021 (4)	0.002 (3)	0.000 (3)	−0.004 (3)
C14	0.030 (4)	0.013 (3)	0.028 (4)	0.005 (3)	−0.002 (3)	0.004 (3)

C15	0.010 (3)	0.017 (4)	0.030 (4)	0.000 (3)	0.001 (3)	0.005 (3)
C16	0.034 (4)	0.020 (4)	0.010 (3)	0.001 (3)	−0.005 (3)	−0.003 (3)
C17	0.014 (3)	0.026 (4)	0.019 (4)	−0.003 (3)	0.000 (3)	−0.003 (3)
C18	0.016 (3)	0.013 (3)	0.018 (4)	−0.002 (3)	−0.007 (3)	−0.002 (2)
C19	0.022 (4)	0.019 (3)	0.010 (3)	−0.002 (3)	−0.002 (3)	−0.001 (3)
C20	0.022 (4)	0.020 (3)	0.024 (4)	−0.006 (3)	0.006 (3)	−0.001 (3)
C21	0.020 (3)	0.016 (3)	0.014 (3)	−0.003 (3)	−0.006 (3)	−0.002 (3)
C22	0.019 (4)	0.015 (3)	0.019 (4)	0.001 (3)	−0.005 (3)	−0.004 (2)
C23	0.031 (4)	0.016 (4)	0.018 (3)	−0.004 (3)	−0.003 (3)	0.004 (3)
C24	0.015 (3)	0.018 (4)	0.019 (3)	−0.001 (3)	−0.002 (3)	−0.002 (3)
C25	0.028 (4)	0.017 (4)	0.021 (4)	−0.003 (3)	−0.003 (3)	−0.002 (3)
C26	0.023 (4)	0.024 (4)	0.016 (4)	0.002 (3)	0.000 (3)	−0.005 (3)
C27	0.024 (4)	0.020 (4)	0.025 (4)	0.003 (3)	0.002 (3)	0.001 (3)
C28	0.015 (4)	0.016 (3)	0.011 (3)	0.000 (3)	−0.003 (3)	−0.007 (3)
C29	0.021 (4)	0.020 (4)	0.023 (4)	0.006 (3)	−0.001 (3)	0.000 (3)
C30	0.038 (4)	0.015 (3)	0.018 (4)	0.004 (3)	−0.004 (3)	−0.004 (3)
C31	0.023 (4)	0.029 (4)	0.035 (4)	0.003 (3)	0.006 (4)	0.016 (4)
C32	0.028 (4)	0.037 (5)	0.021 (4)	0.000 (4)	0.010 (3)	0.001 (3)
C33	0.015 (3)	0.021 (4)	0.030 (4)	0.000 (3)	−0.006 (3)	0.003 (3)
C34	0.023 (4)	0.032 (4)	0.016 (4)	0.004 (3)	0.001 (3)	0.008 (3)
C35	0.020 (4)	0.024 (4)	0.029 (4)	0.010 (3)	−0.007 (3)	−0.004 (3)
C36	0.016 (4)	0.018 (4)	0.023 (4)	0.001 (3)	−0.003 (3)	−0.006 (3)
C37	0.032 (4)	0.030 (4)	0.015 (4)	0.006 (3)	−0.006 (3)	0.004 (3)
C38	0.040 (5)	0.023 (4)	0.026 (4)	0.008 (4)	0.007 (4)	0.003 (3)
C39	0.027 (4)	0.028 (4)	0.015 (3)	−0.002 (3)	0.002 (3)	0.000 (3)
C40	0.018 (3)	0.017 (4)	0.017 (3)	0.002 (3)	−0.001 (3)	−0.001 (3)
C41	0.014 (3)	0.044 (5)	0.032 (5)	0.002 (3)	0.002 (3)	−0.002 (4)
C42	0.018 (3)	0.020 (4)	0.012 (3)	−0.001 (3)	0.001 (3)	−0.001 (3)

C43	0.021 (4)	0.024 (4)	0.022 (4)	−0.002 (3)	−0.002 (3)	0.004 (3)
C44	0.036 (4)	0.029 (4)	0.021 (4)	0.004 (4)	0.007 (4)	0.009 (3)

Table S4.19. Bond lengths [Å], bond angles [º], and torsion angles [º] for **21**.

U1—N1	2.317	(5)	C7—C43	1.506	(10)
U1—N2	2.322	(6)	C8—C36	1.405	(10)
U1—C19	2.772	(7)	C9—C17	1.507	(10)
U1—C18	2.785	(7)	C10—C27	1.390	(11)
U1—C2	2.800	(6)	C10—C40	1.395	(10)
U1—C21	2.801	(6)	C11—C19	1.512	(10)
U1—C42	2.804	(7)	C12—C15	1.393	(11)
U1—C7	2.815	(6)	C12—C38	1.394	(11)
U1—C1	2.818	(6)	C13—C22	1.495	(10)
U1—C17	2.822	(7)	C14—C21	1.502	(10)
U1—C22	2.827	(7)	C15—C16	1.403	(10)
U1—C28	2.831	(7)	C16—C34	1.385	(10)
N1—C24	1.402	(9)	C17—C19	1.394	(10)
N1—C15	1.424	(9)	C18—C28	1.400	(10)
N2—C8	1.396	(9)	C18—C22	1.423	(9)
N2—C10	1.419	(9)	C18—C25	1.504	(10)
C1—C17	1.392	(10)	C19—C42	1.410	(10)
C1—C2	1.450	(8)	C20—C29	1.389	(10)
C1—C37	1.505	(10)	C20—C23	1.399	(10)
C2—C42	1.422	(10)	C21—C22	1.421	(10)
C2—C39	1.494	(9)	C26—C42	1.491	(10)
C3—C41	1.390	(10)	C27—C32	1.380	(11)
C3—C24	1.417	(9)	C29—C36	1.393	(10)
C4—C30	1.375	(10)	C30—C35	1.381	(11)
C4—C24	1.399	(10)	C31—C32	1.377	(12)

C5—C28	1.494 (9)	C31—C33	1.387 (12)
C6—C23	1.390 (10)	C33—C40	1.386 (10)
C6—C8	1.418 (10)	C34—C44	1.380 (12)
C7—C21	1.421 (9)	C35—C41	1.386 (12)
C7—C28	1.432 (10)	C38—C44	1.376 (12)
N1—U1—N2	114.2 (2)	C1—C2—U1	75.7 (3)
N1—U1—C19	89.3 (2)	C39—C2—U1	126.4 (4)
N2—U1—C19	86.8 (2)	C41—C3—C24	120.3 (7)
N1—U1—C18	87.4 (2)	C30—C4—C24	122.1 (7)
N2—U1—C18	90.1 (2)	C23—C6—C8	121.6 (6)
C19—U1—C18	174.1 (2)	C21—C7—C28	107.8 (6)
N1—U1—C2	124.27 (18)	C21—C7—C43	123.7 (6)
N2—U1—C2	99.6 (2)	C28—C7—C43	126.7 (6)
C19—U1—C2	48.4 (2)	C21—C7—U1	74.8 (4)
C18—U1—C2	137.2 (2)	C28—C7—U1	75.9 (4)
N1—U1—C21	101.5 (2)	C43—C7—U1	127.7 (5)
N2—U1—C21	123.7 (2)	N2—C8—C36	123.5 (6)
C19—U1—C21	137.3 (2)	N2—C8—C6	119.4 (6)
C18—U1—C21	48.3 (2)	C36—C8—C6	117.0 (6)
C2—U1—C21	93.7 (2)	C27—C10—C40	117.5 (7)
N1—U1—C42	118.6 (2)	C27—C10—N2	121.5 (7)
N2—U1—C42	77.0 (2)	C40—C10—N2	120.9 (7)
C19—U1—C42	29.3 (2)	C15—C12—C38	120.1 (7)
C18—U1—C42	153.8 (2)	C12—C15—C16	118.2 (7)
C2—U1—C42	29.4 (2)	C12—C15—N1	121.5 (7)
C21—U1—C42	122.0 (2)	C16—C15—N1	120.2 (6)
N1—U1—C7	126.7 (2)	C34—C16—C15	121.5 (7)
N2—U1—C7	96.2 (2)	C1—C17—C19	109.2 (6)

C19—U1—C7	137.2 (2)	C1—C17—C9	127.0 (7)
C18—U1—C7	48.1 (2)	C19—C17—C9	122.8 (7)
C2—U1—C7	89.2 (2)	C1—C17—U1	75.5 (4)
C21—U1—C7	29.31 (19)	C19—C17—U1	73.6 (4)
C42—U1—C7	110.0 (2)	C9—C17—U1	126.3 (5)
N1—U1—C1	96.39 (18)	C28—C18—C22	109.2 (6)
N2—U1—C1	125.4 (2)	C28—C18—C25	125.2 (6)
C19—U1—C1	47.9 (2)	C22—C18—C25	124.4 (6)
C18—U1—C1	137.39 (19)	C28—C18—U1	77.4 (4)
C2—U1—C1	29.92 (17)	C22—C18—U1	77.0 (4)
C21—U1—C1	89.6 (2)	C25—C18—U1	122.2 (5)
C42—U1—C1	48.5 (2)	C17—C19—C42	108.9 (6)
C7—U1—C1	99.9 (2)	C17—C19—C11	125.9 (7)
N1—U1—C17	77.0 (2)	C42—C19—C11	124.5 (7)
N2—U1—C17	115.6 (2)	C17—C19—U1	77.6 (4)
C19—U1—C17	28.8 (2)	C42—C19—U1	76.6 (4)
C18—U1—C17	153.7 (2)	C11—C19—U1	120.5 (5)
C2—U1—C17	48.09 (19)	C29—C20—C23	118.2 (7)
C21—U1—C17	113.8 (2)	C22—C21—C7	108.2 (6)
C42—U1—C17	47.8 (2)	C22—C21—C14	125.7 (6)
C7—U1—C17	128.5 (2)	C7—C21—C14	124.4 (7)
C1—U1—C17	28.6 (2)	C22—C21—U1	76.4 (4)
N1—U1—C22	78.6 (2)	C7—C21—U1	75.9 (4)
N2—U1—C22	119.3 (2)	C14—C21—U1	125.8 (5)
C19—U1—C22	153.9 (2)	C21—C22—C18	107.1 (6)
C18—U1—C22	29.36 (19)	C21—C22—C13	127.1 (6)
C2—U1—C22	121.9 (2)	C18—C22—C13	124.4 (6)
C21—U1—C22	29.2 (2)	C21—C22—U1	74.4 (4)

C42—U1—C22	150.9 (2)	C18—C22—U1	73.7 (4)
C7—U1—C22	48.2 (2)	C13—C22—U1	128.0 (5)
C1—U1—C22	110.0 (2)	C6—C23—C20	120.6 (7)
C17—U1—C22	125.0 (2)	C4—C24—N1	119.5 (6)
N1—U1—C28	116.2 (2)	C4—C24—C3	116.9 (6)
N2—U1—C28	76.7 (2)	N1—C24—C3	123.6 (6)
C19—U1—C28	153.5 (2)	C32—C27—C10	121.9 (7)
C18—U1—C28	28.9 (2)	C18—C28—C7	107.6 (6)
C2—U1—C28	113.81 (19)	C18—C28—C5	124.0 (6)
C21—U1—C28	48.3 (2)	C7—C28—C5	127.1 (6)
C42—U1—C28	125.0 (2)	C18—C28—U1	73.7 (4)
C7—U1—C28	29.4 (2)	C7—C28—U1	74.7 (4)
C1—U1—C28	129.2 (2)	C5—C28—U1	127.4 (4)
C17—U1—C28	157.8 (2)	C20—C29—C36	121.8 (7)
C22—U1—C28	48.0 (2)	C4—C30—C35	120.6 (7)
C24—N1—C15	112.9 (5)	C32—C31—C33	119.7 (7)
C24—N1—U1	125.2 (4)	C31—C32—C27	119.8 (7)
C15—N1—U1	121.8 (4)	C40—C33—C31	120.1 (7)
C8—N2—C10	114.2 (6)	C44—C34—C16	119.3 (7)
C8—N2—U1	126.4 (5)	C30—C35—C41	118.9 (7)
C10—N2—U1	119.4 (4)	C29—C36—C8	120.8 (7)
C17—C1—C2	107.4 (6)	C44—C38—C12	120.6 (7)
C17—C1—C37	126.9 (6)	C33—C40—C10	121.0 (7)
C2—C1—C37	123.9 (6)	C35—C41—C3	121.2 (7)
C17—C1—U1	75.9 (4)	C19—C42—C2	107.5 (6)
C2—C1—U1	74.4 (3)	C19—C42—C26	124.8 (7)
C37—C1—U1	127.9 (4)	C2—C42—C26	126.5 (6)
C42—C2—C1	107.0 (6)	C19—C42—U1	74.1 (4)

C42—C2—C39	127.0 (6)	C2—C42—U1	75.1 (4)
C1—C2—C39	124.3 (6)	C26—C42—U1	126.4 (5)
C42—C2—U1	75.5 (4)	C38—C44—C34	120.4 (7)